United States
Environmental Protection
Agency

Environmental Research
Laboratory
Athens GA 30613

EPA/600/6-85/002b
September 1985
Revised

Research and Development

EPA

Water Quality Assessment:

A Screening Procedure for Toxic and Conventional Pollutants in Surface and Ground Water—Part II (Revised 1985)

EPA/600/6-85/002b
September 1985

WATER QUALITY ASSESSMENT:
A Screening Procedure for Toxic and Conventional Pollutants
(Revised 1985)

Part II

by

W.B. Mills, D.B. Porcella, M.J. Ungs, S.A. Gherini, K.V. Summers,
Lingfung Mok, G.L. Rupp, and G.L. Bowie
Tetra Tech, Incorporated
Lafayette, California 94549

and

D.A. Haith
Cornell University
Ithaca, New York 14853

Produced by:

JACA Corporation
Fort Washington, Pennsylvania 19034

Contract No. 68-03-3131

Prepared in Cooperation with U.S. EPA's

Center for Water Quality Modeling
Environmental Research Laboratory
Athens, Georgia

Monitoring and Data Support Division
Office of Water Regulations and Standards
Office of Water
Washington, D.C.

Technology Transfer
Center for Environmental Research Information
Cincinnati, Ohio

ENVIRONMENTAL RESEARCH LABORATORY
OFFICE OF RESEARCH AND DEVELOPMENT
U.S. ENVIRONMENTAL PROTECTION AGENCY
ATHENS, GEORGIA 30613

DISCLAIMER

Mention of trade names or commercial products does not constitute endorsement or recommendation for use by the U.S. Environmental Protection Agency.

ABSTRACT

New technical developments in the field of water quality assessment and a reordering of water quality priorities prompted a revision of the first two editions of this manual. The utility of the revised manual is enhanced by the inclusion of methods to predict the transport and fate of toxic chemicals in ground water, and by methods to predict the fate of metals in rivers. In addition, major revisions were completed on Chapter 2 (organic toxicants), Chapter 3 (waste loadings), and Chapter 5 (impoundments) that reflect recent advancements in these fields.

Applying the manual's simple techniques, the user is now capable of assessing the loading and fate of conventional pollutants (temperature, biochemical oxygen demand-dissolved oxygen, nutrients, and sediments) and toxic pollutants (from the U.S. EPA list of priority pollutants) in streams, impoundments, estuaries, and ground waters. The techniques are readily programmed on hand-held calculators or microcomputers. Most of the data required for using these procedures are contained in the manual.

Because of its size, the manual has been divided into two parts. Part I contains the introduction and chapters on the aquatic fate of toxic organic substances, waste loading calculations, and the assessment of water quality parameters in rivers and streams. Part II continues with chapters on the assessment of impoundments, estuaries, and ground water and appendices E, H, I, and J. Appendices D, F, and G are provided on microfiche in the EPA-printed manual. Appendices A, B, and C, which appeared in the first two editions, are now out of date and have been deleted.

This report is submitted in fulfillment of Contract No. 68-03-3131 by JACA Corp. and Tetra Tech, Inc. under the sponsorship of the U.S. Environmental Protection Agency. Work was completed as of May 1985.

TABLE OF CONTENTS

LIST OF FIGURES

PART II

LIST OF TABLES

PART II

CHAPTER 5

IMPOUNDMENTS

5.1 INTRODUCTION

This chapter contains several methods for assessing water quality and physical conditions in impoundments. The general topics covered are sediment accumulation, thermal stratification, DO-BOD, eutrophication, and toxicant concentrations. These topics cover the major water problems likely to occur in impoundments. The methods developed are easy to use and require readily obtainable data. Because the methods depend upon a number of simplifying assumptions, estimates should be taken only as a guide pending further analysis. Also, since pollutant inputs are dependent on previous calculations, familiarity with the methods in previous chapters will be very helpful and expand understanding of the various processes.

Some of the techniques are more mechanistic and reliable than others. For example, the thermal stratification technique is based upon output of a calibrated and validated hydrothermal model. The model has been shown to be a good one, and to the extent that physical conditions in the studied impoundments resemble those of the model, results should be very reliable. On the other hand, the methods for predicting eutrophication are empirical and based upon correlations between historical water quality conditions and algal productivity in a number of lakes and reservoirs. Because algal blooms are sensitive to environmental factors and the presence of toxicants and factors other than those involved in the estimation methods, the methods for predicting eutrophication will occasionally be inapplicable. Additional approaches have been developed to broaden the applicability of these empirical models.

In using the techniques to be presented, it is important to apply good "engineering judgment" particularly where sequential application of methods is likely to result in cumulative errors. Such would be the case, for example, in evaluating impoundment hypolimnion DO problems resulting from algal blooms. If methods presented below are used to evaluate hypolimnion DO, the planner should determine when stratification occurs, the magnitude of point and nonpoint source BOD loads, and algal productivity and settling rates. From all of this, he may then predict BOD and DO levels in the hypolimnion. Since each of these techniques has an error associated with it, the end result of the computation will have a significant error envelope and results must be interpreted accordingly. The best way to use any of the techniques is to assume a range of values for important coefficients in order to obtain a range of results within which the studied impoundment is likely to fall.

Although scientists and engineers are familiar with the metric system of units, planners, local interest groups, and the general public are more accustomed to the English system. Most morphometric data on lakes and impoundments are in English

units. The conversion tables in Appendix H should be thoroughly familiar before using these techniques and users should be able to perform calculations in either system even though metric units are simpler to use. Also, dimensional analysis techniques using unit conversions are very helpful in performing the calculations.

The methods presented below are arranged in an order such that the planner should be able to use each if he has read preceding materials. The order of presentation is:

- Impoundment stratification (5.2)
- Sediment accumulation (5.3)
- Eutrophication (5.4)
- Impoundment dissolved oxygen (5.5)
- Fate of Priority Pollutants (Toxics) (5.6).

It is strongly recommended that all materials presented be read and examples worked prior to applying any of the methods. In this way a better perspective can be obtained on the kinds of problems covered and what can be done using hand calculations. A glossary of terms has been placed after the reference section so that equation terms can easily be checked.

The final section (5.7) is an example application to a selected site. This example allows the user to have an integrated view of an actual problem and application. Also "the goodness of fit" to measured results can be evaluated.

5.2 IMPOUNDMENT STRATIFICATION

5.2.1 Discussion

The density of water is strongly influenced by temperature and by the concentration of dissolved and suspended matter. Figure V-1 shows densities for water as a function of temperature and dissolved solids concentration (from Chen and Orlob, 1973).

Regardless of the reason for density differences, water of lowest density tends to move upward and reside on the surface of an impoundment while water of greatest density tends to sink. Inflowing water seeks an impoundment level containing water of the same density. Figure V-2 shows this effect schematically.

Where density gradients are very steep, mixing is inhibited. Thus, where the bottom water of an impoundment is significantly more dense than surface water, vertical mixing is likely to be unimportant. The fact that low density water tends to reside atop higher density water and that mixing is inhibited by steep gradients often results in impoundment stratification. Stratification, which is the establishment of distinct layers of different densities, tends to be enhanced by quiescent conditions. Conversely, any phenomenon encouraging mixing, such as wind stress, turbulence due to large inflows, or destabilizing changes in water temperature will tend to reduce or eliminate strata.

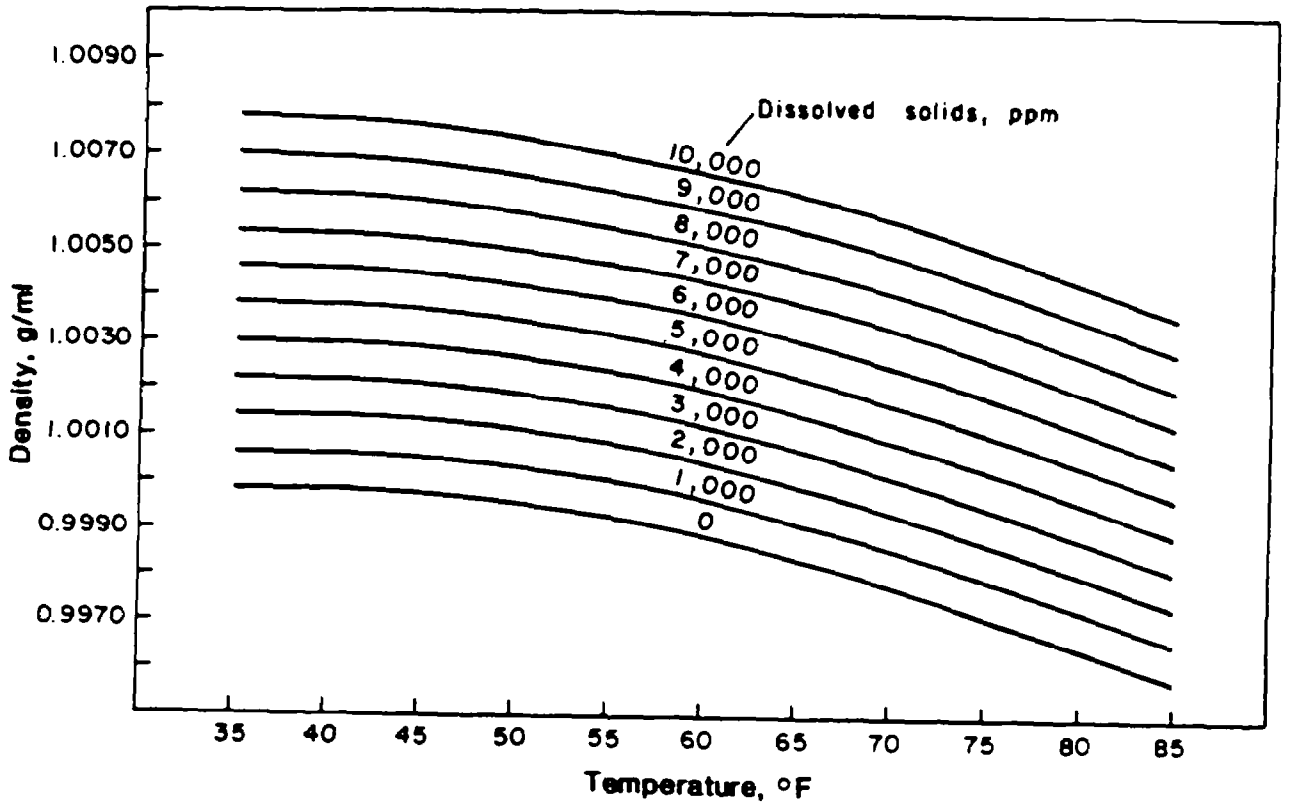

FIGURE V-1 WATER DENSITY AS A FUNCTION OF TEMPERATURE AND DISSOLVED SOLIDS CONCENTRATION (FROM CHEN AND ORLOB, 1973)

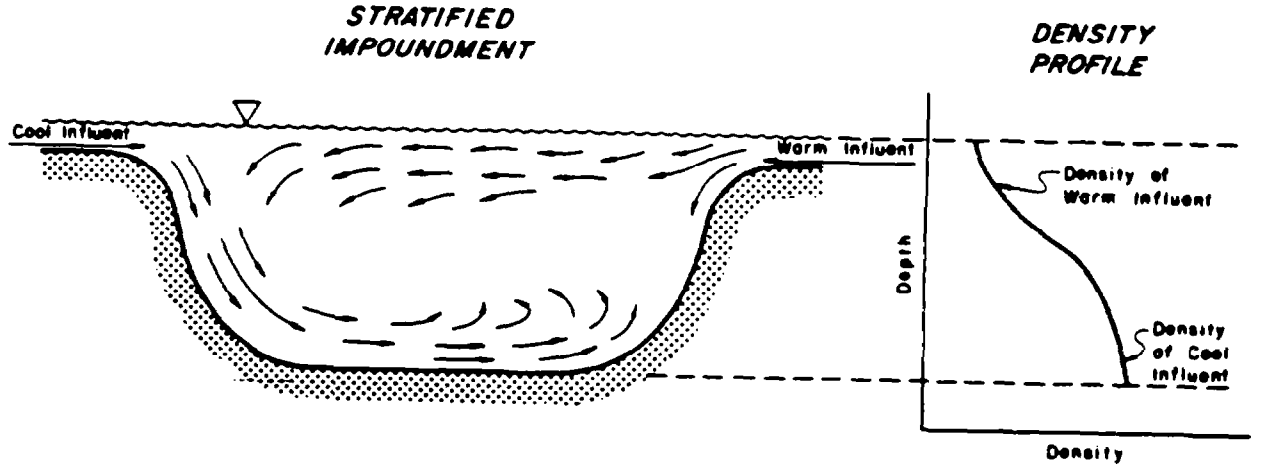

FIGURE V-2 WATER FLOWING INTO AN IMPOUNDMENT TENDS TO MIGRATE TOWARD A REGION OF SIMILAR DENSITY

5.2.1.1 Annual Cycle in a Thermally Stratified Impoundment

Figure V-3 shows schematically the processes of thermal stratification and overturn which occur in many impoundments. Beginning at "a" in the figure (winter), cold water (at about 4°C) flows into the impoundment which may at this point be considered as fully mixed. There is no thermal gradient over depth and the impoundment temperature is about 6°C. During spring ("b"), inflowing water is slightly warmer than that of the impoundment because of the exposure of the tributary stream to warmer air and increasingly intense sunlight. This trend continues during the summer ("c"), with tributary water being much warmer and less dense than the deep waters of the impoundment. At the same time, the surface water of the impoundment is directly heated by insolation. Since the warm water tends to stay on top of the impoundment, thermal strata form.

As fall approaches ("d"), day length decreases, air temperatures drop, and solar intensity decreases. The result is cooler inflows and a cooling trend in the surface of the impoundment. The bottom waters lag behind the surface in the rate of temperature change, and ultimately the surface may cool to the temperature of the bottom. Since continued increases in surface water density result in instability, the impoundment water mixes (overturns).

5.2.1.2 Monomictic and Dimictic Impoundments

The stratification and overturn processes described in Figure V-3 represent what occurs in a monomictic or single-overturn water body. Some impoundments, especially those north of 40°N latitude and those at high elevation, may undergo two periods of stratification and two overturns. Such impoundments are termed "dimictic." In addition to the summer stratification and resulting fall overturn, such impoundments stratify in late winter. This occurs because water is most dense near 4°C, and bottom waters may be close to this temperature, while inflowing water is colder and less dense. As the surface goes below 4°C, strata are established. With spring warming of the surface to 4°C, wind induced mixing occurs.

5.2.1.3 Importance of Stratification

Stratification is likely to be the single most important phenomenon affecting water quality in many impoundments. Where stratification is absent, water mixes vertically, and net horizontal flow is significant to considerable depths. Since the water is mixed vertically, DO replenishment usually occurs even to the bottom and anoxic (literally "no oxygen") conditions are unlikely. Generally speaking, fully mixed impoundments do not have DO deficiency problems.

When stratification occurs, the situation is vastly different. Flow within the impoundment is especially limited to the epilimnion (surface layer). Thus surface velocities are somewhat higher in an impoundment when stratified than when unstrati-

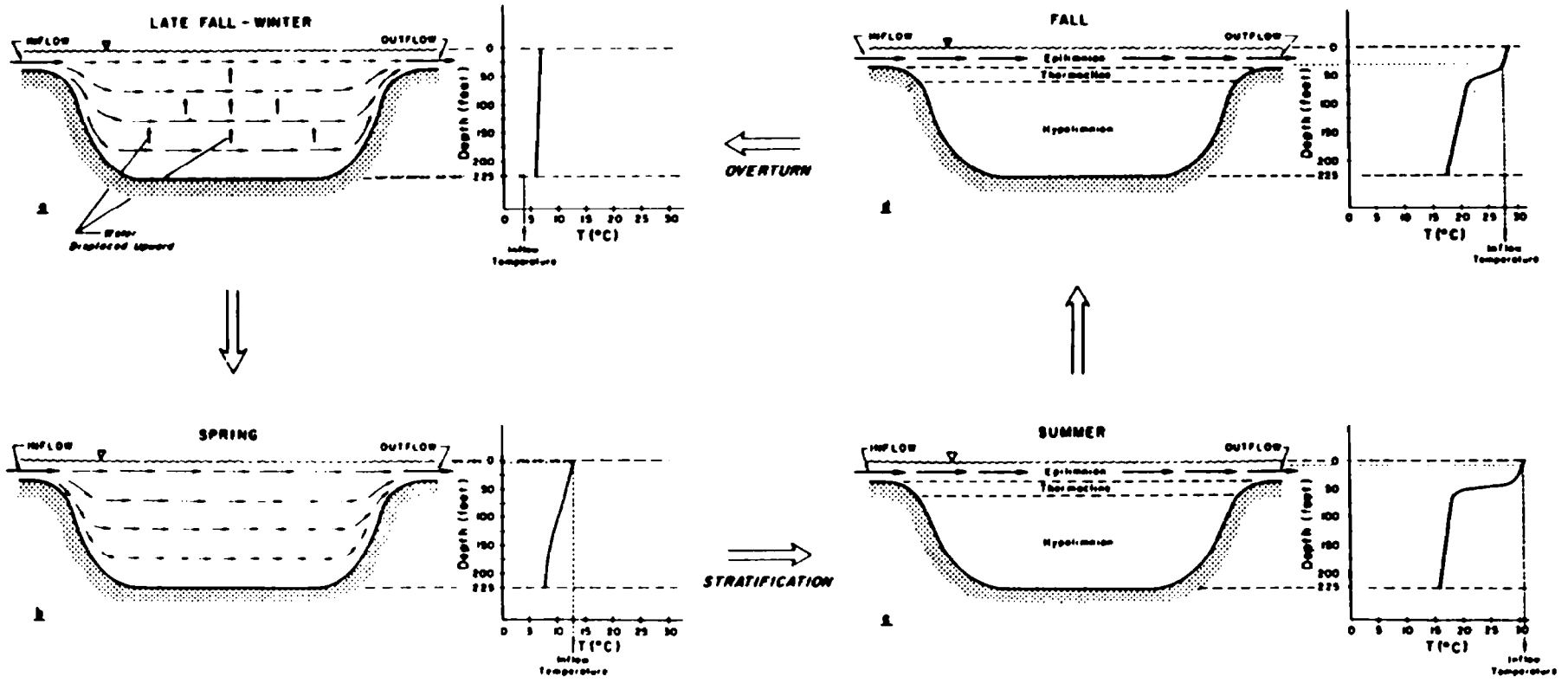

FIGURE V-3 ANNUAL CYCLE OF THERMAL STRATIFICATION AND OVERTURN IN AN IMPOUNDMENT

fied. Since vertical mixing is inhibited by stratification, reaeration of the hypolimnion (bottom layer) is virtually nonexistent. The thermocline (layer of steep thermal gradient between epilimnion and hypolimnion) is often at considerable depth. Accordingly, the euphotic (literally "good light") zone is likely to be limited to the epilimnion. Thus photosynthetic activity does not serve to reoxygenate the hypolimnion. The water that becomes the hypolimnion has some oxygen demand prior to the establishment of strata. Because bottom (benthic) matter exerts a further demand, and because some settling of particulate matter into the hypolimnion may occur, the DO level in the hypolimnion will gradually decrease over the period of stratification.

Anoxic conditions in the hypolimnion result in serious chemical and biological changes. Microbial activity leads to hydrogen sulfide (H_2S) evolution as well as to formation of other highly toxic substances, and these may be harmful to indigenous biota.

It should be noted that the winter and spring strata and overturn are relatively unimportant here since the major concern is anoxic conditions in the hypolimnion in summer. Thus all impoundments will be considered as monomictic.

Strong stratification is also important in prediction of sedimentation rates and trap efficiency estimates. These topics are to be covered later.

5.2.2 Prediction of Thermal Stratification

Computation of impoundment heat influx is relatively straightforward, but prediction of thermal gradients is complicated by prevailing physical conditions, physical mixing phenomena, and impoundment geometry. Such factors as depth and shape of impoundment bottom, magnitude and configuration of inflows, and degree of shielding from the wind are much more difficult to quantify than insolation, back radiation, and still air evaporation rates. Since the parameters which are difficult to quantify are critical to predicting stratification characteristics, no attempt has been made to develop a simple calculation procedure. Instead, a tested model (Chen and Orlob, 1973; Lorenzen and Fast, 1976) has been subjected to a sensitivity analysis and the results plotted to show thermal profiles over depth and over time for some representative geometries and climatological conditions. The plots are presented in Appendix D.

The plots show the variation in temperature (°C) with depth (meters). Temperature is used as an index of density. Engineering judgment about defining layers is based on the pattern of temperature with depth. If stratification takes place, the plot will show an upper layer of uniform or slightly declining temperature (epilimnion), an intermediate layer of sharply declining temperature (thermocline), and a bottom layer (hypolimnion). A rule of thumb requires a temperature change of at least 1°C/meter to define the thermocline. However, this can be tempered by the observation of a well defined mixed layer.

To assess thermal stratification in an impoundment, it is necessary only to determine which of the sets of plots most closely approximates climatic and hydrologic conditions in the impoundment studied. Parameters which were varied to generate the plots and values used are shown in Table V-1.

Table V-2 shows the climatological conditions used to represent the geographic locales listed in Table V-1. For details of the simulation technique, see Appendix E.

5.2.2.1 Using the Thermal Plots

Application of the plots to assess stratification characteristics begins with determining reasonable values for the various parameters listed in Table V-1. For geographic locale, the user should determine whether the impoundment of interest is near one of the ten areas for which thermal plots have been generated. If so, then the set of plots for that area should be used. If the impoundment is not near one of the ten areas, then the user may obtain data for the parameters listed in Table V-2 (climatologic data) and then select the modeled locale which best matches the region of interest.

Next, the user must obtain geometric data for the impoundment. Again, if the impoundment of interest is like one for which plots have been generated, then that set should be used. If not, the user should bracket the studied impoundment. As an example, if the studied impoundment is 55 feet deep (maximum), with a surface area of about 4×10^7 feet^2, then the 40 and 75 foot deep impoundment plots should be used.

Mean hydraulic residence time (τ_w, years) may be estimated using the mean total inflow rate (Q, m^3/year) and the impoundment volume (V, m^3):

$$\tau_w = V/Q \qquad \text{(V-1)}$$

Again, the sets of plots bracketing the value of τ_w should be examined. Where residence times are greater than 200 days, the residence time has little influence on stratification (as may be verified in Appendix D) and either the 200 day or infinite time plots may be used.

Finally, the wind mixing coefficient was used to generate plots for windy areas (high wind) and for very well protected areas (low wind). The user must judge where his studied impoundment falls and interpolate in the plots accordingly (See Appendix D).

TABLE V-1

PARAMETER VALUES USED IN GENERATION OF THERMAL GRADIENT PLOTS (APPENDIX D)

Parameter	Value		
Geographic Locale	Atlanta, Georgia Billings, Montana Burlington, Vermont Flagstaff, Arizona Fresno, California Minneapolis, Minnesota Salt Lake City, Utah San Antonio, Texas Washington, D.C. Wichita, Kansas		
Geometry	Depth (maximum, feet)	Surface Area ($feet^2$)	Volume ($feet^3$)
	20	8.28×10^6	7.66×10^7
	40	3.31×10^7	6.13×10^8
	75	1.16×10^8	4.04×10^9
	100	2.07×10^8	9.58×10^9
	200	8.28×10^8	7.66×10^{10}
Mean Hydraulic Residence Time	Days		
	10		
	30		
	75		
	250		
	∞		
Wind Mixing*	High		
	Low		

*See Appendix E.

TABLE V-2

TEMPERATURE, CLOUD COVER, AND DEW POINT DATA
FOR THE TEN GEOGRAPHIC LOCALES USED TO DEVELOP THERMAL
STRATIFICATION PLOTS (APPENDIX D). SEE FOOT OF TABLE FOR NOTES.

	Temperature (^{o}F)			Dew Point (^{o}F)	Cloud Cover Fraction	Wind (MPH)
	Max.	Mean	Min.			
	Atlanta (Lat:33.8^{o}N, Long:84.4^{o}W)					
January	54	45	36	34	.63	11
February	57	47	37	34	.62	12
March	63	52	41	39	.61	12
April	72	61	50	48	.55	11
May	81	70	57	57	.55	9
June	87	77	66	65	.58	8
July	88	79	69	68	.63	8
August	88	78	68	67	.57	8
September	83	73	63	62	.53	8
October	74	63	52	51	.45	9
November	62	51	40	40	.51	10
December	53	44	35	34	.62	10
	*Billings (Lat:45.8^{o}N, Long:108.5^{o}W)					
January	27	18	9	11	.68	13
February	32	22	12	16	.68	12
March	38	27	16	20	.71	12
April	51	38	26	28	.70	12
May	60	47	34	38	.64	11
June	68	54	40	46	.60	11
July	79	63	46	48	.40	10
August	78	61	45	46	.42	10
September	67	52	37	38	.54	10
October	55	42	30	31	.56	11
November	38	29	20	22	.66	13
December	32	22	14	15	.66	13

TABLE V-2 - CONT.

	Temperature (^{o}F)			Dew Point (^{o}F)	Cloud Cover Fraction	Wind (MPH)
	Max.	Mean	Min.			
	Burlington (Lat:44.5^{o}N, Lat:73.2^{o}W)					
January	27	18	9	12	.72	10
February	29	19	10	12	.69	10
March	38	29	20	20	.66	10
April	53	43	33	32	.67	10
May	67	56	44	43	.67	9
June	54	66	77	54	.61	9
July	82	71	59	59	.58	8
August	80	68	57	58	.57	8
September	71	60	49	51	.60	8
October	59	49	39	40	.65	9
November	44	38	29	30	.79	10
December	31	23	15	17	.78	10
	Flagstaff (Lat:35.2^{o}N, Long:111.3^{o}W)					
January	40	27	14	14	.59	8
February	43	30	17	16	.49	9
March	50	36	22	17	.50	11
April	59	43	28	20	.49	12
May	68	51	34	22	.41	11
June	77	60	42	25	.24	11
July	81	66	50	43	.54	9
August	79	64	49	43	.53	9
September	75	59	42	35	.29	8
October	63	47	31	25	.31	8
November	51	36	21	20	.34	8
December	44	30	17	15	.44	7

TABLE V-2 CONT.

	Temperature (°F)			Dew Point (°F)	Cloud Cover Fraction	Wind (MPH)
	Max.	Mean	Min.			
	Fresno (Lat:36.7°N, Long:119.8°W)					
January	55	46	37	38	.67	6
February	61	51	40	41	.61	6
March	68	55	42	41	.53	7
April	76	61	46	44	.44	7
May	85	68	52	45	.34	8
June	92	75	57	48	.19	8
July	100	81	63	51	.11	7
August	98	79	61	52	.11	6
September	92	74	56	51	.15	6
October	81	65	49	46	.28	5
November	68	54	40	42	.44	5
December	57	47	38	40	.70	5
	Minneapolis (Lat:45.0°N, Long:93.3°W)					
January	22	12	3	6	.65	11
February	26	16	5	10	.62	11
March	37	28	18	20	.67	12
April	56	45	33	32	.65	13
May	70	58	46	43	.64	12
June	79	67	56	55	.60	11
July	85	76	61	60	.49	9
August	82	71	59	59	.51	9
September	72	61	49	50	.51	10
October	60	48	37	40	.54	11
November	40	31	21	25	.69	12
December	27	18	9	13	.69	11

TABLE V-2 CONT.

	Temperature (°F)			Dew Point (°F)	Cloud Cover Fraction	Wind (MPH)
	Max.	Mean	Min.			
Salt Lake City (Lat:40.8°N, Long:111.9°W)						
January	37	27	18	20	.69	7
February	42	33	23	23	.70	8
March	51	40	30	26	.65	9
April	62	50	37	31	.61	9
May	72	58	45	36	.54	10
June	82	67	52	40	.42	9
July	92	76	61	44	.35	9
August	90	75	59	45	.34	10
September	80	65	50	38	.34	9
October	66	53	39	34	.43	9
November	49	38	28	28	.56	8
December	40	23	32	24	.69	7
San Antonio (Lat:29.4°N, Long:98.5°W)						
January	62	52	42	39	.64	9
February	66	55	45	42	.65	10
March	72	61	50	45	.63	10
April	79	68	58	55	.64	11
May	85	75	65	64	.62	10
June	92	82	72	68	.54	10
July	94	84	74	68	.50	10
August	94	84	73	67	.46	8
September	89	79	69	65	.49	8
October	82	71	60	56	.46	8
November	70	59	49	46	.54	9
December	65	42	54	41	.57	9

TABLE V-2 CONT.

	Temperature (°F)			Dew Point (°F)	Cloud Cover Fraction	Wind (MPH)
	Max.	Mean	Min.			
	Washington, D.C. (Lat:38.9°N, Long:77.0°W)					
January	44	37	30	25	.61	11
February	46	38	29	25	.56	11
March	54	45	36	29	.56	12
April	60	56	46	40	.54	11
May	76	66	56	52	.54	10
June	83	74	65	61	.51	10
July	87	78	69	65	.51	9
August	85	77	68	64	.51	8
September	79	70	61	59	.48	9
October	68	59	50	48	.47	9
November	57	48	39	36	.54	10
December	46	43	31	26	.58	10
	Wichita (Lat:37.7°N, Long:97.3°W)					
January	42	32	22	21	.50	12
February	47	36	26	25	.51	13
March	56	45	33	30	.52	15
April	68	57	45	41	.53	15
May	77	66	55	53	.53	13
June	88	77	65	62	.46	13
July	92	81	69	65	.39	12
August	93	81	69	53	.38	11
September	84	71	59	55	.39	12
October	72	60	48	43	.40	12
November	34	55	44	33	.44	13
December	45	36	27	25	.50	12

TABLE V-2 CONT.

Notes: Mean: Normal daily average temperature, ^{o}F.
Max.: Normal daily maximum temperature, ^{o}F.
Min.: Normal daily minimum temperature, ^{o}F.
Wind: Mean wind speed, MPH
Dew Point: Mean dew point temperature, ^{o}F.

*Complete data were not available for Billings. Tabulated data are actually a synthesis of available data for Billings, Montana and Yellowstone, Wyoming.

All data taken from Climatic Atlas of the U.S., 1974.

EXAMPLE V-1

Thermal Stratification

Suppose one wants to know the likelihood that hypothetical Limpid Lake is stratified during June. The first step is to compile the physical conditions for the lake in terms of the variables listed in Table V-1. Table V-3 shows how this might be done. Next, refer to the indexes provided in Appendix D to locate the plot set for conditions most similar to those of the studied impoundment. In this case, the Wichita plots for a 200-foot deep impoundment with no inflow and high mixing rate would be chosen (see Table V-3). Figure V-4 is a reproduction of the appropriate page from Appendix D.

TABLE V-3

LIMPID LAKE CHARACTERISTICS

Item	Limpid Lake	Available Plot
Location	Manhattan, Kansas	Wichita, Kansas
Depth, ft (maximum)	180	200
Volume, ft^3	6×10^{10}	7.66×10^{10}
Mean residence time (τ_w)	500 days	∞ (no inflow)
Mixing	high (windy)	high coefficient

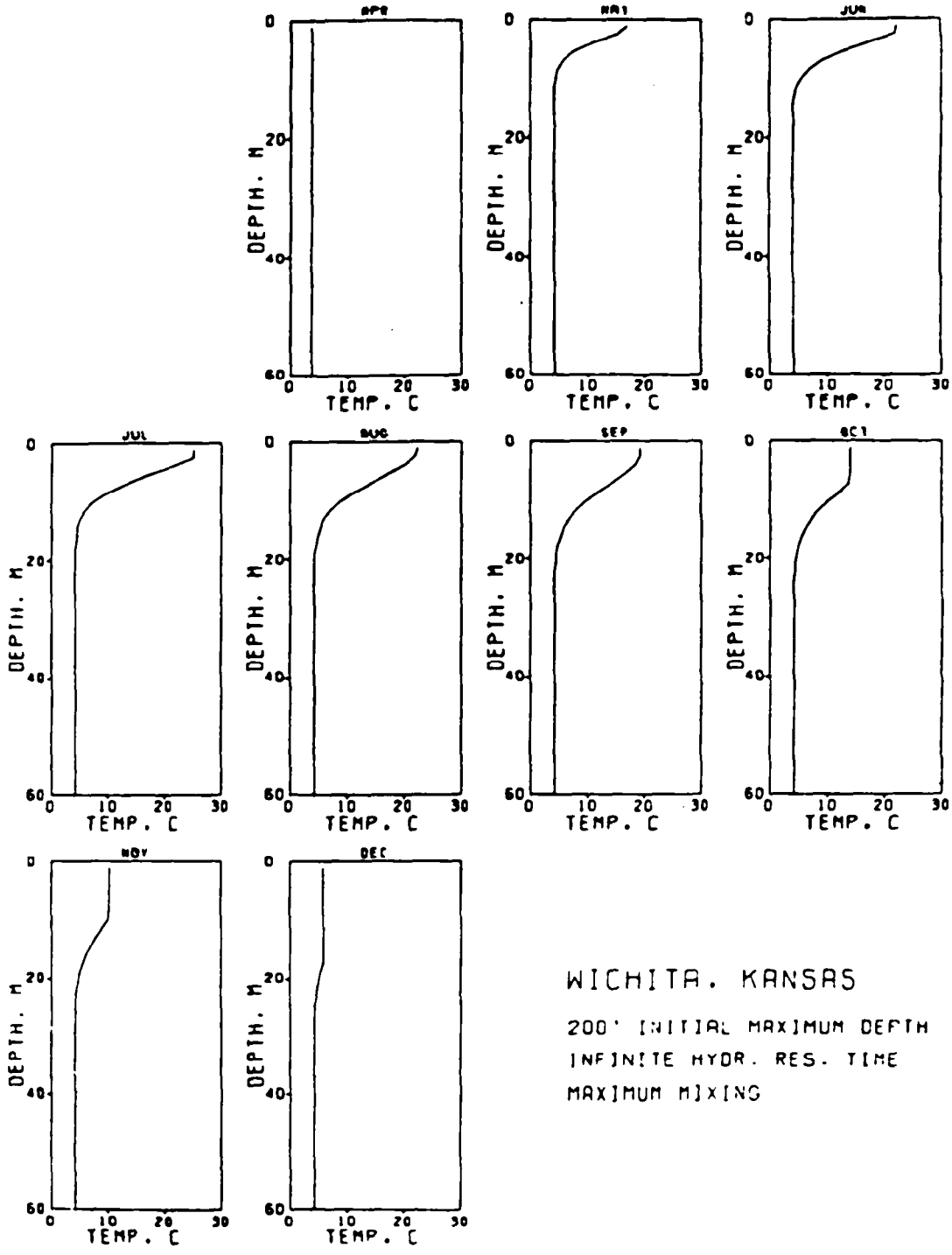

FIGURE V-4 THERMAL PROFILE PLOTS USED IN EXAMPLE V-1

According to the plots, Limpid Lake is likely to be strongly stratified in June. Distinct strata form in May and overturn probably occurs in December. During June, the epilimnion should extend down to a depth of about eight or ten feet, and the thermocline should extend down to about 30 feet. The gradient in the thermocline should be about 1° C per meter.

END OF EXAMPLE V-1

EXAMPLE V-2

Thermal Stratification

What are the stratification characteristics of Lake Smith?

The hypothetical lake is located east of Carthage, Texas, and Table V-4 shows its characteristics along with appropriate values for the thermal plots.

TABLE V-4

PHYSICAL CHARACTERISTICS OF LAKE SMITH

Item	Lake Smith	Plot Values
Location	15 miles east of Carthage Texas	
Depth, ft (maximum)	23	20
Volume, ft^3	3×10^8	1.66×10^8
Mean residence time	250 days	∞
Mixing	low (low wind)	low mixing coefficient

From the available data for Lake Smith, it appears that plots for a 20-foot deep impoundment with no inflow and low mixing coefficient should give a good indication of the degree of summertime stratification. The one remaining problem is climate. Data for nearby Shreveport, Louisiana compare well with those of Atlanta (Table V-5), for which plots are provided in Appendix D, and latitudes are similar. Shreveport is somewhat warmer and insolation is higher, but this is a relatively uniform difference over the year. The net effect should be to shift the thermal plots to a slightly higher temperature but to influence the shape of the plots and the timing of stratification little. As a result, the plots for

TABLE V-5

COMPARISON OF MONTHLY CLIMATOLOGIC DATA
FOR SHREVEPORT, LOUISIANA AND ATLANTA, GEORGIA
DATA ARE PRESENTED AS SHREVEPORT/ATLANTA
(CLIMATIC ATLAS OF THE U.S., 1974)

	Temperature, °F			Dew Point, °F	Cloud Cover, Fraction	Wind, MPH
	Max.	Mean	Min.			
January	57/54	48/45	38/36	38/34	.60/.63	9/11
February	60/57	50/47	41/37	40/34	.58/.62	9/12
March	67/63	57/52	47/41	44/39	.54/.61	10/12
April	75/72	65/61	55/50	54/48	.50/.55	9/11
May	83/81	73/70	63/57	62/57	.48/.55	9/9
June	91/87	81/77	71/66	69/65	.44/.58	8/8
July	92/88	82/79	72/69	71/68	.46/.63	7/8
August	94/88	83/78	73/68	70/67	.40/.57	7/8
September	88/83	78/73	67/63	65/62	.40/.53	7/8
October	79/74	67/63	55/52	55/51	.38/.45	7/9
November	66/62	55/51	45/40	45/40	.46/.51	8/10
December	59/53	50/44	40/35	39/34	.58/.62	9/10

Shreveport Lat:32.5°N, Long:94°W

Atlanta Lat:33.8°N, Long:84.4°W,

Atlanta may be used, bearing in mind that the temperatures are likely to be biased uniformly low. Figure V-5 (reproduced from Appendix D) shows thermal plots for a 20-foot deep Atlanta area impoundment having no significant inflow and low wind stress. From the figure, it is clear that the lake is likely to stratify from April or May through September, the epilimnion will be very shallow, and the thermocline will extend down to a depth of about 7 feet. The thermal gradient is in the range of about 7°C per meter, as an upper limit, during June. Bottom water warms slowly during the summer until the impoundment becomes fully mixed in October.

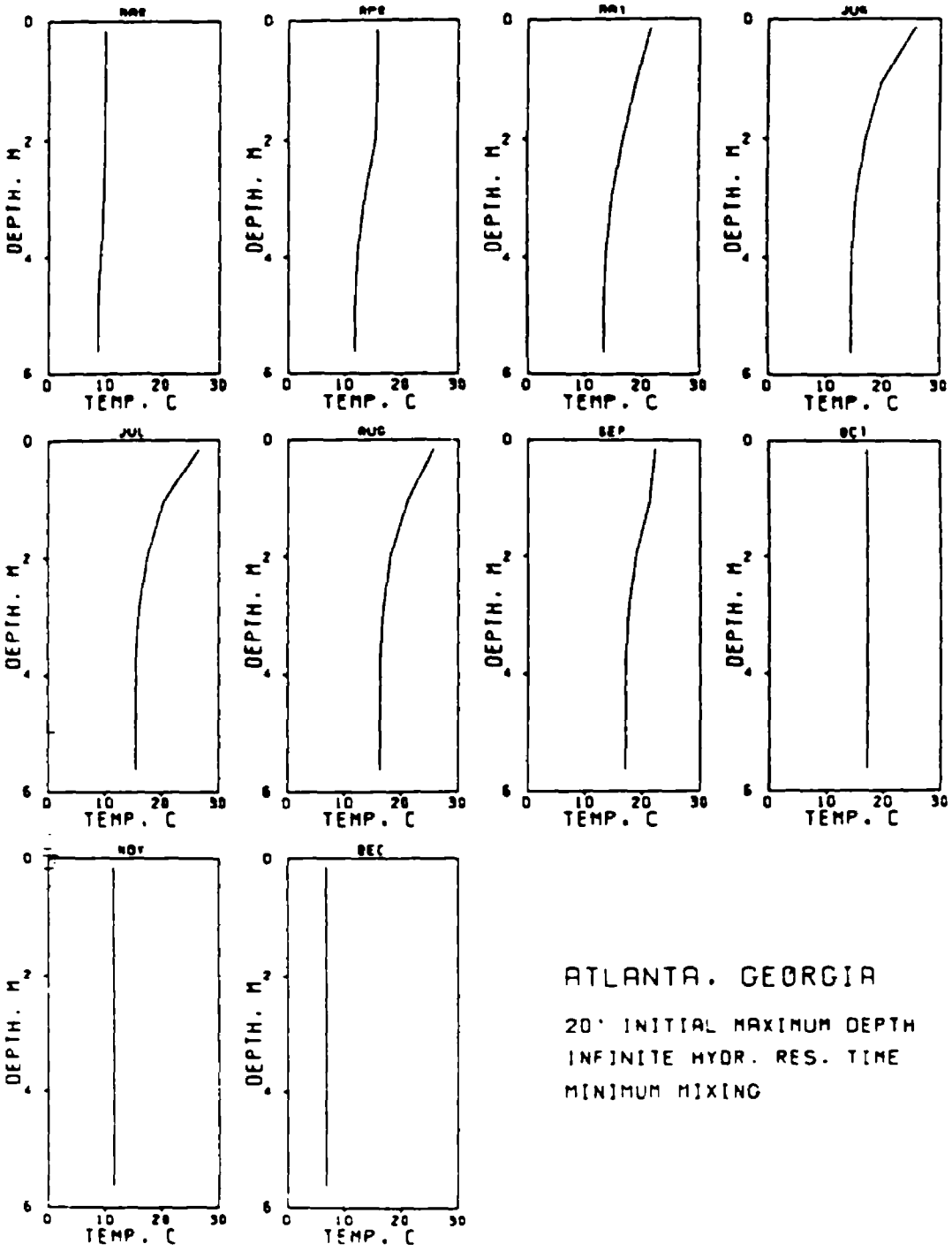

FIGURE V-5 THERMAL PROFILE PLOTS APPROPRIATE FOR USE IN EXAMPLE V-2

END OF EXAMPLE V-2

5.3 SEDIMENT ACCUMULATION

5.3.1 Introduction

Reservoirs, lakes, and other impoundments are usually more quiescent than tributary streams, and thus act as large settling basins for suspended particulate matter. Sediment deposition in impoundments gradually diminishes water storage capacity to the point where lakes fill in and reservoirs become useless. In some cases, sediment accumulation may reduce the useful life of a reservoir to as little as ten to twenty years (Marsh, et al., 1975).

Just how much suspended matter settles out as water passes through an impoundment, as well as the grain size distribution of matter which remains suspended, is of interest to the planner for several reasons. Suspended sediment within an impoundment may significantly reduce light penetration thus limiting algal and bottom-rooted plant (macrophyte) growth. This, in turn, can adversely affect food availability for indigenous fauna, or may slow plant succession, as part of the natural aging process of lakes.

Settling of suspended matter may eliminate harborage on impoundment bottoms thus reducing populations of desirable animal species. More directly, suspended particulates impinging on the gills of fish may cause disease or death.

Some minerals, particularly clays, are excellent adsorbents. As a result, farm chemicals and pesticides applied to the land find their way to an impoundment bottom and into its food chain. The sediment which settles is likely to have a substantial component of organic matter which can exert an oxygen demand, and under conditions of thermal stratification, anoxic conditions on the impoundment bottom (in the hypolimnion) can result in generation of toxic gases. Indigenous biota may be harmed or even killed as a result.

Knowing the rate of sediment transport and the deposition within an impoundment allows for effective planning to be initiated. If sedimentation rates are unacceptable, then the planner can begin to determine where sediments originate, and how to alleviate the problem. For example, densely planted belts may be established between highly erodible fields and transporting waterways, farming and crop management practices may be changed, or zoning may be modified to prevent a worsening of conditions.

These considerations, along with others relating to sediment carriage and deposition in downstream waterways, make estimates of sedimentation rates of interest here. Impoundment sediment computation methods discussed in this section will permit the planner to estimate annual impoundment sediment accumulation as well as short term accumulation (assuming constant hydraulic conditions). Application of the methods will permit the planner to estimate the amount of sediment removed from transport in a river system due to water passage through any number of impoundments.

5.3.2 Annual Sediment Accumulation

Three different techniques are used to estimate annual sediment accumulation: available data, sediment rating curves, and a three step procedure to determine short-term sedimentation rates. As discussed under each technique, caution should be used in selecting one method or another. If data are not available, it may not be feasible to use one or more techniques. When drawing conclusions, the uncertainty in the results should be considered in drawing conclusions based on whichever analysis that is selected. In addition, each technique has its own degree of uncertainty, which should be considered when drawing conclusions.

5.3.2.1 Use of Available Data

Data provided in Appendix F permit estimation of annual sediment accumulation in acre-feet for a large number of impoundments in the U.S. The data and other materials presented provide some basic impoundment statistics useful to the planner in addition to annual sediment accumulation rates.

To use Appendix F, first determine which impoundments within the study area are of interest in terms of annual sediment accumulation. Refer to the U.S. map included in the appendix and find the index numbers of the region within which the impoundment is located. The data tabulation in the appendix, total annual sediment accumulation in acre feet, is given by multiplying average annual sediment accumulation in acre feet per square mile of net drainage area ("Annual Sediment Accum.") by the net drainage area ("Area") in square miles:

$$\text{Total Accumulation} = \text{Annual Sediment Accum.} \times \text{Area} \qquad \text{(V-2)}$$

To convert to average annual loss of capacity expressed as a percent, divide total annual accumulation by storage capacity (from Appendix F), and multiply by 100. Note that this approach and those presented later do not account for packing of the sediment under its own weight. This results in an overestimate in loss of capacity. Note also that other data in Appendix F may be of interest in terms of drainage area estimates for determining river sediment loading and assessment of storm water sediment transport on an annual basis.

5.3.2.2 Trap Efficiency and the Ratio of Capacity to Inflow

Where data are not available in Appendix F for a specific impoundment, the following method will permit estimation of annual or short-term sediment accumulation rates. The method is only useful, however, for normal ponded reservoirs.

To use this approach, a suspended sediment rating curve should be obtained for tributaries to the impoundment. An example of a sediment rating curve is provided in Figure V-6.

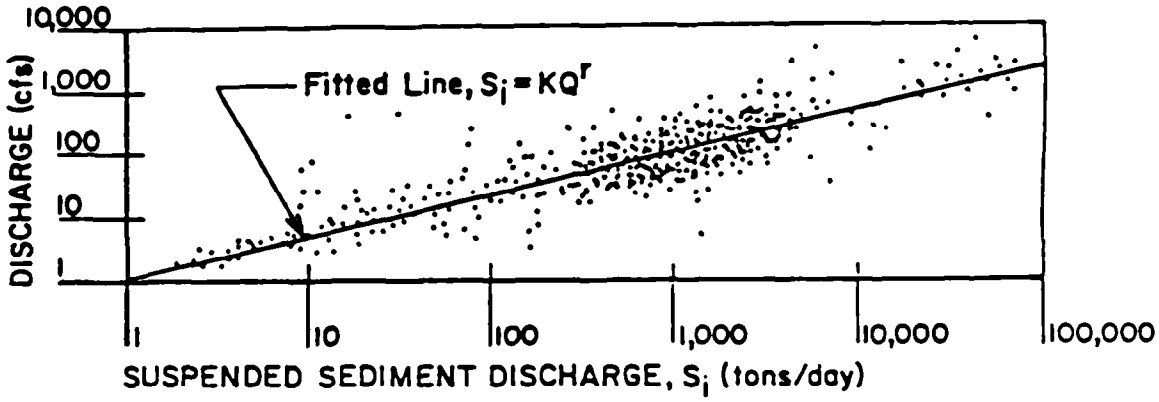

FIGURE V-6 SEDIMENT RATING CURVE SHOWING SUSPENDED SEDIMENT DISCHARGE AS A FUNCTION OF FLOW (AFTER LINSLEY, KOHLER, AND PAULHUS, 1958)

On the basis of such a curve, one can estimate the mean sediment mass transport rate (S_i) in mass per unit time for tributaries. If neither rating curve nor data are available, one may estimate sediment transport rates on a basis of data from nearby channels, compensating for differences by using mean velocities. To a first approximation, it would be expected that:

$$S_i = S_j\left(\frac{V_i}{V_j}\right)^2 \qquad (V\text{-}3)$$

where

S_i = sediment transport rate to be determined in tributary "i" in mass per unit time

S_j = known transport rate for comparable tributary (j) in same units as S_i

V_i = mean velocity for tributary i over the time period

V_j = mean velocity in tributary j over the same time period as V_i.

Once average transport rates over the time period of interest have been determined, the proportion, and accordingly the weight of sediment settling out in the impoundment may be estimated. Figure V-7 is a graph showing the relationship between percent of sediment trapped in an impoundment versus the ratio of capacity to inflow rate. The implicit relationship is:

$$P = f(V/Q_i) \qquad (V\text{-}4)$$

where

P = percent of inflowing sediment trapped

V = capacity of the impoundment in acre-feet

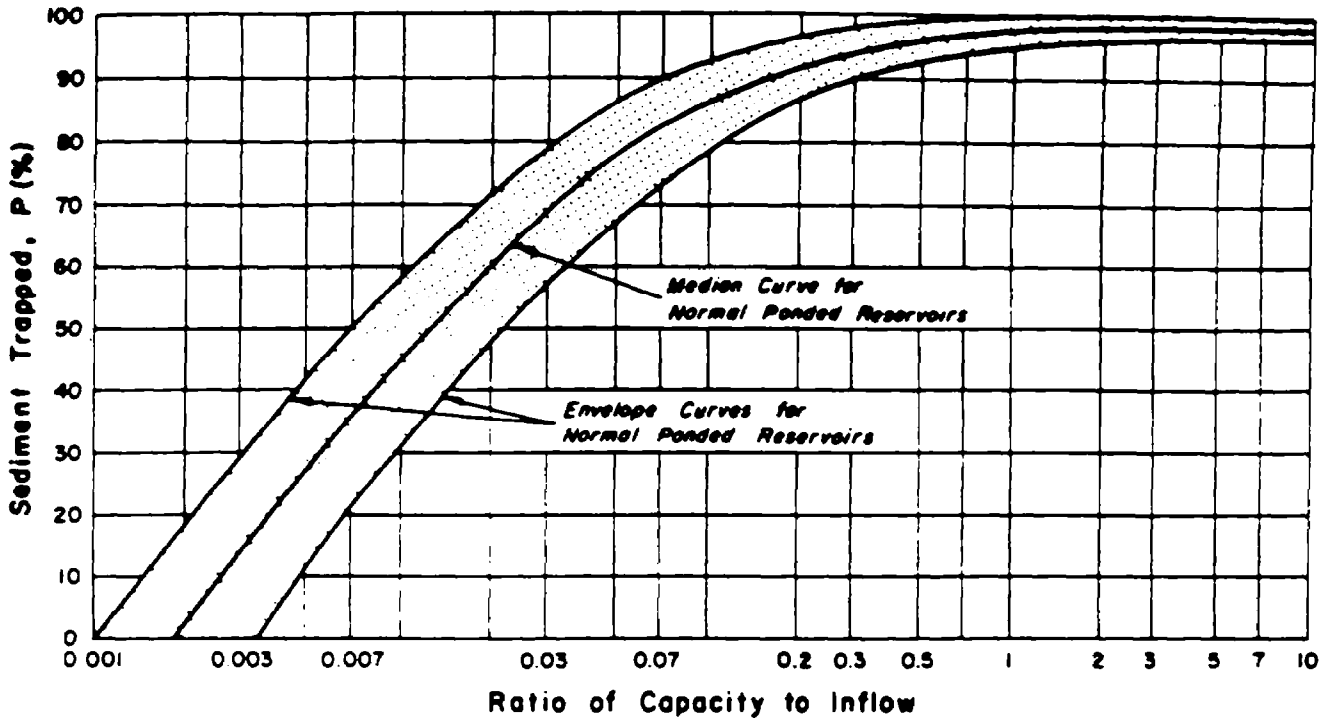

FIGURE V-7 RELATIONSHIP BETWEEN THE PERCENTAGE OF INFLOW-TRANSPORTED SEDIMENT RETAINED WITHIN AN IMPOUNDMENT AND RATIO OF CAPACITY TO INFLOW (LINSLEY, KOHLER, AND PAULHUS, 1958)

Q_i = water inflow rate in acre-feet per year.

Data used for development of the curves in Figure V-7 included 41 impoundments of various sizes throughout the U.S. (Linsley, Kohler, and Paulhus, 1958).

To estimate the amount of suspended sediment trapped within an impoundment using this method, the capacity of the impoundment in acre-feet must first be determined. Next, average annual inflow, or better, average flow for the time period of interest is estimated.

Then:

$$S_t = S_i P \qquad \text{(V-5)}$$

where

S_t = weight of sediment trapped per time period t

P = trap efficiency (expressed as a decimal) from Figure V-7.

A word of caution is in order here. The above described techniques for evaluating sediment deposition in impoundments are capable of providing reasonable estimates, but only where substantial periods of time are involved - perhaps six months or longer. The methods may be used for shorter study periods, but results must then be taken only as very rough estimates, perhaps order-of-magnitude.

5.3.3 Short-Term Sedimentation Rates

The three-step procedure presented below provides a means to make short-term sediment accumulation rate estimates for storm-event analysis and to estimate amounts of different grain-size fractions passing through an impoundment. The steps are:

- Determine terminal fall velocities for the grain size distribution
- Estimate hydraulic residence time
- Compute trap (sedimentation) rate.

5.3.3.1 Fall Velocity Computation

When a particle is released in standing water, it will remain roughly stationary if its density equals that of the water. If the two densities differ, however, the particle will begin to rise or fall relative to the water. It will then tend to accelerate until the drag force imposed by the water exactly counterbalances the force accelerating the particle. Beyond this point, velocity is essentially constant, and the particle has reached terminal velocity. For spheres of specific gravity greater than 1, Stokes' law expresses the relationship between fall velocity (terminal velocity) and several other physical parameters of water and the particles:

$$V_{max} = \frac{g}{18\mu}(\rho_p - \rho_w)d^2 = \frac{1}{18\mu}(D_p - D_w)d^2 \qquad (V\text{-}6)$$

where

V_{max} = terminal velocity of the spherical particle (ft sec^{-1})
g = acceleration due to gravity (32.2 ft sec^{-2})
ρ_p = mass density of the particle (slugs ft^{-3})
ρ_w = mass density of water (slugs ft^{-3})
d = particle diameter (ft)
μ = absolute viscosity of the water (lb sec ft^{-2})
D_p = weight density of particle (lb ft^{-3})
D_w = weight density of water (lb ft^{-3}).

Stokes' law is satisfactory for Reynolds numbers between 1×10^{-4} and 0.5 (Camp, 1968). Reynolds number is given by:

$$R = \frac{vd}{\nu} \qquad (V\text{-}7)$$

where

R = Reynolds number
v = particle velocity
ν = kinematic viscosity of water.

Generally, for particles of diameter less than 3×10^{-2} inches (0.7 mm) this

criterion is met. For large particles, how far conditions deviate from this may be observed using the following approach (Camp, 1968). According to Newton's law for drag, drag force on a particle is given by:

$$F_d = CA\rho_w v^2/2 \qquad (V\text{-}8)$$

where

F_d = the drag force

C = unitless drag coefficient

A = projected area of the particle in the direction of motion.

Equating the drag force to the gravitational (driving) force for the special case of a spherical particle, velocity is given by:

$$V_{max} = \sqrt{\frac{4g\ (\rho_p - \rho_w)d}{3C\quad \rho_w}} \qquad (V\text{-}9)$$

All variables in the expression for V_{max} (Equation V-9) may be easily estimated except C, since C is dependent upon Reynold's number. According to Equation V-7, Reynolds number is a function of v. Thus a "trial and error" or iterative procedure would ordinarily be necessary to estimate C. However, a somewhat simpler approach is available to evaluate the drag coefficient and Reynolds number. First, estimate CR^2 using the expression (Camp, 1968):

$$CR^2 = 4\rho_w\ (\rho_p - \rho_w)\ gd^3/3\mu^2 \qquad (V\text{-}10)$$

Then, using the plot in Figure V-8, estimate R and then C. For R>0.1 use of Equation V-9 will give better estimates of V_{max} than will Equation V-6.

Generally, one of the two approaches for spherical particles will give good estimates of particle fall velocity in an effectively laminar flow field (in impoundments). Occasionally, however, it may prove desirable to compensate for nonsphericity of particles. Figure V-9, which shows the effect of particle shape on the drag coefficient C, may be used to do this. Note that for R < 1, shape of particle does not materially affect C, and no correction is necessary.

A second problem in application of the Newton/Stokes approach described above is that it does not account for what is called hindrance. Hindrance occurs when the region of fluid surrounding a falling particle is disrupted (by the particle motion) and the velocity of other nearby particles is thereby decreased. Figure V-10 shows this effect schematically.

A very limited amount of research has been done to determine the effect of particle concentration on fall velocity (Camp, 1968). Some data have been collected

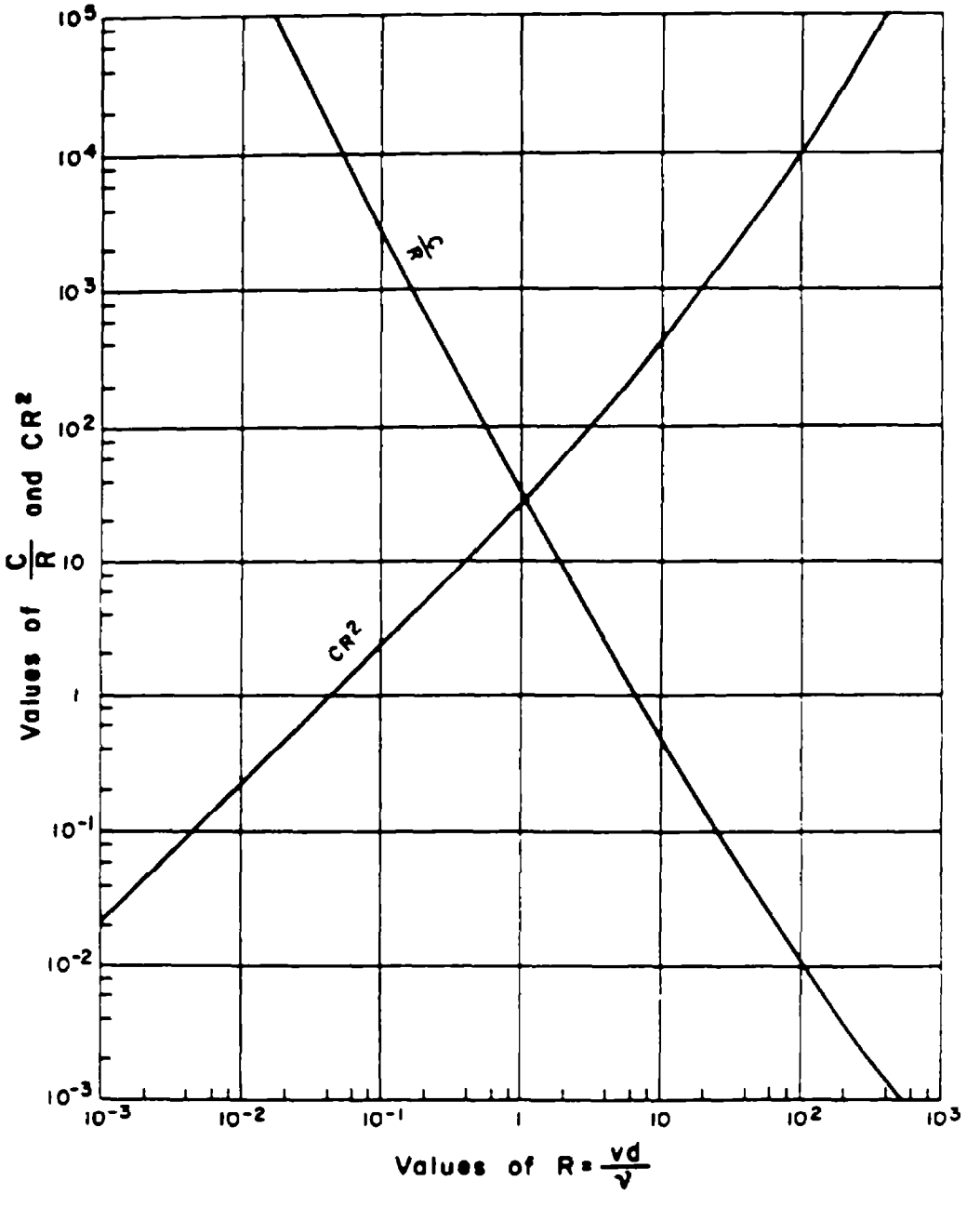

FIGURE V-8 PLOT OF C/R AND CR^2 VERSUS R (CAMP, 1968)

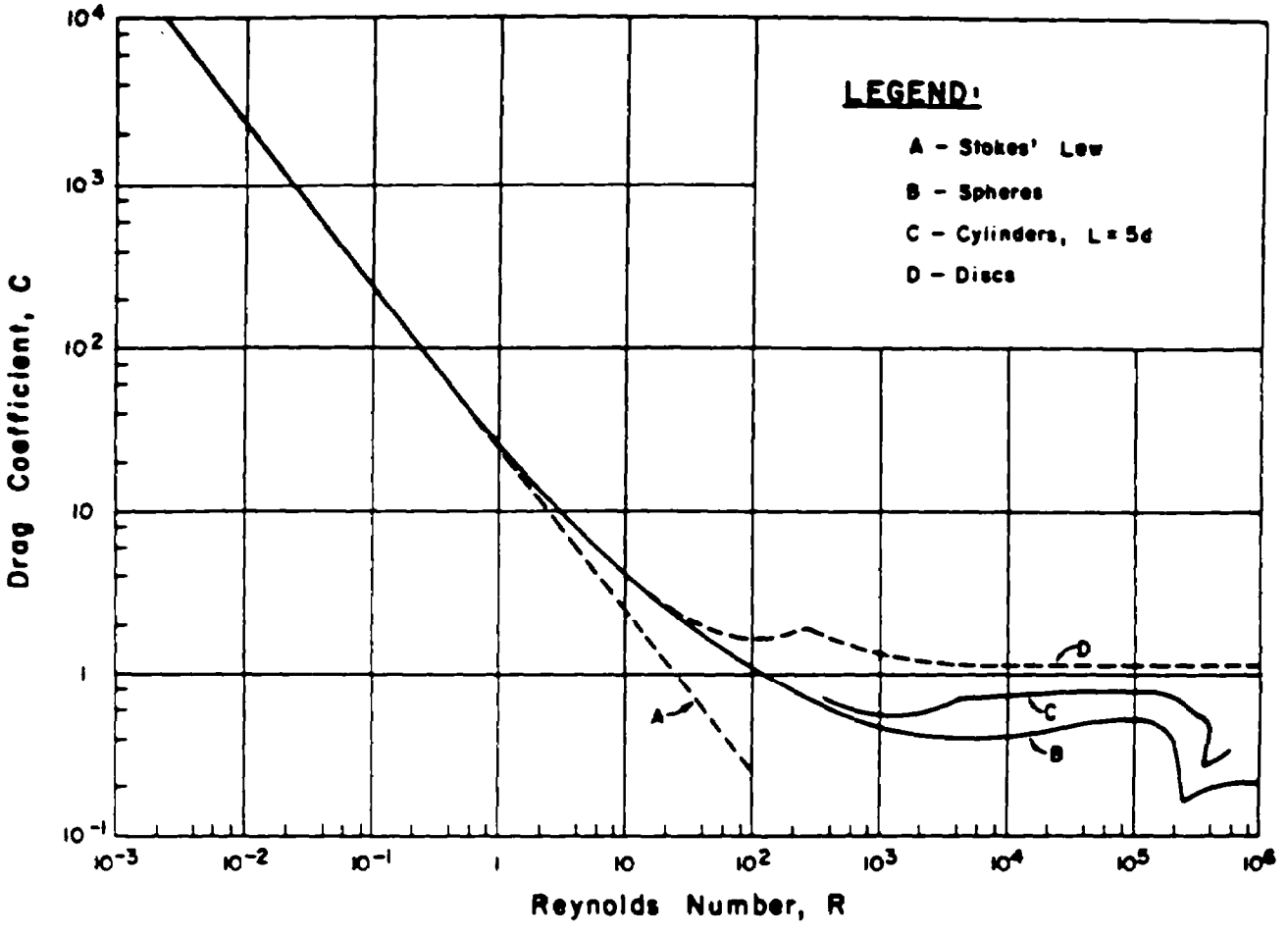

FIGURE V-9 DRAG COEFFICIENT (C) AS FUNCTION OF REYNOLD'S NUMBER (R) AND PARTICLE SHAPE (CAMP, 1968)

however, and Figure V-11 is a plot of a velocity correction factor, v'/v, as a function of volumetric concentration. Volumetric concentration is given by:

$$C_{vol} = \frac{C_{wt}\rho_w}{\rho_p} \qquad (V\text{-}11)$$

where

C_{vol} = volumetric concentration

C_{wt} = weight concentration.

As an approximation, the curve for sand may be used to correct v as a function of C_{vol}.

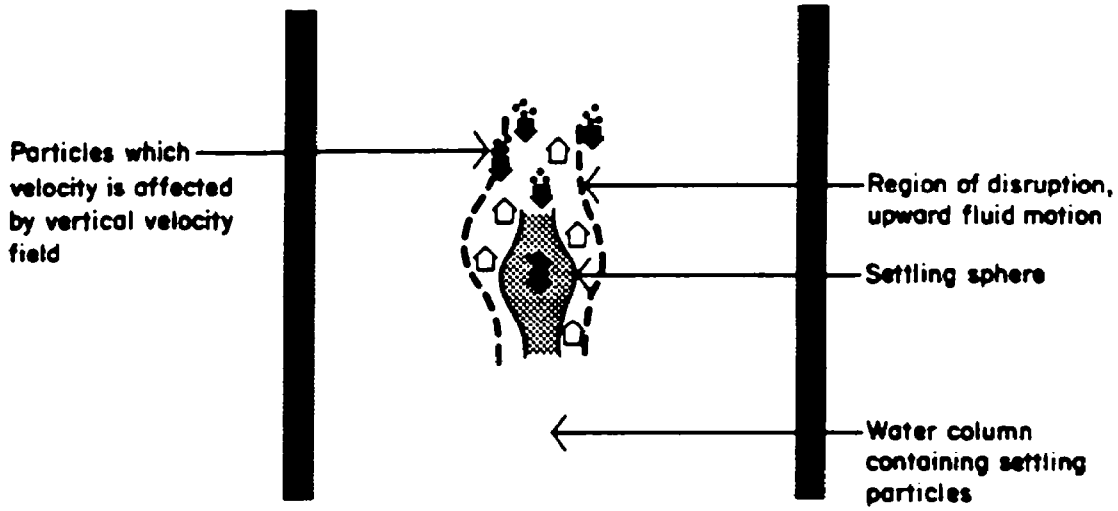

FIGURE V-10 SCHEMATIC REPRESENTATION OF HINDERED SETTLING OF PARTICLES IN FLUID COLUMN

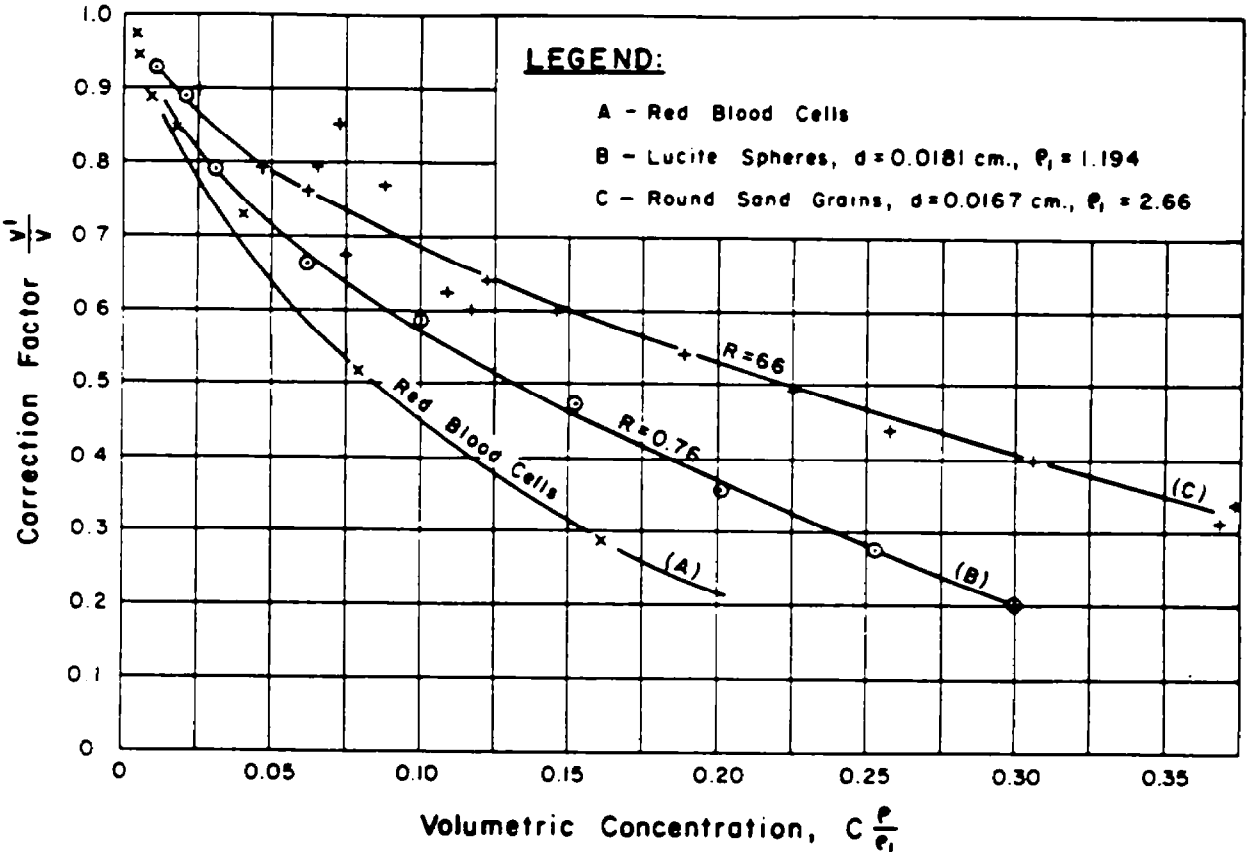

FIGURE V-11 VELOCITY CORRECTION FACTOR FOR HINDERED SETTLING (FROM CAMP, 1968)

EXAMPLE V-3

Settling Velocity

Assume that a swiftly moving tributary to a large reservoir receives a heavy loading of sediment which is mostly clay particles. The particles tend to clump somewhat, and average diameters are on the order of 2 microns. The clumps have a specific gravity of 2.2. Applying Stokes' law for 20°C water:

$$V_{max} = \frac{g}{18\mu} (\rho_p - \rho_w) d^2$$

$$V_{max} = \frac{32.2}{(18 \times 2.1 \times 10^{-5})} \times [(2.2 \times 62.4/32.2) - (62.4/32.2)] \times (6.56 \times 10^{-6})^2$$

$$= 8.53 \times 10^{-6} \text{ ft sec}^{-1} = .03 \text{ ft hr}^{-1}$$

Thus the particles of clay might be expected to fall about nine inches per day in the reservoir. It should be noted that for such a low settling rate, turbulence in the water can cause very significant errors. In fact, the estimate is useful only in still waters having a very uniform flow lacking substantial vertical components.

END OF EXAMPLE V-3

EXAMPLE V-4

Settling Velocity for a Sand and Clay

Suppose a river is transporting a substantial sediment load which is mainly sand and clay. The clay tends to clump to form particles of 10 micron diameter while the sand is of 0.2 mm diameter. The sand particles are very irregular in shape tending toward a somewhat flattened plate form. The specific gravity of the clay is about 1.8 while that of the sand is near 2.8. Given that the water temperature is about 5°C, the terminal velocity of the clay may be estimated as in Example V-3:

$$V_{max} = \frac{g}{18\mu} (\rho_p - \rho_w) d^2$$

$$V_{max} = \frac{32.2}{(18 \times 3.17 \times 10^{-5})} \times (0.8 \times 62.4 / 32.2) \times (3.28 \times 10^{-5})^2$$

$$= 9.4 \times 10^{-5} \text{ ft sec}^{-1}$$

$$= 8 \text{ ft day}^{-1}$$

For the sand, apply Equation V-10:

$$CR^2 = 4\rho_w (\rho_p - \rho_w) gd^3/3u^2$$

$$= 4 \times \frac{62.4}{32.2} \times \frac{1.8 \times 62.4}{32.2} \times \frac{32.2 \times (6.56 \times 10^{-4})^3}{3 \times (3.17 \times 10^{-5})^2}$$

$$CR^2 = 82$$

Referring to Figure V-8, a value of CR^2 equal to 82 represents $R \cong 2.8$ and $C \cong 10.3$. From Figure V-9, the corrected drag coefficient for discs is close to 10.3 (no correction really necessary). Then, using Equation V-9 as an approximation:

$$V_{max} = \sqrt{\frac{49 (\rho_p - \rho_w) d}{3C\rho_w}}$$

$$V_{max} = \sqrt{\frac{4 \times 32.2 \times (1.8 \times 62.4 / 32.2) \times 6.56 \times 10^{-4}}{3 \times 10.3 \times 62.4 / 32.2}}$$

$$V_{max} = 0.07 \text{ ft sec}^{-1} = 252 \text{ ft hr}^{-1}$$

Thus the clay will settle about 8 feet per day while the sand will settle about 6,048 feet per day (252 feet per hour).

END OF EXAMPLE V-4

5.3.4 Impoundment Hydraulic Residence Time

Once settling velocities have been estimated for selected grain sizes, the final preparatory step in estimating sediment deposition rates is to compute hydraulic residence time.

Hydraulic residence time represents the mean time a particle of water resides within an impoundment. It is not, as is sometimes thought, the time required to displace all water in the impoundment with new. In some impoundments, inflowing water may be conceptualized as moving in a vertical plane from inflow to discharge. This is called plug flow. In long, narrow, shallow impoundments with high inflow velocities, this is often a good assumption. As discussed later, however, adoption of this model leads to another problem, namely, is water within the plug uniform or does sediment concentration vary over depth within the plug?

A second model assumes that water flowing into an impoundment instantaneously mixes laterally with the entire receiving layer. The layer may or may not represent the entire impoundment depth. This simplification is often a good one in large surfaced, exposed impoundments having many small inflows.

Regardless of the model assumed for the process by which water traverses an impoundment from inflow to discharge, hydraulic residence time is computed

as in Equation V-1. That is:

$$\tau_w = V/Q$$

The only important qualification is that to be meaningful, V must be computed taking account of stagnant areas, whether these are regions of the impoundment isolated from the main flow by a sand spit of promontory, or whether they are isolated by a density gradient, as in the thermocline and hypolimnion. Ignoring stagnant areas may result in a very substantial overestimate of τ_w, and in sediment trap computations, an overestimate in trap efficiency. Actually τ_w computed in this way is an adjusted hydraulic residence time. All references to hydraulic residence time in the remainder of Section 5.3 refer to adjusted τ_w.

Hydraulic residence time is directly influenced by such physical variables as impoundment depth, shape, side slope, and shoaling, as well as hydraulic characteristics such as degree of mixing, stratification, and flow velocity distributions. The concepts involved in evaluating many of these factors are elementary. The evaluation itself is complicated, however, by irregularities in impoundment shape and data inadequacies. Commonly, an impoundment cannot be represented well by a simple 3-dimensional figure, and shoaling and other factors may restrict flow to a laterally narrow swath through the water body.

In most cases, hydraulic residence time may be estimated, although it is clear that certain circumstances tend to make the computation error-prone. The first step in the estimation process is to obtain impoundment inflow, discharge, and thermal regime data as well as topographic/bathymetric maps of the system. Since a number of configuration types are possible, the methods are perhaps best explained using examples.

EXAMPLE V-5

Hydraulic Residence Time in Unstratified Impoundments

The first step in estimating hydraulic residence time for purposes of sedimentation analysis is to determine whether there are significant stagnant areas. These would include not only regions cut off from the main flow through the body, but also layers isolated by dense strata. Consequently, it must be determined whether or not the impoundment stratifies. Consider Upper Lake located on the Carmans River, Long Island, New York. The lake and surrounding region are shown in Figure V-12, and hypothetical geometry data are presented in Table V-6. Based upon Upper Lake's shallowness, its long, narrow geometry, and high tributary inflows, it is safe to assume that Upper Lake is normally unstratified. Also, because of turbulence likely at the high flows, one can assume that the small sac northeast of the discharge is not stagnant and that Upper Lake represents a slow

TABLE V-6

HYPOTHETICAL PHYSICAL CHARACTERISTICS AND
COMPUTATIONS FOR UPPER LAKE, BROOKHAVEN, SUFFOLK COUNTY, NEW YORK

Distance Downstream from Inflow Miles (feet)	D Average Depth ft.	W Average Width ft.	CSA Cross-sectional Area, D x W ft^2
0.05 (264)	3	63	189
0.10 (528)	4	110	440
0.15 (792)	6	236	1,416
0.20 (1,056)	7	315	2,205
0.25 (1,320)	7	340	2,380
0.30 (1,584)	8	315	2,520
0.35 (1,848)	7	550	3,850
0.40 (2,112)	8	550	4,400
0.45 (2,376)	7	354	2,478
0.50 (2,640)	10	350	3,500
			mean 2,338

Total length = 0.5 mi. (2,640 ft.)
Inflow from upstream = 380 cfs
Outflow to downstream = 380 cfs } (steady-state)

Computation

Volume (Vol) = Total length x mean cross-sectional area
= 2,640 ft. x 2,338 ft^2 = 6.17 x 10^6 ft^3

Residence time (τ_w) = Vol/flow
= 6.17 x 10^6 ft^3/(380 ft^3/sec) = 1.62 x 10^4 sec (4.5 hr)

Velocity (Vel) = length/τ_w
= 2,640 ft/1.62 x 10^4 sec = .163 ft/sec

moving river reach. With these assumptions, the computation of hydraulic residence time is as shown in Table V-6.

Also shown in Figure V-12 is Lower Lake. According to the hypothetical data presented in Table V-7, Lower Lake is much deeper than Upper Lake. Its volume is significantly greater also, but the inflow rate is similar. In this case, particularly during the summer, it should be determined if the lake stratifies. For this example, however, we will assume that the time of the year makes stratifica-

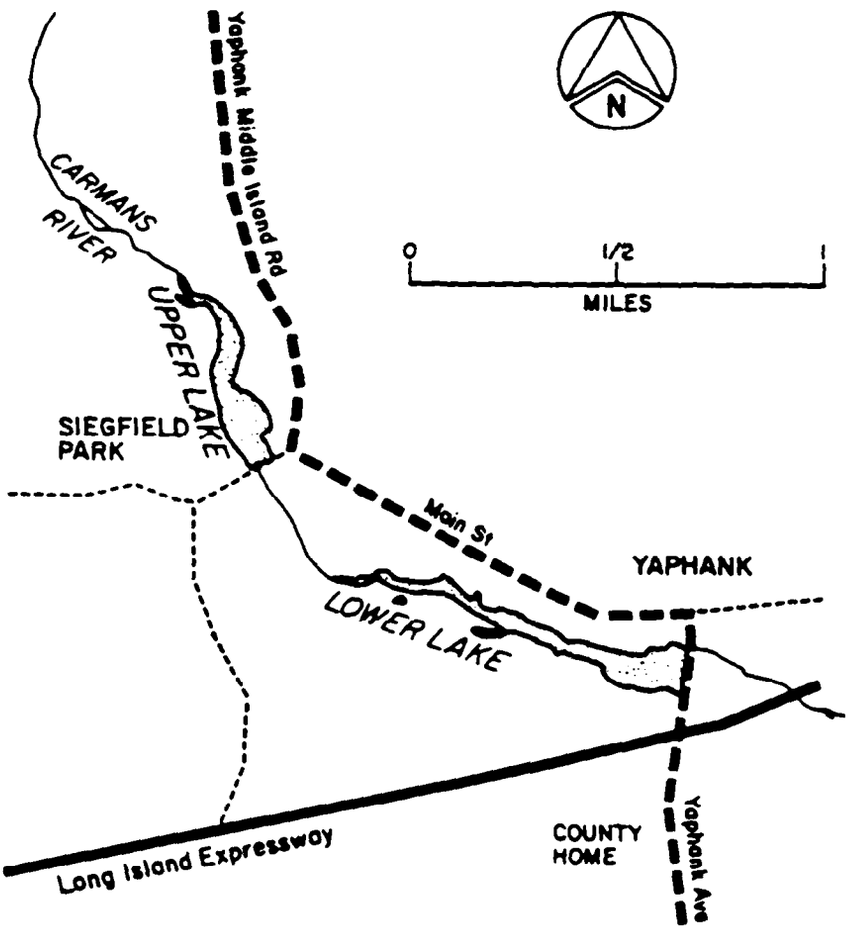

FIGURE V-12 UPPER AND LOWER LAKES AND ENVIRONS, LONG ISLAND, NEW YORK

tion very unlikely, and that Lower Lake is a slow moving river reach. We then compute hydraulic residence time as shown in Table V-7. Figure V-13, in particular diagram 1, shows what these assumptions mean in terms of a flow pattern for both lakes.

TABLE V-7

HYPOTHETICAL PHYSICAL CHARACTERISTICS AND
COMPUTATIONS FOR LOWER LAKE, BROOKHAVEN, SUFFOLK COUNTY, NEW YORK

Distance Downstream from Inflow Miles (feet)	D Average Depth ft.	W Average Width ft.	CSA Cross-sectional Area, D x W ft^2
0.075 (396)	15	157	2,355
0.150 (792)	20	165	3,300
0.225 (1,188)	20	173	3,460
0.300 (1,584)	25	197	4,925
0.375 (1,980)	35	197	6,895
0.450 (2,376)	30	228	6,840
0.525 (2,772)	35	232	8,120
0.600 (3,168)	35	197	6,895
0.675 (3,564)	40	220	8,800
0.750 (3,960)	42	315	13,230
0.825 (4,356)	41	433	17,753
0.900 (4,752)	51	591	30,141
0.975 (5,148)	42	551	23,142
1.050 (5,544)	40	433	17,320
1.125 (5,940)	37	323	11,951
			mean 11,008

Total length = 1.125 mi (5,940 ft.)

Inflow from upstream 400 cfs
Outflow to downstream 390 cfs
} (surface rising)

Average flow = 395 cfs

Computation

Volume (Vol) = Total length x mean cross-sectional area
= 5,940 ft. x 11,008 ft^2 = 6.54 x 10^7 ft^3

Residence Time (τ_w) = Vol/flow
= 6.54 x 10^7/(395 ft^3/sec) = 1.65 x 10^5 sec (46 hr)

Velocity (Vel) = length/τ_w
= 5,940 ft/1.65 x 10^5 sec = .036 ft/sec

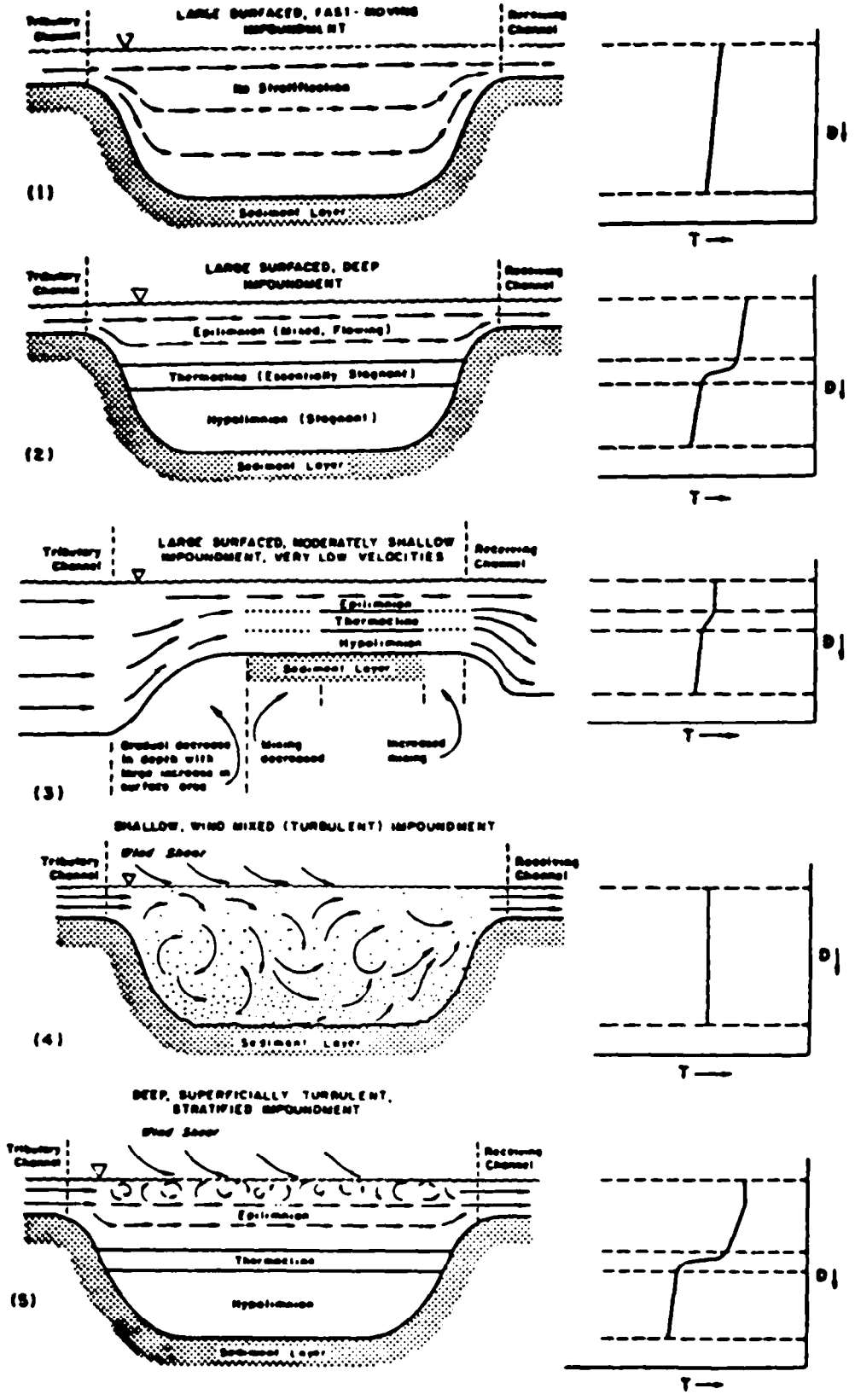

FIGURE V-13 IMPOUNDMENT CONFIGURATIONS AFFECTING SEDIMENTATION

END OF EXAMPLE V-5

EXAMPLE V-6

Assume for this example that Lower Lake is stratified during the period of interest. This significantly changes the computation of residence time. To a first approximation, one can merely revise the effective depth of the impoundment to be from the surface to the upper limit of the thermocline rather than to the bottom. Figure V-13 shows schematically what this simple model suggests for Lower Lake as a stratified impoundment (diagram 2 or possibly 3). The figure also shows wind-driven shallow, and deep impoundments. To the right of each diagram is a plot of the temperature profile over depth. Actually, the profile could represent a salinity gradient as well as a thermal gradient.

Table V-8 shows the procedure to estimate travel time for stratified Lower Lake. The upper boundary of the thermocline is assumed to be at a depth of 10 feet. For all later computations of sediment accumulation, this same 10 foot depth would be adopted. Such an assumption is valid presuming that the thermocline and hypolimnion are relatively quiescent. Thus once a particle enters the thermocline it can only settle, and cannot leave the impoundment.

END OF EXAMPLE V-6

EXAMPLE V-7

Large, Irregular Surface Impoundment

Figure V-14 shows Kellis Pond and surrounding topography. This small pond is located near Bridgehampton, New York and has a surface area of about 36 acres. From the surface shape of the pond, it is clear that it cannot be considered as a stream reach.

Figure V-15 shows a set of hypothetical depth profiles for the pond. From the profiles, it is evident that considerable shoaling has resulted in the formation of a relatively well defined flow channel thorugh the pond. Peripheral stagnant areas have also formed. Hypothetical velocity vectors for the pond are presented in Figure V-16. Based upon them, it is reasonable to consider the pond as being essentially the hatched area in Figure V-15. To estimate travel times, the hatched area may be handled in the same way as for the Upper Lake example presented above. It should be noted, however, that this approach will almost certainly result in underestimation of sediment deposition in later computations. This is true for two reasons. First, estimated travel time will be smaller than the true value since impoundment volume is underestimated. Second, since the approach ignores the low flow velocities to

TABLE V-8

HYPOTHETICAL PHYSICAL CHARACTERISTICS AND
COMPUTATIONS FOR LOWER LAKE, BROOKHAVEN, SUFFOLK COUNTY, NEW YORK
(ASSUMING AN EPILIMNION DEPTH OF 10 FEET)

Distance Downstream from Inflow Miles (feet)	D Average Depth ft.	W Average Width ft.	CSA Cross-sectional Area, D x W ft^2
0.075	10	160	1,600
0.150	10	170	1,700
0.225	10	175	1,750
0.300	10	200	2,000
0.375	10	198	1,980
0.450	10	230	2,300
0.525	10	233	2,330
0.600	10	200	2,000
0.675	10	222	2,220
0.750	10	316	3,160
0.825	10	435	4,350
0.900	10	590	5,900
0.975	10	552	5,520
1.050	10	435	4,350
1.125	10	325	3,250

Total length = 1.125 mi (5,940 ft.) mean CSA = 2,961 ft^2

Inflow from upstream 397 cfs
Outflow to downstream 393 cfs
} (steady-state surface, difference due to loss to water table)

Average flow = 395 cfs

Computation

Volume (Vol) = Total length x mean cross-sectional area
= 5,940 ft. x 2,961 ft^2 = 1.76×10^7

Residence Time (τ_w) = Vol/flow
= $1.76 \times 10^7 / (395\ ft^3/sec) = 4.46 \times 10^4$ sec (12.3 hr)

Velocity (Vel) = length/τ_w
= 5,940 ft/4.46×10^4 sec = 0.133 ft/sec

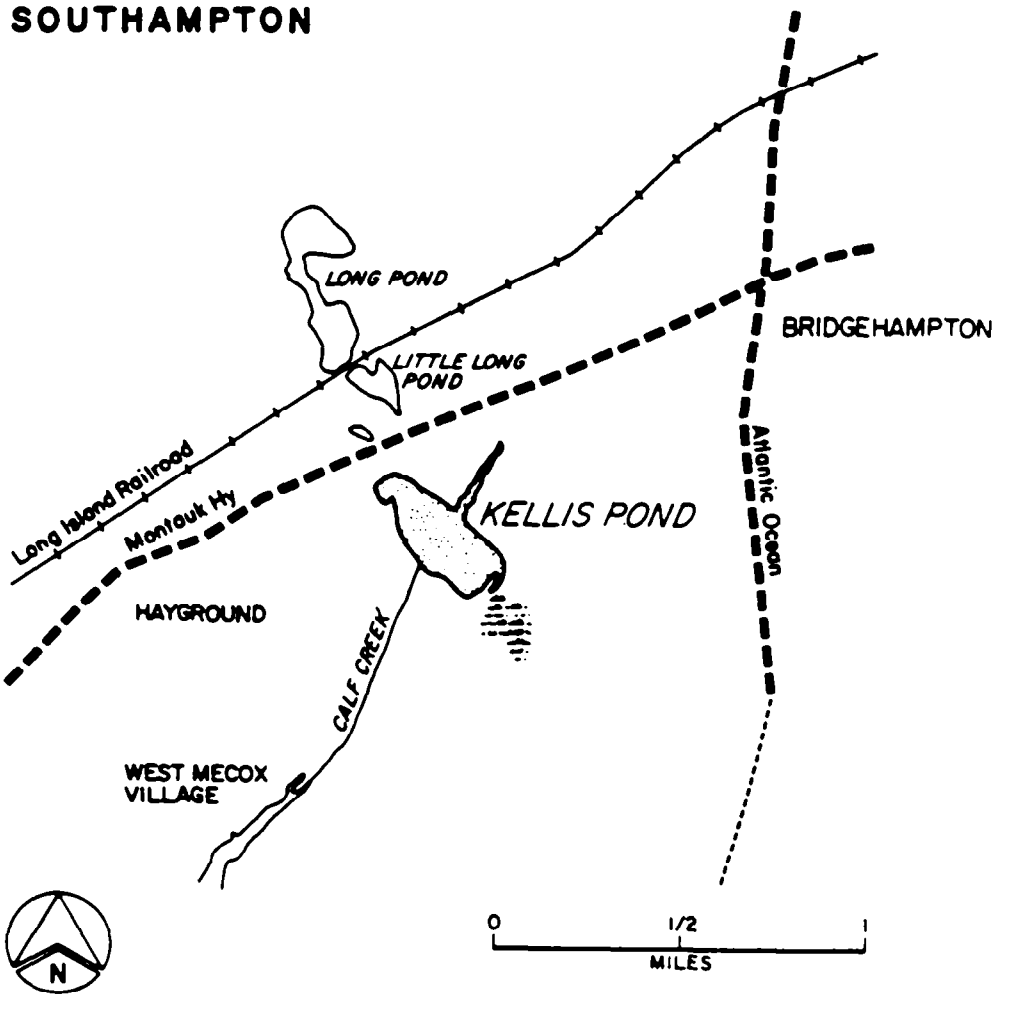

FIGURE V-14 KELLIS POND AND SURROUNDING REGION, LONG ISLAND, NEW YORK

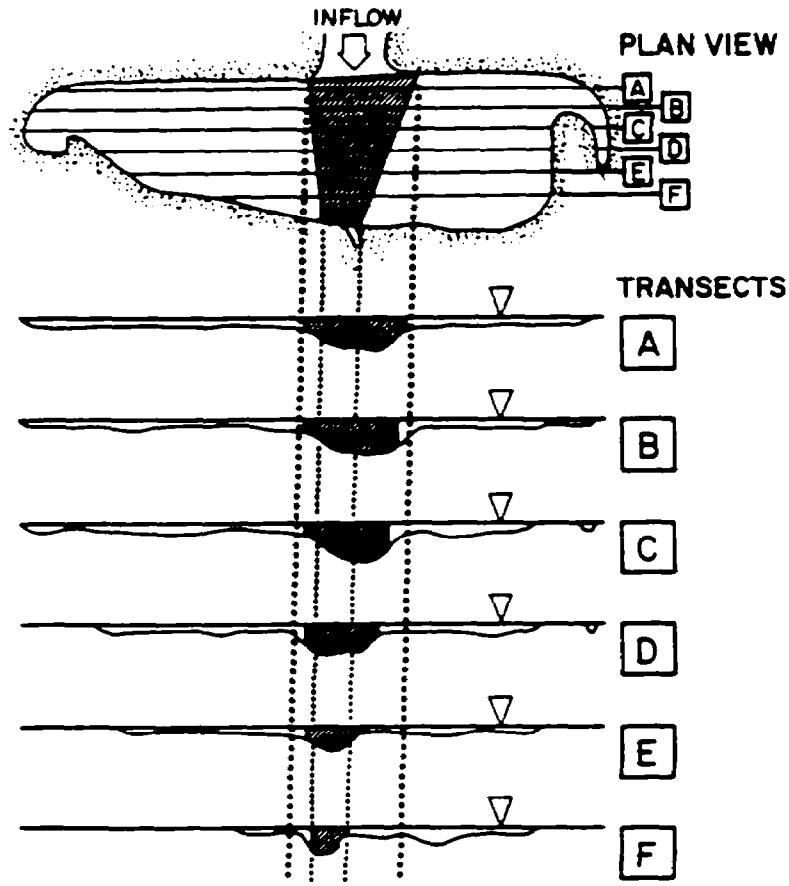

FIGURE V-15 HYPOTHETICAL DEPTH PROFILES FOR KELLIS POND

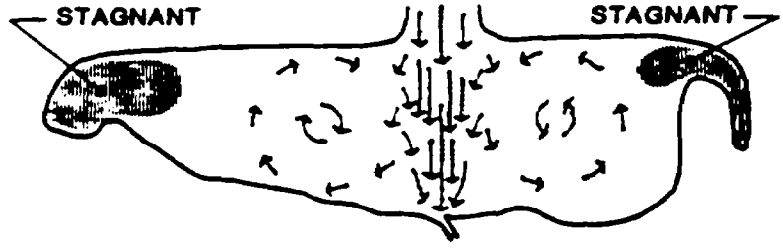

FIGURE V-16 HYPOTHETICAL FLOW PATTERN IN KELLIS POND

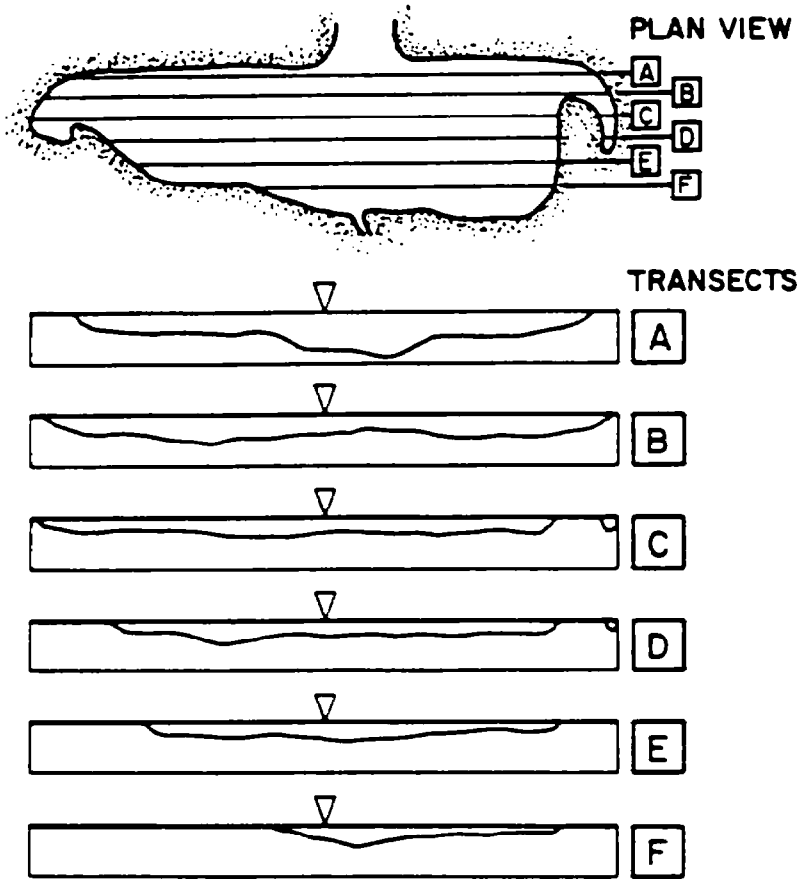

FIGURE V-17 HYPOTHETICAL DEPTH PROFILES FOR KELLIS POND NOT SHOWING SIGNIFICANT SHOALING

either side of the central channel and nonuniform velocities within it, heavier sedimentation than computed is likely.

Still more difficult to evaluate is the situation where shoaling and scour have not resulted in formation of a distinct central channel. Figure V-17 shows hypothetical depth profiles for Kellis Pond for such a case.

Here, velocity distribution data should be obtained, particularly if the impoundment is of much importance. If such data are not available but it is deemed worthwhile to do field studies, methods available for evaluating flow patterns include dye tracing and drogue floats. A simple but adequate method (at least to evaluate the surface velocity distribution) is to pour a large number of citrus fruits (oranges, grapefruit) which float just below the surface, into the impoundment, and to monitor both their paths and velocities. Although it is true that surface velocities may be greater than the velocity averaged over depth, this

will permit estimation of hydraulic residence time directly or generation of data to use in the prescribed method. In the latter case, the data might be used to define the major flow path through an impoundment of a form like Kellis Pond.

END OF EXAMPLE V-7

EXAMPLE V-8

Complex Geometries

The final hydraulic residence time example shows the degree of complexity that sediment deposition problems may entail. Although it is possible to make rough estimates of sediment accumulation, it is recommended that for such impoundments more rigorous methods be used - mathematical modeling and/or detailed field investigations.

Figure V-18 shows Lake Owyhee in eastern Oregon. This impoundment is well outside the range of complexity of water bodies which can be evaluated using these calculation methods. Because of geometry, the number of tributaries, and size, it is not feasible to conceptually reduce the impoundment in such a way as to estimate travel times. Flow patterns are likely to be very complex, and sediment deposition is difficult to predict both in terms of quantity and location.

In contrast, Figure V-19 shows New Millpond near Islip, New York and surrounding features. Although this water body does not have a simple surface geometry, it can be reduced to three relatively simple components as shown in the figure. Bearing in mind the limitations imposed by wind mixing, stratification, and the presence of stagnant regions described in earlier examples, deposition might nevertheless be estimated in arms A, B, and C. Because of the difficulty of predicting velocities and turbulence in section D, estimates of sedimentation cannot be reliably made there. However, it is likely that much of inflowing sediments will have settled out by the time water flows through the arms and into section D.

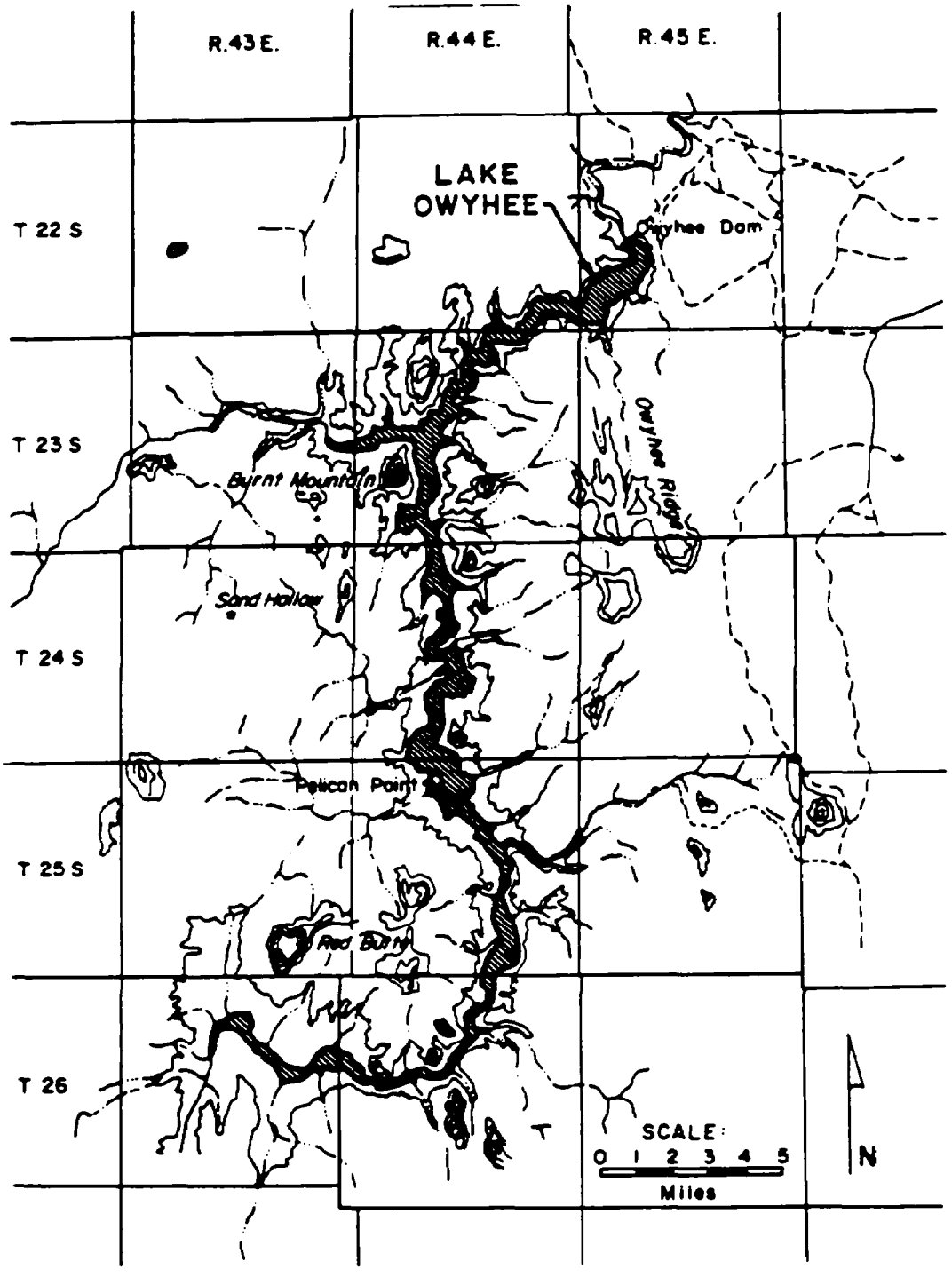

FIGURE V-18 LAKE OWYHEE AND ENVIRONS

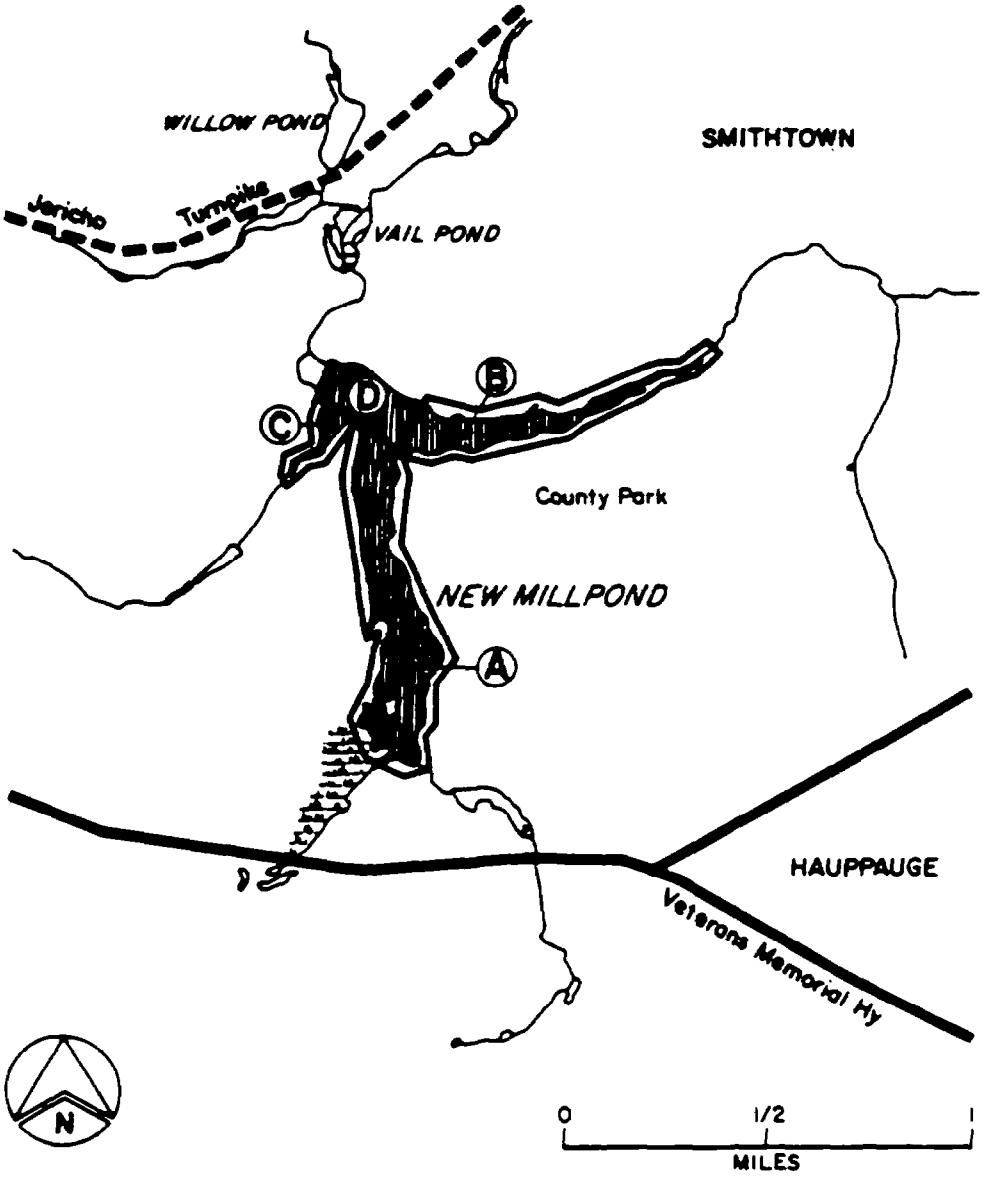

FIGURE V-19 NEW MILLPOND AND ENVIRONS. NEW MILLPOND IS SUBDIVIDED FOR PURPOSES OF ESTIMATING SEDIMENTATION IN REGIONS A, B, AND C.

END OF EXAMPLE V-8

5.3.5 Estimation of Sediment Accumulation

Estimation of quantities of sediment retained in an impoundment follows directly from the computations of settling velocity and travel time, although the computation depends upon whether the adopted model is plug flow, or a fully mixed layer or impoundment.

In the case of plug flow, one of two subordinate assumptions is made: that the plug is fully mixed as in turbulent flow, or that it moves in a "laminar" flow through the impoundment. In terms of sediment accumulation estimates, the fully mixed plug assumption is handled in the same way as the fully mixed impoundment model. Thus we have two kinds of computations:

Case A • Plug flow with the plug not mixed vertically.

Case B
- Plug flow assuming a vertically mixed plug
- A fully mixed impoundment or stratum.

Equation V-12 is pertinent to both cases A and B. It defines the mass of sediment trapped as a function of trap efficiency and inflowing sediment mass. Equation V-13 should be used for case A, and Equation V-14 for case B:

$$S_t = S_i P \tag{V-12}$$

$$P = \left((\tau_w v) + D'' - D \right) / D'' \tag{V-13}$$

$$P = \frac{v\tau_w}{D'} \tag{V-14}$$

where

P = mean proportion of S_i trapped ($1 \geq P \geq 0$)
S_t = mass of sediment trapped per unit time
S_i = mass of sediment in inflows per unit time
v = particle settling velocity
D = discharge channel depth
D' = flowing layer depth
D'' = inflow channel depth.

Figure V-20 shows the significance of the various depth measures D, D', D'', and the assumed sedimentation pattern. In case B, in the absence of substantial erratic turbulence and unpredicted vertical velocity components, and within the constraints of available data, it is clear that this approach can give reasonable estimates of trap efficiencies. In case A, however, small changes in D or D'' can strongly affect trap efficiencies. It is important to remember in applying case A that P is a mean, preferably used over a period of time. It is also important to recognize that conditions within an impoundment leading to selection of case A or B are subject to change, thus affecting estimates.

For convenience, Figure V-21 is included to provide estimates of v_{max}

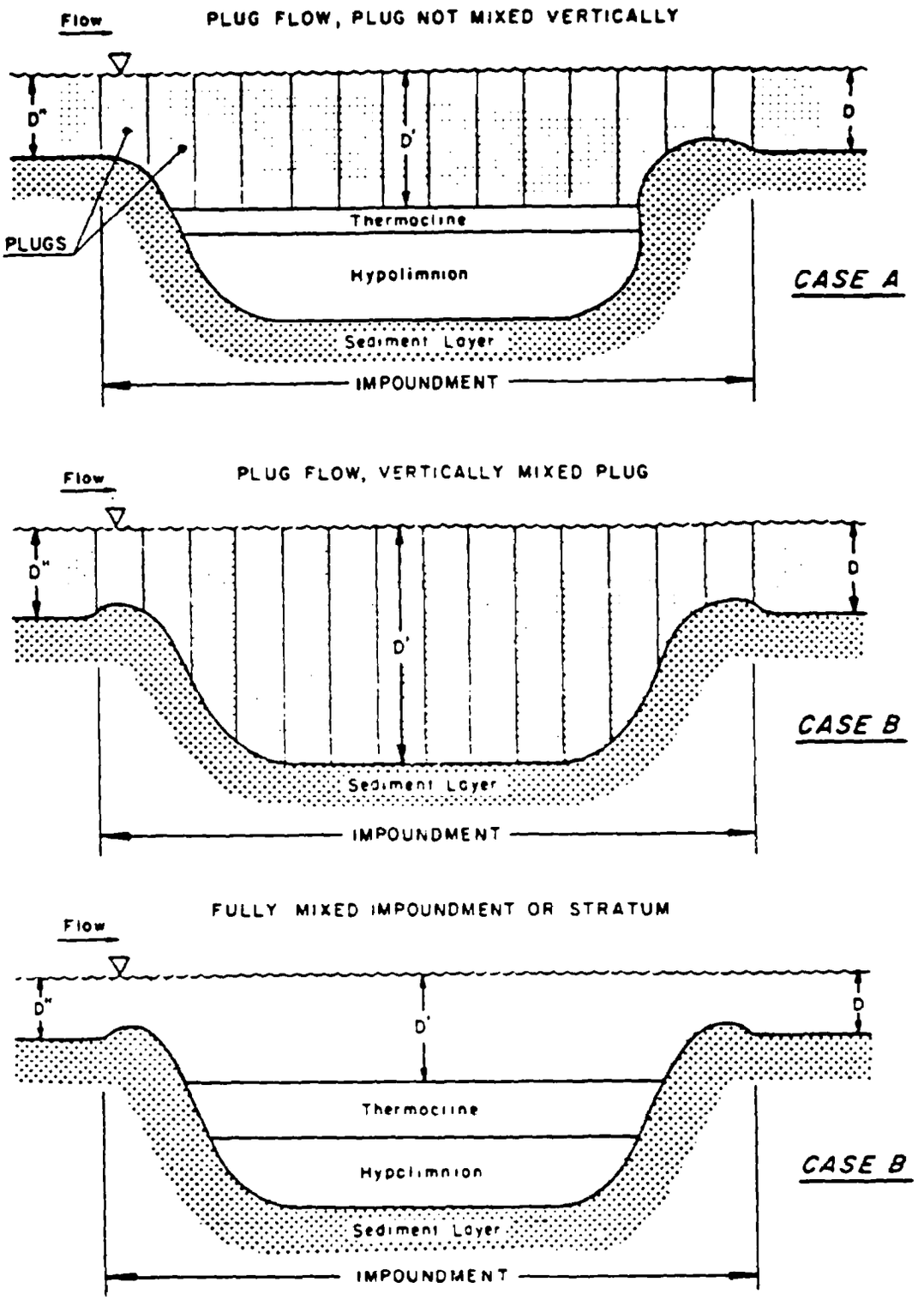

FIGURE V-20 SIGNIFICANCE OF DEPTH MEASURES D, D', AND D'', AND THE ASSUMED SEDIMENTATION PATTERN

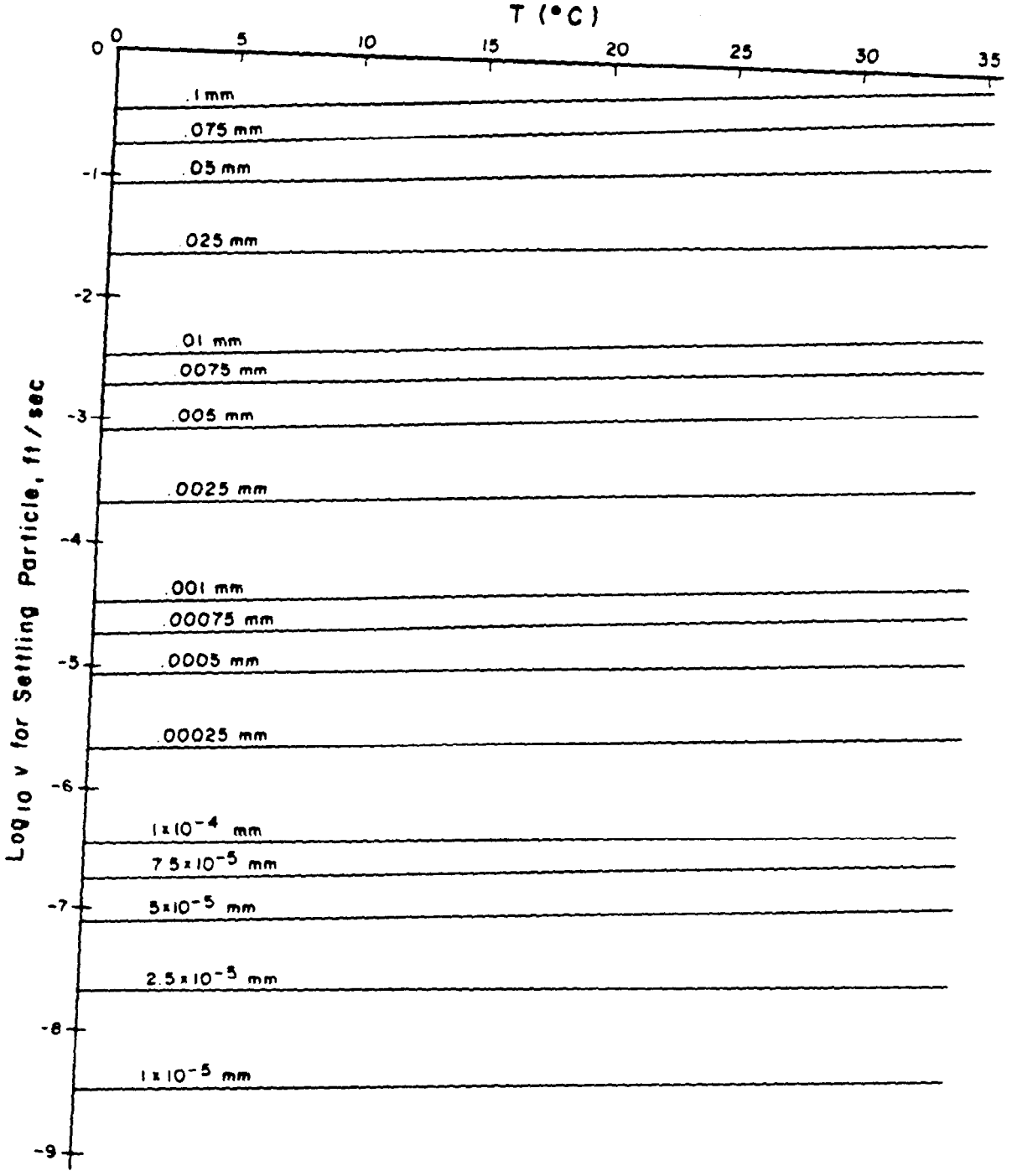

FIGURE V-21 SETTLING VELOCITY FOR SPHERICAL PARTICLES

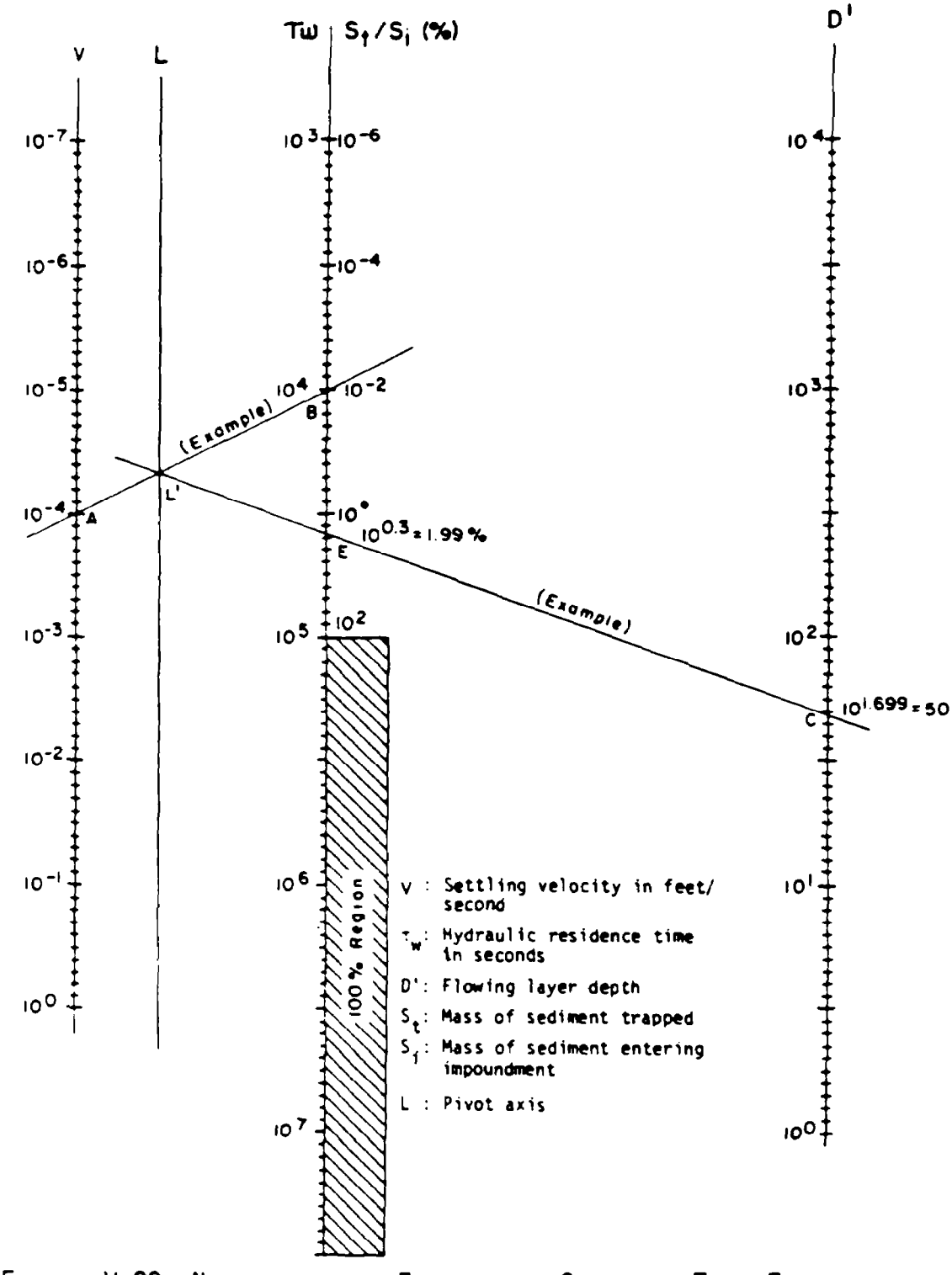

FIGURE V-22 NOMOGRAPH FOR ESTIMATING SEDIMENT TRAP EFFICIENCY

for spherical particles of 2.7 specific gravity. The data are presented as a function of particle diameter and temperature. Figure V-22 is a nomograph relating trap efficiency, P (in percent) to depth D', V_{max}, and τ_w. The nomograph is useful only for case B assumptions.

EXAMPLE V-9

Sedimentation in Upper and Lower Lakes

Using the data from Table V-6 and settling velocities for the clay and sand of Example V-4, for case A:

$$\tau_w = 1.6 \times 10^4 \text{ sec}$$

V_{max} for clay = 8 ft day^{-1}

V_{max} for sand = 252 ft hour^{-1}

Although it is not specified in Table V-6, the inflow channel depth at the entrance to Upper Lake is 3 feet. The discharge channel depth is 10 feet. Assuming "laminar" flow with minimal vertical components (Case A), for clay:

$$P = \frac{[(T_w \times v) + D'' - D]}{D''}$$

$$P = \frac{[(1.6 \times 10^4 \times 9.3 \times 10^{-5}) + 3 - 10]}{3}$$

$$= -5.5$$

The negative value implies that the proportion settling out is virtually zero. Thus the clay will to a large extent pass through Upper Lake. However, τ_w for this example is very small (4.5 hours). Many impoundments will have substantially larger values.

For the sand:

$$P = \frac{[(1.6 \times 10^4 \times 7 \times 10^{-2}) + 3 - 10]}{3}$$

$$= 371$$

All of the sand will clearly be retained. Note that a clay or very fine silt of $V_{max} = 5 \times 10^{-4}$ ft sec^{-1} would be only partially trapped:

$$P = \frac{[(1.6 \times 10^4 \times 5 \times 10^{-4}) + 3 - 10]}{3}$$

$$= 0.33$$

Thus about one-third of this sediment loading would be retained. Note that if D is large, trap efficiency drops using this algorithm. For the silt, a discharge channel depth (at the outflow from Upper Lake) of 11 feet rather than 10 would give:

$$P = \frac{[(1.6 \times 10^4 \times 5 \times 10^{-4}) + 3 - 11]}{3}$$

$$= 0$$

Thus with D = 11, all silt exits the impoundment. If D is only 9 feet, then:

$$P = \frac{[(1.6 \times 10^4 \times 5 \times 10^{-4}) + 3 - 9]}{3}$$

$$= .66$$

Two-thirds of the silt is retained. Remember that P represents a mean value. Clearly during some periods none of the silt will be retained (due to turbulence, higher velocities) while during other periods, all of the silt will be trapped. The key here is the word "mean."

If the impoundment is assumed to be vertically mixed (case B), compute the mean depth $\bar{D}$:

$$\bar{D} = \sum_{i=1}^{n} D_i/n$$

where

n = the number of cross-sections

D_i = depth at the ith cross-section.

For Upper Lake:

$$\bar{D} = 6.7 = D'$$

Then:

$$P = \frac{v\,\tau_w}{D'}$$

For the clay:

$$P = \frac{9.3 \times 10^{-5} \times 1.6 \times 10^4}{6.7}$$

$$= 0.22$$

About one-fourth of the clay is retained:

For the sand:

$$P = \frac{7 \times 10^{-2} \times 1.6 \times 10^4}{6.7}$$

$$= 167$$

All of the sand will be trapped within about 1/167 times the length of the lake. If the daily influent loading of sand is one ton, while the loading of clay is fifteen tons, then the daily accumulation will be one ton of sand and 0.22 x 15 = 3.3 tons of clay.

Finally, as an example of use of Figures V-21 and V-22, assume that the sediment loading consists primarily of silt particles in the size range of .002mm diameter, and that the water temperature is 5°C. Further, assume τ_w has been estimated as 2.77 days (10^4 seconds), and that D' = 50 feet. From Figure V-21, the settling velocity is about 1×10^{-4} feet per second.

In Figure V-22, draw a line from 10^{-4} on the V axis to 10^{4} on the τ_w axis. The point of intersection with axis L is L'. Next, compute $\log_{10}50 = 1.699$. Draw a line from this point on the D' axis to L'. Where this line crosses the S_t/S_i (%) axis gives the log of the percent of the sediment trapped. This is $10^{0.3} = 1.99 \cong 2\%$.

END OF EXAMPLE V-9

5.4 EUTROPHICATION AND CONTROL

5.4.1 Introduction

Eutrophication is the process of increasing nutrients in surface waters. The presence of nutrients in an impoundment generally favors plant growth. Depending upon antecedent conditions, the relative abundance of nitrogen, phosphorus, light, and heat, and the status of a number of other physical and chemical variables, the predominant forms may be diatoms, other microscopic or macroscopic algae, or bottom-rooted or free-floating macrophytes. The quantity of plant matter present in an impoundment is important for several reasons. First, plant cells produce oxygen during photosynthesis, thereby providing an important source of dissolved oxygen to the water column during daylight hours. Plant cells also consume oxygen through the process of respiration. Respiration occurs along with photosynthesis during the day, but occurs at night when photosynthesis does not. Oxygen consumed at night may be considerable, not only because it serves to sustain the plant cells, but because the cells actively perform various vital metabolic functions in the dark. Also, cells that fall below the photic zone will consume additional oxygen irrespective of the time of day.

Plant growth within an impoundment is also important because plant biomass is a major source of nutrition for indigenous fauna, and the growth of plants constitutes what is called "primary production." The stored energy and nutrients provide food for various grazers higher in the food chain, either through direct consumption of living plant tissue by fishes and zooplankton or through consumption of detritus by fishes, microorganisms, and zooplankton. The grazers, in turn, provide food for predatory fishes, mammals, insects, and other higher forms. The kinds and amounts of primary producers affect the other members of the food chain resulting in a good sport fishery or "trash fish," depending on nutrient conditions.

Finally, plant development in impoundments is important because it tends to accelerate impoundment aging. As plants grow, organic matter and sediment accumulate. As the impoundment fills with rock fragments, soil, and plant detritus, an excellent substrate forms upon which more suspended matter may be trapped and which may ultimately support the growth of higher plants and trees. The gradual filling in of an

impoundment in this way reduces its usefulness, and may finally eliminate the impoundment completely.

5.4.2 Nutrients, Eutrophy, and Algal Growth

Eutrophy means literally a state of good nutrition. Plants require a number of nutrients, but to vastly different degrees. Some nutrients, such as carbon, nitrogen, potassium, and phosphorus, are needed in large quantity. These are termed macronutrients. The micronutrients, e.g. iron, cobalt, manganese, zinc, and copper, are needed in very small amounts. In nature, the micronutrients, carbon, and potassium are usually in adequate supply (although not always), while nitrogen and phosphorus are commonly growth limiting.

Nitrogen, particularly as nitrate and ammonium ions, is available to water-borne plant cells to be used in synthesis of proteins, chlorophyll *a*, and plant hormones. Each of these substances is vital for plant survival.

Phosphorus, an element found in a number of metabolic cofactors, is also necessary for plant nutrition. The biosynthesis and functioning of various biochemical cofactors rely on the availability of phosphorus, and these cofactors lie at the very foundation of plant cell metabolism. Without adequate phosphorus, plant cells cannot grow.

Since nitrogen and phosphorus are commonly in limited supply, many impoundments tend inherently to be clear and essentially free of clogging algae and vascular plants. Over long periods of time and depending on geological conditions, natural sources of nutrients may lead to eutrophication in lakes. Because of society's ever-increasing size and need for food, chemical sources of nitrogen and phosphorus are synthesized and spread over vast tracts of farmland. Stormwater washes off these nutrients, which then flow through streams and into natural and artificial impoundments. Also, excessive nutrients occur in wastewaters from municipalities and industry. Due to the fact that many impoundments have very low flow velocities, impoundments represent excellent biological culturing vessels, and often become choked with plant life when nutrients increase.

Since a plant cell has at any point in time a specific need for nitrogen and for phosphorus, one or the other or both may limit cell growth or replication. Where nitrogen is the nutrient that restricts the rate of plant growth, that is, where all other nutrients and factors are present in excess, we say that nitrogen is growth limiting. In general, N:P mass ratios in the range of 5 to 10 are usually associated with plant growth being both nitrogen and phosphorus limited. Where the ratio is greater than 10, phosphorus tends to be limiting, and for ratios below 5, nitrogen tends to be limiting (Chiaudani, *et al.*, 1974). In most lakes, phosphorus is the limiting nutrient. In many nitrogen-limited lakes, phosphorus is still controlling because of the process of nitrogen fixation. Thus, the focus in this manual is on phosphorus.

In addition to nitrogen and phosphorus, any necessary nutrient or physical condition may limit plant growth. For example, in high nutrient (eutrophic) waters, algal biomass may increase until light cannot penetrate, and light is then limiting. At such a point, a dynamic equilibrium exists in which algal cells are consumed, settle or lyse (break) at the same rate as new cells are produced. In other cases, light may be limiting due to non-algal particulate material.

To summarize, the process of eutrophication (or fertilization) is enrichment of a lake with nutrients, particularly nitrogen and phosphorus. However, the problems of eutrophication are caused by increased plant biomass as a result of enrichment. Therefore, the objective is to predict plant biomass as related to nutrient concentrations. The method for predicting plant biomass is based on the rate of phosphorus supply (loading), the concentration of phosphorus in the lake, and the amount of plant biomass that is predicted based on the phosphorus concentration. The plant biomass is exemplified by the phytoplankton (algae) concentration but macrophytes (aquatic weeds) are also of concern. The plant biomass and related variables define the scalar relationships of eutrophication.

5.4.3 Predicting Algal Concentrations

Predicting algal blooms or predominance of macrophytes using a mechanistic approach can be a very complex problem, and most methods are not suited to a simple hand calculation technique. However, relationships regarding algal productivity have been derived that permit an evaluation of the eutrophic state of an impoundment. Because the methods permit algal biomass to be estimated with relatively little, easily obtained data, and because algae are very important in assessing impoundment water quality, these techniques are useful here. The methods presented below are based upon the fact that in most cases (perhaps 60 percent) phosphorus is the biomass limiting nutrient (EPA, 1975). One such approach has been developed by Vollenweider (Vollenweider, 1976; Vollenweider and Kerekes, 1981; Lorenzen, 1976). It may be used to predict the degree of impoundment eutrophication as a function of phosphorus loading.

5.4.3.1 Nutrient Limitation

Before considering application of any of the methods to assess eutrophication, it is important to examine the nitrogen to phosphorus ratio. This indicates whether any of the methods presented below is likely to give realistic results. Generally, an average algal cell has an elemental composition for the macronutrients of $C_{106}\ N_{16}\ P_1$. With 16 atoms of nitrogen for each atom of phosphorus, the average composition by weight is 6.3 percent nitrogen and 0.87 percent phosphorus or an N/P ratio of 7.2/1. Although all nutrient requirements must be met, the relative rate of supply is significant and must be determined to know which is limiting. For N/P

ratios greater than 7.2, phosphorus would be less available for growth ("limiting") and when less than 7.2, nitrogen would be limiting. In paractice, values of less than 5 are considered nitrogen limiting, greater than 10 are phosphorus limiting, and between 5 and 10, both are limiting.

In many cases of eutrophic lakes, nitrogen is not limiting because of the process of nitrogen fixation. Some blue-green algae, a particularly noxious type of algae, have enzymatic processes for the biochemical conversion of dissolved elemental nitrogen into reduced nitrogen (amine groups) suitable for growth and metabolism. Special cells called heterocysts perform this process and only appear when nitrogen is limiting. It can be argued that in general nitrogen is not limiting (Schindler, 1977) and a "worst case" analysis can be made for a screening approach using phosphorus. This is the basis for the eutrophication screening method. However, it should be remembered that the chlorophyll produced is affected by the N/P ratio as are the algal species (Smith, 1979).

5.4.3.2 Nutrient Availability

Availability of nutrients is also important. Particulate nitrogen and phosphorus in the inflowing tributaries generally settle and can therefore be considered unavailable. Few estimates of bioavailable nutrients have been made. The estimates have been made primarily for phosphorus using algal assay techniques. Cowen and Lee (1976) indicated that 30 percent or less of urban runoff phosphorus was available to algae while Dorich et al. (1980) found a value of 20 to 30 percent for sediment bound phosphorus (as would occur in rural runoff). It appears that a fraction of 0.3 would provide a conservative estimate of bioavailable phosphorus in the absence of actual measurements.

5.4.4 Mass Balance of Phosphorus

A material entering a lake or impoundment will partition between the aqueous and solid phases. The solid phase can settle and become bottom sediment or outflow can remove suspended and aqueous phase material. A diagrammatic presentation of the concept of inflow, partitioning and settling, and outflow is shown in Figure V-23. The concentration of the material can be calculated very simply after making several assumptions: the lake is completely mixed, the lake is at steady state and inflowing water equals outflow, and the annual average rates are constant. Although these assumptions are not met entirely for phosphorus, they are satisfied well enough to meet requirements for a screening analysis of eutrophication. Based on its historical development the eutrophication screening method is termed the "Vollenweider Relationship".

As shown in Figure V-23, any of three different forms of the steady state equation can be used to predict phosphorus concentrations in lakes. Each form may be

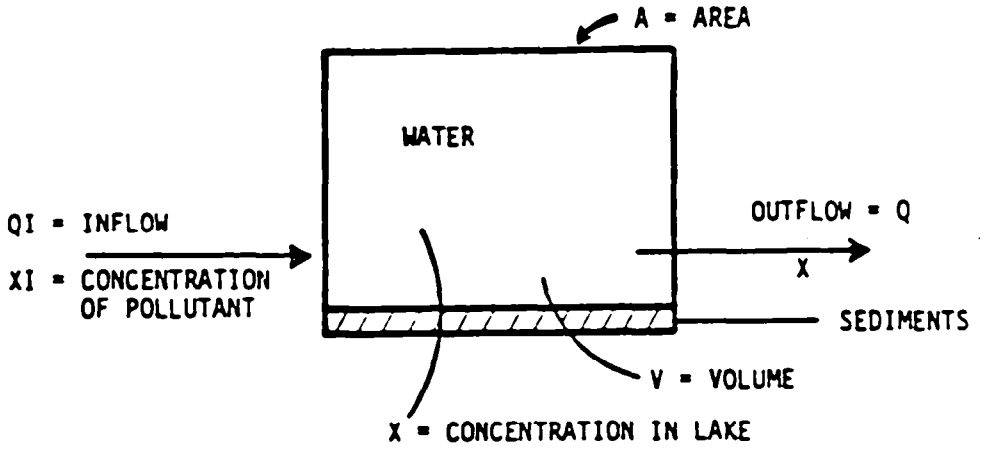

For Example - Phosphorus, P = X

LOADING

$$Lp = QI \cdot PI / A, \ mg/m^2 \ year$$

MASS BALANCE

Assumptions: completely mixed, steady state, $Q \cong QI$, annual average rates are constant

Definitions: Mean depth, $\bar{Z} = V/A$; hydraulic flushing or dilution rate, $D = Q/V$; hydraulic loading, $q_s = Q/A$; $M = QI \cdot PI$; K = net rate of solid phase removal and release (proportional to P), typically negative when averaged over the annual cycle.

$$\frac{dP}{dt} = \frac{Q \cdot PI}{V} - \frac{Q \cdot P}{V} - KP = 0$$

Solving for P,

$$P = \frac{D \cdot PI}{D + K} \quad \text{(Mass Balance Form)} \quad (1)$$

$$P = \frac{M}{Q}\left(\frac{D}{D + K}\right) \quad \text{(Mass Inflow Form)} \quad (2)$$

$$P = \frac{Lp}{\bar{Z}(D + K)} \quad \text{(Loading Form)} \quad (3)$$

FIGURE V-23 FORMULATIONS FOR EVALUATING MANAGEMENT OPTIONS FOR POLLUTANTS IN LAKES AND RESERVOIRS

more or less suitable for a specific data set. The important variables are the hydraulic flushing or dilution rate (Q/V, inverse of residence time), lake volume to area ratio (V/A, equals mean depth), phosphorus in the influent (PI), and the net rate of removal (K).

The variables Q, V, A must be determined from other data. The influent phosphorus can be based on measurements or estimated from calculations performed as in Chapter 3 and including any municipal and industrial effluents. Generally, effluents are considered totally available for growth. Nonpoint sources should be assessed as 100 percent available and as 30 percent available to provide limits for screening purposes.

Estimation of the net rate of removal (K) is not as clear. Vollenweider (1976) and Larsen and Mercier (1976) independently estimated the net rate of removal as a function of dilution rate:

$$K = \sqrt{D}$$

This is the most accepted approach for screening. Jones & Bachmann (1976) estimated that K = 0.65 by least squares fitting of data for 143 lakes.

Equivalently, Vollenweider and Kerekes (1981) provide a derivation of the mass balance equation (Equation 1, Figure V-23) in terms of phosphorus residence time and based on regression analysis:

$$P = \frac{1}{1 + \sqrt{D}} (PI) = \frac{PI}{1 + \sqrt{D}}$$

Regression of predicted phosphorus and actual phosphorus for 87 lakes showed a reasonable correlation (r = 0.93) but indicated that there was a predicted slight underestimate at low concentrations (<8 μg/l) and a slight overestimate at higher concentrations (<20 μg/l) (Vollenweider and Kerekes, 1981).

Also the value of K can be estimated from the ratio (R) of the measured mass phosphorus retained (in minus out) and the mass inflow:

$$R = \frac{QI \cdot PI - Q \cdot P}{QI \cdot PI} \cong \frac{PI - P}{PI}$$

$$K = \frac{Lp}{P \cdot \bar{Z}} (R)$$

To assess the placement of a specific lake relative to a set of lakes, phosphorus loading (Lp) is graphed as a function of hydraulic loading (q_s) (Figure V-24). The data for 49 measurements of U.S. lakes are shown. (Some lakes occur more than once because of multi-year studies.)

More recently, Vollenweider and Kerekes (1981) have presented the OECD Eutrophication Program results showing that lakes can be classified into discrete groups according to their eutrophication characteristics (Table V-9). However, as they note, there is overlap between the different categories showing that these characteristics are not complete descriptors of trophic state but are relative indicators.

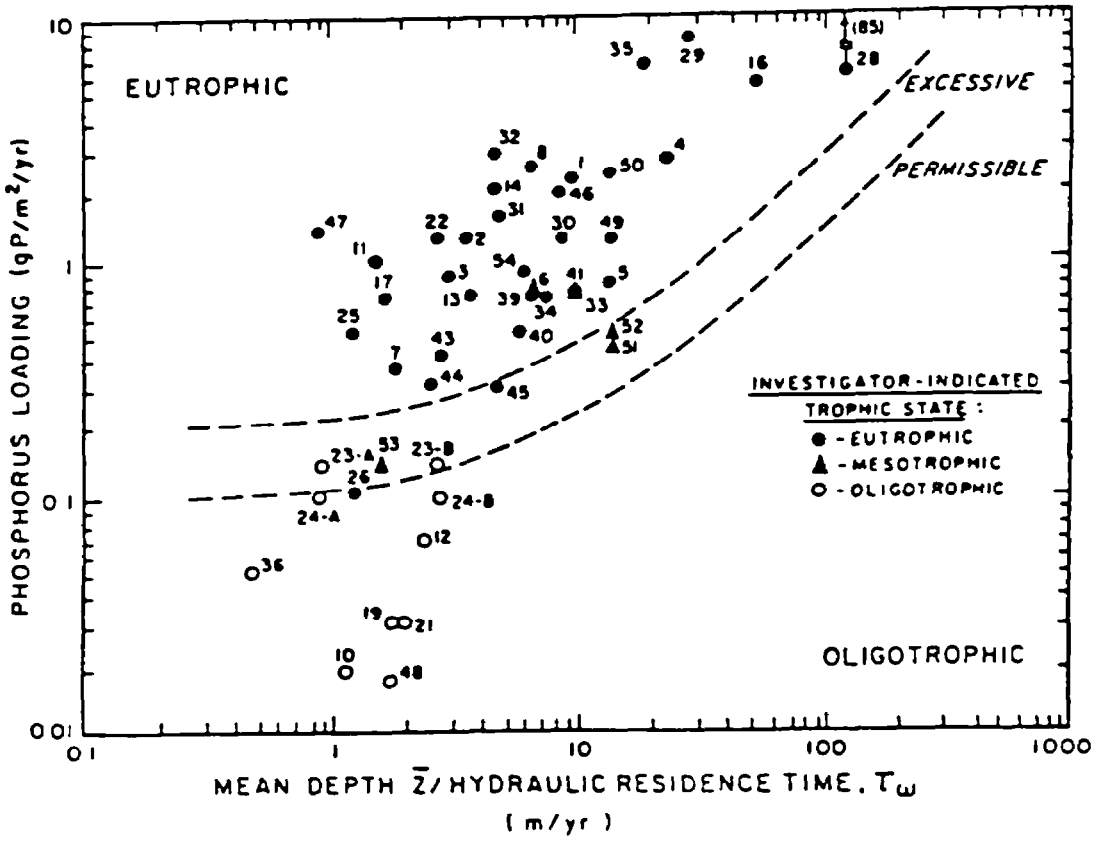

FIGURE V-24 US OECD DATA APPLIED TO VOLLENWEIDER (1976) PHOSPHORUS LOADING AND MEAN DEPTH/HYDRAULIC RESIDENCE TIME RELATIONSHIP (TAKEN FROM RAST AND LEE, 1978)

TABLE V-9

PRELIMINARY CLASSIFICATION OF TROPHIC STATE BASED ON INVESTIGATOR OPINION
(ADAPTED FROM VOLLENWEIDER AND KEREKES, 1981)

Variable*	Oligotrophic	Mesotrophic	Eutrophic
Total Phosphorus			
mean	8	27	84
range (n)	3-18(21)	11-96(19)	16-390(71)
Total Nitrogen			
mean	660	750	1900
range (n)	310-1600(11)	360-1400(8)	390-6100(37)
Chlorophyll *a*			
mean	1.7	4.7	14
range (n)	0.3-4.5(22)	3-11(16)	2.7-78(70)
Peak Chlorophyll *a*			
mean	4.2	16	43
range (n)	1.3-11(16)	5-50(12)	10-280(46)
Secchi Depth, m			
mean	9.9	4.2	2.4
range (n)	5.4-28(13)	1.5-8.1(20)	0.8-7.0(70)

* $\mu g/l$ (or mg/m^3) except Secchi depth; means are geometric annual means (log_{10}), except peak chlorophyll *a*.

EXAMPLE V-10

Big Reservoir and
The Vollenweider Relationship

To use the Vollenweider relationship for phosphorus loading, data on long-term phosphorus loading rates must be available. It is also important that the rates represent average loading conditions over time because transient phosphorus loading pulses will give misleading results. Big Reservoir is a squarish reservoir and has the following characteristics:

Big Reservoir

Available Data (all values are means):

Length	2.0 mi = 3.22 km
Width	5. mi = .805 km
Depth (Z)	200 ft = 20 m
Inflow (Q)	50 cfs = 1.42 cms

Total phosphorus concentration in water column	0.482 ppm
Total nitrogen concentration in water column	2.2 ppm
Total phosphorus concentration in the inflow	1.0 ppm

In order to apply the plot in Figure V-24, the first step is to make as certain as possible that algal growth is phosphorus limited. In this case, the weight to weight N:P ratio is 2.2/.48 = 4.6. Presumably, algal growth in Big Reservoir is not phosphorus limited, and the Vollenweider relationship for phosphorus is not a good one to use. In this case a rigorous model should be used. If nitrogen fixation is observed to occur (heterocystous blue-green algae), an estimate of the potential problem can be obtained by assuming phosphorus to be limiting:

V = length · depth · width

= 3220m · 805m · 20m = 51.8 million m^3

$$D = \frac{1.42\ m^3}{sec\ 51.8Mm^3} \cdot \frac{86400\ sec}{day} \cdot \frac{365\ day}{yr} = \frac{0.865}{yr}$$

τ_w = 1.16 years

$K = \sqrt{D} = 0.93/yr$

$$P = \frac{D \cdot PI}{D + K} = 0.482\ mg/l$$

$Lp = Q \cdot PI/A = 17.3\ g/m^2\ yr$

$q_s = Q/A = \bar{Z}/\tau w = 20/1.16 = 17.2\ m/yr$

Plotting Lp and q_s on Figure V-24 shows that the reservoir could be extremely eutrophic.

END OF EXAMPLE V-10

EXAMPLE V-11

Bigger Reservoir and
The Vollenweider Relationship

The physical characteristics of Bigger Reservoir are:

Bigger Reservoir

Available Data (all values are means):

Length	20 mi = 32.2 km
Width	10 mi = 16.1 km
Depth ($\bar{Z}$)	200 ft = 61 m
Inflow (Q)	500 cfs
Total phosphorus concentration in inflow	0.8 ppm
Total nitrogen concentration in inflow	10.6 ppm

As in the preceding example, first determine whether phosphorus is likely to be growth limiting. Since data are available only for influent water, and since

no additional data are available on impoundment water quality, N:P for influent water will be used.

N:P = 10.6/0.8 = 13.25

Thus algal growth in Bigger Reservoir is probably phosphorus limited.

Compute the approximate surface area, volume and the hydraulic residence time.

Volume (V) = 20 mi x 10 mi x 200 ft x 5280^2 =
$1.12 \times 10^{12} ft^3 = 3.16 \times 10^{10} m^3$

Hydraulic residence time (τ_w) = V/Q =
$1.12 \times 10^{12} ft^3 / 500\ ft^3 sec^{-1} = 2.24 \times 10^9 sec = 71\ yr$

Surface area (A) = 20 mi x 10 mi x 5280^2 =
$5.57 \times 10^9 ft^2 = 5.18 \times 10^8 m^2$

Next, compute q_s

$q_s = \bar{Z}/\tau_w$

$q_s = 61\ m/71\ yr = 0.86\ m\ yr^{-1}$

Compute annual inflow, Q_y

$Q_y = Q \times 3.15 \times 10^7\ sec\ yr^{-1}$

$Q_y = 1.58 \times 10^{10} ft^3\ yr^{-1}$

Phosphorus concentration in the inflow is 0.8 ppm or 0.8 mg/l. Loading (Lp) in grams per square meter per year is computed from the phosphorus concentration, in mg/l:

$$Lp = \frac{28.31\ell}{ft^3} \times \frac{1\ g}{1000 mg} \times \frac{0.8\ mg}{\ell} \times \frac{1}{5.18 \times 10^8 m^2} \times 1.58 \times 10^{10}\ \frac{ft^3}{yr}$$

$Lp = 0.70\ gm^{-2} yr^{-1}$

Now, referring to the plot in Figure V-24, we would expect that Bigger Reservoir is eutrophic, possibly with severe summer algal blooms.

END OF EXAMPLE V-11

EXAMPLE V-12

The Vollenweider Relationship
Using Monthly Inflow Quality Data

Is Frog Lake eutrophic? Frog Lake's physical characteristics are as shown below:

Frog Lake

Available Data:

Mean length	2 mi
Mean width	1/2 mi
Mean depth	25 ft

Available Inflow Water Quality Data:

	Q (monthly mean, cfs)		Total P (mg/l)		Inorganic N (mg/l)	
Month	1972	1974	1972	1974	1972	1974
October	50	65	0.1	0.08	7.2	6.0
November	80	90	0.02	0.02	6.3	2.4
December	40	40	0.03	0.04	3.1	1.5
January	-	-	-	-	-	-
February	-	-	-	-	-	-
March	60	58	0.01	0.02	2.0	1.9
April	80	80	0.01	0.01	2.3	0.50
May	75	76	0.04	0.05	0.55	0.52
June	40	70	0.03	0.08	1.20	1.35
July	-	25	-	0.11	-	2.01
August	38	20	0.09	0.04	3.50	1.29
September	38	25	0.06	0.05	2.80	1.00

First, estimate the mean annual flow and the hydraulic residence time. To compute mean annual flow,

$$Q = \left(\sum_{i=1}^{y} \sum_{j=1}^{n_i} Q_{i,j} \right) / \sum_{i=1}^{y} n_i$$

where

$Q_{i,j}$ = the individual flow measurements

y = the number of years of data

n_i = the number of observations per year

Q = 1050/19 = 55.3 cfs = $1.75 \times 10^9 ft^3/yr$

Now estimate the volume, surface area, hydraulic residence time, and q_s

$$V = 2 \text{ mi} \times 1/2 \text{ mi} \times 25 \text{ ft} \times \frac{(5280 \text{ ft})^2}{\text{mi}} = 6.97 \times 10^8 ft^3 = 1.98 \times 10^7 m^3$$

$$A = 2 \text{ mi} \times 1/2 \text{ mi} \times \frac{(5280 \text{ ft})^2}{\text{mi}} = 2.79 \times 10^7 ft^2 = 2.59 \times 10^6 m^2$$

$$\tau_w = V/Q = 6.97 \times 10^8 ft^3/55.3 \text{ cfs} = 1.26 \times 10^7 \text{ sec} = 0.4 \text{ yr}$$

$$q_s = \bar{Z}/\tau_w$$

$$q_s = 25 \text{ ft.} \frac{0.3048 \text{ m}}{\text{ft}}/0.4 \text{ yr} = 19.05 \text{ m/yr}$$

Next, calculate the weighted mean inflow phosphorus and nitrogen concentrations $\bar{P}$ and $\bar{N}$ as follows:

$$\bar{P} \text{ (or } \bar{N}) = \left(\sum_{i=1}^{y} \sum_{j=1}^{n_i} Q_{i,j} \times C_{i,j}\right)/\left(\sum_{i=1}^{y} \sum_{j=1}^{n_i} Q_{i,j}\right)$$

$$\bar{P} = 43.86/1050 = 0.042 \text{ mg/l}$$

$$\bar{N} = 2671.902/1050 = 2.54 \text{ mg/l}$$

The N:P ratio in the inflows is 60. Therefore if one of the two is growth limiting, it is probably phosphorus. Compute the phosphorus loading, Lp.

$$L_p = \frac{28.31\ell}{ft^3} \times \frac{1 \text{ g}}{1000 \text{mg}} \times \frac{0.042 \text{ mg}}{\ell} \times \frac{1}{2.59 \times 10^6 m^2} \times \frac{1.75 \times 10^9 ft^3}{\text{yr}}$$

$$Lp = 0.80 \text{ g/m}^2 \text{ yr}$$

Now, referring to the plot in Figure V-24 with Lp = 0.80 g/m^2 yr and q_s = 19 m/yr, the impoundment is well into the mesotrophic region.

---------- END OF EXAMPLE V-12 ----------

5.4.5 Predicting Algal Productivity, Secchi Depth, and Biomass

The prediction of eutrophication effects is based primarily on prediction of chlorophyll *a* concentrations from phosphorus concentrations rather than on general impoundment trophic status. The method has been advanced by several researchers including Sakamoto (1966), Lund (1971), Dillon (1974), and Dillon and Rigler (1975). Originally, the method related mean summer chlorophyll *a* concentrations to spring mean total phosphorus. As shown in Figure V-25, the relationship is highly correlated, and a regression of the log of summer mean chlorophyll *a* on the log of spring mean phosphorus is linear (units are μg/l). Using a least squares method gives the equation of the line as (Lorenzen, 1978):

$$\log (\text{chl } a) = 1.5 \log (P) - 1.1$$

or

$$\text{chl } a = 0.08(P)^{1.5} \text{ for } P \leq 250 \text{ mg/m}^3 = 0.25 \text{ ppm}$$

More recently (Vollenweider and Kerekes, 1981), additional data have been compiled and equations have been derived for predicting annual average chlorophyll *a* from annual average total phosphorus ($r = 0.88$, $n=78$):

$$\text{chl } a = 0.27(P)^{0.99} \qquad \text{(V-15)}$$

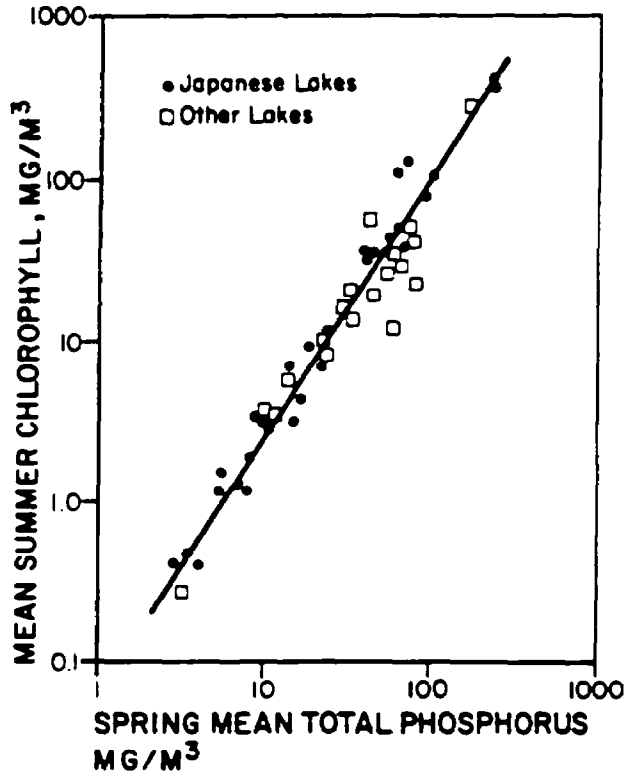

FIGURE V-25 RELATIONSHIP BETWEEN SUMMER CHLOROPHYLL AND SPRING PHOSPHORUS (FROM LORENZEN, UNPUBLISHED)

Perhaps more important from a water quality point of view, peak chlorophyll *a* can be computed from annual average total phosphorus ($r = 0.89$, $n=51$):

$$\text{peak chl } a = 0.58(P)^{1.07} \qquad \text{(V-16)}$$

The peak is approximately 2-3 times as much as the average chlorophyll *a*. If the relationships are computed from phosphorus loading equations, the equations change:

$$\text{chl } a = 0.37(P_L)^{0.79}$$

and

$$\text{peak chl } a = 0.74(P_L)^{0.8}$$

One of the major diagnostic tools in analysis of eutrophication is measurement of water transparency. Algal blooms decrease light penetration by light absorption and scattering that can be approximated by the Beer-Lambert law.

A simple method of estimating light penetration in the vertical direction is with a Secchi disk, where the disappearance depth is defined as the Secchi depth (SD) (Hutchinson, 1957):

$$\ln(I_{SD}/I_o) = -k * SD$$

where

I_o = initial light intensity, light units
I_{SD} = intensity at Secchi depth, light units
SD = Secchi depth, m
k = extinction coefficient, 1/m.

Algal blooms reduce transparency. Algal blooms are measured using the average summertime (July-August) chlorophyll *a* concentration (CA, μg/l) in the mixed layer epilimnion) since non-plant materials do not contain chlorophyll. Lorenzen (1973, 1980) showed that the extinction coefficient (k) could be considered in two parts; that is, light attenuation would be the result of absorption and scattering by algal cells and by the water and non-algal materials in the water column:

$$k = a + b * CA$$

Hutchinson (1957) and others have shown that the Secchi depth occurs over a relatively narrow range of light intensity ratios (I/I_o). If it is assumed that this ratio is a constant ($\ln(I/I_o) = R$), we can substitute ($A = a/R$; $B = b/R$), and solve for Secchi depth as a function of chlorophyll *a*:

$$1/SD = A + B * CA$$

In the equation, A represents non-algal attenuation while B*CA represents attenuation by chlorophyll *a*. Larsen and Malueg (1981) used data from several lakes to compute this relationship. Similarly, data from 226 lakes were used to obtain the following equation:

$$1/SD = 0.02\ CA + 0.6$$

However, B is considered a constant (B = 0.02, Megard *et al.*, 1980), while A will vary with the background light attenuation in the water due to dissolved and particulate matter (Lorenzen, 1980). It should be noted that as the particulate matter increases, the relationship will be less likely to hold.

Figure V-26 shows a plot of maximal primary production in terms of milligrams carbon incorporated in algae per square meter per day as a function of phosphate phosphorus levels. As was the case with predicting chlorophyll *a* concentrations, the relationship appears to be reasonably robust and therefore useful.

Because dried algae contain very roughly 3 percent chlorophyll *a* (J.A. Elder, pers. comm., 1977), dry algal biomass may be estimated from chlorophyll *a* concentration by multiplying by thirty-three. Similarly, carbon productivity, as in the plot in Figure V-26, may be converted to total algal biomass. Since approximate analysis of dried algae has been determined as (Stumm and Morgan, 1970):

$$C_{106}H_{263}O_{110}N_{16}P_1$$

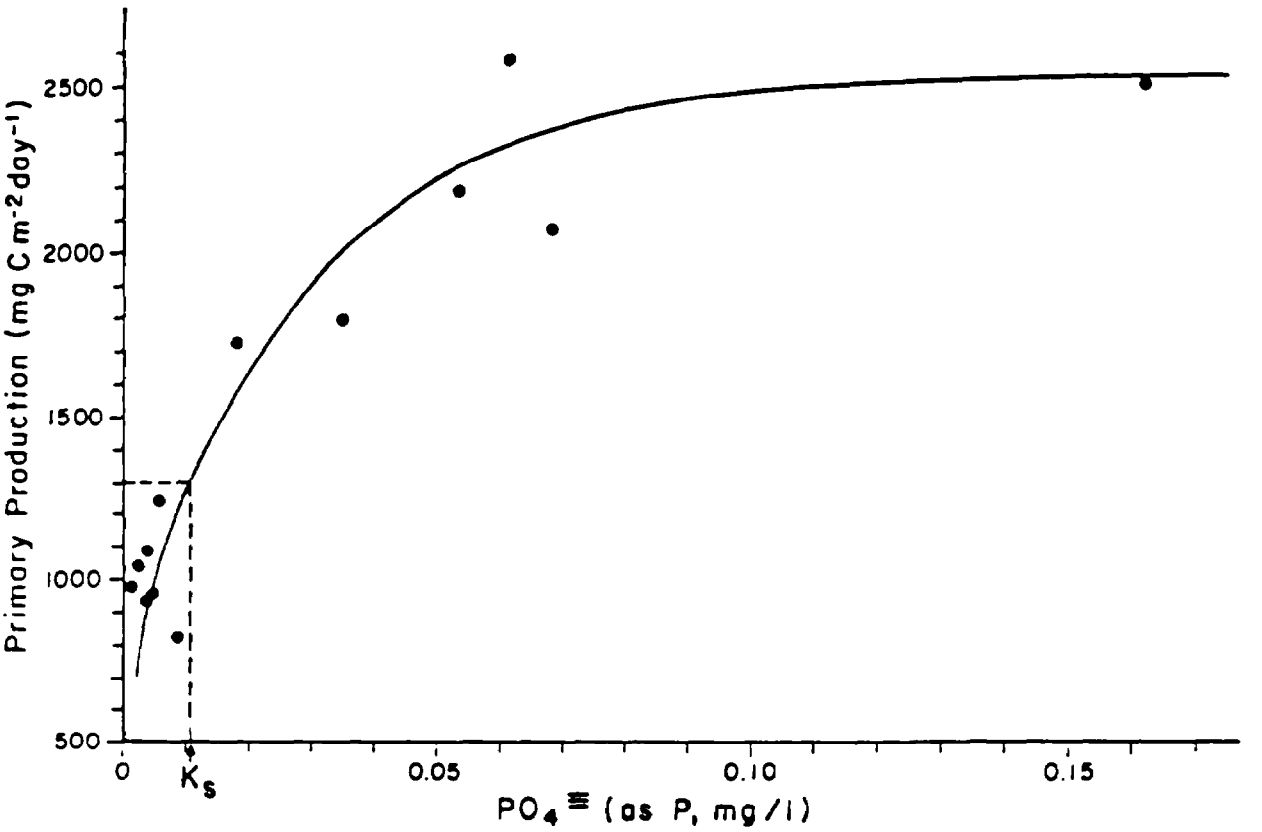

FIGURE V-26 MAXIMAL PRIMARY PRODUCTIVITY AS A FUNCTION OF PHOSPHATE CONCENTRATION (AFTER CHIAUDANI, ET AL., 1974)

the gravimetric factor is $\frac{3550}{1271} \simeq 2.8$. Thus, maximal carbon productivity may be multiplied by 2.8 to give a rough estimate of maximal algal biomass productivity.

The user should bear in mind that applying this technique can only lead to rough estimates. If it is desired to predict biomass or productivity with accuracy, more sophisticated approaches may be necessary.

EXAMPLE V-13

Phosphorus and Summer Chlorophyll a

Lake Sara mean annual total phosphorus concentration, P = .03 mg/l = 30 mg/m^3

$$\text{chl } a = 0.27(P)^{0.99}$$

$$\text{chl } a = 7.8 \text{ mg/m}^3$$

$$\text{algal dry biomass} \cong 7.8 \times 33 = 258 \text{ mg/m}^3$$

Peak chlorophyll a would be 22 mg/m^3. If calculated from loading rates, the

numbers would differ. Secchi depth would be approximately 1.3 meters assuming that the average background light extinction was 0.6.

END OF EXAMPLE V-13

In the absence of measured data, the in-lake concentration (P) can be computed based on the various point and nonpoint loadings (n):

$$Lp = \sum_{i=1}^{n} Q_i PI_i$$

$$P = \left(\frac{PI}{1 + \sqrt{D}} \right)$$

Then chlorophyll a can be estimated as shown in the previous paragraphs.

5.4.6 Restoration Measures

Control of eutrophication in lakes can be evaluated by a variety of approaches (Table V-10). Some methods are directed at external sources (PI) and others at recycling from in-lake sources (K). Changes in volume (V) and inflow (Q) obviously will affect predicted results. For example, on a long term basis dredging will decrease the return of phosphorus for the sediments (i.e. increase K) and increase the volume (and therefore decrease the dilution rate, D). If the input concentration (PI) is the critical variable, then source controls should be investigated. If internal sources are involved, then in-lake controls should be evaluated. In many lakes, both source and in-lake controls will be needed.

Problem treatment is directed at the productivity directly. These controls are often the only alternative for many lake situations. These methods are evaluated only in a qualitative way. Indexes for evaluating lake restoration have been developed (Carlson, 1977; Porcella et al., 1980). These are useful for prioritizing lake restoration projects and for evaluating progress.

5.4.7 Water Column Phosphorus Concentrations

The relationships described in 5.4.5 for predicting algal biomass are predicated on phosphorus levels within the impoundment. A more precise mechanism for estimating phosphorus lake concentrations based on interactions between bottom sediments and overlying water has been developed.

Lorenzen, et al. (1976) developed a phosphorus budget model (Figure V-27) which may be used to estimate water column and sediment bound phosphorus in a fully mixed system. A mass balance on both sediment and water column phosphorus concentrations

TABLE V-10

CLASSIFICATION OF LAKE RESTORATION TECHNIQUES

I. Source Controls
   - A. Treatment of inflows
   - B. Diversion of inflows
   - C. Watershed management (land uses, practices, nonpoint source control, regulations and/or treatments).
   - D. Lake riparian regulation or modification
   - E. Product modification or regulation

II. In-Lake Controls
   - A. Dredging
   - B. Volume changes other than by dredging or compaction of sediments
   - C. Nutrient inactivation
   - D. Dilution/Flushing
   - E. Flow adjustment
   - F. Sediment exposure and dessication
   - G. Lake bottom sealing
   - H. In-lake sediment leaching
   - I. Shoreline modification
   - J. Riparian treatment of lake water
   - K. Selective discharge

III. Problem Treatment (directed at biological consequences of lake condition)
   - A. Physical techniques (harvesting, water level fluctutations, habitat manipulations)
   - B. Chemical (algicides, herbicides, pesticides)
   - C. Biological (predator-prey manipulations, pathological reactions).
   - D. Mixing (aeration, mechanical pumps, lake bottom modification)
   - E. Aeration (add DO; e.g. hypolimnetic aeration)

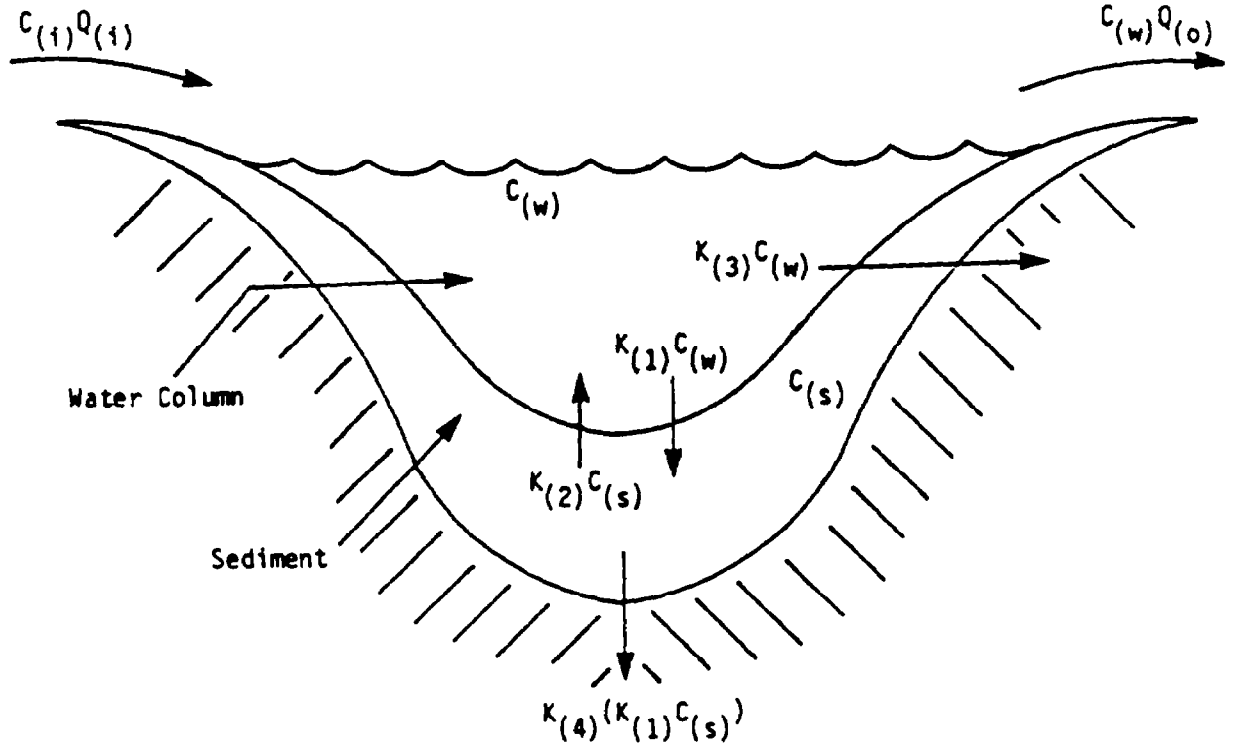

FIGURE V-27 CONCEPTUALIZATION OF PHOSPHORUS BUDGET MODELING (LORENZEN ET AL., 1976)

yields the coupled differential equations:

$$\frac{dC_w}{dt} = \frac{M}{V} + \frac{K_2AC_s}{V} - \frac{K_1AC_w}{V} - \frac{C_wQ}{V} \qquad (V\text{-}17)$$

$$\frac{dC_s}{dt} = \frac{K_1AC_w}{V_s} - \frac{K_2AC_s}{V_s} - \frac{K_1K_3AC_w}{V_s} \qquad (V\text{-}18)$$

C_w = average annual total phosphorus concentration in water column (g/m^3)
C_s = total exchangeable phosphorus concentration in the sediments (g/m^3)
M = total annual phosphorus loading (g/yr)
V = lake volume (m^3)
V_s = sediment volume (m^3)
A = lake surface area (m^2) - sediment area (m^2)
Q = annual outflow (m^3/yr)
K_1 = specific rate of phosphorus transfer to the sediments (m/yr)
K_2 = specific rate of phosphorus transfer from the sediments (m/yr)
K_3 = fraction of total phosphorus input to sediment that is unavailable for the exchange process

When the differential equations relating water column phosphorus to the various controlling phenomena are solved analytically, the following equation results for steady-state water column phosphorus concentration:

$$C_w = \frac{C_{in}}{1 + \frac{K_1 K_3 A}{Q}} \qquad (V\text{-}19)$$

or

$$C_w = \frac{M}{Q + K_1 K_3 A} \qquad (V\text{-}20)$$

where

C_w = steady-state water column phosphorus concentration in ppm

C_{in} = steady-state influent phosphorus concentration in ppm

The steady-state sediment phosphorus concentration is then given by:

$$C_s = \frac{C_{in} K_1 (1 - K_3)}{K_2 (1 + (K_1 K_3 A/Q))} \qquad (V\text{-}21)$$

It is important to observe that these relationships are valid only for steady-state conditions. Where phosphorus loading is changing with time, where sediment deposition or physical characteristics are changing, or where there are long-term changes in physical conditions, the steady-state solutions are not applicable.

Lorenzen applied the model to Lake Washington data and obtained very good results. With their data set, the most satisfactory coefficients had the following values:

K_1 = 43 m/yr

K_2 = 0.0014 m/yr

K_3 = 0.5

It should be recognized, however, that this model is relatively untested and that coefficient values for other impoundments will vary from those cited here.

EXAMPLE V-14

A Comprehensive Example

Impoundment Water Column Phosphorus

What will be the steady-state concentration of phosphorus in the water column of Lake Jones following diversion of flow? How will this affect algal abundance?

Lake Jones:

Area, A. $20 \text{ miles}^2 = 5.6 \times 10^8 \text{ft}^2 = 5.2 \times 10^7 \text{m}^2$

Volume, V. $3.08 \times 10^{11} \text{ft}^3 = 8.73 \times 10^9 \text{m}^3$

Available Data (prior to diversion):

Inflows:

		Mean Annual Flow, cfs	Mean P, mg/l
1.	Janes River	75	.15
2.	Jennies River	22	.07
3.	Johns Creek	5	.21
4.	Direct stormwater influx (nominal, may be disregarded)		

The diversion, which is for irrigation purposes, has decreased the mean annual inflow from Jennies River to 1 cfs with an average annual phosphorus concentration of 0.01 mg/l. Additionally, there is a reduction of flow in Janes River to 55 cfs. but the mean P concentration stays the same.

To apply the Vollenweider relationship, first to the prediversion status of Lake Jones, compute q_s:

$$q_s = \frac{\bar{z}}{\tau_w}$$

$$\bar{z} = \frac{8.73 \times 10^9 \text{m}^3}{5.2 \times 10^7 \text{m}^2} = 168 \text{ m}$$

Based upon the conceptualization (see Figure V-27), it is reasonable that the coefficients interact. For example, K_1, the rate of phosphorus uptake by the sediment must be related to the rate of phosphorus release by the sediment. The model requires however, that the product K_1K_3 be constant. The value used by Lorenzen, et al. was 21.6. As they point out, the coefficients must satisfy certain conditions, specifically those established by the derived equations. The equations are:

$$C_w = \frac{M}{Q + K_1K_3A} \qquad \text{(V-22)}$$

and

$$\frac{C_w}{C_s} = \frac{K_2}{K_1(1-K_3)} \qquad \text{(V-23)}$$

From (V-22)

$$K_1K_3 = \frac{M - QC_w}{C_wA} \qquad \text{(V-24)}$$

Computation of K_1, therefore, requires a value for K_3. This coefficient, (K_3) unfortunately, is usually unavailable. It represents the fraction of phosphorus entering the sediment which is not returned to the water column. Processes contributing to this phenomenon are burial caused by steady-state sediment accumulation, and steady-state chemical precipitation of phosphorus, such as with iron to form $Fe_3(PO_4)\cdot 8H_2O$ (vivianite). Lorenzen's value for Lake Washington was 50 percent. Because the fraction is likely to vary significantly from system to system and because the coefficient is difficult to evaluate, the planner is advised to use 30 percent as the lower limit, 50 percent as a probable value, and 70 percent as an upper limit for estimating sediment phosphorus content. The water column concentration is independent of changes in K_3 because the product of K_1 and K_3 is a constant.

Using Equation (V-24), K_3 uniquely defines K_1. Then, from Equation (V-23):

$$K_2 = \frac{C_w K_1 (1-K_3)}{C_s}$$

K_2 is therefore also defined by fixing K_3, providing C_w and C_s are known.

$$M = \left[\left(\frac{75 ft^3}{Sec} \times \frac{0.15 mg}{\ell}\right) + \left(\frac{22 ft^3}{Sec} \times \frac{.07 mg}{\ell}\right) + \left(\frac{5 ft^3}{Sec} \times \frac{.21 mg}{\ell}\right)\right] \times \frac{28.31 \ell}{ft} \times \frac{1 g}{1000 mg} \times \frac{3.16 \times 10^7 sec}{yr}$$

$$M = 1.24 \times 10^7 \ gP/yr$$

$$Q = \frac{(75+22+5) ft^3}{sec} \times \frac{3.16 \times 10^7 sec}{yr} = \frac{3.22 \times 10^9 ft^3}{yr} = \frac{9.13 \times 10^7 m^3}{yr}$$

$$\tau_w = 8.73 \times 10^9 m^3 / 9.13 \times 10^7 m^3 yr^{-1} = 95.6 \ yr$$

$$q_s = 168/95.6 = 1.76 \ m \ yr^{-1}$$

Compute phosphorus loading:

$$Lp = \frac{M}{A}$$

$$Lp = \frac{1.24 \times 10^7 \ g \ yr^{-1}}{5.2 \times 10^7 \ m^2} = 0.24 \ gm^{-2} yr^{-1}$$

Referring to Figure V-24 with $q_s = 1.76$ and Lp = 0.24, one can see that this lake may have eutrophication problems under pre-diversion conditions.

After the diversion,

$$\tau_w = \frac{8.73 \times 10^9 m^3}{6.98 \times 10^7 m^3/yr} = 125 \text{ yr}$$

Assuming the lake depth is not materially changed over the short term,

$$q_s = 168/125 = 1.34 \frac{m}{yr}$$

For the new conditions,

$$M = 8.33 \times 10^6 \text{ gP yr}^{-1}$$

$$Lp = \frac{8.33 \times 106 \text{ g yr-1}}{5.2 \times 10^7 m^2} = .16 \text{ gP/m}^2\text{yr}$$

Now, according to the Vollenweider plot (Figure V-24), this is in the region between "dangerous" and "permissible" - the mesotrophic region. Under the new circumstances, algal blooms are less likely than before the flow diversions were established, but blooms are by no means to be ruled out.

Turning now to an estimate of algal biomass under pre-diversion conditions, we must calculate the inlake concentration (P).

$$\text{First,} \quad D = 1/\tau w = 1/125 = 0.008; \quad K = \sqrt{D} = 0.09$$

Since our data are already in the loading form:

$$P = \frac{PL}{Z} \frac{1}{D+K}$$

$$= \frac{0.24}{168} \frac{1}{0.008+0.09} = 15 \text{ mg/m}^3$$

Based on annual average chlorophyll *a*,

$$\text{chl } a = 0.37(P)^{0.79}$$

$$\text{chl } a = 3.1 \text{ mg/m}^3$$

Under post-diversion conditions,

$$P = \frac{0.16}{168} \frac{1}{0.008+0.09} = 10 \text{ mg/m}^3$$

$$\text{chl } a = 2.3 \text{ mg/m}^3$$

Note that these low levels of chlorophyll *a* almost certainly mean that the lake is oligotrophic to mesotrophic, and that the Vollenweider method suggests worse conditions than may actually exist in this case (Table V-9).

Consequently, one might choose to use the Lorenzen model to evaluate K_1 and K_3 and determine whether the impoundment is at steady state with respect to phosphorus levels in the water column and sediment. Generally, this is the case where K_1K_3 lies in the range of 20 to 40. If K_1K_3 is outside of

this range, field data should be obtained for current water column phosphorus.

Sediment volume, V_s	Irrelevant for steady-state solution
Phosphorus (water column)	.15 mg/l

$$K_3 = 0.5$$

$$K_1 = \frac{M - QC_w}{K_3 C_w A}$$

$$C_w = 0.15 \text{ mg/l} = .015 \text{ g/m}^3$$

$$K_1 = \left(\frac{1.24 \times 10^7 \text{ gP}}{\text{yr}} - \frac{9.13 \times 10^7 \text{ m}^3}{\text{yr}} \times \frac{.015 \text{g}}{\text{m}^3}\right) \Big/ \left(.5 \times \frac{.015 \text{g}}{\text{m}^3} \times 5.2 \times 10^7 \text{ m}^2\right) = 28.3 \frac{\text{m}}{\text{yr}}$$

$$K_1 K_3 = 44 \times 0.5 = 14$$

This result, therefore, gives reason to suspect non steady-state conditions for water column phosphorus. If more definitive answers are needed, additional field data should be collected.

END OF EXAMPLE V-14

5.5 IMPOUNDMENT DISSOLVED OXYGEN

Organic substances introduced into an impoundment with inflowing water, falling onto its surface, or generated in the water column itself through photosynthesis, may be oxidized by indigenous biota. The process consumes oxygen which may, in turn, be replenished through surface reaeration, photosynthetic activity, or dissolved oxygen in inflowing water. The dynamic balance between DO consumption and replenishment determines the net DO concentration at any point in time and at any location within the water column.

These processes result in characteristic dissolved oxygen (DO) concentrations in the water columns of stratified lakes and reservoirs (Figure V-28). During stratification, typically during summer months, the DO is highest on the surface due to photosynthesis and reaeration. It decreases through the thermocline and then, in the hypolimnion, the DO decreases to zero in those lakes that have high organic matter concentrations.

During spring, after turnover, when lakes are not stratified, the DO is essentially uniform. However, in highly organic lakes benthic processes can already begin to deplete oxygen from lower depths, as shown in Figure V-28.

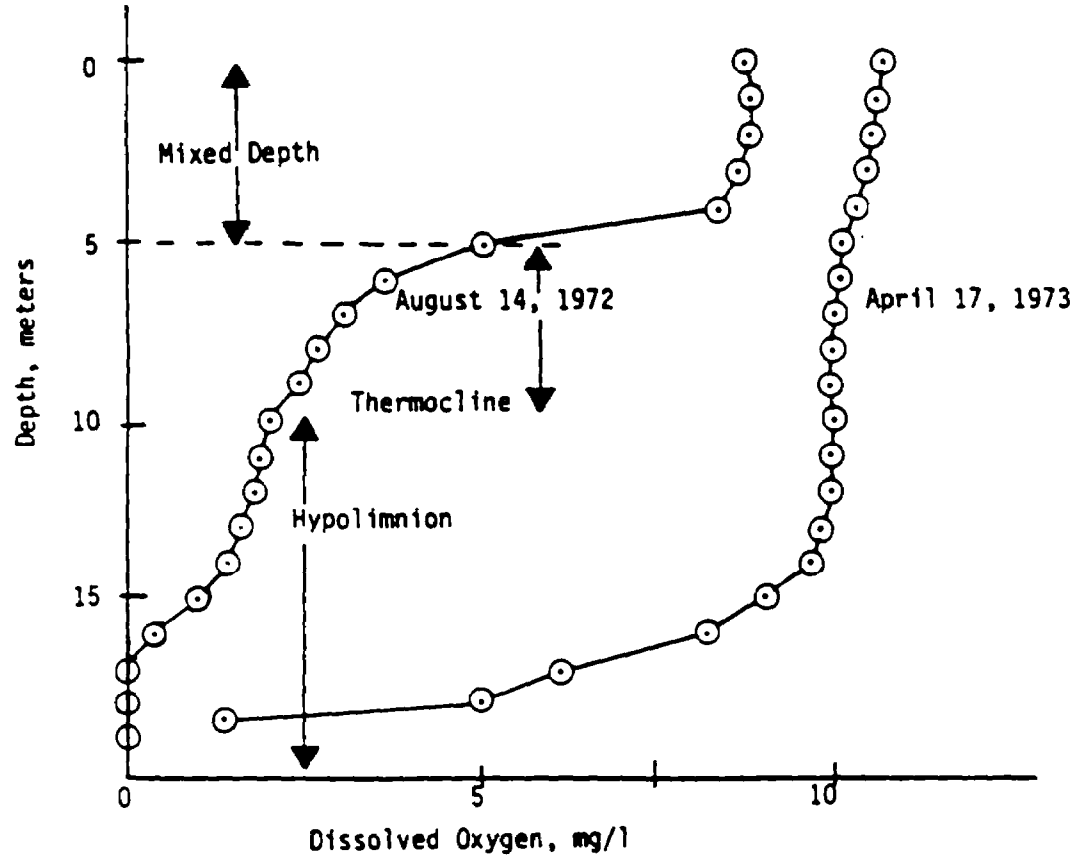

FIGURE V-28 TYPICAL PATTERNS OF DISSOLVED OXYGEN (DO) IN HYRUM RESERVOIR (DRURY, ET AL., 1975)

Essentially, the patterns result from processes that are restricted due to incomplete mixing. The overall effects of such patterns as shown in Figure V-28, are to restrict fishery habitat and create water quality problems for downstream users, especially for deep water discharge.

BOD exertion is not the only sink for DO. Some important sources and sinks of impoundment dissolved oxygen are listed below:

Sources	Sinks
Photosynthesis	Water Column BOD
Atmospheric reaeration	Benthic BOD
Inflowing water	Chemical oxidation
Rainwater	Deoxygenation at surface
	Plant and animal respiration

Many of the processes listed above have a complex nature. For example, the atmospheric reaeration rate is dependent in part upon the near-surface velocity gradient over depth. The gradient, in turn, is influenced by the magnitude, direc-

tion, and duration of wind, as well as the depth and geometry of the impoundment.

Photosynthetic rates are affected by climatological conditions, types of cells photosynthesizing, temperature, and a number of biochemical and biological factors. Exertion of BOD is dependent upon the kind of substrate, temperature, dissolved oxygen concentration, presence of toxicants, and dosing rate.

Despite this degree of complexity, a number of excellent models of varying degrees of sophistication have been developed which include simulation of impoundment dissolved oxygen.

5.5.1 Simulating Impoundment Dissolved Oxygen

Because an unstratified impoundment generally may be considered as a slow-moving stream reach, only stratified impoundments are of interest here. For estimating DO in unstratified impoundments, one should refer to the methods described in Chapter 4.

To understand the phenomena affecting dissolved oxygen in a stratified impoundment and to gain an appreciation of both the utility and limitations of the approach presented later, it is useful to briefly examine a typical dissolved oxygen model. Figure V-29 shows a geometric representation of a stratified impoundment. As indicated in the diagram, the model segments the impoundment into horizontal layers. Each horizontal layer is considered fully mixed at any point in time, and the model advects and diffuses mass vertically into and out of each layer. The constituents and interrelationships modeled are shown schematically in Figure V-30.

The phenomena usually taken into account in an impoundment DO model include:

- Vertical advection
- Vertical diffusion
- Correction for element volume change
- Surface replenishment (reaeration)
- BOD exertion utilizing oxygen
- Oxidation of ammonia
- Oxidation of nitrite
- Oxidation of detritus
- Zooplankton respiration
- Algal growth (photosynthesis) and respiration
- DO contribution from inflowing water
- DO removal due to withdrawals.

Many of the processes are complex and calculations in detailed models involve simultaneous solution of many cumbersome equations. Among the processes simulated are zooplankton-phytoplankton interactions, the nitrogen cycle, and advection-diffusion. Thus it is clear that a model which is comprehensive and potentially capable of simulating DO in impoundments with good accuracy is not appropriate for hand calculations. A large amount of data (coefficients, concentrations) are needed

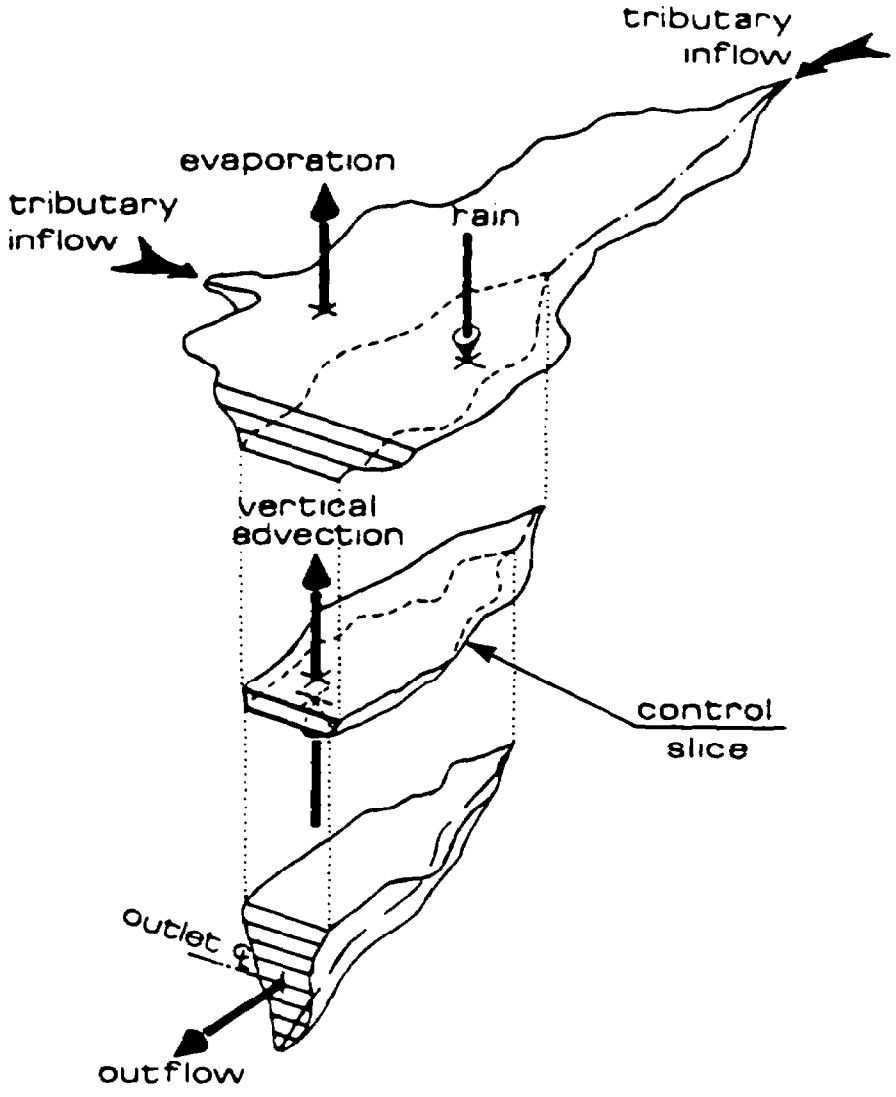

FIGURE V-29 GEOMETRIC REPRESENTATION OF A STRATIFIED IMPOUNDMENT (FROM HEC, 1974)

to apply such a model, and solution is most easily done by computer. Furthermore, some of the terms in the model equation of state do not improve prediction under some circumstances. This is true, for example, where there are no withdrawals or in an oligotrophic impoundment where chlorophyll a concentrations are very low.

Hand calculations must be based upon a greatly simplified model to be practical. Since some DO-determining phenomena are more important than others, it is feasible to develop such a model if some assumptions are made about the impoundment itself.

5.5.2 A Simplified Impoundment Dissolved Oxygen Model

For purposes of developing a model for hand calculations, the following assump-

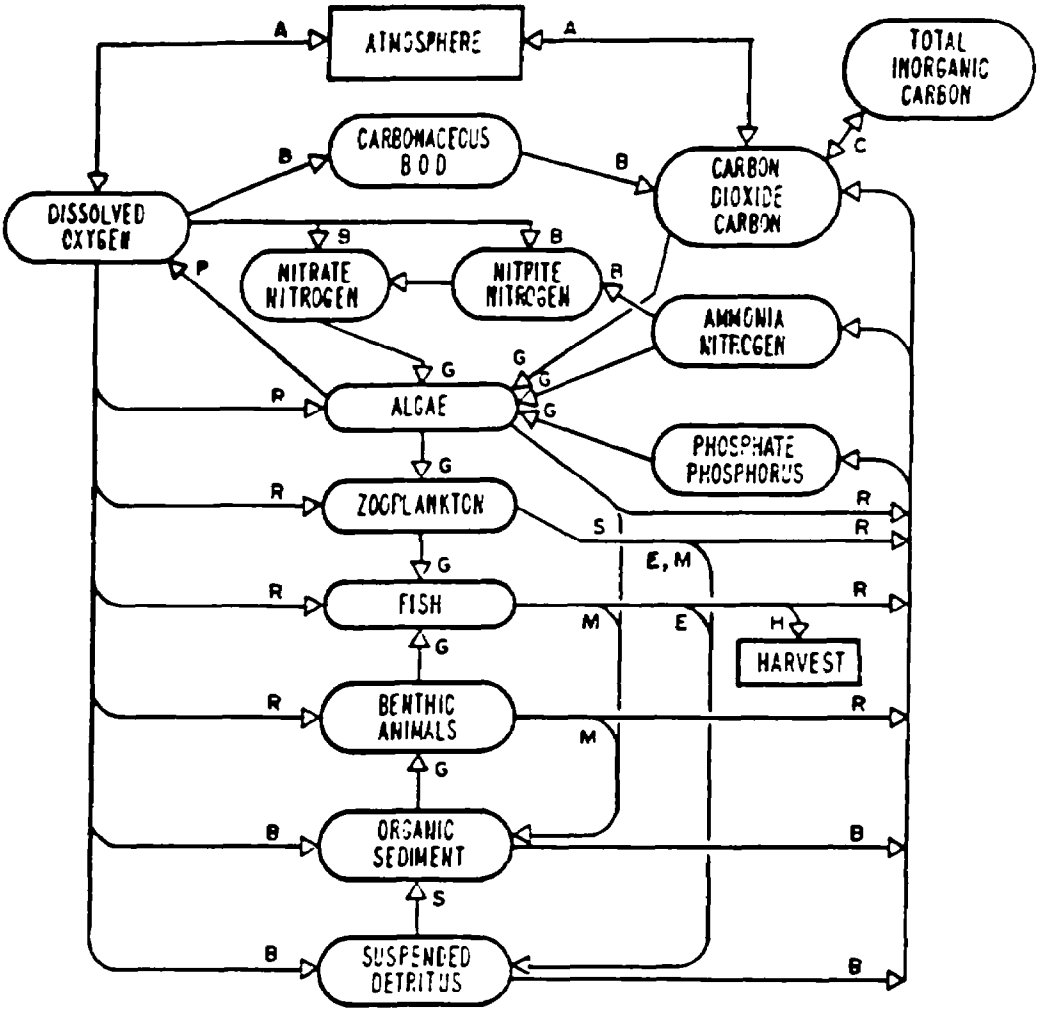

FIGURE V-30 QUALITY AND ECOLOGIC RELATIONSHIPS (FROM HEC, 1974)

tions are made:

- The only condition where DO levels may become dangerously low is in an impoundment hypolimnion and during warm weather.
- Prior to stratification, the impoundment is mixed. After strata form, the epilimnion and hypolimnion are each fully mixed.
- Dissolved oxygen in the hypolimnion is depleted essentially through BOD exertion. Significant BOD sources and sinks to the water column prior to stratification are algal mortality, BOD settling, and outflows. A

minor source is influent BOD. Following formation of strata, sources and sinks of BOD are BOD settling out onto the bottom, water column BOD at the time of stratification, and benthic BOD.

- Photosynthesis is unimportant in the hypolimnion as a source of DO.
- Once stratification occurs (a thermocline gradient of 1°C or greater per meter of depth) no mixing of thermocline and hypolimnion waters occurs.
- BOD loading to the unstratified impoundment and to the hypolimnion are in steady-state for the computation period.

5.5.2.1 Estimating a Steady-State BOD Load to the Impoundment

Equation V-25 is an expression to describe the rate of change of BOD concentration as a function of time:

$$\frac{dC}{dt} = k_a - k_s C - k_l C - \frac{QC}{V} \qquad \text{(V-25)}$$

where

C = the concentration of BOD in the water column in mgl^{-1}

k_a = the mean rate of BOD loading from all sources in mgl^{-1} day^{-1}

k_s = the mean rate of BOD settling out onto the impoundment bottom in day^{-1}

k_l = the mean rate of decay of water colunm BOD in day^{-1}

Q = mean export flow rate in liters day^{-1}

V = impoundment volume in liters.

Integrating Equation V-25 gives:

$$C_t = \frac{(k_a + k_b C_o)e^{(k_b t)} - k_a}{k_b} \qquad \text{(V-26)}$$

where

C_t = concentration of BOD at time t

C_o = initial concentration of BOD

$k_b = -k_s - k_l - \frac{Q}{V}$

To estimate the steady-state loading of BOD, we set dc/dt = 0 and obtain:

$$C_{ss} = -\frac{k_a}{k_b} \qquad \text{(V-27)}$$

where

C_{ss} = steady-state water column BOD.

Thus Equation V-27 may be used to estimate a steady-state water column BOD concentration and Equation V-26 may be used to compute BOD as a function of time, initial concentration of BOD, and the various rates.

5.5.2.2 Rates of Carbonaceous and Nitrogenous Demands

The rate of exertion of BOD and therefore the value of k_1 is dependent upon a number of physical, chemical, and biological factors. Among these are temperature, numbers and kinds of microorganisms, dissolved oxygen concentration, and the kind of organic substance involved. Nearly all of the biochemical oxygen demand in impoundments is related to decaying plant and animal matter. All such material consists essentially of carbohydrates, fats, and proteins along with a vast number of minor constituents. Some of these are rapidly utilized by bacteria, for example, the simple sugars, while some, such as the celluloses, are metabolized slowly.

Much of the decaying matter in impoundments is carbonaceous. Carbohydrates (celluloses, sugars, starches) and fats are essentially devoid of nitrogen. Proteins, on the other hand, are high in nitrogen (weight of carbon/ weight of nitrogen $\simeq$ 6) and proteins therefore represent both carbonaceous and nitrogenous demands.

The rate of exertion of carbonaceous and nitrogenous demands differ. Figure V-31, which shows the difference graphically and as a function of time and temperature, may be considered to represent the system response to a slug dose of mixed carbonaceous and nitrogenous demands. In each two-section curve, especially where concentrated carbonaceous wastes are present, the carbonaceous demand is exerted first, and this represents the first stage of deoxygenation. Then nitrifiers increase in numbers and ammonia is oxidized through nitrite and ultimately to nitrate. This later phase is called the second phase of deoxygenation.

BOD decay (either nitrogenous or carbonaceous alone) may be represented by first order kinetics. That is, the rate of oxidation is directly proportional to the amount of material remaining at time t:

$$\frac{dC}{dt} = -kC \qquad (V-28)$$

The rate constant, k, is a function of temperature, bacterial types and numbers, composition and structure of the substrate, presence of nutrients and toxicants, and a number of other factors. The value of the first stage constant k_1 was first determined by Phelps in 1909 for sewage filter samples. The value was 0.1 (Camp, 1968). More recent data show that at 20°C, the value can range from 0.01 for slowly metabolized industrial waste organics to 0.3 for relatively fresh sewage (Camp, 1968).

The typical effect of temperature on organic reactions is to double reaction rates for each temperature rise of 15°C. The relationship for correcting k_1 for temperature is:

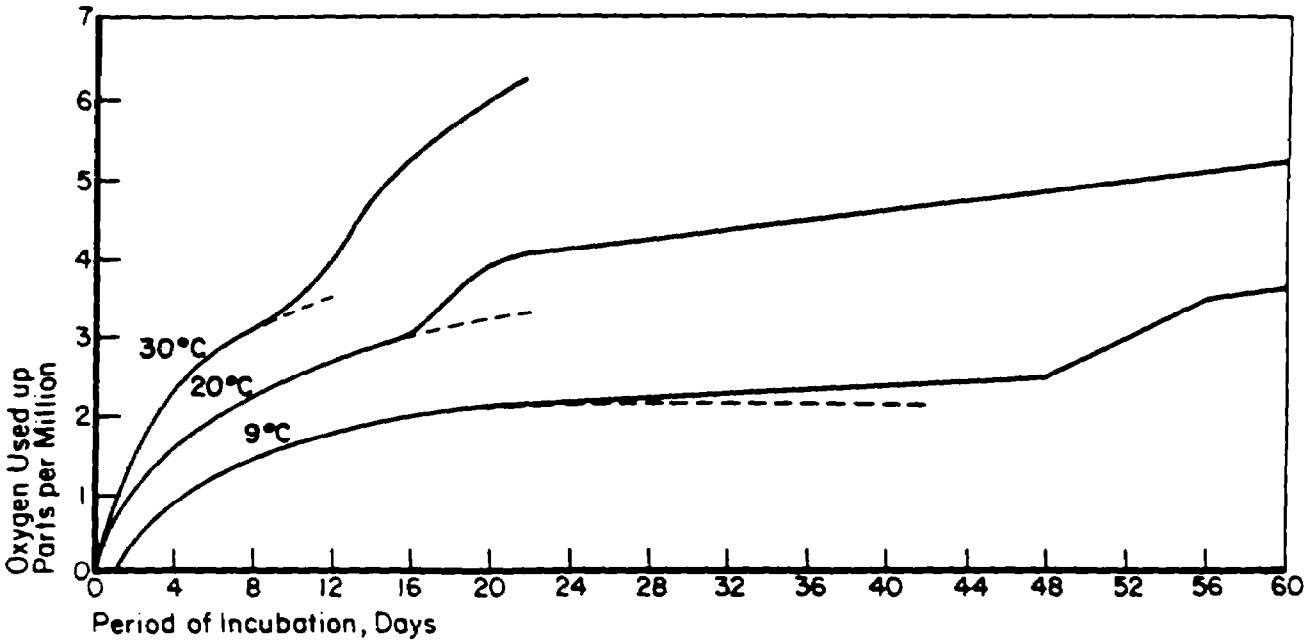

FIGURE V-31 RATE OF BOD EXERTION AT DIFFERENT TEMPERATURES SHOWING THE FIRST AND SECOND DEOXYGENATION STAGES

$$k_{1,(T)} = k_{1,(20°C)}\ \theta^{(T-20)} \qquad \text{(V-29)}$$

where

T = the temperature of reaction

θ = correction constant = 1.047.

However, Thereault has used a value for θ of 1.02, while Moore calculated values of 1.045 and 1.065 for two sewages and 1.025 for river water (Camp, 1968).

Streeter has determined the rate of the nitrification or second deoxygenation stage in polluted streams. At 20°C, k_1 for nitrification is about 0.03 (Camp, 1968). Mobre found the value to be .06 at 20°C and .035 at 10°C (Camp, 1968). For purposes of this analysis, BOD exertion will be characterized as simple first order decay using a single rate constant.

Benthic demand, which is important in later computations, may vary over a wide range because in addition to the variability due to the chemical nature of the benthic matter, rates of oxidation are limited by upward diffusion rates of oxidizable substances through pores in the benthos. Since the nature of the sediment is highly variable, benthic oxygen demand rates vary more than values for k_1 in the water column. In a study using sludges through which oxygenated water was passed, initial rates of demand ranged from 1.02 g/m^2 day (see Table V-11) for a sludge depth of 1.42 cm up to 4.6g g/m^2 day for a sludge depth of 10.2 cm (Camp, 1968).

TABLE V-11

OXYGEN DEMAND OF BOTTOM DEPOSITS
(AFTER CAMP, 1968)

Benthic Depth (mean) cm	Initial Volume of Solids, kom^{-2}	Initial Area Demand L (gm^{-2})	Initial Demand $om^{-2}day^{-1}$	day^{-1} $k_{4(20^oC)}$
10.2	3.77	739	4.65	.0027
4.75	1.38	426	3.09	.0031
2.55	0.513	227	1.70	.0032
1.42	0.188	142	1.08	.0033
1.42	0.188	134	1.02	.0033

In that study, the values found were for initial demand since the sludge was not replenished. The rate per centimeter of sludge depth, then, can vary from a low of 0.46 g/m^2 day for 10.2 centimeter depth sludge up to 0.76 g/m^2 day for 1.42 centimeter depth sludge.

The constant loading rate (k_a) used in Equation V-25 is best estimated from historical data. Alternatively, inflow loading (see Chapter IV) and algal productivity estimates (this chapter) may be used. In the latter case, a value must be adopted for the proportion of algal biomass ultimately exerted as BOD. To a first approximation, k_a may be estimated using this value and adopting some percentage of maximal primary productivity (see Figure V-25). Thus:

$$k_a(algae) = SMP \times 10^{-3}/D \qquad (V\text{-}30)$$

where

$k_{a(algae)}$ = algal contribution to BOD loading rate

S = stoichiometric conversion from algal biomass as carbon to BOD = 2.67

M = proportion of algal biomass expressed as an oxygen demand (unitless)

P = Primary production in $mgCm^{-2}day^{-1}$.

The difference between algal biomass and the parameter M representing the proportion of algal biomass exerted as BOD may be conceptualized as accounting for such phenomena as incorporation of algal biomass into fish tissue which either leaves the impoundment or is harvested, loss of carbon to the atmosphere as CH_4, and loss

due to outflows.

The settling rate coefficient, k_s in Equation V-25 must be estimated for the individual case. It represents the rate at which dead plant and animal matter (detritus) settles out of the water column prior to oxidation. Clearly, this coefficient is sensitive to the composition and physical characteristics of suspended matter and the turbulence of the system. Quiescence and large particle sizes in the organic fraction will tend to give high values for k_s while turbulence and small organic fraction particle sizes will give small values for k_s.

5.5.2.3 Estimating a Pre-Stratification Steady-State Dissolved Oxygen Level

Prior to stratification, the impoundment is assumed to be fully mixed. One of the important factors leading to this condition is wind stress, which also serves to reaerate the water. As a rule, unless an impoundment acts as a receiving body for large amounts of nutrients and/or organic loading, dissolved oxygen levels are likely to be near saturation during this period (D.J. Smith, pers. comm., November, 1976). Table V-12 shows saturation dissolved oxygen levels for fresh and saline waters as a function of temperature and chloride concentrations, and DO levels may be estimated accordingly.

The hypolimnetic saturation dissolved oxygen concentration is determined by using the average (or median) temperature for the hypolimnion as determined during the period of interest throughout the depth of the hypolimnion. Information on the hypolimnion is obtained using the procedures described in Section 5.2. For example, hypolimnetic water at the onset of stratification might be 4-5°C and during the critical summer months be 10°C. The value 10°C should be used having a saturation DO of 11.3 mg/l.

Most lakes are near sea level (<2000 ft elevation) and are relatively fresh (<2000 mg TDS/l). For lakes that do not meet these criteria, corrections for atmospheric pressure differences and salting out due to salinity might be needed. Pressure effects can be approximated by using a ratio of barometric pressure (B) for the elevation of interest and sea level (BSTP) as follows:

e.g. B at 4600 ft elevation,

$$\frac{B}{BSTP} = \frac{640}{760}, \text{ in mm Hg,}$$

$$= 0.84$$

$$\text{DOsat at } 10°C = 0.84 \times 11.3$$

$$= 9.5 \text{ mg/l.}$$

Chloride is an estimator of dilutions of sea water in fresh water where 20000 mg Chloride/l is equivalent to 35000 mg salt (TDS/l), that is, typical ocean water.

TABLE V-12

SOLUBILITY OF OXYGEN IN WATER (STANDARD METHODS, 1971)

Temp. in °C	Chloride Concentration in Water - mg/l					Difference per 100 mg Chloride
	0	5,000	10,000	15,000	Sea Water	
	Dissolved Oxygen - mg/l					
0	14.6	13.8	13.0	12.1	11.3	0.017
1	14.2	13.4	12.6	11.8	11.0	0.016
2	13.8	13.1	12.3	11.5	10.8	0.015
3	13.5	12.7	12.0	11.2	10.5	0.015
4	13.1	12.4	11.7	11.0	10.3	0.014
5	12.8	12.1	11.4	10.7	10.0	0.014
6	12.5	11.8	11.1	10.5	9.8	0.014
7	12.2	11.5	10.9	10.2	9.6	0.013
8	11.9	11.2	10.6	10.0	9.4	0.013
9	11.6	11.0	10.4	9.8	9.2	0.012
10	11.3	10.7	10.1	9.6	9.0	0.012
11	11.1	10.5	9.9	9.4	8.8	0.011
12	10.8	10.3	9.7	9.2	8.6	0.011
13	10.6	10.1	9.5	9.0	8.5	0.011
14	10.4	9.9	9.3	8.8	8.3	0.010
15	10.2	9.7	9.1	8.6	8.1	0.010
16	10.0	9.5	9.0	8.5	8.0	0.010
17	9.7	9.3	8.8	8.3	7.8	0.010
18	9.5	9.1	8.6	8.2	7.7	0.009
19	9.4	8.9	8.5	8.0	7.6	0.009
20	9.2	8.7	8.3	7.9	7.4	0.009
21	9.0	8.6	8.1	7.7	7.3	0.009
22	8.8	8.4	8.0	7.6	7.1	0.008
23	8.7	8.3	7.9	7.4	7.0	0.008
24	8.5	8.1	7.7	7.3	6.9	0.008
25	8.4	8.0	7.6	7.2	6.7	0.008
26	8.2	7.8	7.4	7.0	6.6	0.008
27	8.1	7.7	7.3	6.9	6.5	0.008
28	7.9	7.5	7.1	6.8	6.4	0.008
29	7.8	7.4	7.0	6.6	6.3	0.008
30	7.6	7.3	6.9	6.5	6.1	0.008
31	7.5					
32	7.4					
33	7.3					
34	7.2					
35	7.1					

5.5.2.4 Estimating Hypolimnion DO Levels

The final step in use of this model is preparation of a DO-versus-time plot for the hypolimnion (or at least estimation of DO at incipient overturn) and estimation of BOD and phosphorus loadings which result in acceptable hypolimnion DO levels. An equation to compute DO at any point in time during the period of stratification is:

$$\frac{dO}{dt} = -k_1C - k_4L/D \qquad (V-31)$$

where

O = dissolved oxygen in ppm

k_4 = benthic decay rate in day^{-1}

L = areal BOD load in gm^{-2}

D = depth in m.

The second term in the equation requires that an estimate be made of the magnitude of BOD loading in benthic deposits. To do this within the present framework, it is assumed that BOD settles out throughout the period of stratification. Although many different assumptions have been made concerning benthic BOD decay, it was assumed that benthic demand was a function of BOD settling and the rate of benthic BOD decay. This BOD includes that generated in the system by algal growth and that which enters in tributaries and waste discharges. Based upon the rate of settling used earlier in estimating a steady-state BOD concentration (Equation V-25) and rate of decay for conditions prior to stratification, the rate of benthic matter accumulation is:

$$\frac{dL}{dt} = k_sC_{ss}D - k_4L \qquad (V-32)$$

where

C_{ss} = concentration of BOD in the water column in gm^{-3} at steady-state.

The assumption of steady-state BOD concentration reduces Equation V-32 to the same form as Equation V-25 and integration gives:

$$L_t = \frac{(k_sDC_{ss} - k_4L_o)e^{-k_4t} - k_sDC_{ss}}{-k_4} \qquad (V-33)$$

For steady-state deposition ($dL/dt = 0$, Dk_sC_{ss} = constant):

$$L_{ss} = \frac{k_sC_{ss}D}{k_4} \qquad (V-34)$$

where

L_{ss} = steady-state benthic BOD load in gm^{-2}.

Application of Equation V-34 with k_s and k_4 appropriately chosen for the month or two preceding stratification will give an estimate of the benthic BOD load upon stratification. Application of Equation V-33 gives the response of L to different water column BOD (steady-state) loading rates and changes in rate coefficients.

After strata form, benthic matter decays while hypolimnion water column BOD decays and settles. The change in L over the period of stratification is:

$$\frac{dL}{dt} = -k_4L + Dk_sC \qquad (V-35)$$

Since

$$\frac{dC}{dt} = -k_sC - k_1C = -(k_1+k_s)C \qquad (V-36)$$

and

$$C_t = C_o\, e^{-(k_1 + k_s)t} \qquad (V-37)$$

$$\frac{dL}{dt} = -k_4L + Dk_sC_oe^{-(k_1 + k_s)t} \qquad (V-38)$$

then

$$L_t = \left(L_o + \frac{Dk_sC_o}{k_s+k_1-k_4}\right)e^{-k_4t} - \left(\frac{Dk_sC_o}{k_s+k_1-k_4}\right)e^{(-k_s-k_1)t} \qquad (V-39)$$

Water column BOD in the hypolimnion is given by Equation V-36 and the integrated form is Equation V-37.

Note that k_s, the settling coefficient is equal to v_s/D where v_s is the settling velocity of the BOD, and D is the depth of the hypolimnion (or when the impoundment is unstratified, D is the depth of the entire impoundment). Also note that we usually assume that the DO is at saturation at the onset of stratification. Thus we can ignore the assumptions and calculations (Equation V-32 to V-34) done for periods prior to onset.

The equation presented earlier (Equation V-31) for hypolimnion DO was:

$$\frac{dO}{dt} = -k_1C - k_4L/D$$

Equation V-31 is not integrable in its present form, but since L and C are defined as functions of t (Equations V-39 and V-37 respectively), it is possible to determine dissolved oxygen in the water column. The equation for oxygen at time t is:

$$O_t = O_o - \Delta O_L - \Delta O_c \qquad (V\text{-}40)$$

where

O_t = dissolved oxygen at time t
O_o = dissolved oxygen at time t = 0
ΔO_L = dissolved oxygen decrease due to benthic demand
ΔO_c = dissolved oxygen decrease due to hypolimnion BOD.

From Equation V-39, and using L_{ss} as L_o and C_{ss} as C_o:

$$\Delta O_L = \left(\frac{L_{ss}}{D} + \frac{k_s C_{ss}}{k_s+k_1-k_4}\right)\left(1-e^{-k_4 t}\right) - \left(\frac{k_s C_{ss}}{k_s+k_1-k_4}\right)\left(\frac{k_4}{k_s+k_1}\right)\left(1-e^{-(k_s+k_1)t}\right) \qquad (V\text{-}41)$$

and from Equation V-37:

$$\Delta O_c = \frac{k_1 C_{ss}}{k_1+k_s}\left(1-e^{-(k_1+k_s)t}\right) \qquad (V\text{-}42)$$

Solution of Equation V-40 gives an estimated DO concentration in the hypolimnion as a function of time.

To compute equation V-40, a simpler form of equation V-41 can be derived by substituting as follows:

since $L_{ss} = \frac{k_s C_{ss} D}{k_4}$,

$$\Delta O_L = \left(\frac{k_s C_{ss}}{k_s+k_1-k_4}\right)\left(\frac{k_s+k_1}{k_4}\right)\left(1-e^{-k_4 t}\right)$$

$$\left(\frac{k_4}{k_s+k_1}\right)\left(1-e^{-(k_s+k_1)t}\right) \qquad (V\text{-}43)$$

To simplify computations, the following stepwise solutions can be made:

$$A = \frac{k_s C_{ss}}{k_s+k_1-k_4}$$

$$B = \frac{k_s+k_1}{k_4}$$

$$C = 1-e^{-k_4 t}$$

$$E = 1-e^{-(k_s+k_1)t}$$

$$F = \frac{k_1 C_{ss}}{k_1+k_s}$$

then

$$\Delta D_L = A \left(B \cdot C - \frac{E}{B} \right)$$

$$\Delta D_c = E \cdot F$$

5.5.3 Temperature Corrections

All reactions are computed on the basis of the optimum temperature, but the environment is often at different temperatures. Some rate coefficients for chemical and biological reactions vary with temperature. A simple correction for such rate coefficients to 20°C is as follows:

$$K_T = K_{T20} \times 1.047^{(T - 20°C)}$$

For example, if a rate at 20°C - 0.01 and the lake is at 10°C, then:

$$K_T = 0.01 \times 1.047^{(10 - 20)}$$

$$K_T = 0.00632.$$

Generally the following optima are used:

k_1 - first order decay rate for water column BOD, use 20°C

k_4 - benthic BOD decay, use 20°C

P - productivity rate, use 30°C.

In the screening methods we do not have to correct for temperature except in the oxygen calculation for the rate coefficients, K_1, K_4, P and in the toxics section (5.6) for the biodegradation rate coefficients.

EXAMPLE V-15

Quiet Lake

(Comprehensive Example)

Quiet Lake is located a few miles south of Colton, New York. The lake is roughly circular in plan view (Figure V-32) and receives inflows from three tributaries. There is one natural outlet from the lake and one withdrawal used for quarrying purposes.

The first step in evaluation of lake hypolimnion DO levels is physical and water quality data collection. Table V-13 shows characteristics of Quiet Lake, Table V-14 shows tributary discharge data along with withdrawal and outflow levels, and Table V-15 provides precipitation and runoff information.

In order to evaluate hypolimnion DO as a function of time, the very first question to be answered is, does the impoundment stratify? If so, what are the beginning and ending dates of the stratified period, how deep is the upper surface

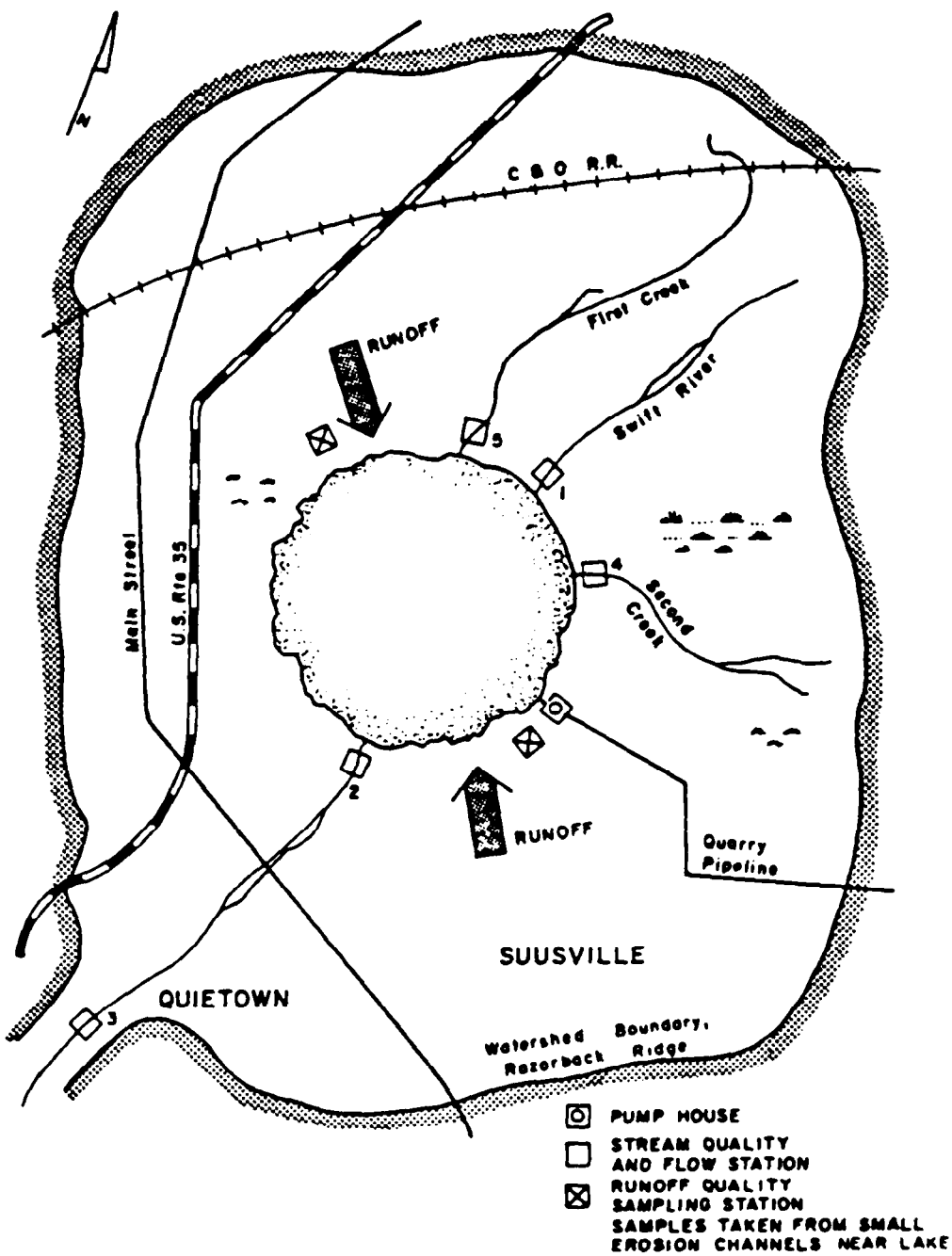

FIGURE V-32 QUIET LAKE AND ENVIRONS

TABLE V-13

CHARACTERISTICS OF QUIET LAKE

Length (in direction of flow)	3.5 miles = 18,480 ft.
Width	4.0 miles = 21,120 ft.
Mean Depth	22 ft.
Maximum Depth	27 ft.
Water Column P	$0.014 \leq P \leq .032$

TABLE V-14

WATER QUALITY AND FLOW DATA FOR TRIBUTARIES TO QUIET LAKE. DATA REPRESENT MEAN FIGURES FOR 1970-1975.

Swift River (Station 1, above Quiet Lake)				
Month	Mean Flow, cfs	Total N	Total P	BOD
			ppm	
October	54	2.2	0.2	3
November	38	4.1	0.08	4
December	10	5.3	0.10	6
January	5	6.1	0.20	12
February	2	5.0	0.15	10
March	8	4.3	0.08	12
April	40	3.3	0.04	10
May	55	2.1	0.02	8
June	85	2.8	0.02	4
July	150	2.9	0.02	2
August	70	1.0	0.02	1
September	85	2.4	0.03	1

TABLE V-14 (Continued)

First Creek (Station 5)

Month	Mean Flow, cfs	Total N	Total P	BOD
			ppm	
October	5	1.0	.01	0.5
November	3	2.0	.01	1.0
December	2	0.5	.02	1.5
January	2	1.2	.01	1.0
February	3	1.3	.02	0.8
March	4	2.3	.01	0.6
April	6	2.0	.01	0.5
May	8	1.8	.02	0.6
June	10	1.6	.01	0.8
July	8	1.4	.01	0.8
August	6	1.5	.00	1.0
September	4	0.8	.00	1.2

Second Creek (Station 4)

Month	Mean Flow, cfs	Total N	Total P	BOD
			ppm	
October	14.0	15	.15	7
November	13.0	16	.08	8
December	12.5	10	.20	10
January	5.0	9	.15	7
February	1.2	12	.12	7
March	2.0	13	.10	6
April	2.5	8	.11	7
May	4.0	6	.07	9
June	8.0	5	.08	12
July	12.0	7	.20	3
August	8.0	6	.22	4
September	5.5	8	.25	8

TABLE V-14 (Continued)

Swift River (Stations 2 and 3) and Pumped Withdrawal

Month	Pumped Withdrawal, cfs	Mean Monthly Flow, cfs	
		Station 2	Station 3
October	22.6	69.5	77.0
November	22.0	50.0	55.0
December	3.5	20.0	22.0
January	1.2	7.5	9.0
February	0.8	1.2	1.4
March	0.4	9.1	10.1
April	12.0	44.5	48.75
May	24.0	63.2	69.5
June	30.7	100.0	110.0
July	89.5	168.5	184.8
August	29.8	80.6	88.5
September	43.9	91.3	100.25

Notes: All three tributaries have their headwaters within the shed. The net inflow-outflow to the groundwater is known to be close to zero in the two creeks. Swift River is usually about 10% effluent over its entire length (10% of flow comes into the river from the groundwater table).

of the hypolimnion, and what is its volume, and what is the distribution of hypolimnion mean temperatures during the period? To answer these questions, either use field observation data, or apply some computation technique such as that presented earlier in this section. Assuming that methods presented earlier are used, the selection of appropriate thermal profile curves hinges around three factors. These are:

- Climate and location
- Hydraulic residence time
- Impoundment geometry.

TABLE V-15

PRECIPITATION AND RUNOFF DATA FOR QUIET LAKE WATERSHED. VALUES ARE MEANS OF DATA COLLECTED FROM BOTH STATIONS (SEE FIGURE V-31). THE WATERSHED HAS AN AREA OF 55 SQUARE MILES INCLUDING THAT OF THE LAKE

	Mean Total Monthly Precipitation, inches	Runoff Quality		
		Total N	Total P	BOD
		ppm		
October	3.0	6.0	0.1	27
November	2.4	6.5	0.2	37
December	1.0	4.0	0.1	46
January	0.5	3.0	0.008	34
February	0.3	1.0	0.07	33
March	0.6	1.5	0.1	30
April	2.0	2.5	0.15	40
May	2.8	3.2	0.25	50
June	4.2	3.6	0.20	40
July	7.6	7.0	0.40	37
August	3.5	7.8	0.60	45
September	4.2	9.2	0.80	50
Total	32.1			

Note: Infiltration to the water table on a monthly basis accounts for roughly 30% of precipitation volume.

In terms of climate and location, the Quiet Lake area is similar to Burlington, Vermont. Examination of the Burlington plots from Appendix D reveals that a 20-foot maximum depth impoundment can stratify in an area shielded from the wind. The area surrounding Quiet Lake does provide good shielding, so the next task is to estimate the hydraulic residence time to select a specific set of plots.

Inspection of all Burlington plots indicates that stratification is likely to occur at most from May to August. Accordingly, for purposes of plot selection, we are most interested in a mean hydraulic residence time based on flows in the period from about March to August. Since hydraulic residence time (τ_w) is given by $\tau_w = V/Q$, we compute mean Q ($\bar{Q}$). $\bar{Q}$ represents the

average of tributary inflows during this period, computed as follows:

$$\bar{Q} = \underbrace{\frac{8 + 40 + 55 + 85 + 150 + 70}{6}}_{\text{(Swift River)}} + \underbrace{\frac{4 + 6 + 8 + 10 + 8 + 6}{6}}_{\text{(First Creek)}} + \underbrace{\frac{2 + 2.5 + 4 + 8 + 12 + 8}{6}}_{\text{(Second Creek)}}$$

$$= 68 + 7 + 6.08 = 81.1 \text{ cfs}$$

However, in order to fully account for mass transport as well as properly estimate hydraulic residence time, one more factor should be considered. This is non-point inflow. At this point, we have enough information to estimate the stormwater contribution directly to Quiet Lake. In view of the available data, the computation is as follows:

$$Q_s = APK(1-L) - \left(\sum_{i=1}^{n} Q_i(1-I_i)\right)$$

where

Q_s = stormwater or non-point inflow in cfs (excluding rivers and creeks)

A = area of shed in square miles

n = number of tributaries

Q_i = monthly mean pickup (in cfs) in the ith tributary

P = monthly total precipitation, in inches per month

I_i = percent (expressed as a decimal) of flow contributed by exfiltration (from the water table into the channel)

L = the proportion of precipitation lost by infiltration into the soil (expressed as a decimal)

K = unit correction = 0.895 $ft^3 mo\ mi^{-2} in^{-1} sec^{-1}$.

As an example, the computation for October is:

$$Q_s = 55 \text{ mi}^2 \times 3.0 \frac{\text{in}}{\text{mo}} \times 0.896 \frac{\text{ft}^3\text{mo}}{\text{mi}^2\text{in sec}} \times (1-0.3) -$$

$$\left(54(1-0.1) + 5(1-0.0) + 14(1-0.0) + (77-69.5)(1-0.1)\right) = 29.1 \text{ cfs}$$

Now, since we know the pumped withdrawal rates as well as the difference between flows at stations 2 and the sum of 1, 4, and 5, and that the impoundment surface is at steady-state over the mouth, we also can estimate the net infiltration rate from the lake into the groundwater. The infiltration rate is (again, for October):

$$\text{Net efflux} = Q_{(\text{sta } 1 + 4 + 5)} - Q_2 + Q_s - Q_w$$
$$= 73.0 - 69.5 + 29.1 - 22.6 = 10.0 \text{ cfs}$$

Note that the pickup in each channel above Quiet Lake is equal to the flow at the pertinent sampling station. This is the case because the three channels

have their headwaters within the watershed. If one were concerned about a subshed with tributary headwaters above the subshed boundary, the difference in Q between each of stations 1, 4, and 5 and the respective flows at the upstream subshed boundary would be used.

To estimate hydraulic residence time add the mean stormwater contribution over the months of interest to that of the tributaries, as computed earlier. The individual stormwater computations are not shown. The method is as just described.

$$\bar{Q}_{total} = 81.1 + \frac{6.6 + 20.7 + 29.4 + 41.4 + 92.5 + 36.6}{6} = 119 \text{ cfs}$$

Then the hydraulic residence time is given by:

$$\tau_w = V/Q = \pi r^2 D/Q$$

$$r = \left[\frac{L+W}{4} \times 5280 \right]$$

where

L = length of the lake in mi
W = width of the lake in mi
D = mean depth in ft
r = radius in ft.

$$\tau_w = 3.14 \times \left[\frac{3.5+4}{4} \times 5280 \right]^2 \times 22/119$$

$$= 5.69 \times 10^7 \text{ sec} = 658 \text{ days}$$

Accordingly, the infinite hydraulic residence time plots for a 20-foot deep, wind-protected, Burlington, Vermont, impoundment should suffice. Note that the entire impoundment volume was used in the above computation. Strictly, one should use the epilimnion volume during stratification. In this case, such a change would not alter selection of the plots because τ_w would still be greater than 200 days. A reproduction of the appropriate plot from Appendix D is presented in Figure V-33. As indicated, Quiet Lake is likely to be weakly stratified from May to August inclusive, with a thermocline temperature gradient of about $1°ft^{-1}$. The hypolimnion should extend downward to the bottom from a depth of about 3-1/2 meters, giving a mean hypolimnion depth of:

$$D_H = \frac{22 \text{ ft}}{3.29 \text{ ft m}^{-1}} - 3.5 \text{ m} = 3.2 \text{ meters}$$

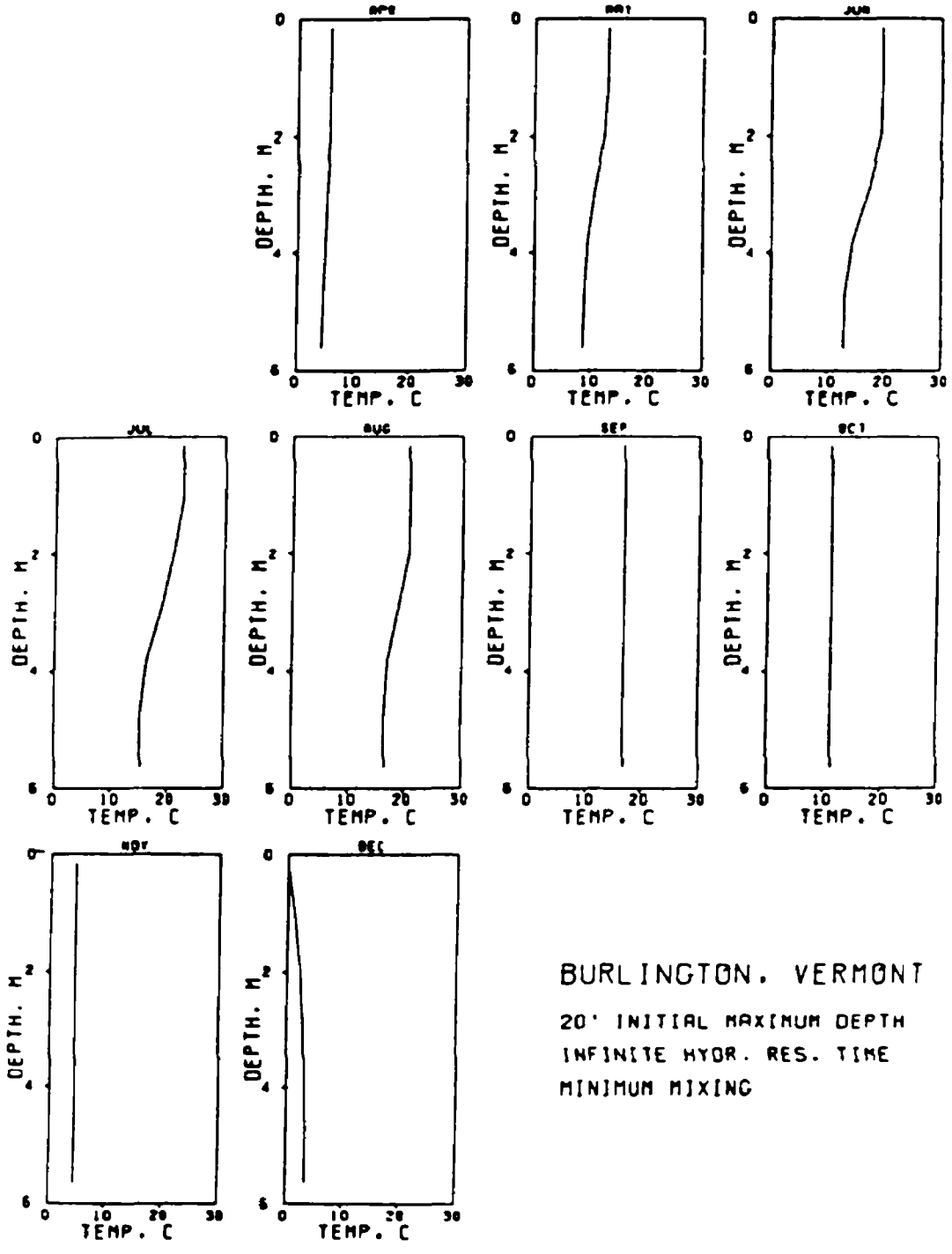

FIGURE V-33 THERMAL PROFILE PLOTS FOR USE IN QUIET LAKE EXAMPLE

The approximate hypolimnion volume, then, is:

$$V_H = \frac{D_H}{D_{Total}} \times V_{Total}$$

$$V_H = \frac{3.2m}{6.7m} \times 1.9 \times 10^{11}\ell = 9.2 \times 10^{10}\ell$$

Over the period of interest, the hypolimnion mean temperature distribution is:

Month	Mean Temperature, °C
March	2.0
April	5.5
May	9.5
June	12.5
July	14.0
August	15.5

The next step in use of the DO model is to determine a steady-state or mean water column BOD loading (k_a) and DO level prior to stratification. This is a multi-step process because of the several BOD sources. The sources are tributaries, runoff, and primary productivity. First, we estimate algal productivity using methods of this chapter (or better, field data).

Using the curve in Figure V-26 and phosphorus data from Table V-14, the maximal primary productivity should be in the range 1,400 mg $Cm^{-2}day^{-1}$ to 1,900 mg$Cm^{-2}day^{-1}$. To convert to loading in $mgl^{-1}day^{-1}$, divide by (1000 lm^{-3} x 6.7m). This gives the loading as 0.21 to 0.28 $mgl^{-1}day^{-1}$.

Now assuming that maximal productivity occurs at about 30°C and that productivity rates obey the same temperature rule as BOD decay, temperature-adjusted estimates of productivity rates can be made. Using the maximal rate range of 0.21 to 0.28$mgl^{-1}day^{-1}$, the adjusted rates are:

$$\text{Productivity} = (0.21, 0.28) \times 1.047^{(3.75-30)}$$
$$= (.06, .08)\ mgl^{-1}\ day^{-1}$$

Then, according to Equation V-30 and assuming M = 1, k_a due to algae is estimated by:

$$k_{a(algae)} = 2.67 \times (.06, .08) = (.16, .21)\ mgl^{-1}day^{-1}$$

The next contributor to water column BOD is BOD loading of inflowing waters. The value to be computed is the loading in milligrams per liter of impoundment water per day:

$$\text{Daily BOD loading rate} = \left(\sum_{i=1}^{n} \sum_{j=1}^{L_i} d_i Q_{i,j} C_{i,j} \right) \Big/ V \sum_{k=1}^{n} d_k$$

where

n = the number of time periods of measurement

V = volume of impoundment in liters

d = the number of days per time period

L = the number of inflows.

For all inflows, the value is therefore approximately:

$$k_{a(Trib)} = (2185 + 48.3 + 643.9 + 14240) \times 2.45 \times 10^{6} \times \frac{1}{1.9 \times 10^{11}}$$

(Swift River; First Creek; Second Creek; Storm water Runoff; Units Conversion; Impoundment Volume)

$$= 0.22 \text{ mgl}^{-1}\text{day}^{-1}$$

Now, summing the two contributions:

$$k_a = k_a \text{ (algae)} + k_{a(Trib)}$$

$$k_a = (.16, .21) + .22 = (.38, .43) \text{ mgl}^{-1}\text{day}^{-1}$$

The value of k_1 will be assumed as 0.1 at 20°C with θ in Equation (V-29) equal to 1.047. Then at 3.75°C:

$$k_{1(3.75°C)} = k_{1(20°C)} \times 1.047^{(3.75-20)}$$

$$= .1 \times 1.047^{(-16.25)} = 0.047$$

Now $Q_{(discharge)}$ (mean for March and April) and V are known, with:

$$Q_{(discharge)} = 26.8 \text{ (Swift River, Station 2)} + 6.2 \text{ (pumped withdrawal)} \times \frac{28.32\,\ell}{ft^3} = 935\,\ell \text{ sec}^{-1}$$

$$V = 1.9 \times 10^{11}\ell$$

then

$$C_{ss} = \frac{.38, .43}{(0.3 + .047 + (935/1.9 \times 10^{11}))} = 4.94, 5.58$$

For further computations, $C_{ss} = 5.25$ will be assumed.

Since k_s has been defined as .03, a steady-state areal concentration of benthic BOD prior to stratification can be estimated. If $k_{4(20°C)} = .003$ and $C_{ss} = 5.25$, using Equation (V-34):

$$L_{ss} = \frac{k_s C_{ss} D}{k_{4(3.75°C)}}$$

$$k_{4(3.75°C)} = .003 \times 1.047^{(3.75-20)}$$

$$= .0014$$

$$L_{ss} = \frac{.03 \times 5.25 \times 6.7}{.0014}$$

$$= 754\ gm^{-2}$$

The next step in evaluating hypolimnion DO depression is to estimate pre-stratification DO levels. If we assume saturation at the mean temperature in April (5.5°C), the dissolved oxygen concentration at onset of strata should be about 12.7 (from Table V-12).

Now we have all values needed to plot hypolimnion DO versus time using Equations V-40 through V-42.

Using

$L_o = L_{ss}$

$C_o = C_{ss}$

$k_1 = 0.1 \times 1.047^{(9.5-20)} = .062$, (T = 9.5°C for May)

$k_s = 0.03$

$k_4 = .003 \times 1.047^{(9.5-20)} = .002$

$t = 5$ days

and applying Equation V-42:

$$\Delta O_c = \frac{k_1 C_{ss}}{k_1 + k_s}\left(1 - e^{-(k_1+k_s)t}\right)$$

$$\Delta O_c = \frac{0.062 \times 5.25}{0.062 \times 0.03}\left(1 - e^{-(0.062+0.03)5}\right) = 1.30$$

then, according to Equation V-41:

$$\Delta O_L = \left(\frac{L_{ss}}{D} + \frac{k_s C_{ss}}{k_s + k_1 - k_4}\right)\left(1 - e^{-k_4 t}\right) - \left(\frac{k_s C_{ss}}{k_s + k_1 - k_4}\right)\left(\frac{k_4}{k_s + k_1}\right)\left(1 - e^{-(k_s+k_1)t}\right)$$

$$\Delta O_L = \left(\frac{754}{3.2} + \frac{0.03 \times 5.25}{0.03 + 0.062 - 0.002}\right)\left(1 - e^{-0.002 \times 5}\right) - \left(\frac{0.03 \times 5.25}{0.03 + 0.062 - 0.002}\right)$$

$$\left(\frac{0.002}{0.062 + 0.03}\right)\left(1 - e^{-(0.062+0.03)5}\right) = 2.35$$

then from Equation V-40:

$$O_t = O_o - \Delta O_c - \Delta O_L$$

$$O_5 = 12.7 - 1.30 - 2.35 = 9.05$$

Solving the same equations with increasing t gives the data in Table V-16. If it has been necessary to develop more data for the remainder of the stratified period, appropriately updated coefficients might be used starting at the beginning of each month.

TABLE V-16

DO SAG CURVE FOR QUIET LAKE HYPOLIMNION

Date	ΔO_L	ΔO_c	O_t
t = 0	0	0	12.70
5/5	2.35	1.30	9.05
5/10	4.68	2.13	5.89
5/15	6.99	2.65	3.06
5/20	9.22	2.98	0.50
5/25	11.54	3.18	0.00

Finally, if it is desired to evaluate the impact of altered BOD or phosphorus loadings, the user must go back to the appropriate step in the evaluation process and properly modify the loadings.

END OF EXAMPLE V-15

5.6 TOXIC CHEMICAL SUBSTANCES

Although reasonably accurate and precise methods have been prepared for screening only a few of the many priority pollutants (Hudson and Porcella, 1981), a reasonable approach for assessing priority pollutants in lakes based on the methods presented in Chapter 2 can be made if certain assumptions are made:

- The major processes affecting the fate and transport of toxicants in aquatic ecosystems are known
- That reasonable safety factors are incorporated by making reasonable most case analyses
- Because it is a screening approach, prioritization can be done to identify significant constituents, lakes where human health or ecological problems can realistically be expected, and processes which might require detailed study.

The major processes affecting toxicants are listed in Table V-17. The primary measure of the impact of a toxic chemical in a lake depends on its concentration in the water column. Thus, these screening methods are primarily directed at fate and

TABLE V-17

SIGNIFICANT PROCESSES AFFECTING
TOXIC SUBSTANCES IN AQUATIC ECOSYSTEMS

Processes	Rate Coefficient Symbol, $time^{-1}$
Physical-Chemical Processes	
Sorption and sedimentation	SED
Volatilization	k_v
Hydrolysis	k_h
Photolysis	k_p
Oxidation	not assessed
Precipitation	not assessed
Biological Processes	
Biodegradation	B
Bioconcentration	BCF (unitless)

transport of toxic chemicals. A secondary target is the concentration in aquatic biota, principally fish. Because of the complexity of various routes of exposure and bioaccumulation processes, the approach of bioconcentration is used to identify compounds likely to accumulate in fish. These can be applied to lakes using the following method:

- A fate model is used that incorporates sediment transport, sorption, partitioning, and sedimentation
- Significant processes include the kinetic effects of sedimentation, volatilization and biodegradation
- Significant biochemical processes can affect the fate of a toxic chemical as well as affect biota, such, as, bioaccumulation, biodegradation, and toxicity
- In keeping with the conservative approach of the toxics screening methodology, some important processes are neglected for simplicity; for example, lake stratification, photolysis, oxidation, hydrolysis, coagulation-flocculation, and precipitation are neglected. Also, it is assumed that the organic matter is associated with inorganic particles and therefore organic matter settles with the inorganic particles.

Generally the toxic chemical concentrations are calculated conservatively, that is, higher concentrations are calculated than would occur in nature because of the assumptions that are made. The water column concentrations are calculated as the

primary focus of the screening method. Then bioconcentration is estimated, based on water concentration. To determine concentration and bioaccumulation, point and nonpoint source loadings of the chemicals being studied are needed. Other data (hydrology, sediments, morphology) are obtained from the problems previously done in earlier chapters or sections of this chapter. The person doing the screening would have to compile or calculate such data.

Occasionally, such information must be estimated based on production, use, and discharge data. Information on chemical and physical properties is important to determine the significance of these estimates.

5.6.1 Overall Processes

Several processes affecting distribution of toxic chemicals are more significant than others. Equilibrium aquatic processes include suspended sediment sorption of chemicals. Organics in sediments can have a significant effect on chemical sorption. Hydrolysis and acid-base equilibria can alter sorption equilibria. Volatilization is an equilibrium process that tends to remove toxic chemicals from aquatic ecosystems. Removal processes include settling of toxics sorbed on sediments, volatilization, and biodegradation. Chemical reactions for hydrolysis and photolysis are included and precipitation and redox reactions could be included if refinement of the method were desired. Generally, bioaccumulation will be neglected as a removal process.

These removal processes are treated as first-order reactions that are simply combined for a toxicant (C, mg/l) to give:

$$dC/dt = - K \times C \qquad \text{(V-44)}$$

where

$K = SED + B + k_v + k_p + k_h$

SED = sedimentation rate, toxicant at equilibrium with sediments

k_v = volatilization rate

B = biodegradation rate

k_p = photolysis rate

k_h = hydrolysis rate.

This equation is analogous to the BOD decay rate equation used in the hypolimnetic DO screening method.

The input of toxic chemical substances is computed simply (refer to Figure V-23):

$$\frac{dC}{dt} = \frac{Q}{V} \times C_{in} - \frac{C}{\tau_w} \qquad \text{(V-45)}$$

where

C_{in} = the concentration in the inflow (tributary or discharge);
flow (Q), volume of reservoir (V) and time (t) are as defined previously.

At steady state, accounting for inflow ($Q \cdot C_{in}$) and outflow ($Q \cdot C$), and using $Q/V = 1/\tau_w$:

$$\frac{dC}{dt} = \frac{1}{\tau_w} (C_{in} - C) - K \times C = 0 \qquad \text{(V-46)}$$

and solving:

$$C = C_{in}/(1 + \tau_w \times K) \qquad \text{(V-47)}$$

To determine the concentration at any time during a non-steady state condition (assuming C_{in} is a constant):

$$C = \frac{C_{in}}{f} (1 - e^{-ft/\tau_w}) + C_o e^{-ft/\tau_w} \qquad \text{(V-48)}$$

where

f = $1 + \tau_w \times K$

C_o = reservoir concentration at $t = 0$.

5.6.1.1 Sorption and Sedimentation

Suspended sediment sorption is treated as an equilibrium reaction which includes partitioning between water (C_w) and the sediment organic phases (C_s). The concentration sorbed on sediment can be computed as follows:

$$\frac{C_s}{C} = a \times K_p \times S \qquad \text{(V-49)}$$

where

C = the total concentration ($C_w + C_s$), mg/l

S = input suspended organic sediment = $OC \times So$, mg/l

OC = fraction of organic carbon.

So = input of suspended sediment, mg/l

K_p = distribution coefficient between organic sediment and water

a = fraction of pollutant in solution

= $1/(1 + (K_p \times S))$.

If K_p is large, essentially all of the compound will be sorbed onto the sediments. Note that S and C must be estimated or otherwise obtained.

The organic matter content of suspended sediment and the lipid solubility of the compound are important factors for certain organic chemicals. Other sorption can be ignored for screening. A simple linear expression can be used to calculate the sediment partition coefficient (K_p) based on the organic sediment carbon concentration (OC) and the octanol-water coefficient (kow) for the chemical:

$k_p = 0.63\ (kow)\ (OC)$

The sedimentation rate (SED) of a toxic chemical is computed as follows:

$$SED = a \times D \times K_p \qquad (V\text{-}50)$$

where

D = $P \times S \times Q/V$, sedimentation rate constant

P = sediment trapping efficiency

Q/V = $1/\tau_w$

5.6.1.2 Biodegradation

The biodegradation rate (B) is obtained from the literature or is computed as follows:

$$B = -\frac{\Delta C}{C \Delta t} \qquad (V\text{-}51)$$

Modification to the rate can be made for nutrient limitation using phosphorus (C_p) as the limiting nutrient:

$$B\ limited = \frac{B\ (0.0277) C_p}{1 + 0.177 \times C_p} \qquad (V\text{-}52)$$

Temperature correction can be performed using the following equation:

$$B(T) = B(20°C) \times 1.072^{(T-20)} \qquad (V\text{-}53)$$

Previous exposure to the pollutant is important for most toxic organic compounds. Higher rates of degradation occur in environments with frequent or longterm loading (discharges, nonpoint sources, frequent spills) than infrequent loadings (one-time spills). In pristine areas, rates of one to two orders of magnitude less should be used.

It is assumed that the suspended sediment decay rate is the same as aqueous phase decay. Also benthic decay is disregarded because bottom sediment release may be negligible.

5.6.1.3 Volatilization

Many organics are not volatile so this process is applied only to those which are. It is assumed that the mass flux of volatile organics is directly proportional to the concentration difference between the actual concentration and the concentration at equilibrium with the atmosphere. The latter can be neglected in lakes.

Also, only the most volatile are assessed.
Thus:

$$\frac{dC}{dt} = - k_v \times C \qquad (V\text{-}54)$$

where

k_v = volatilization rate constant, hr^{-1}

The rate coefficient is derived from the 2 resistance model for the liquid-gas interface, but it can be estimated using correlation with the oxygen reaeration coefficient (based on Zison et al., 1978):

$$k = Ka\ (Dw/Do) \qquad (V\text{-}55)$$

and estimate $(Dw/Do) = (32/mw)^{1/2}$

and the surface film thickness, $SFT = (200\text{-}60 \cdot \sqrt{w}) \times 10^{-6}$

and $Kal = Do/SFT$

$Ka = Kal/ZB$

where

Ka = reaeration rate, hr^{-1}

Dw = pollutant diffusivity in water

Do = diffusivity of oxygen in water (2.1×10^{-9} m^2/sec, 20°C)

mw = pollutant molecular weight

$\bar{w}$ = wind speed, m/sec

$\bar{Z}$ = mean depth, m.

The volatilization rate coefficient (k_v, hr^{-1}) is determined by $k_v = Ka \times k$ where k is obtained from literature values or computed as above ($\sqrt{Dw/Do}$). The rate should be corrected for temperature (k_{vt}) even though temperature has only a relatively small effect:

$$k_{vt} = k_v \times 1.024^{(T-20)} \qquad (V\text{-}56)$$

5.6.1.4 Hydrolysis

Not all compounds hydrolyze and those that do can be divided into three groups: acid catalyzed, neutral, and base catalyzed reactants. A pseudo first-order hydrolysis constant (k_h) is estimated for the hydrolysis of the compound:

$$\frac{dC}{dt} = -k_h \cdot C \qquad (V\text{-}57)$$

The rate constant (k_h) is pH dependent and varies as discussed in Chapter 2.
The typical pH of the lake for the appropriate season should be obtained for the

necessary calculations. Generally, the pH is a common measurement and is available for most lakes. If not, pH values for most open lakes lie between 6-9 and can be estimated based on the following empirical values based on Hutchinson, (1957):

	Hardness (or Alkalinity)	pH
acid lakes	<25	6 - 6.5
neutral lakes	25 - 75	6.5 - 7.5
hard water lakes	75 - 200	7.5 - 8.5
eutrophic and alkaline lakes	0 - 300	8.0 - 10.0

Median values on a range of values can be used to evaluate the significance of hydrolysis as a factor affecting the fate of compounds.

5.6.1.5 Photolysis

Generally, photolysis is a reaction between ultraviolet light (UV, 260 to 380 nm is most important) and photosensitive chemicals. Not all compounds are subject to photolysis nor does UV light penetrate significantly in turbid lakes. In the absence of turbidity data, light transmission can be estimated by seasonally averaged Secchi disk readings according to the following equation:

$$\ln (ISD/Io) = -ke(SD) - \ln 0.1 = -2.3$$

$$ke = 2.3/SD$$

where

$\underset{\sim}{ke}$ = the extinction coefficient

$\bar{SD}$ = the Secchi depth in meters

$(ISD/Io = 0.1)$ = relative intensity based on Hutchinson (1957).

Photolysis for appropriate chemicals (discussed in detail in Chapter 2) depends on a first order rate constant (k_p) incorporating environmental variables (solar irradiance, Io) and chemical variables (quantum yield, Φ, and absorbance, E). Turbidity effects are included as estimated as above since turbidity data are generally not available. These values are incorporated into the rate constant and the concentration reduced as described in Chapter 2:

$$\frac{dC}{dt} = -k_p C \qquad (V\text{-}58)$$

where

$$k_r = f(Io, \Phi, E, ke, \bar{Z})$$

and

$$k_p = \frac{k_r}{ke \cdot \bar{Z}}$$

where

k_r = photolysis rate constant uncorrected for depth and turbidity of the lake.

Depth (Z) is generally applied only to the photic zone; mean depth (Z) is an appropriate measure since it approximates the mixed depth and the photic zone.

5.6.1.6 Bioconcentration

Bioconcentration is a complex subject that depends on many variables. The simplest approach has been developed for organic compounds using the octanol-water coefficient (kow) to calculate tissue concentrations (Y):

$$Y = BCF \times C, \text{ g/kg fresh weight of fish flesh} \qquad (V\text{-}59)$$

where

BCF = Bioconcentration factor

log BCF = 0.75 log kow - 0.23

(The coefficients for the equation (0.75, - 0.23) are median estimates obtained from correlation equations and are default values for occasions where no other data are available.)

5.6.2 Guidelines for Toxics Screening

Generally metals do not biodegrade nor volatilize. However, pH, hardness, alkalinity and other ions are very important and can cause their removal by precipitation. The conservative approach is taken here and metals are calculated without removal (K = 0).

Organics may have variable sorption, volatilization, and biodegradation rates. If data are available in the literature, these should be used. Otherwise, a conservative approach should be used and calculations made without removal (K = 0). For chlorinated (and other halogens) compounds or refractory compounds, biodegradation should be assumed to be zero.

EXAMPLE V-16

Estimating Trichloroethylene and Pyrene Concentrations in an Impoundment

An impoundment with a single tributary is located in a windy valley. The following conditions are known for E.G. Lake:

Mean tributary flow rate = $3.6 \times 10^4 m^3$/hour

Total volume = $1.1 \times 10^8 m^3$

Mean depth = 11 m

Tributary average sediment load = 200 mg/l

Sediment average organic carbon content = .05

Inlet average pyrene concentration = 50 μg/l

Inlet average trichloroethylene concentration = 100 μg/l

Lake average phosphorus concentration = 50 μg/l

Mean water temperature = 15°C

Mean wind speed = 6 m/sec (35 mph)

Secchi depth = 1 m

Determine the steady state concentration of pyrene and trichloroethylene in the lake, assuming V max for the sediment (mostly clay) is 3.2×10^{-5} feet/second. The trapping efficiency is obtained from Figure V-34.

Other data	Pyrene	Trichloroethylene
kow	148000	190
B	1×10^{-4}	-
k_v	-	0.45xKa

The processes of photolysis and hydrolysis can be neglected because turbidity prevents photolysis (SD = 1 meter) and these compounds have negligible hydrolysis (see Chapter 2).

We use the summary equation V-47 for the analysis:

$$C = C_{in}/(1 + \tau_w \cdot K)$$

The hydraulic residence time of E.G. Lake is:

$$\tau_w = 1.1 \times 10^8 m^3/(3.6 \times 10^4 m^3/hr)$$

= 3048 hours

= 127 days

= .349 year

= 1.1×10^6 seconds

Sedimentation

First, the suspended sediment concentration in E.G. Lake must be estimated. The trapping efficiency of the impoundment is estimated from Figure V-34.

Data:		log 10
V max	= 5×10^{-6} fps	-5.30
τ_w	= 1.1×10^6 sec	6.04
D^1	= 11 m = 36.1 ft	1.56

A value of $10^{1.95}$ is obtained which yields:

$$P \cong 90 = 0.9$$

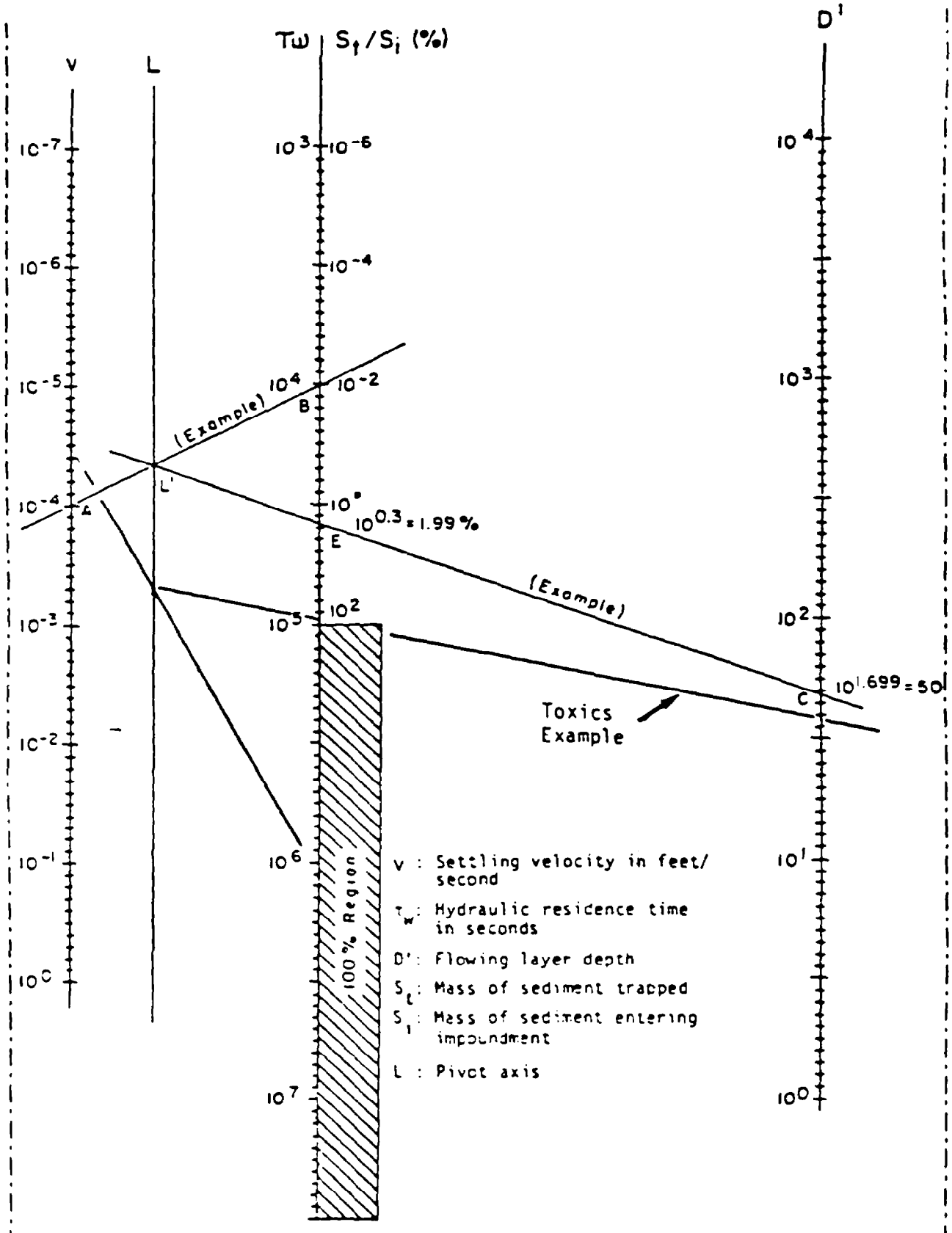

FIGURE V-34 NOMOGRAPH FOR ESTIMATING SEDIMENT TRAP EFFICIENCY

In the inflowing stream, the toxicants are assumed to be at equilibrium with the organic matter. Thus:

$$S = OC \times So = .05 \times 200 \times 10^{-6} = 1 \times 10^{-5} \text{ kg/l}$$

Therefore, for pyrene:

$$K_p = 0.63 \times 148000 \times 0.05 = 4660$$
$$a = 1/(1 + 4660 \times 1 \times 10^{-5}) = 0.955$$
$$\frac{Cs}{C} = 0.955 \times 4660 \times 1 \times 10^{-5} = 0.044$$

and

$$SED = a \times D \times K_p$$
$$D = P \times S \times Q/V$$
$$D = 0.9 \times 200 \times 10^{-6} \times \frac{1}{3048} \text{ hours}$$
$$D = 5.91 \times 10^{-8} \text{ hour}$$
$$SED = .955 \times 5.91 \times 10^{-8} \times 4660$$
$$SED = 2.63 \times 10^{-4} \text{ hr}^{-1}$$

For trichloroethylene:

$$K_p = .63 \times 190 \times 1 \times .05 = 6$$
$$a = 1/(1 + 6 \times 1 \times 10^{-5}) = 1$$
$$\frac{Cs}{C} = 1 \times 6 \times 1 \times 10^{-5} = 6 \times 10^{-5} \approx 0$$

and

$$SED = 1 \times 5.91 \times 10^{-8} \times 6$$
$$SED = 3.54 \times 10^{-7} \text{ hr}^{-1}$$

Biodegradation

Assume that the presence of trichloroethylene does not affect the biodegradation of pyrene. Trichloroethylene does not biodegrade. The temperature corrected and nutrient limited rate constant for microbial decay of pyrene are:

$$Bo = 1. \times 10^{-4} \text{ hr}^{-1}$$
$$B = .0277 \times 50/ (1 + .0277 \times 50)$$
$$= .58$$
$$B(15) = .58 \times 1. \times 10^{-4} \times 1.072^{(15-20)}$$
$$= 4.1 \times 10^{-5} \text{ hr}^{-1}$$

Volatilization

The reaeration coefficient for E.G. Lake will be estimated for trichloroethylene only, because pyrene does not volatilize:

$$Kal = 2.1 \times 10^{-9} / (200 - 60 \times 6^{1/2}) 10^{-6}$$
$$= 3.96 \times 10^{-5} \text{ m/sec}$$
$$= .143 \text{ m/hr}$$

$$Ka = (.143\ m/hr) / 11\ m = .013\ hr^{-1}$$

For trichloroethylene (TCE):

$$k_v = [MW(TCE)/MW(O_2)]^{1/2} \cdot Ka = .45 \times .013 = .0058\ hr^{-1}$$

When adjusted for temperature:

$$k_v = .0058 \times 1.024^{(15-20)}$$
$$= .0052\ hr^{-1}$$

Volatilization for pyrene may be neglected.

Pollutant Mass Balance

The overall decay rate constants are: $K = SED + B + k_v$

Pyrene: $K = 2.63 \times 10^{-4} + 4.1 \times 10^{-5}$
$= .000304\ hr^{-1}$

Trichloroethylene: $K = 3.54 \times 10^{-7} + 0 + 0.0051$
$= .0052\ hr^{-1}$

Using the steady state equation:

$$C = C_{in} / (1 + \tau_w K)$$

For Pyrene:

$$C = 50\ \mu g/l\ /\ (1 + 3048\ hr \times .000304\ hr^{-1})$$
$$C = 27\ \mu g/l$$

Note: WQC for human health is 0.0028 µg/l at 10^{-6} Risk (FR: 11/28/80 p. 79339).

For Trichloroethylene:

$$C = 100\ \mu g/l\ /\ (1 + 3048\ hr \times .0052\ hr^{-1})$$
$$= 5.9\ \mu g/l$$

Note: WQC for human health is 2.7 µg/l at 10^{-6} Risk (FR: 11/28/80 p. 79341)

Tissue burdens (Y) can be calculated:

$$Y = BCF \times C$$

where

$$\log BCF = .75 \log kow - 0.23$$

For Pyrene:

$$Y = 4330 \times 27 = 120000\ \mu g/kg\ fish\ flesh$$

For Trichloroethylene:

$$Y = 30 \times 6 = 180\ \mu g/kg\ fish\ flesh$$

Comments

Several conclusions are apparent from this analysis:

- Certain processes dominate the overall fate for a specific toxic

chemical so that, practically speaking, errors in estimating coefficients are negligible except for the important processes. After identifying the important processes, the coefficients can be varied to determine the range of concentrations. For example, sedimentation of trichloroethylene can be ignored; however, volatilization should be studied.

- The more stringent Water Quality Criteria are for toxicants that have significant bioconcentration; e.g. compare pyrene to trichloroethylene.
- Volatilization of trichloroethylene would be investigated in detail since this process might not be significant in this lake because of its depth. Also, the physical properties are important; e.g. trichloroethylene has a specific gravity of about 1.5. Thus, it may accumulate on the bottom of the reservoir and remain there unless it is completely dispersed.
- Based on this analysis, sources of pyrene would be assessed first, then trichloroethylene.
- What other observations can you draw from this analysis?

END OF EXAMPLE V-16

5.7 APPLICATION OF METHODS AND EXAMPLE PROBLEM

This chapter has presented several approaches to evaluation of five impoundment problem areas. These are thermal stratification, sediment accumulation, eutrophication, hypolimnion DO/BOD, and toxic chemicals. Figure V-35 shows how the different approaches are linked together with their data needs. In studying any or all of the potential problem areas in an impoundment, the user should first define the potential problems as clearly as he can. Often the nature of a problem will change entirely when its various facets are carefully described and examined en masse.

Once the decision is made that an aspect of impoundment water quality should be evaluated and the problem is clearly stated, the user should examine available solution techniques presented both in this document and elsewhere. The examination should address the questions of applicability, degree of accuracy, and need for data. The user will generally know what funds are available for data collection as well as the likelihood of procuring the needed data from previously developed bases. Also, the decision concerning needed accuracy rests with the user, and he should make decisions based upon the way in which his results will be used.

Once appropriate methods have been selected, the next task is to set down the data and to manipulate it according to computational requirements. Data are best displayed first in tabular form and then plotted in some meaningful way. Careful tabulation of data and graphing can themselves sometimes provide a solution to a

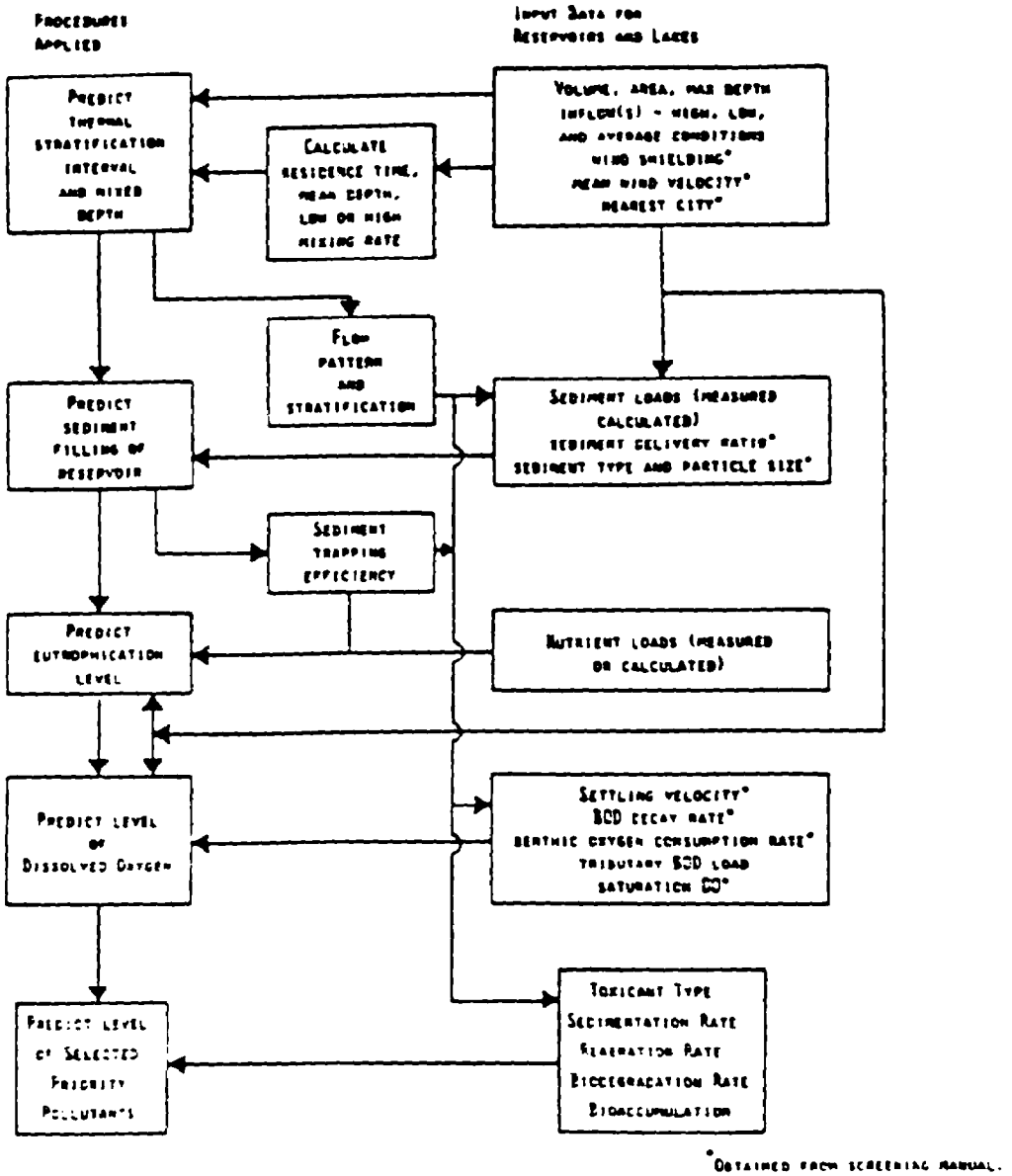

FIGURE V-35 GENERALIZED SCHEMATIC OF LAKE COMPUTATIONS

problem, negating need for further analysis. To illustrate these steps, a comprehensive application to a river basin system was performed in this section.

5.7.1 The Occoquan Reservoir

The Occoquan River basin in Virginia was used to demonstrate the screening approach. A basin map is shown in Figure V-36. Because the Occoquan Reservoir is a public drinking water supply downstream from metropolitan areas, water quality data were available to compare to the screening method's outputs.

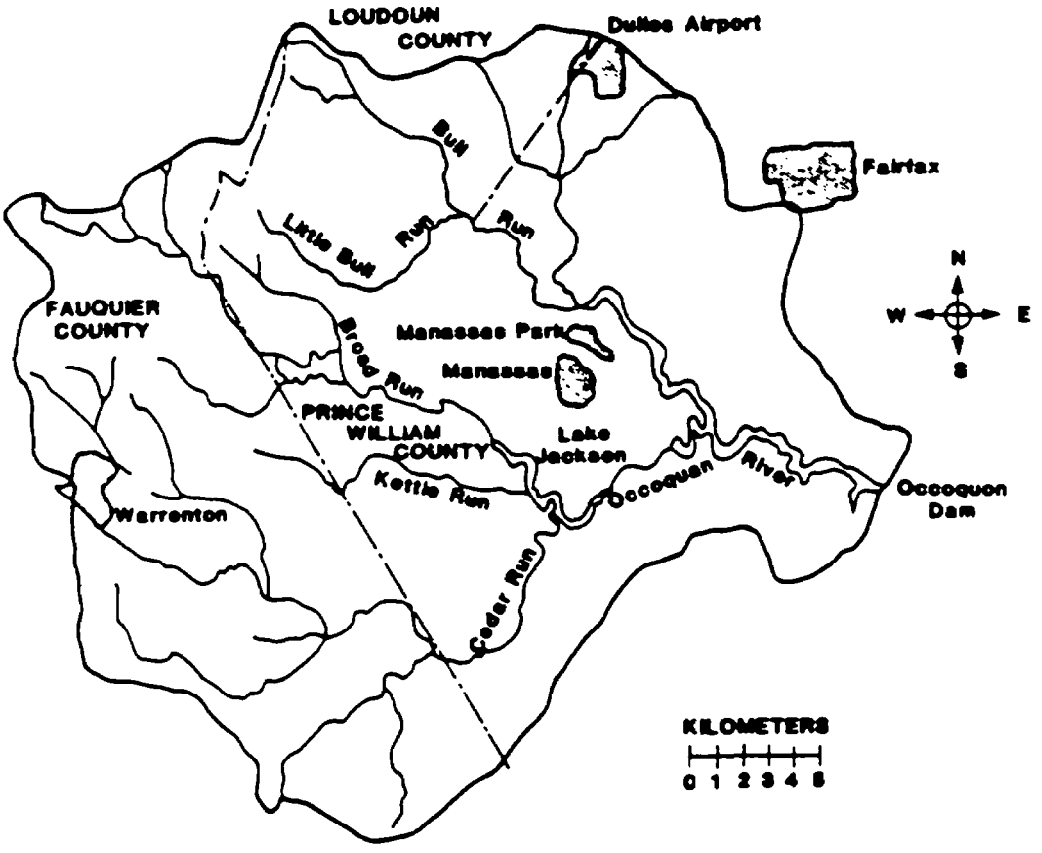

FIGURE V-36 THE OCCOQUAN RIVER BASIN

5.7.2 Stratification

Occoquan Reservoir is about 32 km southwest of Washington, D.C. and has the following morphometric characteristics:

Volume, m^3 = 3.71×10^7

Surface area, m^2 = 7.01×10^6

Maximum depth, m = 7.1 (Occoquan Dam)

Mean depth, m = 5.29

Based upon the above geometry and the thermal plots, determine whether the lake will stratify, the thickness of the epilimnion and the hypolimnion, the depth to the thermocline, and the interval and starting and ending date of stratification. Also note the temperature of the hypolimnion at the onset of stratification.

Predicting the extent of shielding from the wind requires use of topographic maps. The reservoir is situated among hills that rise 25 meters or more above the lake surface within 200 meters of the shore. The relief provides little access for wind to the lake surface. Average annual wind speeds are 15.6 km/hr in Washington, D.C. and 12.6 km/hr in Richmond, VA. Inflow comes essentially from two creeks, the

Occoquan River and Bull Run River (Figure V-35).

First, determine needed information and then do metric/English conversions as necessary.

The first step in assessing impoundment water quality is to determine whether the impoundment thermally stratifies. This requires knowledge of local climate, impoundment geometry, and inflow rates. Using this information, thermal plots likely to reflect conditions in the prototype are selected from Appendix D.

For the thermal plots to realistically describe the thermal behavior of the prototype, the plots must be selected for a locale climatically similar to that of the area under study. Because the Occoquan Reservoir is within 32 kilometers of Washington, D.C., the Washington thermal plots (Appendix D) should best reflect the climatic conditions of the Occoquan watershed.

The second criterion for selecting a set of thermal plots is the degree of wind stress on the reservoir. This is determined by evaluating the amount of protection from wind afforded the reservoir and estimating the intensity of the local winds. Table V-2 shows annual wind speed frequency distribution for Washington, D.C. and Richmond, Virginia. The data suggest that winds in the Occoquan area are of moderate intensity.

Predicting the extent of shielding from the wind requires use of topographic maps. The reservoir is situated among hills that rise 25 meters or more above the lake surface within 200 meters of the shore. The relief provides little access for wind to the lake surface. The combination of shielding and moderate winds implies that low wind stress plots are appropriate.

The geometry of the reservoir is the third criterion used in the selection of thermal plots. Geometric data for the Occoquan Reservoir are summarized in the problem. The volume, surface area, and maximum depth are all nearly midway between the parameter values used in the 40-foot and 75-foot maximum-depth plots. However, the mean depth is much closer to the mean depth of the 40-foot plot.

The mean depth represents the ratio of the volume of the impoundment to its surface area. Because the volume and surface area are proportional to the thermal capacity and heat transfer rates respectively, the mean depth should be useful in characterizing the thermal response of the impoundment. It follows that the 40-foot thermal profiles should match the temperatures in the Occoquan Reservoir more closely than the 75-foot profiles. However, it is desirable to use both plots in order to bracket the actual temperature.

Flow data provide the final information needed to determine which thermal plots should be used. The inflow from the two tributaries adds up to be 20.09 m^3/sec.

The hydraulic residence time can be estimated by using the expression:

$$\tau_w = \frac{V}{Q} = \frac{3.71 \times 10^7 \text{ m}^3}{20.09 \frac{\text{m}^3}{\text{sec}} \times 86400 \frac{\text{sec}}{\text{day}}} = 21.4 \text{ days}$$

Since the residence time is midway between the thermal plot parameter values of 10 and 30 days, both should be used to bracket the mean hydraulic residence time in the prototype. It should be noted that these flow estimates do not include runoff from the area immediately around the lake. However, the upstream Occoquan watershed is large enough relative to the immediate runoff and direct precipitation to justify the assumption that the contribution of the immediate area is not significant.

The likelihood that the Occoquan Reservoir thermally stratifies can now be evaluated. For a hydraulic residence time of ten days, the thermal plots show that stratification is not likely for maximum depths of 40 to 75 feet. In the case of a 30-day hydraulic residence time, the profiles suggest that the reservoir develops a thermal gradient between 1°C m^{-1} and 3°C m^{-1} for either value of maximum impoundment depth. The 40-foot plots (Figure V-37) indicate stratification occurs from May to August at 5-7 meters depth. However, the 75-foot plots predict that the impoundment will have a thermal gradient greater than 1°C m^{-1} only at depths greater than 17 meters. Since the Occoquan Reservoir is 17.1 meters deep at the deepest station, this suggests that the impoundment does not stratify.

The mean hydraulic residence time can be computed using either the average annual flow rate or the flow rate just prior to stratification. In order to use the latter method, the flow rate during the months of March and April should be computed. The flow rate for this period, 25.4 m^3 sec^{-1}, reduces the hydraulic retention time to 17 days. Since the model predicts no stratification for a ten-day residence time, the judgment as to whether stratification occurs becomes difficult.

Because lower flows occur during the summer, the 30-day residence time, 40 foot depth and minimum mixing should be used. In borderline cases such as this, the reservoir will almost certainly stratify during some part of the summer.

The temperatures predicted by the thermal plots match those actually measured in the reservoir quite closely. A comparison of predicted and observed monthly mean temperatures (1974-1976) in both the epilimnion and hypolimnion can be made using observed data (Table V-18) and the plot of the 40 foot, 30 day residence time, minimum mixing (Figure V-37). The difference between the two epilimnion temperatures averages 1.0°C and varies between 0.2 and 1.8°C. The difference in the hypolimnion temperatures averages 1.0°C and ranges from 0.2 to 2.7°C.

The close agreement of the predicted and observed impoundment temperatures probably results from the relatively long hydraulic residence times observed in two of the three years on which the averages are based. In 1974, 1975, and 1976, the mean hydraulic residence times were 31, 18, and 25 days, respectively. The 30-day

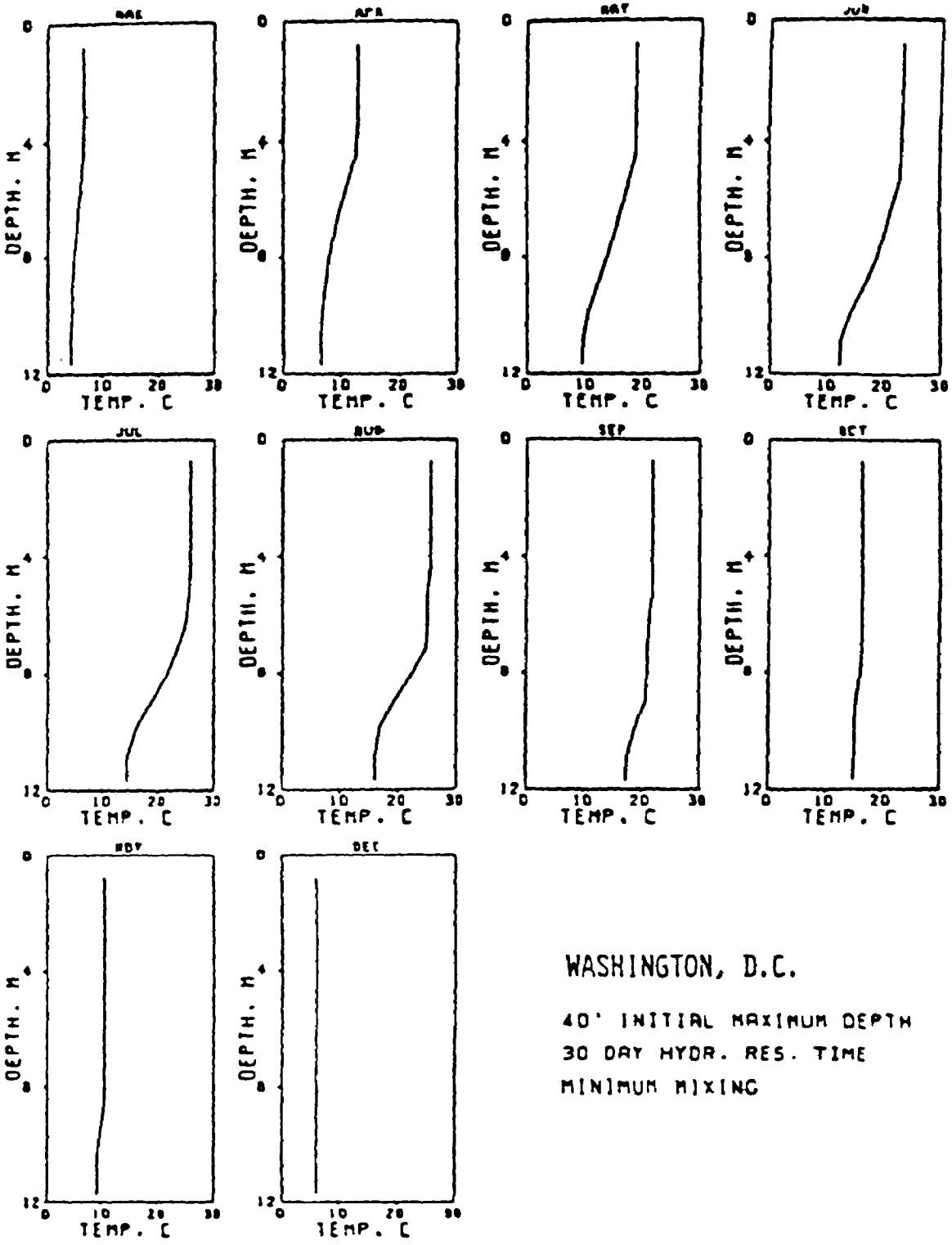

FIGURE V-37 THERMAL PROFILE PLOTS FOR OCCOQUAN RESERVOIR

TABLE V-18

COMPARISON OF MODELED THERMAL PROFILES TO OBSERVED TEMPERATURES IN OCCOQUAN RESERVOIR

Month	Mean Epilimnion Temp., °C		Mean Hypolimnion Temp., °C,		Epilimnion Depth (m)
	40-foot Plot[a]	Observed[c]	40-foot Plot[b]	Observed[c]	40-foot Plot[b]
March	7	8.4	6	6.3	--
April	13.5	12.6	10	9.2	--
May	19	20.5	15	14.4	4.5
June	24	24.8	18	17.2	5.0
July	26	26.6	20	21.2	6.5
August	26	26.5	21	23.7	7
September	22	23.8	20	20.2	--
October	17	17.2	16	15.8	--
November	11	12.2	10	11.6	--
December	7	6.2	7	5.8	--

Source: Northern Virginia Planning District Commission. January, 1979.

[a]Mean temperatures in epilimnion from thermal plots with τ_w = 30 days and a maximum depth of 40 feet.

[b]Mean temperatures in thermocline and hypolimnion from thermal plots with τ_w = 30 days and a maximum depth of 40 feet.

[c]Means of observed temperatures in "upper" and "lower" layers of Occoquan Reservoir for 1974-1976, at Sandy Run.

thermal plots should predict results relatively close to the two low-flow years. The differences expected for 1975 would be less pronounced when averaged with the other two.

In conclusion, Occoquan Reservoir does apparently stratify, the depth to the thermocline or the epilimnion approximates the mean depth (5.29), the hypolimnion has a depth of 11.8 m (17.1-5.3), and the interval of stratification approximates May 1 to mid September or 138 days. The hypolimnetic temperature is about 11 degrees C, typically.

5.7.3 Sedimentation

To evaluate potential sedimentation problems, Appendix F is examined to see if any data exist on the upstream reservoir (Jackson) or Occoquan Reservoir (Figure V-36). Some data exist for Jackson but not for Occoquan Reservoir (Figure V-38 taken

DATA SHEET NUMBER	RESERVOIR	STREAM	NEAREST TOWN	DRAINAGE AREA (SQUARE MILES) TOTAL	NET	DATE OF SURVEY	PERIOD BETWEEN SURVEYS (YEARS)	STORAGE CAPACITY (ACRE-FT)	CAPACITY AVG ANN INFLOW RATIO (ACRE FT PER ACRE FT)	SPECIFIC WEIGHT (DRY) (LB PER CU FT.)	AVG. ANN SEDIMENT ACCUMULATION PER SQ. MI. OF NET DR. AREA FOR PERIOD SHOWN AC.-FT.	TONS	AGENCY SUPPLYING DATA
						POTOMAC, RAPPAHANNOCK, YORK, AND JAMES RIVER BASINS							
5-1a	Lake Barcroft	Trib. of Potomac River	Falls Church, Va.	16.3	16.3	Jan. 1915	—	1/3,067	.162	--	—	—	SCS
	-do-	-do-	-do-	—	—	Feb. 1950	33.1	1/1,763	.136	60	.277	336	
	-do-	-do-	-do-	—	—	Aug. 1957	19.5	2/2,092	.166	—	.730	950	
5-2	Pedlar	Pedlar River	[illegible], Va.	33.71	33.07	Feb. 1907	—	1,860	—	—	—	—	SCS
	-do-	-do-	-do-	—	—	Feb. 1938	31	1,733	—	--	.136	—	
5-3	Burnt Mills	N. W. Br. Anacostia River	Silver Spring, Md.	27.0	26.97	May 1930	—	101	—	—	—	—	SCS
	-do-	-do-	-do-	—	—	Mar. 1938	7.8	99	—	60	.608	933	
5-4b	Greenbelt Lake	Trib. of Indian Creek	Greenbelt, Md.	10/.83	.79	July 1936	—	196	.313	—	—	—	SCS
	-do-	-do-	-do-	--	—	Feb. 1938	1.6	186	.296	60	7.98	10,337	
	-do-	-do-	-do-	--	—	Aug. 1957	19.5	152	.260	60	2.27	2,970	
	-do-	-do-	-do-	--	—	June 1968	10.0	11/167	.736	60	1.53	1,965	
5-5a	Staunton	North River	Staunton, Va.	25	25	Dec. 1925	—	385	—	—	—	—	SCS
	-do-	-do-	-do-	—	--	Jan. 1940	14	373	--	--	.036	—	
	-do-	-do-	-do-	—	--	June 1957	17.5	350	--	--	.053	—	
5-6	Jackson	Occoquan Creek	Manassas, Va.	337	330.6	July 1930	—	6,900	—	--	--	—	SCS
	-do-	-do-	-do-	—	--	Aug. 1937	7.2	6,150	—	60	.166	186	
5-7b	Triadelphia L. (Brighton D.)	Patuxent River	Brighton, Md.	81.6	80.0	Jan. 1943	—	13/20,222	.327	—	—	—	SCS
	-do-	-do-	-do-	--	—	Oct. 1950	8.3	20,089	.326	50	.20	210	
	-do-	-do-	-do-	—	--	Sept. 1958	7.9	19,633	.327	50	.72	786	
	-do-	-do-	-do-	--	—	Aug. 1964	5.9	19,065	.300	64.3	1.25	1,663	
5-8	Gordon Lake	Evitts Creek	Cumberland, Md.	66	15/6	Sept. 1913	—	3,129	—	—	—	—	SCS
	-do-	-do-	-do-	—	—	Apr. 1960	46.6	3,006	--	—	16/.040	—	
5-9	Thomas V. Koon Lake	-do-	-do-	60	59.6	Mar. 1932	—	7,367	—	—	--	—	SCS
	-do-	-do-	-do-	—	—	Apr. 1960	8.1	7,296	—	—	.036	—	
5-10	Savage River Dam	Savage River	Bloomington, Md.	105.0	104.66	Mar. 1952	--	20,300	.172	—	—	--	SCS
	-do-	-do-	-do-	—	—	Mar. 1958	6.0	20,020	.169	60	.463	840	
5-11	Rocky Gorge	Patuxent River	Laurel, Md.	132.0	50.16	Mar. 1954	—	23,300	—	—	—	—	SCS
	-do-	-do-	-do-	—	—	Aug. 1964	10.4	20,309	—	67	1.15	1,670	
5-12	South River, Site 26	Jack Branch	Waynesboro, Va.	2.2	2.2	May 1956	—	810.6	.20	—	—	—	SCS
	-do-	-do-	-do-	—	--	Nov. 1970	14.5	807.0	.20	60	.087	110	
5-13	Wilde Lake	Trib. Little Patuxent	Columbia, Md.	1.09	1.05	Sept. 1966	—	196.97	.160	--	—	--	SCS
	-do-	-do-	-do-	--	—	Aug. 1968	1.9	178.99	.172	60	15/7.986	18/11,270	
	-do-	-do-	-do-	--	—	Aug. 1969	1.0	163.77	.117	60	3.93	5,133	
						CHOWAN, ROANOKE, TAR, NEUSE, AND CAPE FEAR RIVER BASINS							
6-1	Lake Apex	Swift Creek	Apex, N. C.	6.0	6.0	— 1925	—	100	—	--	—	—	SCS
	-do-	-do-	-do-	—	—	June 1961	36	96	--	--	.19	—	
6-2	Franklinton	Little Cedar Creek	Franklinton, N. C.	1.13	1.12	Jan. 1925	—	36.7	—	—	—	—	SCS
	-do-	-do-	-do-	--	--	May 1938	13.3	27.3	—	67	.509	963	
6-3	Greensboro (L. Brandt)	Reedy Fork	Greensboro, N. C.	76.1	73.6	Feb. 1923	--	2,070	--	—	—	—	SCS
	-do-	-do-	-do-	—	--	Aug. 1934	11.5	2,610	—	60	.300	400	
6-4	High Point	Deep River	High Point, N. C.	62.0	62.3	Jan. 1928	--	6,354	--	--	—	—	SCS
	-do-	-do-	-do-	—	—	Aug. 1934	6.5	6,135	—	50.6	.541	595	
	-do-	-do-	-do-	—	--	Apr. 1938	3.75	6,038	--	—	.416	450	

1/ Includes estimated 112 acre-feet passing through Shenandoah Tunnel.
2/ Includes 101 acre-feet of sediment dredged in 1937-1939.
3/ Partial survey covering segments 1-16 in Strong Branch Arm Only.
4/ Net sediment contributing area was 299.6 sq. mi. until 1933 when Prettyboy Dam was completed. This area was used in the 1961 calculations.
5/ Revised after 1961 survey.
6/ Conservation or sediment pool only.
7/ Not determined - assumed equal to that determined in 1961.
8/ Based on original spillway crest elevation 204 feet m. s. l.
9/ Based on spillway crest elevation 210 feet m. s. l. and estimated capacity of 7,300 acre-feet resulting from 1963 addition to top of dam.

10/ Revised 1960.
11/ 9 acre-feet gained by dredging.
12/ Revised due to movable control gates.
13/ Koon Lake, upstream, was built in 1932.
14/ Based on total sediment in both Gordon Lake and Koon Lake.
15/ Does not include 6.36 acre-feet dredged.
16/ Includes 6.36 acre-feet dredged in early spring 1968.
18/ Estimated or assumed.

FIGURE V-38 SUMMARY OF RESERVOIR SEDIMENTATION SURVEYS MADE IN THE UNITED STATES THROUGH 1970

from Appendix F). Thus, we can determine the trapping of sediment in Jackson Reservoir but trapping must be calculated for the Occoquan. To refine the analysis, calculations on Jackson Reservoir will also be made and the results calibrated.

To apply the Stokes' law approach to a reservoir, we need to know the loading first. The necessary sediment loading estimates for the tributaries were provided by the methods in Chapter 3 and are listed in Table V-19 (Dean et al., 1980) Before they are used in further computations, a delivery factor must be applied to these values. This factor (the sediment delivery ratio or SDR) accounts for the fact that not all the sediment removed from the land surface actually reaches the watershed outlet. Nonpoint loads from urban sources are presumed to enter the reservoir through Bull Run River since most of the urbanized portion of the watershed lies in this sub-basin.

Computing the annual sediment load into Occoquan Reservoir is complicated by the presence of Lake Jackson immediately upstream from the reservoir. The trap efficiency must be computed for Lake Jackson as well in order to determine the amount of sediment entering the Occoquan Reservoir from Lake Jackson. The steps involved are to compute the sediment delivered (Table V-20), the size range, the fraction trapped for each size range and the total amount trapped. A table has been devised to simplify these steps (Table V-21).

Soil types provide an indication of the particle sizes in the basin under study. Soils in the Occoquan basin are predominately silt loams. Particle size data on the principal variety, Penn silt loam, are given in Table V-22. These data and all calculations are transcribed into Table V-23.

Some effort can be conserved by first calculating the smallest particle size that will be completely trapped in the impoundment. To do so, P, the trap efficiency, must first be computed. Because both reservoirs are long and narrow and have relatively small residence times, the flow will be assumed to approximate vertically mixed plug flow (Case B1). In this case, P is found from the expression:

$$P = \frac{V_{max}\,\tau_w}{D'}$$

where

D' = mean flowing layer depth, m.

To calculate the smallest particle that is trapped in the impoundment, P is set equal to unity and the above equation is solved for V_{max}:

$$V_{max} = \frac{D' \cdot 1.0}{\tau_w}$$

This expression for V_{max} is then substituted into the fall velocity equation (Stokes' law), which in turn is solved for d:

TABLE V-19

ANNUAL SEDIMENT AND POLLUTANT LOADS IN OCCOQUAN WATERSHED IN METRIC TONS PER YEAR[a]

Type of Load	Kettle Run	Cedar Run	Broad Run	Bull Run	Occoquan River	Urban Runoff
Sediment	46,898	396,312	142,241	232,103	139,685	12,699
Total Nitrogen	164.46	1,457.42	518.91	789.24	469.46	12.88
Available Nitrogen	16.45	145.74	51.89	78.92	46.05	5.38
Total Phosphorus	39.01	341.95	114.22	202.71	119.42	2.59
Available Phosphorus	2.18	14.95	5.57	12.50	8.43	1.27
BOD_5	328.92	2,925.63	1,042.45	1,578.47	925.85	77.47
Rainfall Nitrogen	0.72	5.50	2.00	3.92	2.48	-

[a] Estimates provided by Midwest Research Institutes Nonpoint Source Calculator. These values have not yet had a sediment delivery ratio (SDR) applied to them. We will use 0.1 and 0.2 as lower and upper bounds. The SDR does not apply to rainfall nitrogen.

Note: A large number of significant figures have been retained in these values to ensure the accuracy of later calculations.

TABLE V-20

SEDIMENT LOADED INTO LAKE JACKSON, 1,000 Kg/Year

Tributaries to Lake Jackson	Total Available Sediment	Sediment Delivered to Lake Jackson	
		Case I (SDR=0.1)	Case II (SDR=0.2)
Kettle Run	46,898	4,690	9,380
Cedar Run	396,312	39,630	79,260
Broad Run	142,241	14,220	28,440
Total		58,540	117,080

TABLE V-21

CALCULATION FORMAT FOR DETERMINING SEDIMENT ACCUMULATION IN RESERVOIRS (NOTE UNITS)

Size Fraction	Percent Composition	Density		Mean Particle Diameter	V_{max}	Fraction Trapped (P)		Test Case	Incoming Sediment	Trapped Sediment
		Absolute	Bulk			A	B			

TABLE V-22

PARTICLE SIZES IN PENN SILT LOAM

Particle Size (mm)	% of Particles Smaller Than (By Weight)
4.76	100
2.00	99
0.42	93
0.074	84
0.05	78
0.02	50
0.005	26
0.002	16

$$V_{max} = \frac{4.8 \times 10^6 (D_p - D_w) d^2}{\mu} = \frac{D'}{\tau_w}$$

The resulting expression is:

$$d = \sqrt{\frac{D' \mu}{4.8 \times 10^6 (D_p - D_w) \cdot \tau_w}}$$

The trap efficiency of Lake Jackson is calculated first. The data required for these calculations are:

$V = 1.893 \times 10^6 m^3$

$Q = 12.47\ m^3 sec$

$\bar{D} = 3.34\ m$

$\mu = 1.11$ (Assuming T = 16°C as in Occoquan Reservoir)

and $\tau_w = \frac{V}{Q} = \frac{1.893 \times 10^6\ m^3}{12.47\ m^3 \cdot sec^{-1} \cdot 86400\ sec \cdot day^{-1}} = 1.76$ days

The minimum particle size for 100 percent trapping is computed as:

$$d = \sqrt{\frac{3.34\ m \times 1.11}{4.8 \times 10^6 (2.66 - 1.0) \cdot 1.76}} = 5.14 \times 10^{-4}\ cm$$

TABLE V-23

CALCULATION FORMAT FOR DETERMINING SEDIMENT ACCUMULATION IN RESERVOIRS (NOTE UNITS)

Size Fraction	Percent Composition	Density		Mean Particle Diameter	V_{max}	Fraction Trapped (P)		Test Case		m ton/yr	
		Absolute	Bulk			A	B			Incoming Sediment	Trapped Sediment
cin					m/day						m^3/yr
.000514	0.3	2.66	2.24	N/A	1.90	N/A	1.00	I		176	176 79
								II		352	352 158
.00050	5	2.66	2.24	N/A	1.79	N/A	0.94	I		2927	2751 1228
								II		5854	5502 1356
.00035	5	2.66	2.24	N/A	0.88	N/A	0.46	I		2927	601
								II		5854	2582 1209
.00020	16	2.66	1.28	N/A	0.29	N/A	0.15	I		9366	1405 1098
								II		18732	2810 2196
>.000518	73.7	2.66	2.33 (average)	N/A	-	N/A	1.00	I		43144	43144 19000
								II		86288	86288 37000
					Totals Trapped			I	mtons/yr	48822	
								II	mtons/yr	97644	
								I	m^3/yr	21523	
								II	m^3/yr	43046	

Example Calculation

SDR = 0.115

Vol = 24750 m^3/yr

Vol of Jackson Reservoir last per year = $\frac{24750 m^3/yr}{1893000 m^3}$ = 1.3%/year

(75 yrs lifetime)

The amount trapped of each size fraction is computed separately for Case B-1 from the equation:

$$P = \frac{V_{max}\ \tau_w}{D'}$$

For example, for size fraction 0.00035 cm:

$$P = \frac{(0.88)(1.76)}{(3.34)} = 0.46$$

A composite trapping efficiency can be obtained by determining the total percent trapped (48822/58540 = 0.83).

The sediment accumulated in Lake Jackson for each size range is determined from the expression:

$$S_t = P \cdot S_i$$

where

P = trap efficiency

S_i = sediment load from tributary i

S_t = sediment trapped.

For the two cases (I, II):

S_t = (0.1, 0.1) x 0.83 [46898 + 132241] metric tons/year
= (48822, 97644) metric tons/year.

Data obtained from Appendix F of the screening manual show that the estimated rate of sedimentation in Lake Jackson is 56,153 metric tons/year. This indicates that an SDR of 0.115 would be appropriate.

Bulk density (g/cc) includes the water that fills pore spaces in sediment that has settled to the bottom and this must be accounted for when determining volume lost due to sedimentation. Bulk density varies with particle size and some approximate values for the size ranges for sand (0.005-0.2 cm), silt (0.0002-0.005 cm), and clay (<0.0002 cm) are as follows: 2.56 for sand, 2.24 for silt and 1.28 for clay. Thus, using an SDR of .115, 24,750 m^3 (or 1.3%) of reservoir volume would be lost per year. In comparing to Appendix F data, we find that this value is conservative. The loss of volume was estimated by the SCS to be 47.5 acre feet/year while these calculations show only 20 acre feet/year being lost. The estimated bulk density used by the SCS was 0.93 g/cc and we used a more conservative value. If the SCS figure is used, the volume lost is determined to be 46.4 acre feet/year.

Now we compute the sedimentation in Occoquan Reservoir. The minimum particle size that is completely trapped is computed using the following values:

D' = 5.29

μ = 1.11 (T = 16°C = mean of Table V-18)

$D_w = 2.66\ g\ cm^{-3}$

$D_w = 1.0\ g\ cm^{-3}$

$\tau_w = 21.4$ days.

Under stratified conditions, the epilimnion thickness should be used for D'. Since stratification is uncertain in this case and the predicted average hypolimnion thickness, 5.75 m, is greater than the mean depth, the latter value will be used. All particles with diameter, d, such that:

$$d = \sqrt{\frac{5.29 \times 1.11}{4.8 \times 10^6 (2.66 - 1.0) \cdot 21.4}} = 1.86 \times 10^{-4}\ cm$$

will be completely trapped in the Occoquan Reservoir. Because this value is smaller than the smallest size calculated for Lake Jackson (2×10^{-4} cm), our computations are simple. We assumed that 84 percent of the sediment is totally trapped and the remainder is trapped at an efficiency calculated for particle sizes of 0.0001 cm:

$$V_{max} = \frac{4.8 \times 10^6 (2.66 - 1.)(1 \times 10^{-4})^2}{1.11}$$

$$= 0.072\ m/day$$

$$P = \frac{V_{max} \tau_w}{D'} = \frac{0.072 \cdot 21.4}{5.29} = 0.29$$

The annual sediment trapped is:

$$S_t = P \cdot S_i$$

but corrections for sources and SDR must be made:

S_i = SDR x sediment from each source.

S_i = 13390 (Lake Jackson, already corrected for SDR) 0.115 (232103) (Bull Run) + 0.115 (139685) (Occoquan River) + 12699 (Urban Runoff

S_i = 68845 metric tons/year

Assuming the distribution of particle sizes for all sources are essentially the same and accounting for the fractions (f) of material that are in the two different size ranges:

$$S_i = f_1 P_1 S_i + f_2 P_2 S_i$$

$$S_t = (0.84)(1.0)(68845) + (0.16)(0.29)(68845)$$

S_t = 57830 ; 3194 = 61024 metric tons

The volume lost is $\frac{61024}{0.93} = 65620\ m^3$/year or 0.2 percent per year of the reservoir volume.

5.7.4 Eutrophication

What would be the consequences to eutrophication in Occoquan Reservoir of instituting 90 percent phosphorus removal at the treatment plant? If, in addition to

phosphorus removal, nonpoint source (NPS) phosphorus was reduced by 90 percent by instituting urban runoff and erosion control, green belts, and other NPS controls, would an improvement in lake quality occur?

Several assumptions concerning pollutants in the Occoquan watershed-reservoir system are necessary in order to calculate the desired annual loads:

- The unavailable phosphorus is adsorbed on sediment particles. Therefore, of the unavailable forms coming into Lake Jackson, only the fraction (1 - P_c [Jackson]) is delivered to the Occoquan Reservoir; available P gets through Jackson.
- All of the phosphorus and nitrogen from the sewage treatment plants (STPs) is in available form.
- The output of STPs outside the Bull Run sub-basin is negligible compared to that of the STPs in Bull Run. This is justified by the fact that during the period: under study, the plants in Bull Run had a combined capacity several times larger than the few plants outside the sub-basin.
- The problems of eutrophication depend on loading of phosphorus.

By applying these assumptions to the nonpoint source data in Tables V-19 and V-24 the total load of each pollutant type may be calculated (Table V-25). The computation for the total annual phosphorus load in Occoquan Reservoir is computed in the following paragraphs. First the quantity of total phosphorus coming into the Occoquan Reservoir through Lake Jackson is calculated by:

$$TP_{Jackson} = (1 - P_{c_{Jackson}}) \times [\text{Total P} - \text{Available P}] + \text{Available P}$$

The total phosphorus from Broad run, Cedar Run, and Kettle Run are summed and the available phosphorus loads are subtracted to give the unavailable load. This load is multiplied by the trap efficiency of the lake, $P_c = 0.83$, which yields the unavailable load passing through. This value, plus the available load, is an estimate of the total phosphorus entering Occoquan Reservoir from Lake Jackson. This quantity is 103.24 metric tons yr^{-1} (Table V-25). This value is added to the non-urban, nonpoint source loads from Bull Run and areas adjacent to the Occoquan Reservoir (Table V-18):

$$T_{NPNU} = 202.71 + 119.42 + 103.24$$
$$= 425.37 \text{ metric tons } yr^{-1}$$

This quantity is modified by the sediment delivery ratio. The urban nonpoint loads and STP (Table V-24) loads are added to complete the calculation:

$$TP = (0.115)\ (425) + 2.59 + 11.92$$
$$= 63.3 \text{ metric tons } yr^{-1}$$

Similarly the SDR was applied to nonpoint sources of nitrogen and BOD . The results of load calculations are summarized in Table V-25.

The calculated annual total phosphorus and nitrogen loads (Table V-25) may

TABLE V-24

SEWAGE TREATMENT PLANT POLLUTANT LOADS
IN BULL RUN SUB-BASIN IN METRIC TONS PER YEAR[a]

Total Nitrogen	Total Phosphorus	BOD_5
108.0	11.92	54.80

Source: Northern Virginia Planning District Commission, March 1979.
[a]Averages for July 1974 - December 1977

TABLE V-25

CALCULATED ANNUAL POLLUTANT LOADS TO OCCOQUAN RESERVOIR

	Metric Tons/Year				
Load Source	Total N	Avail.N	Total P	Avail.P	BOD_5
Urban runoff	12.38	5.38	2.59	1.27	77.47
Sewage treatment	108.00	108.00	11.92	11.92	54.80
Rainfall	14.62	14.62	-	-	-
Other Nonpoint Source*	391.00	39.10	48.83	2.65	802.00
TOTAL	526.50	167.10	63.34	15.84	934.27
Nonpoint Source %	80	35	81	25	94
Point Source %	20	65	19	75	6

* Used SDR of 0.115.

be compared with the observed loads listed in Table V-26. The loads observed are 1.5 to 6 times higher than highest calculated loads for nitrogen. Comparison of loadings (kg/ha year) with literature values suggest that Grizzard is most accurate (Likens et al., 1977).

The first method of predicting algal growth is known as the Vollenweider Relationship. In the graph of total phosphorus load (g m^{-2} yr^{-1}) versus mean

TABLE V-26

OBSERVED ANNUAL POLLUTANT LOADS TO OCCOQUAN RESERVOIR

Period	Mean Flow[a] Rate ($m^3\ sec^{-1}$)	Total Nitrogen Load (metric tons $year^{-1}$)	Total Phosphorus Load (metric tons $year^{-1}$)
10/74 - 9/75	24.7	805[b]	110[b]
7/75 - 6/76	24.0	1905[c]	188[c]
7/76 - 6/77	10.4	4763[c]	454[c]

[a] Source: USGS Regional Office, Richmond, Virginia.

[b] Grizzard et al., 1977

[c] Northern Virginia Planning District Commission, March, 1979. Data gathered by Occoquan Watershed Monitoring Laboratory.

depth (m) divided by hydraulic retention time (yrs) (see Figure V-24), areas can be defined that roughly correspond to the nutritional state of the impoundment. For the Occoquan Reservoir, the values of the parameters are:

$$L_p = \frac{(63.34) \times 10^6\ g/yr}{7.01 \times 10^6\ m^2} = 9.04\ g\ m^{-2}\ yr^{-1}$$

$$\frac{\bar{z}}{\tau_w} = \frac{5.29\ m}{0.0586\ yr} = 90\ m\ yr^{-1}$$

According to the Vollenweider Relationship, Occoquan Reservoir is well into the eutrophic region for loading of total phosphorus. Based on these predictions a more in-depth study of the algal productivity seems to be in order.

Solving for the phosphorus concentration in this reservoir:

$$P = \frac{L_p}{\bar{z}} \frac{1}{D+\sqrt{D}} = \frac{9.04\ g\ m^{-2}\ yr^{-1}}{5.29m[(17.1+\sqrt{17.1})yr^{-1}]}$$

$$P = 0.0305\ g/m^3 = 80.5\ \mu g/l.$$

Calculated and observed pollutant concentrations are listed in Table V-27. The mean summer concentrations of phosphorus and nitrogen are closer to the concentrations calculated than would be expected on the basis of the comparison of annual loads.

TABLE V-27

CALCULATED AND OBSERVED MEAN ANNUAL POLLUTANT CONCENTRATIONS IN OCCOQUAN RESERVOIR

	Total Nitrogen[b] ($g\ m^{-3}$)	Available Nitrogen[a] ($g\ m^{-3}$)	Total Phosphorus ($g\ m^{-3}$)
Calculated (SDR = 0.115)	0.831	0.264	0.08
Observed Values[a]			
Mean	0.88	0.16	0.08
Max.	1.50	0.24	0.12
Min.	0.35	0.10	0.04

a Assuming no removal processes for nitrogen.
b Averages for April-October between 1973 and 1977.
Source: Northern Virginia Planning District Commission, March, 1979.

The ratio of nitrogen to phosphorus concentration in the reservoir can be used to estimate which nutrient will limit the rate of plant growth. For the Occoquan Reservoir, the N:P ratios are 10 to 1 for total N to total P. The calculated nutrient ratios and the N:P ratio of the observed data (11.0) indicates that phosphorus is probably growth limiting.

The available data also permits the estimation of the maximal primary production of algae from the Chiaudani and Vighi Curve (Figure V-26). The theoretical phosphorus concentration should be about 0.08 g m according to calculations. The maximal primary production of algae is found from Figure V-26 to be about 2500 mgC m^{-2} day^{-1}. This level of algal production is roughly the maximum production shown on the curve. Both this result and the Vollenweider Relationship suggest algal growth will contribute significantly to the BOD load in the impoundment.

Effects of 90 percent P removal at treatment plant on TP loading:

$M = 52.61$ m ton/yr

$$L = \frac{52.61 \times 10^6 \text{ g/yr}}{7.01 \times 10^6 \text{ m}^2} = 7.50 \text{ g m}^{-2} \text{y}^{-1}$$

$q_s = 90 \text{ m yr}^{-1}$

Although improved, we conclude that loading is still too great according to Figure V-24.

Effects of 90 percent STP removal of TP plus 90 percent NPS removal of TP:

$$M = 6.334 \text{ m ton/yr}$$

$$L_p = \frac{6.334 \times 10^6}{7.01 \times 10^6} = 0.90 \text{ g m}^{-2} \text{ y}^{-1}$$

This would move Occoquan Reservoir into the bottom of the mesotrophic range.

Lake concentrations of total P would be:

$$P = \frac{(7.5)}{(5.29) \cdot (21.2)} = 66.9 \text{ µg/l}$$

$$P = \frac{0.90}{(5.19) \cdot (21.2)} = 8 \text{ µg/l}$$

Although the screening method shows marked improvement in Occoquan eutrophication, 90 percent control of phosphorus NPS would be very expensive. Careful analysis of assumptions made in the screening method and of control alternatives would be necessary before proceeding to map such a control strategy. Moreover, careful study of reservoir TP sources and sinks and of algal productivity would be necessary. The screening method has served to illustrate the feasibility and potential value of such further analysis.

5.7.5 Hypolimnetic DO Depletion

Excessive nutrient loading plus inputs of BODs suggest that DO problems in the hypolimnion could result. We will use the data obtained in the first three problems to determine the hypolimnetic DO. These data are summarized below. All rate coefficients listed have already been corrected for temperature.

Physical/Biological

Area = $7.01 \times 10^6 m^2$

Volume = $3.71 \times 10^7 m^3$

Q = $20.09 \text{ m}^3 \text{ sec}^{-1} = 1.74 \times 10^6 m^3 \text{ day}^{-1}$

Depth to thermocline = 5.29 m (average depth)

Interval of stratification (May to mid-September) = 138 days

BOD loading = $934.27 \ 10^6 g \cdot yr^{-1}$

Algal loading = $1800 \text{ mgCm}^{-2} \text{ day}^{-1}$

BOD concentration = $\frac{934.27 \times 10^6 \text{ g/yr}}{3.71 \times 10 \text{ m} \times 365 \text{ days/yr}} = 0.069 \text{ mg/l}$

Temperature = 10°C

Rates and Input Values

M	= 0.8	k_1	= 0.063 day^{-1}
S	= 2.67	k	= 0.0378 day^{-1}
P	= $0.824 \text{ gC m}^{-2} \text{ day}^{-1}$	k_4	= 0.0019 day^{-1}
$\bar{D}$	= 5.29 m	DO_{sat}	= 11.3 mg/l
τ_w	= 21.4 day	t	= 138

The simplified model used to predict hypolimnion dissolved oxygen levels assumes that the only substantial dissolved oxygen sinks are water column and benthic deposit BOD (Section 5.5). Additionally, all sources of oxygen, photosynthesis, etc., are neglected in the hypolimnion after the onset of stratification. Thus, the procedure requires that pre-stratification levels of BOD and dissolved oxygen be estimated in order to compute the post-stratification rates of oxygen disappearance. The pre-stratification concentration of water column BOD is determined first. A simple mass balance leads to the following relationship, if steady state conditions are assumed:

$$C_{ss} = -\frac{k_a}{k_b}$$

where

C_{ss} = steady state concentration of BOD in water column, mg/l^{-1}

k_a = mean rate of BOD loading from all sources $g\ m^{-3}\ day^{-1}$

$k_b = -k_s - k_1 - \frac{1}{\tau_w}$

where

$k_s = V_s/\bar{Z}$ = mean rate of BOD settling out onto impoundment bottom, day^{-1}

k_1 = mean rate of decay of water column BOD, day^{-1}

Q = mean export flow rate, $m^3\ day^{-1}$

V = impoundment volume, m^3

V_s = settling velocity, $m\ day^{-1}$

$\bar{Z}$ = impoundment mean depth, m.

The BOD load to the impoundment originates in two principal sources: algal growth and tributary loads. The algal BOD loading rate is computed from the expression:

$$k_{a(algae)} = SMP/\bar{Z}$$

where

S = stoichiometric conversion from algal biomass as carbon to BOD = 2.67

M = proportion of algal biomass expressed as oxygen demand

P = algal primary production, $g\ m^{-2}$ day.

Since the Chiaudani and Vighi curve (Figure V-26) gives the maximal algal production, a correction should be made for the actual epilimnion temperature. If the maximal rate occurs at 30°C and the productivity decreases by half for each 15°C decrease in temperature, the algal production can be corrected for temperature using the expression:

$$P_{(T)} = P_{(30)} \times 1.047^{(T-30°C)}$$

According to the data in Table 1, the epilimnion temperature during the month prior to stratification is approximately 13°C. Thus:

$$P_{(13°)} = (1.8)\ gC\ m^{-2}\ day^{-1} \times 1.047^{(13°C-30°C)}$$
$$= 0.824\ gC\ m^{-2}\ day^{-1}$$

If M is assumed to be 0.8, then:

$$k_{a(algae)} = \frac{2.67 \times 0.8 \times 0.824 \text{ gC m}^{-2} \text{ day}^{-1}}{5.293 \text{ m}}$$

$$= 0.333 \text{ g m}^{-3} \text{ day}^{-1}$$

The BOD load borne by tributaries is found by the expression:

$$k_{a(trib)} = \frac{\text{Mean Daily BOD from Tributaries (Table V-18)}}{\text{Impoundment Volume}}$$

$$= \frac{034.27 \times 10^{6} \text{ g yr}^{-1}}{3.71 \times 10^{7} \text{m}^{3}} \times \frac{1 \text{ yr}}{365 \text{ days}}$$

$$= 0.069 \text{ g m}^{-3} \text{ day}$$

The total BOD load to Occoquan Reservoir is then:

$$k_a = k_a(\text{algae}) + k_a(\text{trib})$$

$$= 0.33 \text{ g m}^{-3} \text{ day}^{-1} + 0.069 \text{ g m}^{-3} \text{ day}^{-1}$$

$$= 0.402 \text{ g m}^{-3} \text{ day}^{-1}$$

Before the water column BOD concentration can be computed, the constants comprising k_b must be evaluated. The first of these, k_s, requires knowledge of the settling velocities of BOD particles. Ideally these would be determined by using values of the physical properties of the particles and the water in the settling velocity equation, V-6. Because such data are lacking, a settling velocity of 0.2 m day^{-1} reported for detritus will be substituted. The reported values lie between 0 and 2 meters day^{-1}, with most values close to 0.2 m day^{-1} (Zison et al., 1978). Then:

$$k_s = 0.2 \text{ m day}^{-1}/5.29 \text{ m} = 0.0378 \text{ day}^{-1}$$

The second constant comprising k_b is the first-order decay rate constant for water column BOD. Reported values of k_1 vary widely depending on the degree of waste treatement. Zison et al. (1978)[1] presents data for rivers, but contains only two values for k_1 in lakes and estuaries. Both are $k_1 = 0.2 \text{ day}^{-1}$. Camp (1968) reports values from 0.01 for slowly metabolized industrial wastes to 0.3 for raw sewage. Because there is considerable sewage discharge into the Occoquan Reservoir, k_1 may be assumed to be in the upper range of these values, between 0.1 and 0.3 or 0.15 day^{-1}. Like the algal production rate, k_1 must be corrected for the water temperature. In April, the mean water temperature is about 11°C. Then:

$$k = 0.095 \text{ day}^{-1} \times 1.047^{(11°C-20°C)}$$

$$= 0.063 \text{ day}^{-1}$$

Finally, k_b is evaluated as follows:

$$k_b = -0.0378 \text{ day}^{-1} - 0.063 \text{ day}^{-1} - \frac{1}{21.4 \text{ days}}$$

$$= -0.148 \text{ day}^{-1}$$

Next, k_a and k_b may be substituted into the following equation to obtain C_{ss}.

$$C_{ss} = -\frac{k_a}{k_b}$$

$$= \frac{0.402}{0.148} = 2.72 \text{ g m}^{-3}$$

Once the water column BOD concentration is known, the benthic BOD is computed from the expression:

$$L_{ss} = \frac{k_s C_{ss} \overline{D}}{k_4}$$

where

k_4 = mean rate of benthic BOD decay, day^{-1}

Values for the benthic BOD decay rate constant span a greater range than those for water column BOD. Camp (1968), however, reports values of k_4 very near 0.003 day^{-1} for a range of benthic depth from 1.42 to 10.2 cm (Table V-10). Assuming this to be a good value, a temperature-corrected value of k_4 may be computed at an April hypolimnion temperature of 10°C (Table V-18):

$$k_4 = 0.003 \text{ day}^{-1} \times 1.047^{(10-20)} = 0.0019 \text{ day}^{-1}$$

Then:

$$L_{ss} = \frac{0.0378 \text{ day}^{-1} \times 2.72 \text{ g m}^{-3} \times 5.29 \text{ m}}{0.0019 \text{ day}^{-1}}$$

$$= 286 \text{ g m}^{-2}$$

Prior to stratification the impoundment is assumed to be fully mixed and saturated with oxygen. During April, the hypolimnion temperature is 10°C. Saturated water at this temperature contains 11.3 ppm oxygen (Table V-12).

Finally, the dissolved oxygen level in the hypolimnion may be predicted during the period of stratification. The applicable expressions are:

$$\Delta O_L = \overset{A}{(1.04)} \left[\overset{B}{(53.1)} \overset{C}{(0.231)} - \overset{E}{(1/53.1)}\right] \overset{B}{}$$

$$\Delta O_L = 12.74$$

$$\Delta O_c = \overset{F}{(1.7)} \overset{E}{(1)} = 1.7$$

$$O_t = 11.3 - 12.74 - 1.7$$

Therefore the hypolimnion is depleted of oxygen at the end of the stratification period (138 days). By selecting different conditions for decay rates and for time of stratification a family of curves was generated that can be compared with actual observations (Figure V-39). As can be seen situations 3 and 4 (BOD decay of 0.3 later corrected for temperature and a total BOD loading of 0.36 or 0.57 g · m^{-3} day^{-1}) gave a reasonable fit of observed data at the deepest station (Occoquan Dam, 1973).

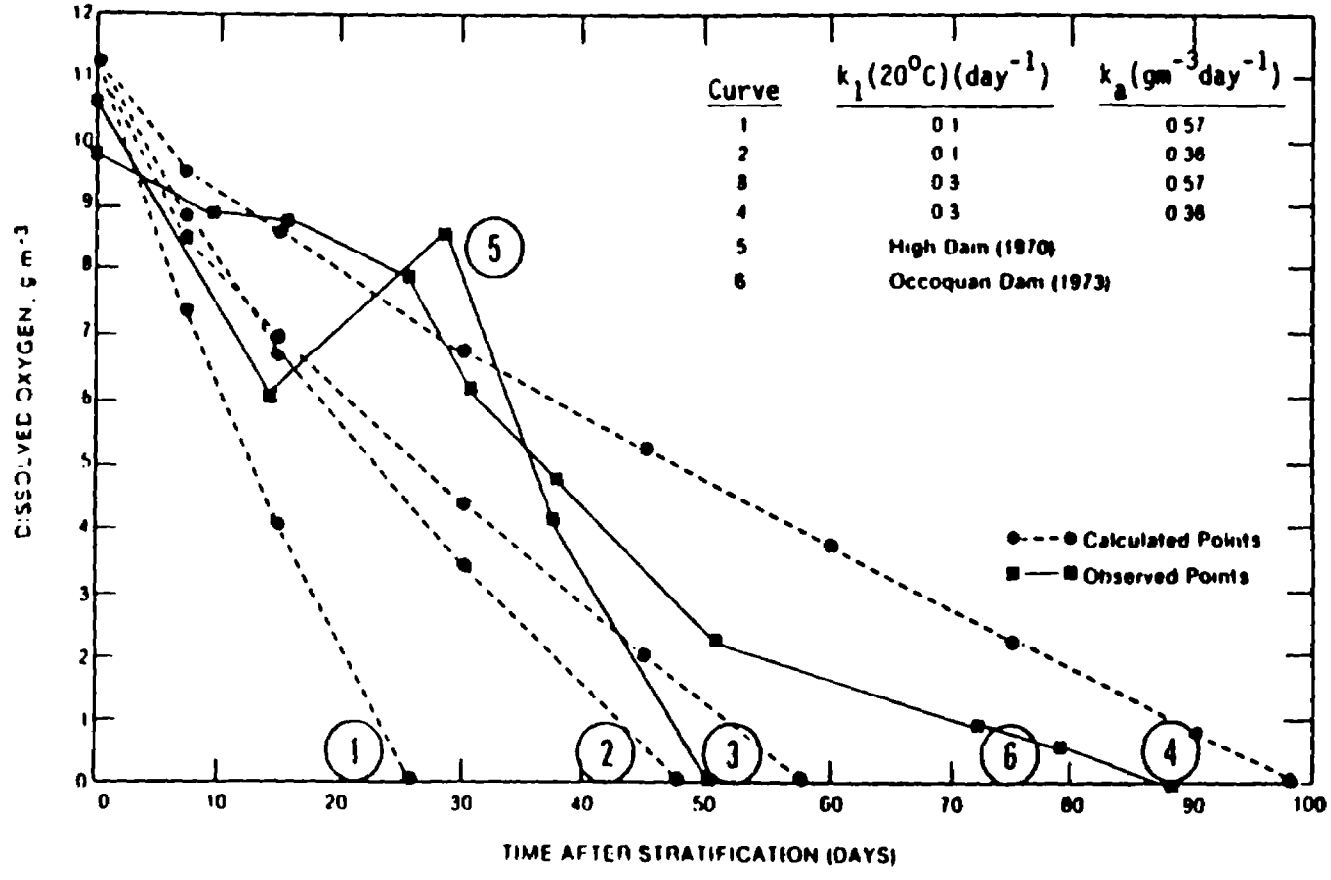

FIGURE V-39 DISSOLVED OXYGEN DEPLETION VERSUS TIME IN THE OCCOQUAN RESERVOIR

Interpretation of the dissolved oxygen-time data at High Dam in 1970 presented in Figure V-39 is complicated by the introduction of fresh oxygen after the onset of stratification. Although a direct comparison of oxygen depletion times is not possible, the rates of oxygen level follows curve 2 of Figure V-39 very closely, while during the second period of oxygen consumption the oxygen concentrations closely match those of curve 1. Since the reservoir is shallowest at High Dam and the substantially lower than average flow rate in 1970 resulted in strongly stratified conditions, the oxygen depletion rates in this case should be among the highest likely to be observed in the impoundment. Curve 1 represents the fastest decay rates predicted by the model. Thus, the observed oxygen consumption times should be greater than the lower limit predicted by the model in nearly all cases.

The above agreement of the observed with the predicted limits for the range of oxygen depletion times in Occoquan Reservoir implies that the typical or average time must also fall within the predicted range. Since it was for "average" conditions that the impoundment was modeled, it may be concluded that the model does accurately describe the behavior of the Occoquan Reservoir.

5.7.6 Toxicants

It was not possible to obtain data on toxicants in Occoquan Reservoir. In order to provide a problem with some realism, published data on a priority pollutant in another reservoir were obtained. In Coralville Reservoir, Iowa, commercial fishing was banned in 1976 because of excessive accumulation of dieldrin residues in flesh of commercially important bottom feeding fish (Schnoor, 1981). The dieldrin arose from biodegraded aldrin, an insecticide in wide use along with dieldrin before cancellation of registration of both pesticides by USEPA in 1975.

After 1976 there was steady diminution of dieldrin in the waters, fish, and bottom sediments of Coralville Reservoir, until the late 1970's when dieldrin levels in fish flesh declined to less than 0.3 mg/kg (Food & Drug Administration guideline). In 1979, the fishing ban was rescinded.

Using the screening methods and data abstracted from Schnoor's paper, the potential dieldrin problem can be evaluated in Coralville Reservoir. Available and back-calculated data include the following values:

Reservoir		Dieldrin	
τ_w	= 14 days = 336 hrs	kow	= 305000
$\bar{Z}$	= 8 feet = 2.4 m	koc	= 35600
C	= 0.05 µg/l dieldrin	solubility in fresh water	≅ 200 µg/l
OC	= 0.05 (estimate)		
So	= 200 µg/l (estimate)		
	= 200×10^{-6} kg/kg		
P	= 0.9 (estimate)		

Assuming that conditions remained constant, the steady state concentration of dieldrin can be computed using the approach described in Section 5.6 as follows:

$$C = C_{in} / (1 + \tau_w \cdot k)$$

where

$$K = SED + B + k_v + k_p + k_h$$

Evaluation of K depends on estimation of the separate rate constants. Information in Chapter 2 and in Callahan, et al. (1977) indicate that the biodegradation rate (B) in aquatic systems is extremely small. Similarly volatilization (k_v) and hydroloysis (k_h) are negligible processes affecting the fate of dieldrin. Photolysis (k_p) can be significant in some circumstances but the high turbidity in Coralville Reservoir indicates that minimal photolysis takes place. Consequently, K ≅ SED. These assumptions are supported by Schnoor (1981).

Calculation of the sedimentation rate constant (SED) is as follows:

$$SED = a \times D \times K_p$$

$$k_p = 0.63 \times kow \times OC$$
$$= 0.63 \times 305000 \times 0.05$$
$$= 9610$$

$$D = P \times 50 \times \frac{1}{\tau_w}$$

$$D = 0.9 \times 200 \times 10^{-6} \times \frac{1}{336} = 5.36 \times 10^{-6} m^{-1}$$

$$a = 1/ (1 + k_p S)$$

$$S = OC \times 50 = .05 \times 200 \times 10^{-6} = 1 \times 10^{-5}$$

$$a = 0.912 \times 5.36 \times 10^{-5} \times 9610$$
$$= 0.0047\ m^{-1}$$

The steady state concentration of dieldrin in Coralville Reservoir is estimated to be:

$$C = 0.05\ \mu g/l\ (1 + (0.0047\ hr^{-1} \times 336\ hr))$$

$$C = 0.019\ \mu g/l$$

This value is much greater than the present fresh water quality criteria of 0.0023 dieldrin µg/l (Federal Register: 79318-79379. Nov. 28, 1980) and would indicate a serious potential problem in the reservoir that would require significant action and study.

Evaluation of bioconcentration supports this conclusion:

$$Y = BCF \times C$$

If the default estimate is used (Section 5.6.1.6):

$$\log BCF = 0.75 \log KOW - 0.23$$
$$= 3.88$$

$$BCF = 7642$$

$$Y = 7642 \times 0.019 = 145\ \mu g/kg\ fish\ flesh$$

This value would be less than the FDA guideline. However, two published BCF values are available: 35600 from Chapter 2; 70000 from Schnoor (1981). These values produce much higher tissue burdens, both of which violate the FDA guideline:

$Y = 35600 \times 0.019 = 676\ \mu g/kg$

$Y = 70000 \times 0.019 = 1330\ \mu g/kg$

In 1979, it is estimated that $C_{in} = 0.01$ (calculated from Schnoor, 1981). Therefore, assuming other conditions are constant:

$C = 0.01/ (1 + (.0047 \times 336))$

$= 0.0039\ \mu g/l$

A value about double the water quality criterion. Flesh concentration would be (using BCF = 70000):

$Y = 70000 \times 0.0039 = 270\ \mu g/kg$

This value (0.27 µg/kg) would be less than the FDA guidelines of 0.3 µg/kg and support the conclusion to lift the fishing ban. Schnoor (1981) shows the following measured data that can be compared to the screening results:

	1970		1979	
	Water	Fish	Water	Fish
Screening	0.019	1300	0.04	270
Measured	0.015	1100	0.005	250

REFERENCES

Callahan, M., M. Slimak, N. Gabel, I. May, C. Fowler, R. Freed, P. Jennings, R. Durfee, F. Whitmore, B. Maestri, W. Mabey, B. Holt, C. Gould. 1979. Water-Related Environmental Fate of 129 Priority Pollutants, Volumes 1 and 2. U.S. Environmental Protection Agency Report. EPA 440/4-79-029a, b. NTIS Reports: PB80 204373, PB80 204381.

Camp, T.R. 1968. Water and Its Impurities. Reinhold Book Corporation, New York.

Carlson, R.E. 1977. A Trophic State Index for Lakes. Limnol. Oceanogr. 22:361-369.

Chen, C.W., and G.T. Orlob. 1973. Ecologic Study of Lake Koocanusa Libby Dam. U.S. Army Corps of Engineers, Seattle District.

Chiaudani, G., and M. Vighi. 1974. The N:P Ration and Tests with Selenastrum to Predict Eutrophication in Lakes. Water Research 8:1063-1069.

Cowen, W.F., and G.F. Lee. 1976. Phosphorus Availability in Particulate Materials Transported by Urban Runoff. JWPCF 48:580-591.

Dean, J.D., R.J.M. Hudson, and W.B. Mills. 1979. Chesapeake-Sandusky: Non-designated 208 Screening Methodology Demonstration. Midwest Research Institute, Kansas City, MO. U.S. Environmental Protection Agency Rept. for Env. Res. Lab, Athens, GA. In Press.

Dillon, P. 1974. A Manual for Calculating the Capacity of a Lake for Development. Ontario Ministry of the Environment.

Dillon, P., and F. Rigler. 1975. Journal Fisheries Research Board of Canada 32(9).

Dorich, R.A., D.W. Nelson, and L.E. Sommers. 1980. Algal Availability of Sediment Phosphorus in Drainage Water of the Black Creek Watershed. J. Environ. Qual. 9:557-563.

Drury, D.D., D.B. Porcella, and R.A. Gearheart. 1975. The Effects of Artificial Destratification on the Water Quality and Microbial Populations of Hyrum Reservoir. PRJEW011-1. Utah State University, Logan, UT.

Grizzard, T.J., J.P. Hartigan, C.W. Randall, J.I. Kim, A.S. Librach, and M. Derewianka. 1977. Characterizing Runoff Pollution-Land Use. Presented at MSDGC-AMSA Workshop, Chicago. VPISU, Blacksburg, VA. 66 pp.

Hudson, R.J.M., and D.B. Porcella, 1980. Selected Organic Consent Decree Chemicals: Addendum to Water Quality Assessment, A Screening Method for Non-designated 208 areas. U.S. Environmental Protection Agency Rept. for Env. Res. Lab, Athens, GA. In Press.

Hutchinson, G.E. 1957. A Treatise on Limnology, Volume I. John Wiley & Sons, New York. 1015 pp.

Hydrologic Engineering Center (HEC), Corps of Engineers. 1974. Water Quality for River-Reservoir Systems. U.S. Army Corp of Engineers.

Jones, J.R., and R.W. Bachmann. 1976. Prediction of Phosphorus and Chlorophyll Levels in Lakes. JWPCF 48:2176-2182.

Larsen, D.P., and K.W. Malueg. 1981. Whatever Became of Shagawa Lake? In: International Symposium on Inland Waters and Lake Restoration. U.S. Environmental Protection Agency. Washington, D.C. p. 67-72. EPA 440/5-81-010.

Larsen, D.P., and H.T. Mercier. 1976. Phosphorus Retention Capacity of Lakes. J. Fish. Res. Board Can. 33:1731-1750.

Likens, G.E. et al. 1977. Biogeochemistry of a Forested Ecosystem. Springer-Verlog, New York. 146 pp.

Linsley, R.K., M.A. Kohler, and J.H. Paulhus. 1958. Hydrology for Engineers. McGraw-Hill, New York.

Lorenzen, M.W. 1978. Phosphorus Models and Eutrophication. In press.

Lorenzen, M.W. 1980. Use of Chlorophyll-Secchi Disk Relationships. Limnol. Oceanogr. 25:371-3727.

Lorenzen, M.W., and A. Fast. 1976. A guide to Aeration/Circulation Techniques for Lake Management. For U.S. Environmental Protection Agency, Corvallis, OR.

Lorenzen, M.W. et al. 1976. Long-Term Phosphorus Model for Lakes: Application to Lake Washington. In: Modeling Biochemical Processes in Aquatic Ecosystems. Ann Arbor Science, Ann Arbor, MI. pp. 75-91.

Lund, J. 1971. Water Treatment and Examination 19:332-358.

Marsh, P.S. 1975. Siltation Rates and Life Expectancies of Small Headwater Reservoirs in Montana. Report No. 65, Montana University Joint Water Resources Research Center.

Megard, R.O., J.C. Settles, H.A. Boyer, and W.S. Combs, Jr. 1980. Light, Secchi Disks, and Trophic States. Limnol. Oceanogr. 25:373-377.

Porcella, D.B., S.A. Peterson, and D.P. Larson. 1980. An Index to Evaluate Lake Restoration. Journal Environmental Engineering Division ASCE 106:1151-1169.

Rast, W., and G.F. Lee. 1978. Summary Analysis of the North American (US Portion) OECD Eutrophication Project. U.S. Environmental Protection Agency, Corvallis, OR. 454 pp. EPA-600/3-78-008.

Sakamoto, M. 1966. Archives of Hydrobiology 62:1-28.

Schnoor, J.L. 1981. Fate and Transport of Dieldrin in Coralville Reservoir: Residues in Fish and Water Following a Pesticide Ban. Science 211:804-842.

Smith, V.H., and J. Shapiro. 1981. Chlorophyll-Phosphorus Relations in Individual Lakes: Their Importance to Lake Restoration Strategies. Env. Sci. and Tech. 15:444-451.

Stumm, W., and J.J. Morgan. 1970. Aquatic Chemistry. Wiley-Interscience, New York.

Vollenweider, R.A. 1976. Advances in Defining Critical Loading Levels for Phosphorus in Lake Eutrophication. Mem. Ist. Ital. Idrobiol. 33:53-83.

Vollenweider, R.A., and J.J. Kerekes. 1981. Background and Summary Results of the OECD Cooperative Program on Eutrophication. In: International Symposium on Inland Waters and Lake Restoration. U.S. Environmental Protection Agency, Washington, D.C. p. 25-36. EPA 440/5-81-010.

U.S. Department of Commerce. 1974. Climatic Atlas of the United States. U.S. Department of Commerce, Environmental Sciences Services Administration, Environmental Data Service, Washington, D.C.

U.S. Environmental Protection Agency. 1975. National Water Quality Inventory, Report to Congress. EPA-440/9-75-014.

Zison, S.W., W.B. Mills, D. Deimer, and C.W. Chen. 1978. Rates, Constants, and Kinetics Formulations in Surface Water Quality Modeling. U.S. Environmental Protection Agency, Athens, GA. 316 pp. EPA-600/3-78-105.

GLOSSARY OF TERMS

Significant variables are shown with typical units. Units must be compatible or use conversion factors (Chapter 1). Note that some symbols are used for more than one term.

A	Lake surface area, m^2 - sediment area, m^2
a	Fraction of pollutant in solution = $1/(1+K_p \times S)$), unitless
B	Biodegradation rate, hr^{-1}
B(T)	Biodegradation rate, corrected for temperature T, hr^{-1}
BCF	Bioconcentration factor, unitless
Bo	Initial microbial biodegradation rate, uncorrected for temperature or nutrient concentration, hr^{-1}
C	Reservoir concentration at time, t, mgl^{-1}
C_o	Initial concentration, mgl^{-1}
C_p	Concentration of phosphorus, μgPl^{-1}
C_s	Total exchangeable phosphorus concentration in the sediments, g m^{-3}
C_s	Toxicant concentration sorbed on sediment, mg l^{-1}
C_t	Concentration of BOD at time t, mg l^{-1}
C_w	Concentration in water phase, mg l^{-1}
C_w	Steady-state water column phosphorus concentration, mg l^{-1}, gm^{-3}
C_{in}	Steady state influent concentration, mg/l
C_{ss}	Steady-state water column BOD, g m^{-3}
C_{wt}	Weight concentration
C_{vol}	Volumetric concentration
D	Depth, m
D	Discharge channel depth, ft
D	Sedimentation rate constant = P x S x Q/V, mg $l^{-1}day^{-1}$
D	Dilution rate, day^{-1}
D'	Flowing layer depth, ft
D"	Inflow channel depth, ft
$\bar{D}$	Mean depth, m
$\bar{D}$	Depth to thermocline, m
D_h	Mean hypolimnion depth, m
D_i	Depth at the ith cross-section, m
Do	Diffusivity of oxygen in water (2.1×10^{-9} m^2 sec^{-1}, 20°C)
D_p	Weight density of a particle, lb ft^{-3}
D_w	Weight density of water, lb ft^{-3}, g cm^{-3}
D_w	Pollutant diffusivity in water, m^2 sec^{-1}
d	Number of days per time period, days
d	Particle diameter, cm

f	$1 + (\tau_w \times K)$, unitless)
g	Acceleration due to gravity, 32.2 ft sec^{-2}
I_{SD}	Intensity of light at Secchi depth, relative units
I_o	Initial intensity of light at surface, relative units
K	Pollutant removal rate, = SED + B + k_v + k_p + k_h, hr^{-1}
K	Net rate of phosphorus removal, hr^{-1}
K_1	Specific rate of phosphorus transfer to the sediments, m yr^{-1}
K_2	Specific rate of phosphorus transfer from the sediments, m yr^{-1}
K_3	Fraction of total phosphorus input to sediment that is available for the exchange process, unitless
K_a	Reaeration rate, hr^{-1}
Ka_1	Reaeration coefficient, m hr^{-1}
K_p	Distribution coefficient between organic sediment and water, unitless
K_1	First order decay rate for water column BOD at 20°C, day^{-1}
K_4	Benthic BOD decay rate at 20°C, day^{-1}
K_a	Mean rate of BOD loading from all sources, g $m^{-3}day^{-1}$
$K_{a(algae)}$	Algal contribution to BOD loading rate, g $m^{-3}day^{-1}$
$K_{a(trib)}$	Tributary or point source contribution to BOD loading rate, g $m^{-3}day^{-1}$
K_b	$= -K_s - K_1 - (1/\tau_w)$, day^{-1}
k_e	Extinction coefficient, m^{-1}
k_h	Hydrolysis rate, hr^{-1}
k_p	Photolysis rate, hr^{-1}
k_r	Photolysis rate constant uncorrected for depth and turbidity of the lake, m^{-1}
k_s	Mean rate of BOD settling out onto the impoundment bottom, day^{-1}
k_v	Volatilization rate, hr^{-1}
koc	Organic carbon based partition coefficient, unitless
kow	Octanol-water coefficient, unitless
L	Areal BOD load, gm^{-2}
L_p	Phosphorus loading, g $m^{-2}yr^{-1}$
L_{ss}	Steady-state benthic BOD load, g m^{-2}
M	Total annual phosphorus loading, g yr^{-1}
M	Proportion of algal biomass expressed as an oxygen demand (unitless)
MW	Molecular weight, g $mole^{-1}$
OC	Sediment organic carbon fraction, unitless
ΔO_c	Dissolved oxygen decrease due to hypolimnion BOD, mg l^{-1}
ΔO_L	Dissolved oxygen decrease due to benthic demand, mg l^{-1}

O_o	Dissolved oxygen at time t = 0, mg l^{-1}
O_t	Dissolved oxygen at time t, mg l^{-1}
p	Sediment trapping efficiency, unitless $1 \geq P \geq 0$
P	Primary productivity rate, g Carbon m^{-2} day^{-1}
P	Total phosphorus in the water column, mg m^{-3}
PI	Influent phosphorus, mg l^{-1}
QI	Mean annual inflow, m^3 yr^{-1}
Q	Mean annual outflow, m^3 yr^{-1}
q_s	Hydraulic loading $(\bar{Z}/\tau_w)$, m yr^{-1}
R	Reynolds number, unitless
r	Radius, ft
S	Stoichiometric conversion from algal biomass as carbon to BOD, 2.67, unitless
S	Input suspended organic sediment = OC x So, mg l^{-1}
S_i	Mass of sediment in inflow per unit time, mg l^{-1}
S_o	Input of suspended sediment, mg l^{-1}
S_t	Sediment trapped, metric tons yr^{-1}
SD	Secchi depth, m
SDR	Sediment delivery ratio, unitless
SED	Sorption and sedimentation rate (toxicant at equilibrium with sediments), hr^{-1}
T	Temperature, degrees centrigrade
V	Lake or impoundment volume, m^3
V_H	Hypolimnion volume, l
V_s	Sediment volume, m^3
V_{max}	Terminal velocity of a spherical particle, ft sec^{-1}
W	Wind speed, m sec^{-1}
Y	Tissue concentration of pollutant, g kg^{-1} fish flesh
y	Number of years
Z	Depth, m
$\bar{Z}$	Mean depth, m
μ	Absolute viscoscity of water, lb sec ft^{-2}, g sec cm^{-2}
ρ_p	Mass density of a particle, slugs ft^{-3}
ρ_w	Mass density of water, slugs ft^{-3}
τ_w	Mean hydraulic residence time (V/Q), days

CHAPTER 6

ESTUARIES

6.1 INTRODUCTION

6.1.1 General

Estuaries are of primary social, economic, and ecologic importance to America. Forty-three of 110 of the Department of Commerce's Standard Metropolitan Statistical Areas are on estuaries (DeFalco, 1967). Estuaries are the terminal or transfer point for essentially all waterborne national and international commerce in this country, and biologically are more productive on a mass per unit area basis than any other type of water body. Essentially all conservative wastes and much of the nonconservative wastes discharged into any inland stream in America eventually pass into an estuary. Yet these coastal formations on which there is such a demand for services are less stable geologically than any other formation found on the continent (Schubel, 1971). Sedimentation processes, for example, are filling, destroying, or at least altering all estuaries. While this process is always rapid in a geological sense, the actual length of time required for complete estuarine sedimentation is a function primarily of the stability of the sea level, the rate of sediment influx, and the intra-estuarine circulation pattern (Schubel, 1971). The instability, variation, and complexity of estuaries make water quality assessment and prediction especially difficult, yet the demands placed on estuaries require a most active water quality management program.

This chapter will describe a systematic approach which may be used to provide estuarine water quality assessment and prediction. Its purpose is two-fold. First, the planner will be provided the capability of making elementary assessments of current estuarine water quality. Second, methodologies are presented by which the planner can evaluate changes in water quality which might result from future changes in waste loading.

Chapter 3 provided methodologies for assessing the waste load directly entering an estuary. Chapter 4 provided methodologies which can be used to assess the water quality of a river or stream as it enters an estuary. The output of these chapters will provide information about present and projected estuarine water quality which can be used to identify regions having greatest water quality problems, water quality parameters of special concern, and areas for which subsequent computer study is necessary. Methods presented below comprise a screening tool which may be used by the planner to focus attention on critical spatial regions and water quality parameters. These can then be fully assessed using computer models or other techniques, as desired.

6.1.2 Estuarine Definition

It is difficult to provide a concise, comprehensive definition of an estuary. The basic elements included in most current definitions are that an estuary is:

- o A semi-enclosed coastal body of water
- o Freely connected to the open sea
- o Influenced by tidal action
- o A water body in which sea water is measurably diluted with fresh water derived from land drainage (Pritchard, 1967; Pritchard and Schubel, 1971).

The seaward end of an estuary is established by the requirement that an estuary be semi-enclosed. Because this boundary is normally defined by physical land features, it can be specifically identified. The landward boundary is not as easily defined, however. Generally tidal influence in a river system extends further inland than does salt intrusion. Thus the estuary is limited by the requirement that both salt and fresh water be measurably present. Accordingly, the landward boundary may be defined as the furthest measurable inland penetration of sea salts. The location of this inland boundary will vary susbstantially from season to season as a function of stream flows and stream velocities and may be many miles upstream from the estuarine mouth (e.g., approximately 40 miles upstream on the Potomac River, 27 miles on the James River, and approximately 16 miles upstream for the small Alsea Estuary in Oregon) (Pritchard, 1971). This definition also separates estuaries from coastal bays (embayments) by the requirement for a fresh water inflow and measurable sea water dilution.

6.1.3 Types of Estuaries

While the above definition provides adequate criteria for segregating estuaries from other major types of water bodies, it does not provide a means to separate the various types of estuaries from one another. The variations in estuarine circulation patterns and resulting variations in pollution dispersion from estuary to estuary make classification a necessary part of any water quality assessment. Two basic estuarine classification systems have been used in recent years to accomplish estuarine subclass separation: a topographical system and a physical processes system (Dyer, 1973, Chapter 2 or Ippen, 1966, Chapter 10).

6.1.3.1 Topographical Classification

Under a topographical system, estuaries are divided into four subclasses. These are briefly described below.

- • Drowned River Valley (Coastal Plain Estuary). These estuaries are the result of a recent (within the last 10,000 years) sea level rise

which has kept ahead of sedimentation processes at a river's mouth. Such estuaries are, quite literally, rivers whose lower basins have been drowned by the rising oceans. Coastal plain estuaries are characteristically broad, relatively shallow estuaries (rarely over 30 m deep) with extensive layers of recent sediment.

- Fjord-like Estuaries. These estuaries are usually glacially formed and are extremely deep (up to 800 m) with shallow sills at the estuarine mouth. Fjord-like estuaries are restricted to high latitude mountainous regions and are not found in the United States outside of Alaska and Puget Sound in the state of Washington.
- Bar-built Estuaries. When offshore barrier sand islands build above sea level and form a chain between headlands broken by one or more inlets, a bar-built estuary is formed. These estuaries are characteristically very shallow, elongated, parallel to the coast, and frequently are fed by more than one river system. As a result bar-built estuaries are usually very complex hydrodynamically. A number of examples of bar-built estuaries can be found along the southeast coast of the United States.
- Tectonic Process Estuaries. Tectonic estuaries exist as the result of major tectonic events (movement of tectonic plates with associated faulting or subsidence and coastal volcanic activity). San Francisco Bay is a good example of an American estuary of this type.

Based on this topographic classification system, the vast majority of American estuaries fall into the drowned river class. As a result, this system is not functional for categorization of American estuaries. The classification system described below is based on physical processes and is more useful. Further, the parameters used in physical classification are directly applicable to estuarine pollution analysis. Consequently, a physical parameter classification system will be used for the water quality assessment approach to be presented.

6.1.3.2 Physical Process Classification

Physical process classification systems are generally based on the velocity and salinity patterns in an estuary. Using these two parameters, estuaries can be divided into three classes, each of which is of potential importance to planners concerned with American coastal plain estuaries. The classes are: stratified, partially mixed, and well mixed.

The general behavior of salinity and velocity regimes in the three types of estuaries has been described by a number of researchers (Glenne, 1967, Duxbury, 1970, Pritchard, 1960, and Dyer, 1973, among others) and is summarized below:

- Stratified (Salt Wedge) Estuary. In this type of estuary, large fresh water inflows ride over a salt water layer which intrudes landward

along the estuary bottom. Generally there is a continuous inland flow in the salt water layer as some of this salt water is entrained into the upper seaward-moving fresh water flow. Tidal action is not sufficient to mix the separate layers. Salinity (S) and Velocity (U) profiles and a longitudinal schematic of this flow pattern are shown in Figure VI-1. The Mississippi River Estuary is usually a salt wedge estuary.

- Well Mixed. In a well mixed estuary, the tidal flow (or the tidal prism*) is much greater than the river outflow. Tidal mixing forces create a vertically well mixed water column with flow reversing from ebb to flood at all depths. Typical salinity and velocity profiles and a longitudinal flow schematic for a well mixed estuary are shown in Figure VI-2. As examples, the Delaware and Raritan River estuaries are both normally well mixed.
- Partially Mixed. Partially mixed estuaries lie between stratified and well mixed in terms of flow and stratification characteristics. Tide-related flows in such estuaries are substantially greater than river flows. Significant salinity gradients exist as in fully stratified estuaries, but are much less steep. While velocity at all depths normally reverses with ebb and flood tide stages, it is possible for net inland flow to be maintained in the lowest layers. Typical salinity and velocity profiles and a longitudinal schematic flow diagram are shown in Figure VI-3. There are many partially mixed coastal plain estuaries in the United States; the lower James River Estuary is typical.

Classification primarily depends on the river discharge at the time of classification. Large river flows result in more stratified estuaries while low flow conditions in the same estuaries can lead to full mixing. Thus the classification of any single estuary is likely to vary from season to season as river flows vary. As examples, many West Coast estuaries are partially mixed in winter when river flows are high and are well mixed in summer when river flows are very low.

6.1.4 Pollutant Flow in an Estuary

The importance of understanding the basic types of estuarine systems may be appreciated by briefly reviewing the general advective movements of a pollutant released into each of the three types of estuaries (summarized from Pritchard, 1960). The associated spatial and temporal variability of pollutant levels have water system management as well as water quality implications.

If a pollutant flow of density greater than the receiving water column is introduced into a salt wedge type estuary, the pollutant tends to sink into the

*The tidal prism is that volume of water which enters an estuary during an incoming (flood) tide and equals high tide estuarine volume minus low tide volume.

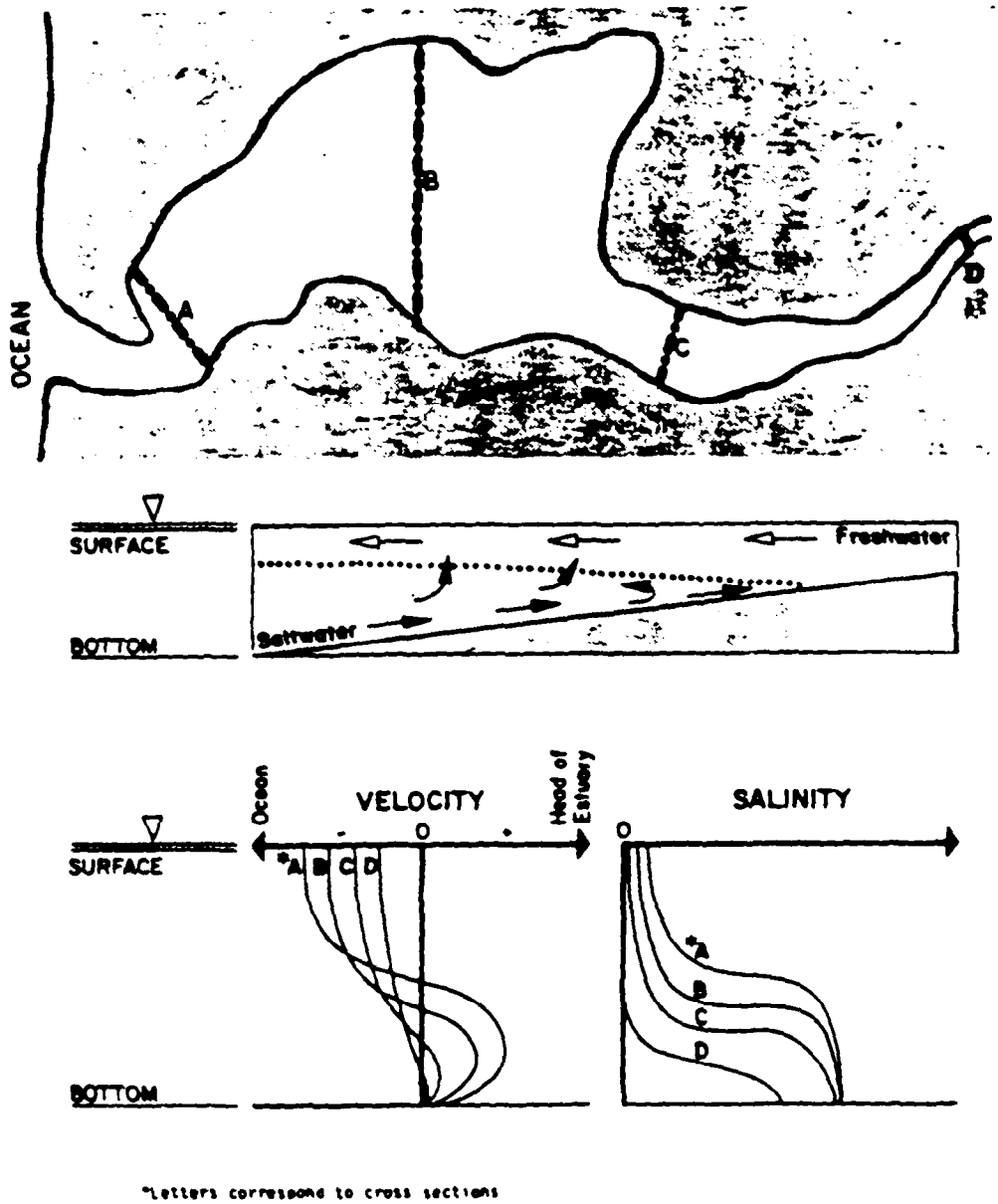

*Letters correspond to cross sections

FIGURE VI-1 TYPICAL MAIN CHANNEL SALINITY AND VELOCITY FOR STRATIFIED ESTUARIES

bottom salt water layer and a portion can be advectively carried inland toward the head of the estuary. Frictionally induced vertical entrainment of the pollutant into the surface water flow is slow, residence time of the pollutant is high, and the time required to flush the pollutant from the estuary is also high. Some pollutants which are sufficiently dense and stable remain in or settle to the bottom layer of water, and are not transported out of a salt wedge estuary. Such constituents build up in the estuarine sediment layer.

Conversely, if a pollutant of lower density than the receiving water column is introduced into a salt wedge estuary, it remains in the surface layer and is readily

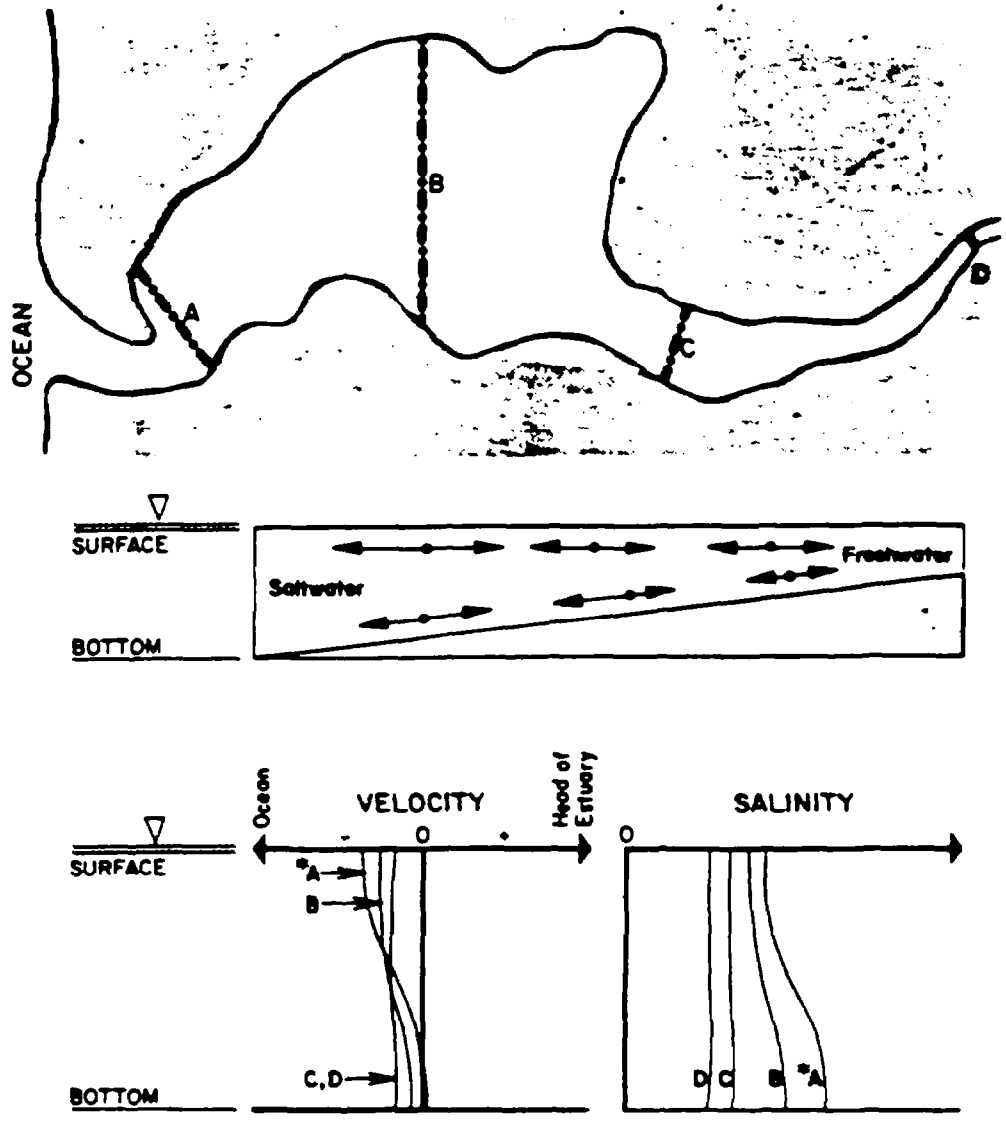

*Letters correspond to channel cross-sections.

FIGURE VI-2 TYPICAL MAIN CHANNEL SALINITY AND VELOCITY PROFILES FOR WELL MIXED ESTUARIES

flushed from the system. This is the case because seaward flows strongly predominate in this layer.

At the opposite end of the estuary classification scale, a pollutant introduced into a well mixed estuary is advectively transported in a manner independent of the pollutant's density. Tidal forces cause turbulent vertical and lateral mixing. The pollutant is carried back and forth with the oscillatory motion of the tides and is slowly carried seaward with the net flow.

Pollutants introduced into partially mixed estuaries are dispersed in a manner

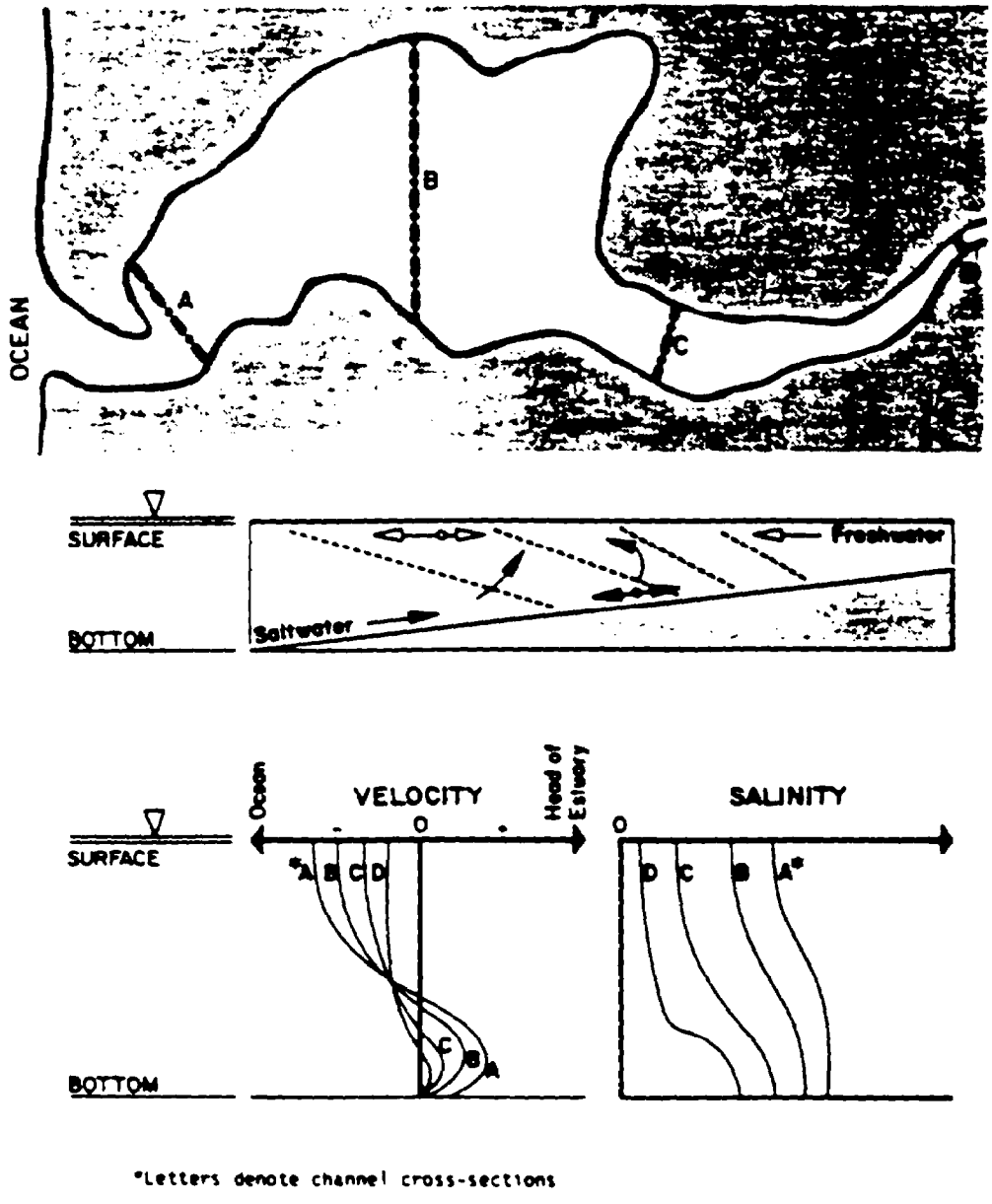

*Letters denote channel cross-sections

FIGURE VI-3 TYPICAL MAIN CHANNEL SALINITY AND VELOCITY PROFILES FOR PARTIALLY MIXED ESTUARIES

intermediate between the transport patterns exhibited in well mixed and stratified estuaries. Pollutant transport is density dependent but nevertheless involves considerable vertical mixing. Eventual flushing of the pollutant from an estuary in this case depends on the relative magnitudes of the net river outflow and the tidal seawater inflow.

6.1.5 Estuarine Complexity and Major Forces

Before outlining the complexities of estuarine systems, a brief review of the nomenclature used in this chapter will be helpful. This information is shown in Figure VI-4. This figure shows top, side, and cross sectional views of an estuary and indicates the basic estuarine dimensions. Additionally, the relationship between tidal elevation (or tidal stage) and surface water velocity is shown in the upper right quadrant of Figure VI-4.

The complexities of estuarine hydrodynamics are evident from even the brief qualitative descriptions presented above. Many variations in flow pattern and many of the forces acting on an estuarine water column have been omitted in order to permit a verbal description of the normally predominant phenomena, and it should be understood that the descriptions do not fully account for the complexities of estuarine motion. Estuarine circulation may be conceived as a three-dimensional flow field with variations possible in salinity and velocity along the longitudinal, the vertical, and the lateral axes. As a result of this complexity, and because an estuary is a transitional zone between fresh water and marine systems, great variations in a number of major water quality and physical parameters are possible. For example:

- pH. Typical concern pH is 7.8 to 8.4. Typically, rivers are slightly acidic (pH<7). Thus the pH can change from slightly acidic to basic across an estuary with resulting major changes in chemical characteristics of dissolved and suspended constituents. pH variations from 6.8 to 9.25 across an estuary have been recorded (Perkins, 1974, p. 29).
- Salinity. Over the length of an estuary, salinity varies from fresh water levels (typically less than 1 ppt) to oceanic salinity levels (usually 32 ppt to 34 ppt)*. Moreover, salinity at any given location in an estuary may vary substantially over one tidal cycle and over the depth of the water column at any single point in time. Salinity variations are especially significant in estuarine calculations for a variety of reasons. First, salinity distribution can be used to predict the distribution of pollutants; second, salinity is a prime determinant of water density; and third, variations in salinity affect other major water quality parameters. For example, the saturated dissolved oxygen concentration normally diminishes by 2 mg/l as salinity increases from 0 to 35 ppt.
- River Flow. River flow is a major determinant of estuarine circulation and flushing characteristics. Instantaneous flow rates for some western rivers vary by orders of magnitude from winter high flow to summer low flow periods (Goodwin, et al., 1970). These differences in river flow result in major variations in estuarine water quality characteristics.

*ppt represents parts per thousand by mass. Sometimes the symbol $^{o}/_{oo}$ is used.

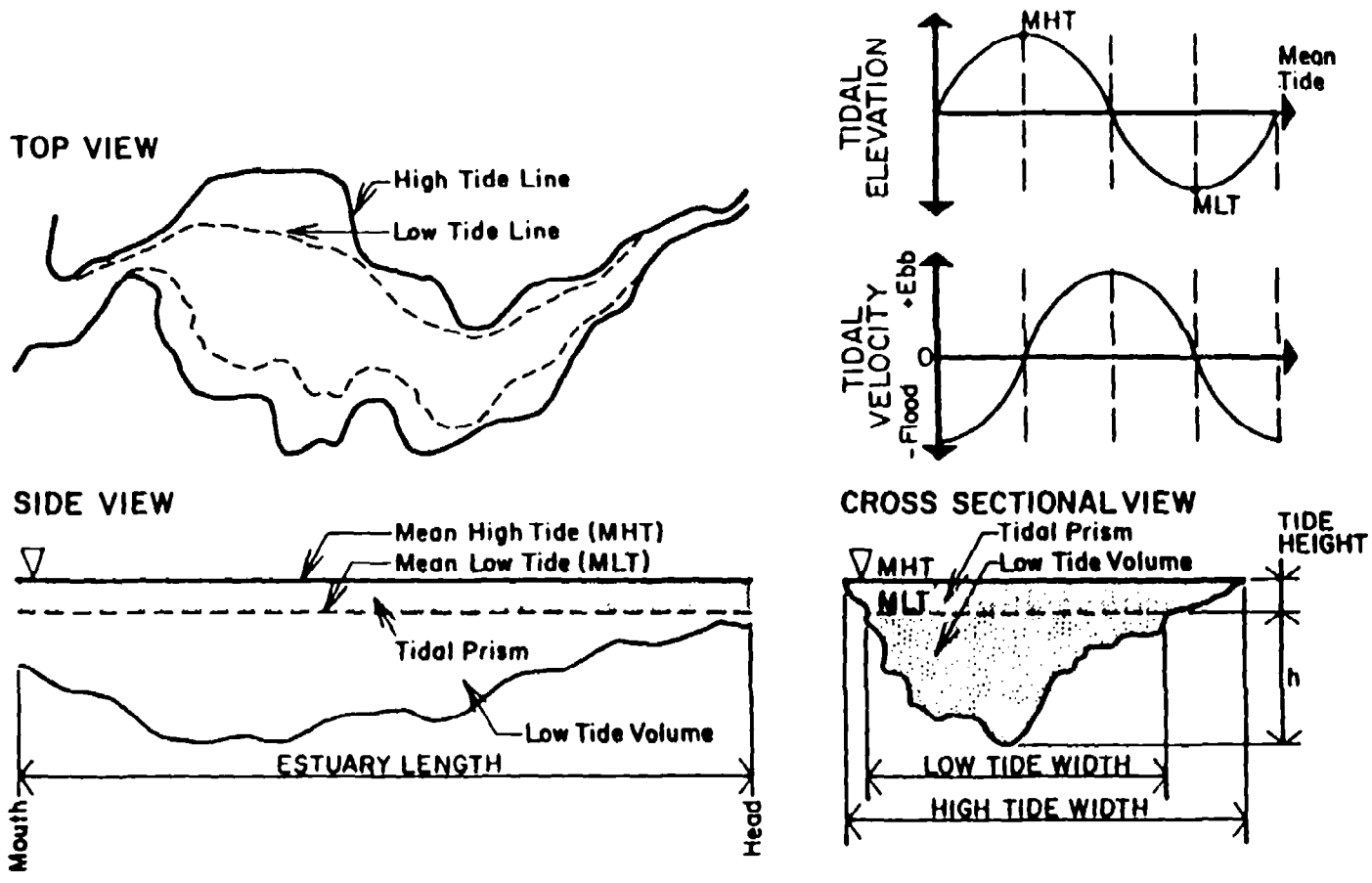

FIGURE VI-4 ESTUARINE DIMENSIONAL DEFINITION

- Time. Estuarine water quality parameters vary over several separate time scales. First, variations occur with each tidal cycle over a period of hours. Second, tidal cycles vary in mean amplitude from spring (maximum amplitude) to neap tides (minimum amplitude) every two weeks. This affects water quality since flushing characteristics are in part dependent on the tidal prism which is, in turn, dependent on tide stage. Third, there are seasonal variations in river flow, temperature and waste loadings.

The four factors just listed affecting the range and rate of variation of estuarine parameters pose part of the difficulty in analyzing estuarine water quality. In order to avoid large errors, both small time increments and small spatial increments must be used. This, in turn, necessitates a large number of individual calculations to fully analyze the variation of even a single parameter over the estuary and sometimes requires the use of a computer model.

Further complicating the analytical process is the large number of independent forces acting on the estuarine water column which should be considered. This group includes (from Harleman and Lee, 1969):

- Ocean tides
- Local wind stresses
- Bottom roughness and bottom sediment types
- Channel geometry
- Coriolis forces*
- Nearby coastal features and coastal processes.

6.1.6 Methodology Summary

A variety of techniques are presented in this chapter to assess water quality in estuaries. Table VI-1 summarizes the techniques and indicates if they are applicable to one-dimensional (well-mixed) or two-dimensional (vertically stratified) estuaries. Many of the techniques can be applied to conventional or toxic pollutants. If decay rates for toxic pollutants are needed, Chapter 2 can be used.

It is redundant to describe in detail each method at this point in the chapter, because the procedures are presented later. As a general statement, however, most of the methods for prediction of water quality apply to continuous, steady-state discharges of pollutants. The discharges can be located anywhere within the estuary,

*Coriolis forces reflect the effect of a rotating reference plane (the earth) on particle motion. The net effect is to cause a water flow to drift to one side as it moves down a channel. The same effect tends to laterally segregate fresh water flows (moving from head to mouth) and salt water inflows (moving from mouth to head) in an estuary and in the northern hemisphere to create a counterclockwise flow pattern with fresh water to the right (looking from the head of the estuary toward the mouth) flowing toward the sea and salt water on the left flowing toward the head of the estuary.

TABLE VI-1

SUMMARY OF METHODOLOGY FOR ESTUARINE WATER QUALITY ASSESSMENT

Calculations	Methods	Type of Estuary Applicable*
Estuarine Classification	• Hansen and Rattray	one- or two-dimensional
	• Flow ratio	one- or two-dimensional
Flushing Time	• Fraction of freshwater	one-dimensional
	• Modified tidal prism	one-dimensional
Pollutant Distribution	• Fraction of freshwater (conservative pollutants)†	one-dimensional
	• Modified tidal prism (conservative or first-order decay pollutants)†	one-dimensional
	• Dispersion-advection equations (conservative, first-order decay pollutants,† and dissolved oxygen)	one-dimensional
	• Pritchard's Box Model (conservative pollutants)†	two-dimensional
	• Initial dilution	one- or two-dimensional
	• Pollutant concentration at completion of initial dilution (conservative pollutants,† pH, dissolved oxygen)	one- or two-dimensional
	• Farfield distribution (conservative and first-order pollutants,† and dissolved oxygen)	two-dimensional
Thermal Pollution	• ΔT of water passing through condenser	not applicable
	• Maximum discharge temperature	not applicable
	• Thermal block criterion	one- or two-dimensional
	• Surface area criterion	one- or two-dimensional
	• Surface temperature criterion	one- or two-dimensional
Turbidity	• Turbidity at completion of initial dilution	one- or two-dimensional
	• Suspended solids at the completion of initial dilution	one- or two-dimensional
	• Light attenuation and turbidity relationship	one- or two-dimensional
	• Secchi disk and turbidity relationship	one- or two-dimensional
Sedimentation	• Description of sediment movement	one- or two-dimensional
	• Settling velocity determination	one- or two-dimensional
	• Null zone calculations	two-dimensional

*One dimensional means a vertically well mixed system. A two dimensional estuary is vertically stratified.
†These methods apply to either conventional or toxic pollutants.

from head to mouth. Multiple sources of pollutants can be analyzed by applying the method of superposition, which is illustrated subsequently.

Although no single sequence of calculations must be followed to use the methodology, Figure VI-5 shows a suggested procedure. It is often useful to begin by classifying the estuary by season to find out when it is well mixed and when it is stratified. If the estuary is never well mixed, then the tools listed in Table VI-1 pertaining to one-dimensional estuaries should not be used.

Users are cautioned that the methods in this chapter are of a simplified nature, and consequently there are errors inherent in the calculations. Additionally, inappropriate data can produce further systematic errors. Data used should be appropriate for the period being studied. For example, when salinity profiles are needed, they should correspond to steady flow periods close to the critical period being analyzed.

Even though the methods presented in this chapter are amenable to hand calculations, some methods are more difficult to apply than others. The fraction of freshwater and modified tidal prism methods are relatively easy to apply, while the advective-dispersion equations offer greater computational challenge. Since the advective-dispersion equations require numerous calculations, the user might find it advantageous to program the methods on a hand calculator (e.g. TI-59 or HP-41C).

6.1.7 Present Water-Quality Assessment

The first step in the estuarine water quality assessment should be the evaluation of existing water quality. Before an analysis of the impact of future waste load changes is made, the planner should know whether or not current estuarine water quality is acceptable, marginal, or substandard.

By far the best way to assess existing water quality is to measure it. The planner should attempt to locate other agencies which might have already collected acceptable samples and/or data. Candidate organizations include the United States Geologic Survey, the U.S. Army Corps of Engineers, state water quality control and monitoring agencies, and engineering and oceanographic departments of local colleges and universities. If such data cannot be located, a data collection program could be undertaken. If at all possible, high tide, and especially low tide in-situ measurements and samples should be collected along the full length of the estuary's main channel and in all significant side embayments. Analyses should then be made in an appropriate laboratory facility. If funds for such data collection efforts are not available, the use of a mathematical estimation of existing water quality is an alternative. The methods presented in subsequent sections and applied to the existing discharges can be used. However, it should be remembered that actual data are preferable to a mathematical estimate of existing water quality.

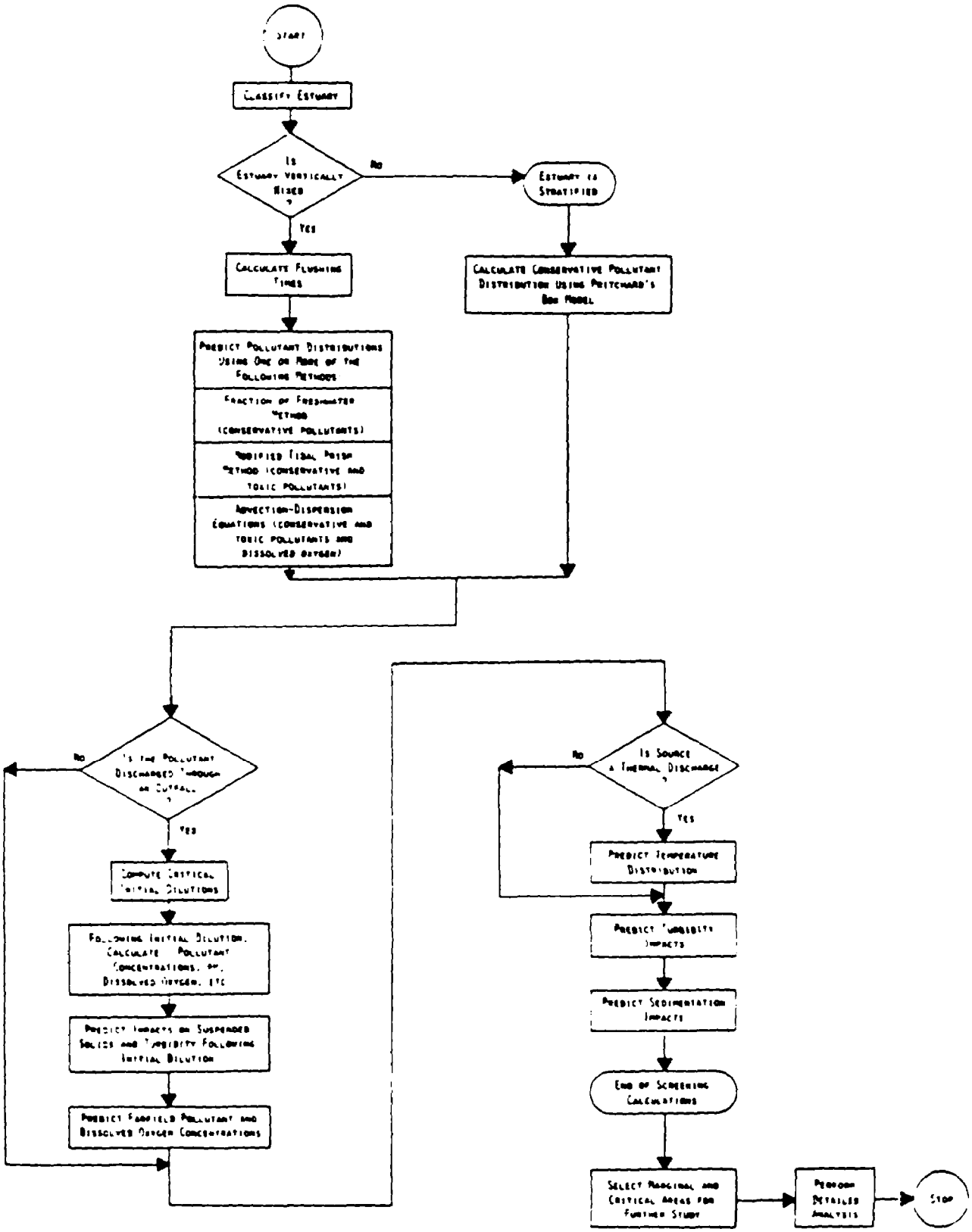

FIGURE VI-5 SUGGESTED PROCEDURE TO PREDICT ESTUARINE WATER QUALITY

6.2 ESTUARINE CLASSIFICATION

6.2.1 General

Section 6.1.7 discussed making a first estimate of current estuarine water quality. This section begins a calculation methodology designed to look at the effect of future changes in waste loading patterns.

The goal of the classifications process presented below is to predict the applicability of the hand calculations to be presented. The classification process is normally the first step to be taken in the calculation procedure since it reveals which techniques can be applied.

6.2.2 Classification Methodology

The classification system recommended for purposes of hand calculations is based on salinity and velocity profiles within the estuary. As both of these parameters vary seasonally and spatially for each estuary, their use will result in a range of values rather than in one single classification number. The following section will describe in detail the procedure for use of this system, and show examples of the procedure.

6.2.3 Calculation Procedure

Hansen and Rattray (1966) developed an estuarine classification system using both salinity stratification and water circulation patterns (based on water column velocities). This procedure involves the calculation of values for two parameters at various points along the main estuarine channel and the plotting of these intersections on the graph shown in Figure VI-6. Figure VI-7 shows plots made by Hansen and Rattray for various estuaries at a single point in time. It should be noted that each estuary is not represented by a point but by a line connecting the points calculated for the mouth and head areas.

The area designations (e.g. 1a, 1b, 2b) on Figure VI-6 were related by Hansen and Rattray to previously used classification titles (e.g. stratified, well mixed). In general, area 1a corresponds to well mixed estuaries. Area 1b has the water circulation pattern of a well mixed estuary yet shows increased stratification. Areas 2 and 3 correspond to the "partially mixed" class of estuaries with area 3 showing more significant vertical circulation within the estuary. Designations 2a/b and 3a/b, as was true of 1a and 1b, indicate increasing degrees of vertical stratification. Type 3b includes fjord-type estuaries. Area 4 represents highly stratified salt wedge estuaries.

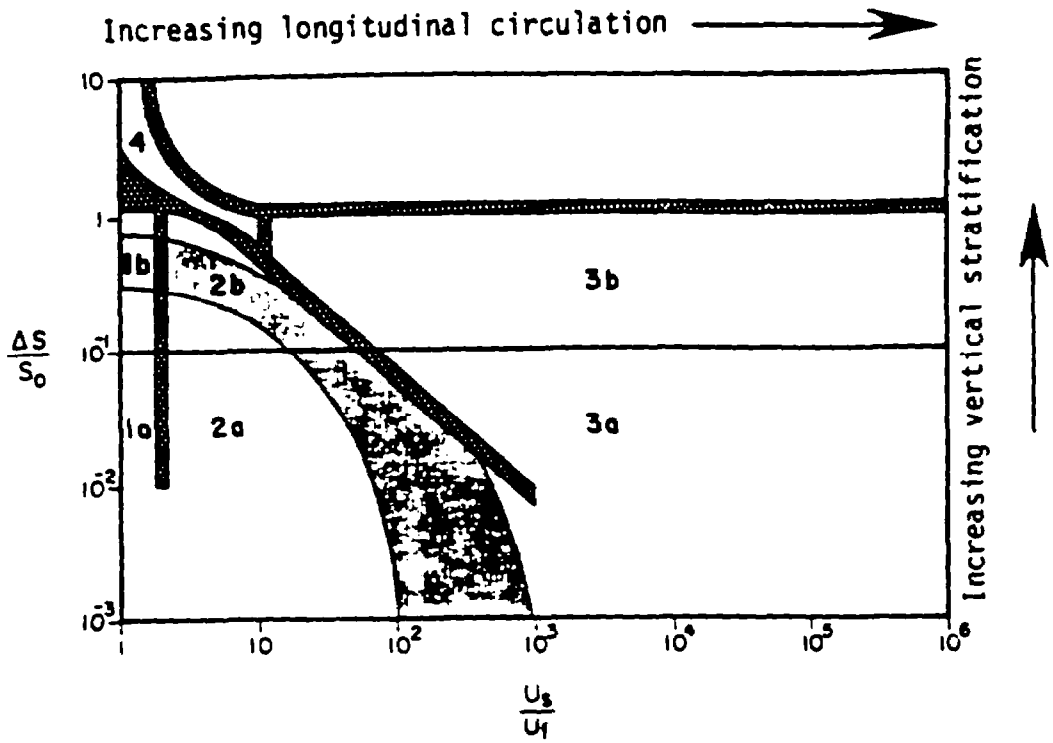

FIGURE VI-6 ESTUARINE CIRCULATION-STRATIFICATION DIAGRAM

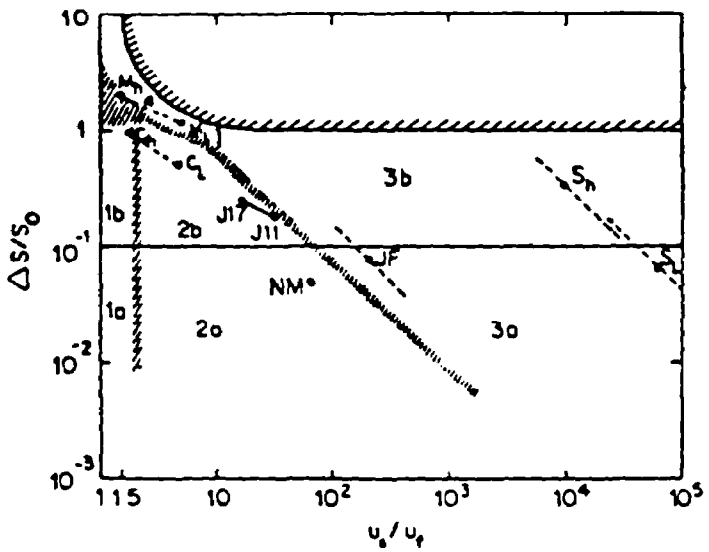

(Station code: M, Mississippi River mouth; C, Columbia River estuary; J, James River estuary; NM, Narrows of the Mersey estuary; JF, Strait of Juan de Fuca; S, Silver Bay. Subscripts h and l refer to high and low river discharge; numbers indicate distance (in miles) from mouth of the James River estuary.

FIGURE VI-7 EXAMPLES OF ESTUARINE CLASSIFICATION PLOTS (FROM HANSEN AND RATTRAY, 1966)

6.2.4 Stratification-Circulation Diagram Interpretation

The closer an estuary falls to the lower left hand corner of a stratification-circulation diagram, the more vertically and laterally homogeneous it is. On the stratification-circulation diagram (Figure VI-6), two types of zonal demarcation can be seen. First are the diagonally striped divisions between adjacent estuarine classifications used by Hansen and Rattray to indicate a transitional zone between separate classifications. The second is a wide solid band arching around the lower left corner of the diagram. Estuaries falling primarily inside of this band (to the lower left of the band) are those for which the one dimensional calculation methods may be applied to obtain reasonably accurate results. If an estuary falls outside of this band, the planner should use only the methods presented which pertain to stratified estuaries, or use computer analyses. Within the band is a borderline of marginal zone. Calculations for one-dimensional estuaries can be used for estuaries falling principally within this zone, however the accuracy of the calculations will be uncertain.

The two parameters used with the stratification-circulation diagram are described below:

a. Stratification Parameter: The stratification parameter is defined as:

$$\text{Stratification Parameter} = \frac{\Delta S}{S_o} \qquad \text{(VI-1)}$$

where

ΔS = time averaged difference in salinity between surface and bottom water ($S_{bottom} - S_{surface}$), ppt

S_o = cross-section mean salinity, ppt.

The diagrammatic relationship of these values is shown in Figure VI-8.

b. Circulation Parameter: The circulation parameter is defined as:

$$\text{Circulation Parameter} = \frac{U_s}{U_f} \qquad \text{(VI-2)}$$

where

U_s = net non-tidal sectional surface velocity (surface velocity through the section averaged over a tidal cycle) measured in ft/sec. See Figure VI-8 for a diagrammatic representation of U_s.

U_f = mean fresh water velocity through the section, ft/sec.

In equation form:

$$U_f = \frac{R}{A} \qquad \text{(VI-3)}$$

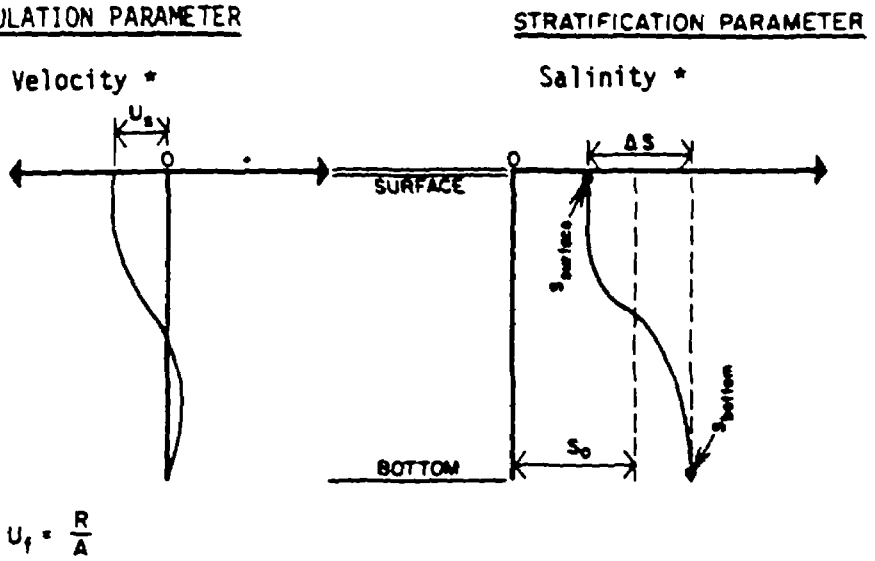

*Both velocity and salinity values for these profiles are averaged over a tidal cycle (net velocity and salinity) rather than being instantaneous values. Of the two the stratification parameter is much less sensitive to variations over a tidal cycle and can be approximated by mean tide values for salinity. Surface velocity (U_s) must be averaged over a tidal cycle.

FIGURE VI-8 CIRCULATION AND STRATIFICATION PARAMETER DIAGRAM

where

R = fresh water (river) inflow rate, ft^3/sec

A = cross-sectional area of the estuary through the point being used to calculate the circulation pattern and stratification parameters based on a mean tide surface elevation, ft^2.

If good cross-sectional area data are not available, cross-sectional profiles can be approximated from the U.S. Geological Survey (USGS) coastal series topographical maps, or, more recently, from NOAA National Ocean Survey charts. The circulation and stratification parameters should be plotted for high and low river flow periods and for stations near the mouth and head of the estuary. The area enclosed by these four points should then include the full range of possible instantaneous estuary hydrodynamic characteristics. In interpreting the significance of this plotted area, by far the greater weight should be given to the low river flow periods as these periods are associated with the poorest pollutant flushing characteristics and the lowest estuarine water quality. The interpretation of the circulation-stratification diagrams will be explained more fully after an example of parameter computation.

EXAMPLE VI-1

Calculation of Stratification and Circulation Parameters

The estuary for this example is the Stuart Estuary which is shown in Figure VI-9. The estuary is 64,000 feet long, is located on the U.S. west coast, and is fed by the Scott River. Two stations were selected for parameter calculation (A and B) with station A located on the southern edge of the main channel 6,500 feet from the estuary's mouth and station B in center channel 47,500 feet from the mouth (16,500 feet from the head of the estuary).

Necessary salinity data were obtained from the coastal engineering department of a nearby university. USGS gage data were available for river flow, and, as a result of its own dredging program, the local district office of the U.S. Corps of Engineers could provide cross-sectional profiles in the approximate areas of both stations. The cross-sections are labeled (1) and (2) on Figure VI-9. The mean low tide depth reading on NOAA Coastal charts was used to verify Corps data. Current meters were tied to buoy channel markers at A and B to provide velocity data. The information obtained from these various sources is shown in graphical form in Figure VI-10.

The calculations proceed as follows:

a. Stratification Parameter:

$$\frac{\Delta S}{S_o} = \frac{S_{bottom} - S_{surface}}{S_o} \longrightarrow$$

	STATION A	STATION B
SUMMER	$\frac{33 - 30}{31.5} = .095$	$\frac{14.5 - 10.5}{12.5} = .32$
WINTER	$\frac{31.5 - 24.2}{27.8} = .26$	$\frac{4 - 2.1}{3.25} = .58$

b. Circulation Parameter:

1. Calculate A_i's using cross sectional information on Figure VI-10:

A_a = (630 ft) (20 ft) (1/2) + (630 ft) (20 ft) + (1590 ft) (20 ft) (1/2)
= 34,800 ft

A_b = (2580 ft) (16 ft) (1/2) + (1720 ft) (16 ft) (1/2)
= 34,400 ft

For most cross-sections it is advisable to use more finely divided segments than in the simple example above in order to reduce the error associated with this approximation. The method for this calculation,

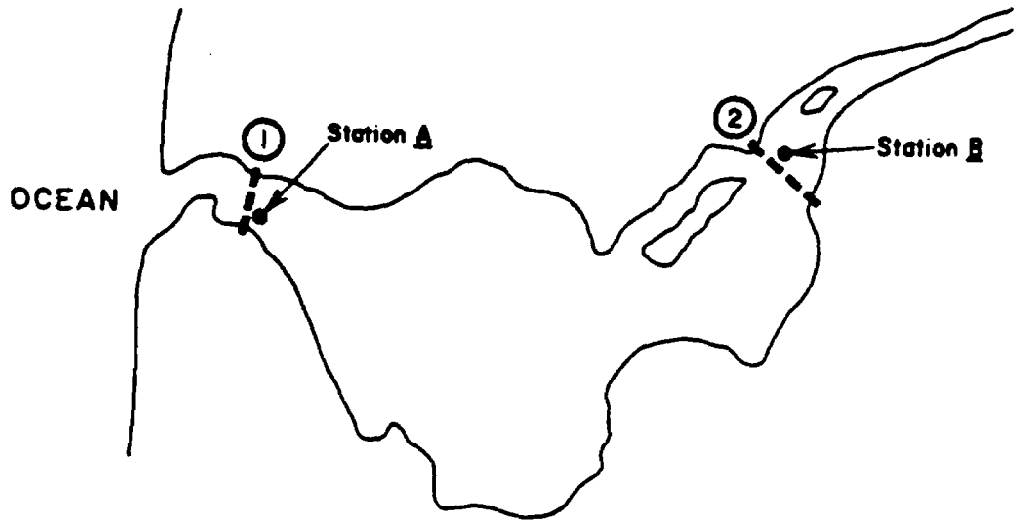

FIGURE VI-9 THE STUART ESTUARY

however, is identical regardless of the number of regular segments used.

2. Calculate U_f's (with R and A_i values obtained from Figure VI-10):

STATION

$U_f = \frac{R}{A_i}$	A	B	
→	$\frac{550\ ft^3/sec}{3.48 \times 10^4 ft^2} = 1.58 \times 10^{-2} ft/sec$	$\frac{550\ ft^3/sec}{3.44 \times 10^4 ft^2} = 1.60 \times 10^{-3} ft/sec$	SUMMER
	$\frac{1800\ ft^3/sec}{3.48 \times 10^4 ft^2} = 5.17 \times 10^{-2} ft/sec$	$\frac{1800\ ft^3/sec}{3.44 \times 10^4 ft^2} = 5.23 \times 10^{-2} ft/sec$	WINTER

3. Calculate $\frac{U_s}{U_f}$'s:

U_s values are read from Figure VI-10. The precise value for U_s is the integral of the velocity curve (area under "ebb" velocity curve minus the area under the "flood" velocity curve) divided by the elapsed time period (length of one tidal cycle). If the elapsed time for flood flow at a station is only slightly below the elapsed time for ebb flow U_s may be approximated as $(U_{ebb(max)} - U_{flood(max)})/2$.

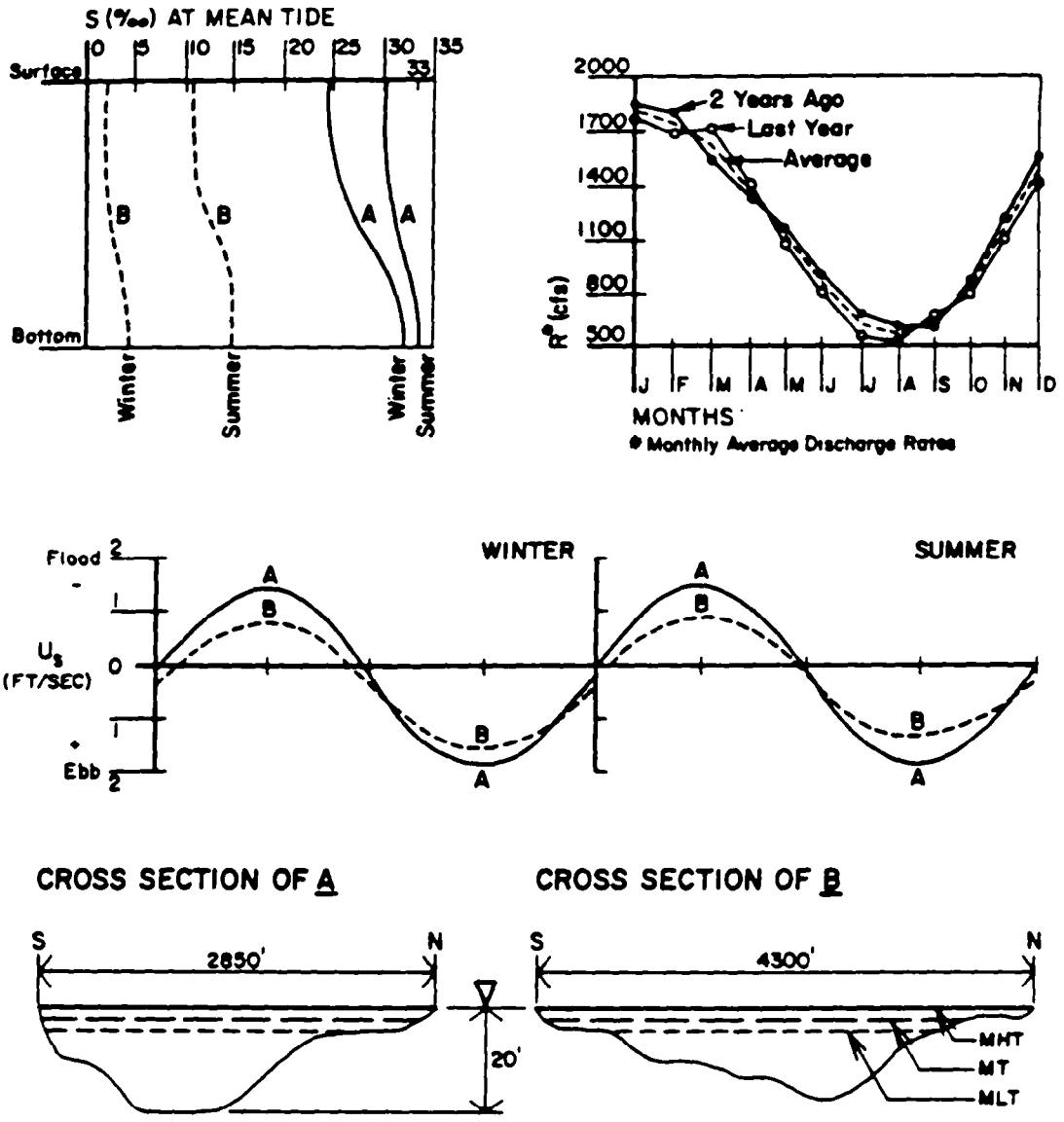

FIGURE VI-10 STUART ESTUARY DATA FOR CLASSIFICATION CALCULATIONS

STATION

$\frac{U_s}{U_f}$ →	A	B	
	$\frac{0.15 \text{ ft/sec}}{1.58 \times 10^{-2} \text{ ft/sec}} = \underline{9.5}$	$\frac{0.3 \text{ ft/sec}}{1.60 \times 10^{-2} \text{ ft/sec}} = \underline{18.8}$	SUMMER
	$\frac{0.2 \text{ ft/sec}}{5.17 \times 10^{-2} \text{ ft/sec}} = \underline{3.9}$	$\frac{0.4 \text{ ft/sec}}{5.23 \times 10^{-2} \text{ ft/sec}} = \underline{7.65}$	WINTER

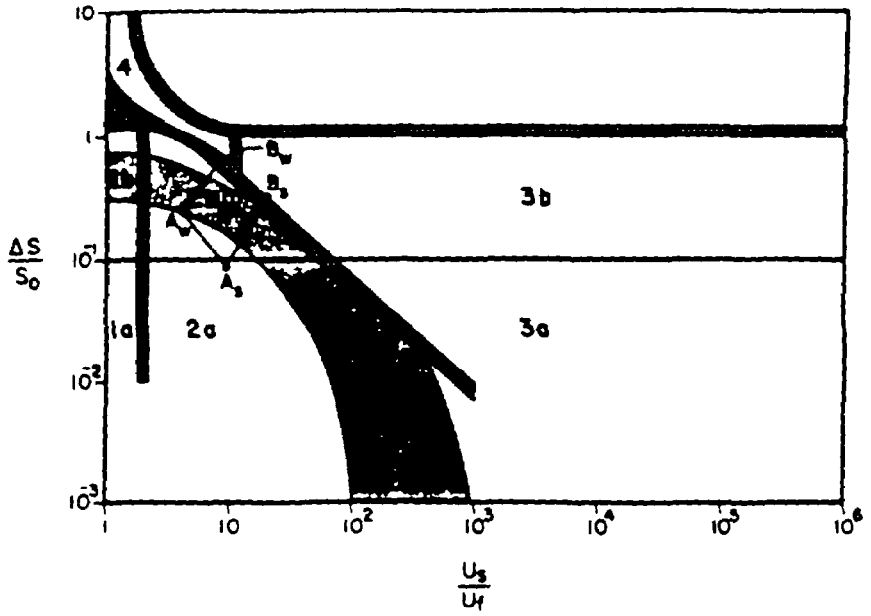

FIGURE VI-11 ESTUARINE CIRCULATION-STRATIFICATION DIAGRAM

The circulation-stratification plots for the Stuart Estuary are shown in Figure VI-11 with points A_s (station A, summer value), A_w (station A, winter Value), B_s (station B, summer value), and B_w (station B, winter value).

As indicated, this estuary shows a significant amount of vertical stratification (especially at station A) but little evidence of major vertical variations in net circulation.

END OF EXAMPLE VI-1

Turning to Figure VI-11, the Stratification-Circulation diagram for the Stuart Estuary, it is apparent that this estuary lies principally within the marginal area. Moreover, the low flow classification (line A_s-B_s) also lies primarily within the marginal area. Thus, the planner for the Stuart Estuary should calculate an additional criterion (see below) to help determine the suitability of using the calculation procedures for well mixed estuaries. If the Stuart Estuary plotted more predominately below the marginal zone, the planner could proceed with flushing time calculations since the estuary would then meet the well mixed classification criteria.

It should be noted that the data for the Stuart Estuary produced a fairly tight cluster of data points. As can be seen in Figure VI-12, the salinity profiles for one west coast estuary (the Alsea River and Estuary along the central Oregon coast) vary considerably more from season to season than those of the Stuart Estuary.

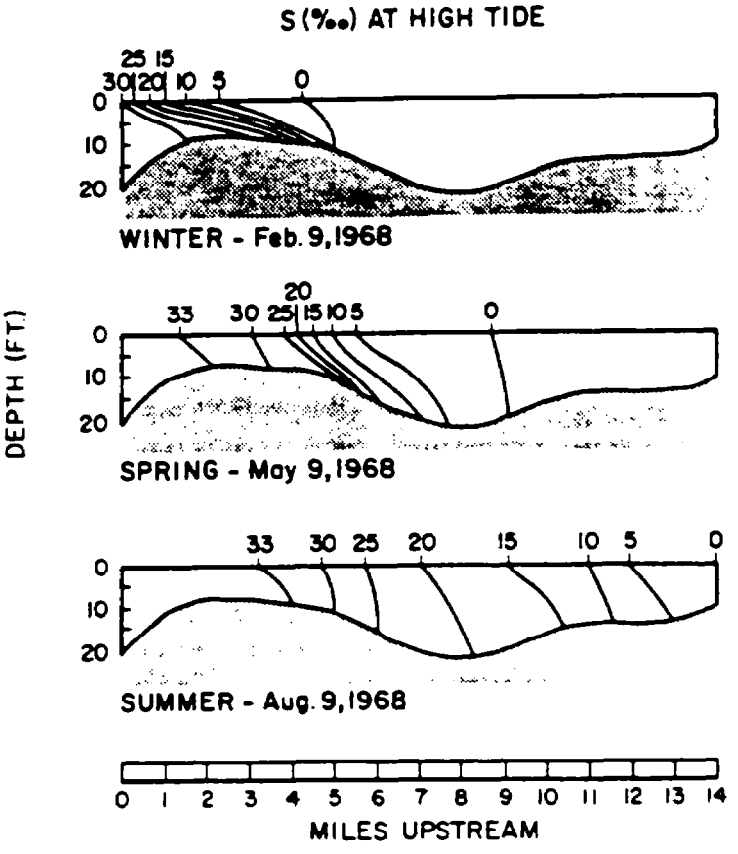

FIGURE VI-12 ALSEA ESTUARY SEASONAL SALINITY VARIATIONS (FROM GIGER, 1972)

This increased variation would produce a far greater spread in the summer and winter $\Delta S/S_0$ parameter values.

6.2.5 Flow Ratio Calculation

If application of the above classification procedure results in an ambiguous outcome regarding estuary classification, another criterion should be applied. This is the flow ratio calculation. Schultz and Simmons (1957) first observed the correlation between the flow ratio and estuary type. They defined the flow ratio for an estuary as:

$$F = \frac{R}{P} \qquad \text{(VI-4)}$$

where

F = the flow ratio,

R = the river flow measured over one tidal cycle (measured in m^3 or ft^3)

P = the estuary tidal prism (in m^3 or ft^3).

Thus the flow ratio compares the tidally induced flow in an estuary with the river induced flow. Schultz and Simmons observed that when this ratio was on the order of 1.0 or greater, the associated estuary was normally highly stratified. Conversely, ratios of about 0.1 or less were usually associated with very well-mixed estuaries and ratios in the range of 0.25 were associated with partially mixed estuaries. A flow ratio of 0.2 or less warrants inclusion of the estuary in the hand calculation process for one dimensional estuaries. Flow ratios in the range 0.2 to 0.3 should be considered marginal. Estuaries with flow ratios greater than 0.3 should not be included in the one-dimensional category.

EXAMPLE VI-2

Calculation of the Flow Ratio for an Estuary

The following data appply to the Patuxent Estuary, Maryland:

R, total river discharge over one tidal cycle = $1.42 \times 10^5 m^3$ (low flow)
$3.58 \times 10^6 m^3$ (high flow)

P, estuary tidal prism volume = $3.51 \times 10^7 m^3$

The flow ratios for the Patuxent Estuary at low and high river flows are thus:

$$F = \frac{R}{P}$$

$$F_{\text{low flow}} = \frac{1.42 \times 10^5 m^3}{3.51 \times 10^7 m^3}$$

$$= 0.004$$

$$F_{\text{high flow}} = \frac{3.58 \times 10^6 m^3}{3.51 \times 10^7 m^3}$$

$$= 0.10$$

Values of $F \leq 0.1$ are usually associated with well mixed estuaries. The F values calculated above indicate a well mixed estuary. However, historical data indicate the Patuxent River Estuary is partially stratified at moderate and high river flows.

END OF EXAMPLE VI-2

When tidal data are not available, NOAA coastal charts may be used to estimate the difference between mean high tide and mean low tide estuary surface areas. As

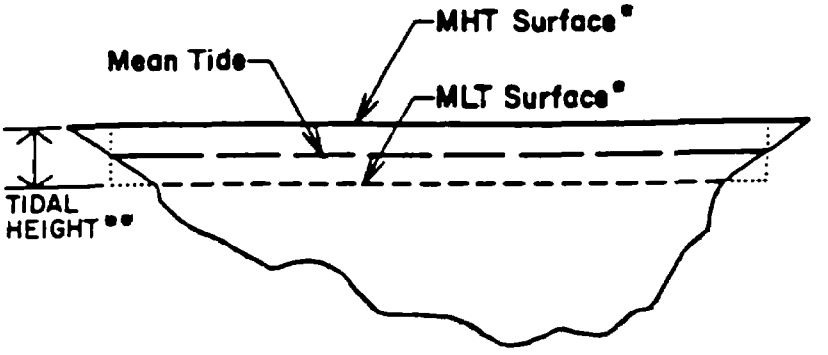

P_i (section i) = section Length x tidal height x $\left(\frac{\text{MHT width} + \text{MLT width}}{2}\right)$

P estuary = $\sum_i P_i$ for all sections

* Widths obtained from NOAA tide table for the area

**Available from local Coast Guard Stations

FIGURE VI-13 ESTUARY CROSS-SECTION FOR TIDAL PRISM CALCULATIONS

can be seen in the cross-section diagram in Figure VI-13 the estuarine tidal prism can be approximated by averaging the MLT and MHT surface areas and multiplying this averaged area by the local tidal height. Mean tidal heights (approximately 1 week before or after spring tides) should be used for this calculation. As indicated in Figure VI-13, the estuary can be conveniently subdivided into longitudinal sections for this averaging process, to reduce the resulting error. Table VI-2 lists tidal prisms estimated for many U.S. estuaries. These values may be used as an alternate to tidal prism calculations.

6.3 FLUSHING TIME CALCULATIONS

6.3.1 General

Flushing time is a measure of the time required to transport a conservative pollutant from some specified location within the estuary (usually, but not always, the head) to the mouth of the estuary. Processes such as pollutant decay or sedimentation which can alter the pollutant's distribution within the estuary are not considered in the concept of flushing time.

It was mentioned earlier in this chapter that the net non-tidal flow in an

TABLE VI-2

TIDAL PRISMS FOR SOME U.S. ESTUARIES

(FROM O'BRIEN, 1969 AND JOHNSON, 1973)

Estuary	Coast	Tidal Prism (ft^3)
Plum Island Sound, Mass.	Atlantic	1.32×10^9
Fire Island Inlet, N.Y.	Atlantic	2.18×10^9
Jones Inlet, N.Y.	Atlantic	1.50×10^9
Beach Haven Inlet (Little Egg Bay), N.J.	Atlantic	1.51×10^9
Little Egg Inlet (Great Bay), N.J.	Atlantic	1.72×10^9
Brigantine Inlet, N.J.	Atlantic	5.23×10^8
Absecon Inlet (before jetties), N.J.	Atlantic	1.65×10^9
Great Egg Harbor Entr, N.J.	Atlantic	2.00×10^9
Townsend Inlet, N.J.	Atlantic	5.56×10^8
Hereford Inlet, N.J.	Atlantic	1.19×10^9
Chincoteague Inlet, Va.	Atlantic	1.56×10^9
Oregon Inlet, N.C.	Atlantic	3.98×10^9
Ocracoke Inlet, N.C.	Atlantic	5.22×10^9
Drum Inlet, N.C.	Atlantic	5.82×10^8
Beaufort Inlet, N.C.	Atlantic	5.0×10^9
Carolina Beach Inlet, N.C.	Atlantic	5.25×10^8
Stono Inlet, S.C.	Atlantic	2.86×10^9
North Edisto River, S.C.	Atlantic	4.58×10^9
St. Helena Sound, S.C.	Atlantic	1.53×10^{10}
Port Royal Sound, S.C.	Atlantic	1.46×10^{10}
Calibogue Sound, S.C.	Atlantic	3.61×10^9
Wassaw Sound, Ga.	Atlantic	8.2×10^9
Ossabaw Sound, Ga.	Atlantic	6.81×10^9
Sapelo Sound, Ga.	Atlantic	7.36×10^9
St. Catherines Sound, Ga.	Atlantic	6.94×10^9
Doboy Sound, Ga.	Atlantic	4.04×10^9
Altamaha Sound, Ga.	Atlantic	2.91×10^9
Hampton River, Ga.	Atlantic	1.01×10^9
St. Simon Sound, Ga.	Atlantic	6.54×10^9
St. Andrew Sound, Ga.	Atlantic	9.86×10^9
Ft. George Inlet, Fla.	Atlantic	3.11×10^8
Old St. Augustine Inlet, Fla.	Atlantic	1.31×10^9

TABLE VI-2 (Cont.)

Estuary	Coast	Tidal Prism (ft^3)
Ponce de Leon, Fla. (before jetties)	Atlantic	5.74×10^6
Delaware Bay Entrance	Atlantic	1.25×10^{11}
Fire Island Inlet, N.Y.	Atlantic	1.86×10^9
East Rockaway Inlet, N.Y.	Atlantic	7.6×10^8
Rockaway Inlet, N.Y.	Atlantic	3.7×10^9
Masonboro Inlet, N.C.	Atlantic	8.55×10^8
St. Lucie Inlet, Fla.	Atlantic	5.94×10^8
Nantucket Inlet, Mass.	Atlantic	4.32×10^8
Shinnecock Inlet, N.Y.	Atlantic	2.19×10^8
Moriches Inlet, N.Y.	Atlantic	1.57×10^9 8.46×10^8
Shark River Inlet, N.J.	Atlantic	1.48×10^8
Manasguan Inlet, N.J.	Atlantic	1.75×10^8
Barnegat Inlet, N.J.	Atlantic	6.25×10^8
Absecon Inlet, N.J.	Atlantic	1.48×10^9
Cold Springs Harbor (Cape May), N.J.	Atlantic	6.50×10^8
Indian River Inlet, Del.	Atlantic	5.25×10^8
Winyah Bay, S.C.	Atlantic	3.02×10^9
Charleston, S.C.	Atlantic	5.75×10^9
Savannah River (Tybee Roads), Ga.	Atlantic	3.1×10^9
St. Marys (Fernandina Harbor), Fla.	Atlantic	4.77×10^9
St. Johns River, Fla.	Atlantic	1.73×10^9
Fort Pierce Inlet, Fla.	Atlantic	5.81×10^3
Lake Worth Inlet, Fla.	Atlantic	9.0×10^8
Port Everglades, Fla.	Atlantic	3.0×10^8
Bakers Haulover, Fla.	Atlantic	3.6×10^8
Captiva Pass, Fla.	Gulf of Mexico	1.90×10^9
Boca Grande Pass, Fla.	Gulf of Mexico	1.26×10^{10}
Gasparilla Pass, Fla.	Gulf of Mexico	4.7×10^8
Stump Pass, Fla.	Gulf of Mexico	3.61×10^8
Midnight Pass, Fla.	Gulf of Mexico	2.61×10^8
Big Sarasota Pass, Fla.	Gulf of Mexico	7.6×10^8
New Pass, Fla.	Gulf of Mexico	4.00×10^8
Longboat Pass, Fla.	Gulf of Mexico	4.90×10^8

TABLE VI-2 (Cont.)

Estuary	Coast	Tidal Prism (ft^3)
Sarasota Pass, Fla.	Gulf of Mexico	8.10×10^8
Pass-a-Grille	Gulf of Mexico	1.42×10^9
Johns Pass, Fla.	Gulf of Mexico	5.03×10^8
Little (Clearwater) Pass, Fla.	Gulf of Mexico	6.8×10^8
Big (Dunedin) Pass, Fla.	Gulf of Mexico	3.76×10^8
East (Destin) Pass, Fla.	Gulf of Mexico	1.62×10^9
Pensacola Bay Entr., Fla.	Gulf of Mexico	9.45×10^9
Perdido Pass, Ala.	Gulf of Mexico	5.84×10^8
Mobile Bay Entr., Ala.	Gulf of Mexico	2.0×10^{10}
Barataria Pass, La.	Gulf of Mexico	2.55×10^9
Caminada Pass, La.	Gulf of Mexico	6.34×10^8
Calcasieu Pass, La.	Gulf of Mexico	2.97×10^9
San Luis Pass, Tex.	Gulf of Mexico	5.84×10^8
Venice Inlet, Fla.	Gulf of Mexico	8.5×10^7
Galveston Entr., Tex.	Gulf of Mexico	1.59×10^{10}
Aransas Pass, Tex.	Gulf of Mexico	1.76×10^9
Grays Harbor, Wash.	Pacific	1.3×10^{10}
Willapa, Wash.	Pacific	1.3×10^{10}
Columbia River, Wash.-Ore.	Pacific	2.9×10^{10}
Necanicum River, Ore.	Pacific	4.4×10^7
Nehalem Bay, Ore.	Pacific	4.3×10^8
Tillamook Bay, Ore.	Pacific	2.5×10^9
Netarts Bay, Ore.	Pacific	5.4×10^8
Sand Lake, Ore.	Pacific	1.1×10^8
Nestucca River, Ore.	Pacific	2.6×10^8
Salmon River, Ore.	Pacific	4.3×10^7
Devils Lake, Ore.	Pacific	1.1×10^8
Siletz Bay, Ore.	Pacific	3.5×10^8
Yaquina Bay, Ore.	Pacific	8.4×10^8
Alsea Estuary, Ore.	Pacific	5.1×10^8
Siuslaw River, Ore.	Pacific	2.8×10^8
Umpqua, Ore.	Pacific	1.2×10^9
Coos Bay, Ore.	Pacific	1.9×10^9
Caquille River, Ore .	Pacific	1.3×10^8
Floras Lake, Ore .	Pacific	6.8×10^7

TABLE VI-2 (Cont.)

Estuary	Coast	Tidal Prism (ft^3)
Rogue River, Ore.	Pacific	1.2×10^8
Chetco River, Ore.	Pacific	2.9×10^7
Smith River, Ca.	Pacific	9.5×10^7
Lake Earl, Ca.	Pacific	5.1×10^8
Freshwater Lagoon, Ca.	Pacific	4.7×10^7
Stove Lagoon, Ca.	Pacific	1.2×10^8
Big Lagoon, Ca.	Pacific	3.1×10^8
Mad River, Calif.	Pacific	2.4×10^7
Humbolt Bay, Calif.	Pacific	2.4×10^9
Eel River, Calif.	Pacific	3.1×10^8
Russian River, Calif.	Pacific	6.3×10^7
Bodega Bay, Calif.	Pacific	1.0×10^8
Tomales Bay, Calif.	Pacific	1.0×10^9
Abbotts Lagoon, Calif.	Pacific	3.5×10^7
Drakes Bay, Calif.	Pacific	2.7×10^8
Bolinas Lagoon, Calif.	Pacific	1.0×10^8
San Francisco Bay, Calif.	Pacific	5.2×10^{10}
Santa Cruz Harbor, Calif.	Pacific	4.3×10^6
Moss Landing, Calif.	Pacific	9.4×10^7
Morro Bay, Calif.	Pacific	8.7×10^7
Marina Del Rey, Calif.	Pacific	6.9×10^7
Alamitos Bay, Calif.	Pacific	6.9×10^7
Newport Bay, Calif.	Pacific	2.1×10^8
Camp Pendleton, Calif.	Pacific	1.1×10^7
Aqua Hedionda, Calif.	Pacific	4.9×10^7
Mission Bay, Calif.	Pacific	3.3×10^8
San Diego Bay, Calif.	Pacific	1.8×10^9

estuary is usually seaward* and is dependent on the river discharge. The non tidal flow is one of the driving forces behind estuarine flushing. In the absence of this advective displacement, tidal oscillation and wind stresses still operate to

*While net flow is always seaward for the estuaries being considered here, it is possible to have a net upstream flow in individual embayments of an estuary. While this occurrence is rare in the United States, an example of such a situation is the South Bay of San Francisco Bay where freshwater inflows are so small that surface evaporation exceeds freshwater inflow. Thus, net flow is upstream during most of the year.

disperse and flush pollutants. However, the advective component of flushing can be extremely important. Consider Tomales Bay, California as an example. This small, elongated bay has essentially no fresh water inflow. As a result there is no advective seaward motion and Pollutant removal is dependent upon dispersion and diffusion processes. The flushing time for the bay is approximately 140 days (Johnson, et al., 1961). This can be compared with the Alsea Estuary in Oregon having a flushing time of approximately 8 days, with the much larger St. Croix Estuary in Nova Scotia having a flushing time of approximately 8 days (Ketchum and Keen, 1951), or with the very large Hudson River Estuary with a short flow flushing time of approximately 10.5 days (Ketchum, 1950).

6.3.2 Procedure

Flushing times for a given estuary vary over the course of a year as river discharge varies. The critical time is the low river flow period since this period corresponds with the minimum flushing rates. The planner might also want to calculate the best flushing characteristics (high river flow) for an estuary. In addition to providing a more complete picture of the estuarine system, knowledge of the full range of annual flushing variations can be useful in evaluating the impact of seasonal discharges (e.g., fall and winter cannery operation in an estuary with a characteristic summer fresh water low flow). Further, storm sewer runoff normally coincides with these best flushing conditions (high flow) and not with the low flow, or poorest flushing conditions. Thus analysis of storm runoff is often better suited for high flow flushing conditions. However, the low flow calculation should be considered for use in primary planning purposes.

There are several ways of calculating flushing time. Two methods are presented here: the fraction of freshwater method and the modified tidal prism method.

6.3.3 Fraction of Fresh Water Method

The flushing time of a pollutant, as determined by the fraction of freshwater method is:

$$T_f = \frac{V_f}{R} \qquad \text{(VI-5)}$$

where

V_f = volume of freshwater in the estuary

T_f = flushing time of a pollutant which enters the head of the estuary with the river flow.

Equation VI-5 is equivalent to the following concept of flushing time which is

more intuitively meaningful:

$$T_f = \frac{M}{\dot{M}} \qquad \text{(VI-6)}$$

where

M = total mass of conservative pollutant contained in the estuary

$\dot{M}$ = rate of pollutant entry into the head of the estuary with the river water.

Since the volume of freshwater in the estuary is the product of the fraction of freshwater (f) and the total volume of water (V), Equation VI-5 becomes:

$$T_f = \frac{fV}{R} \qquad \text{(VI-7)}$$

If the estuary is divided into segments the flushing time becomes:

$$T_f = \Sigma \frac{f_i V_i}{R_i} \qquad \text{(VI-8)}$$

Equation VI-8 is more general and accurate than the three previous expressions because both f_i (the fraction of freshwater in the ith segment) and R_i (the freshwater discharge through the ith segment) can vary over distance within the estuary. Note that the flushing time of a pollutant discharged from some location other than the head of the estuary can be computed by summing contributions over the segments seaward of the discharge.

A limitation of the fraction of freshwater method is that it assumes uniform salinity throughout each segment. A second limitation is that it assumes during each tidal cycle a volume of water equal to the river discharge moves into a given estuarine segment from the adjacent upstream segment, and that an equal volume of the water originally in the segment moves on to the adjacent one downstream. Once this exchange has taken place, the water within each segment is assumed to be instantaneously and completely mixed and to again become a homogeneous water mass. Proper selection of estuarine segments can reduce these errors.

6.3.4 Calculation of Flushing Time by Fraction of Freshwater Method

This is a six step procedure:

1. Graph the estuarine salinity profiles.
2. Divide the estuary into segments. There is no minimum or maximum number of segments required, nor must all segments be of the same length. The divisions should be selected so that mean segment salinity is relatively constant over

the full length of the segment. Thus, stretches of steep salinity gradient will have short segments and stretches where salinity remains constant may have very long segments. Example VI-3 provides an illustration.

3. Calculate each segment's fraction of fresh water by:

$$f_i = \frac{S_s - S_i}{S_s} \qquad \text{(VI-9)}$$

where

f_i = fraction of fresh water for segment "i"

S_s = salinity of local sea water*, °/oo

S_i = mean salinity for segment "i", °/oo.

4. Calculate the quantity of fresh water in each segment by:

$$W_i = f_i \times V_i \qquad \text{(VI-10)}$$

where

W_i = quantity of fresh water in segment "i"

V_i = total volume of segment "i" at MTL.

5. Calculate the exchange time (flushing time) for each segment by:

$$T_i = W_i/R \qquad \text{(VI-11)}$$

where

T_i = segment flushing time, in tidal cycles

R = river discharge over one tidal cycle.

6. Calculate the entire estuary flushing time by summing the exchange times for the individual segments:

$$T_f = \sum_{i=1}^{n} T_i \qquad \text{(VI-12)}$$

where

T_f = estuary flushing time, in tidal cycles

n = number of segments.

Table VI-3 shows a suggested method for calculating flushing time by the fraction of freshwater method.

*Sea surface salinity along U.S. shores vary spatially. Neuman and Pierson (1966) mapped Pacific mean coastal surface salinities as varying from 32.4 °/oo at Puget Sound to 33.9 °/oo at the U.S.-Mexico border; Atlantic mean coastal surface salinities as varying from 32.5 °/oo in Maine to 36.2 °/oo at the southern extreme of Florida; and Gulf coast salinities as varying between 36.2 °/oo and 36.4 °/oo. Surface coastal salinities in Long Island Sound (Hardy, 1972) and off Long Island south coast (Hydroscience, 1974) vary between 26.5 and 28.5 °/oo.

TABLE VI-3

SAMPLE CALCULATION TABLE FOR CALCULATION OF FLUSHING TIME
BY SEGMENTED FRACTION OF FRESHWATER METHOD

Segment Number	Mean Segment Salinity S_i (ppt)	Mean Segment Length (m)	Mean Segment Cross-sectional Area (m^2)	Segment Mean Tide Volume V_i (m^3)	Fraction of River Water $f_i = \frac{Ss-Si}{Ss}$	River Water Volume $W_i = f_i \times V_i$ (m^3)	Segment Flushing Time $T_i = W_i/R$ (tidal cycles)
						$\sum_{i=1}^{n} T_i =$	

Up Estuary ⟵

EXAMPLE VI-3

Flushing Time Calculation by Fraction of Fresh Water Method

This example pertains to the Patuxent Estuary. This estuary has no major side embayments, and the Patuxent River is by far its largest source of fresh water. This estuary therefore lends itself well to analysis by the segmented fraction of fresh water method.

Salinity profiles for July 19, 1978 are used to find segment salinity values. Chesapeake Bay water at the mouth of the Patuxent Estuary had a salinity of 10.7 ppt (S_i). The Patuxent River discharge over the duration of one tidal cycle is:

$$R = (12\ m^3/sec)\ (12.4\ hr/tidal\ cycle)\ (3600\ sec/hr)$$
$$= 5.36 \times 10^3 m\ /tidal\ cycle$$

A segmentation scheme based on the principles laid out above is used to divide the estuary into eight segments; their measured characteristics are shown Table VI-4. The segmentation is shown graphically on the estuary salinity profile (Figure VI-14).

The next step is to find the fraction of fresh water for each segment. For segment 1:

$$f_1 = \frac{S_s - S_1}{S_s}$$

where

f_1 = fraction of fresh water, segment 1
S_s = salinity of local seawater
S = measured mean salinity for segment 1

$$f_1 = \frac{10.7\ ppt - 0.8\ ppt}{10.7\ ppt} = 0.93$$

The calculation is reported in Table IV-4 for segments 2 through 8.

The volume of fresh water (river water) in each segment is next found using the formula:

$$W_i = f_i \times V_i$$

For segment 1:

$$W_1 = f_1 \times V_1 = 0.93\ (0.79 \times 10^7 m^3)$$
$$= 7.35 \times 10^6 m^3$$

The flushing time for each segment is next calculated by:

$$T_i = W_i/R$$

TABLE VI-4

PATUXENT ESTUARY SEGMENT CHARACTERISTICS FOR FLUSHING TIME CALCULATIONS

Segment Number	Mean Segment Salinity S_i, ppt	Segment Length meters	Mean Segment Cross-Sectional Area meter^2	Mean Tide Segment Volume V_i meters^3
8	10.3	10,400	16,000	16.6×10^7
7	9.5	10,400	12,500	13.0×10^7
6	8.7	6,100	11,400	6.95×10^7
5	7.6	6,100	7,500	4.58×10^7
4	5.8	5,800	4,300	2.49×10^7
3	3.3	5,000	3,100	1.55×10^7
2	1.8	4,650	2,200	1.02×10^7
1	0.8	4,650	1,700	0.79×10^7

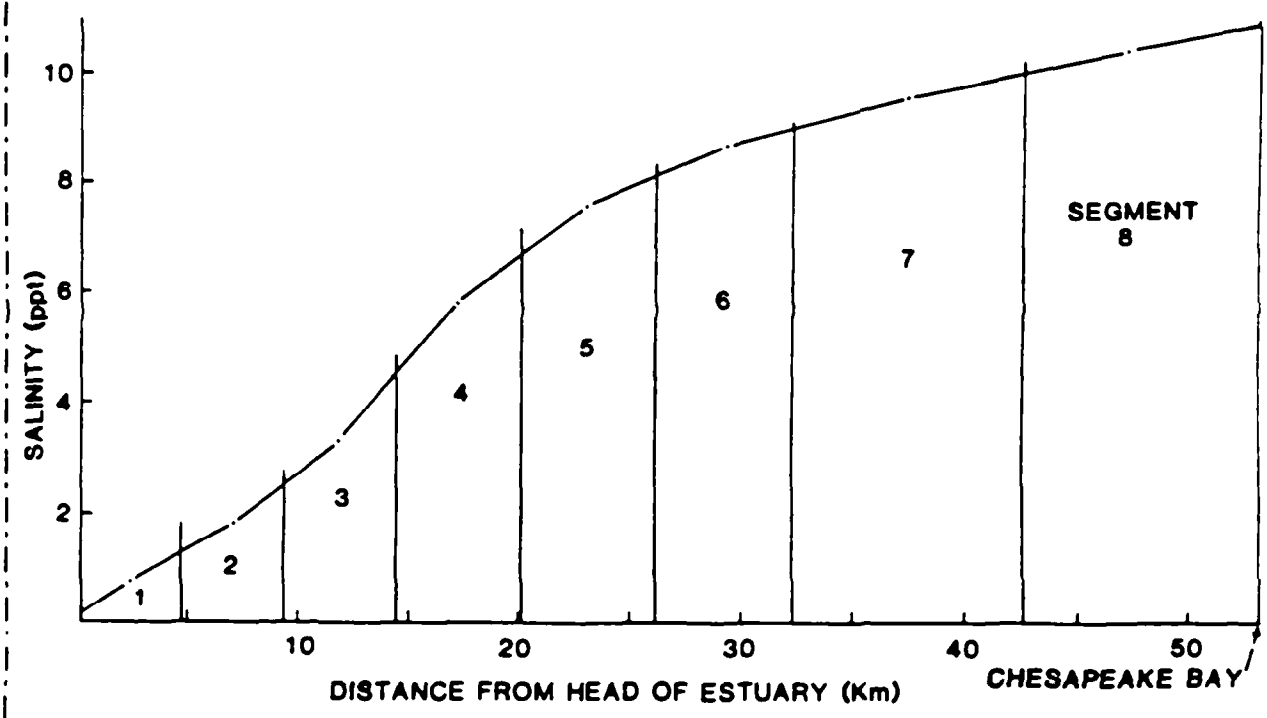

FIGURE VI-14 PATUXENT ESTUARY SALINITY PROFILE AND SEGMENTATION SCHEME USED IN FLUSHING TIME CALCULATIONS.

For segment 1:

$$T_1 = W_1/R = 7.35 \times 10^6 m^3/(5.36 \times 10^5 m^3/\text{tidal cycle})$$
$$= 13.7 \text{ tidal cycles}$$

Fraction of freshwater, river water volume and flushing time values for the eight segments are compiled in Table VI-5.

The final step is to determine the flushing time for the estuary. In this case:

$$T_f = \sum_{i=1}^{8} T_i =$$
$$11.4 + 27.2 + 24.6 + 24.8 + 21.5 + 20.0 + 15.8 + 13.7$$
$$= 159 \text{ tidal cycles, or } 2.74 \text{ months}$$

6.3.5 Branched Estuaries and the Fraction of Freshwater Method

Branched estuaries, where more than one source of freshwater contributes to the salinity distribution pattern, are common. The fraction of freshwater method can be directly applied to estuaries of this description. Consider the estuary shown in Figure VI-15, having two major sources of freshwater (River 1, R_1; and River 2, R_2). The flushing time for pollutants entering the estuary with river flow R_2 is:

$$T_f(R_2) = T_1 + T_2 + T_3 + T_4 + T_5 + T_6 =$$
$$\frac{f_1V_1}{R_2} + \frac{f_2V_2}{R_2} + \frac{f_3V_3}{R_2} + \frac{f_4V_4}{R_2} + \frac{f_5V_5}{R_1+R_2} + \frac{f_6V_6}{R_1+R_2}$$

For the pollutants entering with R_1, the flushing time is:

$$T_f(R_1) = \frac{f_aV_a}{R_1} + \frac{f_bV_b}{R_1} + \frac{f_cV_c}{R_1} + \frac{f_5V_5}{R_1+R_2} + \frac{f_6V_6}{R_1+R_2}$$

The flushing time computations are similar in concept for the case of a single freshwater source, modified to account for a flow rate of $R_1 + R_2$ in segments 5 and 6.

6.3.6 Modified Tidal Prism Method

This method divides an estuary into segments whose lengths are defined by the maximum excursion path of a water particle during a tidal cycle. Within each segment the tidal prism is compared to the total segment volume as a measure of the

TABLE VI-5

FLUSHING TIME FOR PATUXENT ESTUARY

Segment Number	Mean Segment Salinity S_i, ppt	Segment Length meters	Mean Segment Cross-Sectional Area meter^2	Segment Mean Tide Volume V_i meter^3	Fraction of River Water $f_i = \frac{S_s - S_i}{S_s}$ (S_s = 10.7)	River Water Volume $W_i = f_i \times V_i$ (meters^3)	Segment Flush Time $T_i = W_i/R$ tidal cycles
8	10.3	10,400	16,000	16.6×10^7	0.037	6.14×10^6	11.4
7	9.5	10,400	12,500	13.0×10^7	0.112	14.6×10^6	27.2
6	8.7	6,100	11,400	6.95×10^7	0.19	13.2×10^6	24.6
5	7.6	6,100	7,500	4.58×10^7	0.29	13.3×10^6	24.8
4	5.8	5,800	4,300	2.49×10^7	0.46	11.5×10^6	21.5
3	3.3	5,000	3,100	1.55×10^7	0.69	10.7×10^6	20.0
2	1.8	4,650	2,200	1.02×10^7	0.83	8.47×10^6	15.8
1*	0.8	4,650	1,700	0.79×10^7	0.93	7.35×10^6	13.7
							Sum = 159 tidal cycles or 2.74 months

*In this numbering scheme segment 1 is the most upstream segment.

END OF EXAMPLE VI-3

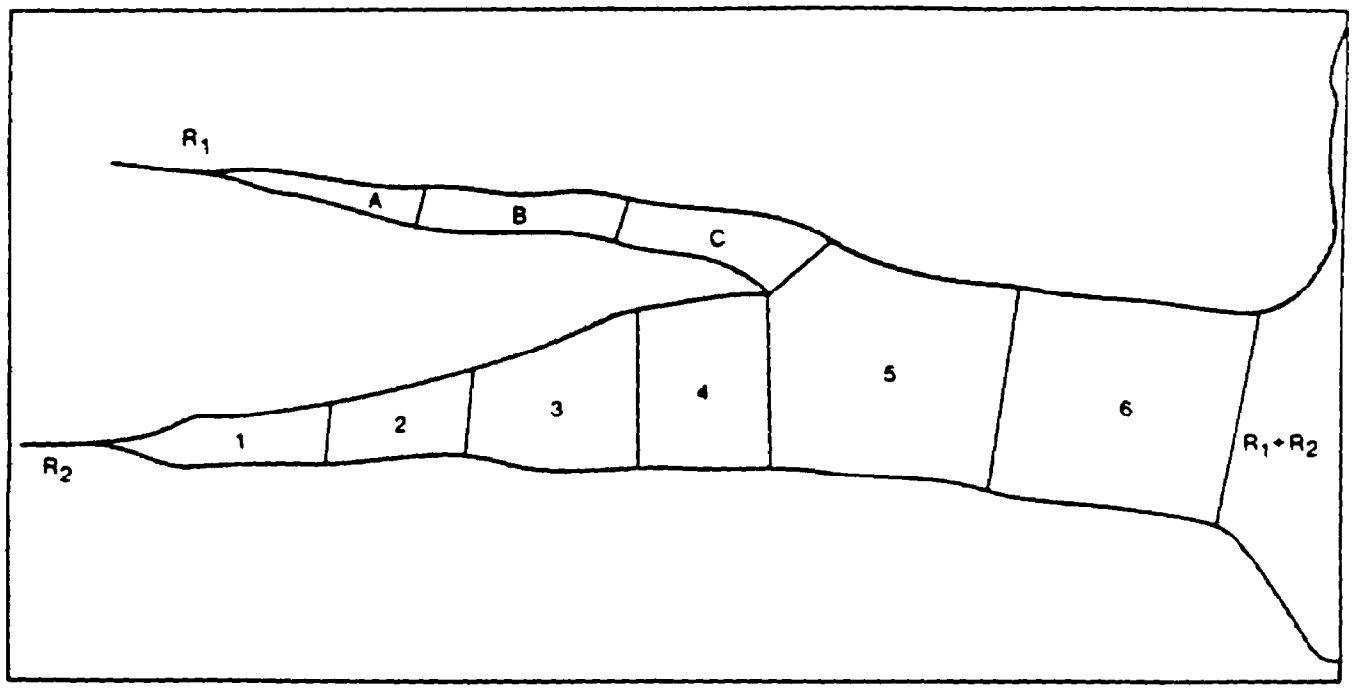

FIGURE VI-15 HYPOTHETICAL TWO-BRANCHED ESTUARY

flushing potential of that segment per tidal cycle (Dyer, 1973). The method assumes complete mixing of the incoming tidal prism waters with the low tide volumes within each segment. Best results have been obtained in estuaries when the number of segments is large (i.e. when river flow is very low) and when estuarine cross-sectional area increases fairly quickly downstream (Dyer, 1973).

The modified tidal prism method does not require knowledge of the salinity distribution. It provides some concept of mean segment velocities since each segment length is tied to particle excursion length over one tidal cycle. A disadvantage of the method is that in order to predict the flushing time of a pollutant discharged midway down the estuary, the method still has to be applied to the entire estuary.

The modified tidal prism method is a four-step methodology. The steps are:

1. Segment the estuary. For this method an estuary must be segmented so that each segment length reflects the excursion distance a particle can travel during one tidal cycle. The innermost section must then have a tidal prism volume completely supplied by river flow. Thus:

$$P_0 = R$$

where

P_0 = tidal prism (intertidal volume) of segment "0"
R = river discharge over one tidal cycle.

The low tide volume in this section (V_0) is that water volume occupying the space under the intertidal volume P_0 (which has just been defined as being equal to R). The seaward limit of the next seaward segment is placed such that its low tide volume (V_1) is defined by:

$$V_1 = P_0 + V_0 \qquad \text{(VI-13)}$$

P_1 is then that intertidal volume which, at high tide, resides above V_1. Successive segments are defined in an identical manner to this segment so that:

$$V_i = P_{i-1} + V_{i-1} \qquad \text{(VI-14)}$$

Thus each segment contains, at high tide, the volume of water contained in the next seaward section at low tide.

2. Calculate the exchange ratio (r) by:

$$r_i = \frac{P_i}{P_i + V_i} \qquad \text{(VI-15)}$$

Thus the exchange ratio for a segment is a measure of a portion of water associated with that segment which is exchanged with adjacent segments during each tidal cycle.

3. Calculate segment flushing time by:

$$T_i = \frac{1}{r_i} \qquad \text{(VI-16)}$$

where

T_i = flushing time for segment "i", measured in tidal cycles.

4. Calculate total estuarine flushing time by summing the individual segment flushing times:

$$T_f = \sum_{i=1}^{n} T_i \qquad \text{(VI-17)}$$

where

T_f = total estuary flushing time

n = number of segments.

Table VI-6 shows a suggested method for calculating flushing time by the modified tidal prism method.

TABLE VI-6

SAMPLE CALCULATION TABLE FOR ESTUARINE FLUSHING TIME BY THE MODIFIED TIDAL PRISM METHOD

← Down Estuary

Segment Number	Segment Dimensions				Subtidal Water Volume, V_j (m^3)	Intertidal Water Volume P_j (m^3)	Segment Exchange Ratio r_j	Segment Flushing Time, T_j (Tidal Cycles)
	Starting Distance Above Mouth (m)	Ending Distance Above Mouth (m)	Distance of Center Above Mouth (m)	Segment Length (m)				
							$\sum_{j=1}^{n} T_j$ =	

EXAMPLE VI-4

Estuary Flushing Time Calculation by the Modified Tidal Prism Method

The Fox Mill Run Estuary, Virginia, was selected for this example. During low flow conditions, the discharge of Fox Mill Run has been measured at 0.031 m^3/sec.

R = river discharge over one tidal cycle
= 0.031 m^3/sec x 12.4 hrs/tidal cycle x 3600 sec/hr
= 1384 m^3/tidal cycle

The estuary flushing time is found in four steps:

1. Segmentation

From bathymetric maps and tide gage data, cumulative upstream volume was plotted for several positions along the estuary (see Figure VI-16).

Since:

$$P_o = R$$
$$P_o = 1384\ m^3$$

Reading across the graph from "a" to the intertidal volume curve, then down the subtidal volume curve and across to "b":

$$V_o = 490\ m^3$$

The known cumulative upstream water volume also establishes the downstream segment boundary. Reading downward from the subtidal volume curve to "c", a V_o of 490 m^3 corresponds to an upstream distance of 2.700 meters for the segment 0 lower boundary.

The low tide water volume for the next segment can be found by the equation:

$$V_1 = P_0 + V_0$$

or

$$V_1 = 1384 + 490 = 1874\ m^3$$

Since the graphs of Figure VI-16 are cumulative curves, it is necessary, when entering a V_i value in order to determine a P_i value, to sum the upstream V_i's. For V_1 the cumulative upstream low-tide volume is:

$$V_0 + V_1 = 490 + 1874 = 2364\ m^3$$

Entering the graph where the subtidal volume is equal to 2,364 m^3 (across from "d"), we can move upward to read the corresponding cumulative intertidal volume "e" on the vertical scale, and downward to read the

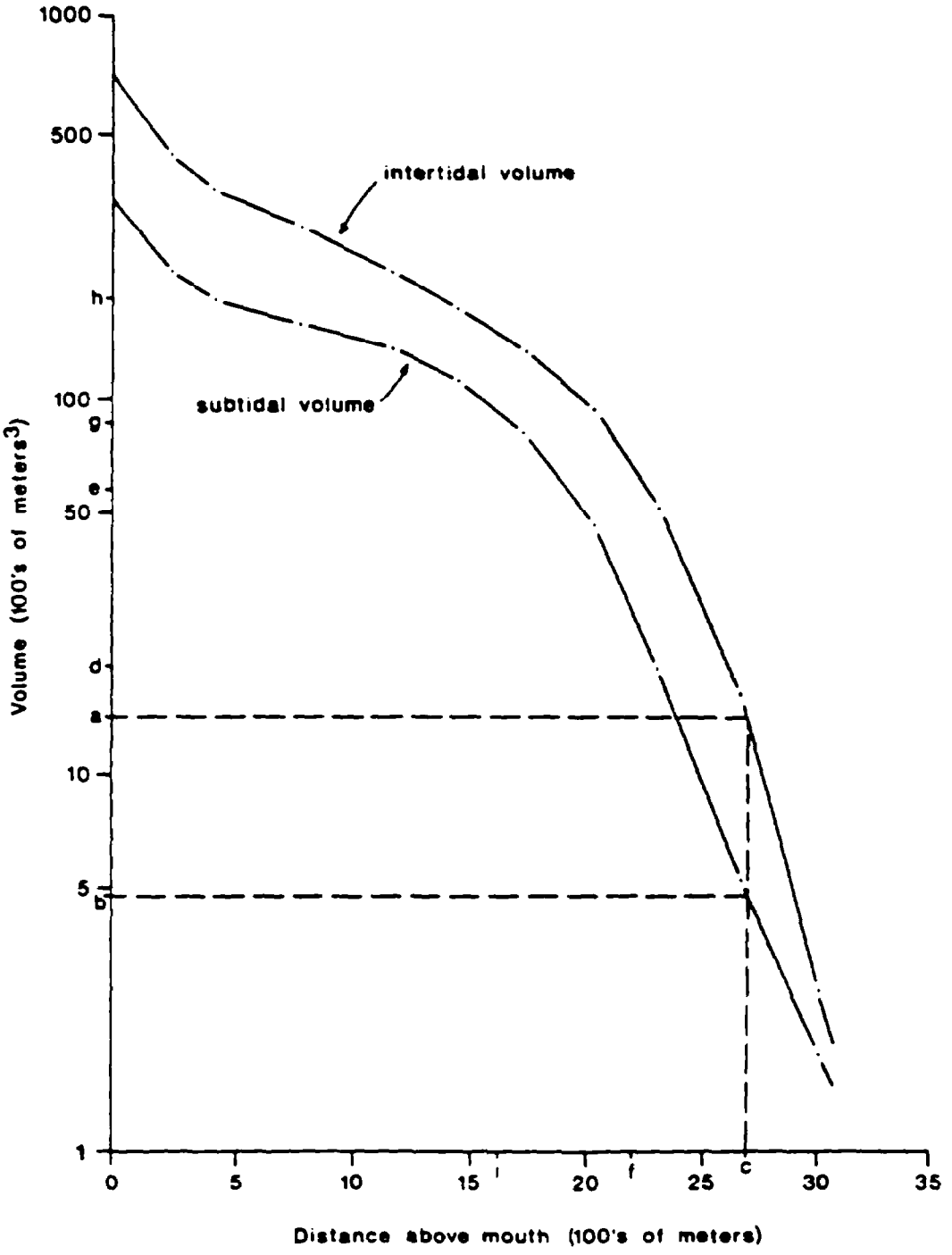

FIGURE VI-16 CUMULATIVE UPSTREAM WATER VOLUME, FOX MILL RUN ESTUARY

downstream boundary of segment 1 at "f" on the horizontal scale. The cumulative upstream intertidal volume is 5900 m^3.

Since:

$$5900\ m^3 = P_0 + P_1$$

$$P_1 = 5900 - 1384 = 4516\ m^3$$

For segment 2:

$$V_2 = P_1 + V_1 = 1874 + 4516 = 6390\ m^3$$

To find P_2, it is necessary to enter the graph at a cumulative subtidal volume of:

$$V_0 + V_1 + V_2 = 490 + 1874 + 6390 = 8759\ m^3 \text{ (across from "g")}$$

This yields a cumulative intertidal volume of 14,000 m^3 (across from "h") and a downstream segment boundary of 1,650 m^3"i".

The tidal prism of Segment 2 is found by:

$$14000 = P_0 + P_1 + P_2$$

or

$$P_2 + 14000 - 1384 - 4516 + 8100\ m^3$$

The procedure is identical for Segment 3. For this final segment:

$$V_3 = 14{,}490\ m^3$$
$$P_3 = 36{,}000\ m^3$$

Dimensions and volumes of the four segments established by this procedure are compiled in Table VI-7.

2. The exchange ratio for segment 0 is found by:

$$r_0 = \frac{P_0}{P_0+V_0} = \frac{1384\ m^3}{1384\ m^3 + 490\ m^3}$$

Exchange ratios are calculated similarly for the other three segments.

3. Flushing time for each segment "i" is given by:

$$T_i = \frac{1}{r_i}$$

so

$$T_o = \frac{1}{r_o} = \frac{1}{0.74} = 1.35$$

Exchange ratios and flushing times for the four segments are shown in Table IV-7.

4. Flushing time for the whole estuary is found by:

$$T_f = \sum_{i=o}^{3} T_i$$

TABLE VI-7

DATA AND FLUSHING TIME CALCULATIONS FOR FOX MILL RUN ESTUARY

Segment Number	Segment Dimensions				Water Volume at Low Tide V_i meters^3	Intertidal Volume P_i meters^3	Exchange Ratio for Segment i r_i	Flushing Time for Segment i T_i
	Starts at this Distance Above Mouth-meters	Stops at this Distance Above Mouth-meters	Center Point Distance Above Mouth-meters	Segment Length meters				
0	3,200	2,700	2,950	500	490	1,384	0.74	1.35
1	2,700	2,240	2,470	460	1,874	4,516	0.71	1.41
2	2,240	1,650	1,945	590	6,390	8,100	0.56	1.79
3	1,650	180	915	1,470	14,490	36,000	0.71	1.41

ΣT = 5.96 tidal cycles

or

$T = 1.35 + 1.41 + 1.79 + 1.41$

= 5.96 tidal cycles

= 73.9 hours

= 3.1 days

END OF EXAMPLE VI-4

6.4 FAR FIELD APPROACH TO POLLUTANT DISTRIBUTION IN ESTUARIES

6.4.1 Introduction

Analysis of pollutant distribution in estuaries can be accomplished in a number of ways. In particular, two approaches, called the far field and near field approaches, are presented here (Sections 6.4 and 6.5, respectively). As operationally defined in this document, the far field approach ignores buoyancy and momentum effects of the wastewater as it is discharged into the estuary. The pollutant is assumed to be instantaneously distributed over the entire cross-section of the estuary (in the case of a well-mixed estuary) or to be distributed over a lesser portion of the estuary in the case of a two-dimensional analysis. Whether or not these assumptions are realistic depends on a variety of factors, including the rapidity of mixing compared to the kinetics of the process being analyzed (e.g. compared to dissolved oxygen depletion rates). It should be noted that far field analysis (either one- or two-dimensional) can be used even if actual mixing is less than assumed by the method. However, the predicted pollutant concentrations will be lower than the actual concentrations.

Near field analysis considers the buoyancy and momentum of the wastewater as it is discharged into the receiving water. Pollutant distribution can be calculated on a smaller spatial scale, and assumptions such as "complete mixing" or "partial mixing" do not have to be made. The actual amount of mixing which occurs is predicted as an integral part of the method itself. This is a great advantage in analyzing compliance with water quality standards which are frequently specified in terms of a maximum allowable pollutant concentration in the receiving water at the completion of initial dilution. (Initial dilution will be defined later in Section 6.5.2.)

The following far field approaches for predicting pollutant distribution are presented in this chapter:

- Fraction of freshwater method
- Modified tidal prism method
- Dispersion-advection equations
- Pritchard's Box Model.

The near field analysis uses tabulated results from an initial dilution model called MERGE. At the completion of initial dilution predictions can be made for the following:

- Pollutant concentrations
- pH levels
- Dissolved oxygen concentrations.

The near field pollutant distribution results are then used as input to an analytical technique for predicting pollutant decay or dissolved oxygen levels subsequent to initial dilution. The remainder of Section 6.4 will discuss those methods applicable to the far field approach.

6.4.2 Continuous Flow of Conservative Pollutants

The concentration of a conservative pollutant entering an estuary in a continuous flow varies as a function of the entry point location. It is convenient to separate pollutants entering an estuary at the head of the estuary (with the river discharge) from those entering along the estuary's sides. The two impacts will then be addressed separately.

6.4.2.1 River Discharges of Pollutants

The length of time required to flush a pollutant from an estuary after it is introduced with the river discharge has already been calculated, and is the estuarine flushing time. Now consider a conservative pollutant continuously discharged into a river upstream of the estuary. As pollutant flows into the estuary, it begins to disperse and move toward the mouth of the estuary with the net flow. If, for example, the estuary flushing time is 10 tidal cycles, then 10 tidal cycles following its initial flow into the estuary, some of the pollutant is flushed out to

the ocean. Eventually, a steady-state condition is reached in which a certain amount of pollutant enters the estuary, and the same amount is flushed out of the estuary during each tidal cycle. The amount of this pollutant which resides in the estuary at steady-state is a function of the flushing time. From the definition of flushing time, the amount of fresh water (river water) in the estuary may be calculated by:

$$W_E = T_f R \qquad \text{(VI-18)}$$

where

W_E = quantity of freshwater in the estuary
T_f = estuary flushing time
R = river discharge over one tidal cycle.

Using the same approach, the quantity of freshwater in any segment of the estuary is given by:

$$W_i = T_i R \qquad \text{(VI-19)}$$

where

W_i = quantity of freshwater in the i^{th} segment of the estuary
T_i = flushing time for the i^{th} segment calculated by the fraction of freshwater method.

If a conservative pollutant enters an estuary with the river flow, it can be assumed that its steady-state distribution will be identical to that of the river water itself. Thus:

$$M_i = W_i C_r = T_i R C_r \qquad \text{(VI-20)}$$

and

$$C_i = W_i/V_i \qquad \text{(VI-21)}$$

where

M_i = quantity of pollutant in estuary segment "i"
C_r = concentration of pollutant in the river inflow
C_i = concentration of pollutant in estuary segment "i" assuming all of pollutant "i" enters the estuary with the river discharge. Thus direct discharges into the estuary are excluded.
V_i = water volume segment "i".

The same values for C_i and M_i may also be obtained by using the fraction of

freshwater, f_i, for each segment by:

$$C_i = f_i C_r \qquad \text{(VI-22)}$$

and

$$M_i = C_i V_i \qquad \text{(VI-23)}$$

Thus both the quantity of a pollutant in each segment and its concentration within each segment are readily obtainable by either of the above methods. The use of one of these methods will be demonstrated in Example VI-5 below for calculation of both C_i and M_i.

EXAMPLE VI-5

Calculation of Concentration of Conservative River Borne Pollutant in an Estuary

The Patuxent Estuary is the subject of this example. The problem is to predict the incremental concentration increase of total nitrogen (excluding N_2 gas) in the estuary, given that the concentration in river water at the estuary head is 1.88 mgN/l.

Assume that total nitrogen is conservative and that the nitrogen concentration in local seawater is negligible. The segmentation scheme used in Example VI-2 (fraction of freshwater calculation) will be retained here. For each segment, the total nitrogen concentration is directly proportional to the fraction of freshwater in the segment:

$$C_i = f_i C_r$$

The total nitrogen concentration for the uppermost segment is therefore given by:

$$C_1 = 0.93\ (1.88\ \text{mgN/l})$$
$$= 1.75\ \text{mgN/l}$$

For the next segment it is:

$$C_2 = 0.83\ (1.88\ \text{mgN/l}) = 1.56\ \text{mgN/l}$$

and so on. Nitrogen concentrations for all the segments are compiled in Table VI-8. Note that these are not necessarily total concentrations, but only nitrogen inputs from the Patuxent River.

The incremental mass of nitrogen in each segment is found by:

$$M_i = W_i C_r$$

TABLE VI-8

POLLUTANT DISTRIBUTION IN THE PATUXENT RIVER

Segment Number*	Fraction of Freshwater* in Segment f_i	Resultant Pollutants** Concentration $=f_i$ x 1.88 mgN/l
8	0.037	0.07
7	0.112	0.21
6	0.19	0.36
5	0.29	0.55
4	0.46	0.86
3	0.69	1.30
2	0.83	1.56
1	0.93	1.88
River	1.00	1.88

*From Example VI-2
**These are the increment concentrations of total nitrogen in the estuary due to the river-borne input.

TABLE VI-9

INCREMENTAL TOTAL NITROGEN IN PATUXENT RIVER, EXPRESSED AS KILOGRAMS
(See Problem VI-5)

Segment Number	River Water Volume $W_i = f_i \times V$ meters	Incremental Total N $M_i = W_i$ (1.88) kilograms
8	6.14×10^6	11,500
7	14.6×10^6	27,400
6	13.2×10^6	24,800
5	13.3×10^6	25,000
4	11.5×10^6	21,600
3	10.7×10^6	20,100
2	8.47×10^6	15,900
1	7.35×10^6	13,800

The W_i values for the eight segments were determined in Example VI-2. For segment 1, the incremental nitrogen is given by:

$$M_1 = W_1 C_r$$
$$= (7.35 \times 10^6 m^3)(1.88 \text{ mgN/l})(10^3 l/m^3)$$
$$= 1.38 \times 10^{10} \text{ mg or } 13{,}800 \text{ kg}$$

Increased total nitrogen (in kilograms) for the entire estuary is shown in Table VI-9.

END OF EXAMPLE VI-5

In this example, low tide volumes were used to calculate M_i since low tide volumes had been used to calculate f_i's. The approach assumes that C_i's are constant over the tidal cycle and that M_i's are constant over the tidal cycle. This leads to the assumption that calculation of a low tide C_i and M_i will fully characterize a pollutant in an estuary. This, however, is not strictly true. Figure VI-17 depicts one tidal cycle in an estuary and shows the periods of the cycle during which a pollutant is flushed out of the estuary and during which river discharge brings pollutants into the estuary. During periods of high tide, rising tidal elevation blocks river discharge and backs up river flow in the lower stretches of the river. Figure VI-17 also shows the resulting quantity of a pollutant in residence in the estuary (W_{pe}) over the tidal cycle. This variation over the tidal cycle as a percentage of M_E is dependent on the flushing time but is usually small. The change in the total volume of water in an estuary over a tidal cycle is equal to the tidal prism which is often of the same magnitude as the low tide volume. As an example, the Alsea Estuary in Oregon has $P_t = 5.1 \times 10^8$ ft^3 while $V_t = 2.1 \times 10^8$ (Goodwin, Emmet, and Glenne, 1970). Thus the variation in estuarine volume is 2.5 times the low tide volume. As a result, estuarine volume variations over a tidal cycle have a much greater impact on variations in pollutant concentrations in the estuary than do changes in the quantity of pollutant present in the estuary over a tidal cycle. It is important to note, however, that low tidal volume and low M_E nearly coincide, so that variations in mean pollutant concentrations are less severe than are estuarine water mass changes.

This qualitative description of pollutant flow into and out of an estuary is somewhat simplistic since it assumes that high tide and low tide at the mouth of an estuary coincide with those at the head of the estuary. This is usually not the case. There is normally a lag time between tidal events at an estuarine mouth and those at its head. Thus river discharge into the estuary which depends on tidal conditions at the head, and tidal discharge which depends on tidal conditions at the mouth, are not as directly tied to each other as indicated in Figure VI-17.

While W_E does not vary substantially over a tidal cycle under steady-state

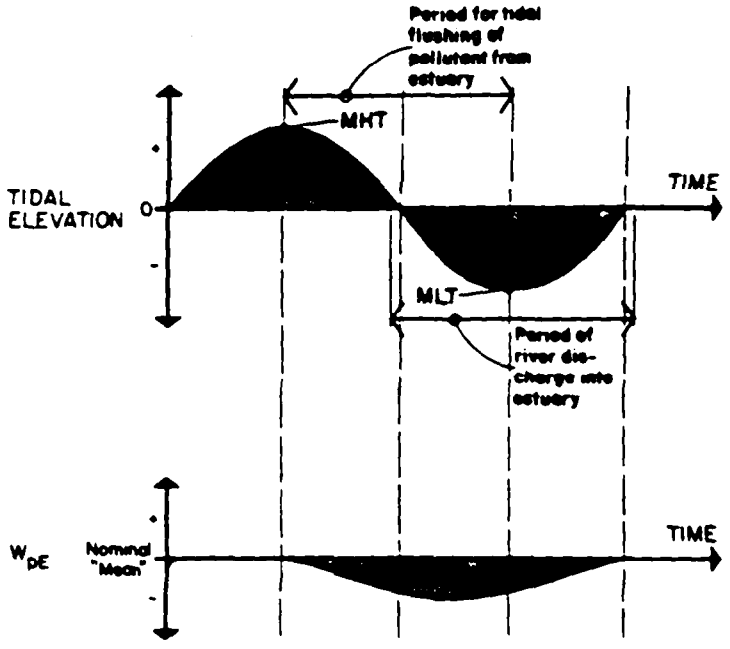

FIGURE VI-17 RIVER BORNE POLLUTANT CONCENTRATION FOR ONE TIDAL CYCLE

conditions, the mean concentration of a pollutant in an estuary (C_E) does. Alsea Estuary data can be used to show this C_E variation over a tidal cycle. Using data for the estuary as a whole (mean concentration), the equations for this comparison are:

$$M_E = W_r T_f \qquad \text{(VI-24)}$$

and

$$C_E = M_E/(V_t + P_t) \qquad \text{(VI-25)}$$

with

$$W_r = (566.4\ \mu g/ft^3)\ (4.64 \times 10^6 ft^3/\text{tidal cycle})$$

or

$$W_r = 2.628 \times 10^9 \mu g/\text{tidal cycle}.$$

Then:

$$M_E = (2.628 \times 10^9 \mu g/\text{tidal cycle})(20.8\ \text{tidal cycle})$$
$$M_E = 5.466 \times 10^{10} \mu g$$

and

$$C_{E(low)} = 5.466 \times 10^{10} \mu g/2.1 \times 10^8 ft^3$$

or

$C_{E(low)}$ = 260.31 $\mu g/ft^3$, or 46 percent of river concentration.

However:

$C_{E(high)} = 5.466 \times 10^{10} \mu g/(2.1 \times 10^8 ft^3 + 5.1 \times 10^8 ft^3)$

$C_{E(high)}$ = 75.92 $\mu g/ft^3$ or 13 percent of river concentration.

In an actual estuary, the concentration of a pollutant is not a stepwise function as indicated by segment C_i values, but is more realistically a continuous spectrum of values. By assigning the longitudinal midpoint of each segment a concentration value equal to that segment's C_i, a resulting continuous curve can be constructed as shown in Figure VI-18. This type of plot is useful in estimating pollutant concentrations within the estuary. It can also be used, however, to estimate maximum allowable C_r to maintain a given level of water quality at any point within the estuary. This latter use of Figure VI-18 is based on determining the desired concentration level (C_x) and then using the ratio of C_x to C_r to calculate an allowable C_r.

6.4.2.2 Other Continuous Conservative Pollutant Inflows

In the previous section, an analysis was made of the steady-state distribution of a continuous flow pollutant entering at the head of an estuary. The result was a graph of the longitudinal pollutant concentration within the estuary (Figure VI-18). This section addresses a continuous, conservative pollutant flow entering along the side of an estuary. Such a pollutant flow (e.g. the conservative elements of a municipal sewer discharge, industrial discharge, or minor tributary) is carried both upstream and downstream by tidal mixing, with the highest concentration occurring in the vicinity of the outfall. Once a steady state has been achieved, the distribution of this pollutant is directly related to the distribution of fresh river water (Dyer, 1973).

The average cross-sectional concentration at the outfall under steady-state conditions is:

$$C_o = \frac{Q_p}{R} f_o \qquad \text{(VI-26)}$$

where

C_o = mean cross-sectional concentration of a pollutant at the point of discharge, mass/volume

Q_p = discharge rate of pollutant, mass/tidal cycle

f_o = segment fraction of freshwater

R = river discharge rate, volume/tidal cycle.

Downstream of the outfall, the pollutant must pass through any cross section at

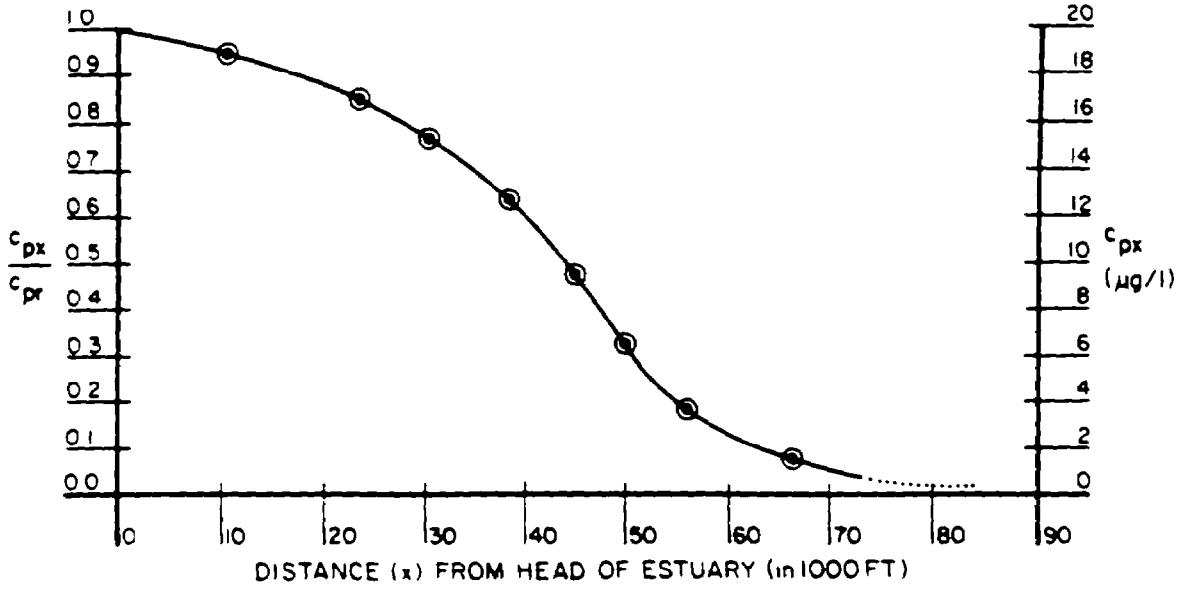

FIGURE VI-18 ALSEA ESTUARY RIVERBORNE CONSERVATIVE POLLUTANT CONCENTRATION

a rate equal to the rate of discharge. Thus:

$$C_x = C_o \frac{f_x}{f_o} = C_o \left(\frac{\frac{S_s - S_x}{S_s}}{\frac{S_s - S_o}{S_s}} \right) = C_o \left(\frac{S_s - S_x}{S_s - S_o} \right) = f_x \frac{Q_p}{R} \qquad \text{(VI-27)}$$

where

S_x, C_x and f_x denote downstream cross-sectional values

S_o, C_o and f_o denote the cross-sectional values at the discharge point (or segment into which discharge is made).

Upstream of the outfall, the quantity of pollutant diffused and advectively carried upstream is balanced by that carried downstream by the nontidal flow so that the net pollutant transport through any cross section is zero. Thus, the pollutant distribution is directly proportional to salinity distribution and (Dyer, 1973):

$$C_x = C_o \frac{S_x}{S_o} \qquad \text{(VI-28)}$$

Downstream of the outfall, the pollutant concentration resulting from a point discharge is directly proportional to river-borne pollutant concentration. Upstream from the discharge point, it is <u>inversely</u> proportional to river-borne pollutant concentrations. Figure VI-19 is a graph of f_x versus distance from the estuary

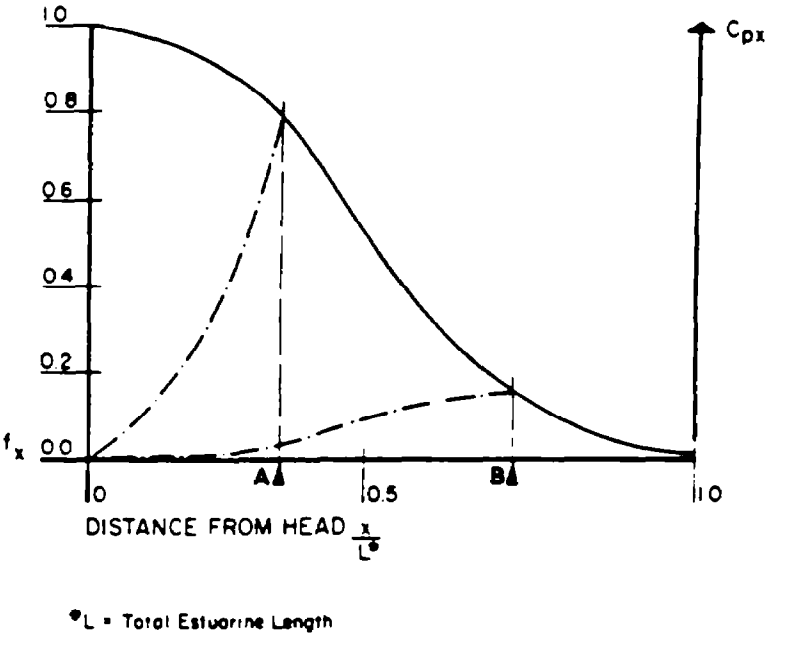

*L = Total Estuarine Length

FIGURE VI-19 POLLUTANT CONCENTRATION FROM AN ESTUARINE OUTFALL (AFTER KETCHUM, 1950)

head for a typical estuary. The solid f_x line is also a measure of pollutant concentration for all points downstream of a pollutant outfall (either discharge location A or B). The actual concentration (C_x) for any point is equal to this f_x value multiplied by Q_p/R which is a constant over all x. Upstream concentrations decrease from C_o in a manner proportional to upstream salinity reduction (see dotted lines). It is important to note how even a small downstream shift in discharge location creates a very significant reduction in upstream steady-state pollutant concentration. Table VI-10 shows a suggested format for tabulating pollutant concentrations by the fraction of freshwater method.

EXAMPLE VI-6

Calculation of Conservative Pollutant Concentration for a Local Discharge

This example will again utilize the eight-segment scheme devised for the Patuxent Estuary in Example VI-2. The objective is to predict the concentration distribution of total nitrogen in the estuary resulting from a discharge of 80,000 mgN/sec into segment 4.

The first step is to determine the nitrogen concentration in segment 4.

TABLE VI-10

SAMPLE CALCULATION TABLE FOR DISTRIBUTION OF A LOCALLY DISCHARGED CONSERVATIVE POLLUTANT BY THE FRACTION OF FRESHWATER METHOD

From Table VI-3					
Segment Number	Fraction of Freshwater f_i	Mean Segment Salinity (ppt)	$\frac{f_i}{f_o}$	$\frac{S_i}{S_o}$	Pollutant Concentrations* (mg/l)
Segment Containing Discharge			1	1	

⟵ Up Estuary

*Pollutant concentration = $\begin{cases} C_o \frac{f_i}{f_o}, & \text{down estuary of the discharge} \\ C_o \frac{S_i}{S_o}, & \text{up estuary of the discharge} \end{cases}$

where $C_o = \frac{W}{R} f_o$

From Equation VI-26:

$$C_o = \frac{Q_p}{R} f_o = \frac{(8\times10^4 \text{ mgN/sec} \times 12.4 \text{ hrs/tidal cycle} \times 3600 \text{ sec/hr})(0.46)}{5.36\times10^5 \text{m}^3\text{/tidal cycle}}$$

$$= \frac{3065 \text{ mgN}}{\text{m}^3} = 3.065 \text{ mgN/l}$$

For segments 1-3, upstream from the discharge, nitrogen concentration is found by Equation VI-28:

$$C_i = C_o \frac{S_i}{S_o}$$

For segment 1:

$$S_1 = 0.8\ ‰$$

$$S_0 = S_4 = 5.8\ ‰$$

$$C_4 = 3.065\ mgN/l$$

so

$$C_1 = 3.065\ mgN/l \left(\frac{0.8\ ‰}{5.8\ ‰}\right) = 0.42\ mgN/l$$

Nitrogen concentrations in segments 2 and 3 are found in an identical way. Table VI-11 summarizes the information used in the calculation.

For the segments downstream of the discharge, total nitrogen concentration is found using Equation VI-27:

$$C_i = C_0 \frac{f_i}{f_0}$$

In segment 5:

$$f_5 = 0.29$$

$$f_0 = f_4 = 0.46$$

TABLE VI-11

NITROGEN CONCENTRATION IN PATUXENT ESTUARY
BASED ON LOCAL DISCHARGE

	Segment Number	Fraction of Freshwater f_i	Mean Segment Salinity	$\frac{S_i}{S_0}$	$\frac{f_i}{f_0}$	Concentration mgN/l
	8	0.037	10.3	-	0.08	0.25
	7	0.112	9.5	-	0.24	0.74
	6	0.19	8.7	-	0.41	1.26
	5	0.29	7.6	-	0.63	1.93
Discharge →	4	0.46	5.8	1	1	3.06
	3	0.69	3.3	0.57	-	1.75
	2	0.83	1.8	0.31	-	0.95
	1	0.93	0.8	0.14	-	0.43

and

$$C_4 = 3.065 \text{ mgN/l}$$

so

$$C_5 = 3.065 \text{ mgN/l} \left(\frac{0.29}{0.46}\right) = 1.93 \text{ mgN/l}$$

The same procedure yields nitrogen concentrations in segments 6-8, also downstream of the discharge.

Figure VI-20 below shows the nitrogen concentration distribution over the entire estuary. Note that the nearer a discharge is to the estuary's mouth, the greater the protection rendered the upstream reaches of the estuary.

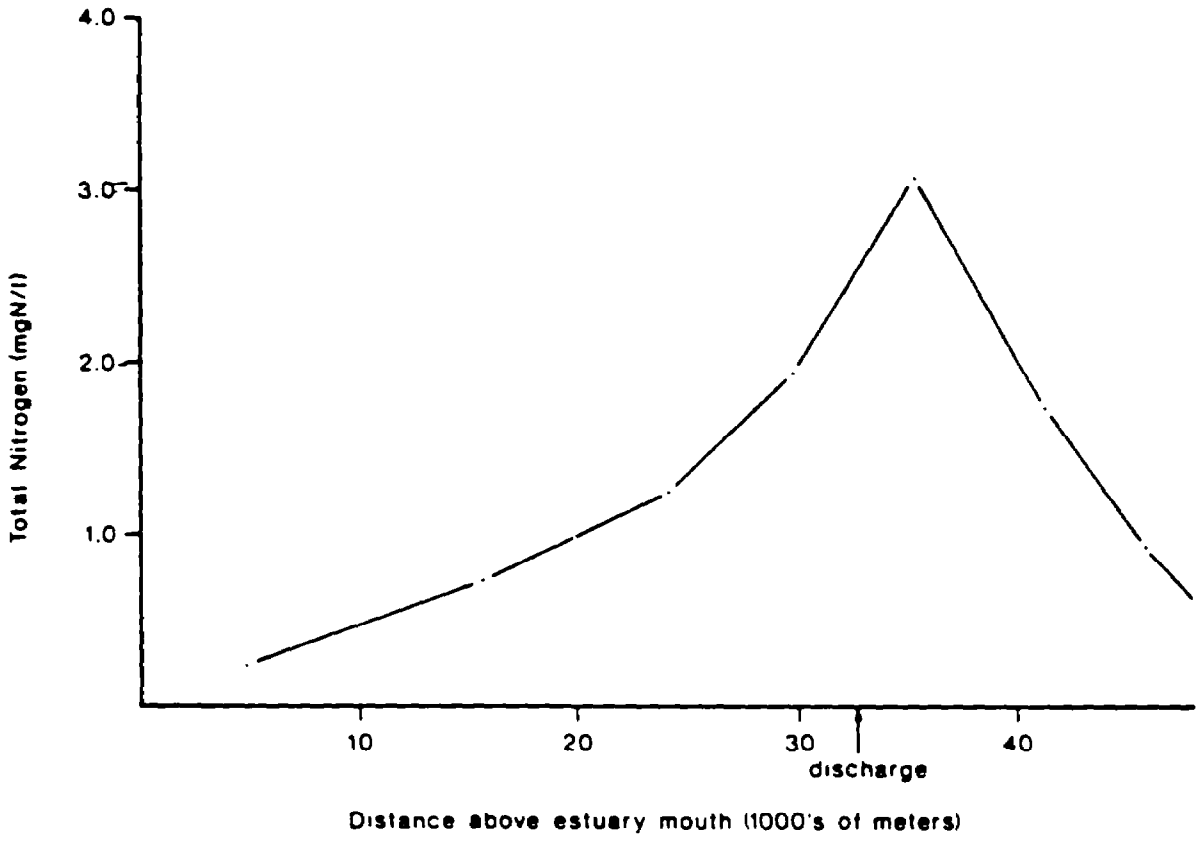

FIGURE VI-20 HYPOTHETICAL CONCENTRATION OF TOTAL NITROGEN IN PATUXENT ESTUARY

END OF EXAMPLE VI-6

6.4.3 Continuous Flow Non-Conservative Pollutants

Most pollutant discharges into estuaries have some components which behave non-conservatively. A number of processes mediate the removal of compounds from natural waters, among these:

- Sorption by benthic sediments on suspended matter
- Partitioning
- Decay (by photolysis or biologically mediated reactions)
- Biological uptake
- Precipitation
- Coagulation.

The latter two processes are particularly significant in estuaries. Thus, in addition to dispersion and tidal mixing, a time-dependent component is incorporated when calculating the removal of non-conservative pollutants from estuarine waters. The concentrations of non-conservative pollutants are always lower than those of conservative pollutants (which have a decay rate of zero) for equal discharge concentrations. The results of the previous section for conservative constituents serve to set upper limits for the concentration of non-conservative continuous flow pollutants. Thus, if plots similar to Figure VI-17 for river discharges and to Figure VI-19 for other direct discharges have been prepared for flow rates equal to that of the non-conservative pollutant under study, some reasonable approximations can be made for steady-state non-conservative pollutant concentrations without requiring additional data. Assuming a first order decay rate for the non-conservative constituent, its concentration is given by:

$$C_t = C_o e^{-kt} \qquad \text{(VI-29)}$$

where

C_t = pollutant concentration at time "t"
C_o = initial pollutant concentration
k = decay rate constant.

For conservative pollutants $k = 0$ and $C = C_o$ under steady-state conditions. Decay rates are determined empirically and depend on a large number of variables. Typical decay rates for BOD and coliform bacteria are shown in Table VI-12. If data are not available for a particular estuary, the use of these average values will provide estimates.

It should be noted that decay rates are dependent upon temperature. The values given assume a temperature of 20°C. Variations in k values for differing temperatures are given by Equation VI-30:

$$k_T = k_{20°}\, \theta^{T-20°} \qquad \text{(VI-30)}$$

TABLE VI-12

TYPICAL VALUES FOR DECAY REACTION RATES 'k'*

Source	BOD	Coliform
Dyer, 1973		.578
Ketchem, 1955		.767
Chen and Orlob, 1975	.1	.5
Hydroscience, 1971	.05-.125	1-2
McGaughhey, 1968	.09	
Harleman, 1971	.069	

*k values for all reactions given on a per tidal cycle basis, 20° C.

where

k_T = decay rate at temperature T

k_{20} = decay rate at 20°C (as given in Table VI-12)

Θ = a constant (normally between 1.03 and 1.05).

Thus an ambient temperature of 10°C would reduce a k value of 0.1 per tidal cycle to 0.074 for a $\Theta = 1.03$.

Decay effects can be compared to flushing effects by setting time equal to the flushing time and comparing the resulting decay to the known pollutant removal rate as a result of flushing. If kt in Equation VI-29 is less than 0.5 for $t = T_f$, decay processes reduce concentration by only about one-third over the flushing time. Here mixing and advective effects dominate and non-conservative decay plays a minor role. When $kT_f > 12$ decay effects reduce a batch pollutant to 5 percent of its original concentration in less than one-fourth of the flushing time. In this case, decay processes are of paramount importance in determining steady-state concentrations. Between these extremes, both processes are active in removing a pollutant from the estuary with $3 < kT_f < 4$ being the range for approximately equal contributions to removal. Dyer (1973) analyzed the situation for which decay and tidal exchange are of equal magnitude for each estuarine segment. Knowing the conservative concentration, the non-conservative steady-state concentration in a segment is given by:

$$C_i = C_o \frac{f_i}{f_o} \prod_{i=1,\ldots,n} \left(\frac{r_i}{1-(1-r_i)e^{-kt}} \right) \quad \text{for segments downstream of the outfall} \qquad \text{(VI-31)}$$

and

$$C_i = C_o \frac{S_i}{S_o} \prod_{i=1,..,n} \left(\frac{r_i}{1-(1-r_i)e^{-kt}} \right) \quad \text{for segments upstream of the outfall} \qquad \text{(VI-32)}$$

where

C_i = non-conservative constituent mean concentration in segment "i"

C_o = conservative constituent mean concentration in segment of discharge

r_i = the exchange ratio for segment "i" as defined by the modified tidal prism method

n = number of segments away from the outfall (i.e. n = 1 for segments adjacent to the outfall; n = 2 for segments next to these segments, etc.)

Other parameters are as previously defined.

In the case of a non-conservative pollutant entering from the river, n = 1, and the only concentration expression necessary is:

$$C_i = C_{i-1} \frac{f_i}{f_{i-1}} B_i \qquad \text{(VI-33)}$$

where

$$B_i = \frac{r_i}{1-(1-r_i)e^{-kt}} \qquad \text{(VI-34)}$$

Table VI-13 shows a suggested format for tabulating pollution concentrations by the modified tidal prism method.

EXAMPLE VI-7

Continuous Discharge of a Non-Conservative Pollutant into the Head of an Estuary

The Fox Mill Run Estuary (see Example VI-3) is downstream of the Gloucester, Virginia, sewage treatment plant. Knowing the discharge rate of CBOD in the plant effluent, the purpose of this example is to determine the concentration of CBOD throughout the estuary.

It is first necessary to determine the concentration of CBOD in Fox Mill Run as it enters the estuary (assume no CBOD decay within the river). The following information has been collected:

C_r, Background CBOD in river = 3 mg/l

TABLE VI-13

SAMPLE CALCULATION TABLE FOR DISTRIBUTION OF A LOCALLY DISCHARGED NON-CONSERVATIVE POLLUTANT BY THE MODIFIED TIDAL PRISM METHOD

From Table VI-6			Mean Salinity (from salinity plot) S_i ppt	Fraction of River Water $f_i = \frac{S_s - S_i}{S_s}$	B_i	Pollutant Concentration $C = C_{i-1} \frac{f_i}{f_{i-1}} - B_i$ (mg/l)
Segment Number	Distance of Center Above Mouth (m)	Segment Exchange Ratio r_i				

← Down Estuary

Q_r, River flow below treatment plant discharge = 0.031 m^3/sec

Q_d, Treatment plant discharge rate = 0.006 m^3/sec

C_d, Treatment plant effluent CBOD = 45 mg/l

The CBOD concentration in the river downstream of the treatment plant is found using the equation:

$$C = \frac{C_r(Q_r-Q_d) + C_dQ_d}{Q_r}$$

or

$$C = \frac{3\ mg/l(.031-.006\ m^3/sec)+45\ mg/l(0.006\ m^3/sec)}{0.031\ m^3/sec}$$

$$= 11.1\ mg/l$$

To find the CBOD concentration distribution in the estuary, the following additional data are used:

S_s, Chesapeake Bay salinity = 19.0 °/oo (at the mouth of Fox Mill Run Estuary)

k, CBOD decay constant = 0.3/day

T, Tidal cycle = 12.4 hours

so

$kt = 0.3/day \times 12.4\ hr \times 1\ day/24\ hours$

$= 0.155$

Also necessary are mean salinity values for each estuary segment. Values for the Fox Mill Run Estuary are summarized in Table VI-14. Fraction of freshwater values for each segment are found using the formula:

$$f_i = \frac{S_s-S_i}{S_s}$$

The variables are as previously defined.

Next, values of the coefficient B_i must be calculated for each segment "i." For segment 0:

r_0, the segment exchange ratio, = 0.74

and

$$B_0 = \frac{r_0}{1-(1-r_0)e^{-kt}} = \frac{0.74}{1-(1-0.74)e^{-0.155}}$$

$$= 0.95$$

Coefficient values for all segments are compiled in Table VI-14.

Finally, CBOD concentrations for the individual segment are calculated, beginning with the uppermost segment and working downstream. The concentration in segment "i" is found by:

$$C_i = C_{i-1}\frac{f_i}{f_{i-1}}B_i$$

TABLE VI-14

SALINITY AND CBOD CALCULATIONS FOR FOX MILL RUN ESTUARY

	From Problem VI-3					
Segment Number	Center Point Distance Above Est. Mouth, Meters	Exchange Ratio For Segment r_i	Mean Segment Salinity S_i, ppt (From Sal. Plot)	Fraction of Fresh (River) $f_i = \frac{S_s - S_i}{S_s}$ (S_s = 19.0)	B_i	Concentration of $CBOD_u$ $C_i = C_{i-1} \frac{f_i}{f_{i-1}} B_i$ (mg/l)
River	(>3200)	-	~0	1.00	-	11.1
0	2950	0.74	4.7	0.75	0.95	8.1
1	2470	0.71	8.6	0.55	0.94	5.5
2	1945	0.56	11.6	0.39	0.90	3.6
3	915	0.71	15.3	0.19	0.94	1.6

For segment 0, the river is taken as segment "i-1", and the calculation is as follows:

$$C_0 = 11.13 \text{ mg/l} \left(\frac{.75}{1.0}\right) 0.95 = 8.1 \text{ mg/l}$$

For segment 1:

$$C_1 = 8.1 \text{ mg/l} \left(\frac{.55}{.75}\right) 0.94 = 5.6 \text{ mg/l}$$

and so on.

Figure VI-21 depicts this estimate of the distribution of CBOD in the estuary. In addition, hypothetical concentrations of a conservative pollutant (k = 0) and coliform bacteria (k = 1.0) are plotted. Downstream concentration diminishes faster for substances having larger decay constants, as might be expected.

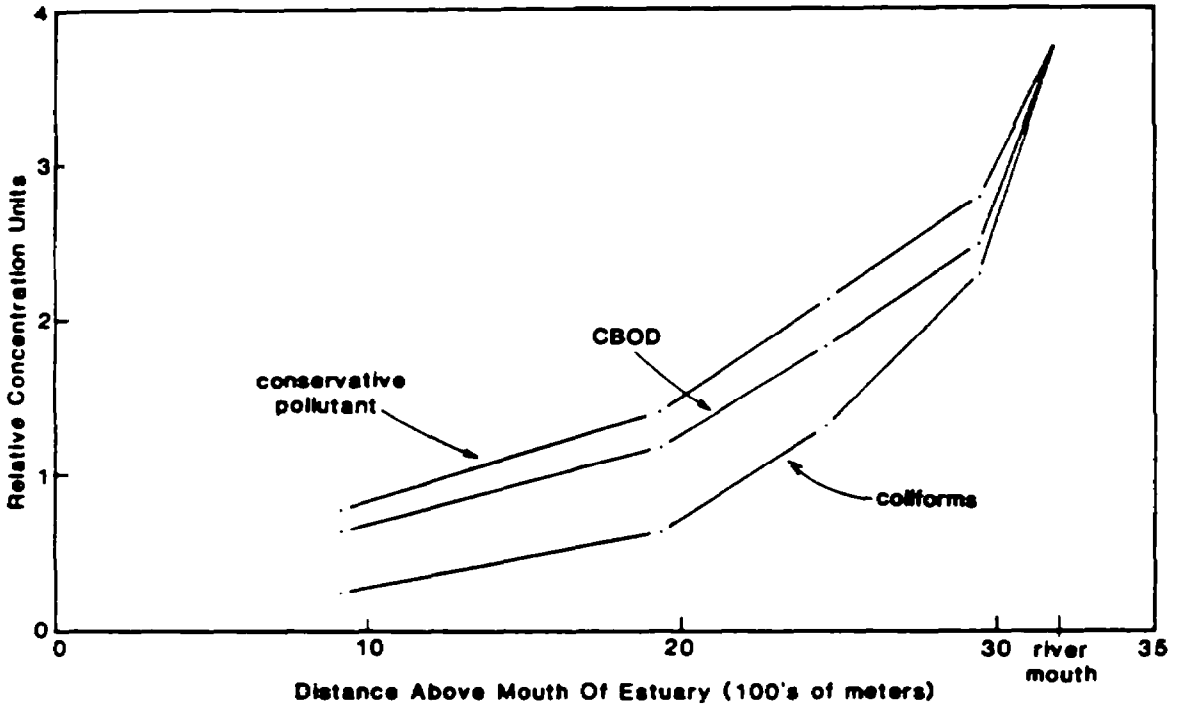

FIGURE VI-21 RELATIVE DEPLETIONS OF THREE POLLUTANTS ENTERING THE FOX MILL RUN ESTUARY, VIRGINIA

END OF EXAMPLE VI-7

6.4.4 Multiple Waste Load Parameter Analysis

The preceding analysis allowed calculation of the longitudinal distribution of a pollutant, either conservative or non-conservative, resulting from a single waste discharge. However, the planner will probably want to simultaneously assess both conservative and non-conservative elements from several separate discharges. This can be accomplished by graphing all desired single element distributions on one graph showing concentration versus length of the estuary. Once graphed, the resulting concentration may be linearly added to obtain a total waste load.

The pollutant concentration increment from each source is calculated by assuming the source is the sole contribution of pollution (i.e. other waste loadings are temporarily set equal to zero). This method, called superposition, is valid as the long as volumetric discharge from any of the sources does not significantly influence the salinity distribution within the estuary. This assumption is typically true, unless the estuary is extremely small and poorly flushed, and the volumetric discharge is large relative to tidal and advective flushing components.

An example of the superposition procedure is shown in Figure VI-22. Three local

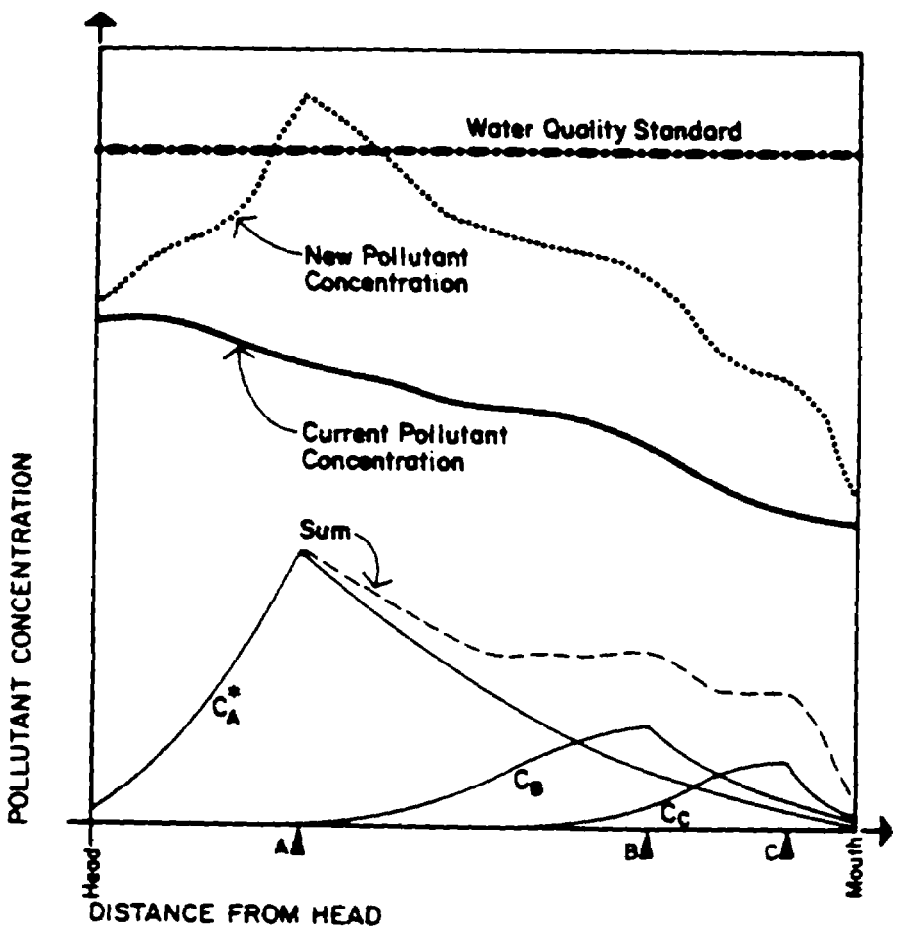

FIGURE VI-22 ADDITIVE EFFECT OF MULTIPLE WASTE LOAD ADDITIONS

point sources of pollutants discharge at locations A, B, and C. A background source enters the estuary with the river discharge. The contribution due to each source can be found from the fraction of freshwater method (assuming the pollutants act conservatively) as follows:

$$C_b = \frac{W_R}{R} f_x \quad , x > 0, \text{ where } x \text{ is measured from the head of the estuary}$$

$$C_A = \begin{cases} \frac{W_A}{R} f_x & , \quad x > A \\ \frac{W_A}{R} f_A \frac{S_x}{S_A} & , \quad x < A \end{cases}$$

$$C_B = \begin{cases} \frac{W_B}{R} f_x & , x > B \\ \frac{W_B}{R} f_B \frac{S_x}{R} & , \quad x < B \end{cases}$$

$$C_C = \begin{cases} \frac{W_C}{R} f_x & , x > C \\ \frac{W_C}{R} f_C \frac{S_x}{R} & , \quad x < C \end{cases}$$

where

C_b = concentration due to river discharge

C_A, C_B, C_C = concentrations due to sources A, B, and C, respectively

R = river flow rate

f_A, f_B, f_C = fraction of freshwater at locations A, B, C, respectively

S_A, S_B, S_C = salinity at locations A, B, C, respectively.

The pollutant concentration (above background) at any location in the estuary is:

$$\text{Sum} = C_A + C_B + C_C$$

and is shown in Figure VI-22. When this is added to the background level, the total pollutant concentration becomes:

$$C_T = (C_A + C_B + C_C) + C_b$$

The dotted line in Figure VI-22 depicts C_T.

The technique of graphing outfall location and characteristics with resulting estuarine pollutant concentration can be done for all anticipated discharges. This will provide the planner with a good perspective on the source of potential water quality problems.

Where the same segmentation scheme has been used to define incremental pollutant distributions resulting from several sources, the results need not even be plotted to determine the total resultant concentrations. In this case, the estuary is evaluated on a segment-by-segment basis. The total pollutant concentration in each segment is calculated as the arithmetic sum of the concentration increments resulting from the various sources.

EXAMPLE VI-8

The previous two example problems involved calculations of nitrogen concentration in the Patuxent Estuary resulting from individual nitrogen sources. The objective of this example is to find the total nitrogen concentration in the estuary resulting from both nitrogen sources.

The eight-segment scheme of Examples VI-6 and VI-7 is retained for this problem. For each segment, the incremental nitrogen increases are summed to give the total concentration:

$$C = C_b + C_A$$

where

C_b = concentration resulting from the N source discharging into the estuary at point A.

For segment 1, the calculation is:

C = 1.75 mg/l (from river) + 0.43 mg/l (from local source)
= 2.18 mg/l total nitrogen

Necessary data and final concentrations for each segment are shown in Table VI-15.

TABLE VI-15

DISTRIBUTION OF TOTAL NITROGEN IN THE PATUXENT ESTUARY DUE TO TWO SOURCES OF NITROGEN

Segment Number	Results From Problem VI-4 Total Nitrogen From River mgN/l, C_b	Results From Problem VI-5 Total Nitrogen From Point A Source (Segment 4) mgN/l, C_A	Resultant Concentration $C=C_b + C_A$ mgN/l
8	0.07	0.25	0.32
7	0.21	0.74	0.95
6	0.36	1.26	1.62
5	0.55	1.93	2.48
4	0.80	3.06	3.92
3	1.30	1.74	3.04
2	1.56	0.95	2.51
1	1.75	0.43	2.18
River	1.88	0.00	1.88

END OF EXAMPLE VI-8

6.4.5 Dispersion-Advection Equations for Predicting Pollutant Distributions

Dispersion-advection equations offer an attractive method, at least theoretically, of predicting pollutant and dissolved oxygen concentrations in estuaries. However, from the point of view of hand calculation, the advection-dispersion equations are usually tedious to solve, and therefore mistakes can unknowingly be incorporated into the calculations.

Dispersion-advection equations have been developed in a variety of forms, including one-, two-, and three-dimensional representations. The equations in this section are limited to one-dimensional representations in order to reduce the amount of data and calculations required.

One-dimensional dispersion-advection equations can be expressed in quite divergent forms, depending on boundary conditions, cross-sectional area variation over distance, and source-sink terms. O'Connor (1965), for example, developed a variety of one-dimensional advection-dispersion equations for pollutant and dissolved oxygen analyses in estuaries, some of which are infeasible for use on the hand-calculation level.

The advection-dispersion equations to be presented subsequently in this chapter can be used to predict:

- Distributions of conservative or non-conservative pollutants
- Polllutant distributions in embayments
- Dissolved oxygen concentrations.

Solutions from advection-dispersion can be superposed to account for multiple discharges. Example VI-9, to be presented subsequently, will illustrate this process.

As the name of the equations implies, dispersion coefficients are needed in order to solve advection-dispersion equations. Tidally averaged dispersion coefficients are required for the steady-state formulations used here. The tidally averaged dispersion coefficient (E_L) can be estimated from the following expression:

$$E_L = \frac{RS}{A\ dS/dx} \tag{VI-35}$$

$$\approx \frac{2RS\Delta x}{A(S_{x+\Delta x} - S_{x-\Delta x})} \tag{VI-36}$$

where

S = tidally and cross sectionally averaged salinity in vicinity of discharge

$2\Delta x$ = distance between the salinity measurements $S_{x+\Delta x}$ (at a distance Δx down estuary) and $S_{x-\Delta x}$ (at a distance of Δx up estuary)

R = freshwater flow rate in vicinity of discharge.

The distance interval $2\Delta x$ should be chosen so that no tributaries are contained within the interval.

In the absence of site specific data, the dispersion coefficients shown in Tables VI-16 and VI-17 can provide estimates of dispersion coefficients.

For pollutants which decay according to first order decay kinetics, the steady state mass balance equation describing their distribution is:

$$E_L \frac{d^2C}{dx^2} - \frac{U\ dC}{dx} - kC = 0 \tag{VI-37}$$

The solution to Equation VI-37 is:

$$C = \begin{cases} C_o\, e^{j_2 x} & x > 0 \text{ (down estuary)} \quad \text{(VI-38a)} \\ C_o e^{j_1 x} & x < 0 \text{ (up estuary)} \quad \text{(VI-38b)} \end{cases}$$

TABLE VI-16

TIDALLY AVERAGED DISPERSION COEFFICIENTS FOR SELECTED ESTUARIES (FROM HYDROSCIENCE, 1971)

Estuary	Freshwater Inflow (cfs)	Low Flow Net Nontidal Velocity (fps) Head - Mouth	Dispersion Coefficient (mi^2/day^*)
Delaware River	2,500	0.12-0.009	5
Hudson River (N.Y.)	5,000	0.037	20
East River (N.Y.)	0	0.0	10
Cooper River (S.C.)	10,000	0.25	30
Savannah R. (Ga., S.C.)	7,000	0.7-0.17	10-20
Lower Raritan R. (N.J.)	150	0.047-0.029	5
South River (N.J.)	23	0.01	5
Houston Ship Channel (Texas)	900	0.05	27
Cape Fear River (N.C.)	1,000	0.48-0.03	2-10
Potomac River (Va.)	550	0.006-0.0003	1-10
Compton_Creek (N.J.)	10	0.01-0.013	1
Wappinger and Fishkill Creek (N.Y.)	2	0.004-0.001	0.5-1

*1 mi^2/day = 322.67 ft^2/sec

where

$$j_2 = \frac{R}{2AE_L}\left(1 - \sqrt{1 + \frac{4kE_L A^2}{R^2}}\right)$$

$$j_1 = \frac{R}{2AE_L}\left(1 + \sqrt{1 + \frac{4kE_L A^2}{R^2}}\right)$$

$$C_o = \frac{W}{R}\frac{1}{\sqrt{1+(4kE_L/U^2)}}$$

U = net velocity

k = decay rate

W = discharge rate of pollutant (at x = 0).

For Equations VI-38a and VI-38b to accurately estimate the pollutant distribution in an estuary, the cross-sectional area of the estuary should be fairly constant over

TABLE VI-17

TIDALLY AVERAGED DISPERSION COEFFICIENTS
(FROM OFFICER, 1976)

Estuary	Dispersion Coefficient Range (ft^2/sec)	Comments
San Francisco Bay Southern Arm Northern Arm	 200-2,000 500-20,000	Measurements were made at slack water over a period of one to a few days. The fraction of freshwater method was used. Measurements were taken over three tidal cycles at 25 locations.
Hudson River	4,800-16,000	The dispersion coefficient was derived by assuming E_L to be constant for the reach studied, and that it varied only with flow. A good relationship resulted between E_L and flow, substantiating the assumption.
Narrows of Mercey	1,430-4,000	The fraction of freshwater method was used by taking mean values of salinity over a tidal cycle at different cross sections.
Potomac River	65-650	The dispersion coefficient was found to be a function of distance below the Chain Bridge. Both salinity distribution studies (using the fraction of freshwater method) and dye release studies were used to determine E_L.
Severn Estuary	75-750 (by Stommel) 580-1,870 (Bowden)	Bowden recalculated E_L values originally determined by Stommel, who had used the fraction of freshwater method. Bowden included the freshwater inflows from tributaries, which produced the larger estimates of E_L.
Tay Estuary	530-1,600 (up estuary) 1,600-7,500 (down estuary)	The fraction of freshwater method was used. At a given location, E_L was found to vary with freshwater inflow rate.
Thames Estuary	600-1,000 (low flow) 3,600 (high flow)	Calculations were performed using the fraction of freshwater method, between 10 and 30 miles below London Bridge.
Yaquina Estuary	650-9,200 (high flow) 140-1,060 (low flow)	The dispersion coefficients for high flow conditions were substantially higher than for low flow conditions, at the same locations. The fraction of freshwater method was used.

distance, and the estuary should be relatively long. For screening purposes the first constraint can be met by choosing a cross-sectional area representative of the length of estuary being investigated. If the estuary is very short, however, pollutants might be washed out of the estuary fast enough to prevent attainment of a steady-state distribution assumed by Equations VI-38a and VI-38b. For shorter estuaries the fraction of freshwater method, modified tidal prism method, or near field approach are more appropriate.

At times when the freshwater flow rate in an estuary is essentially zero pollutant concentrations might increase to substantial levels, if tidal flushing is small. Under these conditions the mass-balance expression for a pollutant obeying first order kinetics is:

$$E_L \frac{d^2C}{dx^2} - kc = 0 \qquad \text{(VI-39)}$$

The solution to this equation is:

$$C = \begin{cases} C_o \exp\left(-\sqrt{\frac{k}{E_L}}\, x\right) & \text{for } x > 0 \text{ (down estuary)} \qquad \text{(VI-40a)} \\ C_o \exp\left(\sqrt{\frac{k}{E_L}}\, x\right) & \text{for } x < 0 \text{ (up estuary)} \qquad \text{(VI-40b)} \end{cases}$$

where

$$C_o = \frac{W}{A\sqrt{4kE_L}} \qquad \text{(VI-41)}$$

When the pollutant is conservative (i.e., k = 0), Equation VI-39 reduces to:

$$E_L \frac{d^2C}{dx^2} = 0 \qquad \text{(VI-42)}$$

The solution is:

$$C = \begin{cases} C_o \text{ , } x < 0 \text{ (up estuary)} & \text{(VI-43a)} \\ \frac{W}{E_L A}(L-x) + C_L \text{ , } x > 0 \text{ (down estuary)} & \text{(VI-43b)} \end{cases}$$

where

$$C_o = C_L + \frac{WL}{E_L A}$$

C_L = background concentration of the pollutant at the mouth of the estuary

L = distance from the discharge location to the mouth of the estuary.

Equation VI-43 illustrates the important concept that the concentrations of conservative pollutants are constant up estuary from the discharge location (when the river discharge is negligible) and decrease linearly from the discharge point to the mouth of the estuary. Equations VI-40 and VI-43 apply to estuaries of constant, or approximately constant, cross-sectional area (e.g. sloughs). If the cross-sectional area increases rapidly with distance toward the mouth, the methods presented in Section 6.5 are more appropriate.

The dissolved oxygen deficit equation (where deficit is defined as the difference between the saturation concentration and the actual dissolved oxygen concentration) for one-dimensional estuaries at steady-state conditions is:

$$\frac{U dD}{dx} = E_L \frac{d^2D}{dx^2} - k_2 D + kL \qquad \text{(VI-44)}$$

where

D = dissolved oxygen deficit
L = BOD concentration
k_2 = reaeration rate
k = BOD decay rate.

Using Equation IV-38 to represent the BOD distribution, the expression for the deficit D is:

$$D = \frac{kh}{A(k_2-k)} \left[\frac{1}{\sqrt{a_1}} \exp\left(\frac{U \pm \sqrt{a_1}}{2E_L} x \right) - \frac{1}{\sqrt{a_2}} \exp\left(\frac{U \pm \sqrt{a_2}}{2E_L} x \right) \right] + \frac{M}{A\sqrt{a_2}} \exp\left(\frac{U \pm \sqrt{a_2}}{2E_L} x \right) \qquad \text{(VI-45)}$$

where

The plus sign (+) is used to predict concentrations up estuary ($x < 0$)
The minus sign (-) is used to predict concentrations down estuary ($x > 0$)

$a_1 = U^2 + 4kE_L$

$a_2 = U^2 + 4k_2E_L$

M = mass flux of dissolved oxygen deficit contained in the discharge.
W = mass flux of ultimate BOD contained in the discharge, $(C_s - C_e)\forall_e$.
C_s = saturation concentration of dissolved oxygen.
C_e = effluent concentration of dissolved oxygen.
$\forall_e$ = effluent flowrate.

The advantage of expressing the dissolved oxygen concentration in terms of the deficit is that the principle of superposition can be invoked for multiple discharges within a single estuary. Specifically:

$$D = \Sigma D_i \qquad \text{(VI-46)}$$

and

$$C = C_s - \Sigma D_i \qquad \text{(VI-47)}$$

where

D_i = dissolved oxygen deficit resulting from the i^{th} discharge

C = final dissolved oxygen concentration

C_s = dissolved oxygen saturation level.

Figure VI-23 shows the relationship between dissolved oxygen saturation and temperature and salinity.

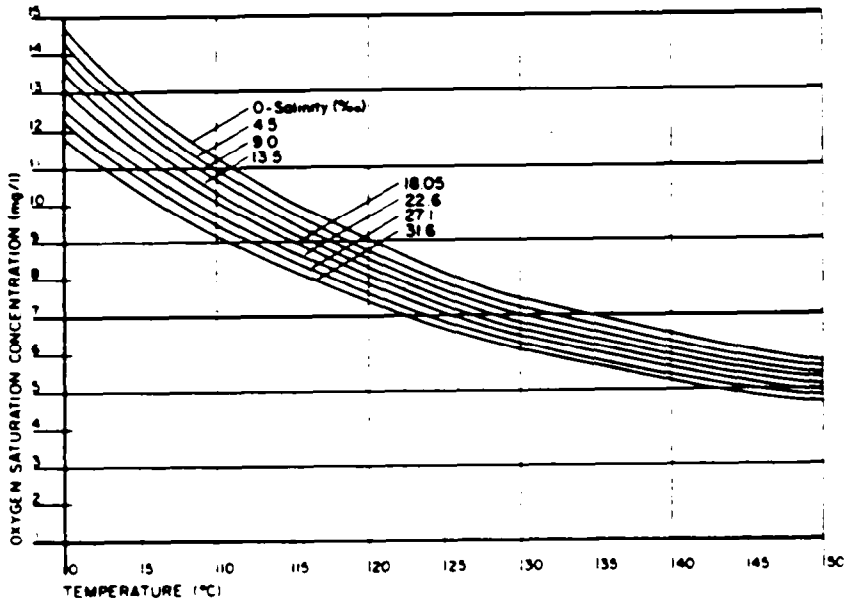

FIGURE VI-23 DISSOLVED OXYGEN SATURATION AS A FUNCTION OF TEMPERATURE AND SALINITY

EXAMPLE VI-9

Dissolved Oxygen Concentration Resulting from Two Sources of BOD

Two municipal wastewater treatment plants discharge significant quantities of BOD into the James River in Virginia. One discharges near Hopewell, and the second 10 miles further down estuary, near West Point. Calculate the dissolved oxygen concentration in the estuary as a function of distance. Pertinent data are:

BOD_5 in Hopewell plant effluent = 69,000 lbs/day

BOD_5 in West Point plant effluent, located 10 miles downstream from Hopewell = 175,000 lbs/day

Freshwater flow rate = 2,900 cfs

Dissolved oxygen saturation = 8.2 mg/l

Cross sectional area = 20,000 ft^2

Reaeration rate = 0.2/day

Deoxygenation rate = 0.3/day

Dispersion coefficient = 12.5 mi^2/day

Effluent dissolved oxygen = 0.0 mg/l.

The dissolved oxygen deficit due to each of the two contributions can be determined independently of the other using Equation IV-45. The results are plotted in Figure VI-24. The deficits are added to produce the total deficit (D(x)) due to both discharges (Figure VI-24a). The distance scale in Figure VI-24a is referenced to the Hopewell plant. The West Point plant is placed at mile 10. When the deficit at this location due to the West Point plant is calculated, set x = 0 in Equation VI-45. The dissolved oxygen concentration then becomes C(x) = 8.2-D(x), and is shown in Figure VI-24b.

One example calculation of dissolved oxygen deficit will be shown to illustrate the process. Consider the deficit produced at mile 0.0, due to the Hopewell plant. The waste loading from the Hopewell plant is:

$$69{,}000 \times 1.46 = 100{,}000 \text{ lbs/day, BOD-ultimate}$$
$$= 1.16 \text{ lbs/sec}$$

When x = 0, Equation VI-45 simplifies to:

$$D = \frac{kW}{A(k_2-k)}\left(\frac{1}{\sqrt{a_1}} - \frac{1}{\sqrt{a_2}}\right)$$

$$a_1 = U^2 + 4k_1E_L\left(\frac{2900}{20000}\right)^2 + \frac{4(.3)(12.5)(5280)(5280)}{81400 \cdot 86400} = .077 \frac{ft^2}{sec^2}$$

so

$$\sqrt{a_1} = .278 \text{ ft/sec}$$

$$a_2 = U^2 + 4k_2E_L = 0.058 \text{ ft}^2/\text{sec}^2$$

so

$$\sqrt{a_2} = .242 \text{ ft/sec}$$

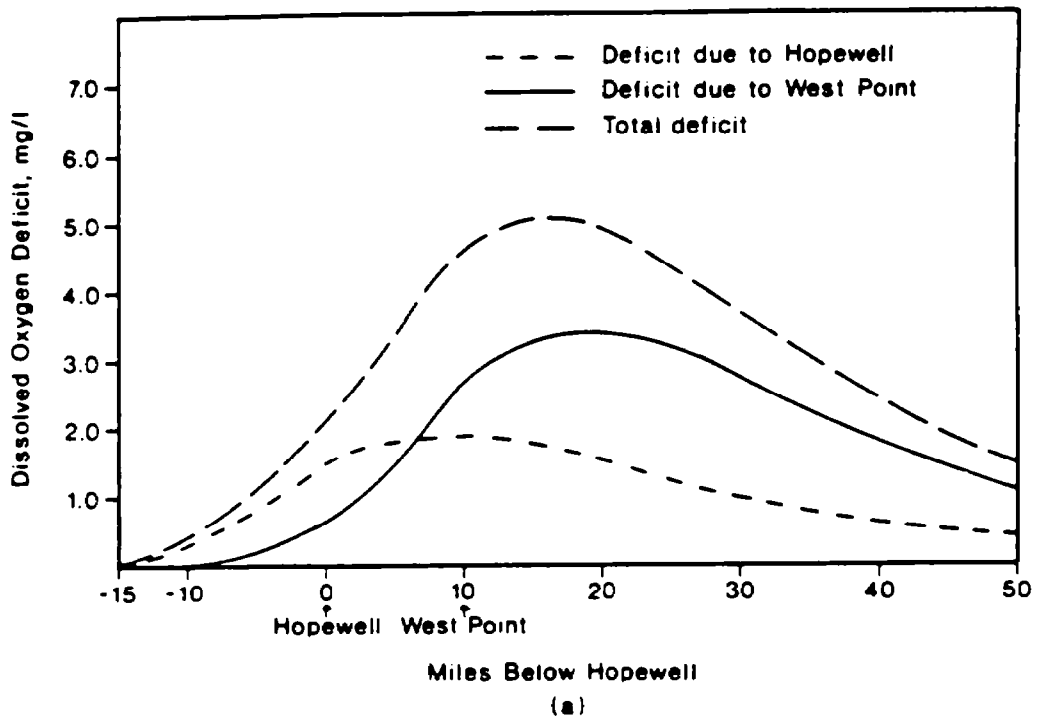

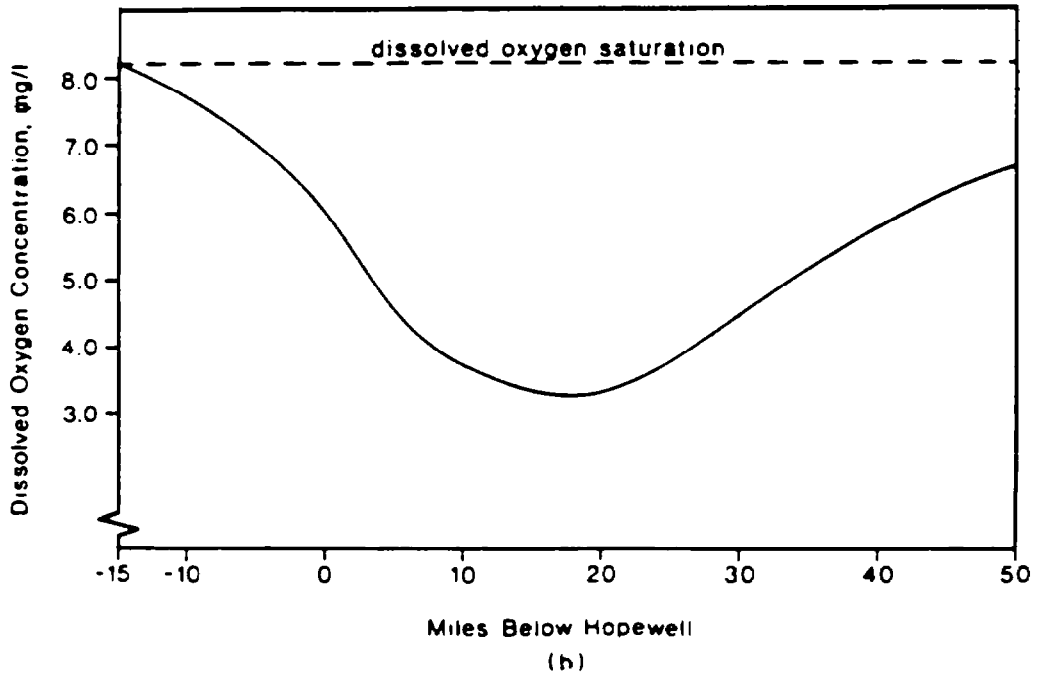

FIGURE VI-24 PREDICTED DISSOLVED OXYGEN PROFILE IN JAMES RIVER

The deficit is:

$$D = \frac{(.3)(1.16)}{20000(.2-.3)}\left[\frac{1}{.278} - \frac{1}{.242}\right] = 9.3 \times 10^{-5}\ lb/ft^3 = 1.5\ mg/l$$

This value is then plotted in Figure VI-24 at mile point 0.0. The deficit at this location due to West Point is evaluated at $x = -10$ miles in Equation VI-45, since West Point is located 10 miles down estuary of Hopewell. A deficit of 0.6 mg/l is found, and is plotted in Figure VI-24 at mile point 0.0. The total deficit at Hopewell is 1.5 + 0.6 = 2.1 mg/l, as shown in the figure.

END OF EXAMPLE VI-9

6.4.6 Pritchard's Two-Dimensional Box Model for Stratified Estuaries

Many estuaries in the United States are either stratified or partially mixed. Because the circulation of stratified systems is fairly complex, few hand calculation methods are available for their analysis. Instead computerized solutions are generally used.

One method developed by Pritchard (1969) which predicts the distribution of pollutants in partially mixed or stratified estuaries is suitable for hand calculations provided the user does not require too much spatial resolution. This method, called the "two-dimensional box model," divides the estuary horizontally from head to mouth into a series of longitudinal segments. Each segment is divided into a surface layer and a bottom layer. The analysis results in a system of n simultaneous linear equations with n unknowns, where n equals twice the number of horizontal segments. The unknowns are the pollutant concentrations in each layer.

Division of the estuary into only two horizontal segments results in four simultaneous equations, which is probably the most one would like to solve entirely by hand. However, many programmable hand calculators contain library routines for solving systems of 10 or more simultaneous equations, which would allow the estuary to be divided into 5 or more horizontal segments. If many more segments are desired, the solution could be easily implemented on a computer using a numerical technique such as Gaussian elimination to solve the resulting system of simultaneous linear equations.

The following information is required for the two-dimensional box analysis: 1) the freshwater flow rate due to the river; 2) the pollutant mass loading rates; and 3) the longitudinal salinity profiles along the length of the estuary in the upper and lower layers, and the salinity at the boundary between these two layers. The upper layer represents the portion of the water column having a net nontidal flow directed seaward, and the lower layer represents the portion of the water column having net nontidal flow directed up to the estuary. If no velocity data are avail-

able, these layers can generally be estimated based on the vertical salinity profiles.

Figure VI-25 shows the parameters used in the analysis, which are defined as follows:

n	= segment number, increasing from head toward mouth
$(S_u)_n$	= salinity in upper layer of segment n
$(S_l)_n$	= salinity in lower layer of segment n
$(S_v)_n$	= salinity at the boundary between the upper and lower layers of segment n
$(S_u)_{n-1,\ n}$	= salinity in the upper layer at the boundary between segments n-1 and n
$(S_l)_{n-1,\ n}$	= salinity in the lower layer at the boundary between segments n-1 and n
$(Q_u)_{n-1,\ n}$	= net nontidal flow rate in the upper layer from segment n-1 to n
$(Q_l)_{n-1,\ n}$	= net nontidal flow rate in the lower layer from segment n to n-1
$(Q_v)_n$	= net upward vertical flow from the lower to the upper layer of segment n
E_n	= vertical exchange coefficient between the lower and upper layers of segment n
R	= freshwater flow rate due to river
$(q_u)_n$	= pollutant mass loading rate to upper layer of segment n (from external sources)
$(q_l)_n$	= pollutant mass loading rate to lower layer of segment n (from external sources)
$(C_u)_n$	= pollutant concentration in the upper layer of segment n)
$(C_l)_n$	= pollutant concentration in the lower layer of segment n.

Pritchard's two-dimensional box analysis as presented here requires the following assumptions:

- Steady-state salinity distribution
- The pollutant is conservative
- The concentration of the pollutant is uniform within each layer of each segment and
- The pollutant concentration at the boundary between segments or layers is equal to the average of the concentrations in the two adjacent segments or layers.

Application of the two-dimensional box model involves six steps. These are:

1. Plot the longitudinal salinity profiles in the upper and lower

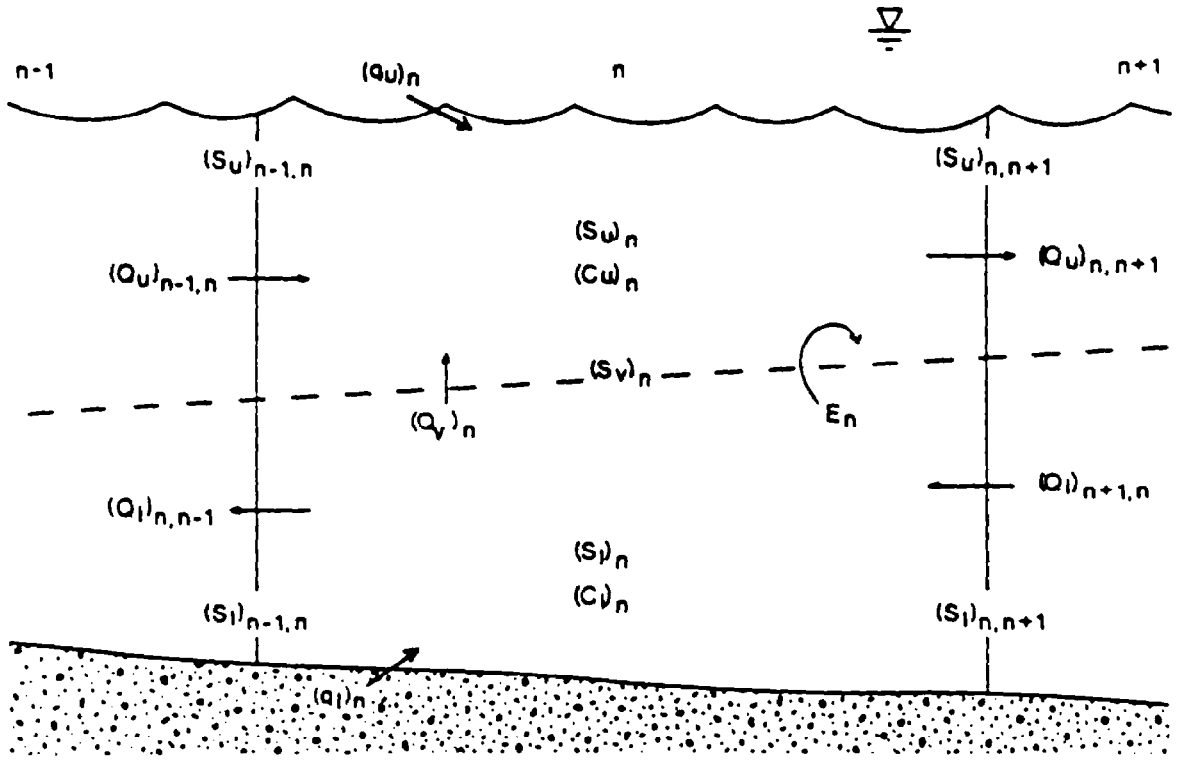

FIGURE VI-25 DEFINITION SKETCH FOR PRITCHARD'S TWO-DIMENSIONAL BOX MODEL

layers, and at the interface between the two layers. If information on the net nontidal velocity distribution is not available to define the layers, the boundary may be estimated for a given section of the estuary as the depth at which the vertical salinity gradient is maximum. The resulting plots will be used to determine the average salinities in each segment and layer, and the salinities at the boundaries between each segment and layer.

2. Segment the estuary. The number of segments will depend on the degree of spatial resolution desired, and the limitations of the hand calculators used to solve the system of simultaneous equations. The accuracy of the results will generally increase with the number of segments used, since the assumptions of the analysis are better satisfied. A minimum of three horizontal segments should probably be used to obtain even a rough estimate of the pollutant distribution in the estuary. This will require the solution of six equations and six unknowns.
3. Compute the net nontidal flows in the upper layer and lower layer at the boundary between each horizontal segment using Knudson's

Hydrographical Theorem (Dyer, 1973):

$$(Q_u)_{n-1,\,n} = R\,\frac{(S_l)_{n-1,\,n}}{(S_l)_{n-1,\,n}-(S_u)_{n-1,\,n}} \qquad \text{(VI-48)}$$

$$(Q_l)_{n,\,n-1} = R\,\frac{(S_u)_{n-1,\,n}}{(S_l)_{n-1,\,n}-(S_u)_{n-1,\,n}} \qquad \text{(VI-49)}$$

At the upstream freshwater boundary of the estuary:

$(Q_l)_{n,\,n-1} = 0.$

4. Compute the net upward vertical flows between layers for each segment using the continuity equation for the upper layer of the segment:

$$(Q_v)_n = (Q_u)_{n,\,n+1} - (Q_u)_{n-1,n} \qquad \text{(VI-50)}$$

5. Compute the vertical exchange coefficients between layers for each segment using the salinity balance equation for the upper layer of the segment, which can be arranged in the following form:

$$E_n = \frac{(Q_u)_{n,\,n+1}\,(S_u)_{n,\,n+1} - (Q_u)_{n-1,\,n}\,(S_u)_{n-1,\,n} - (Q_v)_n\,(S_v)_n}{(S_l)_n - (S_u)_n} \qquad \text{(VI-51)}$$

6. Set up and solve a system of simultaneous linear equations with one equation for each segment and layer where the pollutant concentrations are the unknowns. These equations are based on a pollutant mass balance for each segment and layer. The mass balance equations are:

$$(Q_u)_{n-1,\,n}\left[\frac{(C_u)_{n-1}+(C_u)_n}{2}\right] + (Q_v)_n\left[\frac{(C_u)_n+(C_l)_n}{2}\right] + E_n\left[(C_l)_n-(C_u)_n\right]$$
$$-(Q_u)_{n,\,n+1}\left[\frac{(C_u)_n+(C_u)_{n+1}}{2}\right] + (q_u)_n = 0 \qquad \text{(VI-52)}$$

for the upper layer of segment n and

$$(Q_l)_{n+1,\,n}\left[\frac{(C_l)_{n+1}+(C_l)_n}{2}\right]-(Q_l)_{n,\,n-1}\left[\frac{(C_l)_n+(C_l)_{n-1}}{2}\right]$$

$$-(Q_v)_n\left[\frac{(C_l)_n+(C_u)_n}{2}\right]-E_n\left[(C_l)_n-(C_u)_n\right]+(q_l)_n=0 \qquad \text{(VI-53)}$$

for the lower layer of segment n.

Since most pollutant discharges are buoyant, they should be considered as loadings to the upper layer, even though they may be physically introduced at the bottom. Pollutants which are denser than the upper waters and which would sink to the bottom should be considered as loadings to the lower layer. However, the analysis is not applicable to pollutants which tend to remain near the bottom and accumulate in or react with the bottom sediments.

The above mass balance equations can be simplified and rearranged into the following form:

$$\left[(Q_u)_{n-1,\,n}\right](C_u)_{n-1}+\left[-2E_n\right](C_u)_n+\left[2E_n+(Q_v)_n\right](C_l)_n$$

$$+\left[-(Q_u)_{n,\,n+1}\right](C_u)_{n+1}=-2(q_u)_n \qquad \text{(VI-54)}$$

for the upper layer of segment n and

$$\left[-(Q_l)_{n,\,n-1}\right](C_l)_{n-1}+\left[2E_n-(Q_v)_n\right](C_u)_n+\left[-2E_n\right](C_l)_n$$

$$+\left[(Q_l)_{n+1,\,n}\right](C_l)_{n+1}=-2(q_l)_n \qquad \text{(VI-55)}$$

for the lower layer of segment n. This pair of equations is written for each segment, resulting in a system of simultaneous equations where the concentrations, $(C_u)_n$ and $(C_l)_n$, are the unknowns, the terms enclosed in square brackets are the coefficients, and the terms on the right hand side of the equations are the constants.

However, since each equation involves both the upstream and downstream segments

for a given layer, the boundary conditions at both the upstream and downstream end of the estuary must be applied so that there will not be more unknowns than equations. At the upstream end of the estuary, the following boundary conditions apply:

$(Q_u)_{n-1,\,n}$ = R = river flow rate
$(C_u)_{n-1}$ = C_R = pollutant in river
$(Q_l)_{n,\,n-1}$ = 0 = (no salt water movement upstream into the river).

These conditions simplify the previous equations to:

$$\left[-2E_1\right](C_u)_1 + \left[2E_1 + (Q_v)_1\right](C_l)_1 + \left[-(Q_u)_{1,2}\right](C_u)_2 - (C_u)_1\,R = -2(q_u)_1 - 2RC_R \qquad \text{(VI-56)}$$

for the upper layer of the first upstream segment and

$$\left[2E_1 - (Q_v)_1\right](C_u)_1 + \left[-2E_1\right](C_l)_1 + \left[(Q_l)_{2,1}\right](C_l)_2 = -2(q_l)_1 \qquad \text{(VI-57)}$$

for the lower layer of the first upstream segment.

For the lower layer of the last downstream segment at the ocean end of the estuary, the following boundary condition is used to simplify the equation:

$(C_l)_{n+1}$ = 0 (no pollutant entering the lower layer from the ocean waters outside the mouth of estuary)

which simplifies the corresponding equation to:

$$\left[-(Q_l)_{n,\,n-1}\right](C_l)_{n-1} + \left[2E_n - (Q_v)_n\right](C_u)_n + \left[-2E_n\right](C_l)_n = -2(q_l)_n \qquad \text{(VI-58)}$$

For the upper layer of the last segment at the mouth of the estuary, some assumption must be made about the pollutant concentration in the upper layer just outside the mouth to eliminate the (n + 1) term from the equation. If actual data are available based on field measurements, a measured value of $(C_n)_{n+1}$ can be used. This simplifies the corresponding equation to:

$$\left[(Q_u)_{n-1,\,n}\right](C_u)_{n-1} + \left[-2E_n\right](C_u)_n + \left[2E_n + (Q_v)_n\right](C_l)_n = -2(q_u)_n + (Q_u)_{n,\,n+1}\,C_o \qquad \text{(VI-59)}$$

where C_o is the measured pollutant concentration in the surface waters outside the mouth of the estuary. If no data are available, the simplest assumption that can be made is that the concentration outside the mouth equals the concentration in the surface layer of the last segment inside the mouth, or $(C_u)_{n+1} = (C_u)_n$. Alternatively, the concentration outside the mouth may be assumed to equal some fraction of the concentration inside the mouth, or:

$$(C_u)_{n+1} = f_c\,(C_u)_n$$

where f_c is the selected fraction. The previous assumption $(C_u)_{n+1} = (C_u)_n$ is one case of this second assumption where the fraction equals one ($f_c = 1$).

Using the second more general assumption, the equation of the upper layer of the last downstream segment simplifies to:

$$\left[(Q_u)_{n-1,\,n}\right](C_u)_{n-1} + \left[-2E_n - f_c\,(Q_u)_{n,\,n+1}\right](C_u)_n + \left[2E_n + (Q_v)_n\right](C_i)_n = -2(q_u)_n \qquad \text{(VI-60)}$$

Step (6) of the two-dimensional box analysis involves computing all of the coefficients and constants in the system of equations defining each segment and layer (Equations VI-54 and VI-55) and applying the boundary conditions to produce equations for the first upstream and last downstream segments in the estuary (Equations VI-56 through VI-60). The coefficients and constants are functions of the variables previously computed in steps (3) through (5). The resulting equations are then solved using library routines in programmable hand calculators, or by programming an appropriate numerical technique such as Gaussian elimination on either a programmable hand calculator or a computer.

Since the analysis requires application of the boundary conditions at the freshwater head of the estuary and the coastal mouth of the estuary to obtain the same number of equations as unknowns, the entire estuary must be included in the first cut analysis. The initial analysis will yield the overall pollutant distribution throughout the entire estuary. Once this is determined, the analysis could be repeated to obtain more detail for smaller portions of the estuary by using the first cut results to estimate the pollutant boundary conditions at each end of the region of concern, and then rearranging equations (7) and (8) so the terms involving the concentrations outside the specified regions are treated as constants and moved to the right hand side of the equations.

The Pritchard Model theoretically allows external pollutant loading to be introduced directly into any segment along the estuary. By moving external loadings from the head to near the mouth of the estuary, the planner can predict how pollutant levels are affected. However, experience with the model has shown that when external side loadings are considerably larger than those which enter at the head of the estuary, model instabilities can arise. When this occurs, the pollutant profile oscillates from segment to segment, and negative concentrations can result. It is recommended that the user first run the Pritchard Model by putting all pollutant loading into the head of the estuary. This situation appears to be always stable, and, as the following example shows, reasonable pollutant profiles are predicted.

EXAMPLE VI-10

Pollutant Distribution in a Stratified Estuary

The Patuxent River in Maryland is a partially stratified estuary, where the degree of stratification depends on the freshwater flow rate discharged at the head of the estuary. Table VI-18 shows the salinity distribution within the estuary under low flow conditions for each segment and layer. The location of each layer is shown in Figure VI-26. Also shown in the table is the pollutant distribution by layer and segment for a mass flux of 125 lbs/day (57 kg/day) of conservative pollutant input at the head of the estuary.

The pollutant distribution was predicted by solving on a computer the 12-segment, 2-layer system (24 simultaneous equations). The salinity distribution shown in Table VI-18 was used as input data. As a point of interest, the same network was solved using the model WASP (courtesy of Robert Ambrose, ERL, U.S. Environmental Protection Agency, Athens, Georgia), which is a dynamic two-dimensional estuary model. Instead of using salinity directly, WASP predicts the salinity distribution based on dispersive and advective exchange rates. The salinity distribution predicted by WASP is the same as shown in Table VI-18, which was used as input to Pritchard's Model. After running WASP to steady-state conditions, the pollutant distribution throughout the estuary was virtually the same as predicted by Pritchard's Model.

The pollutant distribution in the Patuxant estuary will be solved in detail using 4 segments instead of 12. The resulting system of 8 simultaneous equations can be solved on a variety of hand-held calculations. The tabulations below show salinities at each segment boundary, and the horizontal flow rates in the upper and lower layers.

Boundary n-1,n	$(S_u)_{n-1,n}$ mg/l-Cl	$(S_l)_{n-1,n}$ mg/l-Cl	$(Q_u)_{n-1,n}$ m^3/sec	$(Q_l)_{n,n-1}$ m^3/sec
0, 1	0.0	0.0	3.3*	0.0
1, 2	4960.	5080.	116.7	113.4
2, 3	9420.	9640.	139.5	136.2
3, 4	11445.	11860.	94.3	91.0
4, 5	13500.	13500.	156.8	153.5

*This is the specified river inflow rate, R.

The flow rates were calculated from Equations VI-48 and VI-49, while the salinities were found directly from Table VI-18.

TABLE VI-18

SALINITY AND POLLUTANT DISTRIBUTION IN PATUXENT ESTUARY UNDER LOW FLOW CONDITIONS

	Salinity (as Chloride, mg/l)		Pollutant Concentration (mg/l)	
Segment Number	Upper Layer	Lower Layer	Upper Layer	Lower Layer
1	496.	524.	0.193	0.192
2	1831.	1940.	0.173	0.171
3	3771.	3970.	0.144	0.141
4	6050.	6280.	0.100	0.108
5	8040.	8220.	0.081	0.078
6	9310	9910.	0.062	0.053
7	10010.	10660.	0.051	0.042
8	10790.	11070.	0.040	0.036
9	11240.	11760.	0.033	0.025
10	11830.	12120.	0.025.	0.020
11	12100.	12650.	0.021	0.013
12	12750.	12850.	0.011	0.009
boundary	13500.	13500.	0.0	0.0

The salinities within each layer, the salinity and flow rate between the interface of each layer, and the exchange coefficients are tabulated below.

Segment n	$(S_u)_n$ mg/l-Cl	$(S_v)_n$ mg/l-Cl	$(s_l)_n$ mg/l-Cl	$(Q_v)_n$ m^3/sec	E_n m^3/sec
1	1830	1890	1940	113.	3260.
2	8040	8130	8220	23.	3140.
3	10790	10930	11070	-45.	930.
4	12100	12380	12650	63.	280.

The flow rates were found from Equation VI-50, and the exchange coefficients from Equation VI-51.

Substituting these data into the pollutant mass balance expressions (Equations

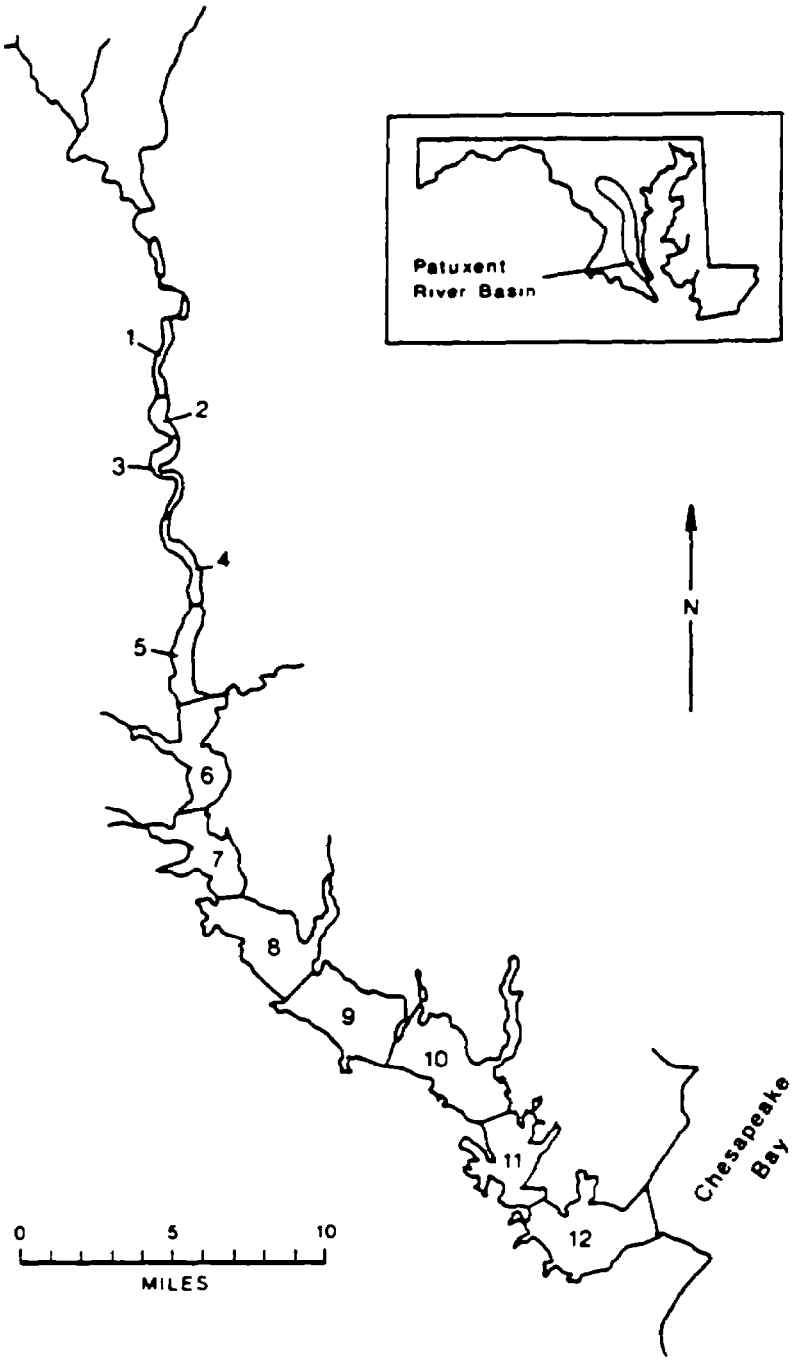

FIGURE VI-26 PATUXENT ESTUARY MODEL SEGMENTATION

VI-54 through VI-59), the following system of equations result:

$$\begin{bmatrix} -6528. & 6638. & -117. & 0. & 0. & 0. & 0. & 0. \\ 6411. & -6525. & 0.0 & 113. & 0. & 0. & 0. & 0. \\ 117. & 0.0 & -6275. & 6297. & -139. & 0. & 0. & 0. \\ 0. & 113. & 6252. & -6275. & 0.0 & 136 & 0. & 0. \\ 0. & 0. & 139. & 0.0 & -1856. & 1811. & -94. & 0. \\ 0. & 0. & 0. & -136. & 1901 & -1856. & 0.0 & 91. \\ 0. & 0. & 0. & 0. & 94. & 0.0 & -561 & 624. \\ 0. & 0. & 0. & 0. & 0. & -91. & 499. & -561 \end{bmatrix} \begin{Bmatrix} (C_u)_1 \\ (C_l)_1 \\ (C_u)_2 \\ (C_l)_2 \\ (C_u)_3 \\ (C_l)_3 \\ (C_u)_4 \\ (C_l)_4 \end{Bmatrix} = \begin{Bmatrix} -1.32 \\ 0. \\ 0. \\ 0. \\ 0. \\ 0. \\ 0. \\ 0. \end{Bmatrix}$$

The value -1.32 in the first row of the right-hand side column vector is twice the loading of pollutant which comes into the upper layer of the first segment, as required in Equation VI-56. The units are in gm/sec to be compatible with the units of the remaining terms in the equations:

$$M = 125 \text{ lbs/day} = 0.66 \text{ gm/sec}$$

so $$2M = 250 \text{ lbs/day} = 1.32 \text{ gm/sec}$$

The pollutant distribution which results from solving the eight linear equations is:

$$(C_u)_1 = (0.17)$$
$$(C_l)_1 = (0.17)$$
$$(C_u)_2 = (0.08)$$
$$(C_l)_2 = (0.08)$$
$$(C_u)_3 = (0.04)$$
$$(C_l)_3 = (0.04)$$
$$(C_u)_4 = (0.02)$$
$$(C_l)_4 = (0.01)$$

These values are nearly the same as found when 12 segments were used, which indicates 4 segments are sufficient to accurately predict pollutant distribution for this problem.

END OF EXAMPLE VI-10

6.5 POLLUTANT DISTRIBUTION FOLLOWING DISCHARGE FROM A MARINE OUTFALL

6.5.1 Introduction

Numerous coastal states have enacted water quality standards which limit the maximum allowable concentration of pollutants, particularly metals and organic

toxicants, which can be discharged into estuarine and coastal waters. The standards normally permit that an exempt area, called a mixing zone, be defined around the outfall where water quality standards are not applicable. For example, the Water Quality Control Plan for Ocean Waters of California (State Water Resources Control Board, 1978) sets forth the following statement directed at toxic substance limitations:

> "Effluent limitations shall be imposed in a manner prescribed by the State Board such that the concentrations set forth . . . as water quality objectives, shall not be exceeded in the receiving water upon the completion of initial dilution."

The mixing zone, or zone of initial dilution (ZID), is non-rigorously defined as the volume of water where the wastewater and ambient saline water mix during the first few minutes following discharge, when the plume still has momentum and buoyancy. As the wastewater is discharged, it normally begins to rise because of its buoyancy and momentum, as illustrated in Figure VI-27.

If the ambient water column is stratified and the water depth is great enough, the rising plume will not reach the surface of the water, but rather will stop at the level where the densities of the plume and receiving water become equal. This level is called the plume's trapping level. (See Figure VI-27.) Due to residual momentum, the plume might continue to rise beyond the trapping level, but will tend to fall back after the momentum is completely dissipated. Once the plume stops rising, the waste field begins to drift away from the ZID with the ambient currents. At this time, initial dilution is considered complete. Section 6.5.2, which follows, shows how initial dilution is calculated, and then Sections 6.5.3 and 6.5.4 illustrate how pollutant concentrations at the completion of initial dilution can be predicted. Sections 6.5.5 and 6.5.6 explain methods of predicting pollutant and dissolved oxygen concentrations, respectively, as the waste field migrates away from the ZID.

The methods presented in Sections 6.5.2 through 6.5.6 are applicable to stratified or non-stratified estuaries, embayments, and coastal waters. The methods assume that reentrainment of previously discharged effluent back into the ZID is negligible. Reentrainment can occur if the wastewater is discharged into a confined area where free circulation is impaired or because of tidal reversals in narrow estuaries.

6.5.2 Prediction of Initial Dilution

6.5.2.1 General

Discharge to bodies of water through submerged diffusers is a common waste water management technique. A diffuser is typically a pipe with discharge ports spaced at regular intervals. Such discharges are often buoyant with high exit velocity relative to the ambient velocity. The resulting waste streams act as plumes or buoyant jets. The velocity shear between ambient and plume fluids results in the

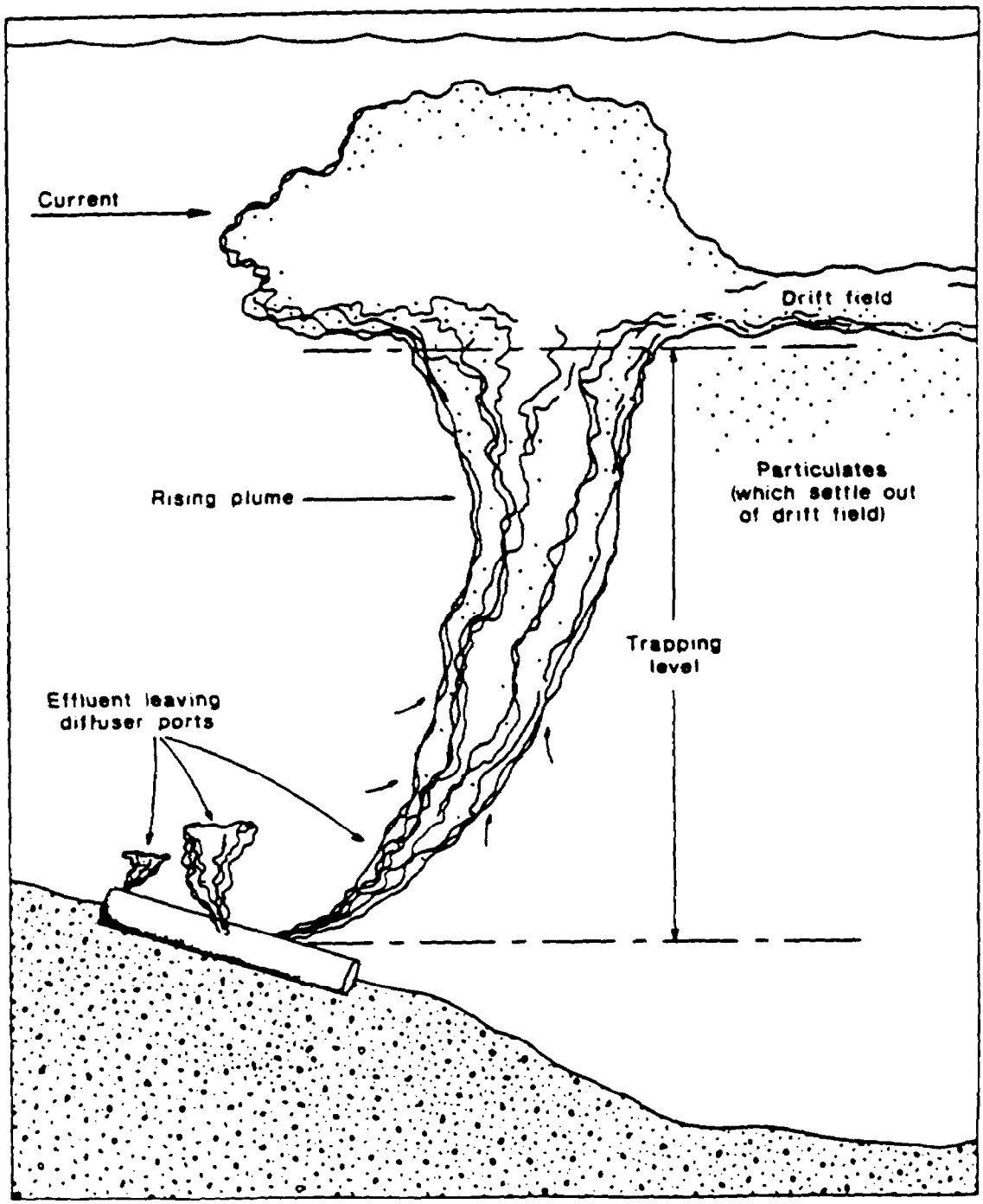

FIGURE VI-27 WASTE FIELD GENERATED BY MARINE OUTFALL

incorporation of ambient fluid into the plume, a process called entrainment. Initial dilution results from the entrainment of ambient fluid into the plume as the plume rises to its trapping level.

The magnitude of initial dilution depends on a number of factors including, but not limited to, the depth of water, ambient density stratification, discharge

rate, buoyancy, port spacing (i.e. plume merging), and current velocity. These factors may be referred to collectively as the diffuser flow configuration or simply the flow configuration. Depending on the flow configuration, the initial dilution may be less than 10 or greater than 500. As attaining water quality criteria may often require relatively high initial dilution, the need to be able to estimate initial dilution for various flow configurations becomes apparent.

Other than actually sampling the water after a facility is in operation, there are various ways to estimate pollutant concentrations achieved in the vicinity of a particular diffuser. A scale model faithful to all similarity criteria could yield the necessary dilution information. Dimensional analysis and empirical formulae may also be very useful. Alternatively, a numerical model based on the laws of physics may be developed. This method is chosen to provide initial dilution estimates here because it is more cost-effective than field sampling and more accurate than a scale model.

Any numerical model used to provide dilution estimates should faithfully replicate the relevant plume relationships and should be verified for accuracy. The plume model MERGE (Frick, 1981c) accounts for the effects of current ambient density stratification and port spacing on plume behavior. In addition, it has been extensively verified (Frick, 1981a, 1981b; Tesche et al., 1980; Policastro et al., 1980; Cavnar et al., 1981).

There are several ways of presenting the initial dilution estimates. MERGE may be run for specific cases or run for many cases spanning a range of conditions and presented in nomogram or tabular form. The latter method is the most compact. The resulting initial dilution tables display values of dilution achieved at the indicated depths and densimetric Froude numbers. One hundred tables are presented in Appendix G for various combinations of port spacing, density stratification, and effluent-to-current velocity ratio.

Before describing the tables in more detail and discussing examples, it may be helpful for some users to read the following, occasionally technical, discussions of the plume model MERGE (Section 6.5.2.2) and of basic principles of similarity (Section 6.5.2.3). Others may want to advance directly to Section 6.5.2.4 describing table usage.

6.5.2.2 The Plume Model MERGE

MERGE is the latest in a series of models whose development began in 1973. Various stages of model development have been recorded (Winiarski and Frick, 1976 and 1978; Frick, 1981c). In the realm of plume modeling, MERGE belongs to the Lagrangian minority since more models are Eulerian. The model can be demonstrated to be basically equivalent to its Eulerian counterparts (Frick and Winiarksi, 1975; Frick, 1981c). Time is the independent variable which is incremented in every program iteration based on the rate of entrainment.

To simplify the problem, many assumptions and approximations are made in plume modeling. In MERGE, steady-state is assumed and the plume is assumed to have a round cross section everywhere.

The MERGE user may input arbitrary current and ambient density profiles. The model includes a compressible equation of continuity so that the predictions are also valid for highly buoyant plumes. It accounts for merging of adjacent plumes but only when the ambient current dilution is normal to the diffuser pipe. In many cases, this is not a significant restriction as many diffusers are oriented to be normal to the prevailing current direction.

The model contains an option for using either constant or variable coeffients of bulk expansion in the equation of state. The water densities in Table VI-19 are generated using the model's density subroutine based on actual temperatures and salinities (i.e. effectively using variable coefficients). If temperature and salinity data are unavailable then the model can be run based on density data alone. The latter method is satisfactory for relatively high temperatures and salinities because the equation of state is relatively linear with these variables in that range. However, for low densities and temperatures gross inaccuracies may result. Unfortunately, the initial dilution tables are based on the latter method. A more accurate representation would greatly increase the number of tables necessary to cover all the cases. Users with applications involving cold, low salinity water are urged to run the more accurate form of the model.

The success of MERGE in predicting plume behavior is primarily attributable to two unique model features. The first of these relates to the expression of forced entrainment. Entrainment may be attributed to the velocity shear present even in the absence of currents, i.e. aspiration, and to current-induced entrainment, sometimes called forced entrainment.

The forced entrainment algorithm in MERGE is based on the assumption that all fluid flowing through the upstream projected area of the plume is entrained. This hypothesis is based on well-established principles and observations (Rawn et al., 1960; Jirka and Harlman 1973). Paradoxically, the hypothesis has never been implemented in numerical models before. The projected area normally contains linear and quadratic terms in plume diameter, whereas in conventional modeling, forced entrainment is generally expressed as a linear function of diameter. It is necessary to include additional sources of entrainment to make up the difference when so expressed.

The second feature is the use of a constant aspiration coefficient. This coefficient is often considered to be variable (e.g. Fan, 1967). The need for a variable coefficient is attributable to the fact that many models predict centerline plume values. For plumes discharged vertically upward into density stratified ambient water, such models are expected to predict the maximum penetration of the plume. To achieve agreement requires a relatively small aspiration coefficient.

TABLE VI-19a

WATER DENSITIES (EXPRESSED AS SIGMA-T)* CALCULATED USING THE DENSITY SUBROUTINE FOUND IN MERGE

Salinity (°/oo)	TEMPERATURE (°C)														
	0		2		4		5		8		10		12		14
0	-0.093	-0.034	.007	.031	.039	.030	.006	-0.032	-0.086	-0.154	-0.235	-0.330	-0.438	-0.558	-0.691
	.721	.776	.814	.835	.839	.827	.800	.758	.702	.632	.548	.450	.340	.217	.082
	1.535	1.586	1.620	1.637	1.638	1.623	1.593	1.548	1.489	1.416	1.329	1.230	1.117	.992	.854
	2.348	2.395	2.425	2.439	2.437	2.419	2.385	2.338	2.276	2.200	2.111	2.008	1.893	1.766	1.626
	3.159	3.203	3.230	3.240	3.234	3.213	3.177	3.126	3.061	2.983	2.891	2.786	2.669	2.539	2.397
5	3.970	4.010	4.033	4.040	4.031	4.007	3.968	3.914	3.847	3.765	3.671	3.564	3.444	3.312	3.168
	4.781	4.817	4.836	4.840	4.818	4.800	4.758	4.701	4.631	4.547	4.450	4.341	4.218	4.084	3.938
	5.590	5.623	5.639	5.639	5.623	5.593	5.548	5.488	5.415	5.329	5.229	5.117	4.992	4.856	4.708
	6.399	6.428	6.441	6.437	6.418	6.385	6.337	6.274	6.199	6.109	6.007	5.893	5.766	5.627	5.477
	7.207	7.233	7.242	7.235	7.213	7.176	7.125	7.060	6.982	6.890	6.785	6.668	6.539	6.398	6.245
10	8.015	8.037	8.042	8.032	8.007	7.967	7.913	7.845	7.764	7.670	7.563	7.443	7.312	7.168	7.014
	8.822	8.840	8.842	8.829	8.801	8.758	8.701	8.630	8.546	8.449	8.340	8.218	8.084	7.939	7.782
	9.628	9.643	9.642	9.625	9.594	9.548	9.488	9.415	9.328	9.228	9.116	8.992	8.856	8.708	8.549
	10.434	10.446	10.441	10.421	10.387	10.338	10.275	10.199	10.109	10.007	9.893	9.766	9.628	9.478	9.317
	11.240	11.248	11.240	11.217	11.179	11.127	11.062	10.983	10.890	10.786	10.669	10.540	10.399	10.247	10.084
15	12.045	12.049	12.038	12.012	11.971	11.916	11.848	11.766	11.671	11.564	11.445	11.313	11.170	11.016	10.851
	12.850	12.851	12.836	12.807	12.763	12.705	12.634	12.549	12.452	12.342	12.220	12.087	11.941	11.785	11.618
	13.654	13.652	13.634	13.602	13.555	13.494	13.420	13.332	13.232	13.120	12.996	12.860	12.712	12.554	12.384
	14.459	14.453	14.432	14.396	14.346	14.282	14.205	14.115	14.013	13.898	13.771	13.633	13.483	13.322	13.151
	15.263	15.254	15.229	15.190	15.137	15.071	14.991	14.898	14.793	14.676	14.547	14.406	14.254	14.091	13.917
20	16.067	16.054	16.027	15.985	15.929	15.859	15.777	15.681	15.573	15.453	15.322	15.179	15.025	14.860	14.684
	16.870	16.855	16.824	16.779	16.720	16.647	16.562	16.464	16.354	16.231	16.097	15.952	15.796	15.628	15.451
	17.674	17.655	17.621	17.573	17.511	17.436	17.347	17.247	17.134	17.009	16.873	16.725	16.566	16.397	16.217
	18.478	18.455	18.418	18.367	18.302	18.224	18.133	18.030	17.914	17.787	17.648	17.498	17.337	17.166	16.984
	19.281	19.225	19.255	19.161	19.093	19.012	18.919	18.813	18.694	18.565	18.424	18.271	18.108	17.935	17.751

TABLE VI-19a

(Continued)

Salinity (°/oo)	TEMPERATURE (°C)														
	0		2		4		5		8		10		12		14
25	20.085	20.056	20.012	19.955	19.884	19.801	19.704	19.596	19.475	19.343	19.199	19.045	18.880	18.704	18.518
	20.888	20.856	20.810	20.749	20.676	20.589	20.490	20.379	20.256	20.121	19.975	19.819	19.651	19.473	19.285
	21.692	21.657	21.607	21.544	21.467	21.378	21.276	21.162	21.037	20.900	20.751	20.592	20.423	20.243	20.053
	22.496	22.457	22.405	22.338	22.259	22.167	22.063	21.946	21.818	21.678	21.528	21.367	21.195	21.103	20.821
	23.300	23.258	23.202	23.133	23.051	22.956	22.849	22.730	22.599	22.458	22.305	22.141	21.967	21.783	21.589
30	24.104	24.059	24.001	23.929	23.843	23.746	23.636	23.514	23.381	23.237	23.082	22.916	22.740	22.554	22.358
	24.908	24.861	24.799	24.724	24.636	24.536	24.423	24.299	24.164	24.017	23.859	23.691	23.513	23.325	23.127
	25.713	25.662	25.598	25.520	25.429	25.326	25.211	25.084	24.946	24.797	24.637	24.467	24.287	24.097	23.897
	26.518	26.464	26.397	26.316	26.223	26.117	25.999	25.870	25.729	25.578	25.416	25.243	25.061	24.869	24.667
	27.324	27.267	27.196	27.113	27.016	26.908	26.788	26.656	26.513	26.359	26.195	26.020	25.836	25.641	25.437
35	28.130	28.070	27.996	27.910	27.811	27.700	27.577	27.422	27.297	27.141	26.974	26.798	26.611	26.414	26.208
	28.936	28.873	28.797	28.708	28.606	28.492	28.366	28.230	28.082	27.923	27.754	27.575	27.387	27.188	26.980
	29.743	29.677	29.598	29.506	29.401	29.285	29.157	19.017	28.867	28.706	28.535	28.354	28.163	27.963	27.753
	30.550	30.482	30.399	30.305	30.197	30.078	29.948	29.806	29.653	29.490	29.317	29.133	28.940	28.738	28.526
	31.358	31.287	31.202	31.104	30.994	30.872	30.739	30.595	30.440	30.275	20.099	29.913	29.718	29.514	29.300
40	32.167	32.092	32.005	31.904	31.792	31.667	31.532	31.385	31.227	31.060	30.882	30.694	30.497	30.290	30.075

*Sigma-t (σ_t) is defined as: (density-1) x 10^3. For example, for seawater with a density of 1.02500 g/cm^3, σ_t = 25.

TABLE VI-19b

WATER DENSITIES (EXPRESSED AS SIGMA-T)* CALCULATED
USING THE DENSITY SUBROUTINE FOUND IN MERGE

Salinity (°/oo)	TEMPERATURE (°C)														
	16		18		20		22		24		26		28		
0	-0.836	-0.993	-1.161	-1.341	-1.532	-1.733	-1.945	-2.167	-2.399	-2.641	-2.893	-3.154	-3.425	-3.704	-3.993
	-0.065	-0.224	-0.394	-0.576	-0.768	-0.971	-1.185	-1.409	-1.642	-1.886	-2.139	-2.402	-2.674	-2.956	-3.246
	.705	.544	.372	.189	-0.006	-0.211	-0.426	-0.651	-0.887	-1.132	-1.387	-1.651	-1.925	-2.208	-2.499
	1.475	1.312	1.138	.952	.756	.550	.333	.106	-0.131	-0.378	-0.635	-0.901	-1.176	-1.460	-1.753
	2.244	2.079	1.903	1.716	1.518	1.309	1.091	.862	.623	.375	.117	-0.150	-0.427	-0.713	-1.007
5	3.012	2.845	2.667	2.478	2.279	2.068	1.848	1.618	1.377	1.127	.868	.599	.321	.034	-0.262
	3.780	3.611	3.431	3.240	2.039	2.827	2.605	2.373	2.131	1.880	1.619	1.348	1.069	.780	.483
	4.548	4.377	4.195	4.002	3.799	3.585	3.362	3.128	2.884	2.631	2.369	2.097	1.816	1.526	1.228
	5.315	5.142	4.958	4.763	4.558	4.343	4.118	3.882	3.637	3.383	3.119	2.846	2.563	2.272	1.972
	6.082	5.907	5.721	5.524	5.317	5.100	4.873	4.636	4.390	4.134	3.868	3.594	3.310	3.017	2.716
10	6.848	6.671	6.483	6.285	6.076	5.857	5.629	5.390	5.142	4.885	4.618	4.342	4.057	3.763	3.460
	7.614	7.435	7.245	7.045	6.835	6.614	6.384	6.144	5.894	5.635	5.367	5.089	4.803	4.507	4.203
	8.379	8.198	8.007	7.805	7.593	7.371	7.139	6.897	6.646	6.385	6.116	5.837	5.549	5.252	4.947
	9.145	8.962	8.768	8.565	8.351	8.127	7.893	7.650	7.397	7.135	6.864	6.584	6.295	5.997	5.690
	9.910	9.725	9.530	9.324	9.108	8.883	8.648	8.403	8.149	7.885	7.613	7.331	7.041	6.741	6.433
15	10.675	10.488	10.291	10.083	9.866	9.639	9.402	9.156	8.900	8.635	8.361	8.078	7.786	7.486	7.176
	11.439	11.251	11.052	10.843	10.623	10.395	10.156	9.908	9.651	9.385	9.109	8.825	8.532	8.230	7.920
	12.204	12.013	11.813	11.602	11.381	11.150	10.910	10.661	10.402	10.134	9.858	9.572	9.278	8.975	8.663
	12.969	12.776	12.573	12.361	12.138	11.906	11.664	11.413	11.153	10.884	10.606	10.319	10.023	9.719	9.406
	13.733	13.539	13.334	13.120	12.895	12.662	12.418	12.166	11.904	11.634	11.354	11.066	10.769	10.464	10.149
20	14.498	14.301	14.095	13.879	13.653	13.417	13.173	12.919	12.656	12.384	12.103	11.813	11.515	11.208	10.893
	15.262	15.064	14.856	14.638	14.410	14.173	13.927	13.671	13.407	13.134	22.851	12.560	12.261	11.953	11.637
	16.027	15.827	15.617	15.397	15.168	14.929	14.681	14.424	14.158	13.884	13.600	13.308	13.007	12.698	12.381
	16.792	16.590	16.378	16.156	15.925	15.685	15.436	15.177	14.910	14.634	14.349	14.056	13.754	13.443	13.125
	17.557	17.353	17.139	16.916	16.683	16.441	16.190	15.931	15.662	15.384	15.098	14.803	14.500	14.189	13.869

TABLE VI-19b

(Continued)

Salinity (°/oo)	TEMPERATURE (°C)														
	16			18		20		22		24		26		28	
25	18.322	18.116	17.901	17.676	17.441	17.198	16.945	16.684	16.414	16.135	15.848	15.552	15.247	14.935	14.614
	19.087	18.880	18.662	18.436	18.200	17.955	17.701	17.438	17.166	16.886	16.597	16.300	15.995	15.681	15.359
	19.853	19.643	19.424	19.196	18.958	18.712	18.456	18.192	17.919	17.637	17.347	17.049	16.742	16.428	16.105
	20.619	20.408	20.187	19.957	19.717	19.469	19.212	18.946	18.672	18.389	18.098	17.798	17.490	17.175	16.851
	21.385	21.172	20.949	20.718	20.477	20.227	19.968	19.701	19.425	19.141	18.849	18.548	18.239	17.922	17.597
30	22.152	21.937	21.713	21.479	21.236	20.985	20.725	20.456	20.179	19.894	19.600	19.298	18.988	18.670	18.344
	22.919	22.702	22.476	22.241	21.997	21.744	21.482	21.212	20.934	20.647	20.352	20.049	19.738	19.419	19.091
	23.687	23.468	23.240	23.003	22.757	22.503	22.240	21.968	21.689	21.401	21.104	20.800	20.488	20.168	19.840
	24.455	24.235	24.005	23.766	23.519	23.263	22.998	22.725	22.444	22.155	21.857	21.552	21.239	20.917	20.588
	25.224	25.001	24.770	24.530	24.281	24.023	23.757	23.483	23.200	22.910	22.611	22.304	21.990	21.668	21.338
35	25.993	25.769	25.536	25.294	25.043	24.784	24.516	24.241	23.957	23.665	23.365	23.058	22.742	22.419	22.088
	26.763	26.537	26.302	26.058	25.806	25.545	25.277	24.999	24.714	24.421	24.120	23.811	23.495	23.171	22.839
	27.534	27.306	27.069	26.824	26.570	26.308	26.037	25.759	25.472	25.178	24.876	24.566	24.248	23.923	23.590
	28.305	28.075	27.837	27.590	27.334	27.071	26.799	26.519	26.231	25.936	25.632	25.321	25.003	24.677	24.343
	29.077	28.846	28.605	28.357	28.100	27.834	27.561	27.280	26.991	26.694	26.390	26.078	25.758	25.431	25.096
40	29.850	29.617	29.375	29.124	28.866	28.599	28.324	28.042	27.751	27.453	27.148	26.835	26.514	26.186	25.851

*Sigma-t (σ_t) is defined as: (density-1) x 10^3. For example, for seawater with a density of 1.02500 g/cm^3, σ_t = 25.

TABLE VI-19c

WATER DENSITIES (EXPRESSED AS SIGMA-T)* CALCULATED
USING THE DENSITY SUBROUTINE FOUND IN MERGE

Salinity (°/oo)	TEMPERATURE (°C)														
	30		32		34		36		38		40		42		44
0	-4.291	-4.597	-4.912	-5.235	-5.567	-5.906	-6.254	-6.610	-6.973	-7.345	-7.723	-8.110	-8.503	-8.904	-9.313
	-3.545	-3.853	-4.169	-4.494	-4.827	-5.168	-5.518	-5.875	-6.240	-6.613	-6.993	-7.381	-7.777	-7.180	-8.590
	-2.800	-3.109	-3.427	-3.753	-4.088	-4.430	-4.781	-5.140	-5.507	-5.881	-6.263	-6.653	-7.050	-7.455	-7.867
	-2.055	-2.366	-2.685	-3.013	-3.349	-3.693	-4.045	-4.405	-4.774	-5.150	-5.534	-5.925	-6.324	-6.730	-7.144
	-1.311	-1.623	-1.943	-2.273	-2.610	-2.956	-3.309	-3.671	-4.041	-4.418	-4.804	-5.197	-5.597	-6.006	-6.421
5	-0.567	-0.880	-1.202	-1.533	-1.872	-2.219	-2.574	-2.937	-3.308	-3.687	-4.074	-4.469	-4.871	-5.281	-5.698
	.177	-0.138	-0.461	-0.793	-1.134	-1.482	-1.839	-2.203	-2.576	-2.956	-3.345	-3.741	-4.145	-4.556	-4.975
	.920	.604	.279	-0.054	-0.396	-0.475	-1.103	-1.469	-1.843	-2.225	-2.615	-3.013	-3.418	-3.831	-4.252
	1.663	1.345	1.019	.685	.342	-0.009	-0.368	-0.736	-1.111	-1.494	-1.886	-2.285	-2.691	-3.106	-3.528
	2.406	2.087	1.759	1.424	1.079	.727	.367	-0.002	-0.379	-0.763	-1.156	-1.556	-1.965	-2.380	-2.804
10	3.148	2.828	2.499	2.162	1.817	1.463	1.101	.731	.354	-0.032	-0.426	-0.828	-1.238	-1.655	-2.080
	3.890	3.569	3.239	2.901	2.554	2.199	1.836	1.465	1.086	.699	.304	-0.099	-0.510	-0.929	-1.355
	4.633	4.310	3.979	3.639	3.291	2.935	2.571	2.199	1.818	1.430	1.034	.629	.217	-0.203	-0.630
	5.375	5.051	4.718	4.378	4.029	3.671	3.306	2.932	2.551	2.161	1.764	1.358	.945	.524	.095
	6.117	5.792	5.458	5.116	4.766	4.408	4.041	3.666	3.284	2.893	2.494	2.088	1.673	1.251	.820
15	6.859	6.532	6.198	5.855	5.503	5.144	4.776	4.400	4.016	3.625	3.225	2.817	2.401	1.978	1.547
	7.601	7.273	6.937	6.593	6.241	5.880	5.511	5.134	4.750	4.357	3.956	3.547	3.130	2.706	2.273
	8.343	8.014	7.677	7.332	6.978	6.617	6.247	5.869	5.483	5.089	4.687	4.277	3.860	3.434	3.001
	9.085	8.755	8.417	8.070	7.716	7.353	6.982	6.604	6.217	5.822	5.419	5.008	4.589	4.163	3.728
	9.827	9.496	9.157	8.809	8.454	8.090	7.718	7.338	6.951	6.555	6.151	5.739	5.320	4.892	4.457
20	10.569	10.237	9.897	9.549	9.192	8.827	8.455	8.074	7.685	7.288	6.884	6.471	6.050	5.622	5.186
	11.312	10.979	10.638	10.288	9.931	9.565	9.191	8.809	8.420	8.022	7.617	7.203	6.782	6.353	5.915
	12.055	11.721	11.378	11.028	10.669	10.303	9.928	9.546	9.155	8.757	8.350	7.936	7.514	7.084	6.646
	12.798	12.463	12.119	11.768	11.408	11.041	10.666	10.282	9.891	9.491	9.084	8.669	8.246	7.816	7.377
	13.541	13.205	12.861	12.508	12.148	11.780	11.403	11.015	10.627	10.227	9.819	9.403	8.980	8.548	8.109

TABLE VI-19c

(Continued)

Salinity	TEMPERATURE (°C)														
(°/oo)	30		32		34		36		38		40		42		44
25	14.285	13.948	13.602	13.249	12.888	12.519	12.142	11.757	11.364	10.963	10.554	10.138	9.714	9.282	8.842
	15.029	14.691	14.345	13.990	13.628	13.258	12.881	12.495	12.101	11.700	11.291	10.874	10.449	10.016	9.576
	15.773	15.434	15.087	14.732	14.369	13.999	13.620	13.233	12.839	12.437	12.027	11.610	11.184	10.751	10.310
	16.518	16.178	15.830	15.475	15.111	14.739	14.360	13.973	13.578	13.175	12.765	12.347	11.921	11.487	11.046
	17.264	16.923	16.574	16.217	15.853	15.481	15.101	14.713	14.317	13.914	13.503	13.084	12.658	12.224	11.782
30	18.010	17.668	17.318	16.961	16.596	16.223	15.842	15.454	15.057	14.654	14.242	13.823	13.396	12.962	12.520
	18.757	18.414	18.063	17.705	17.339	16.965	16.584	16.195	15.798	15.394	14.982	14.563	14.136	13.701	13.258
	19.504	19.160	18.809	18.450	18.083	17.709	17.327	16.937	16.540	16.135	15.723	15.303	14.876	14.441	13.998
	20.252	19.907	19.555	19.195	18.828	18.453	18.070	17.680	17.283	16.878	16.465	16.045	15.617	15.182	14.739
	21.000	20.655	20.302	19.941	19.573	19.198	18.815	18.424	18.026	17.621	17.208	16.787	16.359	15.924	15.481
35	21.749	21.403	21.050	20.688	20.320	19.944	19.560	19.169	18.771	18.365	17.952	17.531	17.103	16.667	16.224
	22.499	22.153	21.798	21.436	21.067	20.690	20.306	19.915	19.516	19.110	18.696	18.276	17.847	17.412	16.969
	23.250	22.903	22.547	22.185	21.815	21.438	21.054	20.662	20.263	19.856	19.442	19.021	18.593	18.157	17.714
	24.002	23.653	23.298	22.935	22.564	22.187	21.802	21.409	21.010	20.603	20.190	19.768	19.340	18.904	18.461
	24.754	24.405	24.049	23.685	23.314	22.936	22.551	22.158	21.759	21.352	20.938	20.517	20.088	19.653	19.210
40	25.508	25.158	24.801	24.437	24.065	23.687	23.301	22.808	22.508	22.101	21.687	21.266	20.838	20.402	19.960

*Sigma-t (σ_t) is defined as: (density-1) x 10^3. For example, for seawater with a density of 1.02500 g/cm^3, σ_t = 25.

However, when the same models are used to predict the trajectories of horizontally discharged buoyant plumes, a larger coefficient is required. Consequently the aspiration coefficient must be variable.

Although relatively advanced, MERGE does have its limitations. Some of these are a result of the assumptions already discussed. For example, the plumes are assumed to be round, whereas some evidence indicates substantial deviation from this idealization (Abramovich, 1963). Other important limitations are listed below:

- Diffuser parallel current: The model does not predict plume dilution for cases of current flowing parallel to the diffuser pipe. This is a severe limitation especially in some ocean applications because this case may be expected to result in the lowest initial dilutions.
- Surface entrainment interference: The model does not properly account for interfacial boundary conditions. Dilutions near the surface or bottom may be overestimated because entrainment will be assumed where water is unavailable for entrainment.
- Horizontal homogeneity: The model assumes homogeneous horizontal current although bottom topography, internal waves, or other factors may cause considerable spatial flow variations. This is in addition to temporal variations which are excluded by virtue of assumed steady-state.
- Uniform discharge: It is assumed that an infinitely long diffuser exists for which there is no port-to-port variation in effluent characteristics.

6.5.2.3 Similarity

The success of a set of tables in describing an infinite number of possible diffuser, effluent, and ambient flow configurations depends on the principles of similarity. Basically, similarity theory states that model and prototype will display equivalent behavior if a limited number of similarity conditions or parameters are preserved. Equivalent behavior means that relative to appropriate measures the behavior will be equal. For example, if all similarity parameters are preserved, then the height of rise predicted by the model and observed in the prototype will be equal when measured in terms of the initial diameters of the corresponding plumes.

The number of similarity conditions is determined by the difference between the number of independent variables and primary variables involved in the problem (Streeter, 1961). Primary variables must include mass, time, and distance. The present problem involves eleven independent variables implying eight similarity conditions. The independent variables, corresponding symbols, units, similarity parameters, and their names are listed in Table VI-20. As the dilution tables are based on a linear equation of state, the effluent and ambient densities ρ_e and ρ_a, respectively, replace four independent variables: the effluent and ambient salinities and temperatures. This effectively reduces the number of similarity conditions by two to six.

Table VI-20.

PLUME VARIABLES, UNITS, AND SIMILARITY CONDITIONS

Variable	Symbol	Units	Dimensionless Sim. Parm	Name
Effluent density	ρ_e	ML^{-3}	none--primary variable	none
Effluent velocity	v	LT^{-1}	none--primary variable	none
Effective diameter	d_o	L	none--primary variable	none
Ambient density	ρ_a	ML^{-3}	ρ_e/ρ_a	density ratio
Reduced gravity	g'	LT^{-2}	$v/\sqrt{g'd_o}$	densimetric Froude number: Fr
Density stratification	$d\rho_a/dz$	ML^{-4}	$\rho_e/(d_o d\rho_a/dz)$	stratification parm.
Current velocity	u_a	LT^{-1}	u_a/v	current to effluent velocity ratio: k
Kinematic viscosity	ν	L^2T^{-1}	d_o/ν	Reynolds number: Re
Port spacing	S_1	L	S_1/d_o	Port spacing parm.: PS

Notes: 1. $g' = ((\rho_a-\rho_e)/\rho_e)g$ where g is the acceleration of gravity (9.807 $msec^{-2}$).

2. In the present application a composite stratification parameter, SP, is used in lieu of the density ratio and the stratification parameter. $SP = (\rho_a-\rho_e)/(d_o d\rho_a/dz)$.

3. The diameter, d_o is taken to be the vena contracta diameter.

It is advantageous to further reduce the number of similarity conditions to minimize the number of tables necessary to represent the flow configurations of interest. From experimental observations, it is found that plume behavior is basically invariant for large Reynolds numbers reducing the number of similarity conditions to five. Finally, the ratio ρ_e/ρ_a and the stratification parameter can be combined in a composite stratification parameter, SP, where:

$$SP = (\rho_a - \rho_e)/(d_o d\rho_a/dz)$$

This is a satisfactory similarity parameter providing that differences in model and prototype densities are not too great. The assumption is valid for discharge of municipal waste water into estuarine or coastal waters. Figures VI-28 and VI-29 demonstrate the effectiveness of this parameter. The same similarity conditions are shared for both cases. The two figures show rise and dilution to be within about a percent of each other even though the stratification and initial buoyancies are much different. With only four similarity conditions to be satisfied, the problem can be represented by considerably fewer model runs than if six similarity conditions were required.

6.5.2.4 Table Usage

To use the dilution tables to estimate dilutions, it is necessary to calculate the appropriate similarity parameters and know the depth of the outfall. Calculation of the four similarity parameters Fr, SP, k, and PS, given in Table VI-20 requires knowledge of all the variables except v. The dilution tables are shown in Appendix G.

The depth used in the dilution tables is expressed in terms of the diameter of the ports; that is, the vena contracta diameter. For bell-mouthed ports, this diameter is approximately equal to the physical diameter of the port. Thus, if the actual depth of water is 10 m and the port diameter is 10 cm, then the depth of water is 100-port diameters.

The dilution tables are numbered from 1 through 100 and are grouped by port spacing as listed below:

Tables	Port Spacing (PS) (Diameters)
1-20	2
21-40	5
41-60	10
61-80	25
81-100	1000 (effluent from each port acts as a single plume)

CASE NUMBER 1

***** TEST OF COMPOSITE STRATIFICATION PARAMETER

INPUT DATA PSEUDO-ECHO

U	V	A	T	S	B	SPC	ALT DEN
7.0200	0.0000	0.1160	0.0000	0.0000	0.0500	100.0000	0.0000

NDP	ITER	IFRQ	NAA	NAB	NAC	IDENSW
2	1000	25	0	0	0	1

(IF IDENSW=1 THEN DENSITY VERSION USED--USE 2ND SIGMAT COL)

AMBIENT STRATIFICATION (AND CALCULATED SIGMAT)

DEPTH(M)	TEMP(C)	SAL(O/OO)	CUR(M/S)	SIGMAT	SIGMAT(DEN VER)
0.000	0.000	0.000	0.000	-0.093	0.000
10.000	0.000	0.000	0.000	-0.093	27.000

EFFLUX TO CURRENT RATIO(R) . . .=	99999.0
DENSIMETRIC FROUDE NO. . . . . .=	43.1
VOLUME FLUX(M**3/S). . . . . .=	0.055
DEPTH AVE STRATIFICATION PARM. .=	3703.7
DEPTH(M) . . . . . .=	10.0
DISCHARGE VELOCITY(M/S). . . . .=	7.02
CURRENT SPEED(M/S) . . . . . .=	0.000
PORT RADIUS(M) . . . . . .=	0.0500
PORT SPACING(M). . . . . .=	100.00

MODEL OUTPUT AFTER -J- ITERATIONS (MKS UNITS)

Q	HOR COR(X)	DEPTH(Z)	DIAMETER	VOL DIL	HOR VEL(U)	VER VEL(V)	TOTAL VEL	DEN DIFF	TIME	CURRENT
1	0.001	10.000	0.100	1.007	6.972	0.000	6.972	26.813	0.000	0.000
25	0.040	10.000	0.118	1.184	5.903	0.001	5.903	22.704	0.006	0.000
50	0.087	10.000	0.140	1.403	4.964	0.003	4.964	19.092	0.015	0.000
75	0.143	10.000	0.167	1.664	4.174	0.004	4.174	16.054	0.027	0.000
100	0.210	10.000	0.198	1.973	3.510	0.006	3.510	13.500	0.045	0.000
125	0.290	10.000	0.235	2.342	2.952	0.008	2.952	11.351	0.070	0.000
150	0.385	9.999	0.279	2.780	2.482	0.010	2.482	9.545	0.105	0.000
175	0.497	9.999	0.332	3.301	2.087	0.012	2.087	8.025	0.155	0.000
200	0.632	9.998	0.395	3.921	1.755	0.015	1.755	6.746	0.226	0.000
225	0.792	9.996	0.469	4.657	1.476	0.018	1.476	5.668	0.326	0.000
250	0.982	9.993	0.558	5.534	1.241	0.021	1.241	4.760	0.468	0.000
275	1.208	9.989	0.663	6.576	1.044	0.026	1.044	3.991	0.668	0.000
300	1.477	9.981	0.788	7.815	0.878	0.031	0.878	3.336	0.951	0.000
325	1.797	9.967	0.936	9.289	0.738	0.037	0.739	2.772	1.352	0.000
350	2.177	9.944	1.113	11.042	0.620	0.043	0.622	2.276	1.917	0.000
375	2.628	9.907	1.321	13.127	0.522	0.051	0.524	1.822	2.715	0.000
400	3.162	9.845	1.568	15.606	0.439	0.058	0.443	1.382	3.839	0.000
425	3.792	9.747	1.859	18.555	0.369	0.065	0.375	0.923	5.416	0.000
450	4.534	9.601	2.202	22.064	0.310	0.067	0.317	0.417	7.624	0.000
NOMINAL TRAPPING LEVEL REACHED										
469	5.184	9.454	2.508	25.169	0.272	0.062	0.279	-0.001	9.877	0.000
475	5.408	9.403	2.615	26.238	0.261	0.059	0.268	-0.135	10.720	0.000
500	6.457	9.196	3.130	31.204	0.219	0.033	0.222	-0.627	15.137	0.000
519	7.407	9.127	3.592	35.809	0.192	0.007	0.192	-0.740	19.789	0.000

FIGURE VI-28 EXAMPLE OUTPUT OF MERGE - CASE 1

CASE NUMBER 2

***** TEST OF COMPOSITE STRATIFICATION PARAMETER

INPUT DATA PSEUDO-ECHO

U	V	A	T	S	B	GPC	ALT DEN
2.3400	0.0000	0.1160	0.0000	0.0000	0.0500	100.0000	0.0000

NDP	ITER	IFRQ	NAA	NAB	NAC	IDENSW
2	1000	25	0	0	0	1

(IF IDENSW=1 THEN DENSITY VERSION USED--USE 2ND SIGMAT COL)

AMBIENT STRATIFICATION (AND CALCULATED SIGMAT)

DEPTH(M)	TEMP(C)	SAL(O/OO)	CUR(M/S)	SIGMAT	SIGMAT(DEN VER)
0.000	0.000	0.000	0.000	-0.093	0.000
10.000	0.000	0.000	0.000	-0.093	0.000

EFFLUX TO CURRENT RATIO(R) . . . .=	99999.0
DENSIMETRIC FROUDE NO. . . . . .=	43.1
VOLUME FLUX(M**3/S). . . . . .=	0.018
DEPTH AVE STRATIFICATION PARM. .=	33333.3
DEPTH(M) . . . . . .=	10.0
DISCHARGE VELOCITY(M/S). . . . .=	2.34
CURRENT SPEED(M/S) . . . . . .=	0.000
PORT RADIUS(M) . . . . . .=	0.0508
PORT SPACING(M). . . . . .=	100.00

MODEL OUTPUT AFTER -J- ITERATIONS (MKS UNITS)

J	HOR COR(X)	DEPTH(Z)	DIAMETER	VOL DIL	HOR VEL(U)	VER VEL(V)	TOTAL VEL	DEN DIFF	TIME	CURRENT
1	0.001	10.000	0.100	1.007	2.324	0.000	2.324	2.979	0.001	0.000
25	0.041	10.000	0.118	1.189	1.968	0.000	1.968	2.523	0.019	0.000
50	0.089	10.000	0.141	1.413	1.655	0.001	1.655	2.121	0.046	0.000
75	0.146	10.000	0.167	1.680	1.391	0.001	1.391	1.784	0.084	0.000
100	0.214	10.000	0.199	1.997	1.170	0.002	1.170	1.500	0.138	0.000
125	0.295	10.000	0.237	2.374	0.984	0.003	0.984	1.261	0.214	0.000
150	0.392	9.999	0.282	2.823	0.827	0.003	0.827	1.061	0.322	0.000
175	0.506	9.999	0.335	3.356	0.696	0.004	0.696	0.892	0.474	0.000
200	0.643	9.998	0.398	3.991	0.585	0.005	0.585	0.749	0.689	0.000
225	0.805	9.996	0.473	4.746	0.492	0.006	0.492	0.630	0.994	0.000
250	0.998	9.993	0.563	5.643	0.414	0.007	0.414	0.529	1.425	0.000
275	1.227	9.988	0.669	6.710	0.348	0.009	0.348	0.443	2.034	0.000
300	1.500	9.980	0.796	7.979	0.293	0.011	0.293	0.370	2.895	0.000
325	1.824	9.966	0.946	9.488	0.246	0.013	0.246	0.308	4.112	0.000
350	2.209	9.942	1.124	11.283	0.207	0.015	0.207	0.252	5.830	0.000
375	2.666	9.902	1.336	13.417	0.174	0.017	0.175	0.201	8.254	0.000
400	3.206	9.838	1.585	15.955	0.146	0.020	0.148	0.152	11.666	0.000
425	3.843	9.736	1.879	18.973	0.123	0.022	0.125	0.100	16.450	0.000
450	4.592	9.585	2.225	22.563	0.103	0.023	0.106	0.043	23.140	0.000
NOMINAL TRAPPING LEVEL REACHED										
468	5.213	9.443	2.518	25.561	0.091	0.021	0.094	-0.002	29.563	0.000
475	5.476	9.382	2.644	26.832	0.087	0.020	0.089	-0.019	32.525	0.000
500	6.537	9.177	3.167	31.909	0.073	0.010	0.074	-0.073	45.931	0.000
517	7.398	9.117	3.583	35.900	0.065	0.000	0.065	-0.083	58.378	0.000

FIGURE VI-29 EXAMPLE OUTPUT OF MERGE - CASE 2

Each group of 20 is further subdivided by current velocity to effluent velocity ratio (k), i.e.:

Tables	Current Velocity to Effluent Velocity Ratio (k)
1-5	0.1
6-10	0.05
11-15	0.02
16-20	0.00 (no current)

Each subgroup of five tables is comprised of tables of varying composite density stratification (SP):

Tables	Composite Stratification Parameter (SP)
1	200 (high stratification)
2	500
3	2000
4	10000
5	infinity (no stratification)

Finally, each table includes densimetric Froude number, Fr = 1, 3, 10, 30, 100, and 1000 to represent cases ranging from highly buoyant plumes to almost pure jets. The dilutions are tabulated with plume rise. The following examples demonstrate how the tables may be applied.

EXAMPLE VI-11

Calculation of Initial Dilution

Example A. This example demonstrates many of the basic features of the dilution tables and their usage. It also includes a method for estimating the plume diameter indirectly using information derived from the tables. The method is used in cases of unmerged or slightly merged plumes and is necessary to better estimate plume dilution when the plume is shown to interact with the water surface.

Given that waste water is discharged horizontally at a depth of 66 m from a simple pipe opening and that:

u_a = the current velocity = 0.15 m/s
v = the effluent velocity = 1.5 m/s
ρ_e = the effluent density = 1000 kg/m^3
ρ_a = the ambient density at discharge depth = 1015 kg/m^3
L = the port spacing = infinite

d_o = the port discharge vena contracta diameter = 1.7 m

dp_a/dz = the ambient density stratification = 0.0441 kg/m^4

The four similarity parameters necessary to use the tables are:

Fr = the densimetric Froude number = 3.0

k = the current to effluent velocity ratio = 0.1

SP = the composite stratification parameter = 200

PS = the port spacing parameter = infinity.

The infinite port spacing indicates that the dilutions will be found in the last 20 tables of the dilution tables in Appendix G, i.e., Tables 81-100. These tables are appropriate because merging does not occur with PS = infinity. The current to effluent velocity ratio of 0.1 indicates that the appropriate dilutions are among the first five of these 20 tables. The stratification parameter 200 identifies the first of these five tables as the correct reference location. Finally, the densimetric Froude number of 3.0 isolates the second column as the one containing the information of interest.

The column of dilutions contains a wealth of information about the plume whose overall behavior is described in Figure VI-30. After rising one diameter (1.7 m), the average plume dilution (expressed in terms of volume dilution) is 2.8. In other words, a given amount of plume volume has been diluted with 1.8 times as much ambient fluid. After rising 2 diameters (3.4 m), the average dilution is 3.7, and so on. At 15 diameters rise, the dilution is 21.4. The next entry follows in a line headed by "T", indicating that the initial trapping level has been reached. This means that the plume and ambient densities are equal at this level and momentary equilibrium has been attained. The "trapping" level dilution is 26.2 and the corresponding plume rise, set off in parentheses to the right of the dilution, is 17.0 diameters. The parentheses are a mnemonic for indicating trapping while values set off in square brackets are merging level plume rises.

When a plume intercepts the water surface, it is deprived of some of its entraining surface and consequently the dilution is less than that indicated in the tables. For well-diluted, unmerged or slightly merged plumes, wih k not equal to zero, the plume diameter, d, may be estimated:

$$d = d_o\sqrt{D/k} \qquad \text{(VI-61)}$$

In dimensionless units, or diameters:

$$d/d_o = \sqrt{D/k} \qquad \text{(VI-62)}$$

In the present case, the diameter at maximum rise calculated in this way is

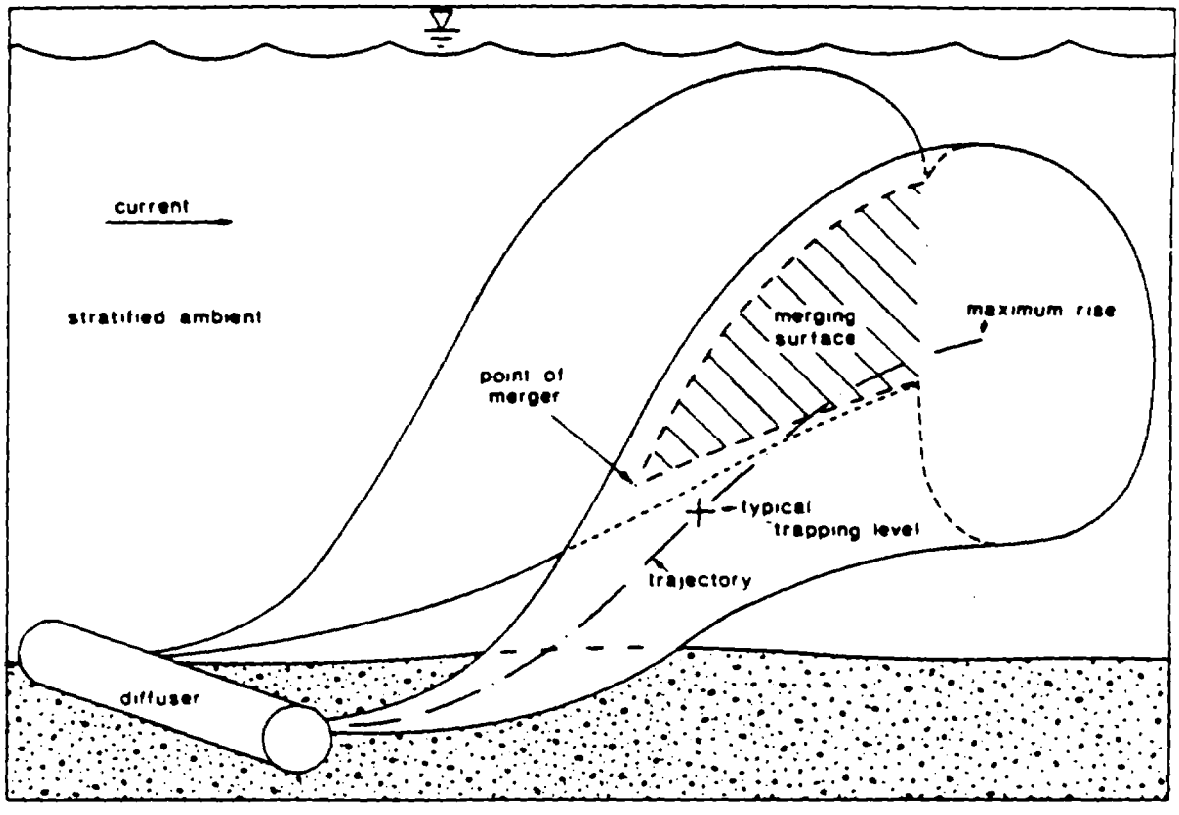

FIGURE VI-30 SCHEMATIC OF PLUME BEHAVIOR PREDICTED BY MERGE IN THE PRESENT USAGE

25.2 diameters (42.8m). Thus the top of the plume is 34.8 diameters (22.2 + 12.6) above the level of the outfall, i.e. 12.6 diameters above the plume centerline, and 4.0 diameters below the surface. Therefore, surface interaction does not occur.

For the sake of comparison, the plume diameter calculated by the program at maximum rise is 23.5 diameters which compares favorably with the simplified estimate made above.

Example B. Suppose that all the conditions given in Example A apply here except that the depth of water is only 29.7 diameters (50.5 m). Table 81 is again used to provide dilution estimates; however, surface interaction does occur. A conservative estimate of initial dilution is obtained by assuming that entrainment stops as soon as the top boundary of the plume intersects the surface. In reality, some additional ambient water could be expected to enter through the sides of the plume.

When the centerline depth of the plume is 20 diameters, its dilution is 37.3 and its approximate diameter is 19.4 diameters (33 m). Consequently, the top boundary of the plume is 29.7 diameters above the level of the outfall and is equal to the depth of water. Thus the dilution of 37.3 provides a conservative

estimate of initial dilution in this case.

Example C. Suppose the following data apply:

u_a = 0.15 m/s
v = 1.5 m/s
ρ_e = 1000 kg/m
ρ_a = 1015 kg/m
S_1 = 0.34 m
d_o = 0.17 m
$d\rho_a/dz$ = 0.0441 kg/m^4

Then, Fr = 9.5, k = 0.1, SP = 2000, and PS = 2, and Table 3 in Appendix G is the appropriate source of dilution information. As the Froude number is almost equal to 10, column 3 information can be used without modification although interpolation may be appropriate in some applications. The plumes merge almost immediately at a dilution of 2.1. The initial trapping level is encountered after the plume rises 89.4 diameters (15.2 m). The maximum dilution is 76.2 after rising 125 diameters (21.3).

For closely spaced plumes, the diameter may be estimated from the relationship:

$$d/d_o = (\pi D)\ (4\ k\ PS) \qquad \text{(VI-63)}$$

The maximum diameter estimated in this way is 299 diameters (50.9 m). In contrast, the program gives a value of 268 diameters (45.5 m). No surface interaction occurs in deep water. In very shallow water, a conservative estimate of dilution may be made by dividing the total flow across the length of the diffuser by the flow through the diffuser. It is conservative because no aspiration entrainment is included in the estimate.

Table 3 contains a blank entry in the second column of the 90-diameter rise line. The previous entry in the column indicates trapping. This means that trapping and the 90-diameter rise level occurred in the same iteration. Therefore, the dilution of 41.3 is the appropriate value for this blank.

Example D. The methods given in Examples A and C for estimating the plume diameter are not accurate when intermediate degrees of merging exist. If surface interaction is important, it may be necessary to run the model to obtain accurate plume diameter predictions.

Example E. Sometimes outfalls or diffusers are located in water only a few port diameters deep and, as a result, initial dilutions may be expected to be quite small. However, after the plumes reach the surface, they still have substantial horizontal velocity and continue to entrain ambient water more vigorously than a plume whose trajectory is unhindered by surface constraints. The workbook by Shirazi and Davis (1976) may be consulted to estimate additional dilution.

Example F. Strong stratification inhibits plume rise. As stratification weakens, plume rise and dilution tend to increase. Predicting large dilutions and plume rises can require more program iterations than used to develop the tables in Appendix G. On the other hand, very large dilutions are usually of lesser interest. Consequently, the number of iterations is arbitrarily limited to 1000 and rise to 300 diameters. Table 94 provides examples in which the runs for each densimetric Froude number are limited by the permitted number of iterations. The final dilutions listed are underlined to remind the user that larger dilutions and plume rises occur. When the rise limitation criterion has been reached, a rise of 300 diameters or slightly more will be indicated.

Example G. Many diffusers have horizontally discharging paired ports on each side of the diffuser. In cross current, the resulting plume behavior appears somewhat like that shown in Figure VI-31. The upstream plume is bent over the counterflowing current and ultimately may be entrained by the downstream plume. The entrainment of pollutant laden fluid will reduce the overall dilution in the merged plumes. Estimates of the magnitude of this effect may be made if it may be assumed that:

- The interaction occurs
- There is merging of adjacent plumes to assure cross diffuser merging and not interweaving of plumes
- The opposite plumes have similar rise and overall entrainment
- There are no surface constraints
- The actual (not permitted) rise is provided in the tables.

The final dilution of the merged plumes, D_f, is approximately:

$$D_f = (D^2)/(2D - D_e) \qquad \text{(VI-64)}$$

where D is the dilution at maximum rise of the downstream plume as given in the tables and D_e is the dilution of the downstream plume upon entry into the bottom of the bent over upstream plume (see Figure VI-31). D_e is estimated by finding the distance in diameters, Z_e, between the depth at entry and the port depth. The dilution at this depth is read from the appropriate line in the dilution tables or interpolated. The maximum radius of the plume is added to the depth at which maximum rise occurs. The difference between the port depth and the depth so calculated is Z_e.

Given that Fr = 3, PS = 25, SP = 2000, and k = 0.1, and that identical plumes are injected into the ambient water from both sides of the diffuser. From Table 63, it is found that the dilution is 270 and the rise is 55.1 diameters. The width of the plumes may be estimated:

$$d/d_o = (\pi 270)/[4(0.1)(25)] = 85$$

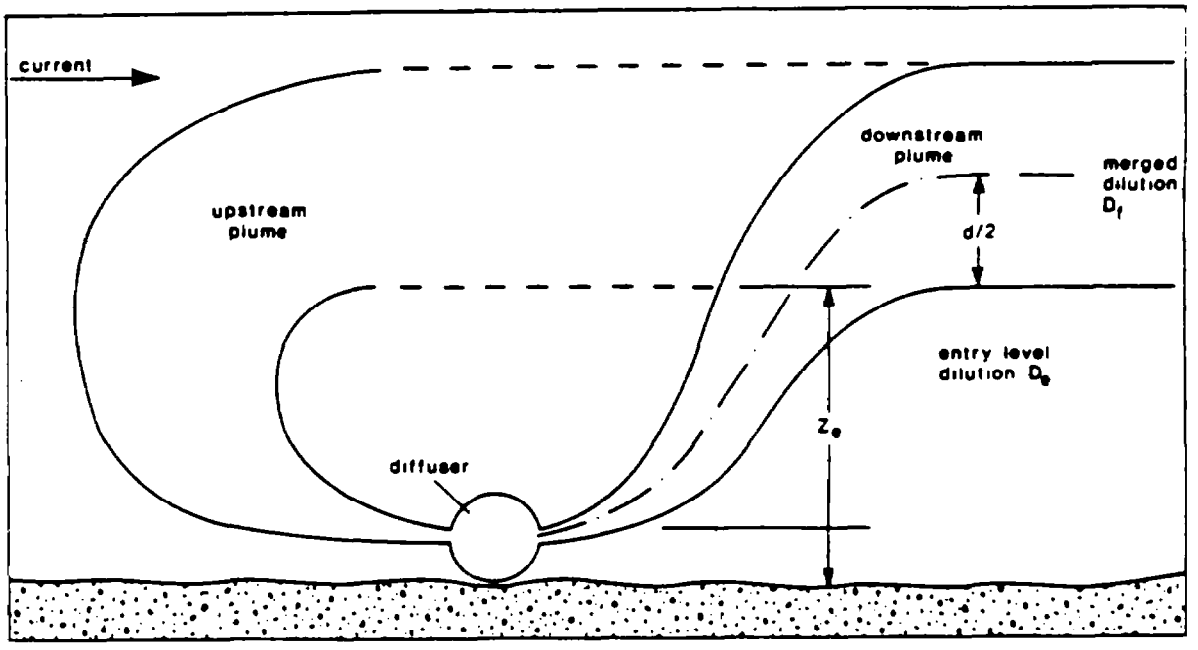

FIGURE VI-31 CROSS DIFFUSER MERGING

(cf. the computer calculated width of 83 diameters). Therefore, the vertical distance between the ports and the plume entry level is 55.1-85/2 = 12.6 diameters, and D_e 15.5 as estimated from the table at rise equal to 12 diameters. D_f may now be calculated:

$$D_f = 270/[2(270) - 15.5] = 139$$

This result may have been anticipated: the dilution is effectively halved. This is the outcome whenever the entry level, Z_e, is small. In many cases, halving the dilution provided in the tables gives an adequate estimate of the overall dilution achieved by the cross diffuser merging plumes.

Example H. Given that PS = 25, SP = 200, k = 0.0, Fr = 10, and that an estimate of the centerline dilution at maximum rise is required. By consulting Table 77, it is found that the average dilution at maximum rise is 26.0. Since there is no current and virtually no merging, this value can be divided by 1.77 to obtain the centerline dilution (based on a gaussian profile, see Teeter and Baumgartner, 1979). The centerline dilution is 14.7.

With identical conditions except for port spacing of 2 instead of 25, Table 16 shows that the dilution at maximum rise is 11.6. The centerline dilution is again smaller but not by the same percentage amount. For the 3/2 power profile, similar to the gaussian, the peak-to-mean ratio in stagnant ambient and complete merging is 1.43 (Teeter and Baumgartner, 1979). Thus the centerline dilution may be found to be 8.1.

The peak-to-mean ratios given above are flow-weighted and are obtained through a straightforward integration. Unfortunately the problem is not as simple when current is present because the gaussian or other arbitrary profiles of velocity are superimposed onto a non-zero average velocity. Hence, in high current, the peak-to-mean ratio for single plumes assuming the 3/2 power profile is 3.89. For merged plumes, the ratio is lower. For intermediate currents, the ratio is between the corresponding extremes depending on the degree of merging and the actual current velocity.

Fortunately, many standards and regulations - for example, the Federal 301(h) regulations - are written in terms of average dilutions. Also, repeated measurements in the field are likely to provide estimates of average concentrations before estimates of maximum concentrations are possible. Thus, the user of MERGE is normally not concerned with centerline dilutions. It is useful to remember that estimating average dilutions using centerline models involves not only the use of variable peak-to-mean ratios but also variable aspiration coefficients.

END OF EXAMPLE VI-11

6.5.3 Pollutant Concentration Following Initial Dilution

The concentration of a conservative pollutant at the completion of initial dilution is expressible as:

$$C_f = C_a + \frac{C_e - C_a}{S_a} \qquad \text{(VI-65)}$$

where

C_a = background concentration, mg/l
C_e = effluent concentration, mg/l
Sa = initial dilution (flux-averaged)
C_f = concentration at the completion of initial dilution, mg/l.

When the background level, C_a, is negligible Equation VI-65 simplifies to:

$$C_f = \frac{C_e}{Sa} \qquad \text{(VI-66)}$$

This expression can be used to predict the increased pollutant concentration above ambient, as long as the effluent concentration greatly exceeds the ambient concentration. It is interesting to note that when the effluent concentration is below ambient, the final pollutant concentration is also below ambient.

Since water quality criteria are often prescribed as maximum values not to be exceeded following initial dilution, it is useful to rearrange Equation VI-65 to

express the maximum allowable effluent concentration as follows:

$$(C_e)_{max} = C_a + (Sa)_{min} (C_c - C_a) \qquad (VI-67)$$

where

$(C_e)_{max}$ = maximum allowable effluent concentration such that water quality criteria are not exceeded

C_c = applicable water quality criterion

$(Sa)_{min}$ = minimum expected initial dilution.

Since initial dilution is a function of discharge and receiving water characteristics, as discussed in detail in Section 6.5.2, finding an appropriate "minimum" initial dilution is not a trivial problem. Most often, initial dilutions are lowest when density stratification is greatest. For a given stratification profile, dilutions generally decrease at lower ambient current speeds and higher effluent flow rates. Based on expected critical conditions in the vicinity of the discharge, the tables in Appendix G can be used to predict $(Sa)_{min}$.

EXAMPLE VI-12

Analysis of the effluent wastewater from a treatment plant discharging into a large west coast estuary revealed that the effluent contained a number of priority pollutants. A few of the pollutants and their measured concentrations are shown below.

Priority Pollutant	Concentrations (µg/l) Dry Weather	Wet Weather	Criterion Level (µg/l)
copper	32.3	61.9	4.0
zinc	33.0	180.0	58.0
mercury	not detected	3.5	0.025
lindane	8.6	not detected	0.16

The critical initial dilution has been determined to be 30. If the criterion levels are designed to be complied with at the completion of initial dilution, determine if the criteria for the four priority pollutants are contravened.

A cursory review of the tabulations above shows that all detected effluent pollutant concentrations (i.e., undiluted concentrations) exceed the criteria levels, other than zinc during dry weather flow conditions. Hence if initial dilutions were to become low enough, each of the four priority pollutants could violate water quality criterion for either dry or wet weather conditions.

Using the minimum initial dilution of 30, the final pollutant levels can be predicted using Equation VI-66, by assuming background levels are neglible. The final pollutant levels compared with the criterion levels are shown below.

Priority Pollutant	Final Concentrations (µg/l) Dry Weather	Wet Weather	Criterion Level (µg/l)
copper	1.1	2.1	4.0
zinc	1.1	6.0	58.0
mercury	-	0.1	0.025
lindane	0.3	-	0.16

Both mercury and lindane violate the criteria while copper and zinc do not. However, copper levels are sufficiently close to the criterion of 4.0 µg/l to warrant further attention.

END OF EXAMPLE VI-12

6.5.4 pH Following Initial Dilution

The pH standard governing wastewater discharges into estuarine or coastal waters is usually quite strict. Typically, state standards require that the pH following initial dilution not deviate by more than 0.2 units from background. A step by step approach is presented here that can be used to determine whether a discharge will comply with a standard of this type.

Step 1. The following input data are required:

- Sa = initial dilution
- Alk_a = alkalinity of receiving water, eq/l
- Alk_e = alkalinity of effluent wastewater, eq/l
- pH_a = pH of receiving water
- pH_e = pH of effluent wastewater
- $K_{a,1}$, $^{c}K_{a,1}$ = equilibrium constant for dissociation of carbonic acid in wastewater and receiving water, respectively (first acidity constants)
- $K_{a,2}$, $^{c}K_{a,2}$ = equilibrium constant for dissociation of bicarbonate in wastewater and receiving water, respectively (second acidity constants)
- K_w, $^{c}K_w$ = ion product for wastewater and receiving water, respectively.

Table VI-21 shows values of the equilibrium constants and ion product of water. For seawater, typical values of pH and alkalinity are 8.3 units and 2.3 meq/l, respectively.

Step 2. Calculate the total inorganic carbon concentrations in the effluent wastewater (C_{te}) and receiving water (C_{ta}):

$$C_{te} = \frac{Alk_e - \frac{K_w}{[H^+]_e} + [H^+]_e}{(\alpha_1 + 2\alpha_2)_e} \qquad \text{(VI-68)}$$

TABLE VI-21

VALUES OF EQUILIBRIUM CONSTANTS AND ION PRODUCT OF WATER AS A FUNCTION OF TEMPERATURE FOR FRESHWATER AND SALT WATER

	$-\log K_{a,1}$		$-\log K_{a,2}$		$-\log K_w$	
Temp., °C	Freshwater	Seawater	Freshwater	Seawater	Freshwater	Seawater
5	6.52	6.00	10.56	9.23	14.63	14.03
10	6.46	5.97	10.49	9.17		
15	6.42	5.94	10.43	9.12	14.35	13.60
20	6.38	5.91	10.38	9.06	14.17	13.40
25	6.35	5.84	10.33	8.99	14.00	13.20

and

$$C_{t_a} = \frac{Alk_a - \frac{c_{K_w}}{[H^+]_a} + [H^+]_a}{(\alpha_1 + 2\alpha_2)_a} \qquad \text{(VI-69)}$$

where

$$\alpha_1 = \frac{[H^+]\, K_{a,1}}{[H^+]^2 + [H^+]\, K_{a,1} + K_{a,1} K_{a,2}} \qquad \text{(VI-70)}$$

$$\alpha_2 = \frac{K_{a,1}\ k_{a,2}}{[H^+]^2 + [H^+]\, K_{a,1} + K_{a,1}\, K_{a,2}} \qquad \text{(VI-71)}$$

Note: $c_{K_{a,1}}$ and $c_{K_{a,2}}$ are used in α_1 and α_2 to calculate C_{ta}.

Step 3. Calculate the akalinity (Alk_f) and total inorganic carbon (C_{tf}) at the completion of initial dilution:

$$Alk_f = Alk_a + \frac{Alk_e - Alk_a}{S_a} \qquad \text{(VI-72)}$$

$$C_{t_f} = C_{t_a} + \frac{C_{t_e} - C_{t_a}}{Sa} \qquad \text{(VI-73)}$$

Step 4. Express the final alkalinity as:

$$Alk_f = C_{t_f} (\alpha_1 + 2\alpha_2)_f + \frac{c_{K_w}}{[H^+]_f} - [H^+]_f \qquad \text{(VI-74)}$$

Rather than solving for $[H^+]_f$ directly in Equation VI-74, it is easier to calculate Alk_f in equation VI-72 for a range of $[H^+]$ values, until the alkalinities computed from equations VI-72 and VI-74 match.

In most cases pH_f will not differ from the ambient pH by more than 0.1 to 0.3 units. Consequently it is usually most expeditious to begin by assuming $pH_f = pH_a$. If $pH_e > pH_a$, then each subsequent calculation should be at 0.1 pH units higher than pH_a. If $pH_e < pH_a$, each subsequent calculation should be 0.1 pH units lower than pH_a.

For typical values of wastewater alkalinity (2.0 meq/l) and receiving water alkalinity (2.3 meq/l), the pH at the completion of initial dilution can be tabulated for selected values of effluent pH, initial dilution, and water temperature. Table VI-22 shows the results, which can be used to provide a quick indication of whether the water quality criterion for pH is violated.

EXAMPLE VI-13

A wastewater treatment plant receives alkaline waste process water, and because of the low level of treatment received in the plant, effluent pH values as high as 11.1 units have been observed. The effluent wastewater is discharged into a water body where the pH standard permits a 0.2 unit deviation from ambient at the completion of initial dilution. Determine if the standard is violated by the discharge. The required pertinent data are:

pH_a = 8.3
Alk_a = 2.3 meq/l
Alk_e = 2.0 meq/l
c_{K_w} = 6.3×10^{-14}, for the ambient water
K_w = 10^{-1}, for the wastewater
$c_{K_{a,1}}$ = 8×10^{-7}, for the ambient water
$K_{a,1}$ = 5×10^{-7}, for the wastewater
$c_{K_{a,2}}$ = 4.68×10^{-10}, for the ambient water
$K_{a,2}$ = 0.5×10^{-10}, for the wastewater
Sa = 20

The dissociation constants for the wastewater α_1, and α_2, are:

$$\alpha_1 = \frac{10^{-11.1} \times 5 \times 10^{-7}}{(10^{-11.1})^2 + 10^{-11.1} \times 5 \times 10^{-7} + 5 \times 10^{-7} \times 0.5 \times 10^{-10}} = .137$$

$$\alpha_2 = \frac{5 \times 10^{-7} \times 0.5 \times 10^{-10}}{(10^{-11.1})^2 + 10^{-11.1} \times 5 + 10^{-7} + 5 \times 10^{-7} \times 0.5 \times 10^{-10}} = .863$$

TABLE VI-22
ESTIMATED pH VALUES AFTER INITIAL DILUTION

Seawater Temp °C	5°C					15°C					25°C				
Seawater pH	Initial Dilution 10	25	50	75	100	Initial Dilution 10	25	50	75	100	Initial Dilution 10	25	50	75	100
Effluent pH = 6.0 Alk = 0.1															
7.0	6.94	6.97	6.98	6.98	6.99	6.95	6.97	6.98	6.99	6.99	6.95	6.98	6.99	6.99	6.99
7.5	7.37	7.44	7.47	7.47	7.48	7.40	7.45	7.47	7.48	7.48	7.42	7.46	7.48	7.48	7.49
7.7	7.56	7.64	7.67	7.67	7.68	7.59	7.65	7.67	7.68	7.68	7.62	7.66	7.68	7.68	7.69
8.0	7.88	7.95	7.97	7.97	7.98	7.91	7.96	7.98	7.98	7.99	7.94	7.97	7.98	7.99	7.99
8.3	8.21	8.26	8.28	8.28	8.29	8.24	8.27	8.28	8.29	8.29	8.25	8.28	8.29	8.29	8.29
8.5	8.43	8.47	8.48	8.48	8.49	8.45	8.48	8.49	8.49	8.49	8.46	8.48	8.49	8.49	8.49
Effluent pH = 6.0 Alk = 0.6															
7.0	6.74	6.87	6.93	6.95	6.96	6.77	6.89	6.94	6.96	6.97	6.77	6.89	6.94	6.96	6.97
7.5	6.98	7.23	7.35	7.40	7.42	7.03	7.27	7.38	7.42	7.44	7.08	7.31	7.40	7.43	7.45
7.7	7.07	7.39	7.53	7.59	7.61	7.16	7.46	7.57	7.61	7.63	7.24	7.51	7.60	7.64	7.65
8.0	7.27	7.70	7.85	7.90	7.93	7.44	7.79	7.90	7.93	7.95	7.60	7.85	7.93	7.95	7.96
8.3	7.66	8.08	8.20	8.23	8.25	7.89	8.15	8.23	8.25	8.26	8.02	8.19	8.24	8.26	8.27
8.5	8.01	8.33	8.42	8.44	8.46	8.18	8.38	8.44	8.46	8.47	8.27	8.41	8.45	8.47	8.47
Effluent pH = 6.0 Alk = 1.0															
7.0	6.63	6.81	6.89	6.92	6.94	6.66	6.83	6.90	6.93	6.95	6.67	6.84	6.91	6.93	6.95
7.5	6.80	7.10	7.27	7.34	7.37	6.86	7.15	7.31	7.36	7.39	6.90	7.20	7.33	7.38	7.41
7.7	6.86	7.23	7.43	7.52	7.56	6.94	7.30	7.49	7.56	7.59	7.01	7.36	7.53	7.58	7.61
8.0	6.98	7.48	7.75	7.83	7.87	7.12	7.63	7.82	7.88	7.91	7.29	7.73	7.86	7.90	7.92
8.3	7.21	7.91	8.12	8.18	8.21	7.51	8.04	8.17	8.21	8.23	7.76	8.10	8.19	8.22	8.23
8.5	7.51	8.20	8.35	8.40	8.42	7.89	8.28	8.39	8.42	8.44	8.06	8.32	8.40	8.42	8.43
Effluent pH = 6.0 Alk = 2.0															
7.0	6.45	6.68	6.81	6.86	6.89	6.48	6.71	6.83	6.88	6.90	6.50	6.72	6.84	6.88	6.91
7.5	6.55	6.88	7.11	7.21	7.27	6.60	6.94	7.16	7.25	7.31	6.64	6.99	7.20	7.29	7.34
7.7	6.58	6.96	7.23	7.36	7.43	6.64	7.04	7.31	7.43	7.50	6.70	7.12	7.39	7.49	7.54
8.0	6.64	7.11	7.49	7.66	7.75	6.73	7.28	7.65	7.77	7.83	6.92	7.45	7.75	7.84	7.88
8.3	6.73	7.41	7.91	8.06	8.12	6.89	7.73	8.06	8.14	8.18	7.11	7.91	8.12	8.18	8.21
8.5	6.83	7.78	8.20	8.31	8.36	7.10	8.07	8.30	8.37	8.40	7.48	8.18	8.36	8.40	8.42
Effluent pH = 6.5 Alk = 0.5															
7.0	6.92	6.96	6.98	6.98	6.99	6.93	6.97	6.98	6.98	6.99	6.93	6.97	6.98	6.98	6.99
7.5	7.32	7.42	7.45	7.47	7.47	7.34	7.43	7.46	7.47	7.48	7.37	7.44	7.46	7.47	7.48
7.7	7.49	7.61	7.65	7.66	7.67	7.53	7.63	7.66	7.67	7.67	7.56	7.64	7.66	7.67	7.67
8.0	7.80	7.92	7.96	7.97	7.97	7.85	7.94	7.96	7.97	7.98	7.88	7.94	7.96	7.97	7.97
8.3	8.15	8.24	8.26	8.27	8.28	8.19	8.25	8.27	8.27	8.28	8.20	8.25	8.26	8.27	8.27
8.5	8.38	8.45	8.47	8.48	8.48	8.40	8.45	8.47	8.47	8.48	8.40	8.44	8.46	8.46	8.46
Effluent pH = 6.5 Alk = 1.0															
7.0	6.85	6.93	6.96	6.97	6.98	6.87	6.94	6.97	6.98	6.98	6.88	6.94	6.97	6.98	6.98
7.5	7.18	7.35	7.42	7.44	7.46	7.22	7.37	7.43	7.45	7.46	7.26	7.40	7.45	7.46	7.47
7.7	7.31	7.53	7.61	7.64	7.65	7.39	7.57	7.63	7.65	7.66	7.45	7.60	7.65	7.66	7.67
8.0	7.60	7.84	7.92	7.95	7.96	7.72	7.89	7.94	7.96	7.97	7.80	7.92	7.96	7.97	7.98
8.3	8.00	8.19	8.24	8.26	8.27	8.09	8.22	8.26	8.27	8.28	8.14	8.24	8.27	8.28	8.28
8.5	8.26	8.41	8.45	8.47	8.47	8.33	8.43	8.46	8.47	8.48	8.36	8.44	8.47	8.48	8.48
Effluent pH = 6.5 Alk = 2.0															
7.0	6.75	6.88	6.93	6.95	6.96	6.78	6.89	6.94	6.96	6.97	6.79	6.90	6.94	6.96	6.97
7.5	6.99	7.23	7.35	7.39	7.42	7.04	7.27	7.37	7.41	7.43	7.08	7.30	7.39	7.42	7.44
7.7	7.07	7.38	7.53	7.58	7.61	7.15	7.44	7.56	7.61	7.63	7.23	7.49	7.59	7.62	7.64
8.0	7.25	7.67	7.84	7.89	7.92	7.41	7.77	7.88	7.92	7.94	7.55	7.82	7.90	7.93	7.94
8.3	7.61	8.06	8.18	8.22	8.24	7.84	8.13	8.21	8.23	8.25	7.96	8.18	8.22	8.24	8.25
8.5	7.95	8.30	8.40	8.43	8.45	8.12	8.35	8.42	8.44	8.45	8.20	8.36	8.42	8.43	8.44
Effluent pH = 9.0 Alk = 2.0															
7.0	7.03	7.01	7.00	7.00	7.00	7.04	7.01	7.00	7.00	7.00	7.04	7.01	7.00	7.00	7.00
7.5	7.52	7.51	7.50	7.50	7.50	7.51	7.50	7.50	7.50	7.50	7.51	7.50	7.50	7.50	7.50
7.7	7.71	7.70	7.70	7.70	7.70	7.70	7.70	7.70	7.70	7.70	7.70	7.70	7.70	7.70	7.70
8.0	8.00	8.00	8.00	8.00	8.00	8.00	8.00	8.00	8.00	8.00	8.00	8.00	8.00	8.00	8.00
8.3	8.30	8.30	8.30	8.30	8.30	8.30	8.30	8.30	8.30	8.30	8.30	8.30	8.30	8.30	8.30
8.5	8.50	8.50	8.50	8.50	8.50	8.50	8.50	8.50	8.50	8.50	8.50	8.50	8.50	8.50	8.50
Effluent pH = 9.0 Alk = 4.0															
7.0	7.07	7.03	7.01	7.01	7.00	7.08	7.03	7.01	7.01	7.00	7.08	7.03	7.01	7.01	7.00
7.5	7.54	7.51	7.50	7.50	7.50	7.54	7.51	7.50	7.50	7.50	7.53	7.51	7.50	7.50	7.50
7.7	7.71	7.70	7.70	7.70	7.70	7.71	7.70	7.70	7.70	7.70	7.70	7.70	7.70	7.70	7.70
8.0	8.00	8.00	8.00	8.00	8.00	8.00	8.00	8.00	8.00	8.00	8.00	8.00	8.00	8.00	8.00
8.3	8.30	8.30	8.30	8.30	8.30	8.30	8.30	8.30	8.30	8.30	8.30	8.30	8.30	8.30	8.30
8.5	8.50	8.50	8.50	8.50	8.50	8.50	8.50	8.50	8.50	8.50	8.50	8.50	8.50	8.50	8.50
Effluent pH = 9.0 Alk = 6.0															
7.0	7.10	7.06	7.02	7.01	7.01	7.11	7.04	7.02	7.01	7.01	7.11	7.05	7.02	7.01	7.01
7.5	7.56	7.52	7.51	7.50	7.50	7.56	7.52	7.51	7.50	7.50	7.54	7.51	7.50	7.50	7.50
7.7	7.72	7.71	7.70	7.70	7.70	7.71	7.70	7.70	7.70	7.70	7.70	7.70	7.70	7.70	7.70
8.0	8.00	8.00	8.00	8.00	8.00	8.00	8.00	8.00	8.00	8.00	8.00	8.00	8.00	8.00	8.00
8.3	8.30	8.30	8.30	8.30	8.30	8.30	8.30	8.30	8.30	8.30	8.30	8.30	8.30	8.30	8.30
8.5	8.50	8.50	8.50	8.50	8.50	8.50	8.50	8.50	8.50	8.50	8.50	8.50	8.50	8.50	8.50

Note Values are shown to 2 decimal places to allow interpolation but should be rounded to 1 decimal place for comparison to standards.

The total inorganic carbon of the wastewater is:

$$C_{t_e} = \frac{.002 - \frac{10^{-14}}{10^{-11.1}} + 10^{-11.1}}{0.137 + 2 \times .863} = 0.000398 \text{ mole/l}$$

The dissociation constants for the ambient water are:

$$\alpha_1 = \frac{10^{-8.3} \times 8 + 10^{-7}}{(10^{-8.3})^2 + 10^{-8.3} \times 8 \times 10^{-7} + 8 \times 10^{-7} \times 4.68 \times 10^{-10}} = 0.909$$

and

$$\alpha_2 = 0.085$$

The total inorganic carbon content is:

$$C_{t_a} = \frac{0.0023 - \frac{6.3 \times 10^{-14}}{10^{-8.3}} + 10^{-8.3}}{.909 + 2 \times 0.085} = .00212 \text{ mole/l}$$

The final alkalinity and inorganic carbon are:

$$\text{Alk} = 0.0023 + \frac{0.002 - 0.0023}{20} = 0.00229 \text{ eq/l}$$

$$C_{t_f} \leftarrow 0.00212 + \frac{0.000398 - 0.00212}{20} = 0.0020 \text{ mole/l}$$

Using Equation VI-74, the alkalinity is calculated for the range of pH values tabulated below, beginning at 8.3 and incrementing by 0.1 units.

pH	Alkalinity, eq/l
8.3	0.00217
8.4	0.00222
8.5	0.00228
8.6	not needed
8.7	not needed
8.8	not needed

The actual and calculated alkalinities match at a pH barely exceeding 8.5. Since this slightly is more than 0.2 units above ambient, the pH standard is violated. The pH problem that results from this discharge could be mitigated in a number of ways, such as increasing initial dilution, or by treating the wastewater in order to lower the effluent pH.

END OF EXAMPLE VI-13

6.5.5 Dissolved Oxygen Concentration Following Initial Dilution

Dissolved oxygen standards in estuarine and coastal waters can be quite stringent. For example, the California Ocean Plan (State Water Resources Control Board, 1978) specifies that:

> "The dissolved oxygen concentration shall not at any time be depressed more than 10 percent from that which occurs naturally, as the result of the discharge of oxygen demanding waste materials."

Since dissolved oxygen concentrations can naturally range as low as 4.0 to 5.0 mg/l at certain times of the year in estuarine or coastal waters, allowable depletions under these conditions are only 0.4 to 0.5 mg/l.

The dissolved oxygen concentration following initial dilution can be predicted using the following expression:

$$DO_f = \overline{DO}_a + \left[\frac{DO_e - IDOD - \overline{DO}_a}{Sa}\right] \qquad \text{(VI-75)}$$

where

DO_f = final dissolved oxygen concentration of receiving water at the plume's trapping level, mg/l

$\overline{DO}_a$ = ambient dissolved oxygen concentration averaged from the diffuser to the trapping level, mg/l

DO_e = dissolved oxygen of effluent, mg/l

IDOD = immediate dissolved oxygen demand, mg/l

Sa = initial dilution.

The immediate dissolved oxygen demand represents the oxygen demand of reduced substances which are rapidly oxidized during initial dilution (e.g. sulfides to sulfates). The procedure for determining IDOD is found in standard methods (APHA, 1976). IDOD values are often between 1 and 5 mg/l, but can be considerably higher. When the effluent dissolved oxygen concentration is 0.0 mg/l and IDOD is negligible (which is a common situation), Equation VI-75 simplifies to:

$$DO_f = \overline{DO}_a \left(1 - \frac{1}{Sa}\right) \qquad \text{(VI-76)}$$

The ambient dissolved oxygen concentration which appears in Equations VI-75 and VI-76 is the concentration in the water column averaged between the location of the diffuser and the trapping level, while the final dissolved oxygen concentration is referenced to the plume's trapping level.

The dissolved oxygen concentration can change significantly over depth, depending on the estuary or coastal system as well as on seasonal influences (e.g. upwelling). As the plume rises during initial dilution, water from deeper parts of the water column is entrained into the plume and advected to the plume's trapping level. If

the dissolved oxygen concentration is much lower in the bottom of the water column than in the top, the low dissolved oxygen water is advected to a region formerly occupied by water containing higher concentrations of dissolved oxygen, and then a "pseudo" dissolved oxygen depletion results, solely caused by entrainment and advection and not consumption of oxygen-demanding material. The following example illustrates this process.

EXAMPLE VI-14

Puget Sound, located in the northwest corner of the state of Washington, is a glacially carved, fjord-type estuary. The average depth of water is about 100 m (330 ft). During periods of upwelling, low dissolved oxygen water enters the estuary at depth and produces a vertical dissolved oxygen gradient throughout much of the estuary. In Commencement Bay, near Tacoma, dissolved oxygen profiles similar to the one shown in Table VI-23 have been observed. Suppose the trapping level is 43 ft (13 m) above the bottom and the minimum initial dilution is 28. Find the final dissolved oxygen concentration and calculate the percent depletion.

TABLE VI-23

DISSOLVED OXYGEN PROFILE IN COMMENCEMENT BAY, WASHINGTON

Depth ft(m)	Temperature, °C	Dissolved Oxygen, mg/l
0 (0)	14.0	7.8
3 (1)	12.0	7.7
7 (2)	12.0	7.6
10 (3)	11.7	7.4
16 (5)	11.7	7.2
23 (7)	11.7	7.0
33 (10)	12.5	6.8
49 (15)	13.5	6.5
66 (20)	11.5	6.1
98 (30)	11.5	5.3
108 (33)	11.5	5.0

The dissolved oxygen concentration varies significantly over depth, from 5.0 mg/l at the bottom to 7.8 mg/l at the water's surface. The average concentration over the plume's trapping level is:

$$\frac{5.0 + 6.1}{2} = 5.6 \text{ mg/l}$$

Using Equation VI-76, the final dissolved oxygen concentration at the trapping level is:

$$DO_f = 5.6 \left(1 - \frac{1}{28}\right) = 5.4 \text{ mg/l}$$

Compared to the ambient concentration at the trapping level (6.1 mg/l), the percent depletion is:

$$\frac{6.1 - 5.4}{6.1} \times 100 = 11 \text{ percent}$$

Compared to the average over the height of rise, the percent depletion is only:

$$\frac{5.6 - 5.4}{5.6} \times 100 = 4 \text{ percent}$$

END OF EXAMPLE VI-14

In contrast to the deep estuaries on the west coast of the United States, those on the east coast are quite shallow. In the Chesapeake Bay, the largest east coast estuary, water depths are often in the 20- to 30-ft (6 to 9 m) range, with channels as deep as 60 to 90ft (18 to 27 m) in places. Because of the shallow water depths, initial dilution is often limited by the depth of the water and can be 10 or less at times of low ambient current velocity.

6.5.6 Far Field Dilution and Pollutant Distribution

After the initial dilution process has been completed, the wastefield becomes further diluted as it migrates away from the ZID. Since concentrations of coliform organisms are often required not to exceed certain specified values at sensitive locations (e.g. public bathing beaches), a tool is needed to predict coliform (or other pollutant) levels as a function of distance from the ZID. This can be accomplished by solving the following expression:

$$u \frac{\partial C}{\partial x} = \varepsilon_y \frac{\partial^2 C}{\partial y^2} - kC \qquad \text{(VI-77)}$$

where

C = pollutant concentration

u = current speed

ε_y = lateral turbulent diffusion coefficient

k = pollutant decay rate.

Figure VI-32 shows how the sewage field spreads laterally as a function of distance from the ZID. The concentration within the wastefield, $C(x,y)$, depends on both x and y, with the maximum concentrations occurring at $y = 0$, for any x value.

It is the maximum concentration $C(x,y = 0)$ which is of interest here. Solving Equation VI-77, the maximum concentration as a function of distance x is:

$$C = C_a + \frac{C_f - C_a}{D_s} \exp\left(-\frac{kx}{u}\right) \qquad \text{(VI-78)}$$

where

D_s = dilution attained subsequent to the initial dilution and is a function of travel time

All other symbols have been previously defined.

The subsequent dilution is unity when $x = 0$ (i.e., at the completion of initial dilution), so $C = C_f$ at $x = 0$, as required. In many instances, the background concentration is negligible, so that Equation VI-78 simplifies to:

$$C = \frac{C_f}{D_s} \exp(-kt) \qquad \text{(VI-79)}$$

Subsequent dilution gradually increases as the wastefield travels away from the ZID and depends on mixing caused by turbulence, shear flows, and wind stresses. Often, dilution caused by lateral entrainment of ambient water greatly exceeds that caused by vertical entrainment. This is assumed to be the case here.

In open coastal areas, the lateral dispersion coefficient is often predicted using the so-called 4/3 law (Brooks, 1960), where the diffusion coefficient increases as the 4/3 power of the wastefield width. In mathematical form:

$$\varepsilon = \varepsilon_o \left(\frac{L}{b}\right)^{4/3} \qquad \text{(VI-80)}$$

where

ε_o = diffusion coefficient when $L = b$

L = width of sewage field at any distance from the ZID

b = initial width of sewage field.

The initial diffusion coefficient can be predicted from:

$$\varepsilon_o = 0.001 b^{4/3} \qquad \text{(VI-81)}$$

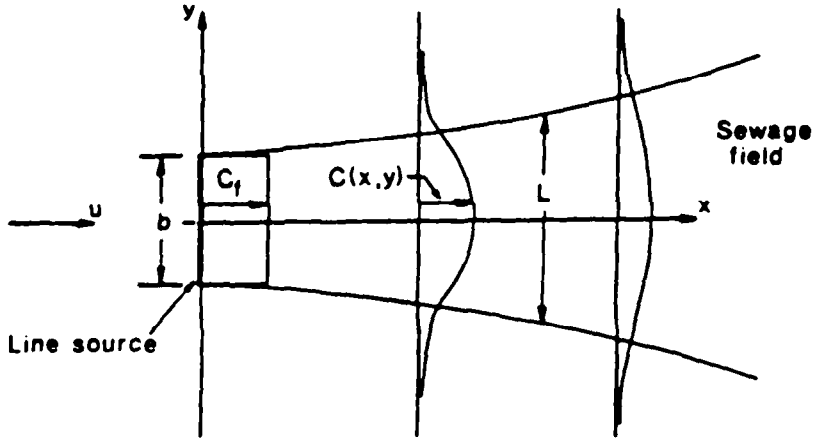

FIGURE VI-32 PLAN VIEW OF SPREADING SEWAGE FIELD

where

ε_o = initial diffusion coefficient, ft^2/sec

b = initial width of sewage field, ft.

Based on Equation VI-80, the centerline dilution, D_s, is given by:

$$D_s = \left[\operatorname{erf} \left(\frac{1.5}{\left(1 + \frac{8\,\varepsilon_o\,t}{b^2} \right)^3 - 1} \right)^{1/2} \right]^{-1} \qquad \text{(VI-82)}$$

where

t = travel time

erf = error function.

The 4/3 law is not always applicable and in confined estuaries might overestimate the diffusion coefficient. Under these circumstances, it is more conservative to assume the diffusion coefficient is a constant. Equation VI-81 can be used to estimate the constant diffusion coefficient, unless the user has better data. Under these circumstances, the subsequent dilution is expressible as:

$$D_s = \left[\operatorname{erf} \left(\frac{b^2}{16\,\varepsilon_o\,t} \right)^{1/2} \right]^{-1} \qquad \text{(VI-83)}$$

Equations VI-82 and VI-83 are cumbersome to use, especially if repeated applications are needed. To facilitate predicting subsequent dilutions, values of D_s are tabulated in Table VI-24 for different initial widths (b) and travel times (t).

TABLE VI-24

SUBSEQUENT DILUTIONS FOR VARIOUS INITIAL FIELD WIDTHS AND TRAVEL TIMES

Travel Time(hr)	Initial Field Width (ft)					
	10	50	100	500	1000	5000
0.5	2.3/ 5.5	1.5/ 2.0	1.3/ 1.6	1.0/ 1.1	1.0/ 1.0	1.0/ 1.0
1.0	3.1/ 13.	2.0/ 3.9	1.6/ 2.6	1.2/ 1.3	1.1/ 1.1	1.0/ 1.0
2.0	4.3/ 32.	2.7/ 8.5	2.2/ 5.1	1.4/ 1.9	1.2/ 1.5	1.0/ 1.0
4.0	6.1/ 85.	3.7/ 21.	3.0/ 11.	1.9/ 3.5	1.5/ 2.3	1.1/ 1.2
8.0	8.5/>100.	5.2/ 53.	4.1/ 29.	2.5/ 7.3	2.0/ 4.4	1.4/ 1.7
12.	10. />100.	6.3/ 95.	5.1/ 50.	3.0/ 12.	2.4/ 6.8	1.6/ 2.3
24.	15. />100.	8.9/>100.	7.1/ 100.	4.2/ 30.	3.4/ 16.	2.1/ 4.4
48.	21. />100.	13. />100.	10. />100.	5.9/ 80.	4.7/ 41.	2.8/10.
72.	26. />100.	15. />100.	12. />100.	7.3/>100.	5.8/ 73	3.4/17.
96.	29. />100.	18. />100.	14. />100.	8.4/>100.	6.6/100.	3.9/24.

*The dilutions are entered in the table as N_1/N_2, where N_1 is the dilution assuming a constant diffusion coefficient, and N_2 is the dilution assuming the 4/3 law.

The initial sewage field widths range from 10 to 5,000 feet and travel times range from 0.5 to 96 hours.

The dilutions presented in the table reveal that as the initial field width increases, the subsequent dilution decreases for a given travel time. For a wider wastefield, a larger time is required to entrain ambient water into the center of the wastefield, so dilutions are lower. This illustrates that a tradeoff exists between large diffusers where initial dilution is high but subsequent dilution low, and small diffusers where initial dilution is low and subsequent dilution high.

The table also reveals that the predicted dilutions are significantly different, depending on whether Equation VI-82 or VI-83 is used. In many cases likely to be evaluated by users of this document, the 4/3 law might overestimate subsequent dilution, even if the outfall is in coastal waters. To attain the subsequent dilutions predicted by the 4/3 law at large travel times, a significant amount of dilution water must be available. Since many outfalls, particularly small ones, are often not too far from shore, the entrainment rate of dilution water can be restricted by the presence of the shoreline and the depth of the water. The wastefield from diffusers located further offshore might entrain water at a rate corresponding to the 4/2 law for an initial period of time. As the wastefield widens significantly, the rate of entrainment could decrease, and the 4/3 law no longer be obeyed.

When travel times are small (e.g., 12 hours or less), there is less discrepancy between the two methods of calculating subsequent dilution, except for the very small initial wastefield widths.

EXAMPLE VI-15

Figure VI-33 shows an outfall which extends about one mile offshore. At the end of the outfall is a multiport diffuser, 800 feet in length. Occasionally, fecal coliform bacteria counts as high as 10,000 MPN/100 ml have been detected in the effluent of the treatment plant.

The allowable fecal coliform level at the shellfish harvesting area inshore of the diffuser is 70 MPN/100 ml. Typically, the ambient current is parallel to shore so that effluent is not carried onshore. However, when wind conditions are right, onshore transport has been observed, and the sustained transport velocity is 4 cm/sec (0.13 ft/sec). Determine whether the coliform standard is likely to be violated or not. Other information needed is:

Coliform decay rate = 1.0/day

Minimum initial dilution = 35

The width of the diffuser is 800 feet and will be used as the initial field width. Note, however, that the diffuser is not exactly perpendicular to shore, so that the initial field width is probably less than 800 feet in the travel direction. Using 800 feet is conservative because subsequent dilution

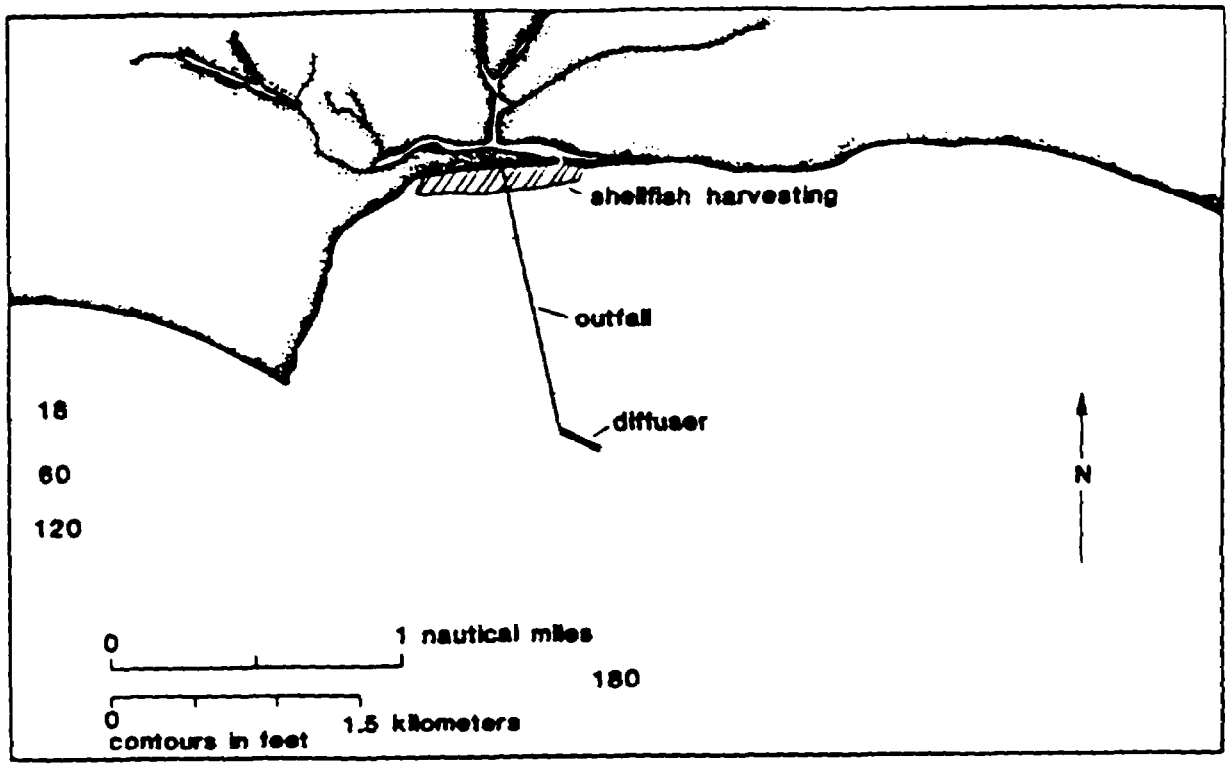

FIGURE VI-35 OUTFALL LOCATION, SHELLFISH HARVESTING AREA, AND ENVIRONS

will be somewhat lower under this assumption.

The coliform count following initial dilution is, using Equation VI-66:

$$C_f = \frac{10000}{35}$$

$$= 290 \text{ MPN/100 ml}$$

The travel time to the shore is:

$$\frac{5280}{0.13 \times 3600} = 11 \text{ hours}$$

Interpolating from Table VI-24, the subsequent dilution is about 2.6.

Using Equation VI-79, the coliform concentration at the shoreline is:

$$C = \frac{290}{2.6} \exp\left[-1 \times \frac{11}{24}\right]$$

$$= 70 \text{ MPN/100 ml}$$

The predicted coliform count is equal to the water quality standard. Since the subsequent dilution was conservatively estimated, it is possible that actual coliform counts will be less than 70 MPN/100 ml. However, the prediction does indicate that careful monitoring of coliform levels at the shoreline is needed to

see that the standard is not violated. Since shoreward transport of effluent is infrequent, sampling has to be conducted at times when the transport is shoreward; otherwise detected coliform levels might not represent worst-case conditions.

END OF EXAMPLE VI-15

6.5.7 Farfield Dissolved Oxygen Depletion

Oxygen demanding materials contained in the effluent of wastewater treatment plants can produce dissolved oxygen deficits following discharge of the effluent into receiving waters. A method will be presented here to predict the depletion following discharge from a marine outfall. The most critical cases occur when the plume and wastefield remain submerged, so that reaeration does not occur. The analysis presented here is applicable to submerged plumes only. When the wastefield is mixed uniformly across the estuary, the methods presented earlier in Section 6.4.5 are applicable.

The oxygen-demanding materials in the wastewater are the sum of the carbonaceous and nitrogenous materials (CBOD and NBOD, respectively). It is possible that the nitrogenous demand might not be exerted if a viable background population of nitrifiers is absent from the receiving water. Under these circumstances, the wastefield is likely to be dispersed before the nitrifying population can increase to numbers capable of oxidizing the NBOD. The user can perform analyses with and without NBOD exertion and then determine whether NBOD is significant or not. If it is, it is suggested that some sampling be conducted to find out whether nitrification is occurring.

The dissolved oxygen concentration in the receiving waters can be expressed as a function of travel time as follows:

$$DO(t) = DO_a + \frac{DO_f - DO_a}{D_s} - \left[\frac{L_f}{D_s}\right][1-\exp(-Kt)] \qquad \text{(VI-84)}$$

where

- $DO(t)$ = dissolved oxygen concentration in a submerged wastefield as a function of travel time t, mg/l
- DO_a = ambient dissolved oxygen concentration, mg/l
- DO_f = dissolved oxygen concentration following initial dilution (see Equation VI-75)
- k = BOD decay rate
- L_f = ultimate BOD concentration above ambient at the completion of initial dilution
- D_s = subsequent centerline dilution.

Equation VI-84 expresses the dissolved oxygen deficit which arises due to an initial deficit at the completion of initial dilution (DO_f-DO_a) plus that caused by

elevated BOD levels in the water column (L_f). The elevated BOD level is either the CBOD or sum of CBOD and NBOD. The initial dissolved oxygen deficit tends to decrease at longer and longer travel times because subsequent dilution increases. However, BOD is being exerted simultaneously and tends to cause the dissolved oxygen level to drop. Depending on the particular case being analyzed, one influence can dominate the other over a range of travel times so that a minimum dissolved oxygen level can occur either immediately following initial dilution, or at a subsequent travel time. The following example illustrates both cases.

EXAMPLE VI-16

A municipal wastewater treatment plant discharges its effluent through an outfall and diffuser system. The maximum daily CBOD value is 270 mg/l, and the critical initial dilution is 114. Limited analyses have been performed on IDOD and the results vary widely, from 0 to 66 mg/l. The length of the diffuser is 500 m (1,640 ft) and can be used as the initial sewage field width. Determine the dissolved oxygen deficit produced by the discharge, assuming the wastefield remains submerged and the ambient dissolved oxygen concentration is 7.0 mg/l.

The BOD concentration at the completion of initial dilution is:

$$\frac{270}{114} = 2.4 \text{ mg/l}, BOD_5$$

$$= 3.5 \text{ mg/l, BOD-ultimate}$$

The dissolved oxygen concentration at the completion of initial dilution is (from Equation VI-75):

$$DO_f = 7.0 + \left[\frac{0.0 - 66. - 7.0}{114}\right]$$

$$= 6.4 \text{ mg/l, when IDOD} = 66$$

or

$$DO_f = 7.0 + \left[\frac{0.0 - 0.0 - 7.0}{114}\right]$$

$$= 6.9 \text{ mg/l, when IDOD} = 0$$

Note that the IDOD of 66 mg/l produces a deficit of 0.6 mg/l.

Since values of IDOD vary widely due to the limited analyses, the far field oxygen depletion curves will be calculated for the following three IDOD's: 0, 40, and 66 mg/l. A BOD decay rate of 0.2/day is used. When IDOD = 66 mg/l, the

following oxygen depletions are predicted:

Travel Time(hr)	D_s (Table VI-24)	$DO_a - DO_t$ (Equation VI-84)
1	1.	0.6
4	1.4	0.5
8	1.9	0.4
12	2.3	0.4
24	3.2	0.4
48	4.6	0.4
72	5.5	0.4
96	6.3	0.4

These results are plotted in Figure VI-34 (Curve A), along with the cases for IDOD = 40 mg/l (Curve B), and IDOD = 0.0 mg/l (Curve C).

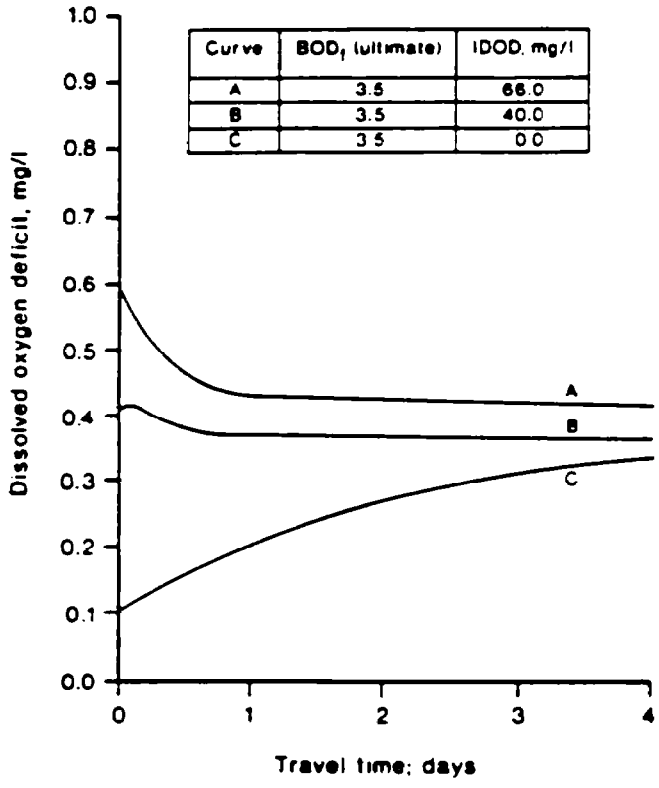

FIGURE VI-34 DISSOLVED OXYGEN DEPLETIONS VERSUS TRAVEL TIME

When the IDOD is 66 mg/l, the maximum dissolved oxygen deficit is 0.6 mg/l and occurs at the completion of initial dilution (a travel time of 0.0 hr). Thus, the processes which occur during initial dilution are more significant than the subsequent BOD exertion. Curve C (IDOD = 0.0 mg/l) shows the opposite situation: farfield BOD exertion is primarily responsible for the maximum oxygen depletion of 0.3 mg/l. The middle curve (Curve B) shows the case when the oxygen depletion remains relatively constant over time and both the near field and farfield processes are important.

In summary, when the IDOD is above 40 mg/l, in this example the maximum oxygen depletion is controlled by the processes occurring during initial dilution. When IDOD is below 40 mg/l, BOD exertion in the far field is primarily responsible for the oxygen depletion. For primary treatment plants, IDOD values of 66 mg/l are atypical; values from 1 to 10 mg/l are much more common. Depending on whether the state dissolved oxygen standard is violated by Curve A, the user might need to make further IDOD determinations to firmly establish the true range of IDOD values.

---------- END OF EXAMPLE VI-16 ----------

6.6 THERMAL POLLUTION

6.6.1 General

The presence of one or more major heat sources can have a significant impact on both the local biotic community and local water quality. As a result, consideration of significant thermal discharges by the planner is essential in any comprehensive water quality analysis. Thermal power plants account for the vast majority of both the number of thermal discharges and the total thermal load. However, some industrial processes generate significant amounts of excess heat.

The most important of the impacts of heat discharge are:

- Ecological Effects: Water temperature increases change the productivity of planktonic and many benthic species. As a result local community structures are altered. Many of the species benefited by warmer conditions (e.g., blue green algae) may be considered to be undesirable. In addition, many species can perform certain life cycle functions only within a limited temperature range. Elevated temperatures may prevent some species from completing one or more life stages, thus disrupting the reproductive cycle and destroying the stability of the population.
- Water Quality Effects: Figure VI-23 showed the relative effect of salinity and ambient temperature on oxygen saturation. From this

figure, note that a 10°C* rise in temperature decreases the oxygen saturation concentration by 1.5 to 2.0 mg/l.

- Sediment Effects: Estuarine sedimentation rates are increased by increasing local water column temperature. The significance of this increase was discussed by Parker and Krenkel (1970). They concluded that not only are sedimentation rates increased, but vertical particle size distribution, particle fall velocity, and thus bottom composition are also affected.
- Beneficial Effects: The effects of thermal discharges are not all negative. It has been shown for example, that marine biofouling is substantially reduced in warmed waters (Parker and Krenkel, 1970). In fact, the recirculation of heated discharge through the condenser has proven to be a less expensive and equally effective method of biofouling control than chlorination for several California coastal power plants. Estuarine contact recreation potentials are increased by increasing local water temperatures, and extreme northern estuaries have reduced winter ice coverage as a result of thermal discharges.

6.6.2 Approach

A number of the algorithms which appear in this section were originally prepared by Tetra Tech, (1979) for the Electric Power Research Institute. The thermal screening approach for estuaries is composed of procedures that can be used to evaluate the following standards:

- The ΔT Criterion: The increase in temperature of water passing through the condenser must not exceed a specified maximum.
- The Maximum Discharge Temperature Criterion: The temperature of the heated effluent must not exceed a specified maximum.
- The Thermal Block Criterion: The cross-sectional area of an estuary occupied by temperatures greater than a specified value must not exceed a specified percentage of the total area .
- The Surface Area Criterion: The surface area covered by isotherms exceeding a specified temperature increment (above ambient) must not exceed a specified maximum .
- The Surface Temperature Criterion: No discharge shall cause a surface water temperature rise greater than a specified maximum above the natural temperature of the receiving waters at any time or place.

Table VI-25 presents a summary of the information needed to apply the thermal screening procedure. Data needed for the T criterion and the maximum discharge temperature criterion were included earlier in the thermal screening section for

*Such a rise is common near power plant thermal plumes.

TABLE VI-25

DATA NEEDED FOR ESTUARY THERMAL SCREENING

Variable	Criteria Where Variable Used	Definition	Default Value
ΔT_c	All	Temperature rise across the condenser (°F)	20
D_p	All	Diameter of discharge pipe or equivalent diameter of discharge canal (m)	--
v_p	Thermal block, surface area	Exit velocity of thermal discharge (m/s)	--
Q_p	All	Flow rate of discharge (m^3/s)	--
ΔT_{tb}	Thermal block	Temperature rise in estuary cross section that constitutes a thermal block (°F)	5
A_{tb}	Thermal block	Portion of estuarine cross-sectional area that constitutes a thermal block (m^2)	25% of the estuarine cross-sectional area
d_{tb}	Thermal block	Average depth of estuary from discharge location to ΔT_{tb} isotherm at slack tide (m)	--
R	Thermal block, surface area	Average freshwater flow rate flowing in the estuary past the power plant site (m^3/s)	$^{70}_{10}$
w	Thermal block, surface area	Width of estuary at power plant site (m)	--
A_t	Thermal block	Cross-sectional area at power plant site (m^2)	--
D_l	Thermal block, surface area	Longitudinal dispersion coefficient (m^2/s)	see text discussion
K	Thermal block, surface area	Surface thermal transfer coefficient ($Btu/m^2 \cdot d \cdot °F$)	--
ρ	Thermal block, surface area, surface temperature	Average mass density of ambient water at power plant site (kg/m^3)	1000 (zero salinity)
C_p	Thermal block, surface area	Specific heat of water ($Btu/kg \cdot °F$)	22
S	Thermal block, surface area	Tidally and cross-sectionally averaged salinity (ppt. $^0/_{00}$)	--
n	Thermal block,	Manning's n ($m^{1/6}$)	0.016 - 0.06
v_{max}	Thermal block, surface area	Maximum tidal velocity over a tidal cycle (m/s)	--
R_h	Thermal block, surface area	Hydraulic radium (cross-sectional area divided by wetted perimeter) (m)	--
ΔT_{sa}	Surface area	Isotherm associated with legal surface area constraint (°F)	4
$\bar{d}_s$	Surface area	Average depth under the surface area calculated for the surface area constraint (m)	--
A_{sa}	Surface area	Legally allowable surface area surrounded by isotherms equalling and exceeding ΔT_{sa} (m^2)	--
g	Surface temperature	Gravitational constant (m/s^2)	9.8
ρ_p	Surface temperature	Mass density of thermal effluent (kg/m^3)	--
h	Surface temperature	Depth to centerline of discharge jet (m)	--
ΔT_{st}	Surface temperature	Maximum legally allowable surface temperature produced by a submerged discharge (°F)	4
ρ_s	Surface temperature	Mass density of water at depth of submerged discharge (kg/m^3)	1000
$\frac{-d\rho}{dz}$	Surface temperature	Linear density gradient over water column depth ($kg/m^3 \cdot m$)	--

rivers and are not repeated here. That the maximum discharge temperature criterion for rivers can be applied to estuaries assumes the intake temperature is near ambient, and that tidal action does not cause significantly elevated temperatures near the intake.

6.6.3 Application

The ΔT criterion and the effluent temperature criterion can be evaluated first following the procedures outlined in the river thermal screening section. The maximum allowable flow rate through the plant, which needs to be identified for use in evaluating those criteria, may not always have a readily determinable upper limit, unlike plants sited on rivers. For estuaries that are essentially tidal rivers, a fraction (say 20%) of the net freshwater flow rate might be used as an upper limit.

The remainder of the estuary physical screening procedure consists of evaluating the following three criteria: the thermal block, the isotherm surface area, and the surface water temperature criteria. Because of the complexity of the flow field in estuaries, slack tide conditions have been chosen as a basis for computations when possible. It is during these conditions that the effects of plume momentum and buoyancy are propagated the greatest distance across the estuary from the discharge site. It is also during slack tide that the thermal block is most likely to occur because of the absence of an ambient current that normally enhances plume entrainment of ambient water.

As the plume spreads across the estuary, the methodology assumes it to be vertically mixed. Although most plumes do not generally exhibit this behavior due to such effects as buoyancy and stratification, this approach will roughly estimate the capacity of the estuary at the power plant location to assimilate the excess heat.

In some instances, when the estuary is relatively narrow, the plume may extend across the estuary's entire width. In these cases (guidelines are given later to determine when this occurs) the near field momentum approach can be used. By using the well mixed assumption (even if the actual estuary is stratified) a lower limit on the expected temperature elevation across the estuary is obtained.

Slack tide conditions will also be used to evaluate the maximum surface temperature produced by a submerged discharge. Both vertically homogeneous and linearly stratified conditions can be evaluated.

6.6.3.1 Evaluating the Thermal Block Constraint

Based upon momentum considerations, the relationship between the ΔT_y

isotherm and the distance (y) it extends from the discharge point is given by (Weigel, 1964):

$$y = \frac{y_o}{2}\left(\frac{\Delta T_c}{\Delta T_y}\right)^2 \quad , \text{for } y \geq y_c \qquad \text{(VI-85)}$$

where

ΔT_c = temperature rise across the condenser (°F)

ΔT_y = temperature excess at a distance y from the discharge outlet (°F)

y = distance measured along the jet axis originating at the discharge point (m)

y_o = virtual source position (m).

The virtual source position is usually about two to ten times the diameter of the discharge orifice. The equivalent diameter of a discharge canal is the diameter of a circle whose cross-sectional area is the same as that of the discharge canal.

Brooks (1972) has shown that for round orifices, the virtual source position is approximately six times the orifice diameter. At the virtual discharge position ($y = y_o$) the average excess temperature is approximately 70 percent that at the discharge location.

Since one of the assumptions used in developing Equation VI-85 is that momentum is conserved along the jet axis, an upper limit on y must be established to prevent the user from seriously violating this assumption. The upper limit can be chosen to be where the plume velocity has decreased to 1 ft/sec or 0.31 meters per second. This implies that the minimum ΔT_y that can be evaluated using the equation is:

$$(\Delta T_y)_{min} = 0.3\,\frac{\Delta T_c}{U_p} \qquad \text{(VI-86)}$$

where

U_p = exit velocity of thermal discharge (m/s)

$(\Delta T_y)_{min}$ = minimum excess temperature that can be evaluated using Equation VI-86 (°F).

This constraint generally does not restrict practical application of Equation VI-85.

Using the value estimated by Brooks (1972) for the virtual source position, Equation VI-85 can be rewritten as:

$$y = 3D_p\left(\frac{\Delta T_c}{\Delta T_y}\right)^2 \quad , \text{for } y \geq 6D_p \qquad \text{(VI-87)}$$

The distance, then, to the ΔT_{tb} isotherm (the isotherm establishing the thermal block) is given as:

$$y_{tb} = 3D_p\left(\frac{\Delta T_c}{\Delta T_{tb}}\right)^2 \quad \text{,for } \Delta T_{tb} \geq (\Delta T_y)_{min} \tag{VI-88}$$

The cross sectional area to the ΔT_{tb} isotherm is (assuming the plume remains vertically mixed):

$$A_c = y_{tb}\,\bar{d}_{tb} \tag{VI-89}$$

where

A_c = cross sectional area measured out to the distance y_{tb} (m^2)

$\bar{d}_{tb}$ = average water depth over the distance y_{tb} (m).

If $A_c < A_{tb}$ (where A_{tb} is the cross sectional area that legally defines a thermal block, e.g., 25% of the total estuary cross sectional area) then a thermal block does not develop.

If the estuary is sufficiently narrow so that y_{tb} as found by Equation VI-88 equals or exceeds the width of the estuary, the approach given above should not be used. Instead, a steady-state well mixed ΔT_{ss} can be found as follows:

$$\Delta T_{ss} = \frac{\Delta T_c\, Q_p}{\sqrt{R^2 + W\, A_t\, E_L\, K/(\rho C_p \cdot 24 \cdot 3600)}} \tag{VI-90}$$

where

ΔT_{ss} = steady state well mixed excess temperature (°F).

In this steady state approach, ΔT_{ss} can no longer be estimated independently of the estuarine flow field characteristics. The surface transfer coefficient K can be determined by reference to the equilibrium temperature discussion in the river thermal screening section. Although the equilibrium temperature does not appear explicitly in Equation VI-90, its effect is indirectly included since K can not be determined independently of E. In the process of finding K, the ambient surface water temperature of the estuary generally should not be assumed to be at equilibrium because of the combined influence of ocean and river water (TRACOR, 1971), each of which may be at different temperatures.

The dispersion coefficient, E_L, is dependent on estuary characteristics. A value obtained from past studies in the vicinity of the power plant site should be used if possible. Alternatively, the methods and data provided earlier in Section 6.4.5 can be used.

6.6.3.2 Surface Area Constraint

The surface area constraint can be evaluated employing the same approach used to evaluate the thermal block constraint. Before beginning, Equation VI-86 should be evaluated to ensure that ΔT_{sa} exceeds $(\Delta T_y)_{min}$, since $(\Delta T_y)_{min}$ establishes the minimum excess isotherm that can be evaluated using these methods.

The distance offshore to the ΔT_{sa} isotherm (the isotherm associated with the legal surface area constraint) can be found as:

$$y_{sa} = 3D_p \left(\frac{\Delta T_c}{\Delta T_{sa}} \right)^2 \quad \text{for } y \geq 6D_p \tag{VI-91}$$

y_{sa} = distance offshore at ΔT_{sa} isotherm (m).

The surface area enclosed by that ΔT_{sa} isotherm can be estimated as:

$$A_s = 6D_p \left(\frac{W_o + D_p}{2} \right) + \left(y_{sa} - 6D_p \right) \frac{W_o}{2} \left(1 + \frac{y_{sa}}{6D_p} \right) \tag{VI-92}$$

where

$$W_o = \frac{2Q_p}{U_p d_s}$$

When the estuary depth drops off rapidly from the outfall location, an appropriate average depth would be the depth to the bottom of the discharge orifice. If $A_s < A_{sa}$, then the surface area constraint is not violated.

When x_a exceeds the width of the estuary, Equation VI-92 should not be used to find A_s. Instead, a surface area based on steady state, well mixed conditions is more appropriate and can be found from the following expression:

$$A_s = W \left[\frac{1}{C_1} + \frac{1}{C_2} \right] \ln \left(\frac{\Delta T_{sa}}{\Delta T_{ss}} \right) \tag{VI-93}$$

where

W = width of estuary (m)

$$C_1 = 1/2 \left[R/(A_t D_1) + \sqrt{(R/A_t D_1)^2 + (4WL/(\rho C_p A_t D \cdot 24 \cdot 3600))} \right]$$

$$C_2 = 1/2 \left[R/(A_t D_1) + \sqrt{(R/A_t D_1)^2 + (WK/(\rho C_p A_t D_1 \cdot 24 \cdot 3600))} \right]$$

ΔT_{ss} was given by Equation VI-90.

When $A_s \leq A_{sa}$ the surface area constraint is not exceeded.

6.6.3.3 Surface Temperature Constraint

This section provides a method for estimating the surface temperature of a buoyant plume resulting from a subsurface discharge. Slack tide conditions and a horizontal discharge configuration are considered. A horizontal configuration

should approximate conditions under which the lowest maximum surface water temperature excess is attained.

When the ambient water density is constant over depth the following two dimensionless parameter groups are needed:

$$G = \frac{h}{D_p} \qquad \text{(IV-94)}$$

and

$$F \text{ (Froude Number)} = \frac{1.07\ U_p}{\sqrt{\frac{\rho - \rho_p}{\rho} D_p g}} \qquad \text{(VI-95)}$$

After calculating G and F, Figure VI-35 can be used to find S_o, the centerline dilution relative to the virtual source position. From this information, the maximum surface temperature elevation can be estimated as:

$$\Delta T_{surface} = \frac{\Delta T_c}{1.15 S_o} \qquad \text{(VI-96)}$$

If $\Delta T_{surface} < \Delta T_{st}$ (the legal allowable surface temperature excess), the surface temperature constraint is not violated.

In cases where the estuary is stratified more often than not at the power plant site, the maximum surface temperature calculation would more appropriately be performed under stratified conditions. If the stratification is substantial, it is possible the discharge may be prevented from reaching the surface entirely. A procedure is given here for a linearly stratified environment. Under stratified conditions the maximum height of rise of the thermal plume can be estimated by (Brooks, 1972):

$$\frac{z_{max}}{D_p} = 3.86\ F^{\frac{1}{4}}\ T^{3/8} \qquad \text{(VI-97)}$$

where

$$F = \frac{1.07\ U_p}{\sqrt{\frac{\rho_s - \rho_p}{\rho_s} D_p g}}$$

$$T = \frac{0.87\ (\rho_s - \rho_p)}{D_p\ (\frac{-d\rho}{dz})}$$

z_{max} = maximum height of rise of thermal plume (m)

$\frac{d\rho}{dz}$ = linear density gradient ($kg/m^3/m$).

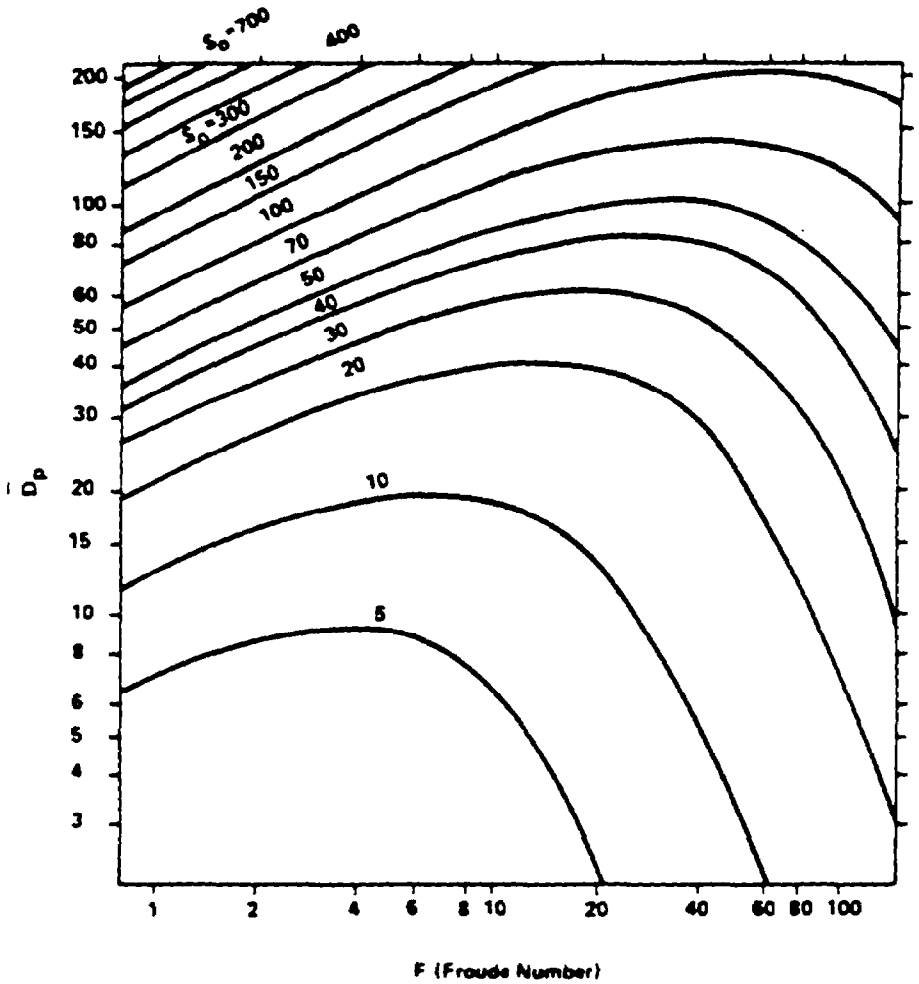

FIGURE VI-35 CENTERLINE DILUTION OF ROUND BUOYANT JET IN STAGNANT UNIFORM ENVIRONMENT (AFTER FAN, 1967)

Using Equation VI-97, the maximum rise of the thermal plume can be estimated. If it is less than the depth of water, the plume remains submerged. If, however, z_{max} exceeds the water depth, the plume will surface. In this case the methods given previously for the nonstratified case can be used to estimate the maximum surface temperature where the ambient water density should be chosen to be the depth-averaged mean.

6.7 TURBIDITY

6.7.1 Introduction

Turbidity is a measure of the optical clarity of water and is dependent upon the light scattering and absorption characteristics of both suspended and dissolved

material in the water column (Austin, 1974). The physical definition of turbidity is not yet fully agreed upon, and varies from equivalence with the scattering coefficient (Beyer, 1969), to the product of an extinction coefficient and measured pathlength (Hodkinson, 1968), and to the sum of scattering and absorption coefficients (VandeHulst, 1957). Turbidity affects water clarity and apparent water odor, and hence is of aesthetic significance. It also affects light penetration, so that increased turbidity results in a decreased photic zone depth and a decrease in primary productivity.

Turbidity levels in an estuary are likely to vary substantially in both temporal and spatial dimensions. Temporal variations occur as a function of seasonal river discharge, seasonal water temperature changes, instantaneous tidal current, and wind speed and direction. Spatially, turbidity varies as a function of water depth, distance from the head of the estuary, water column biomass content, and salinity level. Much of the complexity in the analysis of turbidity results from different sources of turbidity responding differently to the controlling variables mentioned above. As an example, increased river discharge tends to increase turbidity because of increased inorganic suspended sediment load. However, such an increase curtails light penetration, thus reducing water column photosynthesis. This, in turn, reduces the biologically induced turbidity.

Methods employed to monitor turbidity include use of a "turbidimeter". Light extinction measurements are commonly given in Jackson Turbidity Units (JTU) which are based on the turbidity of a standard clay suspension. Once standardized, this arbitrary scale* can be used as a basis to measure changes in turbidity. The turbidity calibration scale is given in APHA (1980). From a measured change in turbidity a relative change in water quality may be inferred. Estuarine water is almost always extremely turbid, especially when compared to ocean or lake waters.

The JTU scale is not the only available turbidity scale. In 1926 Kingsbury and Clark devised a scale based on a Formazin suspension medium which resulted in Formazin Turbidity Units (FTU's). More recently volume scattering functions (VSF) and volume attenuation coefficients have been proposed (Austin, 1974). However, JTU's are still most commonly used as an indicator of estuarine turbidity levels.

As a rough indication of the wide variations possible in turbidity, Figure VI-36 shows suspended solid concentrations for the various sub-bays of San Francisco Bay for one year (Pearson, et al, 1967). The solid line shows annual mean concentrations while the dashed lines indicate concentrations exceeded by 20% and 80% of the samples taken at each station over the one year time period. These variations at stations located near bay heads (left and right extremities of Figure VI-36) typically exceed 300% of the annual 20th percentile values. Use of extreme high/low values would produce correspondingly larger annual variations.

*The JTU scale is an arbitrary scale since it cannot be directly related to physical units when used as a calibration basis for turbidimeter measurement.

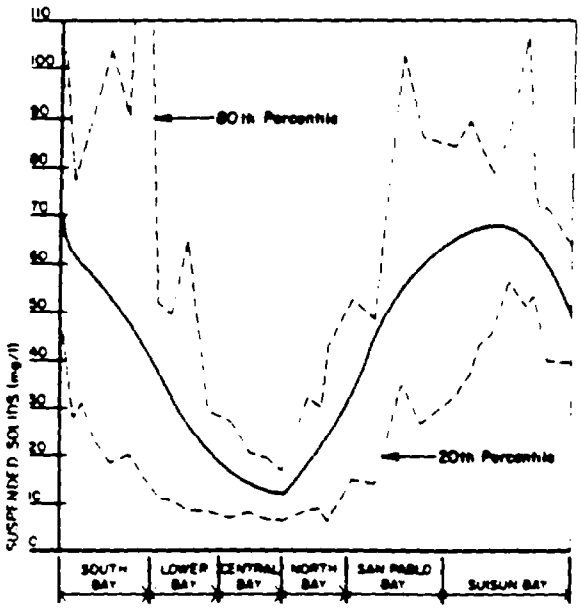

FIGURE VI-36 MEAN SUSPENDED SOLIDS IN SAN FRANCISCO BAY
FROM: PEARSON ET AL., 1967, PG V-15

6.7.2 Procedure to Assess Impacts of Wastewater Discharges on Turbidity or Related Parameters

Numerous states have enacted water quality standards which limit the allowable turbidity increase due to a wastewater discharge in an estuary or coastal water body. The standards, however, are not always written in terms of turbidity, but are sometimes expressed as surrogate parameters such as light transmittance or Secchi disk. The following three standards provide illustrations:

For class AA water in Puget Sound, State of Washington:

> Turbidity shall not exceed 5 NTU over background turbidity when the background turbidity is 50 NTU or less, or have more than a 10 percent increase in turbidity when the background turbidity is more than 50 NTU.

For class A water in the State of Hawaii:

> Secchi disk or Secchi disk equivalent as "extinction coefficient" determinations shall not be altered more than 10 percent.

For coastal waters off the State of California:

> The transmittance of natural light shall not be significantly reduced at any point outside of the initial dilution zone. A significant difference is defined as a statistically significant difference in the means of two distributions of sampling results at the 95 percent confidence level.

These standards illustrate the need for developing interrelationships between turbidity related parameters, since data might be available for one parameter while the state standard is expressed in terms of another. Based on these considerations methods will be presented to:

- Predict the turbidity in the receiving water at the completion of initial dilution
- Predict the suspended solids concentrations in the receiving water at the completion of initial dilution
- Relate turbidity and light transmittance data
- Relate Secchi disk and turbidity data.

By treating turbidity as a conservative parameter the turbidity in the receiving water at the completion of initial dilution can be predicted as:

$$T_f = T_a + \frac{T_e - T_a}{S_a} \qquad \text{(VI-98)}$$

where

T_f = turbidity in receiving water at the completion of initial dilution (typical units: JTU)

T_a = ambient or background turbidity

T_e = effluent turbidity

S_a = initial dilution.

Initial dilution can be predicted based on the methods presented earlier in Section 6.5.2. Equation VI-98 can be used, then, to directly evaluate those standards written in terms of maximum allowable turbidity or turbidity increase.

An expression similar to Equation VI-98 can be used to evaluate the suspended solids concentration in an estuary following completion of initial dilution. Specifically:

$$SS_f = SS_a + \frac{SS_e - SS_a}{S_a} \qquad \text{(VI-99)}$$

where

SS_f = suspended solids concentration at completion of initial dilution, mg/l

SS_a = ambient suspended solids concentration, mg/l

SS_e = effluent suspended solids concentration, mg/l

S_a = initial dilution.

Consider now a situation where light transmittance data have been collected but the state standard is expressed in terms of turbidity. A relationship between the two parameters would be useful. Such a relationship can be developed by first

considering the Beer-Lambert law for light attenuation:

$$T_d = \exp(-\alpha d) \qquad \text{(VI-100)}$$

where

T_d = fraction of light transmitted over a depth d, dimensionless
α = light attenuation, or extinction coefficient, per meter
d = vertical distance between two locations where light is measured, meters.

Austin (1974) has shown that the attenuation coefficient is expressible in terms of turbidity as:

$$\alpha = k \cdot JTU \qquad \text{(VI-101)}$$

where

JTU = turbidity, in Jackson turbidity units
k = coefficient ranging from 0.5 to 1.0.

Combining Equations VI-100 and VI-101 the turbidity is expressible as:

$$JTU = -\frac{1}{kd} \ln T_d \qquad \text{(VI-102)}$$

The increased turbidity (JTU) is expressible as:

$$\Delta JTU = \frac{-1}{kd} \ln \left(\frac{T_{d_2}}{T_{d_1}} \right) \qquad \text{(VI-103)}$$

where

T_{d_2} = light transmittance at the final turbidity
T_{d_1} = light transmittance at the initial turbidity.

EXAMPLE VI-17

Vertical profiles of several water quality parameters, including percent light transmittance, have been collected in the vicinity of a municipal wastewater discharge in Puget Sound. Figure VI-37 shows each of the three profiles. If the maximum allowable turbidity increase is 5 NTU, does the discharge, based on the light transmittance profile shown in Figure VI-37 violate this requirement?

It is known that the wastefield is submerged between about 10 to 20 m below the water's surface. Light transmittances at these depths are about 18 to 20 percent. Deeper within the water column light transmittances are at background values of about 55 percent. Note that in the top few meters the

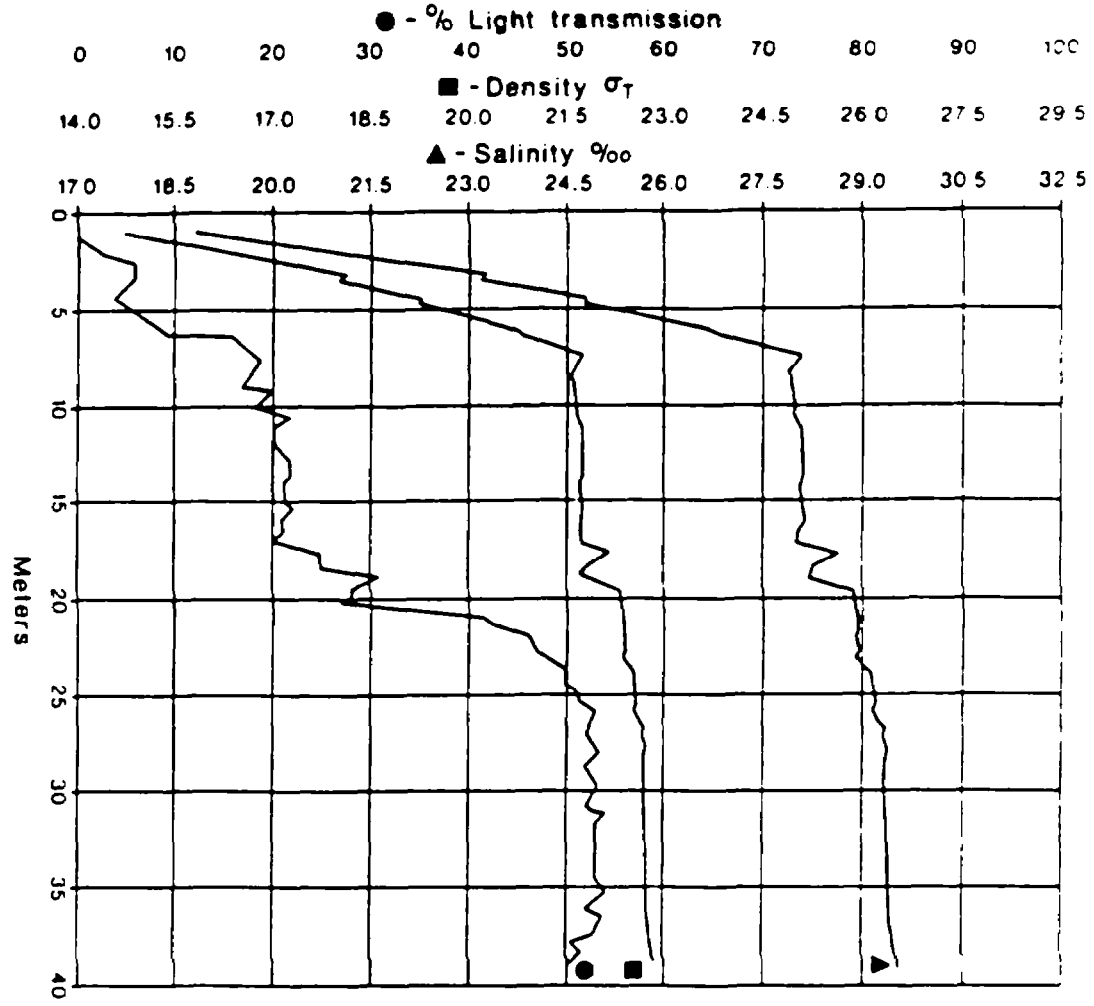

FIGURE VI-37 WATER QUALITY PROFILE OF SELECTED PARAMETERS NEAR A MUNICIPAL OUTFALL IN PUGET SOUND, WASHINGTON

light transmittances are between 0 and 10 percent. These low transmittances are not due to the wastefield, but rather are caused by a lens of turbid freshwater. Consequently, the following data will be used here:

k = 0.5

d = 1 m (i.e., percent transmittance measured over 1 m)

T_{d_2} = 18 percent

T_{d_2} = 55 percent.

The turbidity increase is:

$$\Delta JTU = \frac{-1}{(0.5)\ (1)} \ln \left(\frac{0.18}{0.55}\right) = 2.2 \text{ JTU}$$

Assuming JTU and NTU units are equivalent (EPA, 1979), then the increased turbidity is less than the 5.0 NTU allowable.

It is of interest to calculate the percent light transmittance within the plume that would cause a 5 NTU increase in turbidity. Using a typical background light transmittance of 50 percent found in central Puget Sound, the minimum light transmittance (T_{d_2}) is computed to be:

$$T_{d_2} = \begin{cases} 4 \text{ percent for } k = 0.5 \\ 0.5 \text{ percent for } k = 1.0 \end{cases}$$

Light transmittances as low as 0.5 to 4 percent have been found due to causes other than the plume (e.g. plankton blooms and fresh water runoff), but the lowest light transmittances associated with the plume have been about 18 percent per meter.

END OF EXAMPLE VI-17

Secchi disk and turbidity can be related to each other in the following manner. Assume that the extinction coefficient of visible light (α) is directly proportional to turbidity (T) and inversely proportional to Secchi disk (SD), or:

$$\alpha = k_1 T \tag{VI-104}$$

and

$$\alpha = \frac{k_2}{SD} \tag{VI-105}$$

where k_1 and k_2 are constants which have not yet been specified. These two relationships have theoretical bases, as discussed in Austin (1974) and Graham (1968). Combining those two expressions, the relationship between Secchi disk and turbidity becomes:

$$T = \frac{k_2}{k_1} \frac{1}{SD} \tag{VI-106}$$

Typical values of k_1 and k_2 are:

k_1 = 0.5 to 1.0, where T is expressed in JTU's

k_2 = 1.7 where Secchi disk is expressed in meters.

Thus Equation VI-106 provides a method of correlating turbidity and Secchi disk data.

When state standards are written in terms of Secchi disk, it is convenient

to combine Equations VI-98 and VI-106 to yield:

$$\frac{1}{SD_f} = \frac{1}{SD_a} + \frac{\frac{1}{SD_e} - \frac{1}{SD_a}}{S_a} \qquad \text{(VI-107)}$$

or

$$SD_e = \left[\left(\frac{1}{SD_f} - \frac{1}{SD_a}\right)S_a + \frac{1}{SD_a}\right]^{-1} \qquad \text{(VI-108)}$$

where

SD_f = minimum allowable Secchi disk reading in receiving water such that the water quality standard is not violated

SD_a = ambient Secchi disk reading

Sa = minimum initial dilution which occurs when the plume surfaces

SD_e = Secchi disk of effluent.

Since Secchi disk measurements are made from the water's surface downward, critical conditions (in terms of the Secchi disk standard) will occur when the initial dilution is just sufficient to allow the plume to surface. It is notable that maximum turbidity or light transmittance impacts of a wastewater plume will occur when the water column is stratified, the plume remains submerged, and initial dilution is a minimum. Under these same conditions, however, Secchi disk readings might not be altered at all, if the plume is trapped below the water's surface at a depth exceeding the ambient Secchi disk depth.

EXAMPLE VI-18

A municipality discharges its wastewater through an outfall and diffuser system into an embayment. The state standard specifies that the minimum allowable Secchi disk is 3m. Determine whether the discharge is likely to violate the standard. Use these data:

SD_a = 5 to 10m, observed range

S_a = 75, minimum initial dilution when the plume surfaces

One method of approaching the problem is to assume that violation of the water quality standard is incipient (i.e. SD_f = 3m). Under these conditions the effluent Secchi disk would have to be:

$$SD_e = \left[\left(\frac{1}{3} - \frac{1}{5}\right) 75 + \frac{1}{5}\right]^{-1} = 0.1 \text{ m}$$

$$= 4 \text{ inches}$$

Thus, if the Secchi disk of the effluent exceeds 4 inches, the standards will not be violated even under these critical conditions. It would be a simple matter to measure the Secchi disk of the treated effluent to see whether the standard could be violated or not.

END OF EXAMPLE VI-18

6.8 SEDIMENTATION

6.8.1 Introduction

Like turbidity, sedimentation is a multifaceted phenomenon in estuaries. As in rivers, estuaries transport bed load and suspended sediment. However with the time varying currents in estuaries, no equilibrium or steady state conditions can be achieved (Ippen, 1966). Additionally, while any given reach of a river has reasonably constant water quality conditions, an estuary can vary from fresh water (1 ppt. salinity) to sea water (30 ppt. salinity), and from a normally slightly acidic condition near the head to a slightly basic condition at the mouth. The behavior of many dissolved and suspended sediments varies substantially across these pH and salinity gradients. Many colloidal particles* agglomerate and settle to the bottom. In general, all estuaries undergo active sedimentation which tends to fill them in. It is also true for essentially all U.S. estuaries that the rate of accumulation of sediment is limited not by the available sources of sediment but by the estuary's ability to scour unconsolidated sediments from the channel floor and banks.

6.8.2 Qualitative Description of Sedimentation

Before presenting what quantitative information is available concerning sediment distribution in an estuary, a qualitative description of sediment sources, types and distribution will be helpful. Sediment sources may be divided into two general classes: sources external to the estuary and sources internal to the estuary (Schultz and Simmons, 1957). The major sources of sediment within each category are shown below. By far the largest external contributor is the upstream watershed.

1. External:
   - Upstream watershed
   - Banks and stream bed of tributaries
   - Ocean areas adjacent to the mouth of the estuary
   - Surface runoff from land adjacent to the estuary

*Colloidal particles are particles small enough to remain suspended by the random thermal motion of the water.

- Wind borne sediments
- Point sources (municipal and industrial).

2. Internal:
   - Estuarine marsh areas
   - Wave and current resuspension of unconsolidated bed materials
   - Estuarine biological activity
   - Dredging.

General characterizations of U.S. estuarine sediments have been made by Ippen (1966) and by Schultz and Simmons (1957). Many individual case study reports are available for sediment characterization of most of the larger U.S. estuaries (i.e. Columbia River, San Francisco Bay, Charles Harbor, Galveston Bay, Savannah Harbor, New York Harbor, Delaware River and Bay, etc.). In general, estuarine sediments range from fine granular sand (0.01 in. to 0.002 in. in diameter) through silts and clays to fine colloidal clay (0.003 in. or less in diameter) (Ippen, 1966). Very little, if any, larger material (coarse sand, gravel, etc.) is found in estuarine sediments. Sand plays a relatively minor role in East Coast, Gulf Coast and Southern Pacific Coast estuaries. Usually it constitutes less than 5% by volume (25% by weight) of total sediments for these estuaries with most of this sand concentrated near the estuarine mouth (Schultz & Simmons, 1957). By contrast, sand is a major element in estuarine shoaling for the north Pacific estuaries (i.e., Washington and Oregon coasts). These estuaries are characterized by extensive oceanic sand intrusion into the lower estuarine segments and by extensive bar formations near the estuarine mouth. The relative distribution of silts and clays, of organic and inorganic material within different estuaries, and, in fact, the distribution of shoaling and scour areas within estuaries, varies widely.

6.8.3 Estuarine Sediment Forces and Movement

As sediments enter the lower reaches of a river and come under tidal influence they are subjected to a wide variety of forces which control their movement and deposition. First, net velocities in the upper reaches of estuaries are normally lower than river velocities. Additionally, the water column comes under the influence of tidal action and thus is subject to periods of slack water. During these periods coarse sand and larger materials settle. The scour velocity required to resuspend a particle is higher than that required to carry it in suspension. Thus, once the coarser particles settle out in the lower river and upper estuarine areas, they tend not to be resuspended and carried farther into the estuary (U.S. Engineering District, San Francisco, 1975). Exceptions to this principle can come during periods of extremely high river discharge when water velocities can hold many of these particles in suspension well into or even through an estuary. Table VI-26 lists approximate maximum allowable velocities to avoid scour for various sizes of exposed particles.

TABLE VI-26

MAXIMUM ALLOWABLE CHANNEL VELOCITY TO AVOID BED SCOUR (FPS) (KING, 1954)

Original material excavated	Clear water, no detritus	Water transporting colloidal silts	Water transporting non-colloidal silts, sands, gravels or rock fragments
Fine sand	1.50	2.50	1.50
Sandy loam	1.75	2.50	2.00
Silt loam	2.00	3.00	2.00
Alluvial silts	2.00	3.50	2.00
Ordinary firm loam	2.50	3.50	2.25
Volcanic ash	2.50	3.50	2.00
Fine gravel	2.50	5.00	3.75
Stiff clay	3.75	5.00	3.00
Graded, loam to cobbles	3.75	5.00	5.00
Alluvial silt	3.75	5.00	3.00
Graded, silt to cobbles	4.00	5.50	5.00
Coarse gravel	4.00	6.00	6.50
Cobbles and shingles	5.00	5.50	6.50
Shales and hardpans	6.00	6.00	5.00

Values are approximate and are for unarmored sediment (sediment not protected by a covering of larger material).

Sediments are subject to gravitational forces and have size-dependent settling velocities. In highly turbulent water the particle fall velocities can be small compared to background fluid motion. Thus gravitational settling occurs chiefly in the relatively quiescent, shallow areas of estuaries or during periods of slack water. As mentioned earlier, particle settling attains a maximum in each tidal cycle during high water slack and low water slack tides. During periods of peak tidal velocity (approximately half way between high and low water) resuspension of unconsolidated sediment may occur. Thus during a tidal cycle large volumes of sediment are resuspended, carried upstream with flood flow, deposited, resuspended, and carried downstream on the ebb tide. Only those particles deposited in relatively quiescent areas have the potential for long term residence. Compounding this cyclic movement of sediments are seasonal river discharge variations which alter estuarine hydrodynamics. Thus, sediment masses tend to shift from one part of an estuary to another (Schultz and Simmons, 1975).

As fresh waters encounter areas of significant salinity gradients extremely fine particles (primarily colloidal clay minerals) often destabilize (coagulate) and agglomerate to form larger particles (flocculate). The resulting floc (larger agglomerated masses) then settles to the bottom. Coagulation occurs when electrolytes, such as magnesium sulfate and sodium chloride, "neutralize" the repulsive forces between clay particles. This allows the particles to adhere upon collision (flocculation) thus producing larger masses of material. Flocculation rates are dependent on the size distribution and relative composition of the clays and electrolytes and upon local boundary shear forces (Ippen, 1966, and Schultz and Simmons, 1957). Flocculation occurs primarily in the upper central segments of an estuary in the areas of rapid salinity increase.

Movement of sediments along the bottom of an estuary does not continue in a net downstream direction as it does in the upper layers and in stream reaches. In all but a very few extremely well mixed estuaries upstream bottom currents predominate at the mouth of an estuary. Thus, upstream flow is greater than downstream flow at the bottom. This is counterbalanced by increased surface downstream flow. However, net upstream flow along the bottom results in a net upstream transport of sediment along the bottom of an estuary near the mouth. Thus, sediments and flocs settling into the bottom layers of an estuary near the mouth are often carried back into the estuary rather than being carried out into the open sea. Consequently, estuaries tend to trap, or to conserve sediments while allowing fresh water flows to continue on out to sea. At some point along the bottom, the upstream transport is counter-balanced by the downstream transport from the fresh water inflow. At this point, termed the "null zone," there is essentially no net bottom transport. Here sediment deposition is extensive. In a stratified estuary this point is at the head of the saline intrusion wedge. In a partially mixed estuary it is harder to pinpoint. Nonetheless, sedimentation is a useful parameter to analyze and will be handled in a quantitative manner beginning with Section 6.8.4.

To this point, flow in a fairly regular channel has been assumed. However, in many estuaries geomorphic irregularities exist. Such irregularities (e.g., narrow headlands) create eddy currents on their lee sides. These eddy currents, or gyres, slow the sediment movement and allow local shoaling. Additionally, large shallow subtidal or tidal flatlands exist in many estuaries. Such areas are usually well out of the influence of primary currents. As a result local water velocities are usually low and increased shoaling is possible.

Wind and waves also have a major influence on estuarine sediment distribution. Seasonal wind driven currents can significantly alter water circulation patterns and associated velocities. This in turn determines, to a large extent, the areas of net shoaling and scour throughout an estuary. Local wind driven and oceanic waves can create significant scour forces. Such scour, or particle resuspension, is particularly

evident in shallow areas where significant wave energy is present at the sediment/water interface. Local wind driven waves are a major counterbalancing force to low velocity deposition in many shallow estuarine areas (U.S. Engineering District, San Francisco, 1975).

Finally, oceanic littoral currents (long shore currents) interact with flood and ebb flows in the area of an estuary mouth. Particularly in the Pacific Northwest, sandy sediment fed from such littoral drift is a major source of estuarine sediment, and the interference of littoral drift with normal flood and ebb flows is the major factor creating estuarine bars.

Figure VI-38 shows the schematic flow of annual sediment movement through San Francisco Bay. With the exception of the magnitude of annual dredging, this is typical for most U.S. estuaries. The most important thing to observe is the dominance of resuspension and redeposition over all other elements of sediment movement including net inflow and outflow. Also note that there is a net annual accumulation of deposited sediment in the bay. This figure is also helpful in conceptualizing the sediment trap or sediment concentration characteristic of estuaries. In any year, 8-10 million cubic yards flow into the estuary and 5 to 9 million cubic yards flow out. However, over 180 million cubic yards are actively involved in annual sediment transport within the estuary.

Figure VI-39 is an idealized conceptualization of the various sediment-related processes in an estuary. It must be remembered that these processes actually overlap spatially much more than is shown and that the processes active at any given location vary considerably over time.

From this qualitative analysis, there are some general statements which can be made. Ippen (1966) drew the following conclusions on the distribution of estuarine sediments:

- The major portion of sediments introduced into suspension in an estuary from any source (including resuspension) during normal conditions is retained therein, and if transportable by the existing currents is deposited near the ends of the salinity intrusion, or at locations of zero net bottom velocity.
- Any measure contributing to a shift of the regime towards stratification causes increased shoaling. Such measures may be: structures to reduce the tidal flow and prism, diversion of additional fresh water into the estuary, deepening and narrowing of the channel.
- Sediments settling to the bottom of an estuary are generally transported upstream and not downstream. Such sediments may at some upstream point be resuspended into the upper layers and carried back downstream.
- Sediments accumulate near the ends of the intrusion zone and form shoals. Shoals also form where the net bottom velocity is zero (in the null zone

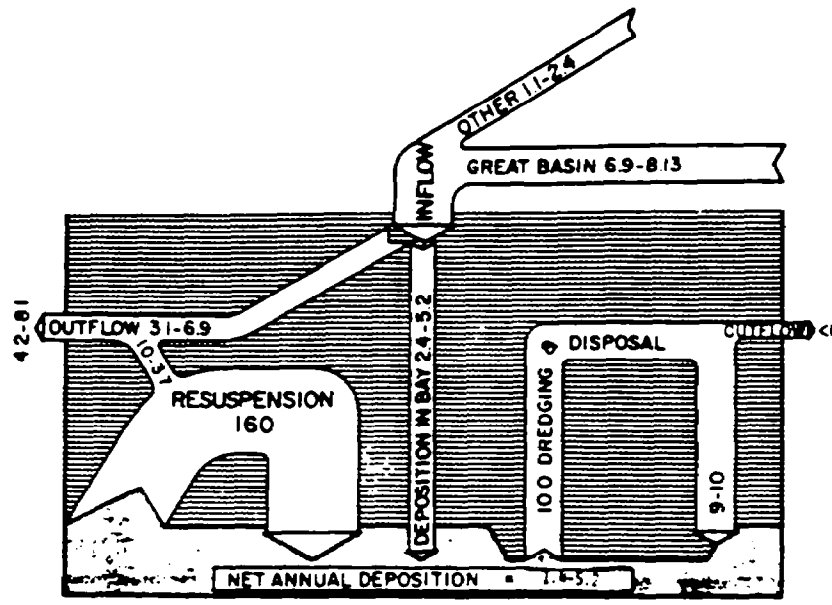

FIGURE VI-38 SEDIMENT MOVEMENT IN SAN FRANCISCO BAY SYSTEM (MILLION CUBIC YARDS), FROM: U.S. ENGINEERING DISTRICT, SAN FRANCISCO, 1975)

The intensity of shoaling is most extreme near the end of the intrusion for stratified estuaries and is lessened in the well mixed estuary. Shoals occur along the banks of the main estuarine channel where water is deep enough to prevent wave induced scour and where velocities are reduced from main channel velocities sufficiently to allow settling.

Schultz and Simmons (1957) made similar conclusions but added the presence of shoaling at the mouth where flood and ebb currents intercept littoral drift.

6.8.4 Settling Velocities

As was stated in the previous section, settling velocities do not play a great role in controlling sedimentation patterns in estuaries as they do in lakes. However, it is informative to assess settling rates for various size particles. The possible size classifications of particles and their general inclusive diameter sizes are shown in Table VI-27. Table VI-28 lists terminal settling velocities for each particle size assuming spherical particles and density of 2.0* in quiescent water. From this table it can be inferred that particles of the medium sand class and coarser probably settle to the bottom within a very short time after entering an estuary.

*The density of many inorganic suspended particles is approximately equal to that of sand (2.7 gm/cm^3) while that of biomass and organic detritus is usually much closer to that of water and can be assumed to be about 1.1 gm/cm^3.

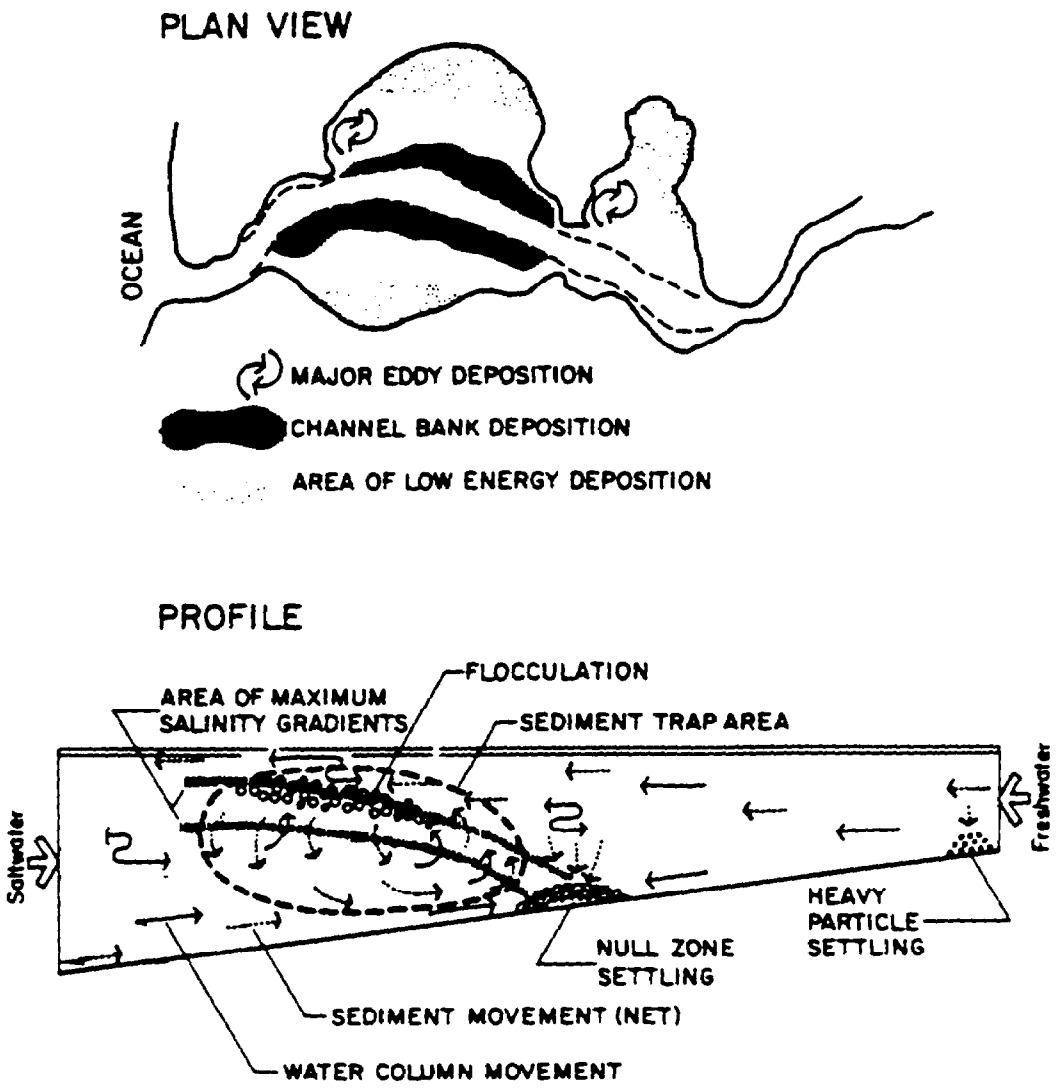

FIGURE VI-39 IDEALIZED ESTUARINE SEDIMENTATION

Turning to the other end of the particle size scale of Table VI-28, particles with a diameter of 10^{-6} mm fall only 3.1×10^{-7} inches per hour in the most favorable environment (calm waters). Such a settling rate is not significant in the estuarine environment. Figure VI-40 shows the quiescent settling rates for particle sizes in between these two extremes since this intermediate size group is of real significance in estuarine management (primarily silts). For particles smaller than those shown in Figure VI-40, gravitational settling is not a significant factor in controlling particle motion. Particles substantially larger than the range shown in Figure VI-40 tend to settle above, or at, the head of an estuary.

Combining Figure VI-40 (fall per tidal cycle)* with known segment flushing

* Based on a 12.4 hour tidal cycle.

TABLE VI-27

SEDIMENT PARTICLE SIZE RANGES (AFTER HOUGH, 1957)

	PARTICLE SIZE RANGE			
	Inches		Millimeters	
	$D_{max.}$	$D_{min.}$	$D_{max.}$	$D_{min.}$
Derrick STONE	120	36	--	--
One-man STONE	12	4	--	--
Clean, fine to coarse GRAVEL	3	1/4	80	10
Fine, uniform GRAVEL	3/8	1/16	8	1.5
Very coarse, clean uniform SAND	1/8	1/32	3	0.8
Uniform, coarse SAND	1/8	1/64	2	0.5
Uniform, medium SAND	--	--	0.5	0.25
Clean, well-graded SAND AND GRAVEL	--	--	10	0.05
Uniform, fine SAND	--	--	0.25	0.05
Well-graded, silty SAND AND GRAVEL	--	--	5	0.01
Silty SAND	--	--	2	0.005
Uniform SILT	--	--	0.05	0.005
Sandy CLAY	--	--	1.0	0.001
Silty CLAY	--	--	0.05	0.001
CLAY (30 to 50% clay sizes)	--	--	0.05	0.0005
Colloidal CLAY (-2μ>50%)	--	--	0.01	10^{-6}

times (in tidal cycles) the size of particles tending to settle out in each segment can be estimated. If such predictions reasonably match actual mean segment sediment particle size, then this method can be useful in predicting changes in sediment pattern. Anticipated changes in river-borne suspended sediment load by particle size can be compared to areas where each size of particle would tend to settle. This would then identify areas which would either be subject to increased shoaling or reduced shoaling and increased scour. This type of analysis has been more successful when applied to organic detritus material than for inorganic suspended loads.

A number of simplifying assumptions have gone into this settling velocity analysis. The most significant of these are:

- Water column density changes have been ignored. Inclusion of this

TABLE VI-28

RATE OF FALL IN WATER OF SPHERES OF VARYING RADII AND CONSTANT DENSITY OF 2[a] AS CALCULATED BY STOKES' LAW[b,c] (MYSELS,1959)

Radius	Terminal velocity	
mm.	cm./sec.	cm./min.
10	(>1)	
1	(>1)	
0.1	(>1)	
0.01	2.2×10^{-2}	1.3
10^{-3}	2.2×10^{-4}	0.013
10^{-4}	2.2×10^{-6}	1.3×10^{-4}
10^{-5}	2.2×10^{-8}	1.3×10^{-6}
10^{-6}	2.2×10^{-10}	1.3×10^{-8}
10^{-7}	(2.2×10^{-12})	

[a] To apply to other conditions, multiply the u value by the pertinent density difference and divide it by the pertinent viscosity in centipoises.

[b] Values in parentheses are calculated by Stokes' law under conditions where this law is not applicable.

[c] Stokes law states that the terminal velocity is proportional to the particle radius squared, the difference in density and inversely proportional to the liquid viscosity.

factor would slightly reduce the settling velocity with increased depth. This effect will be more significant for organic matter because of its lower density.

- Dispersive phenomena and advective velocities have not been considered.
- Table VI-27 and Figure VI-40 are based on the fall of perfectly spherical particles. Non-spherical particles have lower settling velocities.
- Interference between particles has not been considered. However, in a turbulent, sediment-laden estuary such interference is possible (hindered settling). The analysis of the effect of interference on settling velocities was covered in Chapter V for lakes. This analysis is also basically valid for estuaries. The effects introduced there can be applied to Figure VI-40 velocities to adjust for particle interference.

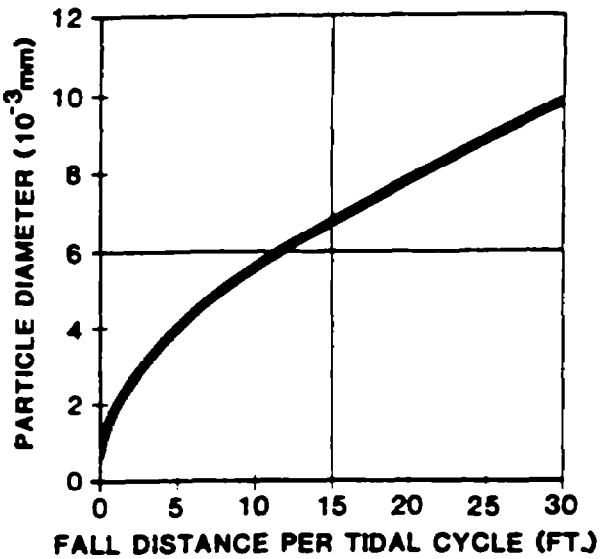

FIGURE VI-40 PARTICLE DIAMETER VS SETTLING FALL PER TIDAL CYCLE (12.3 HRS) UNDER QUIESCENT CONDITIONS (SPHERES WITH DENSITY 2.0 GM/CM^3)

6.8.5 Null Zone Calculations

It was previously mentioned that substantial shoaling occurs in the area of the null zone. It is possible to estimate the location of this zone, and hence the associated shoaling areas, as a function of water depth and river discharge. In addition to the importance of the null zone to shoaling, Peterson and Conomos (Peterson, et al., 1975) established the biological and ecological importance of this area in terms of planktonic production. The null zone, therefore, is both an area of potential navigational hazard and an area of major ecological importance to the planner.

Silvester (1974) summarized the analysis for estimating the location of the null zone with respect to the mouth of an estuary. The basic equation used in this analysis is:

$$\frac{\bar{S}_n}{S_o} = \frac{1000}{0.7 S_o F_n^2} \frac{U_r^2}{gd} \qquad \text{(VI-109)}$$

where

$\bar{S}_n$ = mean salinity (averaged vertically and over a tidal cycle) at the null point (n), (ppt)

S_o = ocean surface salinity adjacent to the estuary in parts per thousand (ppt),

U_r = fresh water flow velocity (ft/sec)

g = gravitational acceleration = 32.2 ft/sec^2,

d = estuarine depth, (ft)

F_n = densimetric Froude number at the null zone where F_n is defined by:

$$F_n = U_r / \sqrt{(\Delta\rho/\rho_n) g d} \qquad \text{(VI-110)}$$

where

$\Delta\rho/\rho_n$ = difference between fresh water density and that at the the null zone (averaged over the depth of the water column) divided by the density at the null zone. This value may be approximated for estuarine waters by:

Combining Equations VI-109 and VI-110 and solving for $\frac{\Delta\rho}{\rho_n}$ yields

$$\frac{\Delta\rho}{\rho_n} = \frac{0.7}{1000} S_n \qquad \text{(VI-111)}$$

This formulation is particularly good for channels which are either maintained at a given depth (dredged for navigation) or are naturally regular, as "d" represents mean cross section channel depth at the null zone.

The use of these equations first requires location of the present null zone. This can most easily be done by measuring and averaging bottom currents over one tidal cycle to locate the point where upstream bottom currents and downstream river velocities are exactly equal, resulting in no net flow. This situation is schematically shown in Figure VI-41.

When this point has been established for one set of river discharge conditions, Equation VI-111 can be substituted into Equation VI-110 to calculate F_n. This F_n value is an inherent characteristic of an estuary and can be considered to be constant regardless of the variations in flow conditions or null zone location (Silvester, 1974).

With this information and a salinity profile for the estuary (S_x plotted against x from x = 0 at the mouth of the estuary to x = L at the head) the location of future null zones may be calculated. Given the new conditions of U_r (changes in river discharge) or of d (changes in channel depth, as by dredging activity), Equation VI-109 will allow calculation of a new S_n. This may be plotted on the salinity profile to calculate the location of a new null zone position. Even though these changes will produce a new estuarine salinity profile, the use of

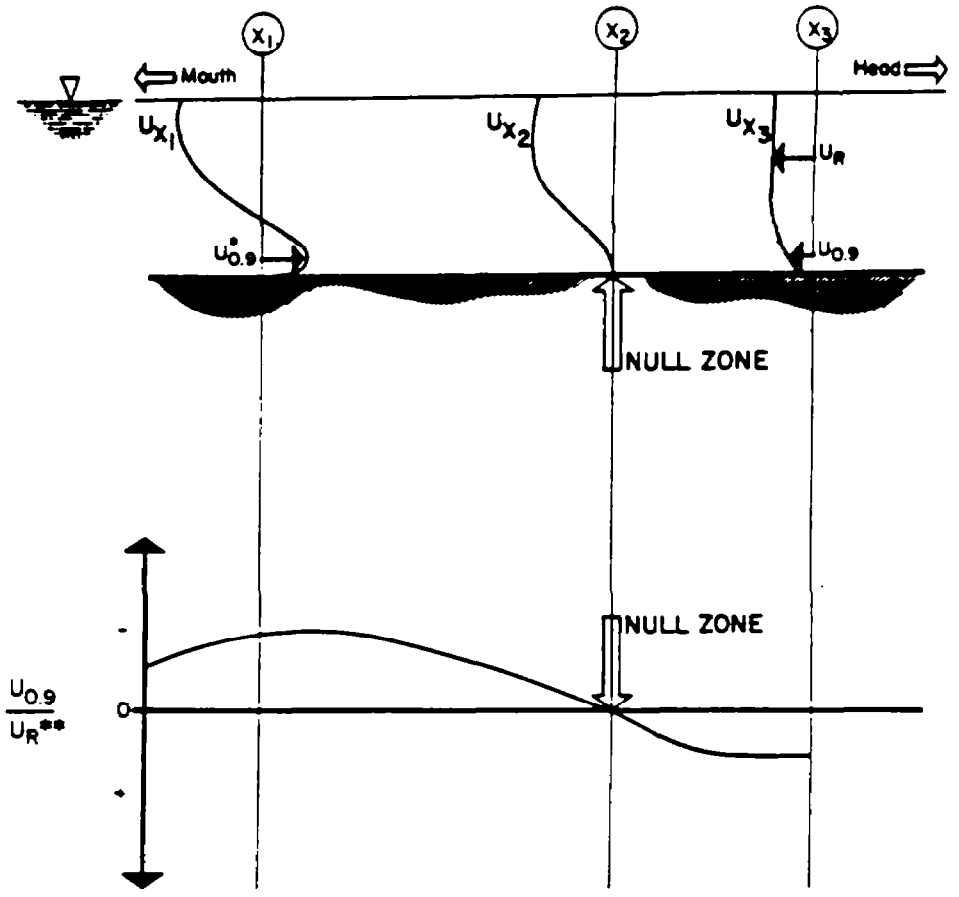

* $U_{0.9}$ = tidally averaged velocity at a depth equal to 0.9 of the water column depth.

** U_R = river flow velocity

FIGURE VI-41 ESTUARINE NULL ZONE IDENTIFICATION

Equation VI-109 and the old (known) salinity profile will produce reasonably good estimates of longitudinal shifts in the location of the null zone. Salinity profiles for appropriate seasonal conditions should be used for each calculation (e.g., low flow profiles for a new low flow null zone calculation).

EXAMPLE VI-19

Estimation of Null Zone Location

An estuary has the tidally averaged salinity profile shown in the Salinity Table below. Mean channel depth in the area of the existing null zone is 18 feet

and the salinity at that point is 10 parts per thousand (ppt). Current (low flow) river discharge velocity is 0.5 ft/sec. Normal winter (high flow) velocity is 1.8 ft/sec. It is desired to know where the null zone will be located in summer and winter if a 30 ft deep channel is dredged up to 70,000 feet from the mouth.

SALINITY DATA FOR EXAMPLE VI-19

Distance from mouth (1000ft)	5	15	25	35	45	55	65	75	85
Salinity (ppt)	30	28	25	20	13	8	6	4	1

From Equation VI-110 and Equation VI-111:

$$F_n = U_r / \sqrt{(.7/1000)\ (\bar{S}_n)\ (g)\ (d)}$$

$$= 0.5 \text{ ft/sec} / \sqrt{(7\text{x}10^{-4})\ (10 \text{ ppt})\ \ (32.2 \text{ ft/sec}^2)\ (18 \text{ ft})}$$

or $F_n = 0.248$

From equation VI-109 the null zone salinity with a deeper channel will be:

$$= \frac{S_o\ 1000\ U_r^2}{S_o\ 0.7\ F_n^2\ gd}$$

$$= (1000)\ (0.5 \text{ ft/sec})^2 / 0.7\ (0.248)^2\ (32.2 \text{ ft/sec}^3)\ (30 \text{ ft})$$

$$= 6.0 \text{ ppt}$$

From the previous tabulation this will occur approximately 65,000 ft from the mouth of the estuary.

Under winter flow conditions:

$$\bar{S}_n = \frac{S_o\ 1000\ U_r^2}{0.7\ F_n^2\ gd}$$

$$= (1000)\ (1.8 \text{ ft/sec}) / 0.7\ (0.248)^2\ (32.2 \text{ ft/sec}^2)\ (30 \text{ ft})$$

$$\bar{S}_n = 77.9 \text{ ppt}$$

This $\bar{S}_n$ is greater than ocean salinity and will not actually be encountered. Thus, null zone shoaling will occur at the mouth if it occurs at all. This condition is common for rivers with seasonally variable flow rates.

END OF EXAMPLE VI-19

REFERENCES

Abramovich, G. 1963. The Theory of Turbulent Jets. MIT Press.

American Public Health Association. 1976. Standard Methods for the Examination of Water and Wastewater. 14th edition.

APHA, AWWA, WPCF. 1980. Standard Methods For the Examination of Water and Wastewater. 15th edition. APHA, Washington, D.C. 1134 pp.

Austin, R.W. 1974. Problems in Measuring Turbidity as a Water Quality Parameter. Proceedings of Seminar on Methodology for Monitoring the Marine Environment. EPA Environmental Monitoring Series. EPA-600/4-74-004.

Beyer, G.L. 1969. Turbidimetry and Nephelometry. Encyclopedia of Chemical Technology. New York. pp. 738-798.

Brooks, N.H. 1972. Dispersion in Hydrologic and Coastal Environments. Report No. KH-R-29, California Institute of Technology, Division of Engineering and Applied Science.

California State Water Resources Control Board. 1978. Water Quality Control Plan for Ocean Waters of California. State Water Resources Control Board Resolution No. 78-2. 15 pp.

Carhart, R.A., A.J. Policastro, S. Ziemer, K. Haake, and W. Dunn. 1981. Studies of Mathematical Models for Characterizing Plume and Drift Behavior from Cooling Towers, Volume 2. Mathematical Model for Single-Source (Single-Tower) Cooling Tower Plume Dispersion. Electric Power Research Institute, CS-1683, Volume 2, Research Project 906-1.

Chen, C.W. and G.T. Orlob. 1975. Ecologic Simulation for Aquatic Environments. Systems Analysis and Simulation in Ecology, Volume 3. Academic Press. New York. pp. 475-558.

DeFalco, Paul, Jr. 1967. The Estuary-Septic Tank of the Megalopolis. In: Estuaries, Ed. G.H. Lauff. American Association for the Advancement of Science. (83):701-707.

Duxbury, A.C. 1970. Estuaries Found in the Pacific Northwest. Proceedings, Northwest Estuarine and Coastal Zone Symposium. Bureau of Sport Fisheries and Wildlife.

Dyer, K.R. 1973. Estuaries: A Physical Introduction. John Wiley and Sons, New York.

Edinger, J.E. 1971. Estuarine Temperature Distributions. Estuarine Modeling: An Assessment. Chapter 4, Environmental Protection Agency Water Pollution Control Research Series, No. 16070DZV 02/71.

Edinger, J.E., and E.M. Polk. 1969. Initial Mixing of Thermal Discharges into a Uniform Current. Water Center Report #1, Vanderbilt University.

Fan, L.N. 1967. Turbulent Buoyant Jets into Stratified or Flowing Ambient Fluids. KH-4-15. California Institute of Technology. W.M. Keck Laboratory, Pasadena, CA.

Fisher, H.B. 1968. Methods for Predicting Dispersion Coefficients in Natural Streams, with Applications to Lower Reaches of the Green and Duwamish Rivers, Washington. U.S. Geological Survey Professional Paper 582-A. U.S. Government Printing Office, Washington, D.C.

Frick, W.E. 1981a. Projected Area in Plume Modeling. Submitted for publication September 1981. Corvallis, OR.

Frick, W.E. 1981b. Comparison of PLUME and OUTPLM Predictions with Observed Plumes. Tetra Tech, Inc., Corvallis, OR.

Frick, W.E. 1981c. A Theory and Users's Guide for the Plume Model MERGE. Tetra Tech, Inc., Corvallis, OR.

Frick, W.E. 1980. Findings and Recommendations on the Use and Modification of the EPA Computer Model DKHPLM. Tetra Tech, Inc., Corvallis, OR.

Frick, W.E., and L.D. Winiarski. 1980. Why Froude Number Replication Does Not Necessarily Ensure Modeling Similarity. In: Proceedings of the Second Conference on Waste Heat Management and Utilization. Miami Beach, FL.

Frick, W.E., and L.D. Winiarski. 1975. Comments on: The Rise of Moist Buoyant Plumes. Journal of Applied Meteorology, 14(3):421.

Giger, R.D. 1972. Some Estuarine Factors Influencing Ascent of Anadromous Cutthroat Trout in Oregon. Proceedings of the Second Annual Technical Conference on Estuaries of the Pacific Northwest. Oregon State University. pp. 18-30.

Glenne, B. 1967. A Classification System for Estuaries. Journal of the Waterways and Harbors Division. February, 1967. pp. 55-61.

Goodwin, C.R., W.D. Emmett, and B. Glenne. 1970. Tidal Studies of Three Oregon Estuaries. Oregon State University Engineering Experiment Station Bulletin No. 45.

Graham, J.J. 1968. Secchi Disc Observations and Extinction Coefficients in the Central and Eastern North Pacific Ocean. Limnology and Oceanography. pp. 184-190.

Green, J. 1968. The Biology of Estuarine Animals. University of Washington Press, Seattle, WA.

Hansen, D.V., and M. Rattray. 1966. New Dimensions in Estuarine Classification. Limnology and Oceanography 11(3):319-316.

Hardy, C.D. 1972. Movement and Quality of Long Island Sound Waters, 1971. Technical Report #17, State University of New York, Marine Sciences Research Center.

Harleman, D.R.F. 1964. The Significance of Longitudinal Dispersion in the Analysis of Pollution in Estuaries. Proceedings 2nd International Conference on Water Pollution Research. Tokyo. Pergamon Press, New York.

Harleman, D.R.F. 1971. Hydrodynamic Model - One Dimensional Models. Estuarine Modeling: An Assessment. EPA Water Pollution Control Research Series, No. 16070 DZV 02/71. pp. 34-90.

Harleman, D., and C.H. Lee. 1969. The Computation of Tides and Current in Estuaries and Canals. U.S. Corps of Engineers Committee on Tidal Hydraulics. Technical Bulletin No. 16.

Hodkinson, J.R. 1968. The Optical Measurement of Aerosols. In: Aerosol Science, Ed. C.N. Davies. Academic Press, New York. pp. 287-357.

Hough, B.K. 1957. Basic Soils Engineering. Ronald Press, New York. p. 69.

Hydroscience, Inc. 1971. Simplified Mathematical Modeling of Water Quality. U.S. Environmental Protection Agency, Water Quality Management Planning Series, Washignton, D.C.

Hydroscience, Inc. 1974. Water Quality Evaluation for Ocean Disposal System - Suffolk County, New York. Bowe, Walsh and Associates Engineers, New York.

Ippen, A.T. 1966. Estuary and Coastline Hydrodynamics. McGraw-Hill, New York.

Jirka, G., and D.R.F. Harleman. 1973. The Mechanics of Submerged Multiport Diffusers for Buoyant Discharges in Shallow Water. Report No. 169, MIT. Ralph M. Parsons Laboratory, Department of Civil Engineering. p. 236.

Johnson, J. 1973. Characteristics and Behavior of Pacific Coast Tidal Inlets. Journal of the Waterways Harbors and Coastal Engineering Division. August, 197. pp. 325-339.

Johnson, R.G., W.R. Bryant, and J.W. Hedgpeth. 1961. Ecological Survey of Tomales Bay: Preliminary Report of the 1960 Hydrological Survey. University of the Pacific, Pacific Marine Station.

Ketchum, B.H. 1950. Hydrographic Factors Involved in the Dispersion of Pollutants Introduced Into Tidal Waters. Journal of the Boston Society of Civil Engineers 37:296-314.

Ketchum, B.H. 1955. Distribution of Coliform Bacteria and Other Pollutants in Tidal Estuaries. Sewage and Industrial Wastes 27:1288-1296.

Ketchum, B.H., and D.J. Keen. 1951. The Exchanges of Fresh and Salt Waters in the Bay of Fundy and in Passamaquoddy Bay. Woods Hole Oceanographic Institution. Contribution No. 593, Reference Number 51-98.

King, H.W. 1954. Handbook of Hydraulics. McGraw-Hill, New York. pp. 7-33.

McGauhey, P.H. 1968. Engineering Management of Water Quality, McGraw-Hill, San Francisco, CA.

McKinsey, D. 1974. Seasonal Variations in Tidal Dynamics, Water Quality, and Sediment in Alsea Estuary. Oregon State University, Dept. of Civil Engineering, Corvallis, OR.

Mysels, K.J. 1959. Introduction to Colloid Chemistry. Interscience New York. p.61.

Neumann, G., and W. Pierson. 1966. Principles of Physical Oceanography. Prentice-Hall, Englewood Cliffs, NJ.

O'Brien, M.P. 1969. Equilibrium Flow Areas of Inlets on Sandy Coasts. Journal of the Waterways and Harbors Division, Proceedings of the American Society of Civil Engineers. pp. 43-51.

O'Connor, D.J. 1965. Estuarine Distribution of Nonconservative Substances. Journal of Sanitary Engineering Division, ASCE. SA1:23-42.

O'Connor, D.J., and R. V. Thomann. 1971. Water Quality Models: Chemical, Physical, and Biological Constituents. Estuarine Modeling: An Assessment, Chapter III. U.S. Environmental Protection Agency Water Pollution Control Research Series No. 16070 DZV 02/71. pp. 102-169.

Parker, F.L., and P.A. Krenkel. 1970. CRC Physical and Engineering Aspects of Thermal Pollution. Chemical Rubber Company Press, Cleveland, OH.

Pearson, E. et al. 1967. Final Report: A Comprehensive Study of San Francisco Bay, Volume V: Summary of Physical, Chemical and Biological Water and Sediment Data. Report No. 67-2, U.C. Berkeley Sanitary Engineering Research Laboratory.

Perkins, E.J. 1974. The Biology of Estuaries and Coastal Waters. Academic Press, London.

Peterson, O.H. et al. 1975. Location of the Non-tidal Current Null Zone in Northern San Francisco Bay. Estuarine and Coastal Marine Science (1975) 3, pp. 1-11.

Policastro, A.J., R.A. Carhart, S.E. Ziemer, and K. Haake. 1980. Evaluation of Mathematical Models for Characterizing Plume Behavior from Cooling Towers. Dispersion from Single and Multiple Source Natural Draft Cooling Towers, NUREG/CR-1581, Volume 1. Argonne National Laboratory, Argonne, IL.

Pritchard, D.W. 1960. The Movement and Mixing of Contaminants in Tidal Estuaries, Proceedings of the First International Conference on Waste Disposal in the Marine Environment. University of California, Berkeley.

Pritchard, D.W. 1967. What is an Estuary: Physical Viewpoint. In: Estuaries, ed, G.H. Lauff. American Association for the Advancement of Science, Publication No. 83. pp. 2-6.

Pritchard, D.W. 1969. Dispersion and Flushing of Pollutants in Estuaries. Journal of Hydraulics Division, ASCE, HY1. pp. 115-124.

Pritchard, D.W., and J.R. Schubel. 1971. What is an Estuary, The Estuarine Environment-Estuaries and Estuarine Sedimentation. American Geological Institute.

Rawn, A.M., F.R. Bowerman, and N.H. Brooks. 1960. Diffusers for Disposal of Sewage in Seawater. Journal of the Sanitary Engineering Division, ASCE, SAR. p. 80.

Schubel, J.R. 1971. The Origin and Development of Estuaries, The Estuarine Environment-Estuaries and Estuarine Sedimentation. American Geological Institute.

Schultz, E.A., and H.B. Simmons. 1957. Freshwater-Salt Water Density Current, a Major Cause of Siltation in Estuaries. Commission on Tidal Hydraulics, U.S. Army Corps of Engineers. Technical Bulletin No. 2.

Serne, R.J., and B.W. Mercer. 1975. Characterization of San Francisco Bay Delta Sediments - Crystalline Matrix Study. Dredge Disposal Study of San Francisco Bay and Estuary, Appendix F. U.S. Army Corps of Engineers, San Francisco District.

Shiraza, M.A., and L.R. Davis. 1976. Workbook of Thermal Plume Predictions: Surface Discharge. U.S. Environmental Protection Agency, Corvallis Environmental Research Laboratory, OR.

Silvester, R. 1974. Coastal Engineering, II: Sedimentation, Estuaries, Tides, Effluents and Modeling, Elsevier Scientific Publishing, New York.

Stommel, H. 1953. Computation of Pollution in a Vertically Mixed Estuary. Sewage and Industrial Wastes, 25(9):1065-1071.

Streeter, V.L. 1961. Handbook of Fluid Dynamics, McGraw-Hill, New York.

Stumm, W., and J.J. Morgan. 1970. Aquatic Chemistry: An Introduction Emphasizing Chemical Equilibria in Natural Waters. Wiley-Interscience, New York. pp. 507-513.

Teeter, A.M., and D.J. Baumgartner. 1979. Prediction of Initial Mixing for Municipal Ocean Discharges, CERL-043. U.S. Environmental Protection Agency, Corvallis Environmental Research Laboratory, OR.

Tesche, T.W., W.D. Jensen, and J.L. Haney. 1980. Modeling Study of the Proposed SMUD Geothermal Power Plant: Model Application Protocol. SAI No. 118-E780-11, Systems Applications, Inc., San Rafael, CA.

Tetra Tech, Inc. 1979. Methodology for Evaluation of Multiple Power Plant Cooling System Effects. General Description and Screening. Electric Power Research Institute Report EA-1111. Pal Alto, CA.

Tracor. 1971. Estuarine Modeling: An Assessment For: Water Quality Office, U.S. Environmental Protection Agency.

U.S. Engineer District - San Francisco. 1975. Draft Composite Environmental Statement for Maintenance Dredging of Federal Navigation Projects in San Francisco Bay Region, California. U.S. Army Corps of Engineers.

U.S. Environmental Protection Agency. 1979. Methods for Chemcial Analysis of Water and Wastes. EPA-600/4-79-020.

Van de Hulst, H.C. 1957. Light Scattering by Small Particles. John Wiley and Sons, New York.

Winiarski, L.D., and W.E. Frick. 1978. Methods of Improving Plume Models. Presented at the Cooling Tower Environment 1978 Conference May 2-4, 1978, at University of Maryland, College Park, MD.

Winiarski, L.D., and W.E. Frick. 1976. Cooling Tower Plume Model. U.S. Environmental Protection Agency Corvallis Environmental Research Laboratory, Corvallis, OR. EPA-600/3-76-100.

CHAPTER 7

GROUND WATER

7.1 OVERVIEW

Ground water now serves as a source of drinking water for over 100 million people in the United States, including an estimated 95 percent of the rural population. Ground water is also used for irrigation, industrial process water, and cooling water. Along with its increased usage has come an awareness of the need for protecting its quality. Recent legislation and policy decisions, including the Resource Conservation and Recovery Act, its amendments, and the U.S. EPA's Ground Water Protection Strategy, attempt to minimize the impacts of waste disposal on ground water quality. Predictive methods are needed to determine the hazards associated with existing sites and proposed waste disposal activities.

7.1.1 Purpose of Screening Methods

The purpose of this chapter is to discuss approaches and hand calculation methods which can be used to predict ground water contamination for common waste disposal techniques and hydrogeologic settings. The screening methods can answer questions such as how long it will take contaminants to reach a downgradient location. For example, are the contaminants likely to reach a water supply well in 1 to 2 days or 10 to 20 years? In addition, an initial assessment of the hazard involved can be made. For example, are the predicted concentrations below detectable levels or several times greater than the drinking water standards? Based on such results, decisions can be made to improve the estimates by collecting additional data, to proceed to more detailed analyses including numerical simulation models, or to proceed to other more critical problems. Guidance is included at the end of this chapter suggesting when numerical simulation models should be used.

The hand calculation methods presented in this chapter have been selected based on a series of criteria similar to those used for the surface water methods presented in earlier chapters. The two primary criteria are 1) that, although the method can be simplified, it must be technically defensible and 2) that it require limited data which can be easily estimated or obtained. One simplification in all the methods presented is the use of spatially and temporally averaged data. To do otherwise requires a grid system, a computer, and most importantly--extensive data. Through careful selection of parameter values and the use of sensitivity analyses, results for both worst case and typical conditions can be obtained. The other criteria are 3) that the method be applicable to a range of waste sources and 4) that the method be applicable to a variety of hydrogeologic settings.

The emphasis of this chapter is on prediction of contaminant migration in porous media. Specific methods for handling solute migration in fractured formations have not

been included in this chapter. While fractured formations are important in some parts of the country, predictions of contaminant behavior in such systems are typically not amenable to screening methods. For porous media, the hand calculation methods presented can predict the time for specific concentrations to occur at downgradient locations, the time for contaminants to reach a specified distance, the concentration at a given time and location, or the maximum likely concentration at any location.

7.1.2 Ground Water vs. Surface Water

To orient readers who are more familiar with surface water than ground water, the major differences in both physical and chemical processes are presented before proceeding to the remainder of the chapter. Most of the differences stem from the fact that surface waters occur in surface depressions exposed to the atmosphere, while most ground water occurs in porous media typically isolated from the atmosphere. Flow velocities in ground water are much slower, on the order of meters per month rather than meters per second. A consequence of the low velocities is that flow in porous media is generally laminar, with the exception of flow in cavernous limestone formations or volcanic formations with lava tubes. The presence of laminar flow simplifies the flow calculations as will be discussed in more detail in Section 7.3. The low velocities also mean that travel times must be carefully considered in selecting sampling well locations and in interpreting previously collected data. The lower velocities of ground water have several important implications with respect to chemical processes. At low velocities, very slow chemical reactions can become important and faster reactions often can be treated as equilibrium processes.

Mixing or dispersion in ground water is more difficult to quantify than in surface water. Estimation of the extent of a mixing zone when contaminants enter an aquifer is hard to determine and depends on local heterogeneities, particularly with respect to hydraulic conductivity. The extent of vertical dispersion can be critical when interpreting data obtained from wells screened over different intervals.

Another factor which is different is that there is far less temperature fluctuation in most ground waters so that rate coefficients do not have to be continuously adjusted for short-term temperature changes. Except in geothermal waters or where a waste discharge has increased the temperature in its immediate vicinity, ground water temperatures are likely to be between 5 and 15^{o}C.

In addition to the above differences, there are differences in the solution characteristics which influence the behavior of contaminants in subsurface waters. The important solution characteristics are total dissolved solids, dissolved oxygen, pH, redox potential, partial pressure of carbon dioxide, and solid/liquid ratio. Total dissolved solids (TDS) concentrations in ground water typically range from 100-1000 mg/l, ionic strengths are generally close to 0, and activity coefficient corrections are usually not necessary for screening calculations. If the TDS concentrations are

greater than 1000 mg/l and the contaminants are metals, the need for activity corrections should be considered. Dissolved oxygen (DO) had traditionally been considered to be absent in ground waters. However, measurements in the last 10 to 15 years have shown levels up to 4 mg/l in some systems (Wilson and McNabb, 1981). The presence or absence of DO can determine whether certain reactions will occur. For example, dehydrochlorination of trichloroethylene into the dichloro isomers and vinyl chloride can occur under anaerobic conditions but not aerobic conditions.

The presence or absence of dissolved oxygen along with other redox species also determines the redox potential. Reducing conditions (no DO, presence of dissolved iron) are common in ground water. Speciation of metals partly depends on redox conditions. The pH of the ground water influences the degree to which metals adsorb onto the permeable media. The occurrence of reducing conditions complicates sampling and can cause metals to precipitate when the ground water is brought to the surface and is exposed to the atmosphere. Another factor which causes problems in sampling, particularly for metals, is that the ground water is typically supersaturated with respect to atmospheric levels of carbon dioxide. When samples are brought to the surface, the weak acid CO_2 may be lost. This causes the sample pH to rise and may thereby change the speciation of metals and allow some to precipitate.

The high solid to liquid ratio in ground water is a major difference from surface water. Interfacial phenomena such as adsorption can be important chemical attenuation processes. Example problems presented in later sections clearly show that solutes with strong affinities for the solid phase do not travel far in porous media. Unlike in surface waters, the particles to which the contaminants adsorb are usually immobile. Because the particles are in continual contact with the flowing water the sorbed contaminants can act as secondary sources and may desorb when the concentrations in the ground water decrease. Desorption can occur in rivers but is less important since most of the sorbed contaminants become part of the bottom sediment.

A final difference between surface and ground waters is in the screening methods themselves. As will be discussed in more detail, considerably more analysis is required prior to the use of a particular screening method to determine the flow paths of the contaminants in ground water. Flow paths for rivers are easily determined by visual observation, whereas in ground water they are based on limited data and calculations.

7.1.3 Types of Ground Water Systems Suitable for Screening Methods

The screening methods presented in this chapter are applicable to porous media where the capacity to transmit water is due to primary permeability (connected pores) rather than due to secondary permeability (e.g., fractures, lava tubes). If fractures in a formation are relatively uniform in size and spatially distributed over the area of interest, these formations could be analyzed using the screening methods by

substituting an equivalent permeability from pump tests. More complex fractured formations (e.g., when the fractures are predominantly in one direction) are not amenable to screening methods.

Major types of aquifers in the United States are shown in Figure VII-1. The divisions shown are unconsolidated and consolidated formations, alluvial aquifers along major rivers, and areas where aquifer yields are less than 0.2 m^3/min (50 gpm) to individual wells. The stratigraphy in an area can range from a layered system such as on Long Island (Figure VII-2) to a complex system of unconsolidated glacial formations overlying several different types of consolidated rock formations such as occur in New Jersey (Figure VII-3). In such complex hydrogeologic systems, some aquifers may be confined (i.e., not open to the atmosphere). In the arid western part of the country, additional complications can occur. Examples include closed basins where evapotranspiration is the only outflow and highly faulted basins which can have large changes in permeability over short distances (Figure VII-4). Infiltration in such basins typically occurs along the basin boundaries, primarily from runoff in the mountains, instead of directly through the valley floor. There are also more likely to be thick unsaturated zones. Screening methods are presented in this chapter which predict the migration of contaminants in both the unsaturated and saturated zones.

7.1.4 Pathways for Contamination

The usual division of waste sources into point and nonpoint sources can be used for ground water but this kind of division does not indicate the variety of ways in which contaminants can enter ground water systems. Waste can enter the ground water directly, through recharge of contaminated surface water, or through leakage from one aquifer to another. In some cases, recharge of contaminated water may not be considered because of the inferred presence of an impermeable layer or confining bed, when in reality the impermeable layer or bed is discontinuous and contamination of an underlying or overlying aquifer has occurred.

Examples of point sources of importance to ground water include surface impoundments, landfills, spills and leaks, and injection wells. The largest number of impoundments are associated with the oil and gas industry, although larger volumes of waste are disposed by the paper, chemical, and metals processing industries (U.S. EPA, 1979). The relative number of impoundments by state is shown in Figure VII-5. Landfills are used to dispose of sludge from municipal waste treatment plants, ash and flue-gas desulfurization sludge from coal-fired utilities, and wastes from other types of industries. The wastes can contain high concentrations of metals, organic chemicals, and acids. Spills and leaks, particularly from underground storage tanks, have recently been recognized as a major source of contamination, especially with respect to organic chemicals (e.g., trichloroethylene and gasoline). Injection wells have been used primarily for oil field brines and the associated "produced waters", but

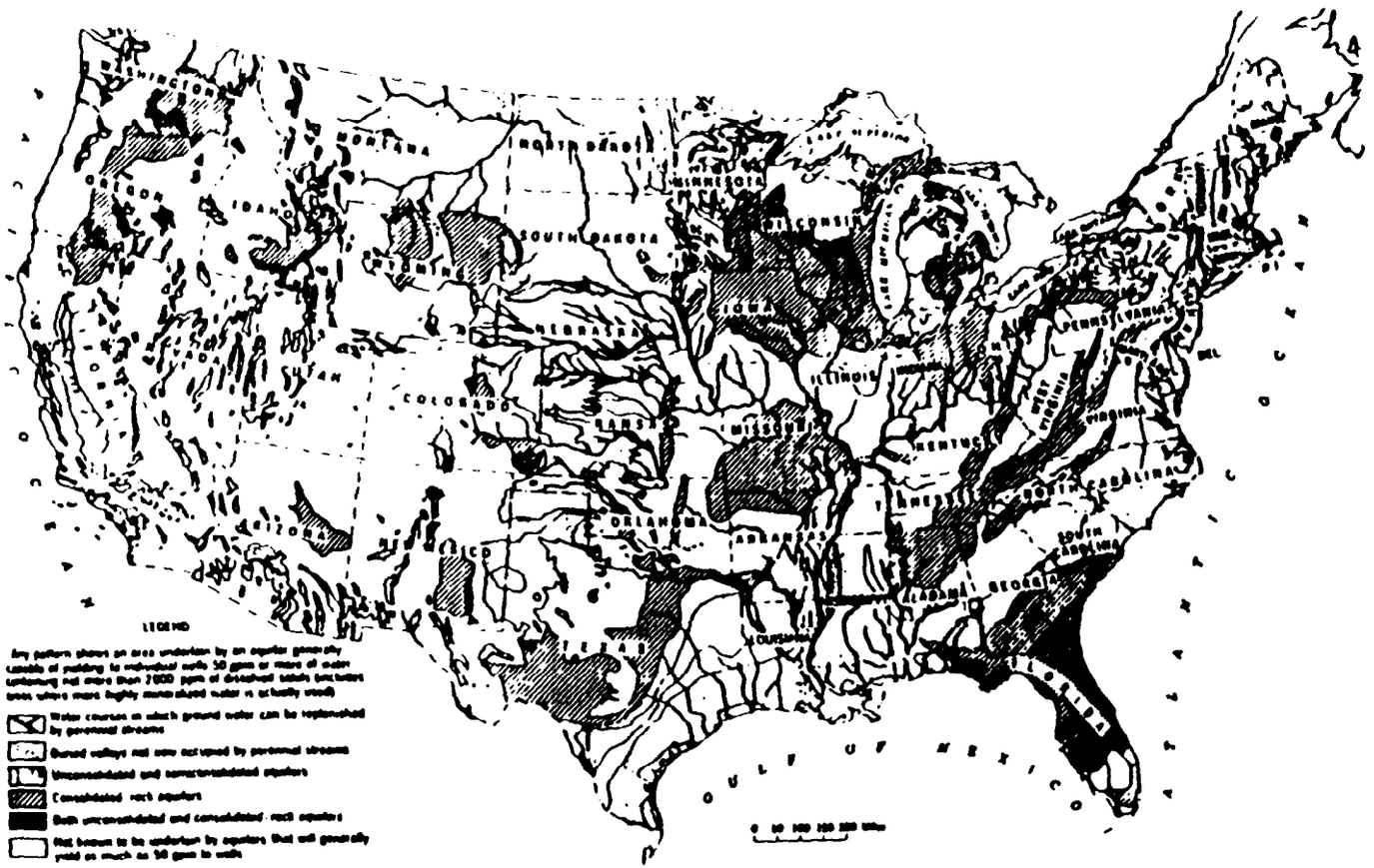

FIGURE VII-1 MAJOR AQUIFERS OF THE UNITED STATES. REFERENCE: THOMAS (1951)

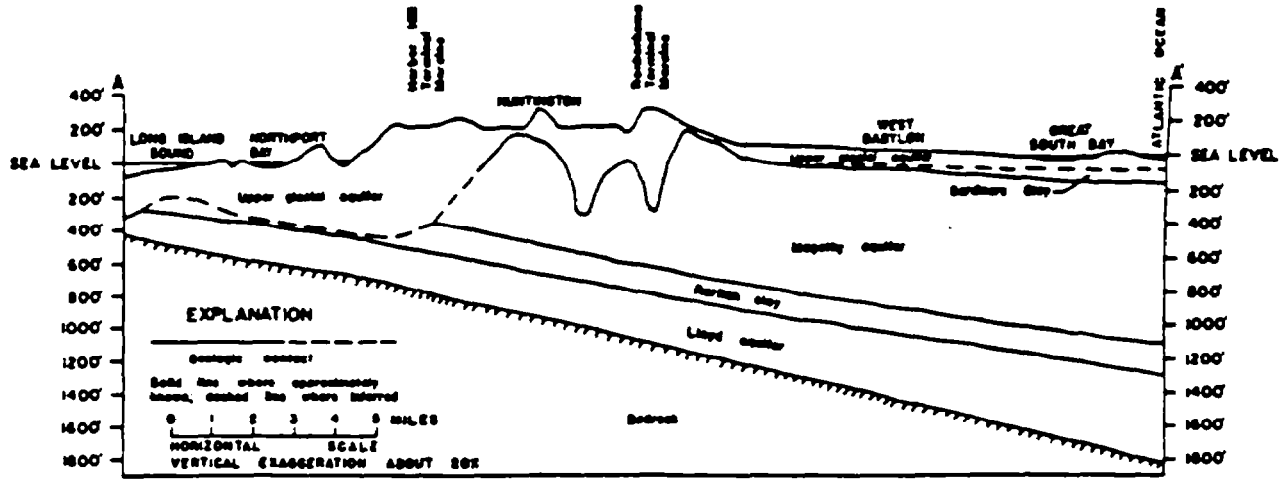

FIGURE VII-2 GEOLOGIC SECTION IN WESTERN SUFFOLK COUNTY, LONG ISLAND, SHOWING BOTH CONFINED AND UNCONFINED AQUIFERS. REFERENCE: TETRA TECH (1977)

some manufacturing process wastes and mining wastes have also been injected into deep aquifers or into dry wells in areas with deep unsaturated zones. Contamination from wells can also occur from migration from one zone or aquifer to another along abandoned or improperly plugged casings.

Nonpoint sources, which result in contaminants being spread over large areas, include seepage from residential areas with septic tank systems, infiltration of runoff, and application of pesticides and fertilizer to agricultural and residential land. The methods presented in this chapter are oriented more towards point sources but can be used to estimate the overall effect on an aquifer of a wide-spread contaminant.

7.1.5 Approach to Ground Water Contamination Problems

The initial step in analyzing a ground water problem is the selection of the spatial and temporal framework for the problem. The spatial representation is determined from the disposal system configuration (i.e., a large pond or landfill versus a leak or an injection well) and the type of question being asked. For example, if the need is to predict the concentration at the water table of a contaminant spilled at the surface, a one-dimensional vertical transport method may be most appropriate. If the need is to predict the areal extent of a ground water plume, a two-dimensional method for flow in the saturated zone would be preferred. The temporal representation of a problem must consider whether a waste source should be considered as a one-time

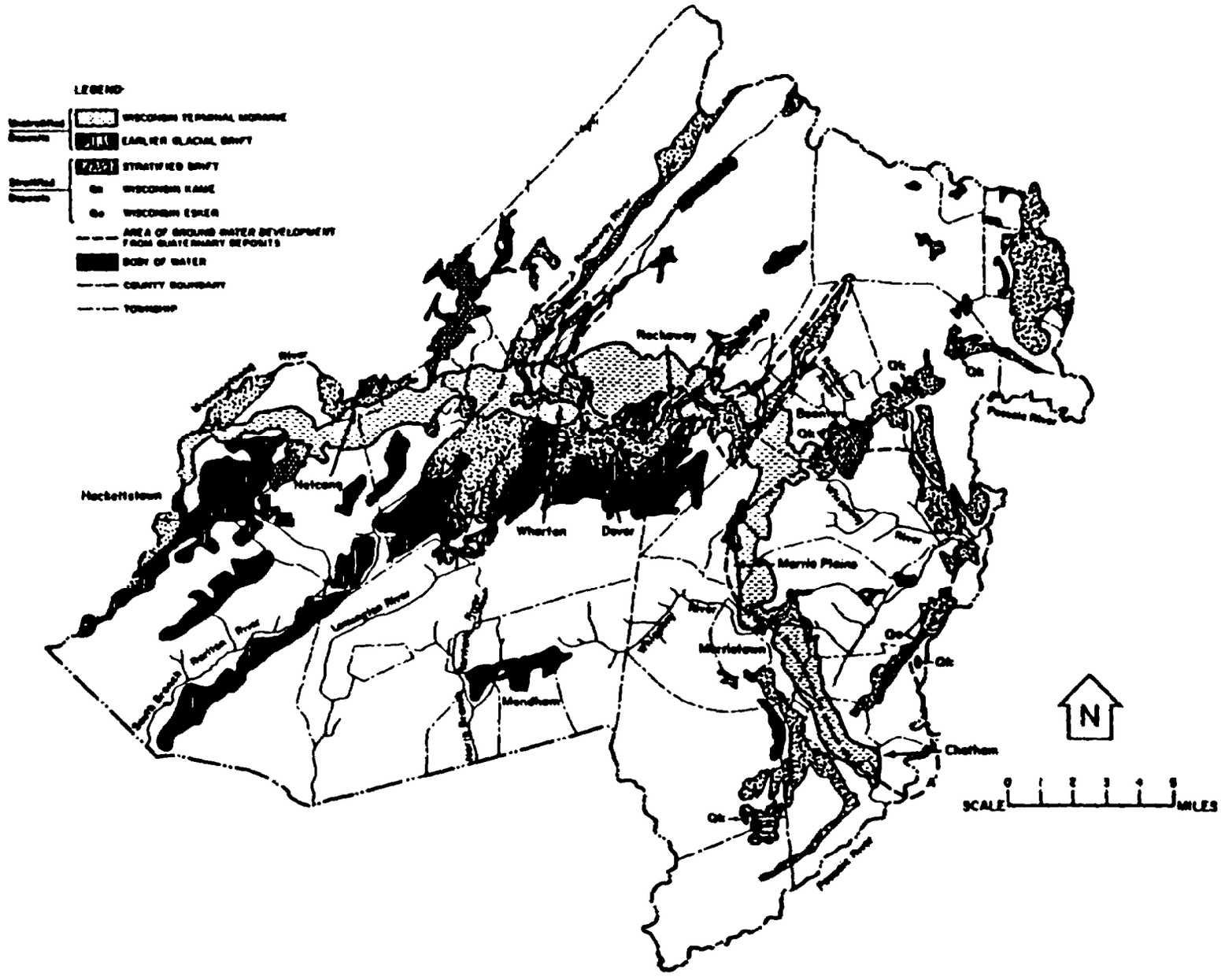

FIGURE VII-3 DETAILED QUATERNARY GEOLOGIC MAP OF MORRIS COUNTY (AFTER GILL AND VECCHIOLI, 1965)

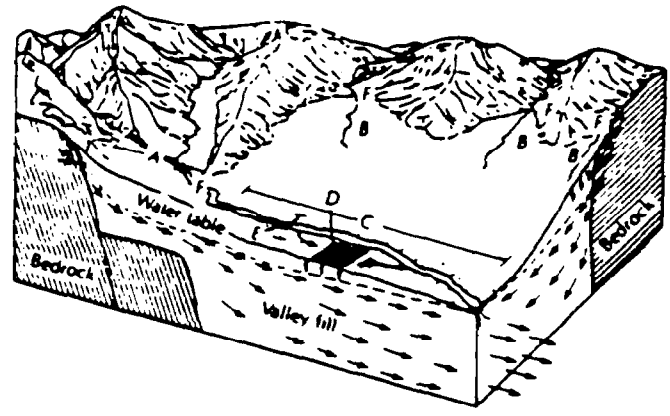

A) VALLEY IN BASIN AND RANGE AREA SHOWING THICK UNSATURATED ZONE OF COARSE SAND AND GRAVEL

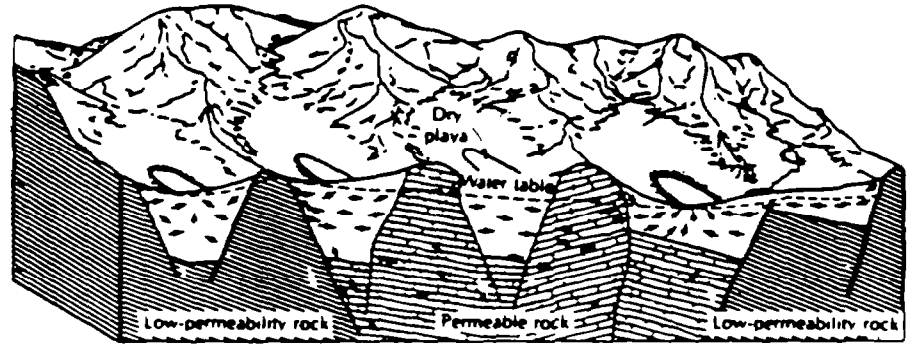

B) FAULTED BASINS WHICH CAN BE CLOSED. RECHARGE IS MOSTLY FROM RUNOFF IN MOUNTAINS NOT RAINFALL DIRECTLY ON VALLEY FLOOR

FIGURE VII-4 GENERALIZED CROSS-SECTIONS SHOWING FEATURES COMMON IN ARID WESTERN REGIONS OF THE UNITED STATES. REFERENCE: EAKIN, PRICE, HARRILL (1976)

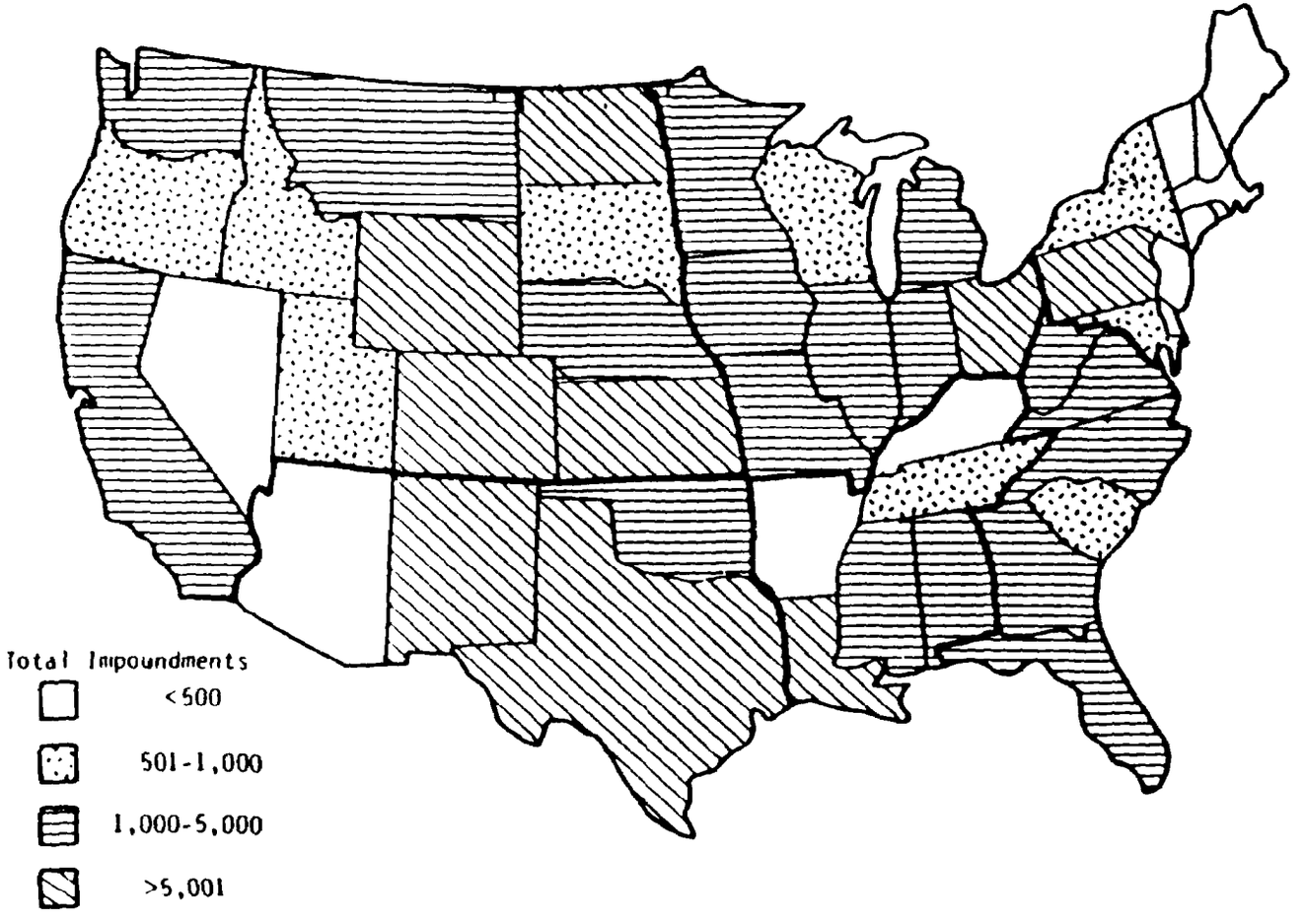

Figure VII-5 Number of Waste Impoundments by State (after U.S. EPA, 1979a)

discharge (slug), as a continuous discharge, or otherwise. This distinction does not have to be made in absolute terms but instead can be made relative to the time scale of the problem. For example, if waste had been discharged to a pond for a one-month period and the objective was to predict concentrations at a downgradient well five years later, the waste source could be considered to act as a slug discharge. Examples of how problems should be proposed (set-up) are given in Section 7.5.

7.1.6 Organization of This Chapter

The remaining sections describe the specific screening methods, how to estimate or obtain the necessary data, and how to interpret the results. Section 7.2, Aquifer Characterization, is intended as a reference section for those readers who may not be familiar with ground water terminology. Parameter nomenclature which may be encountered in the literature is explained, and typical values are provided. Information is also included on methods for estimating the parameters and for quantifying them either in the laboratory or in the field. Section 7.3, Ground Water Flow Regimes, describes detailed procedures for estimating seepage velocities and travel times for conservative constituents and includes example problems. Section 7.4, Pollutant Transport Processes, discusses the major physical and chemical transport processes. A practical approach is provided for estimating dispersion and diffusion. This section also discusses pollutant-soil interactions and the chemical and biological processes which are pertinent to subsurface problems. Methods are described for estimating the necessary rate coefficients and for incorporating them into the screening methods. Section 7.5, Methods for Predicting the Fate and Transport of Conventional and Toxic Pollutants, presents five different calculation methods. The methods predict migration of solutes from a contaminated aquifer to a well, from an injection well out into an aquifer, from the surface down to the water table, and from a one-time or continuous discharge downgradient in the saturated zone. For each method selected the following information is provided:

- Uses of the method
- Brief description of method and its theoretical basis
- Assumptions and simplifications required
- Types of input data needed
- Worked-out example problems
- Limitations of the method.

Finally, Section 7.6, Interpretation of Results, discusses reference criteria which may be of interest, and methods for estimating the uncertainty associated with the results. Guidelines are discussed for suggesting when more detailed analyses, including use of numerical simulation models, are warranted given the relative hazard, the uncertainty associated with the screening results, data availability, and time and budget constraints. Section 7.7, References, includes the references cited in the chapter and a list of additional material which may be helpful, particularly with respect to field sampling.

7.2 AQUIFER CHARACTERIZATION

This section is intended as a reference section for those users of the manual who may not be familiar with the parameters used in ground water investigations. It is anticipated that most readers will use this section only as needed to obtain a typical value for a given parameter or to review methods for measuring the parameters.

Before the transport of contaminants in ground water can be predicted, estimates of key properties of the porous media are needed. Section 7.2 discusses the definition and use of these parameters in the screening methods. The key parameters have been grouped into those characteristic of the porous media (Section 7.2.2), those used to estimate flow in the saturated zone (Section 7.2.3), and those used to estimate flow in the unsaturated zone (Section 7.2.4). Tables of average and typical values for a wide range of geologic formations have been included. The specific parameters are listed in Table VII-1. Additional parameters, also shown in this table, are discussed in Appendix I. The parameters given in Appendix I are not generally needed for the screening methods presented later in this chapter but may be encountered in the ground water literature. Methods for measuring the parameters in the field or laboratory or estimating them from other parameters are presented in Section 7.2.5. A discussion has also been included in this section on sample size and confidence levels.

7.2.1 Physical Properties of Water

For the vast majority of problems of interest, the concentration of dissolved solids in the ground water is so low that it does not affect the physics of fluid flow. Hence, the physical properties of the transport fluid such as density, viscosity, compressibility, etc. are assumed to be independent of the solute concentrations and to be equal to those of pure water. Situations where this assumption may not be true are when the solute concentrations are very high, (e.g., brackish aquifers or where large quantities of pure solute with a density different than water have been mixed with ground water (e.g., oil, gasoline)). The principal physical properties of water that are of interest in ground water flow are density, viscosity, and compressibility. In most situations these properties can be considered constant as shown below:

Compressibility of water at 1 atm and 4°C: 4.96×10^{-11} cm sec^2/g

Density of water at 1 atm and 4°C: 1.000 g/cm^3

Viscosity of water at 1 atm and 4°C: 0.01567 g/cm sec

Values for these properties as a function of temperature are included in Appendix I.

7.2.2 Physical Properties of Porous Media

The physical properties of porous media can be described by the relative state of its three phases or primary components. These are the solid, liquid, and gaseous phases. A schematic representation of a soil's three phases is given in Figure VII-6.

TABLE VII-1

AQUIFER PARAMETERS AND THEIR RELATIVE IMPORTANCE AS SCREENING PARAMETERS

Symbol	Parameter	Section Where Discussed	Relative Importance As A Screening Parameter	
			Low[a]	High[b]
ρ_w	density of water	I-1	X	
μ	viscosity of water	I-1	X	
β_w	compressibility of water	I-1	X	
ρ_s	particle density	I-1	X	
ρ_b	bulk density	7.2.2.1		X
d_e	particle-size distribution	7.2.2.2	X	
p	porosity	7.2.2.3		X
θ	water content	7.2.2.4		X
S_r	specific retention	I-1	X	
S_y	specific yield	I-1	X	
α_s	compressibility of soil	I-1	X	
S_s	specific storage	I-1	X	
S	storativity	I-1	X	
b, m	aquifer thickness	7.2.3.2		X
K, T	hydraulic conductivity and transmissivity:			
	saturated media	7.2.3.2		X
	unsaturated media	7.2.4.3		X
x, y, z	anistropy	7.2.3.2	X	
$\theta(\psi)$	soil-moisture characteristic curve	I-1	X	
θ-ψ	hysteresis	I-1	X	
h	water level elevation	7.3.2		X
Φ_g, ψ_g, H_g	gravitational potential	I-1	X	
Φ_p, ψ_p, H_p	pressure potential	I-1	X	
Φ_o, ψ_o, H_o	osmotic potential	I-1	X	
I	hydraulic gradient	7.3.1		X

[a]Parameter is not essential and/or its value can be easily obtained from tables given in Section 7.2 and Appendix I.

[b]Parameter is essential. Estimates or measurements of its value are used in the methods included in this chapter.

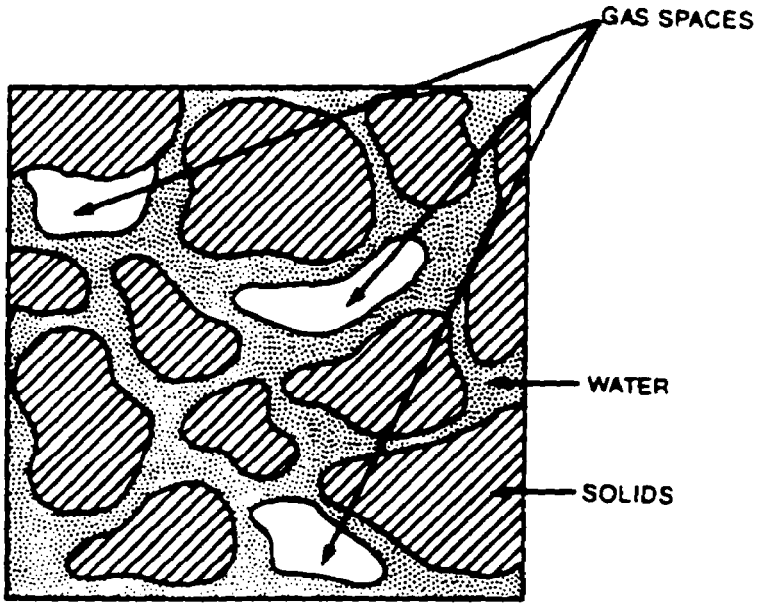

Figure VII-6 Schematic Showing the Solid, Liquid and Gaseous Phases in a Unit Volume of Soil

The solid phase is made up of soil particles that represent the granular skeleton of the aquifer.

A volume of soil V is equal to the sum of the volume of solids V_s, the volume of water V_w, and the volume of gas (vapor phase), V_g:

$$V = V_s + V_w + V_g \qquad \text{(VII-1)}$$

The volume of voids or pores V_v in a soil is defined as the sum of the water and gas volumes:

$$V_v = V_w + V_g \qquad \text{(VII-2)}$$

hence

$$V = V_s + V_v \qquad \text{(VII-3)}$$

The total mass M of these three phases in a volume of soil is the sum of the mass of solids M_s, the mass of water M_w, and the mass of gas M_g (which is negligible):

$$M = M_s + M_w + M_g \qquad \text{(VII-4)}$$

The quantitative relationship between the three phases can be characterized by such variables as the bulk density of the soil, the particle-size distribution and the porosity or water content.

7.2.2.1 Bulk Density

Bulk density is used in describing the phenomenon of sorption and retardation in contaminant transport equations (see Section 7.4.2.1.1). The dry bulk density of a soil $\rho_b(g/cm^3)$ is defined as the mass of a dry soil $M_s(g)$ divided by its bulk or total volume $V(cm^3)$:

$$\rho_b = M_s/V \qquad \text{(VII-5)}$$

The bulk density is affected by the structure of the soil (e.g., its looseness or degree of compaction) as well as its swelling and shrinkage characteristics which are dependent upon its wetness. Loose, porous soils will have low values of bulk density and more compact soils will have higher values. Bulk density values normally range from 1 to 2 g/cm^3. Soils with high organic matter content will generally have lower bulk density values. Very compact subsoils, regardless of texture, may have bulk densities higher than 2 g/cm^3. Moreover, there is a general tendency for the bulk density to increase with depth. The range and mean value of bulk density for various geologic materials are given in Table VII-2.

7.2.2.2 Particle-Size Distribution

Soil type can be used to estimate porosity, hydraulic conductivity, and specific surface area available for sorption. The texture of a soil is usually determined by the relative proportions (by dry weight) of sand, silt and clay present in the soil. A soil-texture trilinear diagram is then used to determine the soil class (Figure VII-7). Alternatively, soil classification can be characterized on the basis of particle or grain-size distribution. Particle-size distribution curves (Figure VII-8) are obtained by plotting the cumulative percentage (by dry weight) of soil particles in a soil as a function of their particle size. Table VII-3 lists the range of particle sizes for various soil classifications.

An effective particle size, d_e, is defined as the grain diameter for which "e" percent of the particles (by dry weight) is equal or smaller in diameter. Normally "e" is set to 10 percent for Hazen's effective grain size d_{10} but d_{20} will often be used to characterize coarse materials. Hence, if d_{10} = 0.6mm (uniform, coarse sand), then 10% of the soil particles of this material (by dry weight) will have a grain diameter less than or equal to 0.6mm. A list of d_{10} effective grain sizes is given for

TABLE VII-2

RANGE AND MEAN VALUES OF DRY BULK DENSITY

Material	Range (g/cm^3)	Mean (g/cm^3)
clay	1.18 - 1.72	1.49
silt	1.01 - 1.79	1.38
sand, fine	1.13 - 1.99	1.55
sand, medium	1.27 - 1.93	1.69
sand, coarse	1.42 - 1.94	1.73
gravel, fine	1.60 - 1.99	1.76
gravel, medium	1.47 - 2.09	1.85
gravel, coarse	1.69 - 2.08	1.93
loess	1.25 - 1.62	1.45
eolian sand	1.33 - 1.70	1.58
till, predominantly silt	1.61 - 1.91	1.78
till, predominantly sand	1.69 - 2.12	1.88
till, predominantly gravel	1.72 - 2.12	1.91
glacial drift, predominantly silt	1.11 - 1.66	1.38
glacial drift, predominantly sand	1.36 - 1.83	1.55
glacial drift, predominantly gravel	1.47 - 1.78	1.60
sandstone, fine grained	1.34 - 2.32	1.76
sandstone, medium grained	1.50 - 1.86	1.68
siltstone	1.35 - 2.12	1.61
claystone	1.37 - 1.60	1.51
shale	2.20 - 2.72	2.53
limestone	1.21 - 2.69	1.94
dolomite	1.83 - 2.20	2.02
granite, weathered	1.21 - 1.78	1.50
gabbro, weathered	1.67 - 1.77	1.73
basalt	1.99 - 2.89	2.53
schist	1.42 - 2.69	1.76

Reference: Morris and Johnson (1967).

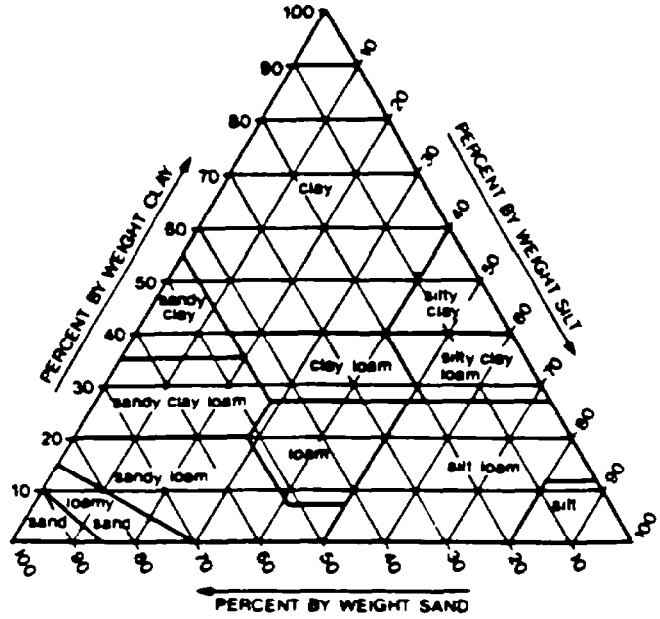

Figure VII-7 Soil Texture Trilinear Diagram Showing Basic Soil Textural Classes. Reference: Hillel (1971)

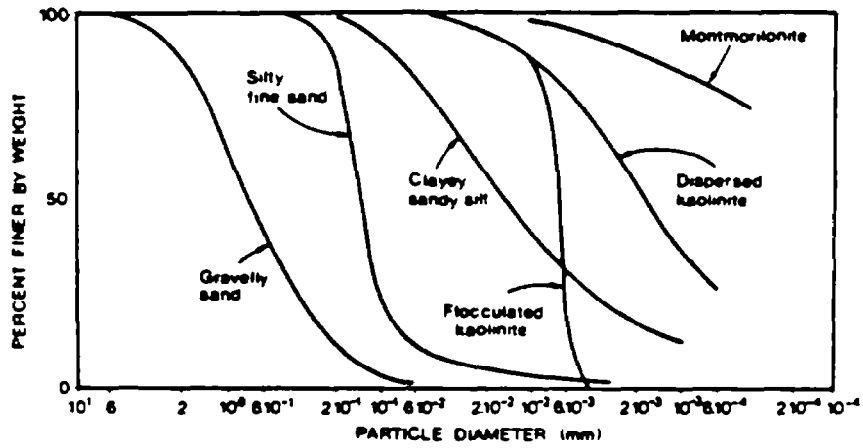

Figure VII-8 Typical Particle-size Distribution Curves for Various Soil Classifications. Reference: Bear (1972)

TABLE VII-3

EFFECTIVE GRAIN SIZE AND THE RANGE OF SOIL PARTICLE SIZES FOR VARIOUS MATERIALS

Material	Effective Grain Size d_{20}(mm)	d_{10}(mm)	Particle Size (mm)
colloidal clay	—	40Å*	10Å-.01
clay (30 to 50% clay sizes)	—	.0003	.0005-.05
silty clay	—	.0015	.001-.05
sandy clay	--	.002	.001-1
uniform silt	--	.006	.005-.05
silty sand	--	.01	.005-2
well-graded, silty sand and gravel	--	.02	.01-5
uniform, fine sand	--	.06	.05-.25
clean, well-graded sand and gravel	--	.1	.05-10
uniform, medium sand	--	.3	.25-.5
uniform, coarse sand	--	.6	.5-2
very coarse, clean, uniform sand	1.5	--	.8-3
fine uniform gravel	3	--	1.5-8
clean, fine to coarse gravel	13	--	10-80
one man stone	150	--	100-300
derrick stone	1200	--	900-3000

*A = angstrom = 1 x 10^{-8} cm.

Reference: Hough (1957).

various materials in Table VII-3. The d_{10} value can be used to predict intrinsic permeability, as shown in Section 7.2.5.2.1.

7.2.2.3 Porosity

Porosity is an important screening parameter in saturated aquifers used in computing the velocity of contaminants in the ground water (seepage velocity, Section 7.3.3.1.2) and the sorption and retardation of contaminants (see Section 7.4.2.1.1). Soil porosity "p" (unitless) is defined as the void or pore volume $V_v(cm^3)$ of the soil divided by the bulk volume $V(cm^3)$ of the soil:

$$p = V_v / V \qquad \text{(VII-6)}$$

The porosity is expressed as either a decimal fraction or as a percent. The void volume of a soil is defined in Equation VII-2 as the sum of the gas and water filled voids or interstices. Typical values of porosity for various geologic materials are given in Table VII-4.

The term effective porosity p_e (unitless) is sometimes used but its meaning depends upon its usage. It can equal the specific yield of a water-table aquifer which is defined as the volume of water obtained under a unit drop in head from a unit area of the aquifer. Alternatively, it can refer to that portion of the porous medium through which flow actually takes place. The last definition is important when the porous matrix includes a large number of dead-end pores and hence part of the fluid in the pore space is immobile (or practically so). In either definition, the effective porosity is always less than or equal to the total porosity ($p_e \leq p$). The porosity of consolidated materials depends mainly on the degree of cementation of the grains. The porosity of unconsolidated materials depends on the packing of the grains, their shape, arrangement and size distribution.

7.2.2.4 Water Content

Water content in the unsaturated zone is in some ways analagous to porosity in the saturated zone of an aquifer. The water content is used in the computation of seepage velocity and the sorption and retardation of contaminants. The water or moisture content of a soil is the amount of water in a given amount of soil. It is a dimensionless quantity and can be expressed on either a gravimetric (mass) or a volumetric (volume) basis. The gravimetric water content θ_g (unitless) is defined as the mass of water M_w (g) divided by the dry mass of the soil M_s (g) (oven dried at 105-110°C):

$$\theta_g = M_w / M_s \qquad \text{(VII-7)}$$

The volumetric water content (unitless) is defined as the volume of water V_w (cm^3) divided by the volume of the soil V (cm^3):

$$\theta = V_w / V \qquad \text{(VII-8)}$$

These two expressions for water content are related as follows:

$$\theta = \theta_g \rho_b / \rho_w \qquad \text{(VII-9)}$$

where ρ_b(g/cm^3) is the dry bulk density of the soil and ρ_w(g/cm^3) is the density of water. The ratio ρ_b/ρ_w is often called the apparent specific gravity of the soil (unitless). Values for ρ_b can be found in Table VII-2 for different geologic materials.

TABLE VII-4

RANGE AND MEAN VALUES OF POROSITY

Material	Range (percent)	Mean (percent)
clay	34.2 - 56.9	42
silt	33.9 - 61.1	46
sand, fine	26.0 - 53.3	43
sand, medium	28.5 - 48.9	39
sand, coarse	30.9 - 46.4	39
gravel, fine	25.1 - 38.5	34
gravel, medium	23.7 - 44.1	32
gravel, coarse	23.8 - 36.5	28
loess	44.0 - 57.2	49
eolian sand (dune sand)	39.9 - 50.7	45
till, predominantly silt	29.5 - 40.6	34
till, predominantly sand	22.1 - 36.7	31
till, predominantly gravel	22.1 - 30.3	26
glacial drift, predominantly silt	38.4 - 59.3	49
glacial drift, predominantly sand	36.2 - 47.6	44
glacial drift, predominantly gravel	34.6 - 41.5	39
sandstone fine grained	13.7 - 49.3	33
sandstone, medium grained	29.7 - 43.6	37
siltstone	21.2 - 41.0	35
claystone	41.2 - 45.2	43
shale	1.4 - 9.7	6
limestone	6.6 - 55.7	30
dolomite	19.1 - 32.7	26
granite, weathered	34.3 - 56.6	45
gabbro, weathered	41.7 - 45.0	43
basalt	3.0 - 35.0	17
schist	4.4 - 49.3	38

Reference: Morris and Johnson (1967).

In general, at saturation the volumetric water content θ_{sat} equals the porosity (i.e., $\theta_{sat} = \rho$). For unsaturated conditions, θ is always less than the porosity. However, for swelling, clayey soils, the volume of water at saturation can exceed the porosity of the dry soil.

The volumetric water content is the most used and probably the most convenient method of expressing water content. It is more directly adaptable to the computation of fluxes and water quantities added or subtracted by seepage through ponds and landfills, irrigation or evaporation.

7.2.3 Flow Properties of Saturated Porous Media

Saturation of a porous medium means that all of the soil voids or pores are filled with water. Complete saturation, however, is not always possible since some gas may be trapped between soil particles.

In an unconfined aquifer the upper surface of the saturated zone is open to the soil atmosphere. This surface is called the water table or phreatic surface. In a well penetrating an unconfined aquifer, the water will rise only to the level of the water table (i.e., when the ground water flow is predominately horizontal). A schematic of an unconfined aquifer is shown in Figure VII-9. Changes in the level of water in such a well result primarily from changes in the volume of water in storage.

In a confined aquifer, the saturated zone is underlain and overlain by relatively impermeable strata. The ground water in a confined aquifer is under a pressure greater than atmospheric. In a well penetrating a confined aquifer, the water may rise above the bottom of the overlying confining stratum. The water level is called the piezometric or potentiometric surface. A schematic of a confined aquifer is also shown in Figure VII-9. Changes in the level of water in such a well result primarily from changes in pressure rather than from changes in storage volumes. If the piezometric surface lies above the ground, a flowing well will result. In a leaky or semiconfined aquifer, the saturated zone is underlain or overlain by a semipervious stratum.

In order to describe flow through saturated porous media, the hydraulic conductivity (or transmissivity) and storativity of the medium must be characterized.

7.2.3.1 Saturated Hydraulic Conductivity

Hydraulic conductivity K (cm/sec) expresses the ease with which a fluid can be transported through a porous medium. Hydraulic conductivity is an imporant parameter used in computing seepage velocity. It is also one of the most difficult parameters to measure accurately and is relatively expensive to obtain. Usually "point" values are measured but large variations can occur within short distances, even in apparently uniform geologic formations. It is a function of properties of both the porous medium and the fluid. The range of values for saturated hydraulic conductivity and intrinsic permeability are given in Table VII-5 for various geologic materials.

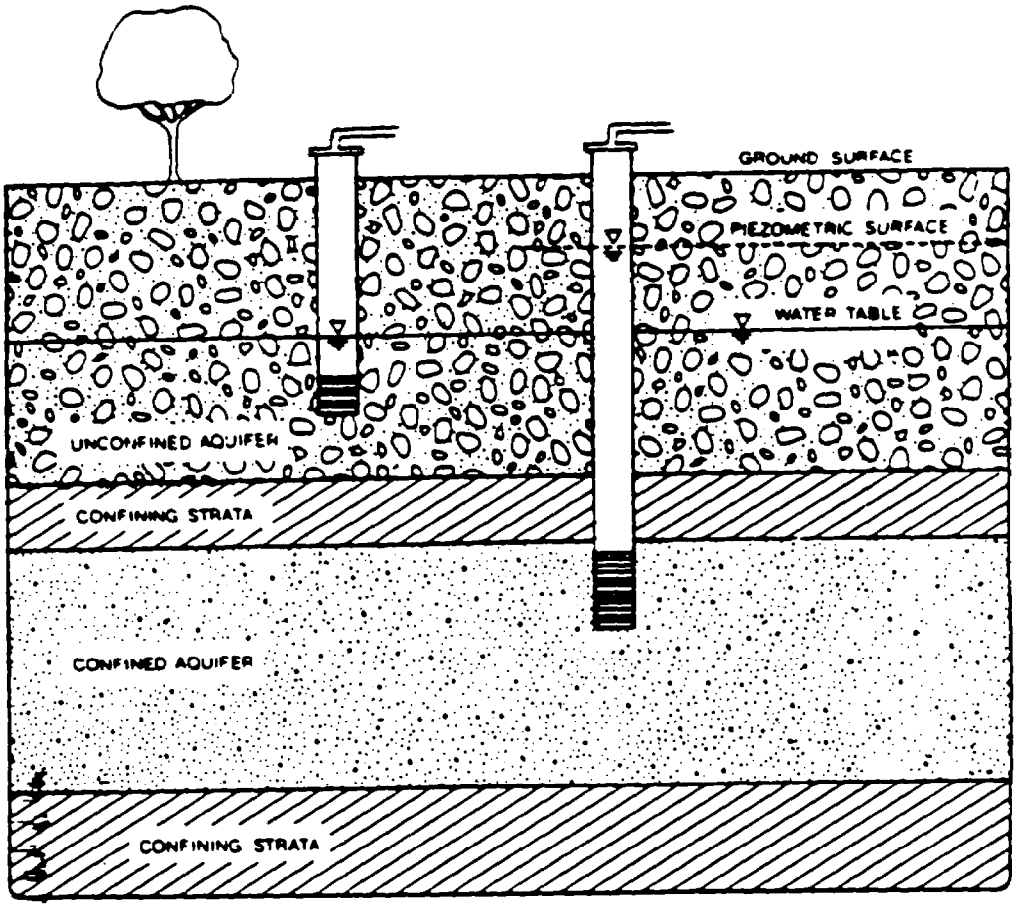

FIGURE VII-9 SCHEMATIC CROSS SECTION SHOWING BOTH A CONFINED AND AN UNCONFINED AQUIFER

These properties can ideally be separated by expressing hydraulic conductivity as follows:

$$K = K_i g \rho_w / \mu \qquad \text{(VII-10)}$$

where K_i is the intrinsic permeability (cm^2), g is the gravitational acceleration (980.7 cm/sec^2), ρ_w is the density of water (g/cm^3) and μ is the viscosity of water (g/cm sec). Values of ρ_w and μ are given in Table I-1 in Appendix I. The intrinsic permeability is only a function of porous medium properties such as the particle-size distribution, grain or pore shape, and tortuosity. However, the expression in Equation VII-10 for saturated hydraulic conductivity assumes that the water and solid matrix of the soil do not interact in such a way as to change the properties of either. In most soils there is no matrix-water interaction. In addition, the intrinsic permeability may vary with time as a result of chemical, physical and biological processes. These may include structural and textural changes

TABLE VII-5

TYPICAL VALUES OF SATURATED HYDRAULIC CONDUCTIVITY AND INTRINSIC PERMEABILITY

Material	Hydraulic Conductivity[a] K(cm/sec)	Intrinsic Permeability[a] K_i(cm^2)
clean gravel	.1 - 100	10^{-6} - 10^{-3}
clean sand	10^{-4} - 1	10^{-9} - 10^{-5}
silty sand	10^{-5} - .1	10^{-10} - 10^{-6}
silt, loess	10^{-7} - 10^{-3}	10^{-12} - 10^{-8}
stratified clay[b]	10^{-7} - 10^{-4}	10^{-12} - 10^{-9}
glacial till	10^{-10} - 10^{-4}	10^{-15} - 10^{-9}
unweathered, marine clay	10^{-11} - 10^{-7}	10^{-16} - 10^{-12}
karst limestone	10^{-4} - 1	10^{-9} - 10^{-5}
permeable basalt	10^{-5} - 1	10^{-10} - 10^{-5}
fractured igneous and metamorphic rocks	10^{-6} - 10^{-2}	10^{-11} - 10^{-7}
limestone and dolomite	10^{-7} - 10^{-4}	10^{-12} - 10^{-9}
sandstone	10^{-8} - 10^{-4}	10^{-13} - 10^{-9}
shale	10^{-11} - 10^{-7}	10^{-16} - 10^{-12}
breccia, granite[b]	10^{-11} - 10^{-9}	10^{-16} - 10^{-14}
unfractured metamorphic and igneous rocks	10^{-12} - 10^{-8}	10^{-17} - 10^{-13}

[a] Reference: Freeze and Cherry (1979).

[b] Reference: Bear (1972).

due to subsidence and consolidation, the development of solution channels, clay swelling, and clogging due to biological growth and by precipitates carried by the water.

If the aquifer properties (e.g., hydraulic conductivity) are independent of position within a geologic formation, the formation is called homogeneous. If the properties are dependent on position within a geologic formation, the formation is called heterogeneous. Heterogeneity is caused by the presence of interlayered deposits, faults, or other large-scale stratigraphic features (such as overburden-bedrock contacts), large scale changes in the sedimentary formations (particularly those which are part of deltas, alluvial fans, and glacial outwash plains) and small-scale layering in an otherwise homogeneous formation.

If hydraulic conductivity is independent of the direction of measurement in a geologic formation, the formation is called isotropic. If the hydraulic conductivity varies with the direction of measurement, the formation is called anisotropic. The primary cause of anisotropy on a small scale is the orientation of clay minerals in sedimentary rocks and unconsolidated sediments. Anisotropy of consolidated geologic materials is governed by the orientation of layers, fractures, solution openings or other structural conditions which may not have a horizontal alignment. Fractured rocks can also be anisotropic because of directional variation in joint aperture and spacing.

The horizontal saturated hydraulic conductivity K_h (cm/sec) in some materials (e.g., alluvium) is normally greater than the vertical conductivity K_v (cm/sec); hence $K_h/K_v \geq 1$. Ratios of K_h/K_v usually fall in the range of 2 to 10 for alluvium and glacial outwash (Weeks, 1969) and 1.5 to 3 for sandstone (Piersol et al., 1940) but it is not uncommon to have values of 100 or more occur where clay layers are present (Morris and Johnson, 1967).

7.2.3.2 Transmissivity

The transmissivity or coefficient of transmissibility T (cm^2/sec) is defined as:

$$T = Kb \qquad \text{(VII-11)}$$

where K is the saturated hydraulic conductivity (cm/sec) and b is the aquifer thickness (cm). Transmissivity has traditionally been expressed in units of gal/(ft day) but this can be converted to the cgs units of cm^2/sec by multiplying the gal/(ft day) by 1.438×10^{-3}. Thus:

$$1 \text{ gal/(ft day)} = 1.438 \times 10^{-3} \text{ cm}^2\text{/sec} \qquad \text{(VII-12)}$$

Transmissivity can be estimated by multiplying the saturated hydraulic conductivity K(cm/sec) given for various geologic materials in Table VII-5 by the aquifer thickness b(cm). Because pumping tests can provide values for transmissivity, this type of data may be more available than saturated hydraulic conductivity.

7.2.3.3 Storativity

Storativity or storage coefficient, S, is defined as the volume of water that is released from storage per unit horizontal area of aquifer per unit decline of hydraulic head. It is a dimensionless quantity. This parameter is obtained in addition to transmissivity from pumping tests. It is used to compute aquifer yields and to compute drawdowns of individual wells.

For confined aquifers, storativity is due to water being released from the compression of the granular skeleton and expansion of the pore water. S is

mathematically defined as the product of the specific storage, S_s (cm^{-1}) and the aquifer thickness, b(cm): $S = S_s b$.

The value of the storativity for confined aquifers is generally small, falling between the range of .00005 to .005 (Todd, 1980). Hence, large pressure changes over an extensive area of aquifer are required before substantial water is released.

7.2.4 Flow Properties of Unsaturated Porous Media

The term unsaturated means that the voids or pores of a porous medium are only partially filled with water. Under these conditions, the pressure within a soil pore becomes less than atmospheric because water is under surface-tension forces. These surface-tension forces increase as the water content decreases. Hence, the flow properties of a porous medium (such as hydraulic conductivity) are functionally dependent on the water content. These functional relationships are a characteristic of the particular porous medium.

7.2.4.1 Soil-Water Energy

To describe the movement and behavior of ground water, the relative energy state of the soil water must be known. This is necessary because flow will occur in the direction of decreasing energy and the soil water tends to equilibrate with its surroundings. As stated above, the relative amount of energy contained in the soil water is important and not the absolute amount of energy (i.e., relative to a standard reference state). Generally, the standard state is defined as a hypothetical reservoir of free water at atmospheric pressure, at the same temperature as that of the soil water, and at a given and constant elevation.

The total energy E of the soil water is equal to the sum of its kinetic E_k and potential E_{pot} energies:

$$E = E_k + E_{pot} \qquad \text{(VII-13)}$$

Kinetic energy E_k is that energy which the soil water has by virtue of its motion. However, under most typical ground water situations, the kinetic energy will be negligible compared to potential energy by virtue of the low velocities generally encountered in subsurface flow.

Potential energy is that energy which soil water has by virtue of its position. Technically the potential energy of soil water is the amount of work that must be done per unit quantity of pure water in order to transport reversibly and isothermally an infinitesimal quantity of water from a pool of pure water at a specified elevation at atmospheric pressure to the soil water at the point under consideration.

The potential energy, E_{pot}, of soil water can be separated into at least three components: gravitational, E_g; pressure, E_p; and osmotic, E_o. The total potential energy is the sum of these three:

$$E_{pot} = E_g + E_p + E_o \qquad \text{(VII-14)}$$

The three components of the potential energy are considered below.

7.2.4.1.1 Gravitational Potential

Gravitational potential energy is the potential for work resulting from the force of gravity acting on a quantity of pure water located at some point in space that is vertically different from a reference point. The strength of this potential energy E_g(erg) depends on the strength of the gravitational force g(cm/sec^2), the density of water ρ_w(g/cm^3) and the vertical elevation of the water from a reference point z(cm). Hence, the gravitational potential energy acting on a volume V_w(cm^3) of water is mathematically defined as:

$$E_g = \rho_w g V_w z \qquad \text{(VII-15)}$$

This potential energy is a positive quantity if the unit volume of soil water is located above the reference level and negative if located below.

7.2.4.1.2 Pressure Potential

Pressure potential energy E_p (erg) is that potential energy due to the pressure of the surrounding fluid acting on it. Mathematically, this can be represented as follows for the case of constant density ρ_w(g/cm^3):

$$E_p = PM_w/\rho_w = PV_w \qquad \text{(VII-16)}$$

where P is the relative or gage pressure (dyne/cm^2) acting on a unit volume V_w(cm^3) or unit mass M_w (g) of soil water.

Note that P is the relative or gage pressure and not the absolute pressure. Hence:

$$P = p_w - p_o \qquad \text{(VII-17)}$$

where p_w is the absolute pressure at the point under consideration and p_o is the absolute pressure at the reference elevation (usually taken to be atmospheric pressure). Thus, pressure potential is a positive quantity under a free-water surface

(saturated zone), a zero potential at the water surface and a negative pressure potential in the unsaturated zone.

In the saturated zone, the pressure potential is a direct result of the weight of overlying water. Hence, the pressure potential at any point in the system is determined by the depth that the point lies below the water table. The relative pressure P (dyne/cm^2) can thus be expressed as:

$$P = \rho_w g h \qquad \text{(VII-18)}$$

where h (cm) is the depth below the water table. The pressure potential is measured in the field with a piezometer. In a confined aquifer, the piezometer head h is measured as the distance between the point under consideration and the free water level in the piezometer.

In the unsaturated zone, the pressure potential is a negative quantity and is often given a special symbol such as ψ and a special name such as the matric potential, capillary potential, matric suction or tension. By convention, suction and tension are considered positive quantities, hence:

ψ = matric potential = - matric suction

Under unsaturated conditions, the pressure potential of soil water results from forces attributable to the soil matrix, such as absorption and capillarity (see Figure VII-10). These forces attract and bind water to the soil by the processes of surface tension, molecular attraction and ion exchange. The net effect of these processes is to reduce the free energy of the soil water in comparison to that of pure, bulk water.

Typical values of pressure potential are given below.

Moisture Level	Pressure Potential* Per Unit Volume (bars)
saturated: confined	greater than 0
saturated: unconfined (at free water surface)	0
field capacity	-.1 to -.2
wilting coefficient	-15
hygroscopic coefficient	-31
molecular bound water to soil solids	-10,000

*1 bar = 0.987 atmosphere

Reference: Brady (1974).

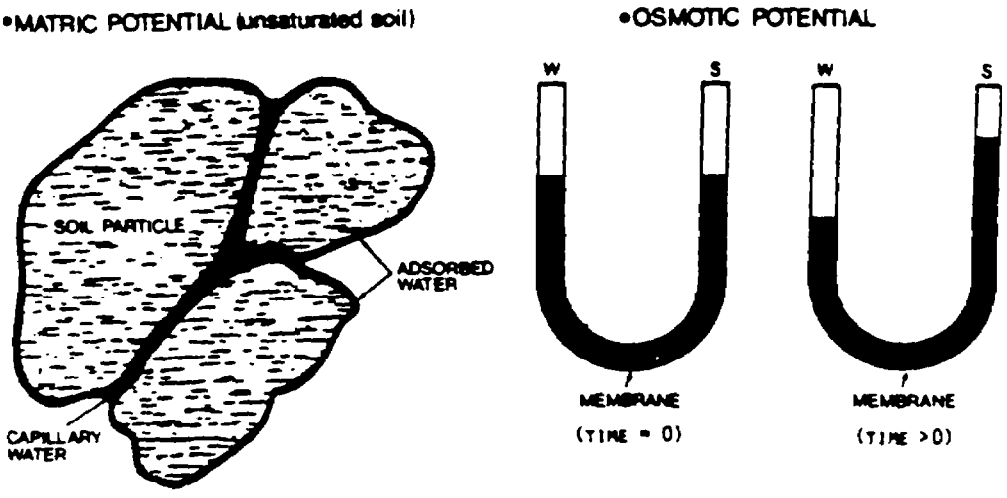

FIGURE VII-10 SCHEMATIC OF MATRIC AND OSMOTIC SOIL-WATER POTENTIAL. REFERENCE: BRADY (1974)

Note that plants cannot obtain water from soil at pressure potentials less than the wilting coefficient and water will not move in liquid form below the hygroscopic coefficient level.

7.2.4.1.3 Osmotic Potential

Osmotic potential energy is that potential energy attributed to the attraction of solutes for water. Attractive forces arising from the polar nature of water tend to orient water around ions. Hence, osmotic potential refers to the work required to pull water away from these attracted ions.

In the absence of a semipermeable membrane, soluble ions will diffuse into a soil solution until the ions are uniformly distributed. With the presence of a semipermeable membrane between two solutions, water molecules will move through the membrane to the side with the higher solute concentration (see Figure VII-10). Water will continue to pass through such a membrane until the hydrostatic pressure difference between the two sides balances the effect of the ion-water attraction forces. Hence, one can measure the osmotic potential of the solute solution by measuring the hydrostatic pressure difference across the membrane. The osmotic potential is a negative quantity because the presence of solutes lowers the vapor pressure and free energy of the soil water and hence lowers the potential energy.

Clays can act as a leaky semipermeable membrane, allowing water to pass more easily than salts. This is sometimes referred to as salt sieving (Nye and Tinker, 1977). Thus in sedimentary basins, osmosis can cause significant pressure differentials across clayey strata (Freeze and Cherry, 1979). The osmotic potential

can also be important in saline soils of arid and semiarid regions (Brady, 1974). In addition, the osmotic potential is important to the uptake of water by plant roots and the movement of water vapor. Both the soil-root and water-gas interfaces act as semipermeable membranes. Except for the above cases, however, the contribution of osmotic potential to the mass movement of water is negligible in most soil systems.

7.2.4.2 Soil-Moisture Characteristic Curves

Consider a sample of soil that is maintained at saturation and is exposed to atmospheric pressure. By definition, the pressure potential of the soil water in this soil sample would be zero. Now consider the case of applying a slight suction or subatmospheric pressure across the soil sample. No water will flow out until a certain critical suction (called the air-entry suction) is reached. At this point, the largest soil pores start to empty. As the suction is further increased, additional water flows as progressively smaller pores empty. Finally, at very high suctions, only the micropores remain filled. As the soil becomes increasingly dry, a nearly exponential increase in suction is required to remove additional water.

The functional relationship between the moisture content and matric or suction potential is a characteristic of a particular soil. This relationship is called the soil-moisture characteristic curve, the soil-moisture retention curve or simply the characteristic curve. The soil-moisture characteristic curves for three different textured soils are shown in Figure VII-11. As previously stated, the absolute value of the matric or suction potential increases as the moisture content decreases. In addition for a given matric potential, a coarse soil (e.g., sand) generally has less water remaining in the soil and has a steeper slope to the curve than a fine soil (e.g., clay). The slope of the soil-moisture characteristic curve (i.e., the change of water content per unit change of matric potential) is called the specific water capacity.

In a coarse, saturated soil, the pores are predominately large and drain quickly under a slight suction. A high suction is required to remove the last water from the remaining, small pores. In a clayey soil, the pore-size distribution is more uniform, so that a more gradual decrease in water content occurs with an increase in suction. In addition, at low suctions (for example, between 0 and 1000 cm H_2O) the amount of water remaining in a soil depends primarily on soil structure (i.e., pore-size distribution and particle aggregation). At higher suctions, however, water retention is due increasingly to adsorption and thus is influenced more by the particle-size distribution and specific surface of a soil.

Unfortunately, the water content and matric potential are not always uniquely related to each other because of hysteresis. Hysteresis means that the characteristic curves are different, depending on whether the soil is being wetted or dried. The characteristic curve during a drying cycle is called the drying, desorption or drainage

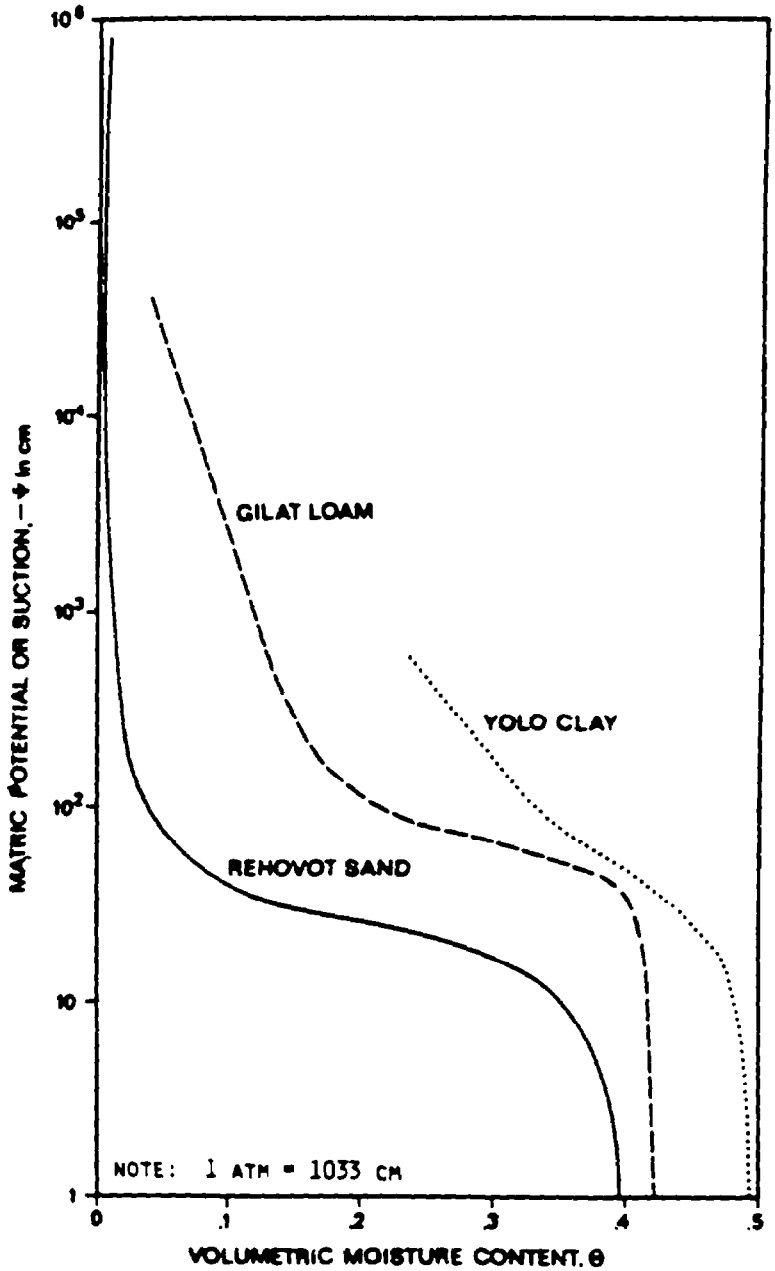

FIGURE VII-11 CHARACTERISTIC CURVES OF MOISTURE CONTENT AS A FUNCTION OF MATRIC POTENTIAL FOR THREE DIFFERENT SOILS. REFERENCE: BRAESTER (1972)

curve; during wetting it is called the wetting, sorption or imbition curve. A soil which is partially wetted, then dried or vice versa will follow an intermediate characteristic curve called a scanning curve, which lies between the envelope formed by the wetting and drying curves.

Figure VII-12 shows an example of hysteresis in a sandy soil. The hysteresis effect may be attributed to the inkbottle effect (geometric nonuniformity of individual pores), the contact-angle or rain drop effect (differences in the contact angle for advancing and receding fluids), entrapped air, and changes in soil structure (e.g., swelling, shrinking or aging phenomena) caused during the wetting or drying of a soil.

7.2.4.3 Unsaturated Hydraulic Conductivity

In Section 7.2.3.1, the saturated hydraulic conductivity was stated to be affected by an intrinsic property of the solid matrix of a soil and by fluid properties. For unsaturated porous media, the hydraulic conductivity is also a function of the energy state of the soil water (i.e., the water content or pressure potential).

The hydraulic conductivity of three different soils is shown in Figure VII-13 as a function of moisture content. The hydraulic conductivity decreases exponentially as the moisture content decreases. The large pores of a porous media are the most conductive, their relative conductivity being proportional to the square of the pore diameter and their volumetric discharge rate being proportional to the fourth power of the pore diameter. As a soil dries out, the large pores empty first, forcing flow to be conducted through a diminishing cross-sectional area.

Since the moisture content is related to the matric or suction potential, through the soil-moisture characteristic curve (see Section 7.2.4.2), the hydraulic conductivity can be expressed as a function of either the moisture content, $K(\theta)$, or of the matric potential, $K(\psi)$. Just as with moisture and pressure, hydraulic conductivity is also not a single valued function. Figure VII-12 showed hysteresis in the hydraulic conductivity of a sandy soil. At a given suction, the hydraulic conductivity is generally lower in a wetting soil than in a drying soil. This is because the wetting soil contains less water than the drying one (for a given suction).

7.2.5 Data Aquisition or Estimation

In Sections 7.2.2 to 7.2.4, the physical and flow properties of porous media were discussed in detail. Tables were included to show what values are typically found in aquifers of various geologic materials. In this section, laboratory and field methods are briefly discussed to show how the properties of a particular aquifer or porous medium can be estimated or measured. Finally, in Section 7.2.5.4 the effect of sample size on measurement precision is discussed from a statistical point of view.

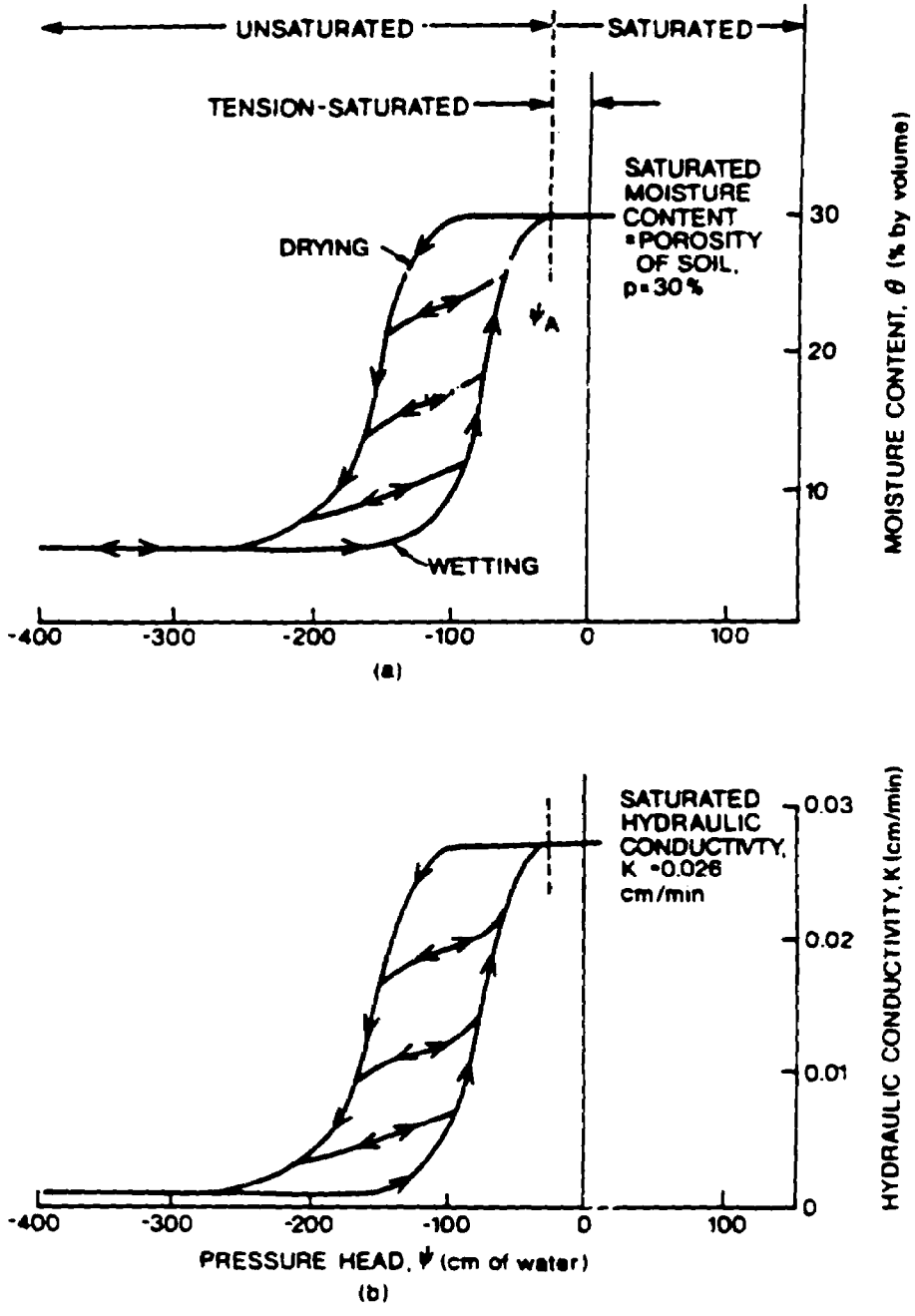

FIGURE VII-12 CHARACTERISTIC CURVES OF (A) MOISTURE CONTENT AND (B) HYDRAULIC CONDUCTIVITY AS A HYSTERETIC FUNCTION OF MATRIC POTENTIAL FOR A NATURALLY OCCURRING SANDY SOIL. REFERENCE: FREEZE AND CHERRY (1979)

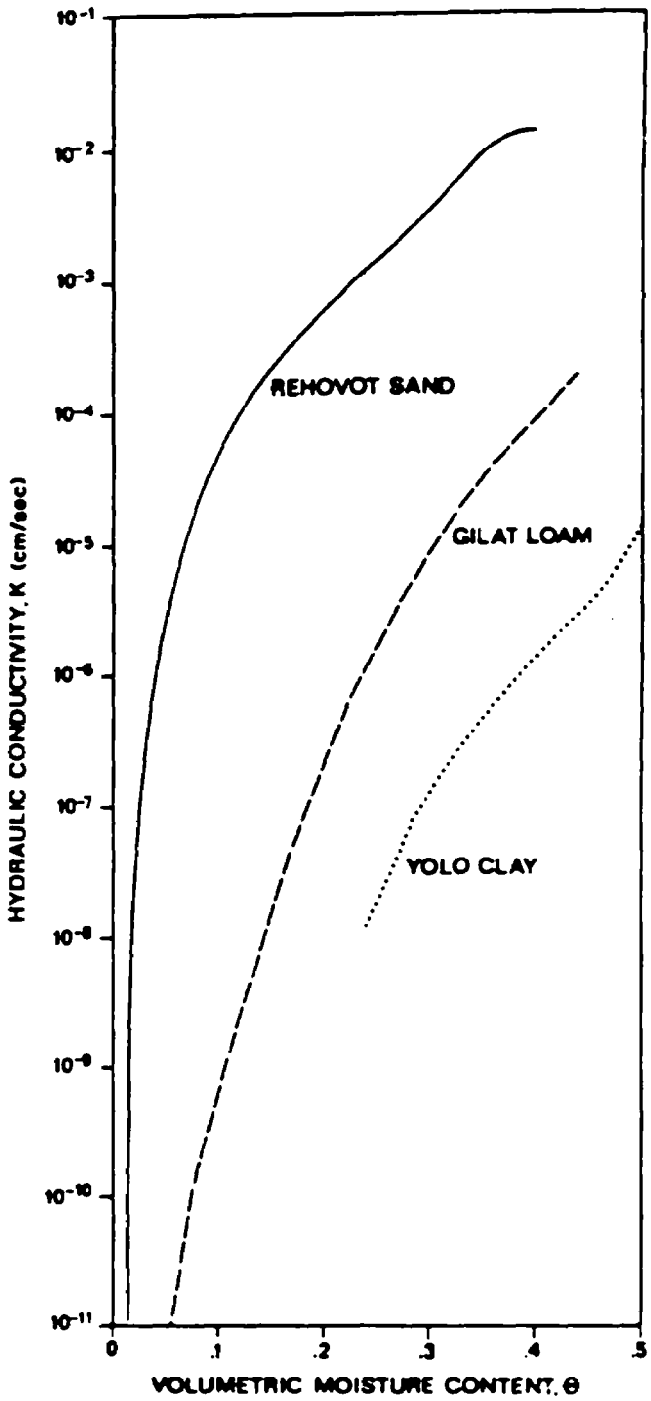

FIGURE VII-13 HYDRAULIC CONDUCTIVITY AS A FUNCTION OF MOISTURE CONTENT FOR THREE DIFFERENT SOILS. REFERENCE: BRAESTER (1972)

7.2.5.1 Methods to Measure the Physical Properties of Porous Media

In Section 7.2.2, the physical properties of bulk density, particle-size distribution, porosity and water content were discussed. Methods to measure and estimate these properties are reviewed below.

Bulk density ρ_b (g/cm^3) of a material is measured by taking an undisturbed sample of the material in the field, using a sampler of known volume. The sample is then dried to a constant weight in an oven at 105-110°C. The bulk density of a sample is thus calculated as its oven dry weight divided by the sample volume (see Equation VII-5). Other methods of measuring bulk density include in-situ measurement by gamma radiation and microscopic methods using paraffin fixation. These methods are discussed in detail by Fox and Page-Hanify (1959), Baver et al. (1972) and Taylor and Ashcroft (1972).

The determination of particle-size distribution is carried out by mechanical or sieve analysis for particles larger than approximately 0.0625 mm, and hydrometer or sedimentation analysis for smaller particles. In the mechanical analysis, the soil sample is shaken on a sieve with square openings of specified size. Successively smaller and smaller screens are used. For particles less than 0.0625 mm, a sedimentation analysis is done. In this method, the size of a particle is defined as the diameter of a sphere that settles in water at the same velocity as the particle (Morris and Johnson, 1967; Taylor and Ashcroft, 1972).

Soil porosity can be measured directly in the laboratory by either an air-picnometer technique, a porosimeter, mercury displacement or a gas expansion method (Klock et al., 1969; Bear, 1972; Baver et al., 1972). Porosity, p (unitless), can also be estimated based on typical values for a given soil or rock type (see Table VII-4).

Soil water content in the laboratory is usually measured by the gravimetric method of determining the soil's moist and dry (oven dried at 105-110°C) weights and then using Equation VII-7 to get the gravimetric water content θ_g (unitless). The volumetric water content θ (unitless) can be found from θ_g through Equation VII-9. Other methods of measuring water content are neutron scattering, gamma ray attenuation, electromagnetic techniques, tensiometric techniques and hygrometric techniques. A summary of the relative advantages and disadvantages of these methods, is given in Table VII-6. For screening calculations, an estimated average water content based on grain-size is usually adequate. If necessary, this estimate could be checked by collecting a few samples and measuring the water content gravimetrically.

7.2.5.2 Methods to Measure the Flow Properties of Saturated Porous Media

The flow properties of saturated porous media are discussed in Section 7.2.3. These properties include specific yield, specific storage, storativity, saturated hydraulic conductivity and transmissivity. The measurement of those properties related to the quantity of water that an aquifer can release or take up (i.e., specific yield,

TABLE VII-6

SUMMARY OF METHODS FOR MEASURING SOIL MOISTURE (θ)

Method	Advantages	Disadvantages	References
gravimetric	easy to take samples most accurate of available methods	destructive sampling provides a point value	Black (1965) Reynolds (1970a,b) Taylor and Ashcroft (1972)
neutron scattering	measures moisture in-situ regardless of its physical state can determine θ versus depth nondestructive can detect rapid changes in θ	depth resolution $\pm$0.5 ft below a depth of 6 in. below land surface expensive and requires a radioactive source	Gardner and Kirkham (1952) van Bavel (1961, 1962) Rawls and Asmussen (1973) Vachaud et al. (1977)
gamma ray attenuation	can determine θ versus depth in-situ easy to obtain temporal changes very good depth resolution (2-3 cm) nondestructive automatic recording is possible	assumes bulk density of soil is known and a constant expensive, complicated instrumentation and requires a radioactive source	Gurr (1962) Ferguson and Gardner (1962) Hofziger (1978)
resistivity and capacitance (i.e., gypsum blocks; geophysical methods)	can determine absolute values of θ versus depth high precision can measure high suction pressures (greater than 800 cm H_2O)	time lag in response some devices can deteriorate sensitive to soil salinity	Thomas (1963) Selig et al. (1975)
tensiometric techniques	easy to design, construct, and install measurement range is between 0 and 800 cm H_2O of tension operable for long time periods rapid response time (with transducers) adaptable to freezing and thawing conditions	gives a direct measure of soil water pressure but an indirect measure of θ instruments can be broken during installation some electronic drift in pressure transducers sensitive to temperature changes	Kirkham (1964) S.J. Richards (1965) Rice (1969) Taylor and Ashcroft (1972) Williams (1978)

Reference: after Schmugge et al. (1980) and Wilson (1981)

specific storage and storativity) are discussed in Appendix I. Those properties that describe the rate at which water can move in the aquifer (i.e., hydraulic conductivity and transmissivity) are discussed below.

7.2.5.2.1 Laboratory Methods of Measuring Hydraulic Conductivity

There are two major ways of assessing saturated hydraulic conductivity K in the laboratory: particle-size analysis and permeameter tests.

In particle-size analysis, soil samples are characterized by their particle-size distribution, and then empirical formulae are used to estimate K. For example, consider the following empirical formula developed by Hazen for intrinsic permeability K_i (cm^2):

$$K_i = C\, d_{10}^2 \qquad \text{(VII-19)}$$

where C is a dimensionless coefficient and d_{10}(mm) is the effective particle diameter obtained from the particle-size gradation curve (see Section 7.2.2.2). The intrinsic permeability is related to hydraulic conductivity through the relation of Equation VII-10. Harleman et al. (1963) found good agreement with experimental values of K_i using $C = 6.54 \times 10^{-6}$ (where d_{10} is in mm and K_i is in cm^2). Krumbein and Monk (1943) found C to equal 6.17×10^{-6}. Hazin's approximation for intrinsic permeability in Equation VII-19 was originally determined for uniformly graded sand, but it can give a rough estimate for soils in the fine sand to gravel range (Freeze and Cherry, 1979).

Hydraulic conductivity can also be determined in the laboratory by a permeameter, in which flow is maintained through a soil core that is held in a metal or plastic cylinder while measurements of flow rate and head loss are made. Either a constant head or a variable head permeameter method can be used (Todd, 1980; Morris and Johnson, 1967). The constant head permeameter is generally used for samples of medium to high permeability and the variable head permeameter for samples of low permeability.

However, permeability results from the laboratory may bear only limited relation to values obtained by in-situ methods in the field. Supposedly uniform deposits, for example clays, more often than not contain thin seams or lenses of silt or fine sand. These thin layers may occur as continuous laminations or be randomly dispersed and discontinuous. As a consequence of this stratification, hydraulic conductivity values calculated in-situ in the field for clay or clay/silt deposits are generally several orders of magnitude larger than those derived from laboratory tests (Milligan, 1976). An order of magnitude difference generally occurs for sand and silt deposits. The greater the heterogenity in a formation, the greater the discrepancy between laboratory and field measured values of saturated hydraulic conductivity. Hence, the most reliable methods are the in-situ or field methods.

7.2.5.2.2 Field Methods of Measuring Hydraulic Conductivity

Field or in-situ determination of saturated hydraulic conductivity can be made by a wide variety of methods. These methods include the auger-hole method, piezometer method, pumping tests, tracer tests, packer tests and the point dilution method. Milligan (1976) reviewed these various in-situ methods as summarized in Table VII-7. Many authors, including Todd (1980) and Milligan (1976), feel that the most reliable in-situ method for estimating hydraulic conductivity is the well pumping test. When such a test is not practical, borehole slug tests can be used to provide adequate estimates for screening calculations. Values of transmissivity T are obtained from pumping tests by superimposing a plot of nonsteady-state drawdown on a family of type curves. Transmissivity is converted to hydraulic conductivity by dividing T by the aquifer thickness. Worked out examples using the various pumping and slug tests are given by Lohman (1972) and Fetter (1980). A detailed discussion on designing the geometry or layout of pumping tests can also be found in Kruseman and deRidder (1970) and Stallman (1971).

7.2.5.3 Methods to Measure the Flow Properties of Unsaturated Porous Media

The methods of measuring soil-water potential, such as the gravitational, pressure and osmotic potentials will be discussed in Section 7.2.5.3.1. Measuring the characteristic curves of soil-water retention and unsaturated hydraulic conductivity will be discussed in Section 7.2.5.3.2.

7.2.5.3.1 Measuring Soil-Water Potential

Gravitational potential is easy to measure since only the vertical distance z(cm) between the reference point and the point under consideration has to be measured. If the point under consideration is above the reference point, the gravitational potential is positive and negative if it lies below the reference point.

Pressure potential is that potential in the soil water due to the pressure of the surrounding fluid acting on the soil water. It is the relative or gauge pressure that is measured (i.e., relative to atmospheric pressure). Hence, the pressure potential is zero at a water surface (e.g., water table) exposed to atmospheric pressure. Pressure potential is positive at any saturated point below a water surface and is generally measured with a piezometer. A piezometer consists of a small diameter casing which has a short section of slotted pipe or well screen at the bottom and is open to the atmosphere at the top. The pressure potential or hydraulic head in a water table aquifer or a confined aquifer is calculated as the distance between the well point and the free water level in the piezometer. Under unsaturated conditions, the pressure potential or matric potential is negative and is measured with a tensiometer. A tensiometer generally consists of a ceramic porous cup attached through an airtight, water filled tube to a manometer. The vacuum created in the tube is a measure of the matric potential of the soil water surrounding the porous cup and is measured by a

TABLE VII-7

TECHNIQUES FOR MEASURING SATURATED HYDRAULIC CONDUCTIVITY

a. Direct testing of in-situ permeability in soils

Method	Technique	Remarks on Application	Method Rating	Reference
(A) Open Augerhole	Shallow uncased hole in unsaturated material above water level	Difficult to maintain water levels in coarse gravels	Poor	USBR (1968)
Test Pit	Square or rectangular test pit (equivalent to circular hole above)		Poor	Lacroix (1960)
(B) Borehole Slug	i) Falling/rising head, Δh in casing measured vs time	Borehole must be flushed Possible fines clog base (falling Δh)	Fair to Good	Hvorslev (1951)
	ii) Constant head maintained in casing, outflow measured, Q vs time	Pumping (rising Δh) where WL lowered excessively		USBR (1968)
(C) Piezometers/ Permeameters (with or without casing)	Piezometer tip pushed into soft deposits/placed in boring, sealed casing withdrawn/pushed ahead of boring. Constant head, outflow measured vs time. Variable heads also possible.	Possible tip 'smear' when pushed. Δh set up in pumping tip Danger of hydraulic fracture		Gibson (1966) Wilkes (1974) Hvorslev (1951) Bjerrum et al. (1972)
(D) Well pumping test	Drawdown in central well monitored in observation wells on at least two 90° radial directions	Screened portion should cover complete stratum tested	Excellent	Todd (1980)

TABLE VII-7 (continued)

b. Direct testing of in-situ permeability in rock

Method	Technique	Remarks on Application	Method Rating	Reference
(A) Borehole (simple tests)	i) Water gain/loss in drilling	i) Gives possible indication of previous zones. Must be supplemented by detailed examination of core.	Poor	USBR (1968)
	ii) Simple variable/constant head tests in open boreholes	ii) Similar to borehole slug tests	Poor	
(B) Borehole packer tests	i) Single packer tests (during advance of boring)	Expanding leather/rubber packers may provide inadequate seal	i) Fair	USBR (1968) Sherard, et al. (1963)
	ii) Double packer tests (in completed boreholes)	Pneumatic packers superior to other types, but limited to pressures <200 lb/sq. in.	ii) Poor to Fair	Sharp (1970)
(C) Permeameters/inserts	Variable head tests in:			
	i) Sealed individual piezometers (local zone)	i) Similar to Piezometers - local zones tested. Limited application	i) Fair to good (local zone)	i) USBR (1968)
	ii) Continuous borehole piezometers	ii) Possible to monitor water pressure variation over complete boring to 200m depth. Needs interpretation to assess K	ii) Fair (Potential good)	ii) Londe (1973)
(D) Well pumping test	Normally carried out in open central well. Observation wells at radii, 90^{θ}	Screen/perforated casing often not required	Excellent	Todd (1980)

TABLE VII-7 (continued)

c. Indirect assessment of in-situ permeability in soils and rocks

Method	Technique	Remarks on Application	Method Rating	Reference
(A) Tests on samples	i) Particle-size distribution ii) Laboratory K	i) D_{10} applicable to uniform sands ii) Often inapplicable to field conditions	Fair Poor	Loudon (1952) Golder, Gass (1963) Rowe (1972)
(B) Geophysical Logging	i) Multi-electrode resistivity ii) Single point resistance potential iii) Fluid conductivity, temperature	Continuous profiling of borings can be carried out at low cost (Requires further correlation with in-situ direct testing)	Fair Future development good	Guyod (1966) Robinson (1974)
(C) Observations of natural or induced seepage	Measurement and analysis of data from: i) Observation wells ii) Piezometers iii) Dyes, tracers, radioactive isotopes	Provides method of assessing permeabilities, in-situ	Excellent	Walker (1955) Terzaghi (1960, 1964) Golder, Gass (1963) Sharp (1970)

Reference: Milligan (1976).

manometer, a vacuum gauge or a transducer. A detailed description of the design and use of tensiometers can be found in Kirkham (1964) and S.J. Richards (1965). Additional discussion is included in Table VII-6.

Osmotic potential is that potential of the soil water due to the physical separation of free water from soil water solutes by a semipermeable membrane. Separate measurement of osmotic potential is not necessary for screening calculations. It is difficult to measure but can be measured with a psychrometer (Richards and Ogata, 1961; Campbell et al., 1966; Taylor and Ashcroft, 1972) or a ceramic conductivity cell (Kemper, 1959).

7.2.5.3.2 Measuring the Characteristic Curves of Soil-Water Retention and Hydraulic Conductivity

The soil-moisture characteristic curve can be obtained in the laboratory by a combination of measurement techniques. The hanging water column or tension plate method is generally used to measure the wet range (0 to 100 cm H_2O suction) of the characteristic curve and a pressure plate or membrane apparatus is generally used for the dry range (100 to 5000 cm H_2O suction). For suctions greater than 5000 cm H_2O, the soil-moisture characteristic curve can be determined by a psychrometer or vapor pressure technique using saturated salt solutions (Taylor and Ashcroft, 1972).

There are several methods of obtaining the characteristic curve of unsaturated hydraulic conductivity. These include direct laboratory methods and quasi-empirical metnods, such as the instantaneous profile and capillary model techniques. The usual laboratory method of measuring unsaturated hydraulic conductivity is to apply a constant hydraulic head or pressure difference across a soil sample and then measuring the resulting steady flux of water. This pressure difference can be created by applying a vacuum in a tension plate or pressure chamber device or by creating a fixed evaporation rate (Taylor and Ashcroft, 1972). Measurements are made at successive levels of suction, so as to obtain the characteristic function $K(\theta)$ or $K(\psi)$. Additional laboratory methods are described in detail by L.A. Richards (1965), Klute (1965) and Bouwer and Jackson (1974).

Various empirical equations have been proposed to relate hydraulic conductivity with matric potential or with percent saturation. The most commonly employed empirical equation is of the following form:

$$K = a/(b + \psi^m) \qquad \text{(VII-20)}$$

where a, b and m are empirical constants, ψ is the absolute value of the matric or suction potential and K is the unsaturated conductivity. The empirical constants a, b and m are found experimentally for each soil by best fit.

The instantaneous profile method can be applied to either laboratory flow columns or to field situations (Klute, 1972). In this method, the unsaturated hydraulic

conductivity is calculated from the measured moisture content profile of a draining soil by averaging the value of the time derivative of the moisture content between successive depths. However, the instantaneous profile method can only determine hydraulic conductivity in the relatively wet range (suctions less than 1000 cm H_2O). In addition, it is experimentally difficult to carry out this method and generally many duplicate measurements are necessary to make the conductivity-water content relationship reliable.

Another method of calculating the unsaturated hydraulic conductivity is to combine the water retention characteristic with the capillary pore-size distribution. This approach, called the capillary model, is based on the Kelvin equation which relates the surface tension and soil water energy to pore radius. A capillary model with a closed form solution for hydraulic conductivity is given by van Genuchten (1980). A review of previous theoretical capillary models is given by Mualem (1976) and a comparison between six recent models is given by Simmons and Gee (1981).

7.2.5.4 Measurement Precision and Sample Size

Many of the methods given in Section 7.2.5 will give an accurate measurement of an aquifer property but this information usually consists of one or two values that are taken at one point in the aquifer. Because of heterogeneity within an aquifer, one or two measurements may not be representative. In this section, a brief discussion is given on how to achieve a specified level of precision and confidence level when estimating aquifer properties.

The number of measurements necessary to reasonably characterize the mean value of an aquifer property or parameter can be determined after some initial data collection. For the methods discussed below, several assumptions must be made. First, the sample mean of an aquifer parameter is assumed to be normally distributed. This means that if random measurements are made of an aquifer parameter, the deviation of the sample mean from the "true population" mean will be normally distributed. Secondly, the variance or standard deviation of the aquifer property will be assumed to be known or measurable. Based on these assumptions, the number of measurements needed to obtain a specified precision and confidence level of an aquifer parameter can be prescribed. However, the number of measurements and tests which can be made is often dictated by time and budget constraints. Comparison to the sample sizes given below indicates the level of confidence which should be placed in the data obtained. For screening calculations, the number of measurements collected will most likely be small.

The precision or margin of error that can be tolerated in measuring the mean value of a variable X with n samples and with confidence level γ is:

$$P_x = (t_{\gamma,n-1})S_x/\sqrt{n} \qquad \text{(VII-21)}$$

where P_x is the precision of measuring variable X, $t_{\gamma,n-1}$ is the student's t-distribution percentile with confidence γ and n-1 degrees of freedom, S_x is the standard deviation of the sample:

$$S_x = \left(\sum_{i=1}^{n^*} \frac{(X_i - \bar{X})^2}{n^* - 1} \right)^{1/2} = \left(\frac{\left(\sum_{i=1}^{n^*} X_i^2 \right) - n^* \bar{X}^2}{n^* - 1} \right)^{1/2} \qquad \text{(VII-22)}$$

X_i is the i-the observed value of variable X, n^* is the number of data measurements or observations used to find an estimate of the sample standard deviation, $\bar{X}$ is the sample mean of variable X:

$$\bar{X} = \sum_{i=1}^{n^*} X_i / n^* \qquad \text{(VII-23)}$$

The precision P_x can also be written as a percent of the sample mean:

$$P_x = \left| \bar{X} \, d/100 \right| \qquad \text{(VII-24)}$$

where d is the allowed deviation of the sample mean from the true mean, expressed as a percent of the true mean (i.e., d can range between 0 and 100).

Upon rearranging Equation VII-21, it is possible to determine the number of measurements necessary to obtain a specified precision and confidence level:

$$n \geq (t_{\gamma,n-1} / e)^2 \qquad \text{(VII-25)}$$

where the variable "e" is defined as:

$$e = P_x / S_x = \left| \bar{X} d / (100 \, S_x) \right| \qquad \text{(VII-26)}$$

The variable "e" is related to the inverse of the coefficient of variation and is dimensionless.

Equation VII-25 has been solved for various confidence levels and tabulated in Table VII-8 as a function of "e". It is quite clear from this table that the sample size "n" grows dramatically as the numerical value of precision decreases and as the desired confidence level increases.

If some value of "e" is desired other than that given in Table VII-8, then an iterative solution is necessary to solve Equation VII-25. This is because the student's t-distribution percentile $t_{\gamma,n-1}$ is also a function of the number of measurements minus one, n-1. As an initial guess to the size of n, the standard normal deviate Z_γ can be used in place of the student's t-distribution in Equation VII-25.

TABLE VII-8

SAMPLE SIZE FOR VARIOUS CONFIDENCE LEVELS USING THE STUDENT'S t-DISTRIBUTION

	Confidence Level γ(%)				
e	50	80	90	95	99
.01	4549	16424	27055	38414	66349
.05	182	657	1082	1537	2654
.10	46	164	271	384	663
.15	21	74	120	173	295
.20	12	42	70	99	171
.25	8	28	45	64	110
.30	6	20	32	45	78
.40	4	12	19	26	45
.50	3	8	13	18	30
.60	2	6	10	13	22
.70	2	5	8	10	17
.80	2	4	7	9	14
.90	2	4	5	7	12
1.00	2	3	5	6	10
1.25	2	3	4	5	8
1.50	2	3	3	4	7
1.75	2	2	3	4	6
2	2	2	3	4	5
3	2	2	3	3	4
4	2	2	2	3	4
5	2	2	2	3	3
6	2	2	2	2	3
7	2	2	2	2	3
29	2	2	2	2	2

Values of Z_γ are given in Table VII-9 as a function of confidence level. Thus, as a first guess to determining the sample size (called n'), solve:

$$n' = (Z_\gamma/e)^2 \qquad \text{(VII-26a)}$$

With n' from Equation VII-26a, calculate the student's t-distribution $t_{\gamma,n'-1}$ and substitute into Equation VII-25. Values of $t_{\gamma,n'-1}$ are given in Table VII-10 as a function of confidence level and degrees of freedom df, where df = n'-1. The correct

TABLE VII-9

STANDARD NORMAL DISTRIBUTION FUNCTION

Confidence Level γ(%)	Deviate z_γ
50	0.67449
80	1.28155
90	1.64485
95	1.95996
99	2.57583

$$\text{where } \gamma = 100 \int_{-z_\gamma}^{z_\gamma} \frac{e^{-y^2/2}}{\sqrt{2\pi}}\, dy$$

Reference: after Abramowitz and Stegun (1964).

Table VII-10

PERCENTAGE POINTS OF THE STUDENT'S t-DISTRIBUTION

$t_{\gamma,df}$

Degrees of Freedom	Confidence Level (%)				
df= n-1	50	80	90	95	99
1	1.000	3.078	6.314	12.706	63.657
2	0.816	1.886	2.920	4.303	9.925
3	0.765	1.638	2.353	3.182	5.841
4	0.741	1.533	2.132	2.776	4.604
5	0.727	1.476	2.015	2.571	4.032
10	0.700	1.372	1.812	2.228	3.169
15	0.691	1.341	1.753	2.131	2.947
20	0.687	1.325	1.725	2.086	2.845
25	0.684	1.316	1.708	2.060	2.787
30	0.683	1.310	1.697	2.042	2.750
40	0.681	1.303	1.684	2.021	2.704
60	0.679	1.296	1.671	2.000	2.660
120	0.677	1.289	1.658	1.980	2.617
infinite	0.674	1.282	1.645	1.960	2.576

n = number of measurements.

Reference: after Abramowitz and Stegun (1964).

sample size "n" can be determined after one or two iterations (i.e., iterate until n'=n).

Hence, in order to determine the correct sample size, the precision and confidence level have to be specified and an estimate made of the standard deviation. The latter can be made from historical data or by making a rough estimate from previous sampling or from a pilot survey. If no data are available, then a two step sampling procedure would be needed. First, a sample of size n* from the initial data set (where n* is at least 2 or more) is made from which the standard deviation is estimated using Equation VII-22. Then, Equation VII-26 and Table VII-8 can be used to find a total sample size "n". This and other sampling strategies are discussed in detail by Cochran (1977) and Nelson and Ward (1981).

An example of a two step sampling problem is shown below. In this example, the proper sample size for measuring hydraulic conductivity will be determined. The aquifer consists of alluvial sand. The drawdown versus elapsed time method of Theis is used to evaluate the horizontal hydraulic conductivity at various observation wells.

EXAMPLE VII-1

Initially, six texts were conducted. The results are shown below:

Field Data			Data Summary	
Saturated, Horizontal			existing data size:	n* = 6
Hydraulic Conductivity			confidence level:	γ = 95%
(cm/sec)			allowed deviation:	d = 10%
0.13	0.12	0.18		
0.13	0.13	0.15		

Based on these six initial measurements, a 95 percent confidence level, and a 10 percent deviation or precision in estimating the true mean, the following parameters were calculated. The sample mean $\bar{X}$ was calculated using Equation VII-23 to give $\bar{X}$ = 0.14 cm/sec, the sample standard deivation S_x from Equation VII-22 gives S_x = 0.022 cm/sec, precision P_x from Equation VII-24 gives P_x = 0.014 cm/sec and variable e was calculated from Equation VII-26 to give e = 0.64. Finally, by using either Equation VII-25 or Table VII-8, it was determined that a total of 12 tests would have to be done (i.e., sample size n = 12). Since six tests had already been done, six additional drawdown tests would have to be performed to obtain the desired degree of precision and confidence level.

Note that this precision and confidence refer to the uncertainty or variability of a single site if all 12 drawdown tests are done using the same observation well. Using 12 different observation wells will show the variability of the aquifer over the region measured.

----------END OF EXAMPLE VII-1----------

Before leaving this section on sampling size, one additional consideration needs to be considered: cost. Virtually all of the field tests used to measure the flow properties of aquifers, such as transmissivity or hydraulic conductivity are costly to perform. Typically, most ground water studies use only a few pumping tests per site or per study area. It is clear from Table VII-8 that two tests can only give results with a low confidence level and/or poor precision and one test provides no information about precision. But a few tests can give an "order of magnitude" value to an aquifer characteristic, such as hydraulic conductivity. An order of magnitude value is adequate for most screening calculations. For detailed investigations more data are needed to provide a greater level of confidence and precision.

7.3 GROUND WATER FLOW REGIME

7.3.1 Approach To Analysis of Ground Water Contamination Sites

The recommended approach to analysis of ground water contamination problems is to first use existing data and screening methods such as presented in this chapter to gain a basic understanding of the site hydrogeologic characteristics and the relative hazard associated with the particular problem. The steps involved are to first characterize the waste sources in terms of type of waste, quantities disposed, disposal method, and dimensions of the disposal area. Next, hydrogeologic data for water levels, hydraulic conductivity, and porosity or moisture content are obtained. The water level data are plotted as ground water elevation contour maps from which flow directions are then determined. The remaining hydrogeologic data are used to estimate vertical and horizontal seepage velocities. Next, these velocities are used to estimate travel times for conservative solutes to nearby wells or surface water bodies. These estimates are compared to observed solute concentration data which can also be plotted as contour maps. The effects of additional processes including dispersion and chemical attenuation are then considered using the methods discussed in Section 7.5. Finally, estimates of uncertainty associated with the predictions should be made. At this point information is available to determine whether additional field sampling or detailed investigations are warranted.

The procedures for conducting the hydrogeologic portion of the analyses are discussed in detail in the following sections. Section 7.3.2 discusses measurement of water levels and determination of flow directions. Section 7.3.3 presents methods for calculating seepage velocities and travel times.

7.3.2 Water Levels and Flow Directions

7.3.2.1 Introduction

Water level data can be found in ground water investigation reports or well logs, by talking to the owners of nearby wells, or by making water level measurements at existing wells. Also, water surface elevations of nearby streams, ponds, lakes, springs, marshes, gravel pits, etc. can be used to estimate water level elevations since these are areas where the ground water table intersects the land surface. (Care should be taken, however, to be sure that these water bodies are not perched.)

In the field, the presence or absence of vegetation common to wet soils and salt tolerant plants (e.g., willow, cottonwood, mesquite, saltgrass, greasewood) may be indicative of discharge areas and hence can be used to locate areas where the ground water table is near the surface. In arid regions, a thicker than normal cover of vegetation or salt outcrop (e.g., saline soils, playas, or salt precipitates) may indicate a discharge area. Field mapping of such occurrences can be valuable in obtaining an initial idea of the depth to water. However, relatively impermeable layers of even small areal extent may result in perched waters, which in turn yield wetlands or ponds. The unforeseen presence of a perched water table may lead to misinterpretations of surface observations.

The following general observations for unconfined water table aquifers in humid areas can be made:

- Ground water discharge zones are in topographic low spots
- Ground water generally flows away from topographic high spots and toward topographic low spots
- The water table may have the same general shape as the land surface.

From the above, it might seem reasonable that the hydraulic gradient (i.e., the change in ground water surface elevation per unit distance) of water table aquifers should vary in a direct relationship with the slope of the land (i.e., the hydraulic gradient is steepest where the land slope is steepest). However, the presence of formations with low hydraulic conductivity, subsurface geologic inhomogeneities and man-made influences (e.g., pumping wells, landfills) can have a profound effect on both the direction and magnitude of ground water flow. Care should be taken in assuming that the direction of the local ground water flow is the same as that of either the surface topography or regional ground water flow directions. For example, the presence of an unknown buried stream channel can cause the local flow to be in the opposite direction of the regional flow. Obtaining reliable water level data from observation wells is indispensable, even in the screening stage of a ground water study.

7.3.2.2 Water Level Measurement

One of the most important measurements in ground water investigations is the determination of water level elevation. Mean sea level is generally taken as the

reference or datum from which water level elevations are measured. Water level elevation is best measured as the height of water in a piezometer or observation well. Such a well has a short, screened interval in the aquifer (confined or unconfined) and is open to the atmosphere at the top. Water level elevation represents the average hydraulic head H at the location of the well screen.

Most measurement techniques involve measuring depth to water (i.e., depth to water from land surface or from the top of the well casing). Depth to water is converted to water elevation by subtracting depth to water from the elevation of the ground surface. Serious errors in data interpretation can occur if the reference point from which the depth to water was measured (i.e., land surface or well casing top) was not noted.

To convert depth to water table to water level elevations, the land surface elevation (or well casing elevation) needs to be known. The required accuracy in measuring or knowing surface elevation depends in part on the ultimate use of the data and on the scale of the problem. Individually surveying each well is the best method. However, for screening purposes, an estimate based on topographic maps and the height of the casing above the land surface may be adequate in some cases.

Water level elevations are usually measured by means of a chalked steel tape or an electric water-level probe, but air lines, pressure transducers and sound reflection methods may also be used.

Great care should be taken when measuring water level elevations, particularly when the hydraulic gradient or aquifer slope is small. In general though, an accuracy of ± 3 centimeters in measuring water level elevation should be sufficient for most ground water applications and is easily obtained.

7.3.2.3 Sources of Error in Water Level Data

There are many possible sources of error and misinterpretation when taking water level data. Some of the most serious errors are those caused by vertical flow in the aquifer, water level fluctuation, unknown screen locations and unknown or excessively long screened intervals. These sources are described in more detail in this section.

7.3.2.3.1 Vertical Flow

Under most conditions, flow in a homogeneous formation is predominately horizontal. Under this assumption, the equipotential (equal energy) lines are vertical. Hence, water will rise to the same level in piezometers that are located side-by-side but which penetrate the aquifer to different depths. However, if flow is not horizontal, such as near a discharge or recharge area, the water will rise to different levels. This is schematically shown in Figure VII-14. The observed water level in a piezometer will decrease as the well tip of the piezometer is located at lower and lower depths in a recharge area (compare wells "a" and "b" in Figure VII-14). The water level will increase in a discharge area (compare wells "d" and "e" in Figure VII-14). This same phenomenon can occur near large pumping wells. Hence, a

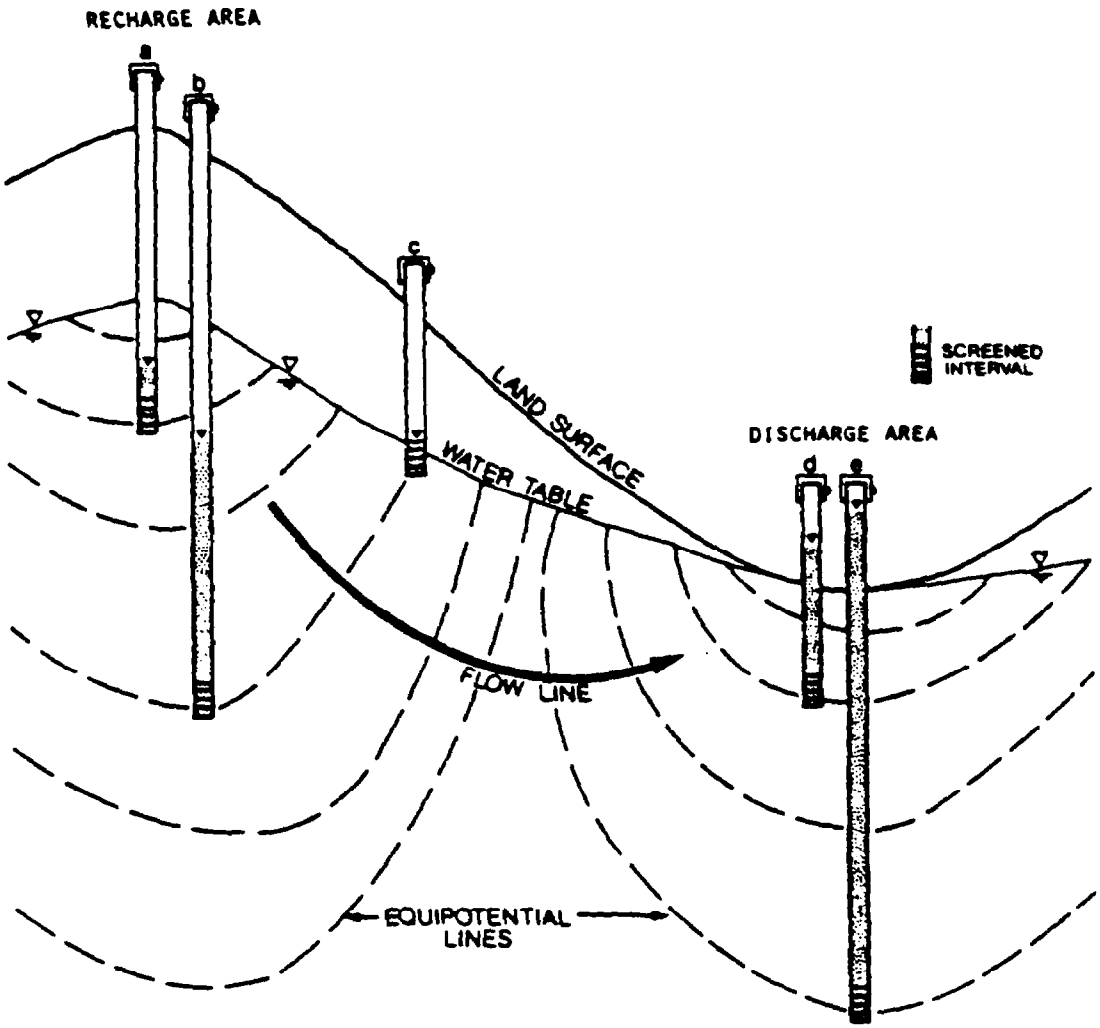

FIGURE VII-14 CROSS-SECTIONAL DIAGRAM SHOWING THE WATER LEVEL AS MEASURED BY PIEZOMETERS LOCATED AT VARIOUS DEPTHS. THE WATER LEVEL IN PIEZOMETER C IS THE SAME AS WELL B SINCE IT LIES ALONG THE SAME EQUIPOTENTIAL LINE

piezometer will only indicate the approximate water table in an unconfined aquifer with vertical flow. What the piezometer does indicate (assuming a short screen length is used) is the exact hydraulic or piezometric head at the point of the well screen. In fact, the vertical flow component of ground water velocity can be determined by placing several piezometers at various depths so that the vertical hydraulic gradient can be measured. This vertical gradient is then multiplied by the vertical hydraulic conductivity to obtain the vertical flow velocity (see Section 7.3.3.1).

Fortunately, the vertical hydraulic gradient in most aquifers is small enough that the component of vertical flow can be ignored. Care must be taken, however, to properly interpret water level data near recharge/discharge areas of the aquifer and near pumping wells. During pumping tests, only short well screens should be used in observation wells to avoid integrating or averaging ground water heads in the vertical direction.

7.3.2.3.2 Water Level Fluctuations

Water levels in wells are usually not static but are constantly fluctuating. The water levels in wells that monitor confined aquifers generally fluctuate more than those in unconfined or water table aquifers. Short term fluctuations in confined aquifers can be caused by many factors, including earthquakes, ocean tides, changes in atmospheric or barometric pressure, changes in surface-water levels and in surface loadings (e.g., a passing train), recharge from precipitation and from drawdown of nearby pumping wells. Water levels in unconfined or water table aquifers are affected by recharge from precipitation (including air entrapment in the unsaturated zone), evapotranspiration, nearby pumping wells and atmospheric pressure changes.

These fluctuations can be observed by maintaining a continuous record of measured water levels over a period of time and then plotting water level as a function of time. The best way to reduce the effect of such fluctuation is to take water level measurements from all observation wells within a 1 to 2 day period. Generally, it is the relative spatial difference in the water level that is the most important information desired (see Section 7.3.3), rather than the absolute water level value.

7.3.2.3.3 Screen Length and Location

Additional interpretation errors may occur when either screen length or screen location of the observation wells are unknown. In addition, excessively long screens (such as used in large production wells and open boreholes) can give conflicting information on water level. Long screens allow flow between different formations within an aquifer and may even penetrate more than one aquifer. Invalid conclusions can also be reached if wells tapping different aquifers are compared. It is important that accurate information be obtained as to screen length and depth. If such information is not obtainable, the water level data should be interpreted most cautiously.

7.3.2.4 Determination of Flow Directions

After water level information has been collected, the data should be plotted as water level elevation contours and used to determine the ground water flow directions.

7.3.2.4.1 Water Level Elevation Contours

A contour map of the water level elevations is prepared from wells screened in the same aquifer. Water level elevation data from the observation wells must all be measured during the same time period (best if measured within a few days) and in the same portion or zone of the aquifer (e.g., upper, middle, lower). A contour map of the water levels can be constructed using the following five steps: 1) plot the spatial location of each well on a map and label each point; 2) write the water level elevation value on the map for every well measured during the same specified time period and in the same aquifer; 3) decide which contour values are desired (e.g., every meter or decimeter change in elevation): 4) locate points on the map corresponding to the contour values chosen in step 3 by interpolating between all of the measured values; 5) draw a line connecting all points of equal value. These lines are drawn so that no two lines ever cross. This process is repeated for each time period and for each aquifer. An example of these steps is shown in Figure VII-15 for a water table aquifer underlying a series of waste ponds.

There are, of course, more sophisticated methods of constructing contour plots, such as contained in several computer programs. SURFACE II is a recent FORTRAN computer program developed by the Kansas Geological Survey (Olea, 1975; Sampson, 1978). This program uses regionalized variable theory or Kriging to perform automatic contouring of point observations. This and many other programs (Davis, 1973) are available but usually hand contouring is more than adequate for screening purposes.

7.3.2.4.2 Water Flow Directions

It was stated in Section 7.2.4.1 that water flows in the direction of decreasing potential energy. In the case of saturated ground water, the potential energy is equal to the water level elevation, as measured by piezometers or wells screened in either confined or unconfined aquifers.

It can be shown that ground water in an isotropic aquifer not only moves in the direction of decreasing water level elevation but also perpendicular to the equipotential lines. Isotropy means that the hydraulic properties (e.g., hydraulic conductivity) of the aquifer are equal in all directions. Hence, if a contour plot of the water level elevation is available and if the horizontal and vertical scales that are used in constructing the contour plot are the same, then the ground water flow direction can easily be found as follows: 1) pick any point along a water level elevation contour or equipotential line; 2) draw a line (called a flow line) from this initial contour line to the next smaller valued contour line, going initially in a direction perpendicular to the first contour line; 3) extend the flow line until it reaches the next contour, making sure that it crosses this new contour line perpendicularly; 4) extend this flow line to as many contour lines as desired, always crossing the contour lines at right angles. Any number of flow lines can be

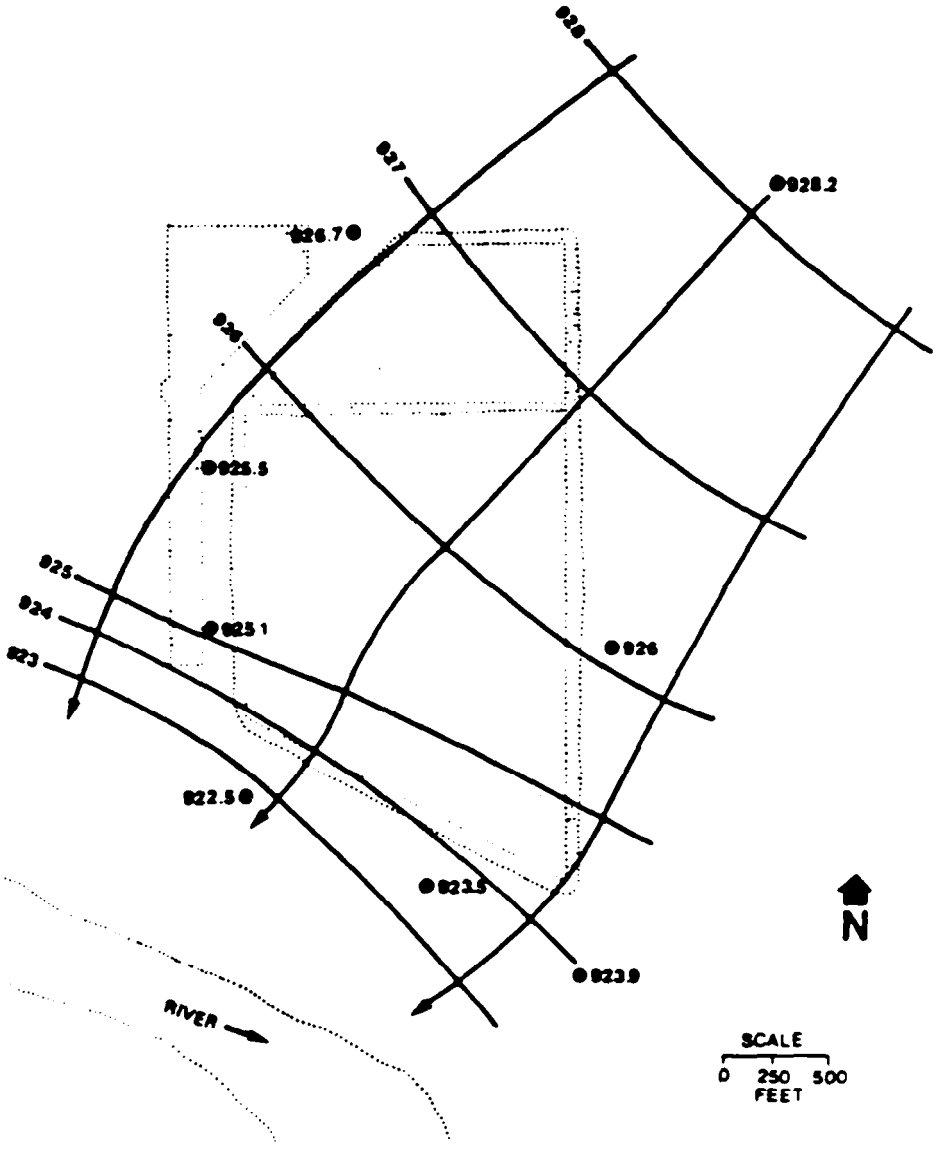

FIGURE VII-15 AN EXAMPLE OF A CONTOUR PLOT OF WATER LEVEL DATA WITH INFERRED FLOW DIRECTIONS. REFERENCE: TETRA TECH, 1985

constructed in this manner. The direction of ground water flow is along these flow lines. An example of constructing flow directions is shown in Figure VII-15, using the water level data shown in the figure. An extensive discussion of graphical methods for constructing flow lines and flow nets can be found in DeWiest (1965).

As shown in Figure VII-16, the graphical construction of flow lines are made by crossing the equipotential lines at right angles. This is always true for isotropic, homogeneous aquifers when the plotted contours are constructed using equal horizontal and vertical scales. However, additional complications or modifications arise if these

conditions are not met. Van Everdingen (1963) discusses the problem of drawing flow lines when the horizontal and vertical scales are not equal as in cross-section diagrams. Liakopoulos (1965) provides theoretical principles for constructing flow lines in homogeneous, anisotropic media (when the hydraulic conductivity varies according to the direction of flow). Fetter (1981) gives a simple graphical method (using a permeability tensor ellipse) to account for anisotropy. Comparison of flow directions in an isotropic aquifer and anisotropic aquifer is shown in Figure VII-16.

The effects of anisotropy and heterogeneity are important but they are difficult to take into account with data generally available during the screening phase of a project. The construction of equipotential and flow lines should be done first assuming a homogeneous and isotropic aquifer. The flow directions could then be adjusted if additional detailed data show this to be necessary.

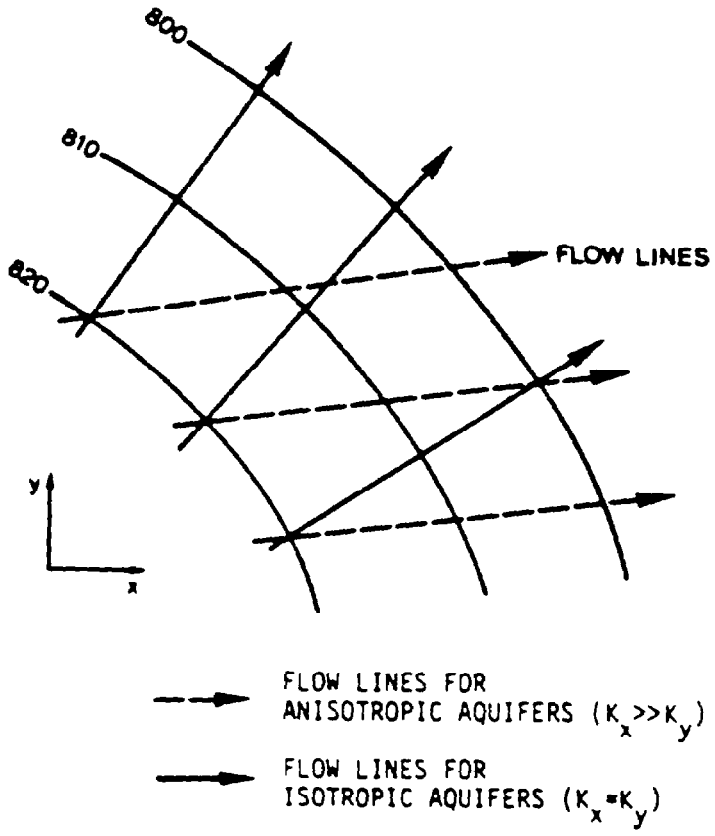

FIGURE VII-16 SCHEMATIC SHOWING THE CONSTRUCTION OF FLOW DIRECTION LINES FROM EQUIPOTENTIAL LINES FOR ISOTROPIC AQUIFERS AND ANISOTROPIC AQUIFERS

7.3.3 Flow Velocities and Travel Times

7.3.3.1 Ground Water Flow Velocities

The direction of ground water flow is discussed in Section 7.3.2.4.2 in terms of water level elevations and hydraulic gradient. To determine the magnitude of ground water flow, Darcy's law is used. Section 7.3.3.1.1 presents Darcy's law for both saturated and unsaturated flow situations. The various forms of representing flow velocity are discussed in Section 7.3.3.1.2 and the applicability or range of validity of Darcy's law is reviewed in Section 7.3.3.1.3. Finally, methods of measuring or estimating ground water flow velocities are discussed in Section 7.3.3.1.4.

7.3.3.1.1 Darcy's Law

In 1856, Henri Darcy discovered by experiment that the flow rate through a saturated porous medium was proportional to the change in head across the medium and inversely proportional to the length of the flow path. Darcy's law can be expressed as:

$$Q = -KA\,\Delta H/\Delta L = -KAI \qquad \text{(VII-27)}$$

where K is a proportionality constant (the hydraulic conductivity, cm/sec), A is the flow cross-sectional area (cm^2) of the soil (measured at a right angle to the direction of flow), ΔH is the change in hydraulic head (cm H_2O) across the soil, ΔL is the distance or length (cm) across the soil (measured parallel to the flow), I is the hydraulic gradient (cm/cm) and Q is the volumetric discharge rate (cm^3/sec). The negative sign in Equation VII-27 indicates that water flows in the direction of decreasing head or potential energy.

Schematics of the experimental set-ups to demonstrate Darcy's law can be seen in Figure VII-17. In Figure VII-17a, flow occurs along an inclined, saturated soil column. The flow is from left to right, going from the upper to the lower reservoir of water. The change in hydraulic head ΔH across the soil column is simply:

$$\Delta H = H_{out} - H_{in} \qquad \text{(VII-28)}$$

where H_{in} is the hydraulic head (cm) at the inlet and H_{out} is the hydraulic head (cm) at the outlet.

Darcy's law is also valid for unsaturated flow, the only difference being that the hydraulic conductivity is now a function of pressure potential H_p or ψ

$$Q = -K(\psi)\,A\,\Delta H/\Delta L \qquad \text{(VII-29)}$$

An example of a demonstration of Darcy's law for unsaturated flow can be seen in Figure VII-17b. This example is the same as shown in Figure VII-17a but now the soil

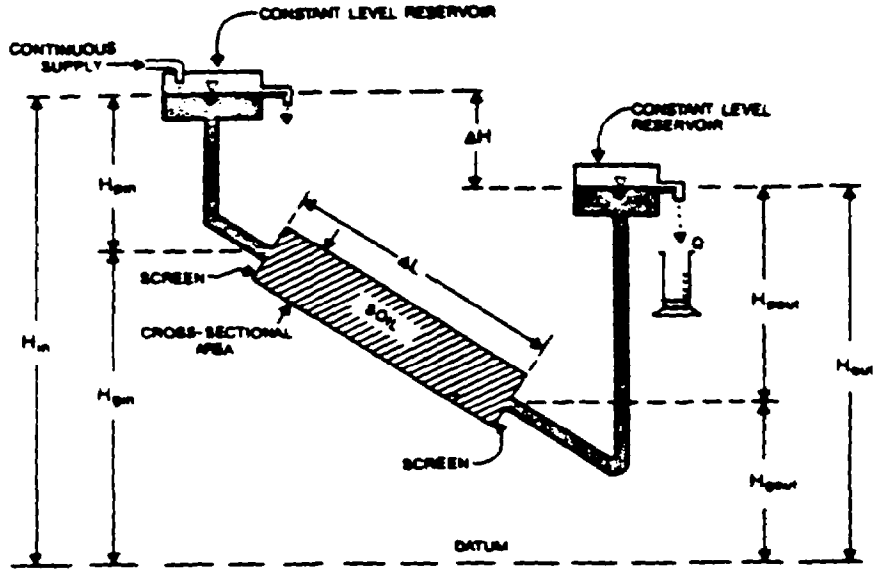

a. Flow in an inclined saturated column of soil.

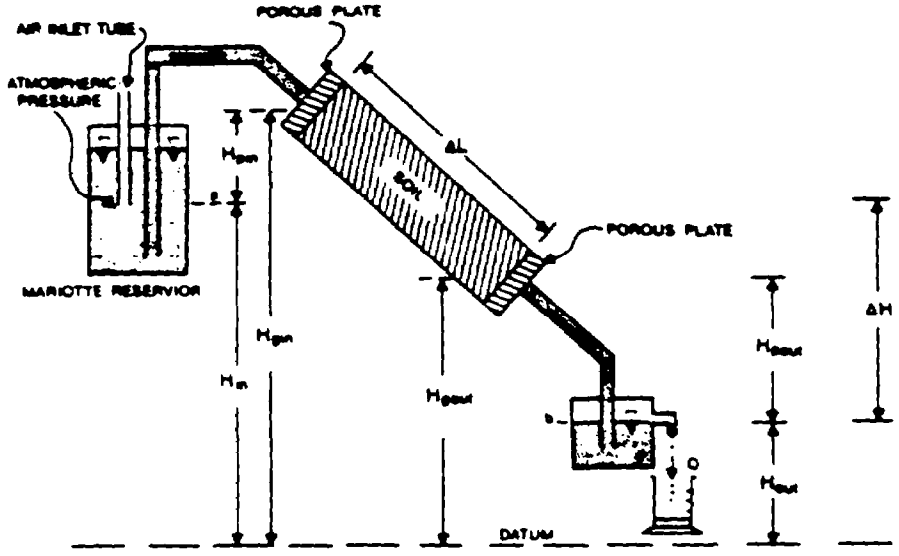

b. Flow in an inclined, unsaturated column of soil. Note that the Mariotte reservoir maintains a constant reference level at atmospheric pressure, even when the inlet water column is under negative pressure.

FIGURE VII-17 SCHEMATIC DIAGRAMS SHOWING PERMEAMETERS TO DEMONSTRATE DARCY'S LAW

is subject to a negative pressure (or a positive suction) potential at both ends of the soil sample by hanging water columns. The hanging water columns will exert a negative pressure potential as long as points "a" and "b" are located below the inlet and outlet, respectively. In general, both the pressure potential and hydraulic conductivity will vary along the soil column. As the absolute value of the pressure potential increases, the hydraulic conductivity will decrease. However, a constant hydraulic conductivity can be made by making the pressure potential H_{pin} equal to H_{pout}.

The total head or potential at any given point is due to the sum of the gravitational and pressure potentials:

$$H = H_g - \left|H_p\right| \qquad \text{(VII-30)}$$

The minus sign was put in front of the absolute value of the pressure potential to avoid any confusion as to the contribution of the pressure potential to the total head in unsaturated soil. Upon substitution of Equation VII-30 into Equation VII-28 and VII-29, Darcy's law for the unsaturated flow case illustrated in Figure VII-17b can be described by:

$$Q = -K^*A(H_{gout} - \left|H_{pout}\right| - H_{gin} + \left|H_{pin}\right|)/\Delta L \qquad \text{(VII-31)}$$

where all of the H terms are expressed in units of length (cm). Since unsaturated hydraulic conductivity is a nonlinear function of pressure potential (see Section 7.2.4.3), the K^* (cm/sec) used in Equation VII-31 represents the hydraulic conductivity for the average matric or pressure potential ψ_{avg}(cm) in the soil column:

$$\psi_{avg} = (H_{pin} + H_{pout})/2 \qquad \text{(VII-32)}$$

Hence, the hydraulic conductivity used in Equation VII-31 becomes:

$$K^* = K(\psi_{avg}) \qquad \text{(VII-33)}$$

7.3.3.1.2 Darcy and Seepage Velocities:

If the volumetric discharge rate Q (cm^3/sec) from Darcy's law is divided by the cross-sectional area A (cm^2), then the ratio Q/A has the units of a velocity, v_d (cm/sec). This "velocity" is called the Darcy velocity or specific discharge:

$$v_d = Q/A = -K\Delta H/\Delta L = -KI \qquad \text{(VII-34)}$$

where I (cm/cm) is defined as the hydraulic gradient. However, the Darcy velocity is not the "true" velocity at which the water moves through the pores of a medium. It is both impractical and unnecessary to determine the actual microscopic velocities through the pore spaces. A more useful macroscopic quantity is called the seepage velocity. Since solutes do not migrate across the entire pore space, we need only consider the water filled portion of it. To take this into account, the Darcy velocity v_d is divided by the volumetric moisture content to yield the seepage velocity, v_s:

$$v_s = v_d/\theta \qquad \text{(VII-35)}$$

Since θ is less than one, the seepage velocity is greater than the Darcy velocity (usually by a factor of 2 or more). The seepage velocity is also called the average interstitial or pore-water velocity.

For saturated flow, like in Figure VII-17a, the volumetric water content equals the porosity p (unitless ratio). Upon substitution of p into Equation VII-35 and v_s into Equation VII-34, the seepage velocity for saturated conditions becomes:

$$v_s = \frac{-K}{p}\frac{\Delta H}{\Delta L} = -KI/p \qquad \text{(VII-36)}$$

where I (cm/cm) is the hydraulic gradient. For unsaturated flow, the seepage velocity is:

$$v_s = \frac{-K}{\theta}\frac{\Delta H}{\Delta L} = -KI/\theta \qquad \text{(VII-37)}$$

where the hydraulic conductivity K is now a function of the moisture content θ.

In general, the Darcy velocity v_d is used in the computation of ground water flow problems and the seepage velocity, v_s, is used in the computation of contaminant or solute transport problems. Great care must be used when obtaining velocity data from published reports since many authors do not state which velocity formulation they are using.

7.3.3.1.3 Applicability of Darcy's Law

Darcy's law is only valid for those conditions in which the flux Q is a linear function of the hydraulic gradient I (i.e., $\Delta H/\Delta L$). This generally corresponds to the condition of laminar flow and when resistance to flow is dominated by viscosity. However, at very high velocities, the flow becomes turbulent and inertial forces become dominant. The Reynolds number R_e is a dimensionless number that expresses the ratio of the inertial to the viscous forces during flow:

$$R_e = d_s \rho_w v_d/\mu \qquad \text{(VII-38)}$$

where ρ_w is the density of water (g/cm^3), μ is the viscosity (cm^2/sec) and d_s is some characteristic length (cm) representing the intergranular flow channels. Bear (1972) suggests using d_{50} (i.e., the average or mean grain size diameter) for d_s but sometimes d_{10} is used (See Section 7.2.2.2). Values for ρ_w and μ are given in Appendix I.

Darcy's law has been shown experimentally to be valid for those conditions for which the Reynolds number is less than 10 when using d_{50} (the average grain-size diameter) for d_s. This covers virtually all natural ground water situations, except perhaps for flow through extremely coarse materials, and in areas of steep hydraulic gradients (gradients greater than 1, such as close to pumping wells). On the other extreme, Darcy's law may also be invalid for extremely low hydraulic gradients and flow through dense clay.

7.3.3.1.4 Methods to Estimate Flow Velocities

There are several ways of estimating the ground water flow velocity. A review of these methods is shown in Table VII-11. The Darcy-based method, as discussed in Sections 7.3.3.1.1 and 7.3.3.1.2, is probably the least expensive and quickest method of estimating flow velocities. From Equation VII-34, the horizontal Darcy velocity v_{dh} (cm/sec) can be calculated between any two points spaced a distance Δx (cm) apart as:

$$v_{dh} = -K_h \Delta H/\Delta x = -K_h I_h \qquad \text{(VII-39)}$$

where I_h (cm/cm) is the horizontal hydraulic gradient, ΔH is the hydraulic head change and K_h (cm/sec) is the horizontal hydraulic conductivity. The vertical Darcy velocity v_{dv} (cm/sec) can be calculated between any two depths spaced a distance Δz (cm) apart as:

$$v_{dv} = -K \Delta H/\Delta z = -K_v I_v \qquad \text{(VII-40)}$$

where I_v (cm/cm) is the vertical hydraulic gradient, K_v (cm/sec) is the vertical hydraulic conductivity and ΔH (cm) is the change in hydraulic head across the points of measurement. Note that in the case of saturated flow (confined or unconfined), ΔH is simply the difference in water level elevations between the measurement points.

The major disadvantage of using the Darcian method for calculating flow velocities is that the hydraulic conductivity needs to be known. Methods of measuring hydraulic conductivity are given in Section 7.2.5.2.2 but large uncertainties are usually associated with these methods. Despite these uncertainties, Darcy's method is best suited for the screening phase of a ground water study.

TABLE VII-11

METHODS FOR MEASURING GROUND WATER FLOW VELOCITY

Technique	Advantages	Disadvantages	References
Darcy-based method	inexpensive simple to calculate can measure horizontal or vertical velocity	need to measure hydraulic conductivity separately	Freeze and Cherry (1979) Fetter (1980)
Direct tracer method	simple in principle only travel time needs to be measured	expensive must adjust for dispersion must know direction of flow and approximate velocity to design well sampling program long times are typically required to obtain data	Knutson (1966) Brown et al. (1972) Gaspar and Oncescu (1972)
Point dilution method	a down-hole method short times needed single observation well is needed	can only measure horizontal velocity	Halevy et al. (1967) Drost et al. (1968) Grisak et al. (1977) Klotz et al. (1978)
Flow meter	a down-hole method for directly measuring horizontal velocity quick, real-time method	under development significant interference from well screens and gravel packs does occur	Kerfoot, 1982

7.3.3.2 Ground Water Travel Times

The distance traveled by an object moving at a constant velocity is:

$$\Delta l = (\Delta t)(\text{Velocity}) \qquad \text{(VII-41)}$$

where Δl is the distance traveled and Δt is the time of travel. If the transport of a non-reactive and non-dispersive solute or contaminant is considered, the "velocity" in the above equation becomes equal to the seepage velocity v_s (which was discussed in Section 7.3.3.1.2). The seepage velocity is used because solutes only travel through the water filled portion of soil pores. The travel time Δt can now be solved from Equation VII-41 to give:

$$\Delta t = \Delta l / v_s \qquad \text{(VII-42)}$$

If the seepage velocity is calculated from Darcy's law, then Equation VII-36 can be substituted into Equation VII-42 to yield the travel time for saturated flow conditions:

$$\Delta t = \frac{-p\Delta l}{KI} \qquad \text{(VII-43)}$$

where Δt (sec) is the travel time, Δl (cm) is the travel distance, p (unitless ratio) is the porosity, K (cm/sec) is the hydraulic conductivity and I (cm/cm) is the hydraulic gradient. Estimated values of porosity are given in Table VII-4 for a variety of geologic materials. Note that the porosity used in Equation VII-43 is to be expressed as a ratio or decimal fraction and not as a percent. For unsaturated flow, the volumetric moisture content θ (unitless ratio) is substituted in place of porosity "p" in Equation VII-43.

It should be remembered that travel times computed from Equations VII-42 and VII-43 are for non-reactive and non-dispersive, conservative solutes moving at a constant velocity. Retardation by sorption and attenuation by other solute-soil interactions may substantially decrease the velocity of solute movement and increase the travel time. Conversely, dispersive processes can either substantially increase or decrease the velocity that a portion of the solute molecules move and hence change the travel time. The processes of sorption and dispersion will be discussed in greater detail in Section 7.4.

In many situations, the flow velocity may vary in both direction and magnitude in an aquifer. Variable velocity and/or variable soil properties can easily be incorporated into the calculation of solute travel time by assuming that solute flow is a constant over a series of finite subregions. If these properties vary by less than 20 percent, discretization is not necessary for screening calculations. Figure VII-18

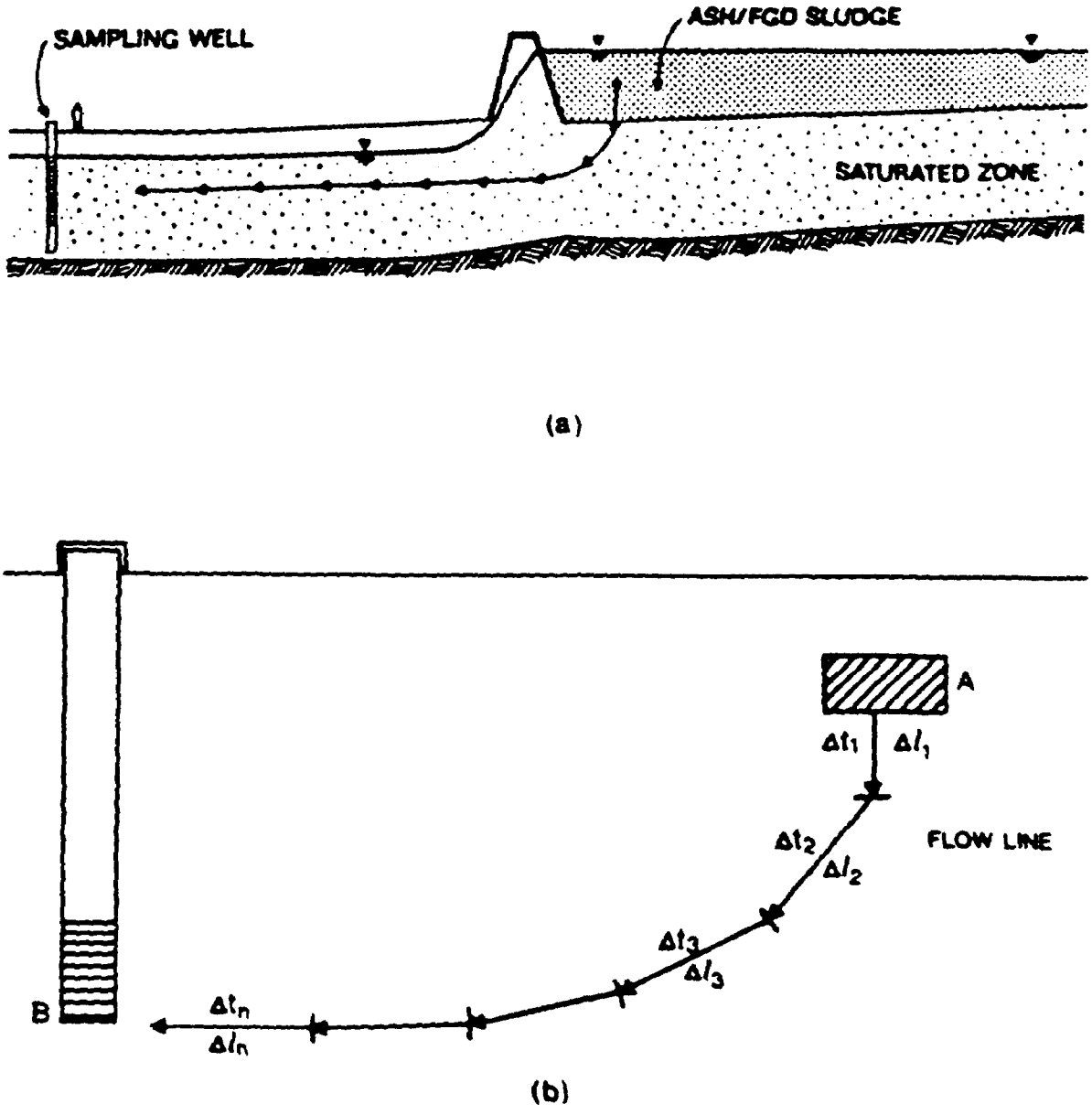

FIGURE VII-18 SCHEMATIC SHOWING HOW TRAVEL TIME CAN BE CALCULATED FOR SOLUTE TRANSPORT WHEN THE FLOW VELOCITY VARIES: A) ORIGINAL PROBLEM, B) DISCRETIZED REPRESENTATION OF THE FLOW LINE. REFERENCE: TETRA TECH (1984)

shows such a discretization process. Equation VII-43 is applied over each "constant" subregion and then all travel times are summed, such that the total travel time T_t is:

$$T_t = \sum_{i=1}^{n} \Delta t_i = -\sum_{i=1}^{n} \left[\frac{p\Delta l}{K_I}\right]_i \qquad \text{(VII-44)}$$

where the subscript "i" refers to the i-th subregion and n is the total number of subregions, p (unitless ratio) is the porosity, Δl (cm) is the travel distance, K (cm/sec) is the hydraulic conductivity and I (cm/cm) is the hydraulic gradient. For unsaturated flow, the volumetric moisture content θ (unitless ratio) is substituted for porosity p. The parameters p, Δl, K and I can be different for each subregion "i". Obviously, a small number of subregions should be chosen at first, and the number increased as more data become available.

Consider the following example illustrating the computation of travel time for ground water from a holding basin to a nearby river.

EXAMPLE VII-2

A buried stream channel is suspected of being beneath the holding basin shown in Figure VII-19. The aquifer underlying the holding basin and the surrounding area is a water table aquifer (unconfined). The hydraulic conductivity measurement from a pump test at well B1 was 0.4 cm/sec and the hydraulic conductivity from a pump test in well B2 was 0.6 cm/sec. The water level elevations in wells B1 and B2 were 2.82×10^4 cm and 2.8140×10^4 cm, respectively. The estimated porosity is 0.3. Calculate the seepage velocity and travel time for sulfate from the edge of the holding basin to the river using the above data. Assume the sulfate does not interact with the soil.
Consider the following steps:

1) Obtain the average hydraulic conductivity from the two pumping tests,

$K = (0.4 + 0.6)/2 = 0.5$ cm/sec

2) Calculate the hydraulic gradient between the basin and the river, where the distance between wells B1 and B2 is 4×10^4 cm,

$$I = \frac{\Delta H}{\Delta L} = \frac{(H_1 - H_2)}{\Delta L} = \frac{(2.8200 \times 10^4 - 2.8140 \times 10^4)}{4 \times 10^4}$$

$= 0.0015$ (cm/cm)

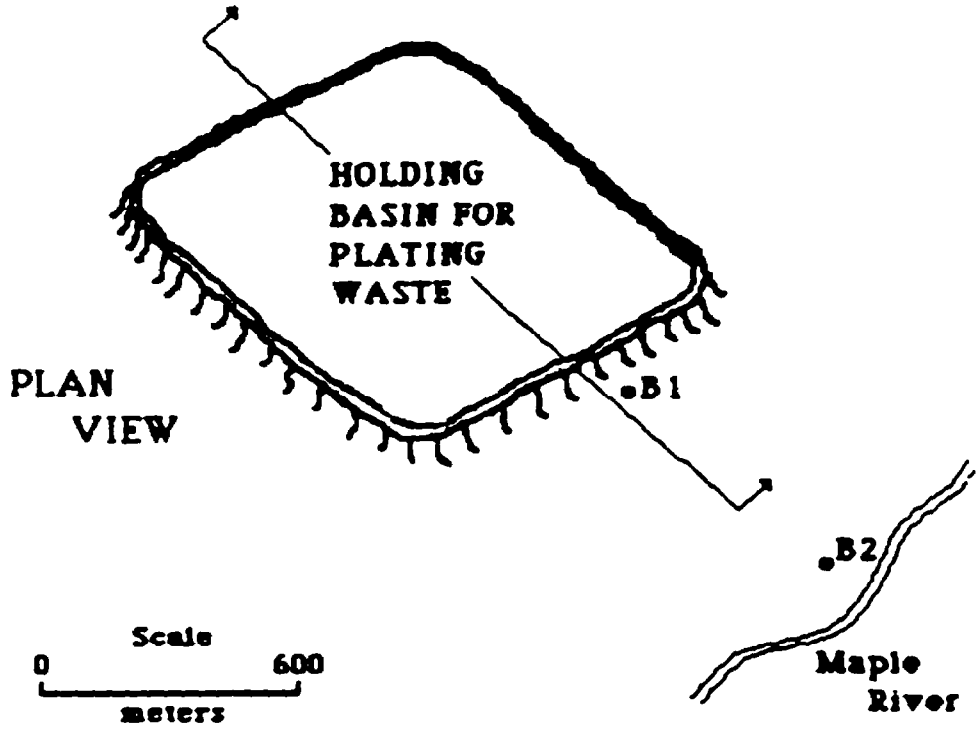

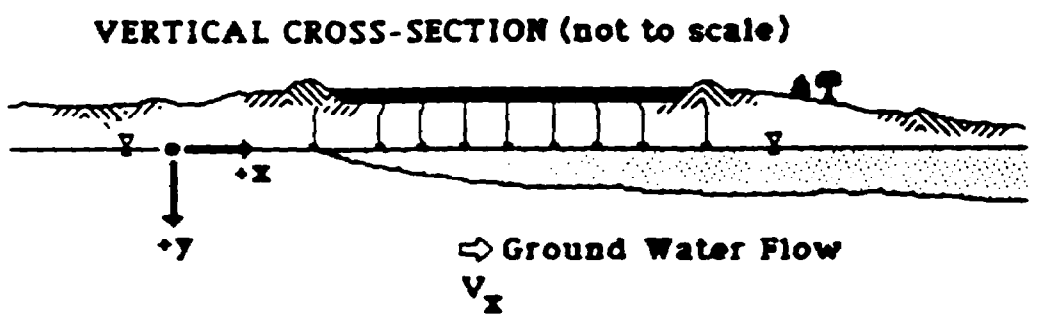

Parameter	Available Data Well No. B1	Well No. B2
H	2.82×10^4 cm	2.814×10^4 cm
K	0.4 cm/sec	0.6 cm/sec
P	0.3	0.3

FIGURE VII-19 EXAMPLE PROBLEM: CALCULATION OF TRAVEL TIME FOR SULFATE FROM HOLDING BASIN TO RIVER

3) Calculate the seepage velocity using Equation VII-36,

$$v_s = \frac{KI}{p} = \frac{(0.5)\ (0.0015)}{(0.3)} = 0.0025 \text{ cm/sec}$$

4) Estimate the travel time to the river using either Equation VII-42 or VII-43, where the distance between the basin and the river is 6×10^4 cm,

$$\Delta t = \Delta l / v_s = \frac{(6 \times 10^4)}{(0.0025)} = 2.4 \times 10^7 \text{ sec}$$

or

$$\Delta t = p \frac{\Delta l}{KI} = \frac{(0.3)(6 \times 10^4)}{(0.5)(0.0015)} = 2.4 \times 10^7 \text{ sec}$$

Hence, the travel time for sulfate, from the basin to the river is 280 days or approximately 9 months.

END OF EXAMPLE VII-2

7.4 POLLUTANT TRANSPORT PROCESSES

The basis for ground water transport of contaminants is discussed in this section. First, the processes of dispersion and diffusion are reviewed in Section 7.4.1. This section includes both the definition and the estimation of these parameters for the one-dimensional and then the two-dimensional case. Finally, chemical and biological processes that affect contaminant transport are discussed in Section 7.4.2. This section discusses how sorption and rate processes can be represented in screening methods.

7.4.1 Dispersion and Diffusion

7.4.1.1 Hydrodynamic Dispersion

Up until this point, the migration of dissolved solutes through porous media was assumed to be only related to the seepage velocity of ground water (see Section 7.3.3). Under this assumption, an injected solute or contaminant would travel through the aquifer by plug flow (e.g., piston-like motion). The concentration profile would resemble a step function. However, experience has shown that solutes do not exhibit true plug flow. Instead, solutes gradually spread out from their initial point of introduction and occupy an ever increasing volume of the aquifer, moving far beyond the region that it would be expected to occupy based on the average seepage velocity alone. This spreading or dispersing phenomenon is called hydrodynamic dispersion.

Hydrodynamic dispersion constitutes a nonsteady, irreversible mixing process. Bear (1972) states that hydrodynamic dispersion is the macroscopic outcome of the

solute's movement due to microscopic, macroscopic and megascopic effects. On the microscopic scale, dispersion is caused by: a) external forces acting on the ground water fluid, b) macroscopic variations in the pore geometry, c) molecular diffusion along solute concentration gradients, and d) variations in the fluid properties, such as density and viscosity.

In addition to inhomogeneity on the microscopic scale (i.e., pores and grains), there may also be inhomogeneity in the hydraulic properties (macroscopic variation). Variations in hydraulic conductivity and porosity introduce irregularities in the seepage velocity with the consequent additional mixing of solute. Finally, over large distances of transport, megascopic or regional variations in the hydrogeologic units or strata are present in the aquifer. The effect of scale on the mechanisms of hydrodynamic dispersion are shown schematically in Figure VII-20. Since the magnitude of dispersion varies significantly with the scale of the physical system, care must be taken to properly define which scale is to be used in any given problem.

The hydrodynamic dispersion coefficient D (cm^2/sec) may be mathematically expressed as the sum of two dispersive processes: mechanical dispersion D_m (cm^2/sec) and molecular diffusion D* (cm^2/sec). Thus, the sum is:

$$D = D_m + D^* \qquad \text{(VII-45)}$$

Molecular diffusion D* is a microscopic and molecular scale process that results from the random thermal induced motion of the solute molecules within the liquid phase. This process is independent of the advective motion of the ground water and can be of significant importance at low flow velocities and very near solid surfaces. Duursma (1966) reported experimentally determined molecular diffusion coefficients that ranged between 2×10^{-6} and 6×10^{-6} cm^2/sec for trivalent and monovalent ions (both positive and negative) in fine sand. However, molecular diffusion is generally specified (Sudicky, 1983; Gillham et al., 1984) as:

$$D^* = 1 \times 10^{-6} \text{ cm}^2/\text{sec} \qquad \text{(VII-46)}$$

Mechanical dispersion D_m occurs predominately on a macro and megascopic scale and is due to the "mechanical mixing" of the solutes. Such mechanical mixing is caused by: a) variations in the velocity profile across the water filled portions of a pore, b) variations in the channel size of the pores, c) the tortuosity, branching and interfingering of pore channels.

7.4.1.2 One-Dimensional Flow

7.4.1.2.1 Introduction

For one-dimensional flow, mechanical dispersion D_m(cm^2/sec) is generally expressed

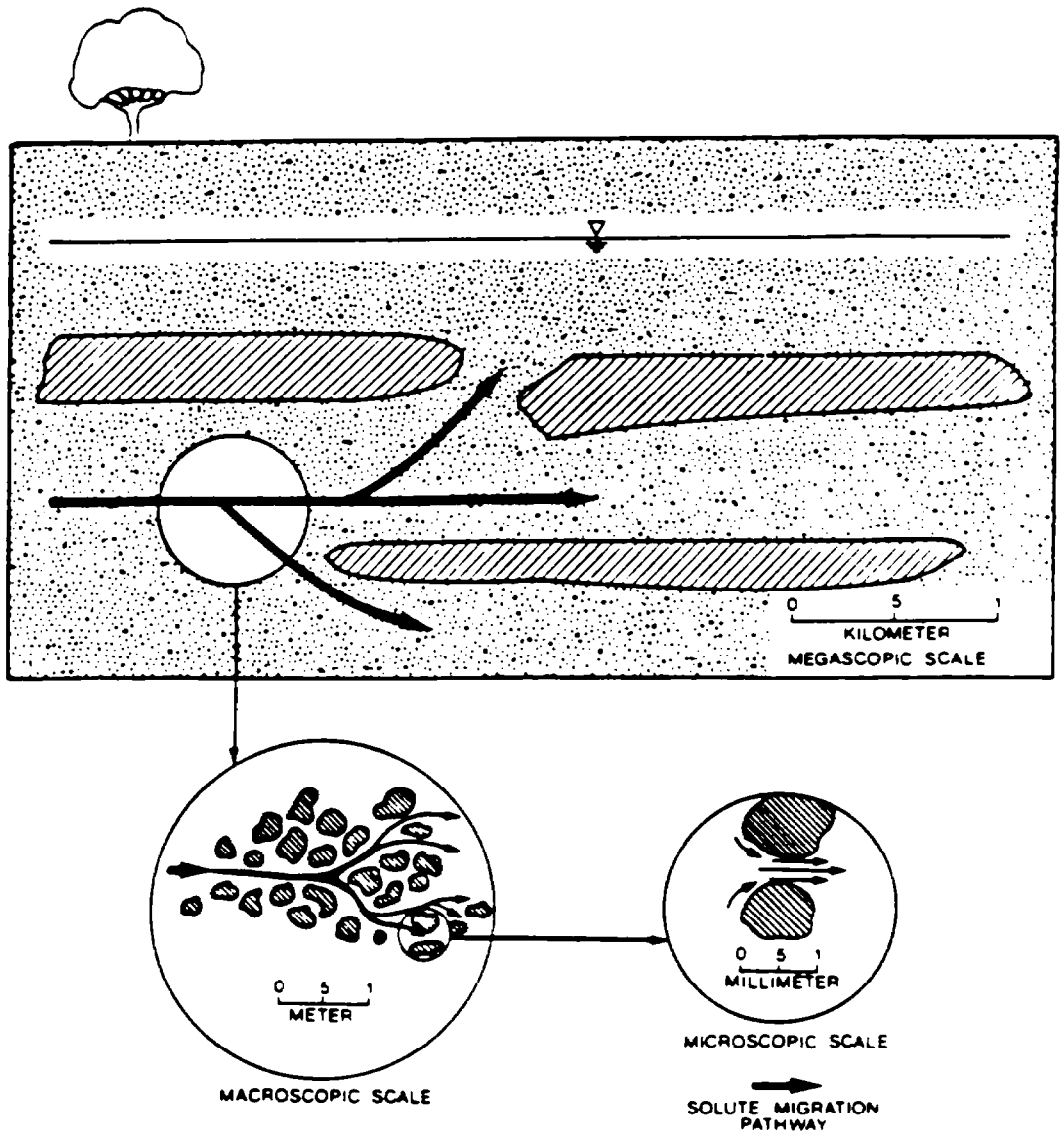

FIGURE VII-20 SCHEMATIC SHOWING THE EFFECT OF SCALE ON HYDRODYNAMIC DISPERSION PROCESSES

as a function of the seepage velocity v_s (cm/sec) with the relationship:

$$D_m = \alpha_l v_s \qquad \text{(VII-47)}$$

where α_l (cm) is the longitudinal dispersivity of the porous medium. Upon substitution of Equation VII-47 into Equation VII-45, the hydrodynamic dispersion coefficient D (cm^2/sec) becomes:

$$D = \alpha_l v_s + D^* \qquad \text{(VII-48)}$$

where the molecular diffusion D^* (cm^2/sec) is given by Equation VII-46.

Unfortunately, dispersivity α_l is not a constant but rather appears to depend on the mean travel distance or scale at which the measurements were taken (Fried, 1975; Pickens and Grisak, 1981 a, b; Sudicky, 1983). For example, laboratory experiments give values of dispersivity in the range of 10^{-2} to 1 cm, while field determined values range from about 10^3 to 10^4 cm.

7.4.1.2.2 Estimating Longitudinal Dispersivity

A rough estimate of longitudinal dispersivity in saturated porous media may be made by setting α_l (cm) equal to 10% of the mean travel distance $\bar{x}$ (cm) (Gelhar and Axness, 1981):

$$\alpha_l = .1\bar{x} \qquad \text{(VII-49)}$$

In Figure VII-21, 48 values of longitudinal dispersivity are plotted as a function of scale length of the experiment for saturated porous media (Lallemand-Barres and Peaudecerf, 1978). Note in Figure VII-21 the line predicted by Equation VII-49. Lallemand-Barres and Peaudecerf (1978) concluded that field-scale dispersivity was independent of both the aquifer material and its thickness. In addition, Equation VII-49 and Figure VII-21 suggest that longitudinal dispersivity increases indefinitely with scale length.

More recently, Gelhar et al. (1985) reviewed the available literature and obtained 77 values of longitudinal dispersivity from saturated field studies and 13 values of longitudinal dispersivity from unsaturated field and laboratory studies. The saturated media results are shown in Figure VII-22 and the unsaturated media results in Figure VII-23. These data also show that longitudinal dispersivity increases with scale length. However, a critical evaluation of saturated site data in terms of reliability (as indicated by the size of the circles in Figure VII-22) led Gelhar et al. (1985) to suggest that no definite conclusion could be reached concerning scales greater than 100 meters. Longitudinal dispersivity probably approaches asymptotically a constant value for very large or megascopic scale lengths (Gelhar and Axness, 1983; Sudicky, 1983). In addition, the 10 percent rule of thumb expression for longitudinal dispersivity given by Equation VII-49 does not hold in the unsaturated zone. Rough approximations of longitudinal dispersivity for unsaturated flow can be made by using Figure VII-23, where scale means the mean travel distance or simply the distance from the origin of the contaminant.

To estimate longitudinal dispersion, an appropriate distance is determined (typically the distance from the contaminant source to the furthest point of interest). The dispersivity is then selected for the chosen distance from either Equation (VII-44) or Figure VII-22 for the saturated zone or Figure VII-23 for the unsaturated zone.

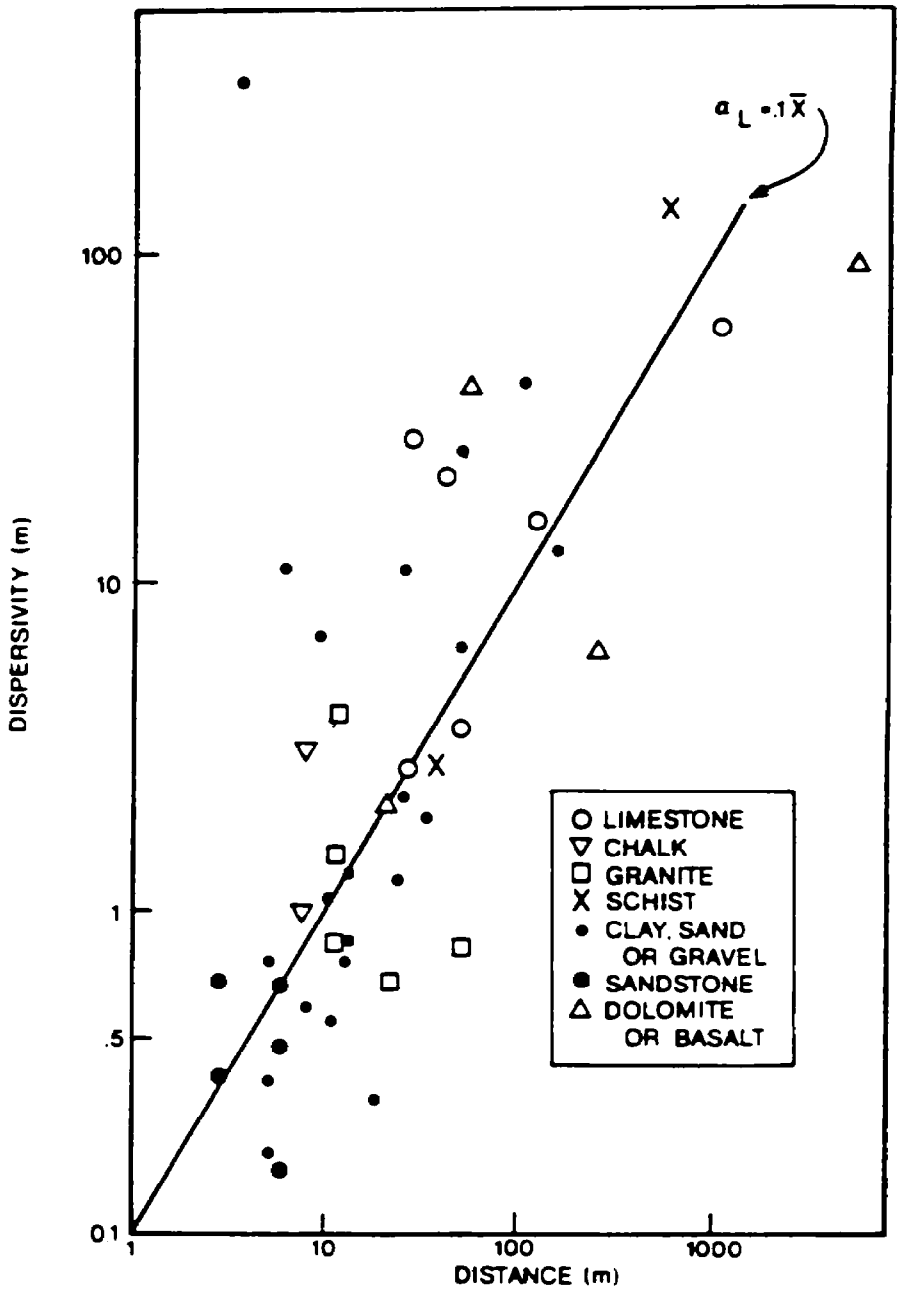

FIGURE VII-21 FIELD MEASURED VALUES OF LONGITUDINAL DISPERSIVITY AS A FUNCTION OF SCALE LENGTH FOR SATURATED POROUS MEDIA. REFERENCE: LALLEMAND-BARRES AND PEAUDECERF (1978)

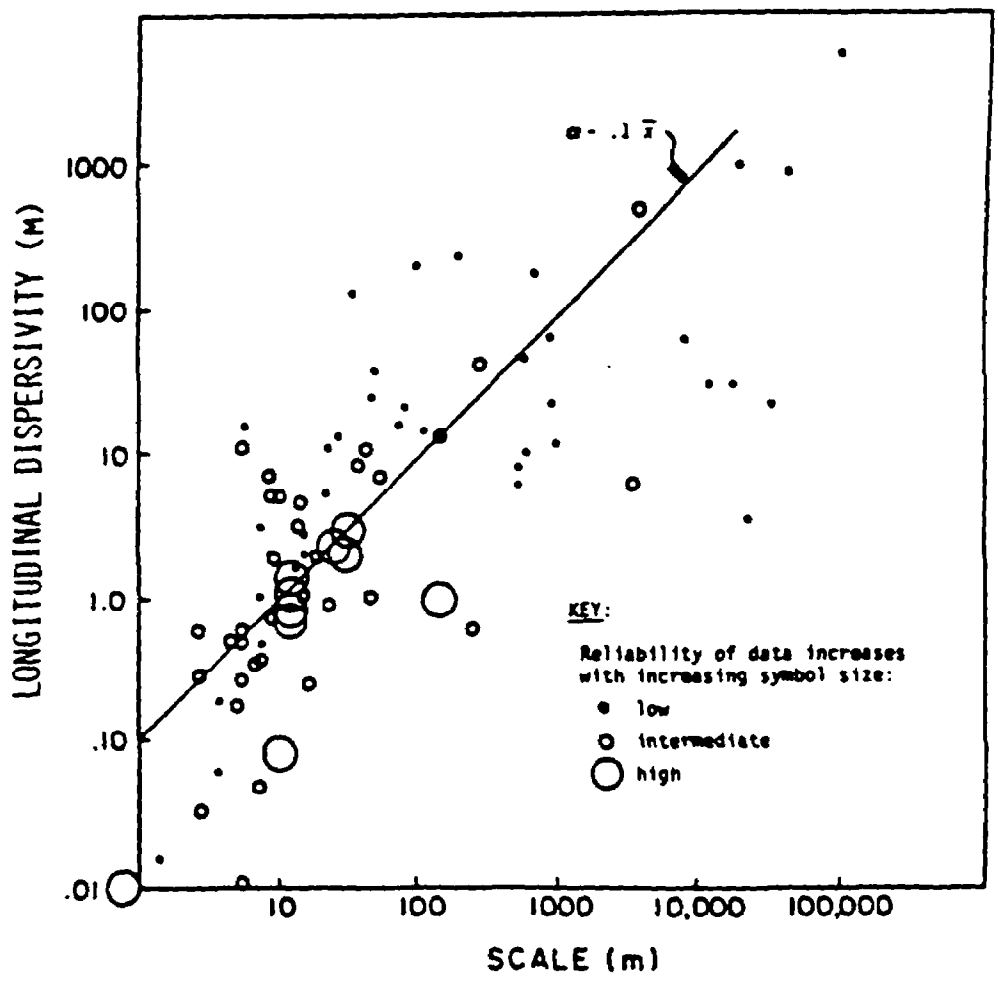

FIGURE VII-22 A PLOT OF LONGITUDINAL DISPERSIVITY VS. SCALE LENGTH FOR SATURATED POROUS MEDIA. REFERENCE: GELHAR ET AL. (1985)

Dispersion is then calculated using Equation (VII-48) or Equation (VII-47) for one-dimensional flow.

7.4.1.2.3 Solute Transport Equation

In order to better visualize the concept of dispersion, a brief discussion is given concerning the equation describing one-dimensional solute transport in ground water flow systems. The partial differential equation describing the one-dimensional, advective-dispersive transport of non-reactive solutes in saturated (or unsaturated), homogeneous porous media is given by:

$$\frac{\partial C}{\partial t} = D \frac{\partial^2 C}{\partial x^2} - v_s \frac{\partial C}{\partial x} \qquad \text{(VII-50)}$$

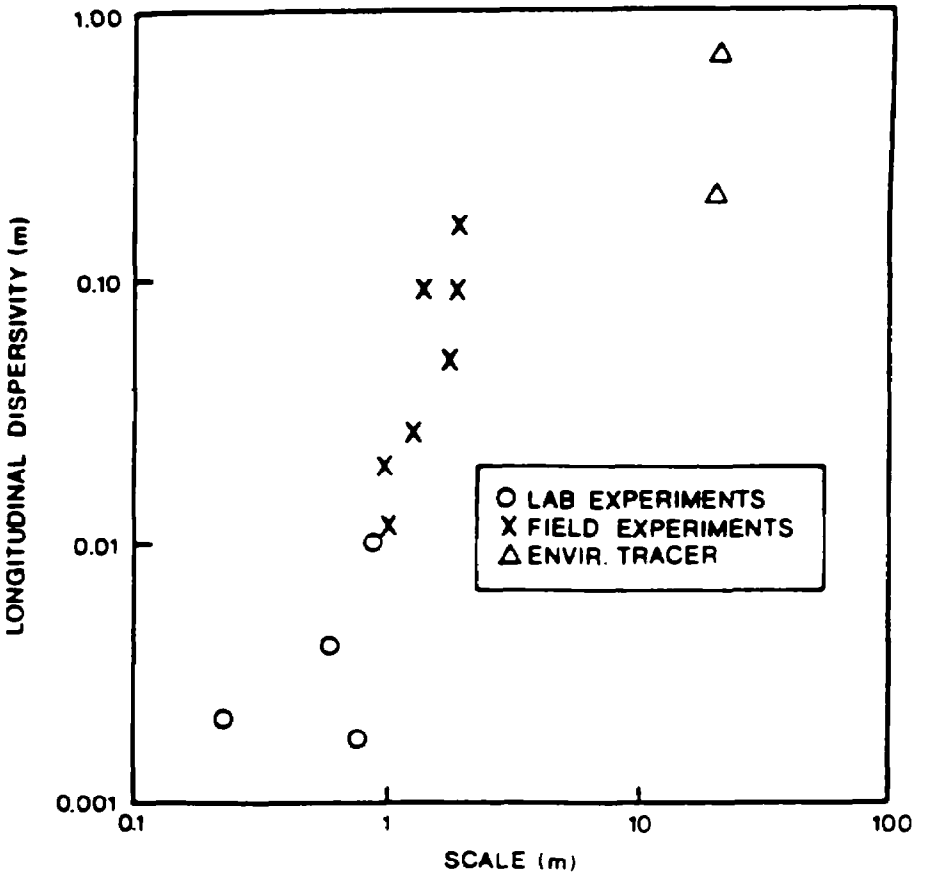

FIGURE VII-23 A PLOT OF LONGITUDINAL DISPERSIVITY VS. SCALE LENGTH FOR UNSATURATED POROUS MEDIA. REFERENCE: GELHAR ET AL., (1985)

where c (g/ml) is the solute concentration at time t (day) and distance x (m), D (m^2/day) is the hydrodynamic dispersion coefficient and v_s (m/day) is the ground water seepage velocity.

If the aquifer is initially assumed to be solute free and if the D and v_s parameters are constant over the distance of interest, then a solution to Equation VII-50 for a step function input (i.e., the initial concentration goes from zero to a value c_o at t = 0) can be obtained (Ogata and Banks, 1961; Ogata, 1970). The analytic solution and a worked out example using an integrated form of Equation VII-50 are given in Section 7.5.4. Note that a constant hydrodynamic dispersion coefficient D was used when solving Equation VII-50 in Section 7.5.4. Yet, Equation VII-49 and Equation VII-50 indicate that D is a function of distance or scale. Unfortunately, no simple analytic solution exists for the general case of a spatially varying dispersivity term. Hence, the distance or scale of the problem is used to compute the longitudinal dispersivity.

Consider the analytic solution to Equation VII-50 from Section 7.5.4, shown schematically in Figure VII-24. The solute concentration is plotted as a function of distance in Figure VII-24a at times t_1 and t_2, where t_2 is greater than t_1. The solute concentration is plotted as a function of time in Figure VII-24b. The solute concentration versus time plot is also known as a breakthrough curve. Each plot in Figure VII-24 also shows the solution to Equation VII-50 for plug flow (i.e., no dispersion).

A comparison between plug flow and dispersive flow in Figure VII-24 shows an "S" shaped curve when dispersion is considered. As time or distance increases, the S shape flattens out. Remember that solutes in plug flow move at the seepage velocity and as a sharp front. Hence, solutes in dispersive flow are spreading out and the leading portion of the solutes are moving faster than the seepage velocity and the trailing portion are moving slower than the seepage velocity. At the point $c/c_0 = 0.5$, the solutes move at a rate approximately equal to the seepage velocity.

In Section 7.3.3.2, the question of travel time was addressed but only for non-reactive, non-dispersive, plug flow. It should now be obvious from the above discussion that ignoring the effect of dispersion can considerably overestimate the travel time of a contaminant. The leading front of a contaminant plume may reach a given location as much as an order of magnitude faster than that predicted by plug or non-dispersive flow. Plug flow only predicts the travel time for the center or centroid of solute mass of the contaminant plume. The travel time estimates given by plug flow in Section 7.3.3.2 are still useful in that it gives a time reference for contaminant transport. What plug flow considerations alone cannot do is to predict time of arrival for the leading edge of a contaminant plume.

Unfortunately, there is no simple, algebraic way to incorporate the effect of dispersion into calculating time of travel and solute concentration profiles. Equation VII-50 has to be solved repeatedly for different times and distances. The example given above plus four other examples of solute transport are discussed with additional detail in Section 7.5.

7.4.1.2.4 Measuring Longitudinal Dispersivity

In Section 7.4.1.2.1, several figures and equations were given as a means of estimating longitudinal dispersivity. These methods of estimation are more than adequate during the screening phase of a ground water project.

A great deal of controversy still exists as to the true meaning of hydrodynamic dispersion, its correct mathematical representation and the proper method to measure it in the field. In Equation VII-49, longitudinal dispersivity was estimated as a linear function of scale distance. However, many other representations are possible (Pickens and Grisak, 1981 a, b). Even stochastic representations are available (Todorovic, 1975; Smith and Schwartz, 1980; Gelhar and Axness, 1983).

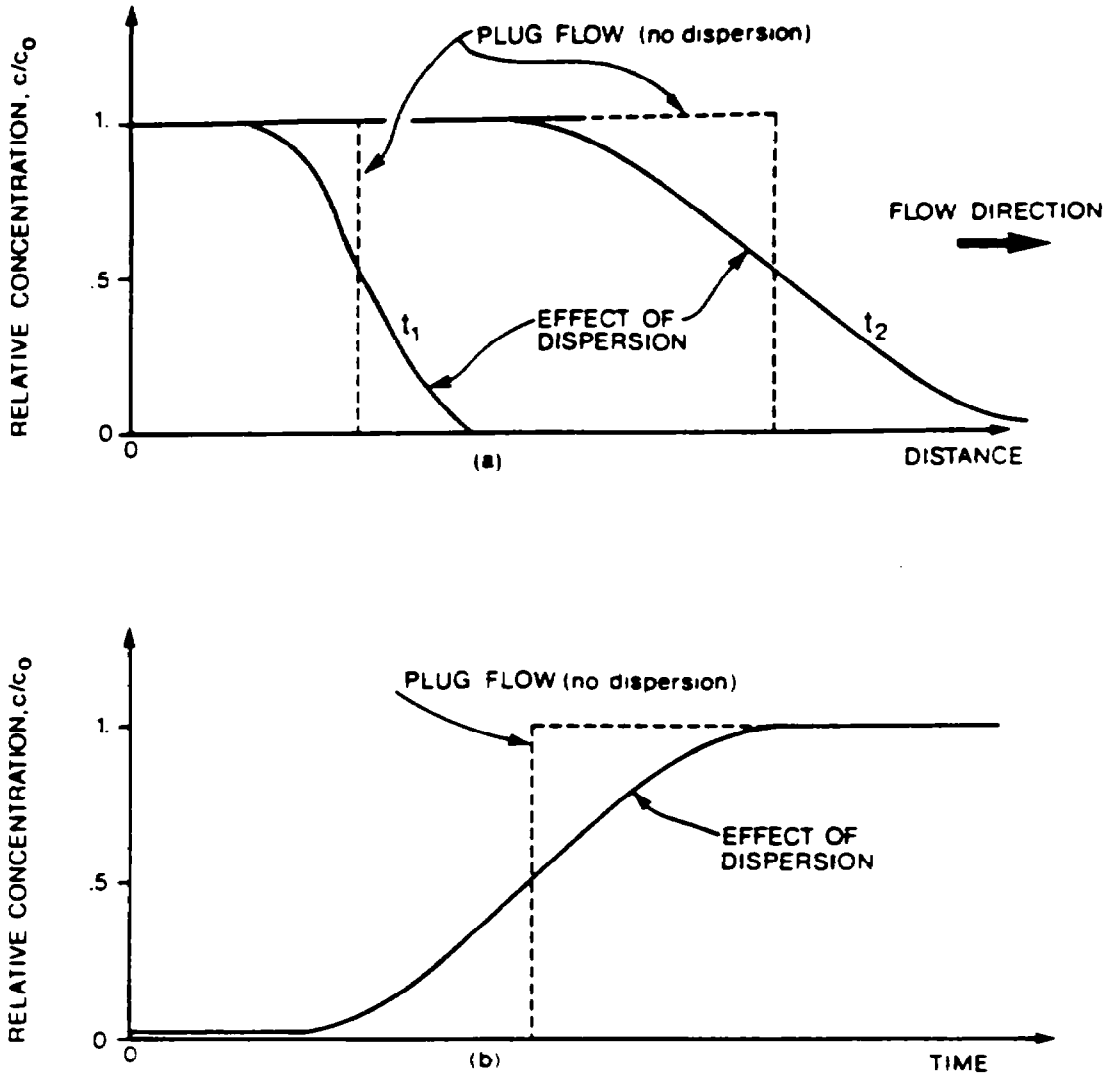

FIGURE VII-24 SCHEMATIC SHOWING THE SOLUTION OF EQUATION VII-50 AND THE EFFECT OF DISPERSION: A) SOLUTE CONCENTRATION AS A FUNCTION OF DISTANCE AT TIMES T_1 AND T_2, B) SOLUTE CONCENTRATION AS A FUNCTION OF TIME (THE BREAKTHROUGH CURVE)

The typical field method to measure longitudinal dispersivity consists of injecting a tracer into the porous medium and then monitoring the arrival time of the tracer concentrations. The experimental data are then fitted or calibrated (using either an analytical or numerical solution of the dispersion equation) to obtain the longitudinal dispersivity or dispersion coefficients. Many analytical methods of fitting the solute breakthrough curve are available, such as those given by Elprince and Day (1977) and Basak and Murty (1979). An extensive discussion on field methods to determine dispersion coefficients is also given by Fried (1975).

7.4.1.3 Multi-Dimensional Flow

7.4.1.3.1 Introduction

In any real ground water system, the point release of a solute or contaminant into the aquifer will produce an expanding, three-dimensional ellipsoid. The concentration profile of such a plume will be approximately Gaussian in shape in the transverse directions (both across and down). The concentration profile will also be approximately Gaussian in shape along the longitudinal direction if the point release is instantaneous (i.e., a slug or short pulse). The component or contribution of dispersion will generally be greatest along the direction of flow (longitudinal) and less in the transverse directions. The longitudinal direction is implicitly taken to be along the principal direction of ground water flow. The transverse directions t and v are perpendicular to the longitudinal but t (lateral-transverse) is in the same plane as that of ground water flow. The v or vertical-transverse direction is perpendicular to the l-t plane but it is not necessarily in the same direction as gravity. The vertical-transverse direction is only along the direction of gravity when the ground water flow is in the horizontal direction.

In a layered, unconsolidated aquifer with horizontal flow, the effect of vertical dispersion will generally be significantly less than from horizontal dispersion. Vertical mixing is a slow process and solute will often remain confined to a narrow horizontal zone in the aquifer. Hence, most analyses, including those of the screening methods, consider one- or two-dimensional analyses of solute transport. If the source of the solute or contaminant is very wide compared to the distance of interest, then one-dimensional analyses (such as is given in Section 7.4.1.2) are adequate.

As in Section 7.4.1.1, the coefficient of hydrodynamic dispersion D is defined as the linear sum of mechanical dispersion and molecular dispersion D^*. However, for an anisotropic, three-dimensional medium, Scheidegger (1961) and Bear (1972) define D as a fourth-rank tensor, containing 81 components. If the coordinate axes are chosen so that they coincide with the principal axes of dispersion, then virtually all of the off-diagonal terms of the tensor are zero.

In a two dimensional, horizontal, isotropic medium, the hydrodynamic dispersion coefficient becomes:

$$D_{xx} = \alpha_l v_{sx}^2/v_s + \alpha_t v_{sy}^2/v_s + D^*$$

$$D_{xy} = D_{yx} = (\alpha_l - \alpha_t) v_{sx} v_{sy}/v_s \qquad \text{(VII-51)}$$

$$D_{yy} = \alpha_t v_{sx}^2/v_s + \alpha_l v_{sy}^2/v_s + D^*$$

where the magnitude of the seepage velocity v_s (cm/sec) is given by:

$$v_s^2 = v_{sx}^2 + v_{sy}^2 \qquad \text{(VII-52)}$$

and where D^* (cm^2/sec) is molecular dispersion (see Equation VII-46); α_l (cm) and α_t (cm) are the dispersivities in the longitudinal and transverse directions, respectively; v_{sx} (cm/sec) and v_{sy} (cm/sec) are the longitudinal and transverse seepage velocity components, respectively; D_{xx}, D_{yy}(cm^2/sec) are the principal components of the hydrodynamic dispersion term; and D_{xy}, D_{yx}(cm^2/sec) are the off-diagonal components of the hydrodynamic dispersion term.

If the Cartesian coordinate system is chosen so that the longitudinal (i.e., the x) axis coincides with the direction of the average seepage velocity v_s, then D reduces to:

$$D_l = \alpha_l v_s + D^*$$

$$D_t = \alpha_t v_s + D^* \qquad \text{(VII-53)}$$

where D_l (cm^2/sec) and D_t (cm^2/sec) are the longitudinal and transverse hydrodynamic dispersion terms, respectively. This orientation of the Cartesian coordinate system is used in most of the problems in Section 7.5. The molecular dispersion term D^* (cm^2/sec) ranges in value between 10^{-6} and 10^{-5} cm^2/sec. The computation of the seepage velocity v_s is discussed in Sections 7.3.3.1, the longitudinal dispersivity term α_l (cm) is given in Section 7.4.1.2.2 and the transverse dispersivity term α_t (cm) is discussed below.

7.4.1.3.2 Estimating the Transverse Dispersivity Components

Whitaker (1967) predicted that for uniform flow in an isotropic, saturated porous medium, that dispersivity would be dominated by the longitudinal dispersivity component α_l and that α_l would be exactly three times the value of the lateral-transverse component α_t. Hence:

$$\alpha_l/\alpha_t = 3 \qquad \text{(VII-54)}$$

The estimate of Equation VII-54 agrees with the field data analyzed recently by Gelhar et al. (1985) for unconsolidated materials. The α_l/α_t ratio ranged between 2.1 and 5 for alluvial and glacial deposits (sand and gravel), the average being 3.5. The ratio of α_l/α_t for limestone was 3.2. The vertical transverse component of dispersivity α_v was generally two orders of magnitude smaller than that of the horizontal components. The α_l/α_v ratio ranged between 30 and 860 for alluvial/glacial deposits, the average being 400 (Gelhar et al., 1985).

The dispersivity components can be estimated for screening purposes as follows: a) use the 10 percent rule of thumb from Equation VII-49 to estimate the longitudinal α_l component for saturated media and Figure VII-23 for unsaturated media, b) then use either Equation VII-54 or the above ratios to estimate the transverse dispersivities α_t and/or α_v.

7.4.1.3.3 Alternative Dispersion Formulations

Before leaving this section on dispersion, one additional comment should be made concerning spatial variability. In both the one-dimensional and two-dimensional representations of solute transport, it is conveniently assumed that the seepage velocity v_s could be averaged and expressed as a constant. However, the seepage velocity may have substantial variations in space. Consider Figure VII-25 which schematically shows how the horizontal seepage velocity $v_s(z)$ may vary dramatically with depth. Such stratification or variations are quite common in aquifers and are caused by the variations in the hydraulic conductivity and porosity in the medium (Sudicky et al., 1983; Gillham et al., 1984). Recently, several researchers such as Molz et al. (1983), Sudicky (1983), Gillham et al. (1984), etc. have suggested that the primary physical mechanism that causes the spreading of solute in the longitudinal direction is due to the vertical variation in the seepage velocity $v_s(z)$. Hence, they argue that the phenomenon of scale-dependent dispersivity and hydrodynamic dispersion is an artifact. They suggest that more emphasis should be placed on the accurate determination of hydraulic conductivity and aquifer inhomogeneities.

Artifact or not, the use of hydraulic dispersion algorithms is currently the only practical method, short of direct measurement, to account for dispersive solute transport. Those who are in the screening phase of a ground water project are unlikely to have access to a detailed survey of the hydraulic conductivity and seepage velocities of the aquifer. The analytic and heuristic methods presented here and in Section 7.5 are the best that are currently available.

7.4.2 Chemical and Biological Processes Affecting Pollutant Transport

Pollutants in ground water can be affected by a number of chemical and biological processes as shown in Figure VII-26. Volatilization generally does not have to be considered in ground water screening problems unless the pollutant is within a few inches of the land surface and the media is highly permeable. Of the remaining

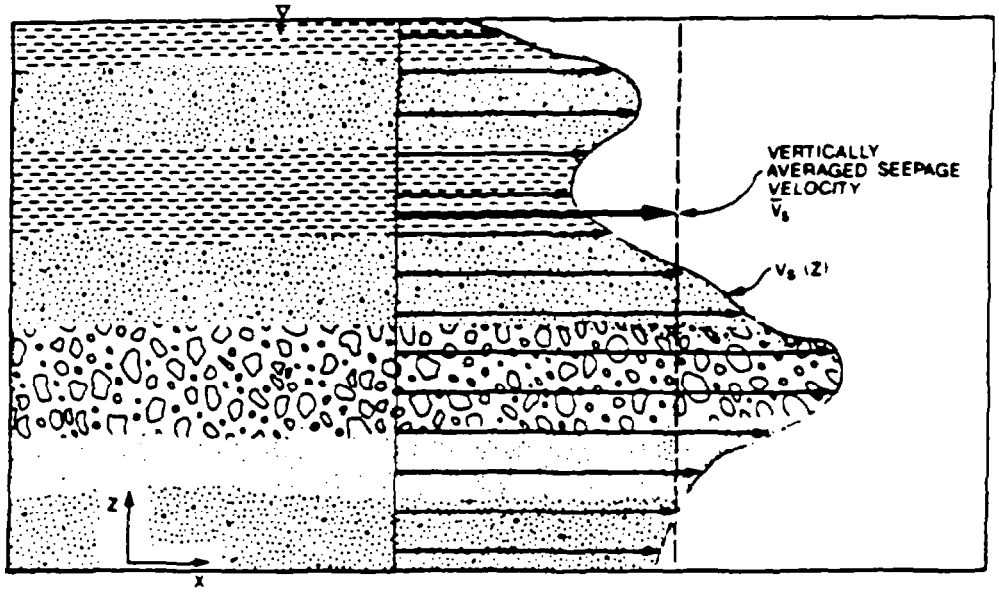

FIGURE VII-25 SCHEMATIC SHOWING HYPOTHETICAL VERTICAL VARIATION IN THE GROUND WATER FLOW VELOCITY

processes shown in Figure VII-26, some can be incorporated directly into the analytical methods to be presented later in this chapter. These processes are sorption-desorption and ion-exchange, hydrolysis, and biodegradation.

Other chemical processes can be considered separately from the analytical methods. Processes which can be evaluated include acid-base reactions, speciation, complexation, oxidation-reduction reactions and precipitation-dissolution. For example, to determine if sorption is important and if so, an appropriate coefficient, the metal speciation must be determined for the pH and redox conditions present in the ground water. This can be done based on Eh-pH diagrams or equilibrium geochemical models. At this point, the transport of the metals can be estimated using the analytical methods discussed in Section 7.5. Next, the extent of precipitation-dissolution can be determined using methods similar to those described in Chapter 4 of this manual. If the calculations show that some metal could precipitate, the transport calculations can be revised using the new dissolved concentration. In most surface and ground waters, revised transport calculations will not be necessary because sorption is the dominant process at typical metal concentrations. However, within a waste material and immediately downgradient of it, metal concentrations can be high so solubility limits should be checked.

7.4.2.1 Sorption

Sorption can be defined as the accumulation of a chemical in the boundary region of the soil-water interface. Sorption-desorption processes are an important

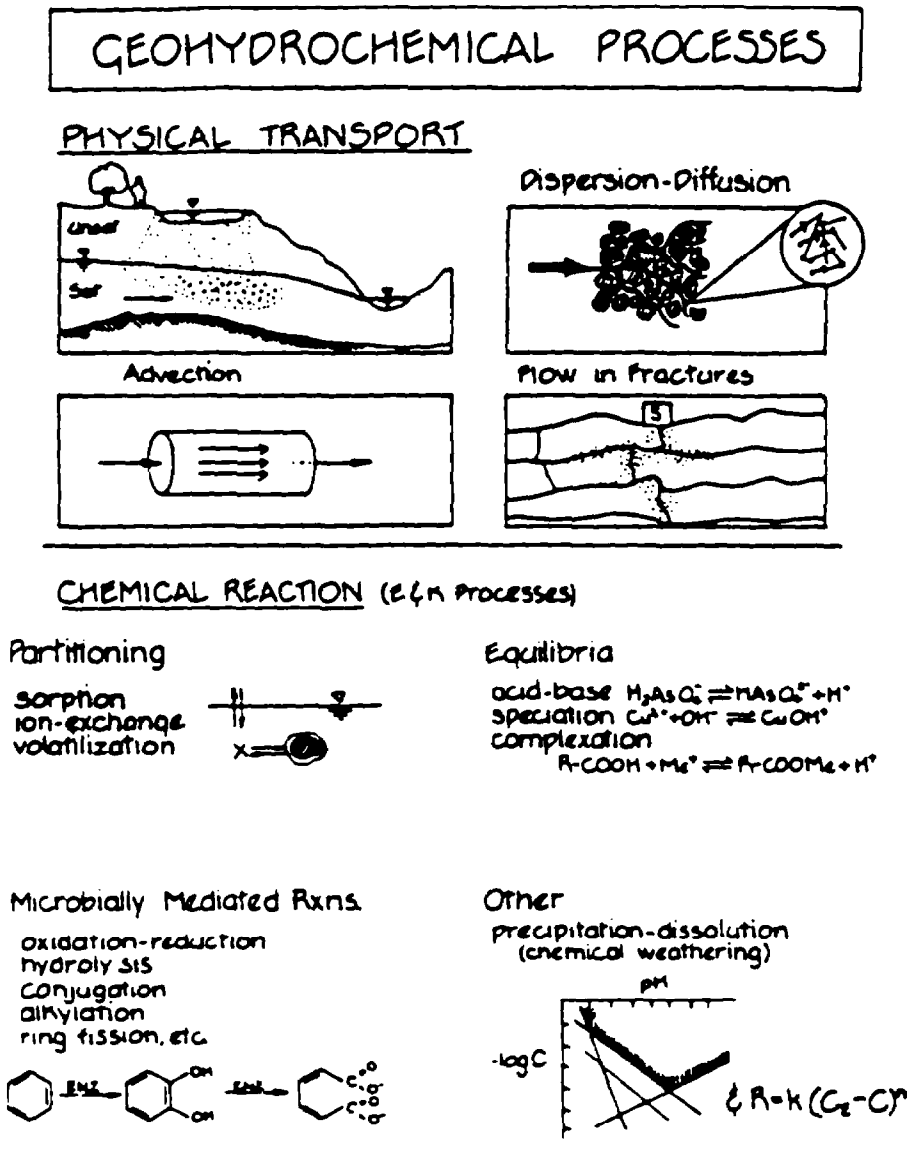

FIGURE VII-26 MAJOR EQUILIBRIUM AND RATE PROCESSES IN NATURAL WATERS. REFERENCE: SCIENCE APPLICATIONS, 1982

determinant of pollutant behavior in the subsurface environment. Because of the much higher solid to liquid ratios in ground waters than in surface waters, the concentration of even a moderately-sorbed pollutant can decrease significantly with distance as it migrates in the ground water. In addition to decreasing the aqueous concentration, there are several other implications of sorption. Volatization, even in the uppermost soil layers, is diminished. Rates of reactions such as microbial degradation can be different for the adsorbed pollutant and the portion remaining in solution. Unlike in surface waters where the adsorbed pollutant may still be advected

downstream associated with suspended sediment, in ground water the adsorbed pollutant is not ususally transported by advection or dispersion (the solid phase is immobile.) However, when the concentration gradient changes, the pollutant can be desorbed over time at the same or a different rate than it was sorbed onto the soil particles. This has important implications for handling waste disposal problems in that when "clean" water flushes an aquifer which previously contained water contaminated with metals or organic chemicals, the concentrations of the pollutants may remain relatively high until the reservoir of adsorbed pollutants has been depleted. In one case of high TCE contamination, the downgradient concentration was predicted to be 80 percent of the existing level even after the aquifer was flushed once with distilled water.

7.4.2.1.1 Retardation Factor

If sorption is modeled as a linear, equilibrium process, it can be incorporated into the analytical methods presented in Section 7.5 as a retardation factor. This factor is defined as follows:

$$R_d = 1 + (K_d \rho_b / p) \qquad \text{(VII-55)}$$

where

R_d = retardation factor (unitless)
K_d = distribution coefficient (ml/g)
ρ_b = bulk density (g/ml)
p = porosity (decimal fraction).

The term, K_d is used in most ground water literature, but it is synonymous with K_p, the partition coefficient, which is more common in chemical and surface water literature. If a pollutant is not sorbed, the retardation factor equals 1 which shows that the pollutant moves at the same speed as the ground water. If the retardation factor is greater than 1, say 2, the pollutant will move half as fast as the water. Typical values for bulk density and porosity for different types of soil materials were included in Table VII-2 and VII-4, respectively.

The K_d term is an empirical coefficient for a specific constituent under a particular set of conditions. For linear, equilibrium sorption, K_d can be measured in the laboratory as:

$$K_d = [s]/[c] \qquad \text{(VII-56)}$$

where K_d = distribution coefficient, ml/g
[s] = concentration of pollutant sorbed on soil, g/g
[c] = concentration of pollutant in solution, g/ml.

K_d may be a function of the concentration of the sorbing chemical species itself, the concentration of any competing species (usually major ions affect trace constituents but not vice-versa), concentrations of any complexing species present (e.g., Cl, organics), pH of solution, the amount and type of adsorbent (e.g., clays, iron oxides, aluminum oxides), and the amount of organic matter associated with the solid phase. Figure VII-27 shows the effect of pH and organic matter on typical adsorption curves. When obtaining values for a pollutant of interest, these and other factors should be as similar as possible to the conditions in the problem being addressed. Selected K_d values for metals have been included in Chapter 4. Available values for Al, Sb, As, Ba, Be, B, Cd, Cr, Cu, F, Fe, Pb, Mn, Hg, Mo, Ni, Se, Na, SO_4, V, and Zn have been compiled from the literature for a variety of conditions (Rai and Zachara, 1984). The values are reported along with characteristics of the absorbent (i.e., type of material, cation exchange capacity, and surface area), concentration of species of interest, and solution characteristics (i.e., composition, molar concentration of adsorbing species and pH).

For organic chemicals, the adsorption coefficients are usually referred to as partition coefficients K_p. The partition coefficient can be calculated from the octanol-water partition coefficient K_{ow} (unitless) and estimates of the organic fraction of sand and silt plus clay (see Section 2.3.2). The octanol-water partition coefficient can also be calculated from solubility data using an empirical relationship. Typical values for solubility and K_{ow} are included in Tables II-5 through II-9 for the 129 priority pollutants. Additional data on pesticides including EDB and DBCP are included in Zalkin et al.(1984) and Bowman and Sans (1983). Partition coefficients and sorption in general are discussed in more detail in Section 2.3.2.

EXAMPLE PROBLEM VII-3

Calculate the retardation factor for anthracene in a silty-clay formation where the organic carbon content of the silty-clay is about 0.01.

From Table II-9, the octanol-water partition coefficient is found to be 28,000 (unitless). The organic carbon partition coefficient is first estimated from Equation II-18 as follows:

$$K_{oc} = 0.63\ K_{ow}$$
$$= (0.63)(28{,}000)$$
$$= 17{,}640\ ml/g$$

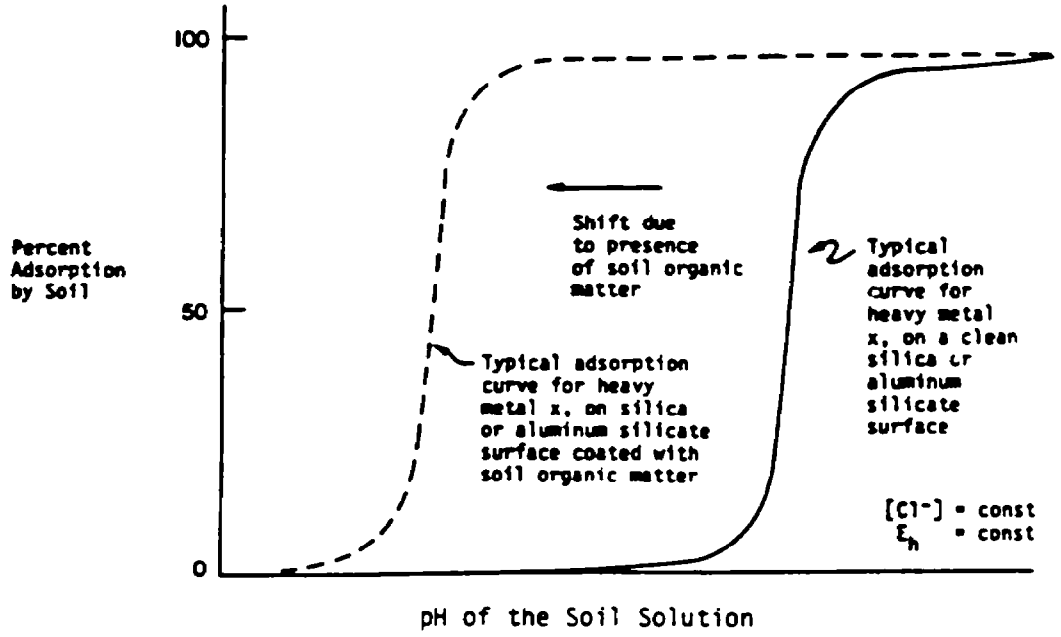

a) Generalized Heavy Metal Adsorption Curve for Cationic Species
(e.g., $CuOH^+$)

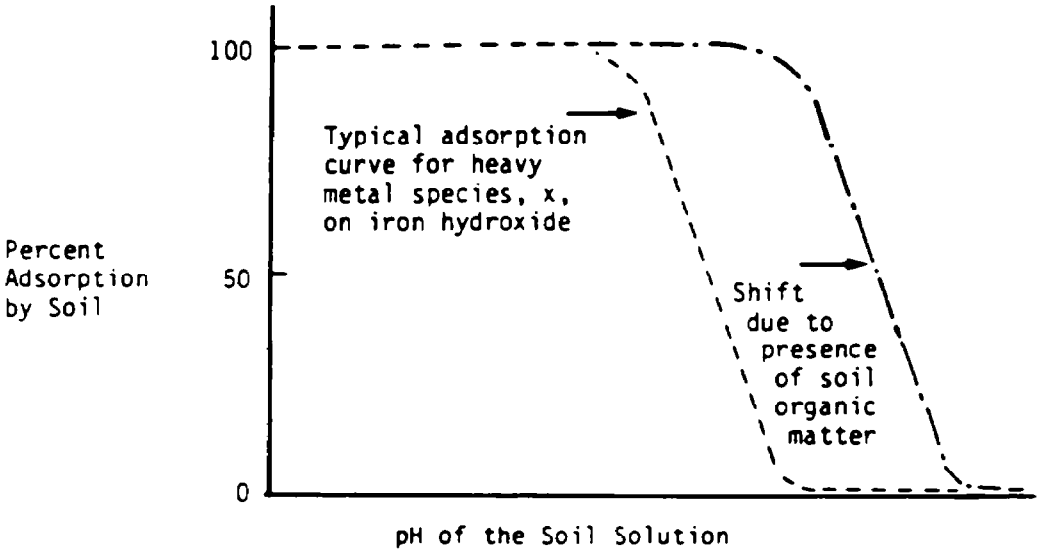

b) Generalized Heavy Metal Adsorption Curve for Anionic Species
(e.g., CrO_4^{2-})

FIGURE VII-27 HYPOTHETICAL ADSORPTION CURVES FOR A) CATIONS AND B) ANIONS SHOWING EFFECT OF pH AND ORGANIC MATTER

where the conversion coefficient 0.63 has units of ml/g.

The partition coefficient, K_p, is calculated next using Equation II-17 as follows:

$$K_p = K_{oc}\left[0.2(1-f)X_{oc}^{s} + fX_{oc}^{f}\right]$$

where

$$f = \frac{\text{mass of silt and clay}}{\text{mass of silt, clay and sand}} \quad (0 \le f \le 1)$$

X_{oc}^{s} = organic fraction of sand ($0 \le X_{oc}^{s} \le 0.1$)

X_{ox}^{f} = organic fraction of silt-clay ($0 \le X_{oc}^{f} \le 0.1$)

Substituting the above data yields the following expression:

$$K_p = 17{,}640\ [0.2(1-1)0 + 1(0.01)]$$
$$= 176 \text{ ml/g}$$

Finally, the retardation factor is calculated as follows using Equation VII-55, where the bulk density and porosity of this formation are 1.6 g/ml and 0.3 (unitless), respectively:

$$R_d = 1 + \frac{K_p \rho_b}{p}$$

$$= 1 + \frac{(176 \text{ ml/g})(1.6 \text{ g/ml})}{0.3}$$
$$= 940$$

The relative amounts of anthracene in the dissolved and sorbed phases can be estimated using a modified form of Equation II-22 as follows:

$$\frac{c}{c_t} = \frac{c}{(c + s\rho_b/p)} = \frac{1}{R_d}$$

where c = total dissolved pollutant concentration
$c_t = c + s\rho_b/p$
s = mass of sorbed pollutant per unit mass of soil
R_d = retardation factor

hence,

$$\frac{c}{c_t} = \frac{1}{940} = 0.001$$

Thus, 0.1 percent of the anthracene is in the dissolved phase and the rest is associated with the solid phase.

END OF EXAMPLE PROBLEM VII-3

7.4.2.1.2 Effect of Sorption on Seepage Velocity and Travel Time

A solute subject to sorption will travel at the following average velocity:

$$v_s^* = v_s / R_d \qquad \text{(VII-57)}$$

where v_s^* (cm/sec) is the velocity of the solute, v_s (cm/sec) is the seepage velocity of the ground water and R_d (unitless) is the retardation factor accounting for sorption. Since the retardation factor R_d is equal to one for no sorption and is greater than one with sorption, the solute velocity v_s^* will always be less than or equal to that of the seepage velocity.

Ground water travel time Δt was defined in Section 7.3.3.2 as the average time that it takes ground water to travel a specified distance. In the case of a solute subject to linear, equilibrium sorption, its travel time will be:

$$\Delta t^* = R_d \Delta t \qquad \text{(VII-58)}$$

where Δt^* (sec) is the travel time of the solute, Δt (sec) is the travel time of ground water and R_d (unitless) is the retardation factor accounting for sorption. Hence, the travel time of a solute will be greater than or equal to that of the ground water. (An insignificant exception may exist for solutes like chloride, which because of anion exclusion by negatively charged soils, may move slightly faster than the ground water itself.)

7.4.2.2 Other Processes

Processes such as biodegradation and hydrolysis can be represented in some of the analytical methods by first-order decay rates. The actual rate constant used should be the sum of the individual first order decay rate for the specific pollutant. Hydrolysis rates are given in Section 2.5.3 for organic chemicals. Biodegradation is presented in Section 2.5.1. Biodegradation for some compounds may be more important in ground waters than in surface waters due to the slow velocities, and hence long travel

times, and the common occurrence of anoxic conditions. Figure VII-28 shows the degradation of tetrachlorethylene and the resulting products of the series of dehydrochlorination reactions which occur under anoxic conditions. Biodegradation rates in ground water for selected organic chemicals are available from Wood et al., 1981 and Wilson and McNabb, 1981.

7.5 METHODS FOR PREDICTING THE FATE AND TRANSPORT OF CONVENTIONAL AND TOXIC POLLUTANTS

7.5.1 Introduction to Analytical Methods

In this section, five analytical models are presented which can be used to predict the extent of contamination in ground water. A summary of these models is given in Table VII-12. For each model, the types of contaminant sources, flow situations, source release characteristics and spatial dimensions are briefly described. A discussion of the assumptions and the mathematical expression for each model is given in Figures VII-29 to VII-33. Finally, a more complete presentation of the derivation and use of each model, plus one or more worked out examples or applications are given in Sections 7.5.2 to 7.5.6. Each model has been programmed for solution on micro-computers (Mills et al., 1985).

Obviously, there exist far more than five analytical models that describe ground water contamination. These five were chosen because they represent many of the typical ground water contamination problems for which solutions could be obtained with hand-held calculators. A more comprehensive collection of one-dimensional analytical transport models is given by van Genuchten and Alves (1982) and multiple-dimension analytical models by Yeh (1981) but these are primarily suitable for solution with large desk-top or main-frame computers. The models chosen in this section are relatively simple to use, yet are powerful in their range of applications.

Analytical methods allow prediction of contaminant concentrations in the aquifer at given times and locations as a result of an individual contaminant source. The simplest methods are based on the theory of flow to a pumping well (see Section 7.5.2). Most analytical methods, however, involve solving some form of the equation of flow in porous media. The complexity of the solutions varies greatly, depending on the number of dimensions included and the simplifying assumptions made. The equations range from simple, one-dimensional advective-transport equations to those simulating contaminant dispersion, diffusion, sorption and decay in two dimensions.

Analytical techniques are based on a number of simplifying assumptions. A key to using and interpreting the results of these methods appropriately, therefore, is understanding the assumptions which need to be made about the aquifer system and the various hydrogeologic parameters. Common assumptions include steady and uniform ground water flow in the saturated zone, aquifer isotropy (equal hydraulic conductivity in all directions), and constant contaminant concentration or mass loading rate from the contaminant source.

The reliability of the predictions generated depends on the inherent limitations

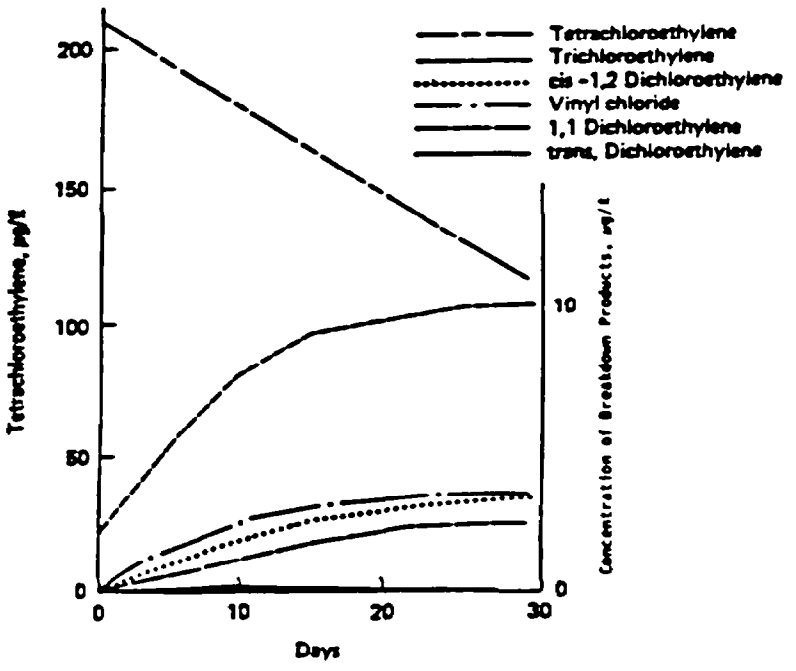

FIGURE VII-28 DEHYDROCHLORINATION RATE OF TETRACHLOROETHYLENE AND THE PRODUCTION RATE OF ITS DECHLORINATION PRODUCTS (AFTER WOOD ET AL., 1931)

of the equations used, the assumptions made, the data used, and the complexity of field conditions. It is critical for the user to understand how reasonable the assumptions of a particular technique are for the aquifer and site being examined. For example, a technique assuming aquifer isotropy may not be well suited for predicting contaminant transport through an aquifer with a well-developed fracture system. In addition, mathematical constraints due to functions used in the algorithms sometimes limit the usefulness of the analytical techniques, restricting them to relatively narrow ranges of input values. Predictions for a number of times and locations in the aquifer can be used to detect aberrant values stemming from those mathematical factors.

Solving the flow and transport equations of analytical methods requires a limited amount of field data. Typically, these data needs include:

- Contaminant concentration (or mass loading rate) at the source
- Effective porosity of the aquifer
- Aquifer thickness
- Soil bulk density
- Ground water velocity
- Hydraulic conductivity
- Dispersion coefficients in longitudinal and transverse directions
- Distribution coefficient (K_d) or retardation factor (R_d)
- Solute decay rate constants, if appropriate.

TABLE VII-12

SUMMARY OF SOLUTION METHODS

Solution Method	Contaminant Source	Contaminant Release	Spatial Dimensions and Coordinate System
Section 7.5.2 Figure VII-29	Migration of contaminant to pumping well	continuous and constant	1-D radial
Section 7.5.3 Figure VII-30	Migration of contaminant from injection well	continuous and constant	1-D radial
Section 7.5.4 Figure VII-31	Migration of contaminant from surface to ground water table, such as from: spills or dumping, leaky ponds or tanks, landfills, surface sites or deposits	continuous or intermittent release with a constant or exponential source strength	1-D cartesian
Section 7.5.5 Figure VII-32	Migration of contaminant in saturated zone, such as from: leaky ponds or tanks, spills, landfills	slug	2-D cartesian
Section 7.5.6 Figure VII-33	Migration of contaminant in saturated zone, such as from: leaky ponds or tanks, spills, landfills, surface sites or deposits	continuous or intermittent release with a constant source strength	2-D cartesian

Techniques specifically for wells also require well pumping or injection rate and duration of the pumping/injection period.

Despite some limitations, the analytical techniques are extremely useful in the assessment of aquifer contamination from point sources. Once the necessary input data are collected, contaminant prediction can be performed quickly and easily. The algorithms can be programmed on hand-held calculators or micro-computers. Once they are programmed, contaminant predictions for a number of times and locations can be generated quickly. In this way, maps of potential aquifer contamination can be prepared. When numerical modeling of a site is being considered, use of analytical calculations can indicate whether there is sufficient contamination potential to justify a major modeling effort and, if so, where the data collection efforts for the model should be concentrated.

Given their ability to address many types of problems, their relative ease of application and low cost, analytical techniques offer potential uses for a variety of

CONTAMINANT TRANSFER TO DEEP WELLS
(SEE SECTION 7.5.2)

Reference: Phillips and Gelhar (1978)

Objective: Compute concentration as a function of time in a deep well drawing water downward or upwards from a contaminated aquifer or layer.

Assumptions:
- uniform, radial flow in saturated media
- no dispersion
- no adsorption or decay of contaminant
- screened interval of well is short (screen-length/depth ratio less than 1/5)
- screen interval is located considerably below or above the base of the contaminant zone

Equation:

$$\frac{c}{c_o} = \left(1 - T^{-1/3}\right)/2$$

where

$$T = \frac{30t}{4\pi H^3 pB} \quad \text{or} \quad t = T\left(\frac{4\pi H^3 pB}{30}\right)$$

and

- c_o = average concentration of the contaminated layer (mg/l)
- c = concentration at well screen (mg/l)
- Q = pumping rate of well (m^3/day)
- t = time (day)
- H = distance from contaminated layer to center of screen (m)
- p = porosity (unitless)
- B = anisotropy ratio = K_x/K_z (unitless)
- K_x, K_z = saturated hydraulic conductivity in the horizontal and vertical directions, respectively (m/day)

FIGURE VII-29 SUMMARY OF MODEL DESCRIBING CONTAMINANT TRANSFER TO DEEP WELLS

SOLUTE INJECTION WELLS: RADIAL FLOW
(SEE SECTION 7.5.3)

References: Hoopes and Harleman (1967), Tang and Babu (1979)

Objective: To determine contaminant concentrations for a given time and location from a continuously discharging, fully penetrating injection well. Regional flow is negligible compared to flow induced by injection well.

Assumptions:
- uniform, radial flow in a confined aquifer
- contaminant enters the aquifer as a line source over the saturated thickness of the aquifer at $r = r_o$
- linear equilibrium adsorption of contaminant
- first-order decay of the contaminant
- concentration of contaminant at well is constant

$$c(r,t) = c_o \frac{\text{erfc}(a)}{\text{erfc}(a_o)} \exp\left(\frac{-kR_d(r^2-r_o^2)}{2A}\right)$$

where

$$a = \frac{(r^2/2 - At/R_d)R_d}{\left(\frac{4}{3}\alpha r^3 + \frac{D^* r^4}{A}\right)^{1/4}}, \quad a_o = \frac{(r_o^2/2 - At/R_d)R_d}{\left(\frac{4}{3}\alpha r_o^3 + D^* \frac{r_o^4}{A}\right)^{1/4}}$$

r = radial distance from center of well (meters)
r_o = radius of well casing (meters)
t = time (days)
α = dispersivity of aquifer (meters)
A = $Q/(2\pi bp)$
D^* = molecular diffusion coefficient (m^2/day)
c = contaminant concentration in the aquifer (mg/l)
c_o = contaminant concentration in the injection well (mg/l)
Q = volumetric rate of injection by the well (m^3/day)
b = saturated thickness of the aquifer (meters)
p = porosity of the aquifer (unitless)
R_d = retardation coefficient for linear adsorption (unitless)
k = total decay rate constant for the contaminant (1/day)

FIGURE VII-30 SUMMARY OF MODEL DESCRIBING RADIAL FLOW FROM AN INJECTION WELL

CONTAMINANT RELEASE ON THE SURFACE WITH 1-D VERTICAL, DOWNWARD TRANSPORT
(SEE SECTION 7.5.4)

Reference: van Genuchten and Alves (1982)

Objective: Compute solute concentration as a function of time and distance for a continuous surface contaminant release with subsequent vertical, downward transport.

Assumptions:
- uniform, steady, vertical, downward flow
- first-order decay and linear, equilibrium adsorption of the contaminant in the aquifer
- constant or first-order decay of the contaminant source at the land surface
- one-dimensional transport in unsaturated or saturated media

$$c(x,t) = \frac{c_o}{2} \exp\left(\frac{v_s x}{2D} - \gamma t\right)\left\{e^{-2ab}\ \text{erfc}\left(-a\sqrt{t} + \frac{b}{\sqrt{t}}\right) + e^{2ab}\ \text{erfc}\left(a\sqrt{t} + \frac{b}{\sqrt{t}}\right)\right\}$$

where

$$a = \sqrt{k - \gamma + \frac{v_s^2}{R_d 4D}} \qquad b = \frac{x}{2}\sqrt{\frac{R_d}{D}}$$

c_o = initial concentration of the contaminant source (mg/l)
c = concentration of the contaminant at a specified time and depth (mg/l)
v_s = seepage velocity, positive vertically downward (m/day)
D = dispersion coefficient in the vertical direction (m^2/day)
x = vertical distance, positive downwards (m)
R_d = retardation coefficient for linear adsorption (unitless)
k = total decay rate constant for the contaminant in the aquifer (1/day)
γ = decay rate of the contaminant source at the land surface (1/day)

FIGURE VII-31 SUMMARY OF MODEL DESCRIBING ONE-DIMENSIONAL, VERTICALLY DOWNWARD TRANSPORT OF A CONTAMINANT RELEASED ON THE SURFACE

TWO-DIMENSIONAL HORIZONTAL FLOW WITH A SLUG SOURCE
(SEE SECTION 7.5.5)

Reference: Wilson and Miller (1978)

Objective: To determine contaminant concentration for a given time and location for an instantaneous discharge from a fully penetrating line source. Contaminant transport is dominated by regional flow.

Assumptions:
- uniform, steady regional flow in the x direction
- contaminant enters the aquifer over the full saturated thickness of the aquifer at $x = 0$, $y = 0$
- linear, equilibrium adsorption of the contaminant
- decay of the contaminant in the aquifer is first-order
- mass loading rate of contaminant is instantaneous

$$c(x,y,t) = \frac{c_o Q'}{b4\pi pt(D_x D_y)^{1/2}} \exp\left(-kt - \frac{(xR_d - v_x t)^2}{4D_x tR_d} - \frac{(yR_d)^2}{4D_y tR_d}\right)$$

where

c_o = initial concentration of discharged contaminant (mg/l)
Q' = volume of contaminant being discharged (m^3)
b = aquifer saturated thickness (m)
p = porosity (unitless)
t = time (days)
D_x, D_y = dispersion coefficients (m^2/day)
v_x = seepage velocity of the regional flow (m/day)
x, y = spatial coordinates (m)
k = total decay rate constant for the contaminant (1/day)
R_d = retardation coefficient for linear adsorption (unitless)

FIGURE VII-32 SUMMARY OF MODEL DESCRIBING TWO-DIMENSIONAL HORIZONTAL FLOW WITH A SLUG SOURCE

TWO-DIMENSIONAL HORIZONTAL FLOW WITH CONTINUOUS SOLUTE LINE SOURCES
(SEE SECTION 7.5.6)

Reference: Wilson and Miller (1978)

Objective: To determine contaminant concentration for a given time and location from a continuously discharging, fully penetrating line source. Contaminant transport is dominated by the regional flow.

Assumptions:
- uniform, steady regional flow in the x direction
- contaminant enters the aquifer over the full saturated thickness of the aquifer at $x = 0$, $y = 0$
- linear, equilibrium adsorption of the contaminant
- decay of the contaminant in the aquifer is first-order
- mass loading rate of contaminant is continuous and constant over the time period of interest

$$c(x,y,t) = \frac{c_o Q}{4\pi p b (D_x D_y)^{1/2}} \exp\left(\frac{v_x x}{2D_x}\right) W\left(u, \frac{r}{B}\right)$$

where

$W(\cdot)$ = the leaky well function of Hantush

$B = 2D_x/v_x$ (m)

$r = \left(\alpha\left(x^2 + y^2\frac{D_x}{D_y}\right)\right)^{1/2}$ (m)

$u = \frac{r^2 R_d}{4\alpha D_x t}$ (unitless)

$\alpha = 1 + 2BR_d k/v_x$ (unitless)

Q = volumetric rate of discharge of the line source (m^3/day)

t = time (days)

(x,y) = spatial coordinates (m)

D_x, D_y = dispersion coefficients (m^2/day)

v_x = seepage velocity of the regional flow (m/day)

p = porosity of the aquifer (unitless)

b = saturated thickness of the aquifer (m)

k = total decay rate constant for the contaminant (1/day)

R_d = retardation coefficient for linear adsorption (unitless)

c_o = concentration of contaminant being discharged (mg/l)

FIGURE VII-33 SUMMARY OF MODEL DESCRIBING TWO-DIMENSIONAL HORIZONTAL FLOW WITH CONTINUOUS SOLUTE LINE SOURCES

ground water management activities. Analytical techniques can be used to predict the migration of plumes and to determine the extent of contaminant mixing in ground water. Four specific questions can be addressed: (1) In what direction will a contaminant plume travel and how will its shape change as it travels? (2) To what extent will concentrations of contaminants be reduced as a result of dispersion, sorption and decay? (3) How far will the plume migrate over time? (4) Where should wells to monitor the plume's movement be located?

Other applications of analytical methods include estimating "worst case" concentrations at a site as a conservative estimate of a site's hazard, guiding the collection and analysis of field data to test hypotheses, checking the results of more sophisticated numerical models, determining design requirements for pump tests and tracer studies, and designing and evaluating the effectiveness of plume control options. Because analytical techniques are relatively quick and inexpensive to apply, they are useful in many phases of ground water activities--facility siting and permitting, site inspection and enforcement, monitoring, estimating the extent and significance of known contamination, and evaluating plume management options. A reliable "worst case" evaluation of a known ground water contamination problem may show that the site poses little near-term risk to the public and that a low-level monitoring program is an appropriate management strategy. Alternatively, an evaluation may indicate significant health or environmental risks, in which case intensive monitoring and/or use of a sophisticated numerical model may be warranted.

An overall summary of analytical methods is given below:

- Provide quantitative estimates of potential contamination at a specific location and time
- Require limited field data
- Predictions can be made quickly using hand calculators
- Require simplifying assumptions
- Cannot handle complex field conditions.

In the remaining portion of Section 7.5, the five analytical models are presented along with worked out examples of their use.

7.5.2 Contaminant Transport to Deep Wells

Many regions of the country obtain their freshwater supply from deep well systems. However, many of these deep wells are now in jeopardy because of the contamination of shallow ground water aquifers from cesspools, septic tanks and overuse of crop and lawn fertilizers. Subsurface sanitary disposal systems discharge wastewaters high in nitrogen and bacteria to the unsaturated zone. Nitrogen and pesticides from fertilizers and herbicides may migrate to the saturated zone where water-supply wells may intercept them. Our objective is to predict the increase in contaminant concentration at a water supply well and to determine how long it would take for a

specified concentration to be reached. Phillips and Gelhar (1978) presented an equation for solving these types of problems. The Phillips and Gelhar equation is appropriate when the well is either far below the existing contaminant zone or far above the contaminant zone. One other restriction is that the length of the well screen must be less than about one-fifth of the well depth. The flow to the well can then be represented as three-dimensional radial flow as shown in Figure VII-34.

For the example shown in the figure, there is an unbounded radial flow system with a contamination zone initially a distance H above the center of the well screen. The equation to represent the movement of the contamination zone is based on fluid displacement in a homogeneous anisotropic porous medium. The effects of dispersion are not included in Phillips and Gelhar's equation. However, Hoopes and Harleman (1965) have shown that dispersion is a secondary effect in such local flow systems.

The analytic solution for the contaminant concentration at the well screen as a function of time is given by:

$$c(t) = (c_o(1 - T^{-1/3}))/2 \qquad \text{(VII-59)}$$

where

$$T = \frac{3Qt}{4\pi H^3 pB} \qquad \text{(VII-60)}$$

or

$$t = \frac{4\pi H^3 pB}{3Q} \; T \qquad \text{(VII-61)}$$

and where

- $c(t)$ = concentration at the well (mg/l)
- c_o = average concentration of the contaminated zone (mg/l)
- Q = constant pumping rate of the well (m^3/day)
- t = time (day)
- T = dimensionless time (unitless)
- H = distance from the contaminated zone to the center of the screened interval of the well (m)
- p = effective porosity of the saturated portion of the aquifer (unitless-decimal fraction)
- B = anisotropy ratio of the aquifer = K_x/K_z (unitless)
- K_x, K_z = saturated hydraulic conductivity in the horizontal and vertical directions, respectively (m/day)

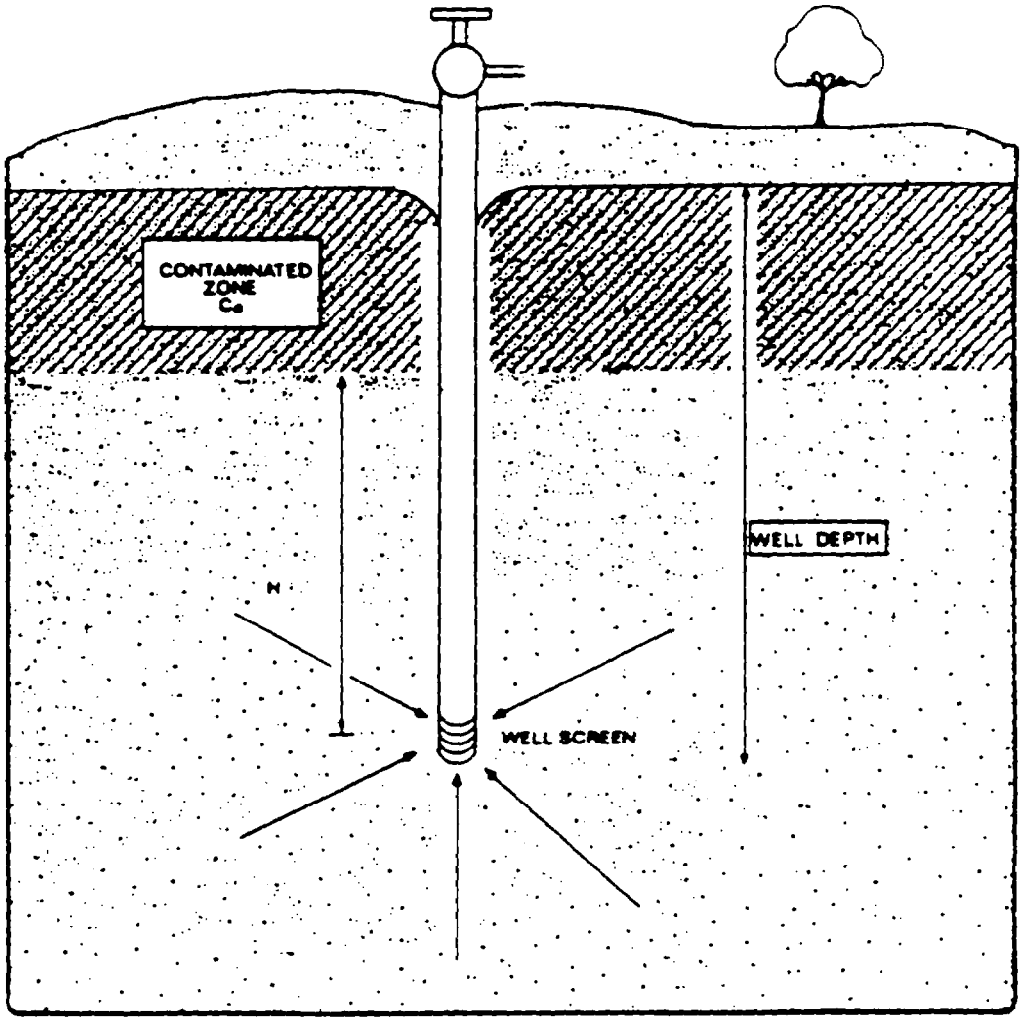

FIGURE VII-34 SCHEMATIC OF FLOW TO A WELL BENEATH A CONTAMINATED ZONE

Equation VII-59 has been solved for various values of T. The results are shown in Figure VII-35. Equation VII-60 and VII-61 can be solved to answer several questions:

- When will shallow contaminated ground water reach a deep pumping well?
- When will the percentage of the contaminant concentration in the well exceed a given value, say 20 percent?
- What is the effect of changing the pumping rate?

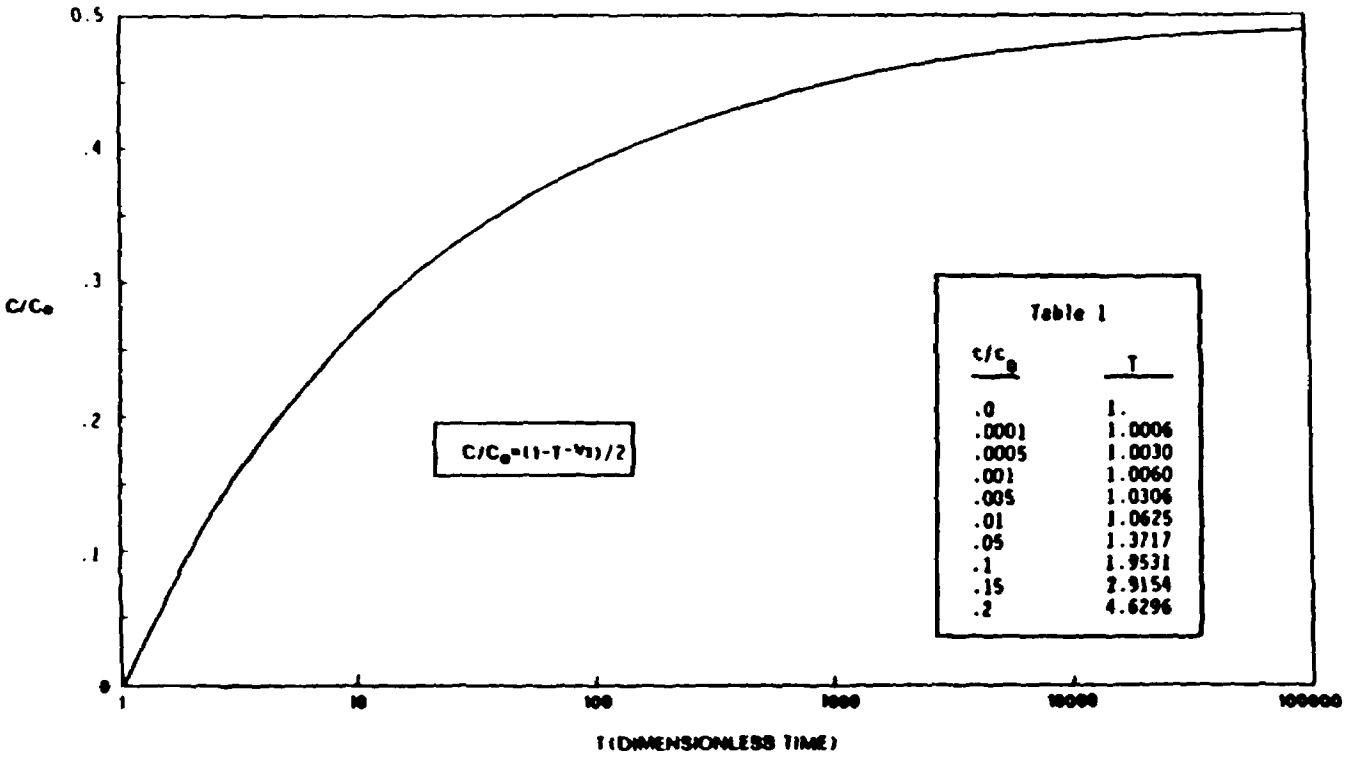

FIGURE VII-35 NORMALIZED SOLUTE CONCENTRATION VS. DIMENSIONLESS TIME

EXAMPLE VII-4

The nitrate concentration in a town's ground water has been increasing for the last several years. The following information is available. A schematic of the problem is shown in Figure VII-36.

The aquifer is unconfined with fine to medium grained quartz sand deposited originally as sand dunes. The storage coefficient is about 0.2 and the ratio of the horizontal to the vertical hydraulic conductivity is 10. This anisotropy is caused by localized cementation and horizontal bedding in the dunes. The municipal well is pumping 3000 m^3/day. The lower tip of the municipal well screen is located 50 meters below the surface of the land. The well is screened over 4 meters. Analysis of the water samples showed that the municipal well had a nitrate-nitrogen concentration of 7.2 mg/l on January 1, 1984. A series of shallow monitoring wells indicated that the upper part of the aquifer has an average concentration of 26 mg/l of nitrate-nitrogen and that the zone of contamination extends down to 20 meters below the surface of the land.

The city council wants to know when the nitrate-nitrogen concentration in the community well will equal or exceed 10 mg/l (the primary drinking water standard).

The steps required to answer this question are given below:

1. Determine the current dimensionless time, T_o, where c/c_o =

   $(1 - T_o^{-1/3})/2 = 7.2/26 = 0.28$

   From Figure VII-35 we find that $T_o = 11.7$.

2. Determine the dimensionless time when the well concentration equals 10 mg/l:

   $c/c_o = (1 - T_{10}^{-1/3})/2 = 10./26 = 0.38$

   From Figure VII-35 we find that $T_{10} = 72.3$.

3. Real time is related to dimensionless time by Equation VII-61:

   $$t = T\left(\frac{4\pi H^3 p B}{3Q}\right)$$

   Hence, the estimated time when the concentration at the pumping well will reach 10 mg/l is given by the difference between t_{10} and t_o:

   $$t_{10}-t_o = (T_{10}-T_o)\,\frac{4\pi H^3 p B}{3Q}$$

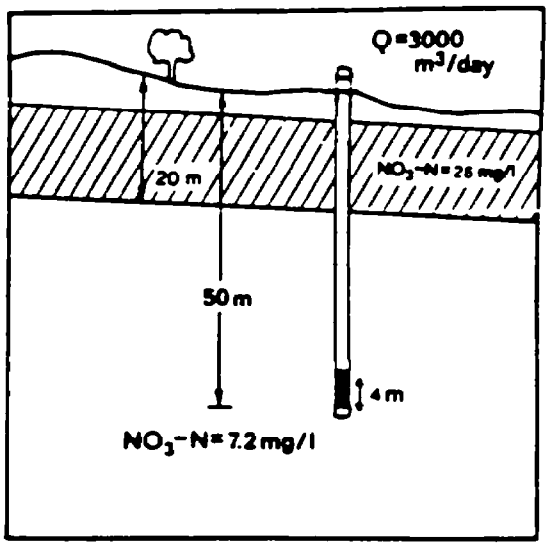

FIGURE VII-36 SCHEMATIC OF EXAMPLE PROBLEM FOR FLOW TO WELL FROM A SHALLOW CONTAMINATED ZONE

4. Calculate H and then substitute H, p, B, Q, T_o and T_{10} into the above equation. Note that H and Q must be expressed in the same units. Also note that H is measured as the distance between the center of the well screen and the bottom of the contamination zone. In this example, H = (50-20-4/2) = 28 meters. The data can now be tabulated as follows:

H = 28 meters	p = 0.2
B = 10	Q = 3000 m^3/day

Substituting the above data into the expression for $t_{10}-t_o$, results in the following:

$$(t_{10}-t_o) = (72.3-11.7)\frac{(4\pi(28)^3(0.2)(10))}{3(3000)}$$

$$= 3715 \text{ days} = 10.2 \text{ years}$$

Hence, the concentration of nitrate-nitrogen is expected to reach 10 mg/l in the municipal well in about ten years.

END OF EXAMPLE PROBLEM VII-4

7.5.3 Solute Injection Wells: Radial Flow

Because of the interest in underground injection, the following analyses will be presented to show how injection wells can be modeled analytically. With the model given below, the concentration of solute from an injection well can be predicted as a function of time and space. This information can then be used to estimate the impact of an injection well on the ground water quality. A schematic view of a typical injection well is given in Figure VII-37.

Both shallow and deep wells have been used for injection of waste into subsurface strata. Storm water, spent cooling water, and sewage effluent have been injected through relatively shallow wells. Sometimes these wells are completed in the unsaturated zone; however, they often penetrate the saturated zone and thus contaminants are discharged directly into the ground water. In addition, large volumes of brine produced by chemical industries, geothermal energy production, and other sources have been injected through deep wells into saline-water aquifers. Acids, spent solvents, and plating solutions containing heavy metals have also been injected.

The following assumptions will be made concerning the injection well system to permit the analytical solution given below to be used. A solute with a constant concentration c_o will be discharged at a constant rate Q into a homogeneous, non-leaky, isotropic aquifer. The aquifer is assumed to be confined by two parallel, impermeable formations and spaced a distance "b" apart. The injection well is screened over the entire thickness of the confined aquifer. The density and viscosity of the injected solute are the same as those of the native water in the aquifer. There is negligible regional flow in the aquifer and the flow field near the well is dominated by the waste being discharged. A schematic view of the problem is given in Figure VII-37.

The seepage velocity, v_s, at any specified radius from the well can be computed from the continuity equation:

$$Q = 2\pi r b v_s p \qquad \text{(VII-62)}$$

where Q is the volumetric rate of injection by the well (m^3/day), r is the radius to a point in the aquifer measured from the center of the well (m), b is the saturated thickness of the aquifer (m), p is the porosity of the aquifer (decimal percent, unitless), and v_s is the radial seepage velocity of the fluid from the well (m/day).

The seepage velocity can thus be expressed as:

$$v_s = \frac{A}{r} \quad \text{with } A = Q/(2\pi bp) \qquad \text{(VII-63)}$$

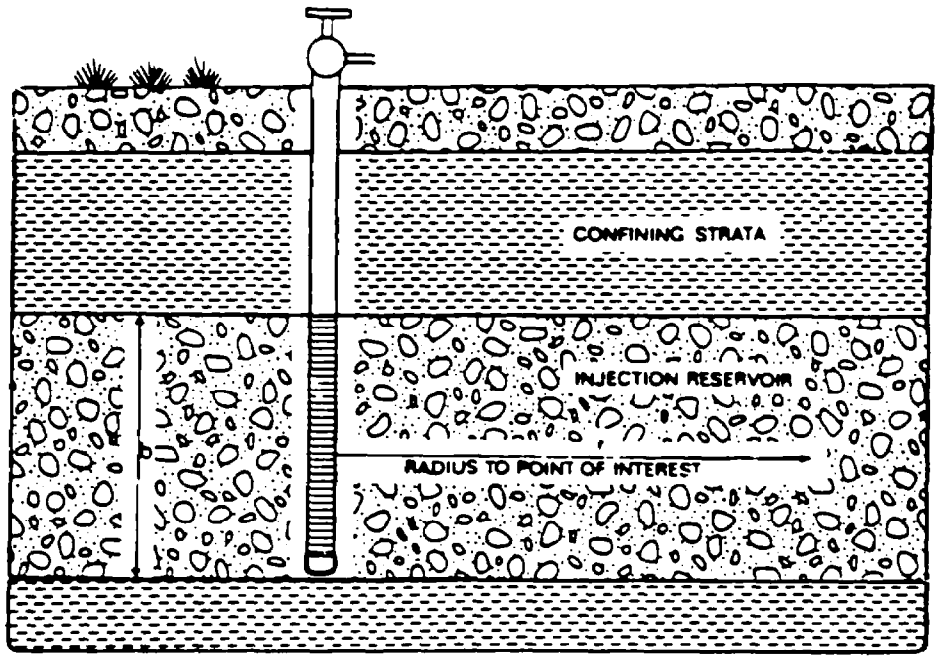

FIGURE VII-37 SCHEMATIC VIEW OF A WELL INJECTING SOLUTE INTO A CONFINED AQUIFER

The governing equation describing the spatial and temporal distribution of a dissolved substance introduced into the saturated zone is:

$$R_d \frac{\partial c}{\partial t} + v_s \frac{\partial c}{\partial r} = \frac{1}{r} \frac{\partial}{\partial r}(D_r r \frac{\partial c}{\partial r}) - kcR_d \qquad \text{(VII-64)}$$

where c is the solute concentration (mg/l), D_r is the radial dispersion coefficient (m^2/day), k is the first-order decay rate of the substance (per day), and R_d is the retardation coefficient for linear, equilibrium adsorption (unitless). The initial concentration in the aquifer is assumed to be zero, the concentration $c = c_o$ is assumed to be held constant at the well.

If the dispersion coefficient is assumed to vary as a function of the radial seepage velocity, then:

$$D_r = \alpha v_s + D^* \qquad \text{(VII-65)}$$

where α is the dispersivity coefficient (m) and D^* is the molecular diffusion coefficient (m^2/day).

The general solution to Equation VII-64 can be found by the Laplace transform method to give:

$$c(\rho,\tau) = c_0 \exp\left[\frac{(\rho-\rho_0)}{2} - k^*\tau\right]\mathcal{L}^{-1}\{f(s)\} \qquad \text{(VII-66)}$$

where $\mathcal{L}^{-1}\{:\}$ is the inverse Laplace transform operator and f(s) is the Laplace solution to Equation VII-64:

$$f(s) = \frac{1}{(s-k^*)} \frac{A_1\left[(R_d s)^{-2/3}(R_d\rho s + 1/4)\right]}{A_1\left[(R_d s)^{-2/3}(R_d\rho_0 s + 1/4)\right]} \qquad \text{(VII-67)}$$

where s is the transformed variable of time; $A_1[:]$ is the Airy function; k^* is the dimensionless decay rate, where $k^* = k\alpha^2$; τ is the dimensionless time, $\tau = t/(A\alpha^2)$; ρ is the dimensionless radial distance from the center of the well, $\rho = r/\alpha$; and ρ_0 is the dimensionless radius of the well casing, $\rho_0 = r_0/\alpha$.

Equation VII-66 has been solved analytically by Tang and Babu (1979) but their solution involves integrating four different types of Bessel functions of fractional order (order 1/3) over three different integrals. Alternatively, one can numerically compute the Laplace inverse of Equation VII-66 by the Stehfest algorithm (Moench and Ogata, 1981). However, if one uses Equation VII-67 in the numerical inversion, a great deal of care must be used in computing the Airy functions to avoid numerical roundoff problems in the solution.

Because of the difficulties in obtaining numerical values from Equation VII-66, several authors have suggested approximate solutions. The method of Raimondi et al. (1959) assumes that at some distance from the source, the influence of dispersion and diffusion on the concentration distribution are small in comparison to the total dispersion that has taken place up to that point. Thus the spatial gradient on the right-hand side of Equation VII-64 is ignored and is substituted by the temporal gradient:

$$\frac{D_r}{v_s^2}\frac{\partial^2 c}{\partial t^2} \qquad \text{(VII-68)}$$

The solution to this approximation was originally given by Tang and Babu (1979). Their solution has been modified to allow for retardation and is shown below:

$$c = c_0 \frac{\text{erfc}(a)}{\text{erfc}(a_0)} \exp\left(\frac{-kR_d(r^2-r_0^2)}{2A}\right) \qquad \text{(VII-69)}$$

where erfc(:) is the complimentary error function (see Appendix J) and

$$a_o = \frac{\left(\frac{r_o^2}{2} - \frac{At}{R_d}\right) R_d}{\left(\frac{4}{3}\alpha r_o^3 + \frac{D^* r_o^4}{A}\right)^{1/4}} \qquad \text{(VII-70)}$$

$$a = \frac{\left(\frac{r^2}{2} - \frac{At}{R_d}\right) R_d}{\left(\frac{4}{3}\alpha r^3 + \frac{D^* r^4}{A}\right)^{1/4}} \qquad \text{(VII-71)}$$

When the radius of the well casing, r_o, is negligible, then $\text{erfc}(a_o)$ is set equal to 2 and Equation VII-69 reduces to:

$$c = \frac{c_o}{2} \text{erfc}(a) \exp\left(\frac{-kR_d(r^2 - r_o^2)}{2A}\right) \qquad \text{(VII-72)}$$

Equation VII-72 is the same as Hoopes and Harleman (1967) when $k = 0$ (i.e., the exponential term drops out). Equation VII-69 and VII-72 satisfy the boundary conditions $c = c_o$ at $r = r_o$ and $c = 0$ at distances far from the well but they do not satisfy the initial condition $c = 0$ at $t = 0$ near the well. Equations VII-69 and VII-72 predict a finite amount of mass in the media at $t = 0$. However, Equations VII-69 and VII-72 are approximately true away from the immediate vicinity of the source. Hoopes and Harleman (1965) carried out an extensive series of laboratory investigations in a sand-filled box and concluded that Equations VII-69 and VII-72 are a good approximation of dispersion in radially diverging flow for distances larger than 20 particle diameters from the well.

A table of the complimentary error function is given in Table J-1 of Appendix J.

EXAMPLE VII-5

A local electronic component factory, called "The Chip Works", was recently constructed in town. It produces electronic circuit boards and micro chips. As part of the manufacturing process, various acids are used to etch and plate the electronic circuits. These acids leach various heavy metals, including cadmium from the metal components and hence must be disposed of. Because of the high toxicity of the plating waste, the local sewer authority will not allow The Chip Works to discharge its waste into the domestic sewer line without pretreatment. After much negotiation, it was finally decided to inject the plating waste directly into a deep aquifer. The following analyses were done to determine if solute injection into the aquifer would allow the drinking water standards to be met in the aquifer without pretreating the plating waste.

The sandstone aquifer is about 30 meters thick. It is confined above and below by impermeable shale. The aquifer lies about 300 meters below the surface of the ground. The velocity in the aquifer is negligible. The plating waste is to be injected at a volumetric rate of 550 m^3/day through a well screened over the entire depth of the aquifer. The casing radius is 0.1 meters. The plating waste contains an average concentration of 50 µg/l of cadmium and has a pH of about 5.5. The dispersivity of the sandstone is about 50 meters, the effective porosity about 0.2 and the molecular diffusion coefficient about 8.7×10^{-5} m^2/day. The cadmium concentration is below solubility limits. To be conservative, adsorption is assumed to be negligible, thus the retardation factor is set equal to 1 (see Equation VII-55 of Section 7.4.2.1.1).

The injection well is located in the center of the property of The Chip Works and the nearest property boundary is 450 meters away. The local pollution agency has specified that the cadmium concentration in the aquifer never exceed 10 µg/l at the property boundary. It is known that the background concentration of cadmium is negligible. A series of monitoring wells have been installed at the property boundary to verify compliance. Will the standard be exceeded and if so, when? A schematic of the above problem is given in Figure VII-38.

We want to know when the cadmium concentration will equal or exceed 10 µg/l. The data can be summarized as follows:

r_o = 0.1 m	R_d = 1
r = 450 m	k = 0/day
α = 50 m	b = 30 m
D^* = 8.7×10^{-5} m^2/day	p = 0.2
Q = 550 m^3/day	c_o = 50 µg/l

The only missing variable is time, t, which can be estimated. The well casing radius r_o is negligible in comparison to the distance of interest, r, and time t is not extremely short (i.e, less than 0.001 days), so Equation VII-72 can be used (i.e., $\text{erfc}(a_o) = 2$). This expression is first solved for "a":

$$\text{erfc}(a) = 2c/c_o = (2)(10)/50 = 0.4$$

Interpolating the complimentary error function in Table J-1 of Appendix J, one can see that the above corresponds to a value of a = 0.59. From Equation VII-71, one can solve for time as a function of "a":

$$t = R_d \frac{r^2}{2A} - \frac{a}{A}\left(\frac{4}{3}\alpha r^3 + D^* \frac{r^4}{A}\right)^{1/2} \qquad \text{(VII-73)}$$

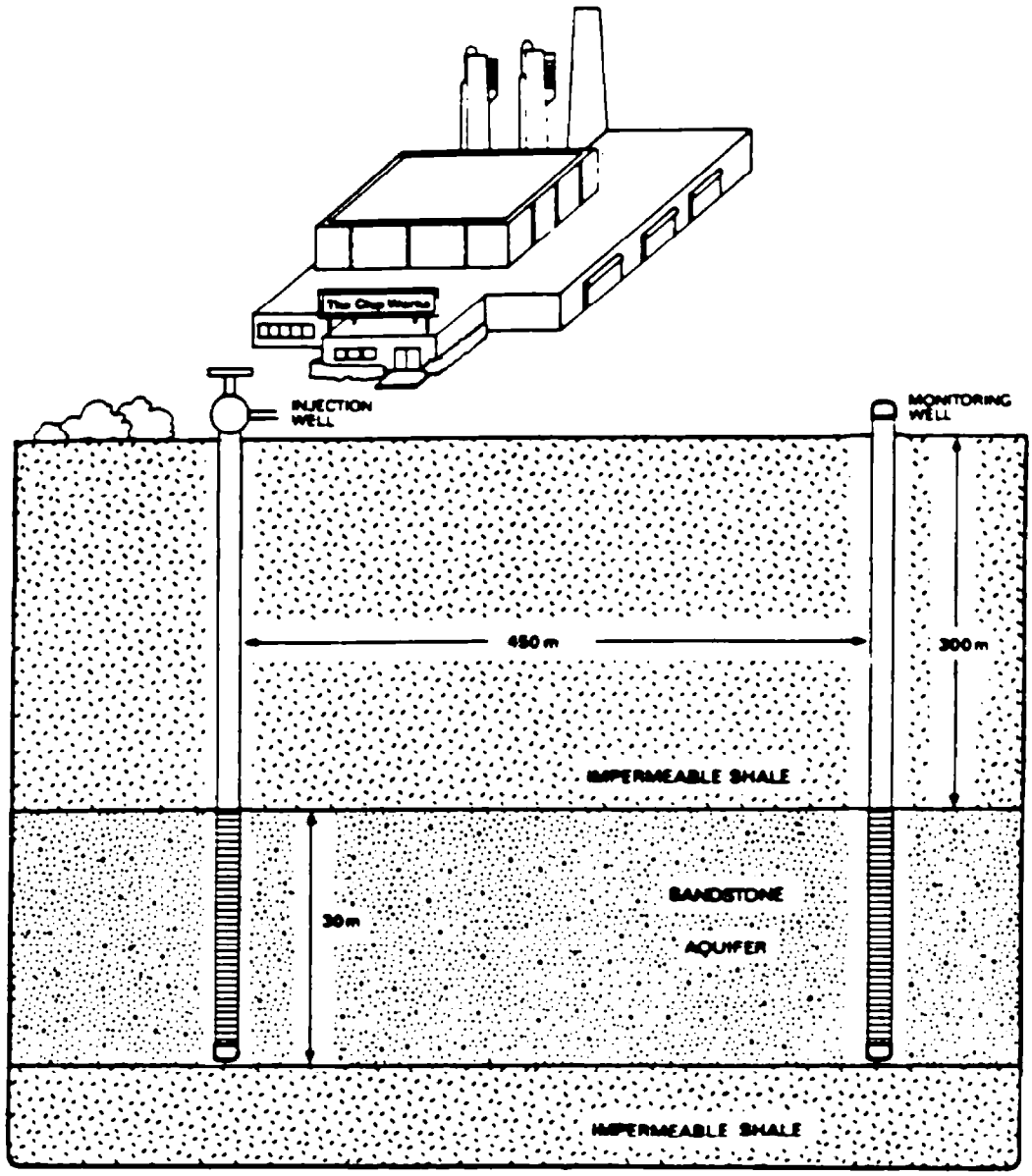

FIGURE VII-38 SCHEMATIC OF THE EXAMPLE PROBLEM SHOWING RADIAL FLOW OF PLATING WASTE FROM AN INJECTION WELL

where

$$A = Q/(2\pi bp) \qquad \text{(VII-74)}$$

Upon substitution of the data into Equations VII-73 and VII-74, we can solve for time, t. Thus:

$$A = \frac{550}{2\pi(30)(0.2)} = 14.6 \text{ m}^2/\text{day}$$

$$t = \frac{(1)(450)^2}{2(14.6)} - \frac{(0.59)}{(14.6)}\left(\frac{4}{3}(50)(450)^3 + (8.7\times10^{-5})\frac{(450)^4}{14.6}\right)^{1/2}$$

= 3780 days or about 10 years

Hence, the cadmium concentration will equal 10 µg/l at the monitoring well after about 10 years of continuous injection. It appears from the calculations that pretreatment of the waste will be necessary prior to disposal.

END OF EXAMPLE VII-5

EXAMPLE VII-6

This example problem considers another metal, zinc, which is present in smaller quantities in this waste. Zinc is weakly adsorbed at a pH of 6.0. The adsorption coefficient K_d for zinc is about 2 ml/g at a pH of 6.0. The bulk density, ρ_b, of sandstone is 2.3 g/ml. Hence, the retardation factor for linear equilibrium adsorption can be calculated using Equation VII-55.

Calculate the concentration of zinc at the property boundary after 3780 days. Assume the waste has been pretreated to a pH of 6.0. The data can now be summarized as follows:

r_o = 0.1 m	ρ_b = 2.3 g/ml
r = 450 m	p = 0.2
α = 50 m	Q = 550 m^3/day
D^* = 8.7 x 10^{-5} m^2/day	b = 30 m
K_d = 2 ml/g	c_o = 5 mg/l
k = 0	t = 3780 days

Step 1. Calculate the retardation coefficient using Equation VII-55:

$$R_d = 1 + \frac{K_d \rho_b}{p} = 1 + \frac{(2)(2.3)}{(0.2)} = 24$$

Step 2. Calculate A using Equation VII-74:

$$A = \frac{Q}{2\pi bp} = \frac{550}{2\pi(30)(0.2)} = 14.6$$

Step 3. Calculate "a" using Equation VII-71:

$$a = \frac{\left(\frac{r^2}{2} - \frac{At}{R_d}\right) R_d}{\left(\frac{4}{3}\alpha r^3 + \frac{D^* r^4}{A}\right)^{1/2}} = \frac{\left(\frac{(450)^2}{2} - \frac{(14.6)(370)}{(24)}\right)(24)}{\left(\frac{4(50)(450)^3}{3} + \frac{(8.7\times10^{-5})(450)^4}{(14.6)}\right)^{1/2}} = 30.5$$

Step 4. Calculate erfc(a) (see Table J-1 of Appendix J):

$$\text{erfc}(a) = \text{erfc}(30.5) = 0$$

Step 5. Calculate c:

$$c = \frac{c_o}{2}\,\text{erfc}(a) = \frac{(5)(0)}{2} = 0 \text{ mg/l.}$$

Hence, the zinc concentration will be zero at the property boundary after 10 years. The difference between the behavior of cadmium and zinc is due to sorption. Without sorption, cadmium moves with the same velocity as does the injected water (i.e., the seepage velocity v_s). With adsorption, zinc moves 24 times slower than the injected water.

END OF EXAMPLE VII-6

7.5.4 Contaminant Release on the Surface with 1-D Vertical Downward Transport

A surface release of a contaminant can be treated in many instances as a one-dimensional flow problem with the contaminant moving vertically downward through the soil as shown in Figure VII-39. This case can be greatly simplified by considering the velocity, moisture content, retardation and dispersion coefficient as constant over a given depth. If the soil has several distinct layers, calculations can be performed for each layer separately. Flow can occur through either saturated or unsaturated soil, as long as the moisture content is assumed to be a constant throughout the soil.

To understand how the analytical method may be used, the governing equation should be briefly reviewed. The equation describing one-dimensional advective transport with dispersion, adsorption and first-order decay is as follows:

$$R_d \frac{\partial c}{\partial t} = D \frac{\partial^2 c}{\partial x^2} - v_s \frac{\partial c}{\partial x} - kcR_d \qquad \text{(VII-75)}$$

Mass Transport Equation

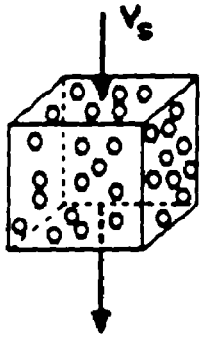

$$\left\{\begin{matrix}\text{net rate of}\\ \text{mass}\\ \text{accumulation}\end{matrix}\right\} = \left\{\begin{matrix}\text{mass flow}\\ \text{by}\\ \text{dispersion}\end{matrix}\right\} + \left\{\begin{matrix}\text{mass flow}\\ \text{by}\\ \text{advection}\end{matrix}\right\} - \left\{\begin{matrix}\text{mass depletion}\\ \text{by}\\ \text{reactions}\end{matrix}\right\}$$

$$R_d \frac{\partial c}{\partial t} = D \frac{\partial^2 c}{\partial x^2} - V_s \frac{\partial c}{\partial x} - k c R_d$$

Waste Pond or Landfill

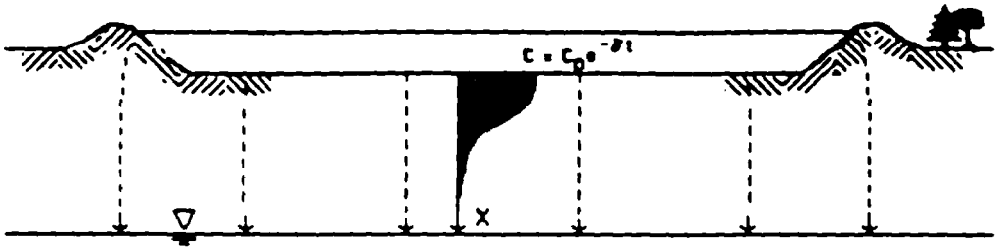

Initial condition: $C(x,t=0) = 0$

Boundary Conditions: $C(\infty,t) = 0$

$$\frac{\partial c}{\partial x}(\infty,t) = 0$$

FIGURE VII-39 SCHEMATIC SHOWING EQUATION FOR 1-D VERTICAL TRANSPORT FROM A SURFACE WASTE SOURCE

where

c = concentration of contaminant in the soil solution (mg/l)

v_s = seepage velocity, positive downward (velocity of fluid flow through interstices of the soil) (m/day)

t = time (days)

x = distance down the soil (positive downward) (m)

D = dispersion coefficient of the contaminant in solution in the soil (m^2 /day)

R_d = retardation factor for linear, equilibrium adsorption (unitless)

k = first-order decay constant of the contaminant in the aquifer (per day)

The terms in Equation VII-75 from left to right represent the time rate of change in the concentration of the contaminant, transport due to dispersion, transport due to advection, and last, a term accounting for adsorption by the soil matrix and chemical reaction (Figure VII-39).

As presented in Equation VII-75, the first-order decay rate, k, assumes that solute in its liquid and solid phases decays at the same rate (i.e., $k = K_{liquid} = k_{solid}$). The liquid phase refers to solute in the aqueous phase and the solid phase refers to solute that has been adsorbed. If the liquid and solid phase decay rates are not the same, the following substitution needs to be made:

$$k = \frac{k_{liquid} + \frac{k_{solid}\, b K_d}{\theta}}{R_d} \qquad \text{(VII-76)}$$

where K_d is the distribution coefficient (unitless) for linear, equilibrium sorption, ρ_b is the soil bulk density (g/ml) and θ is the volumetric moisture content (unitless fraction).

The initial concentration of the contaminant is assumed to be zero in the soil solution:

$$c(x,t) = 0 \quad \text{for } x \geq 0 \text{ and } t = 0$$

At the upper boundary, $x = 0$, the concentration of the contaminant (source) is either held constant or allowed to decrease exponentially with a rate constant γ (for a source concentration which does not change with time, set $\gamma = 0$):

$$c(x,t) = c_o e^{-\gamma t} \quad \text{for } x = 0 \text{ and } t > 0$$

At large distances from the upper boundary, both the concentration and the gradient of the concentration become negligible:

$$c, \frac{c}{x} = 0 \quad \text{when } x \text{ is very large and } t > 0$$

Equation VII-75 can be solved with the above initial and boundary conditions by either the integral transform or Laplace transform techniques. A solution is given by van Genuchten and Alves (1982) as:

$$c(x,t) = \frac{c_o}{2} e^{\left(\frac{v_s x}{2D} - \gamma t\right)} \left\{ e^{-2ab} \operatorname{erfc}\left(-a\sqrt{t} + \frac{b}{\sqrt{t}}\right) + e^{2ab} \operatorname{erfc}\left(a\sqrt{t} + \frac{b}{\sqrt{t}}\right) \right\} \qquad \text{(VII-77)}$$

where

$$a = \sqrt{k - \gamma + \frac{v_s^2}{R_d 4D}} \quad \text{and} \quad b = \frac{x}{2}\sqrt{\frac{R_d}{D}}$$

erfc(:) = the complimentary error function (Appendix J).

EXAMPLE VII-7

A farmhand has just finished spraying a field of potatoes with the insecticide endrin. He then returns the spray rig back to a livestock water well where he washes out the spray tank. After carefully hosing out the inside of the spray tank with fresh water, he opens the tank valve and allows the rinse water to run out on top of the ground. A total of about 0.5 m^3 of rinse water contaminated with endrin drains and forms a pool about 10 m^2 in area. This pool takes about four hours to seep into the ground. Upon draining the spray tank, the farmhand drives back to the ranch.

When the farmhand tells the boss of his activities, the boss becomes furious. Apparently, the well used to clean out the spray tank is also used to water the milk cows. If endrin contaminates the well and then the cows, the cows may have to be destroyed. The boss, his son, and the farmhand quickly drive out to the well site. The son has recently completed a course in contaminant transport and wants to try out some of his new knowledge. Along the way, the son explains to his father he thinks a one-dimensional model of contaminant transport with a constant surface concentration would be sufficient to model the spill. The analytical method would predict the contaminant concentration for any depth and time. To use the method, the following parameters would have to be calculated: vertical pore-water velocity, dispersion coefficient and retardation factor for linear, equilibrium adsorption. Upon arriving at the well site, the following information is estimated from well data and their experience in farming the area. A schematic of the example problem is shown in Figure VII-40. Data

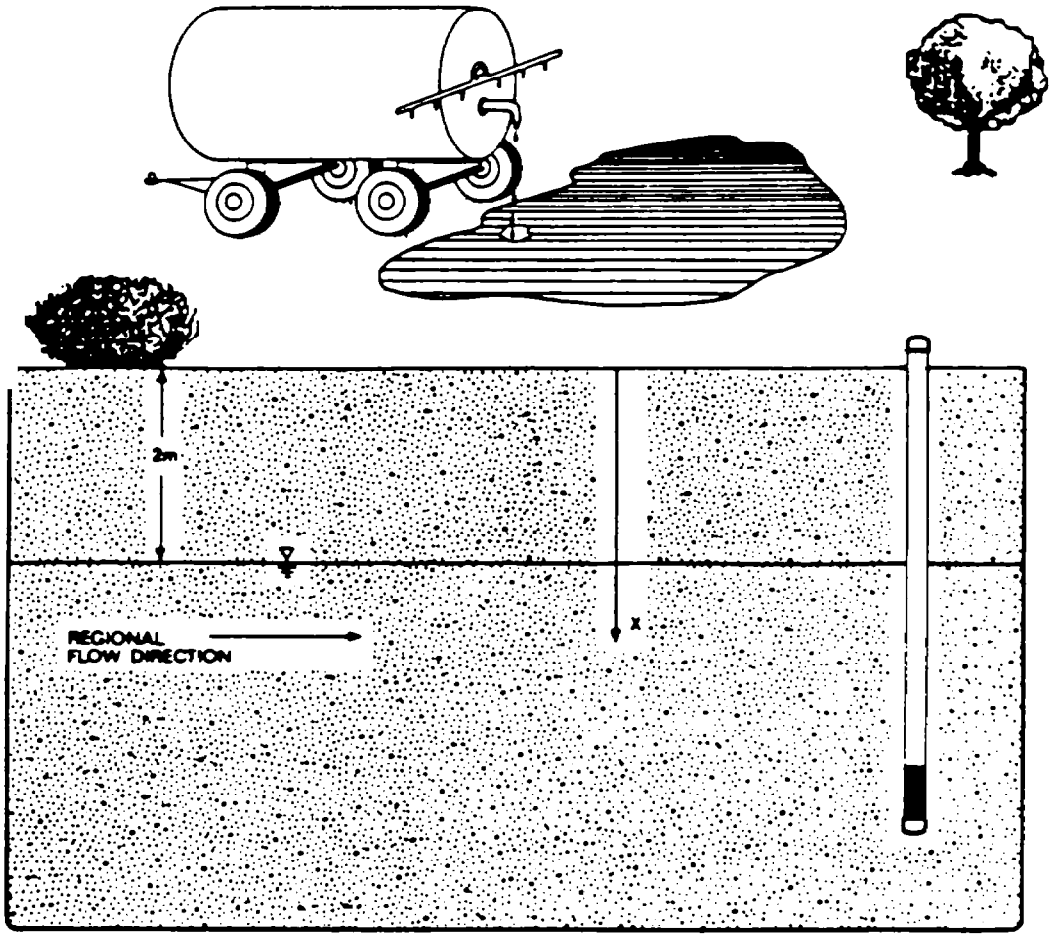

FIGURE VII-40 SCHEMATIC OF EXAMPLE 1-D PROBLEM

are listed below:

Soil type: silty sand with gravel	
Soil fraction silt and clay	f = 0.1
Percent organic carbon in sand	X_{oc}^{s} = 0
Percent organic carbon in silt and clay	X_{oc}^{f} = 0.10
Soil bulk density	ρ_b = 1.8 g/ml
Volumetric moisture content	θ = 0.15
Dispersivity coefficient	a = 0.22 meter
Saturated hydraulic conductivity	K_{sat} = 0.5 m/day
Depth to water table	x = 2 meters
Decay rate in the soil	k = 0/day
Decay rate of the source	γ = 0/day
Time since start of spill	t = 1 day
Contaminant	endrin
Partition coefficient	

for endrin in octanol-water $K_{ow} = 4 \times 10^5$

Surface concentration (rinse water) $c_o = 200$ ppb

To calculate the retardation factor R_d for linear, equilibrium adsorption, one must first calculate the partition coefficient K_p using Equation II-17 and II-18:

$$K_p = K_{oc}(0.2(1-f)X_{oc}^s + fX_{oc}^f)$$
$$K_{oc} = 0.63\ K_{ow}$$
$$K_{oc} = (0.63)(4 \times 10^5) = 2.5 \times 10^5\ ml/g$$
$$K_p = 2.5 \times 10^5(0.2(1-0.1)(0) + (0.1)(0.1)) = 2500\ ml/g$$

Therefore,

$$R_d = 1 + \frac{(1.8)(2500)}{0.15} = 30001$$

One next needs to compute the vertical Darcy velocity and then the vertical seepage velocity. For the case of a large spill into unsaturated medium, the following procedure can be used to estimate the Darcy velocity:

$$v_d = \frac{\text{volume of spill}}{(\text{area of spill})(\text{time to completely drain})}\ (m/day) \qquad \text{(VII-78)}$$

Substitute the above data into Equations VII-35 and VII-78 to get:

$$v_d = \frac{0.5}{(10)(4/24)} = 0.3\ m/day$$

$$v_s = \frac{0.3}{0.15} = 2\ m/day$$

To calculate the dispersion coefficient, dispersion is assumed to be a linear function of the seepage velocity and molecular diffusion is considered to be negligible (Equation VII-47). Thus:

$$D = \alpha v_s \quad (m^2/day)$$

where α is the dispersivity coefficient (meters).

Substituting the data yields:

$$D = (0.22)(2) = .44\ m^2/day$$

The concentration of endrin as a function of time and depth can be calculated from Equation VII-77. Upon rearranging terms, Equation VII-77 becomes:

$$c(x,t) = \frac{c_o e^{-\gamma t}}{2}\left(e^{A_1}\ \text{erfc}(A_2) + e^{A_3}\ \text{erfc}(A_4)\right) \qquad \text{(VII-79)}$$

where

$$A_1 = \frac{x v_s}{2D} - 2ab \qquad \text{(VII-80)}$$

$$A_2 = -a\sqrt{t} + \frac{b}{\sqrt{t}} \qquad \text{(VII-81)}$$

$$A_3 = \frac{x v_s}{2D} + 2ab \qquad \text{(VII-82)}$$

$$A_4 = a\sqrt{t} + \frac{b}{\sqrt{t}} \qquad \text{(VII-83)}$$

and where a and b are as defined previously in Equation VII-77.

For this problem, the concentration of endrin at the water table (i.e., x = 2 meters) is needed for a time period of one day since the spill started (i.e., t = 1 day). The data needed for this problem are summarized below:

$D = 0.44\ m^2/day$	$c_o = 200$ ppb
$v_s = 2$ m/day	$R_d = 30001$
$x = 2$ m	$k = 0$/day
$t = 1$ day	$\gamma = 0$/day

Substitute all of the data into Equation VII-79 to get:

$$a = \left(0\text{-}0 + \frac{2^2}{(30001)(4)(0.44)}\right)^{1/2} = 0.009$$

$$b = \frac{2}{2}\left(\frac{30001}{0.44}\right)^{1/2} = 261$$

$$A_1 = \frac{(2)(2)}{(2)(0.44)} - (2)(0.009)(261) = -0.15$$

$$A_2 = -0.009\sqrt{1} + \frac{261}{\sqrt{1}} = 261$$

$$A_3 = \frac{(2)(2)}{(2)(0.44)} + (2)(0.009)(261) = 9.2$$

$$A_4 = 0.009\sqrt{1} + \frac{260}{\sqrt{1}} = 260$$

Hence,

$$c(2,1) = \frac{200}{2} e^{0(1)} \left(e^{-0.15} \text{erfc}(261) + e^{9.2} \text{erfc}(261) \right)$$

but

$$\text{erfc}(261) = 0$$

Thus

$$c(2,1) = 0 \text{ ppb}$$

The model predicted concentration of endrin two meters down and one day after the spill is essentially zero. Why? Because of the extremely high retardation due to adsorption of endrin onto the soil particles.

---------- END OF EXAMPLE VII-7 ----------

7.5.5 Two-Dimensional Horizontal Flow With A Slug Source

The previous three analytical models only considered one-dimensional flow. Methods for two-dimensional flow will now be introduced. The first 2-D model that will be considered calculates the concentration of a contaminant downgradient of the source. The waste is considered to have been instantaneously discharged at a point. The resultant concentration in the aquifer is assumed to be uniform with depth at the point of discharge. The depth of mixing can be less than the full depth of the aquifer if the contaminant is thought to be only in a particular part of an aquifer. Vertical dispersion is usually small as discussed earlier in Section 7.4.1 on dispersion. Hence, only horizontal variations can be considered. Such an instantaneous discharge is also called a slug source and can be caused by leaky ponds or tanks or by spills. Instantaneous means that the duration of the discharge is very short compared to the time since the discharge. An analytical solution will be given below to model this problem. The solution can be used to answer the following questions:

- What is the maximum concentration of contaminants likely to be at a downgradient well?
- When does the concentration of contaminants at a downgradient well exceed a particular value or become negligible?
- At what distance will the concentration of contaminants remain at negligible concentrations?
- What is the approximate areal extent of the contaminant plume?

Before the analytical model can be given, several additional assumptions need to be stated. These are as follows. The saturated thickness of the aquifer is assumed to be uniform and the hydraulic properties of the aquifer are relatively homogeneous. The density and viscosity of the injected solute are the same as those of the native water in the aquifer. The regional flow in the aquifer is uniform and horizontal. The effect of the source on the seepage velocity is assumed to be negligible compared to the uniform regional flow rate.

The mass transport equation governing advection, dispersion, first-order decay and linear, equilibrium adsorption in two dimensions in the aquifer for the above case is:

$$R_d \frac{\partial c}{\partial t} + v_x \frac{\partial c}{\partial x} = D_x \frac{\partial^2 c}{\partial x^2} + D_y \frac{\partial^2 c}{\partial y^2} - kR_d c + m' \frac{\delta(x)\delta(y)\delta(t)}{p} \qquad \text{(VII-84)}$$

The last term on the right side of Equation VII-84 represents the instantaneous discharge of mass at location x=0, y=0. The $\delta(:)$ represents a Dirac delta function and m' is the strength of the discharge, where $m' = c_o Q'/b$ (i.e., the mass of contaminants injected divided by the thickness of the aquifer). A schematic of the problem is shown in Figure VII-41.

As presented in Equation VII-84, the first-order decay rate, k, assumes that solute in the liquid and solid phases decays at the same rate (i.e., $k = k_{liquid} = k_{solid}$). The liquid phase refers to solute in solution and the solid phase refers to solute that has been adsorbed. If the liquid and solid phase decay rates are not the same, the k value is corrected using Equation VII-76.

The solution to the equation shown in Equation VII-84, with a zero initial condition and zero gradient at large distances, can be found by means of the integral transform or Laplace transform techniques:

$$c(x,y,t) = \frac{c_o Q'}{b4\pi pt(D_x D_y)^{1/2}} \exp\left(-kt - \frac{(xR_d - v_x t)^2}{4D_x tR_d} - \frac{(yR_d)^2}{4D_y tR_d}\right) \qquad \text{(VII-85)}$$

where

c_o = initial concentration of contaminant being discharged (mg/l)
Q' = volume of contaminant being discharged (m^3)
b = saturated thickness of aquifer (m)
p = effective porosity (decimal percent, unitless)
t = time (days)
D_x, D_y = dispersion coefficients in x and y directions, respectively (m^2/day)
v_x = seepage velocity of the regional flow in the x direction (m/day)
x,y = location of point of interest (m), where the source is located at x=0, y=0
k = first-order decay constant of the contaminant in the aquifer (per day)
R_d = retardation coefficient for linear, equilibrium adsorption (unitless)

Equation VII-85 is similar to the solution presented by Wilson and Miller (1978) but linear, equilibrium adsorption has been added.

The maximum concentration at any specified location occurs at time t_{max}. This time is computed as:

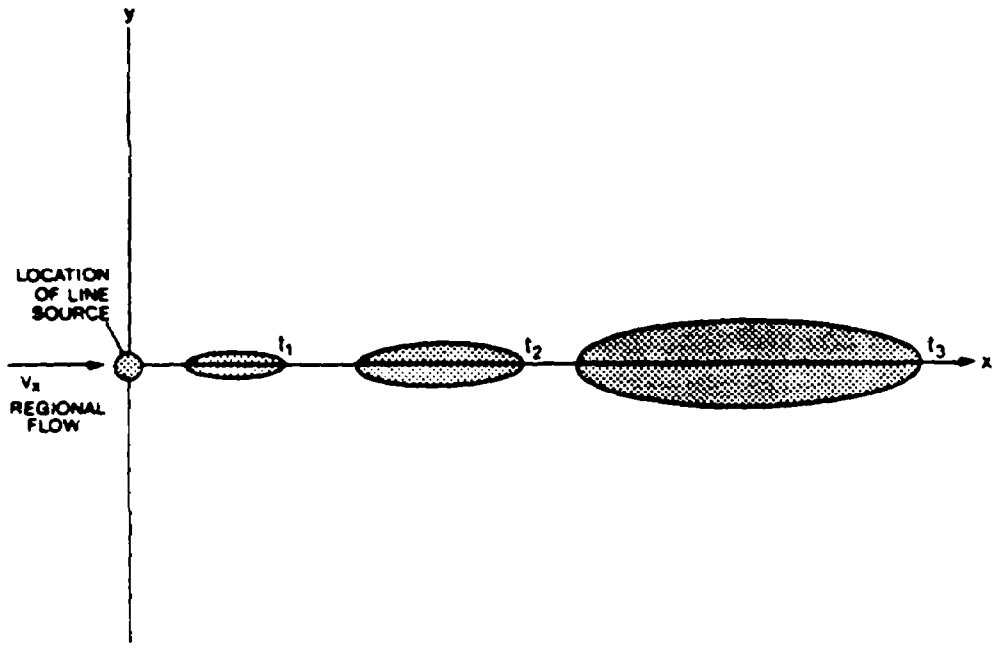

FIGURE VII-41 SCHEMATIC SHOWING A SLUG DISCHARGE OF WASTE INTO A REGIONAL FLOW FIELD

$$t_{max} = \left(- B + (B^2 - 4AC)^{1/2}\right)/(2A) \qquad \text{(VII-86)}$$

where

$$A = (k4D_xD_yR_d + v_x^2D_y) \qquad \text{(VII-87)}$$

$$B = (4D_xD_yR_d) \qquad \text{(VII-88)}$$

$$C = - (x^2R_d^2D_y + y^2R_d^2D_x) \qquad \text{(VII-88a)}$$

Hence, to calculate the maximum concentration that will occur at a point (x,y), substitute t_{max} for t in Equation VII-85.

EXAMPLE VII-8

Consider the problem of an accidental spill inside a chemical warehouse in which a storage drum of chloromethane (methyl chloride) leaks into an industrial sewer. The industrial sewer discharges into an injection well that is screened over the entire saturated thickness of the sandstone aquifer. About 0.1 m^3 of

chloromethane enters the aquifer at a concentration of 1600 mg/l. The sandstone aquifer has the following properties:

Soil fraction silt and clay	$f = 0.01$
Percent organic carbon in the sand fraction	$X_{oc}^{s} = 0.01$
Percent organic carbon in the silt and clay fraction	$X_{oc}^{f} = 0.05$
Soil bulk density	$\rho_b = 2.5$ g/ml
Effective porosity	$p = 0.12$
Saturated thickness	$b = 15$ m
Dispersion coefficient	$D_x = 4$ m^2/day
	$D_y = 1$ m^2/day
Seepage velocity:	$v_x = 0.3$ m/day

In addition, chloromethane has the following adsorption and degradation properties:

Octanol-water partition coefficient	$K_{ow} = 8$ (unitless)
Hydrolysis rate (at a pH of 7)	$K_H = 0.0021$ per day

At a distance of 35 meters downgradient of the injection well is a domestic supply well. What is the maximum concentration of chloromethane expected to reach the domestic well and when will the maximum concentration occur?

To answer these questions, several parameters have to be computed. Chloromethane undergoes both adsorption and degradation in the aquifer. Adsorption is related to the soil properties as described by Equation II-17 and II-18.

Upon substitution of the data into Equations II-17 and II-18, one obtains the adsorption coefficient K_d as shown below:

$$K_{oc} = 0.63(8) = 5 \text{ ml/g}$$

$$K_d = (5)(0.2(1-0.01)(0.01) + (0.01)(0.05)) = 0.012 \text{ ml/g}$$

If we assume adsorption can be described by a linear, equilibrium model, then the retardation coefficient for chloromethane can be computed using Equation VII-55 as shown below:

$$R_d = 1 + \rho_b K_d / p$$

$$R_d = 1 + (2.5)(0.012)/(0.12) = 1.25 \text{ (unitless)}$$

In addition to adsorption, chloromethane in the aqueous phase is subject to hydrolysis. Adsorbed chloromethane does not undergo hydrolysis. The relation between the general degradation rate and the liquid/adsorbed phase rates is given

by Equation VII-76. Thus for this problem, k_{liquid} would equal the hydrolysis rate and k_{solid} would be zero. Upon substitution of the data into Equation VII-76:

$$k = \frac{0.0021 + \frac{(0)(2.5)(0.012)}{(0.12)}}{(1.25)} = 0.0017 \text{ per day}$$

All of the soil and chemical properties can now be given for the problem as follows:

$x = 35$ m	$c_o = 1600$ mg/l
$y = 0$ m	$Q' = 0.1$ m^3
$b = 15$ m	$v_x = 0.3$ m/day
$p = 0.12$	
$R_d = 1.25$	$D_x = 4$ m^2/day
$k = 0.0017$ per day	$D_y = 1$ m^2/day

The time at which the maximum concentration occurs can now be computed upon substitution of the above data into Equation VII-86 to VII-89:

$$A = (k4D_xD_yR_d + v_x^2D_y) = (0.0017)4(4)(1)(1.25) + (0.3)^2(1) = 0.124$$

$$B = (4D_xD_yR_d) = 4(4)(1)(1.25) = 20$$

$$C = -(x^2D_y + y^2D_x)R_d^2 = -\ (35)^2(1) + (0)^2(4)\ \ (1.25)^2 = -1914$$

$$t_{max} = (-B + (B^2 - 4AC)^{1/2})/2A)$$

$$= \left(-20 + \left((20)^2 - 4(.124)(-1914)\right)^{1/2}\right)\ /(2(.124)) = 67.5 \text{ days}$$

Hence, the maximum concentration will occur at the domestic well 68 days after the spill. The value of the maximum concentration is computed by substituting t_{max} and the other data into Equation VII-81:

$$c_{max} = \frac{c_oQ'}{b4\pi pt_{max}(D_xD_y)^{1/2}} \exp\left(-kt_{max} - \frac{(xR_d - v_xt_{max})^2}{4D_xt_{max}R_d} - \frac{(yR_d)^2}{4D_yt_{max}R_d}\right) \qquad \text{(VII-89)}$$

$$c_{max} = \frac{(1600)(0.1)}{(15)4\pi(0.12)(67.5)\ ((4)(1))^{1/2}} \exp\left(-(0.0017)(67.5)\right.$$

$$- \frac{((35)(1.25)-(0.3)(67.5))^2}{4(4)(67.5)(1.25)} - \frac{(\ (0)\ (1.25)\ )^2}{4(1)(67.5)(1.25)}\Bigg)$$

$$= (0.0524)\exp(-0.524) = 0.031 \text{ mg/l}$$

Hence, the maximum concentration of chloromethane that will reach the domestic well is 0.031 mg/l or 31 μg/l. This concentration will occur at the domestic well 68 days after the spill.

END OF EXAMPLE VII-8

EXAMPLE VII-9

Consider a large electric power company that has a coal-burning plant that produces electricity. Its fly ash is deposited as a slurry waste into a large lagoon where the ash is allowed to settle. The lagoon site is above a 2 meter thick water table aquifer that consists of glacial outwash. A layer of impermeable clay lines the bottom of the lagoon. A large river flows nearby.

Next to the lagoon, the electric company has been preparing the ground for another lagoon when a bulldozer accidentally breaches the berm surrounding the lagoon. Very quickly, about 40 m^3 of supernatant spill out and form a pool on top of the ground. The supernatant percolates into the ground after a short time. The greatest concern to the company is the level of boron in the spill water, which had a concentration of about 10 mg/l. They want to know what the maximum concentration of boron will be where the aquifer discharges to the river and when this will occur. The downgradient distance between the spill site and the river is 50 meters.

Since the area of the spill site is very small compared to the area over which the contaminant will travel and since the duration of the spill was short, a slug source model is selected. This model assumes complete vertical mixing of the source in the aquifer. This seems reasonable considering the relative thinness of the glacial outwash aquifer.

After an investigation of the problem, the following information is obtained:

$x = 50$ m	$c_o = 10$ mg/l
$y = 0$ m	$Q' = 40$ m^3
$b = 2$ m	$v_x = 2$ m/day
$p = .15$	
$R_d = 17$	$D_x = 15$ m^3/day
$k = 0$/day	$D_y = 5$ m^3/day

Step 1. The time at which the maximum concentration of boron will reach the river, t_{max} can now be computed by substituting the above data into Equation VII-86 to VII-89:

$$A = (k4D_xD_yR_d + v_x^2D_y) = (0)(4)(15)(17) + (2)^2(5) = 20$$

$$B = (4D_xD_yR_d) = (4)(15)(5)(17) = 5100$$

$$C = -(x^2D_y + y^2D_x)R_d^2 = -\left((50)^2(5) + (0)^2(15)\right)(17)^2 = -3.61\times10^6$$

$$t_{max} = (-B + (B^2-4AC)^{1/2})/(2A)$$

$$= (-5100 + ((5100)^2-4(20)(-3.6\times10^6))^{1/2})/(2(20)) = 316 \text{ days.}$$

Hence, it will take about 320 days for the maximum concentration of boron to reach the river.

Step 2. The value of the maximum concentration of boron that will reach the river is computed by substituting the above data into Equation VII-85:

$$c_{max} = \frac{c_oQ'}{b4\pi t_{max}(D_xD_y)^{1/2}} \exp(g)$$

where

$$g = \left(-kt_{max} - \frac{(xR_d-v_xt_{max})^2}{4D_xt_{max}R_d} - \frac{(yR_d)^2}{4D_yt_{max}R_d}\right)$$

$$g = \left(-(0)(316) - \frac{((50)(17)-(2)(316))^2}{4(15)(316)(17)} - \frac{((0)(17))^2}{4(5)(316)(17)}\right) = -0.15$$

$$c_{max} = \frac{(10)(40)\exp(-.15)}{(2)4\pi(.15)(316)((15)(5))^{1/2}} = 0.033 \text{ mg/l}$$

The maximum concentration of boron that will reach the river is about 0.03 mg/l or 30 μg/l.

END OF EXAMPLE VII-9

7.5.6 Two-Dimensional Horizontal Flow With Continuous Solute Line Sources

In Section 7.5.5, the problem of an instantaneous waste discharge is considered. In this section, a continuous waste discharge into a homogeneous, isotropic aquifer will be considered. The contaminant is discharged continuously and uniformly with depth into the aquifer. The density and viscosity of the discharged solute are the same as those of the native water in the aquifer. The effect of the discharging solute on the seepage velocity is assumed to be negligible compared to the uniform regional flow rate.

The mass transport equation governing advection, dispersion, first-order decay and linear, equilibrium adsorption in two dimensions in the aquifer is:

$$R_d \frac{\partial c}{\partial t} + v_x \frac{\partial c}{\partial x} = D_x \frac{\partial^2 c}{\partial x^2} + D_y \frac{\partial^2 c}{\partial y^2} - kR_d c + g_L \frac{\delta(x)\,\delta(y)}{p} \qquad \text{(VII-90)}$$

The last term on the right-hand side of Equation VII-90 represents the instantaneous discharge of mass by a well screened over the entire depth of the aquifer at location x=0, y=0. The mixed zone can be set equal to the depth screened, rather than the full depth of the aquifer, if vertical mixing above and below the screened zone is thought to be small. The $\delta(\cdot)$ is a Dirac delta function and g_L is the strength of the line source, where $g_L = c_o Q/b$.

As presented in Equation VII-90, the first-order decay rate, k, assumes that solute in its liquid and solid phases decays at the same rate (i.e., $k = k_{liquid} = k_{solid}$). The liquid phase refers to solute in solution and the solid phase refers to solute that has been adsorbed. If the liquid and solid phase decay rates are not the same, Equation VII-76 needs to be substituted.

The solution to Equation VII-90, with a zero initial concentration and zero gradients at large distances can be found by means of the integral transform or Laplace transform techniques:

$$c(x,y,t) = \frac{c_o Q}{4\pi pb(D_x D_y)^{1/2}} \exp\left(\frac{v_x x}{2D_x}\right) W\left(u, \frac{r}{B}\right) \qquad \text{(VII-91)}$$

where

$W(\cdot)$ = the leaky well function of Hantush (see Appendix J)

$B = 2D_x/v_x$ (m)

$r = (B(x^2 + y^2 D_x/D_y))^{1/2}$ (m)

$u = \frac{r^2 R_d}{4BD_x t}$ (unitless)

β = $1 + 2BR_d k/v_x$ (unitless)

Q = volumetric rate discharge into the aquifer by the line source (m^3/day)

t = time (days)

(x,y) = location of point of interest (m), where the line source is located at x=0, y=0

D_x, D_y = dispersion coefficients in the x and y directions, respectively (m^2/day)

v_x = seepage velocity of the regional flow in the x direction (m/day)

p = effective porosity of the aquifer (unitless, decimal percent)

b = saturated thickness of mixed zone (m)

k = first-order decay constant (per day)

R_d = retardation coefficient for linear, equilibrium adsorption (unitless)

c_o = concentration of contaminant being discharged (mg/l)

Note that Equation VII-91 is similar to the solution presented by Wilson and Miller (1978). However, Equation VII-91 allows for linear, equilibrium adsorption. A schematic representation of Equation VII-91 is shown in Figure VII-42.

The leaky well function of Hantush W(u,r/B) is discussed in Appendix J. In addition, a table of values (i.e., Table J-3) and several approximations are given for the W(:) function in Appendix J.

For the special case of steady-state conditions (i.e., large times) and when the ratio r/B is larger than one (i.e., far from the source), then Equation VII-91 reduces to the following simplified form:

$$c(x,y,\text{steady-state}) = \frac{c_o Q}{b2\pi p}\left(\frac{\pi B}{2D_x D_y r}\right)^{\frac{1}{2}} \exp\left(\frac{v_x x}{2D_x} - \frac{r}{B}\right) \qquad \text{(VII-92)}$$

EXAMPLE VII-10

A small community had water from their municipal well checked for trace organics. To their surprise, they found a concentration of 150 µg/l of trichloroethylene (TCE). After much investigation, a local environmental organization found the only major user of TCE to be a semi-conductor manufacturing plant. However, the plant was located over 1000 meters away from the site of the municipal well. At first, few could believe that the plant could be the source of the contamination because of the large distance involved. Hence, a blue-ribbon committee was selected to investigate the problem. What follows are the results of the committee's work.

The solvent TCE has been used continuously by the manufacturing plant for the last 25 years as a degreaser for their equipment. All residual TCE is washed

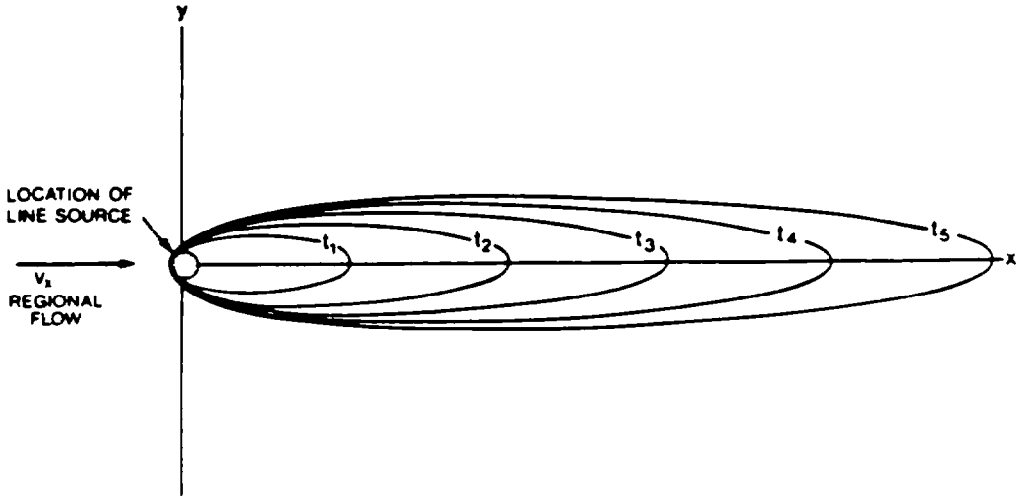

FIGURE VII-42 SCHEMATIC SHOWING A CONTINUOUS DISCHARGE OF WASTE INTO A REGIONAL FLOW FIELD

out of the plant by a large volume of water, which in turn is pumped to a small, unlined pond. The pond receives about 500 m^3 of TCE contaminated wash water per year and the concentration of TCE in the pond is 25,000 µg/l. The wastewater percolates through the bottom of the pond as quickly as it flows in. The depth to the water table is about 2 meters and the underlying aquifer consists of unconsolidated sand. From well logs, observation wells and pumping tests, it was found that the hydraulic conductivity in the unconsolidated sand was 3640 m/yr, the effective porosity 0.2, hydraulic gradient in the aquifer 0.0022 m/m and saturated thickness of the aquifer 20 meters. The unconsolidated sand is underlain by a thick impermeable clay layer. Dispersion tests showed that the dispersivity along the direction of ground water flow is about 50 m and transverse to the flow about 5 m. The background concentration of TCE upgradient of the plant is below detection.

As a first approximation, the TCE is considered to be vertically mixed in the aquifer. Since the dimensions of the pond are small compared to the travel distance, the analytic solution of Wilson and Miller (1978) can be used to simulate the TCE transport.

In addition to the other information already given, the seepage velocity and dispersion coefficients are needed. The seepage velocity is calculated using Equation VII-36:

$$v_s(\text{seepage}) = (K_{sat})(\text{hydraulic gradient})/p$$

$$v_x = (3640)(0.0022)/0.2 = 40 \text{ m/yr}$$

Note that the transverse velocity is zero because we have oriented the x axis along the principal flow direction. If hydrodynamic dispersion is assumed to be a linear function of seepage velocity, then dispersion can be computed as follows from Equation VII-53:

$$D_x = \alpha_x v_x = (50)(40) = 2000 \text{ m}^2/\text{yr}$$

$$D_y = \alpha_y v_x = (5)\ (40) = 200 \text{ m}^2/\text{yr}$$

where α_x and α_y are the longitudinal and transverse dispersivities, respectively.

The committee further assumes that there is negligible adsorption of TCE and that degradation (e.g., dehydrochlorination) is zero because of the aerobic conditions. The amount of TCE entering the aquifer through the pond bottom is estimated to have been constant over the past 25 years.

The information for this example can now be tabulated as follows:

$t = 25$ yrs	$c_o = 25000$ µg/l
$v_x = 40$ m/yr	$Q = 500$ m^3/yr
$D_x = 2000$ m^2/yr	$b = 20$ m
$D_y = 200$ m^2/yr	$p = 0.2$
$x = 1000$ m	$R_d = 1$
$y = 0$ m	$k = 0$ per yr

Determine the concentration of TCE at a distance of 1000 meters from the manufacturing plant after 25 years. This problem is mathematically described by Equation VII-90. Equation VII-91 gives an analytic solution to the problem. To predict the concentration, the committee needs to first evaluate the following terms:

$$B = 2D_x/v_x = (2)(2000)/40 = 100 \text{ m}$$

$$\beta = 1 + 2BR_d k/v_x = 1 + 2(100)(1)(0)/40 = 1$$

$$r = \left(\beta\left(x^2 + y^2 \frac{D_x}{D_y}\right)\right)^{1/2} = \left((1)\left((1000)^2 + (0)^2\frac{(2000)}{200}\right)\right)^{1/2} = 1000 \text{ m}$$

$$r/B = 1000/100 = 10$$

$$u = \frac{r^2 R_d}{4BD_x t} = \frac{(1000)^2(1)}{4(1)(2000)(25)} = 5$$

With the above terms, Equation VII-91 can now be evaluated:

$$c(x,y,t) = \frac{c_o Q}{b4\pi p(D_x D_y)^{1/2}} \exp\left(\frac{v_x x}{2D_x}\right) W\left(u, \frac{r}{B}\right)$$

$$c(1000,0,25) = \frac{(25000)(500)}{(20)4\pi(0.2)((2000)(200))^{1/2}} \exp\left(\frac{(40)(1000)}{2(2000)}\right) W(5,10)$$

$$= (393.2)\exp(10)W(5,10)$$

Unfortunately, the range of parameter values given in Table J-3 of Appendix J does not include the values needed to evaluate the leaky well function of Hantush, W(5,10). However, since the r/B parameter is very large, one can use the Wilson and Miller (1978) approximation to W given in Appendix J:

$$W(u,r/B) = \left(\frac{\pi B}{2r}\right)^{1/2} \exp\left(-\frac{r}{B}\right) erfc\left(-\frac{(r/B-2u)}{2\sqrt{u}}\right)$$

$$W(5,10) = \left(\frac{\pi(100)}{2(1000)}\right)^{1/2} \exp(-10) erfc\left(-\frac{(10-2(5))}{2\sqrt{5}}\right)$$

$$W(5,10) = (0.40)\exp(-10)erfc(0)$$

but erfc(0) = 1, thus

$$W(5,10) = (0.4)(4.54 \times 10^{-5})(1) = 1.82 \times 10^{-5}$$

Therefore, upon substitution of W(5,10) back into our concentration solution (Equation VII-91):

$$c(1000,0,25) = (393.2)(22026.5)(1.82 \times 10^{-5}) = 158\ \mu g/l$$

If one does not use the Wilson and Miller approximation, the exact solution is 154 µg/l.

As mentioned earlier, a concentration of 150 µg/l of TCE was discovered in the municipal water well. The manufacturing plant appears to be the likely source of the TCE contamination.

END OF EXAMPLE VII-10

EXAMPLE VII-11

The previous example showed how the contaminant TCE decreased in concentration with distance and time. Biological and chemical degradation processes were assumed to be negligible. This is true under aerobic conditions for TCE but under anaerobic conditions degradation can take place. It is difficult to provide accurate rates of degradation for field type situations because many variables (e.g., pH, temperature) may affect it. The half life of TCE under anaerobic conditions ranges from 40 to 400 days (Wood et al., 1981). This corresponds to a decay rate of 0.2 to 6 per year.

What is the concentration of TCE at a distance of 1000 m after 25 years if biodegradation at a rate of 0.2 per year is included? The data needed are summarized below:

t = 25 yrs	c_o = 25000 µg/l
v_x = 40 m/yr	Q = 500 m^3/yr
D_x = 2000 m^2/yr	b = 20 m
D_y = 200 m^2/yr	p = 0.2
x = 1000 m	R_d = 1
y = 0 m	k = 0.2 per yr

Step 1. Calculate the following terms in Equation VII-91:

$$B = 2D_x/v_x = 2(2000)/40 = 100$$

$$\beta = 1 + \frac{2BR_d k}{v_x} = 1 + \frac{2(100)(1)(0.2)}{40} = 2$$

$$r = (\beta(x^2 + y^2 D_x/D_y))^{1/2}$$

$$r = (2((1000)^2 + (0)^2(2000)/(200))^{1/2} = 1414$$

$$r/B = 1414/100 = 14.14$$

$$u = \frac{r^2 R_d}{4BD_x t} = \frac{(1414)^2(1)}{4(2)(2000)(25)} = 5$$

Step 2. Is r/B greater than 1? If so, use the Wilson and Miller (1978) approximation given in Appendix J to evaluate W, the leaky well function Hantush. If r/B is less than 1, then use Table J-3 to evaluate W. For example, to use the Wilson and Miller approximation, proceed as follows. Evaluate the terms:

$$\left(-\frac{(r/B-2u)}{2\sqrt{u}}\right) = -\frac{(14.14-2(5))}{2\sqrt{5}} = -0.93$$

$$\text{erfc}\left(-\frac{(r/B-2u)}{2\sqrt{u}}\right) = \text{erfc}(-0.93) = 1.81$$

Note that $\text{erfc}(-a) = 2 - \text{erfc}(a) = 2 - 0.188 = 1.81$

$$W(u,r/B) = \left(\frac{\pi B}{2r}\right)^{\frac{1}{2}} \exp\left(-\frac{r}{B}\right)\text{erfc}\left(-\frac{(r/B-2u)}{2\sqrt{u}}\right)$$

$$W(5,14.14) = \left(\frac{\pi(100)}{2(1414)}\right)^{\frac{1}{2}} \exp(-14.14)(1.81) = 4.36 \times 10^{-7}$$

Step 3. Evaluate the final computation using Equation VII-91:

$$c(x,y,t) = \frac{c_o Q}{4\pi pb(D_x D_y)^{\frac{1}{2}}} \exp\left(\frac{v_x x}{2D_x}\right) W(u, r/B)$$

$$c(1000,0,25) = \frac{(25000)(500)}{4\pi(0.2)(20)((2000)(200))^{\frac{1}{2}}} \exp\frac{(40(1000)}{2(2000)} \quad (4.36 \times 10^{-7})$$

$$c(1000,0,25) = 3.8\ \mu g/l$$

With degradation over a 25-year period, the predicted concentration of TCE is decreased from 185 µg/l to 4 µg/l. However, it should be noted that when TCE undergoes degradation by dehydrochlorination, it produces incomplete degradation products (e.g., the two isomers of dichloroethylene) which are also hazardous.

END OF EXAMPLE VII-11

7.6 INTERPRETATION OF RESULTS

This section discusses the interpretation of results calculated using the screening methods. Section 7.6.1 reviews water quality criteria which are pertinent to ground water. A brief analysis of uncertainty and methods for quantifying it are given in Section 7.6.2. Finally, Section 7.6.3 provides guidance for determining when more detailed analyses such as those involving numerical computer models are appropriate.

7.6.1 Appropriate Reference Criteria

7.6.1.1 Introduction

Federal and state regulations applicable to ground water quality are currently undergoing revision. The trend is toward more regulation at the state level rather

than at the federal level. Pertinent federal laws include the Federal Water Pollution Control Act/Clean Water Act (1972/1977/1982), the Safe Drinking Water Act (1974/1977), the Resource Conservation and Recovery Act (1976/1984), and the Toxic Substances Control Act (1976). The U.S. Environmental Protection Agency recently made public its policy regarding ground water protection in a document referred to as the EPA's Ground Water Protection Strategy (U.S. EPA, 1984). Individual states are also in the process of developing laws and programs related to ground water. For example, Connecticut, Florida, Wisconsin, and New Mexico have ground water classification systems and numerical standards for each classification. Maryland, New Jersey, and New York specify effluent limitations for waste discharges to ground water.

7.6.1.2 Water Quality Standards

The predicted results of the hand calculation methods should be compared to the appropriate standards. The federal standards for drinking water are currently being reviewed (CFR Vol. 48, No. 194, October, 1983). Numerical limits may change and new parameters may be added as shown in Table VII-13. The interim primary drinking water standards are based on human health considerations. The present standards cover ten inorganic chemicals, bacteria, turbidity, organic chemicals and radioactivity.

The interim secondary drinking water standards (Table VII-14) mainly address aesthetic and pragmatic factors rather than public health. The secondary standards cover parameters which affect taste, color, odor and the corrosive properties of water. These standards are not federally enforceable but are considered guidelines for the states.

In addition to the federal drinking water standards, each state may have its own set of water quality standards, which may be equal or more stringent than the federal standards. These regulations may change so it is imperative to check with the local state agencies regarding current values.

The state may specify that standards apply to the ground water at the waste disposal site boundary, at a specified distance downgradient of the site, at a property boundary, or at the point of use. In some states, ground water downgradient of a waste site may have to meet all federal drinking water standards. In addition, if the ground water discharges to a surface water body, surface water standards may apply.

7.6.2 Quantifying Uncertainty

Uncertainty in ground water flow and contaminant transport has been implied throughout this chapter. Part of this uncertainty is due to aquifer heterogeneities and natural variability. Additional uncertainty is introduced by sampling and measurement errors and the assumptions on which the hand calculation methods are based. For numerical models used to compute ground water flow and contaminant transport, uncertainty can also result from the numerical solution techniques.

TABLE VII-13

PRIMARY DRINKING WATER STANDARDS

INORGANIC CHEMICALS

Parameter	Maximum Contaminant Level (mg/l)	Parameters Under Consideration	
Arsenic	0.05	Aluminum	Nickel
Barium	1.0	Antimony	Sodium
Cadmium	0.010	Asbestos	Sulfate
Chromium	0.05	Beryllium	Thallium
Lead	0.05	Copper	Vanadium
Mercury	0.002	Cyanide	Zinc
Nitrate (as N)	10.0	Molybdenum	
Selenium	0.01		
Silver	0.05		
Fluoride	1.4-2.4		

MICROBIOLOGICAL CONTAMINANTS AND TURBIDITY

Parameter	Maximum Contaminant Level (mg/l)	Parameters Under Consideration
Total Coliforms	1/100 ml Monthly Average 4/100 ml Single Sample	Giardia, Legionella, Viruses Standard Plate Count (SPC)
Turbidity	1-5 turbidity units	

ORGANIC CHEMICALS

Parameter	Maximum Contaminant Level (mg/l)	Parameters Under Consideration	
Endrin	0.002	Aldicarb	Dibromochloropropane (DBCP)
Lindane	0.004	Chlordane	1,2-Dichloropropane
Methoxychlor	0.1	Dalapon	Pentachlorophenol
Toxaphene	0.005	Diquat	Pichloram
2,4-D	0.1	Endothall	Dinoseb
2,4, 5-TP Silvex	0.01	Glyphosate	Alachlor
Total Trihalomethanes	0.1	Carbofuran	Ethylene dibromide
		1,1,2-Trichloroethane	Epichlorohydrin
		Vydate	Dibromomethane
		Simazine	Toluene
		PAHs	Xylene
		PCBs	Adipates
		Atrazine	Hexachlorocyclopentadiene
		Phthalates	2,3,7,8-TCDD (Dioxin)
		Acrylamide	

RADIOACTIVITY

Parameter	Maximum Contaminant Level	Parameters under Consideration
Combined radium 226 and radium 228	5 pCi/l	Uranium
Gross alpha particle activities	15 pCi/l	Radon
Beta particle and photon radioactivity from man-made radionuclides	4 millirem/year	

Reference: U.S. EPA (1977a) and Code of Federal Regulations 40 CFR 141.11-141.16 (1982).

TABLE VII-14

INTERIM SECONDARY DRINKING WATER STANDARDS

Parameter	Maximum Contaminant Level
Chloride	250 mg/l
Color	15 color units
Copper	1 mg/l
MBAS*	0.5 mg/l
Iron	0.3 mg/l
Manganese	0.05 mg/l
Odor	Threshold Odor Number 3
pH	6.5-8.5
Sulfate	250 mg/l
Total Dissolved Solids	500 mg/l
Zinc	5 mg/l
Corrosivity	Non-Corrosive

*Methylene blue active substances

Reference: U.S. EPA (1977b) and Code of Federal Regulations 40 CFR 143.3 (1982).

7.6.2.1 Sources of Uncertainty

Uncertainty associated with measured values of a parameter may be due to variability of aquifer characteristics, sampling error, and analytical error. The distinction between these sources can be made by collecting replicate samples, splitting them, and performing at least duplicate analyses of the samples. One common sampling design involves collection of four replicates which are then each split four ways. The uncertainty can then be allocated using a 4 x 4 analysis of variance (ANOVA). The quality of laboratory analyses should also be checked by analysis of blanks, standards, and unknowns. Additional discussion of QA/QC procedures is included in Scalf et al. (1981), U.S. EPA (1979b) and (1980).

Uncertainty in the representation of the physical system may also create uncertainty in the parameters used to describe the system. For example, consider the concept of hydrodynamic dispersion which was discussed in Section 7.4.1. Several figures and tables were given to provide estimates for dispersivity, which itself is used to represent the dispersive characteristics of an aquifer. However, current research indicates that dispersion results from variations in the seepage velocity profile. These variations may not be adequately characterized by existing mathematical formulations.

Additional uncertainty and errors can be introduced by mathematical solutions in the form of overshoot, numerical dispersion, truncation and round-off errors. Overshoot and numerical dispersion are the most important errors generated by finite difference and finite element models of contaminant transport. The term overshoot describes the erroneously high values computed near the upstream side of sharp solute fronts (undershoot is the analogous behavior on the downstream side of sharp fronts). Numerical dispersion, which results from the incomplete approximation of the differential equations, can smear a sharp front and thereby produce a solution indicative of a larger dispersion coefficient (Pinder and Gray, 1977). Truncation errors occur when only a finite number of terms are used to represent the original equations describing flow and mass transport. Finally, round-off errors result from the finite accuracy of computer calculations. It should be noted that even analytic solutions can be subject to truncation and round-off errors.

7.6.2.2 Methods of Estimating Uncertainty

The recognition of uncertainty helps put predicted results in perspective. For example, if the time of arrival of a contaminant at a well is 300 $\pm$ 10 days, then time is available to design a plan of action. However, if our uncertainty analysis predicted a time of arrival of 300 $\pm$ 200 days, a plan of action would have to be developed much sooner.

Several methods are available for estimating the uncertainty associated with calculations. Included are sensitivity analysis, variance analysis, interval analysis, and Monte Carlo analysis. Each of these methods is discussed briefly below.

Sensitivity analysis is the process of determining the variation in a model output variable caused by a change in one of the input parameters. This can be done using a mathematical approach or simply by making repeat calculations using different parameter values. The parameters which most influence the results can thereby be identified.

Consider a sensitivity analysis of the seepage velocity v_s for saturated flow. From Section 7.3.3.1.2, it was shown that the seepage velocity is a function of the hydraulic conductivity K, the hydraulic gradient I and the porosity p. From Equation VII-36 the seepage velocity was shown to be equal to:

$$v_s = -KI/p$$

The total uncertainty in the seepage velocity dv_s can be expressed as:

$$dv_s = \left(\frac{\partial v_s}{\partial K}\right) dk + \left(\frac{\partial v_s}{\partial I}\right) dI + \left(\frac{\partial v_s}{\partial p}\right) dp \qquad \text{(VII-93)}$$

where $(\partial v_s/\partial K)$, $(\partial v_s/\partial I)$ and $(\partial v_s/\partial p)$ are the sensitivity coefficients and dK, dI and dp are the uncertainties associated with these parameters (e.g., $dK = \pm 1 \times 10^{-5}$ cm/sec,

$dI = \pm 0.001$, $dp = \pm 0.05$). Upon substitution of Equation VII-36 into Equation VII-93, the uncertainty dv_s becomes:

$$dv_s = -\left(\frac{I}{p}\right) dK - \left(\frac{K}{p}\right) dI + \left(\frac{KI}{p^2}\right) dp \qquad \text{(VII-94)}$$

The relative or percent uncertainty is found by dividing Equation VII-94 through by v_s. Thus upon substitution:

$$\frac{dv_s}{v_s} = \frac{dK}{K} + \frac{dI}{I} - \frac{dp}{p} \qquad \text{(VII-95)}$$

In the case of the seepage velocity, the uncertainty can be due to K, I, or p. However, the greatest source of uncertainty is generally the hydraulic conductivity term; its value may vary over several orders of magnitude. The above mathematical procedure for computing the sensitivity analysis can in principal be done for any input parameter but it usually becomes too complicated except for simple expressions. The alternative "brute force" method is to repeatedly perform the calculations, systematically varying the parameters, one at a time and in combinations, to determine how the variations in parameter values affect the predicted result.

Another mathematical technique used to quantify uncertainty is based upon determining how the variance of individual equation terms interact with each other. Consider two variables, called X and Y. Let the sum (or difference) of these two variables be called Z. If X and Y are considered as independent random variables, then the variance of Z can be calculated as:

$$Var[Z] = Var[X \pm Y] = Var[X] + Var[Y] \qquad \text{(VII-96)}$$

where Var [ ] is the variance of the variable. (An estimate of the variance can be obtained by squaring the standard deviation S_x. S_x is defined by Equation VII-22 in Section 7.2.5.4). If X and Y are multiplied together to get Z, then the variance of Z for this product will vary as:

$$\begin{aligned} Var[Z] &= Var[XY] \\ &= (E[X])^2 Var[Y] + (E[Y])^2 Var[X] + Var[X]Var[Y] \end{aligned} \qquad \text{(VII-97)}$$

where E [ ] is the expected value of the variable. (An estimate of the expected or mean value is given by Equation VII-23 in Section 7.2.5.4.) If Z is defined as X divided by Y, the variance of Z for this quotient will vary approximately as:

$$Var[Z] = Var[X/Y] \simeq \left(\frac{E[X]}{E[Y]}\right)^2 \left(\frac{Var[X]}{(E[X])^2} + \frac{Var[Y]}{(E[Y])^2}\right) \qquad \text{(VII-98)}$$

From the above expressions, it is obvious that if any independent variables have uncertainty associated with them, then the addition, subtraction, multiplication or division of these variables will always increase the variance of the combined variables. However, if the variables are not mutually independent of each other, the effect on the variance is not as clear since covariance terms need to be included in the above equations. Procedures for adding the covariance terms are included in Mood et al. (1974).

Interval analysis (Ross and Faust, 1982) is similar to sensitivity analysis except that likely ranges for the input parameters of interest are chosen and then these values are substituted into the analytical method to provide likely upper and lower bounds for the desired output parameters. For example, the upper bound could be the predicted contaminant concentration in the aquifer at a point 100 ft downgradient of an injection well using as input data a low retardation factor and minimal dispersion. The lower bound could be the predicted contaminant concentration at this same location when the highest retardation factor and dispersion are used in the calculations. When limited field data are available, this approach can provide at least an estimated range for the output parameters.

Monte Carlo analysis involves solving the ground water flow and solute transport equations using randomly chosen values as input parameters. The random values are selected from specified probability density functions (pdf) of key parameters. Typically, 50 to 300 repetitions of the calculations would be performed with different input parameters. Histograms of the predictions are generated and used to calculate the probability of specific events (e.g., number of times that concentration limits will be exceeded or time for a contaminant plume to reach a given well or surface water body). The principal limitations of this approach are the high cost of doing a large number of calculations, difficulties in estimating the pdf for each of the parameters and the need to include the "worst cases" of interest. The computer program MACRO developed by Kaufman et al. (1980) can be used to calculate pdf's of predicted contaminant concentrations. MACRO works by systematically making repeated model runs with regularly spaced values of the sensitive parameters. This program, however, has only been used for simple cases.

7.6.3 Guidelines for Proceeding to More Detailed Analysis

7.6.3.1 Introduction

There are typically four critical questions to be addressed in ground water contamination studies: a) where are the contaminants; b) when will they arrive at a specific location; c) what are the concentrations of the contaminants; and d) what hazards are posed by the contaminants. Answers to these questions provide a concise statement of the information needed to evaluate the environmental consequences of ground water contamination. To address these types of questions, there are three

general types of assessment tools available: site ranking methods, analytical (hand calculation) methods, and numerical models. These tools are useful for different levels of analysis and thus offer complimentary rather than competing uses. Up to this point, the chapter has addressed only the hand calculation methods. The three approaches are briefly compared below:

- Site ranking methods allow initial assessment of a large number of existing ground water contamination problems. With a minimum amount of information and technical expertise, site ranking methods can be used for evaluating the relative hazard posed by a large number of contamination sources. Because site ranking models do not provide quantitative estimates of contaminant concentrations, they will not be discussed further in this chapter. A review of selected ranking methods is included in Summers and Rupp (1982a).
- Analytical (or hand calculation) methods can predict the migration of contaminants in ground water from potential or existing waste sources. As shown in Section 7.5, these techniques are based on simplified representations of the ground water system. The techniques require limited field data and can be applied rapidly with hand calculators.
- Numerical models, like analytical methods, provide site-specific predictions by solving a series of equations. These models can provide greater temporal and spatial resolution. However, using numerical models generally requires large amounts of data and a computer.

Numerical models will be briefly discussed below. A method for determining when numerical models are appropriate is given in Section 7.6.3.3.

7.6.3.2 Numerical Models

Numerical model results can help address the following questions pertinent to ground water contamination problems:

- What is the maximum areal extent of a plume at a given site?
- What is the approximate time for a plume to reach a given well or surface water body?
- What is the maximum concentration of a contaminant that could occur at a given well or in the ground water discharging into a surface water body?
- How much time would be required to flush contaminants from an aquifer?
- What control methods are technically feasible and cost-effective?
- Is it likely that a contaminant plume would form at a candidate waste disposal site?
- Where should monitoring wells be located?

Flow and solute transport models vary in type and complexity depending upon the system being modeled and the extent to which the model attempts to fully represent that system. Modeling contaminant movement in a homogeneous aquifer is significantly less complex than attempting to model movement in a heterogeneous aquifer, such as one with interbedded clay lenses.

Data requirements for ground water flow and solute transport models are given in Table VII-15. The amount of data needed increases with the number of dimensions modeled and the size of the grid system.

Along with the input data shown in Table VII-15, historical water level and ground water quality data are needed to calibrate the model. Model results are usually compared with historical data and refined accordingly--a process known as calibration or history matching. This does not assure that a model will give accurate predictions for the future when conditions may change (e.g., a confined aquifer could have been pumped enough to change it to an unconfined system).

There are many mathematical models available for predicting ground water flow and solute transport in 1, 2, or 3 dimensions. Numerical solution techniques to choose from include finite difference, finite element, integrated finite difference, and method of characteristics. Detailed reviews of numerical models can be found in the following reports: Kincaid et al. (1983), Bachmat et al. (1978), van Genuchten (1978), Oster (1982) and Thomas et al. (1982). In addition, information and copies of publicly available ground water models may be obtained through the International Ground Water Modeling Center (IGWMC) at the Holcomb Research Institute of Butler University. The IGWMC has developed a computerized data base of over 600 models called the Model Annotation Retrieval System or MARS.

7.6.3.3 Model Selection

In this chapter, three different approaches to assessing ground water contamination problems have been briefly discussed, including site ranking, analytical and numerical models. However, the question of which approach to use is as of yet unanswered. Before a method is selected, an assessment should be made of the complexity of the hydrogeologic system, the type of information needed to meet the study objectives, and the present understanding of the aquifer system. Figure VII-43 shows a general sequence for determining whether a numerical model is needed and alternative approaches. Numerical models should be applied when a detailed assessment of the extent and significance of contamination is needed and when adequate funding and trained personnel are available for the required data collection and modeling effort. The steps involved in applying a model are shown in Figure VII-44. As this figure shows, data collection, interpretation and model application ideally should be an iterative process. Analytical methods should be used at each of these feedback points and to check final model results.

TABLE VII-15

DATA NEEDS FOR NUMERICAL MODELS

Flow Models

- areal extent of the aquifer
- grid type and spacing
- aquifer thickness, by node
- boundary conditions and locations of assigned nodes
- hydraulic conductivities (or permeabilities), by node
- specific storage or specific yield
- initial head, by node
- net recharge rate of the aquifer
- the locations and flow rates of system stresses (e.g. pumping wells)
- relationship to surface water, if present
- water level data for model calibration and verficiation

Solute Transport Models*

- longitudinal, transverse, and vertical dispersivity coefficients
- bulk density of permeable media
- effective porosity of the aquifer
- initial contaminant concentrations in the aquifer
- concentrations and flow rates of waste sources (these may vary by location and time)
- distribution coefficients or retardation factors for the contaminants of interest
- radioactive or biological decay constants, if appropriate
- concentration data for model calibration and verification

*The flow data are also needed to run solute transport models.

The simplest models should be used first to determine sensitive parameters and to identify significant data gaps. Based on the predicted results of the simple models and uncertainty analyses, a decision can then be made as to whether additional data and more complex models are necessary.

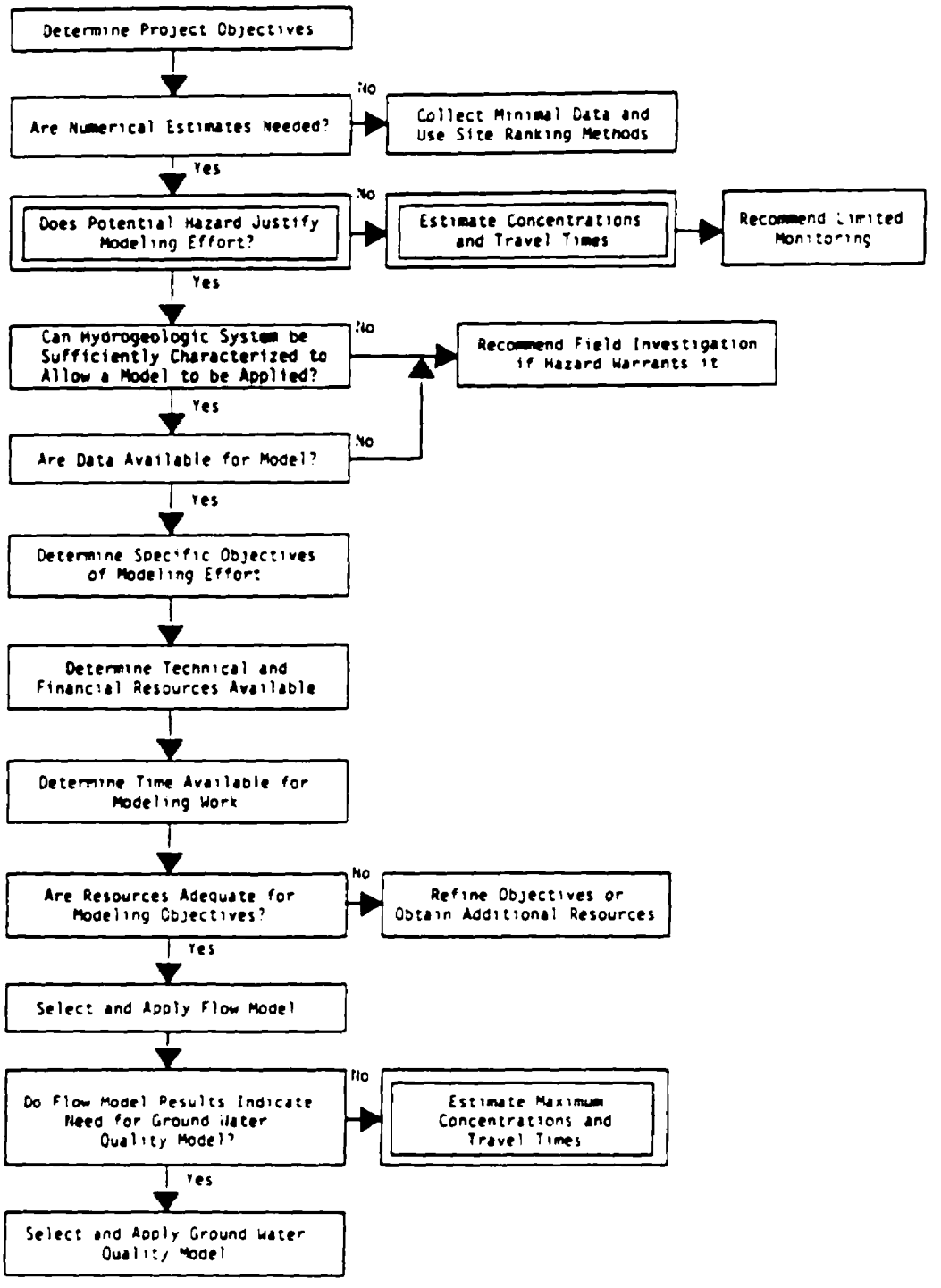

FIGURE VII-43 GENERAL SEQUENCE TO DETERMINE IF A MODELING EFFORT IS NEEDED. REFERENCE: SUMMERS AND RUPP (1982B)

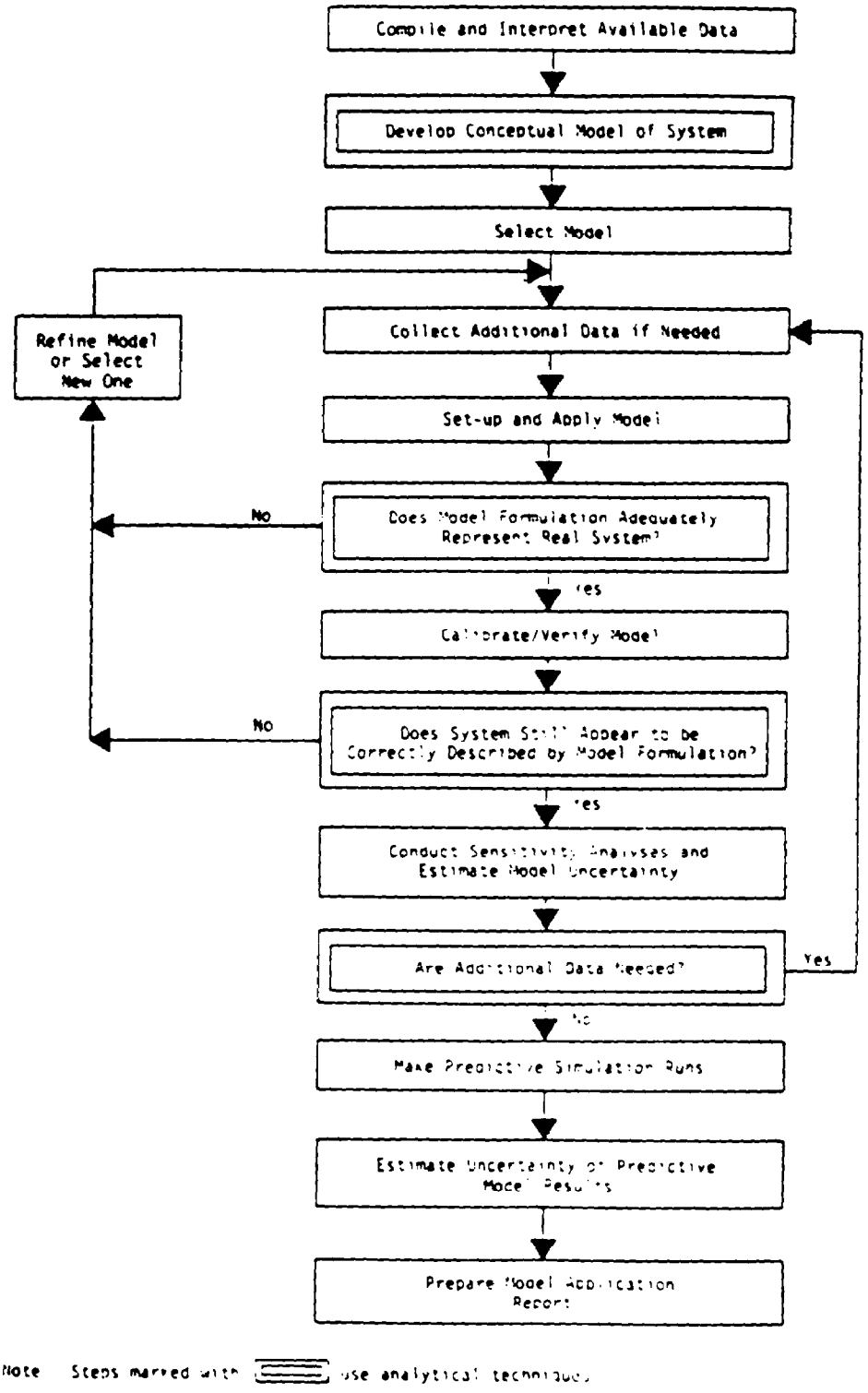

FIGURE VII-44 STEPS INVOLVED IN MODEL APPLICATION. REFERENCE: SUMMERS AND RUPP (1982B)

REFERENCES

References Cited

Abramowitz, M. and I.A. Stegun. 1964. Handbook of Mathematical Functions with Formulas, Graphs and Mathematical Tables. Applied Mathematics Series No. 55, National Bureau of Standards, 1046 p.

Bachmat, Y., B. Andrews, D. Holtz and S. Sebastian. 1978. Utilization of Numerical Ground Water Models for Water Resource Management. EPA-600/8-78-012, U.S. EPA, Robert S. Kerr Environmental Research Laboratory, Ada, Okalhoma.

Basak, P. and V.V. Murty. 1979. Determination of Hydrodynamic Dispersion Coefficients Using "Inverfc". Journal of Hydrology, Volume 41, pp. 43-48.

Baver, L.D., W.H. Gardner and W.R. Gardner. 1972. Soil Physics, Fourth Edition, John Wiley and Sons, Inc., New York, 498 p.

Bear, Jacob. 1972. Dynamics of Fluids in Porous Media. American Elsevier Publishing Co., Inc., New York, 764 p.

Bjerrum, L., J.K. Nash, R.M. Kennard and R.R. Gibson. 1972. Hydraulic Fracturing in Field Permeability Testing. Geotechnique, Volume 22, Number 2.

Black, C.A. 1965. Methods of Soil Analysis: Part 1, Physical and Mineralogical Properties, Including Statistics of Measurement and Sampling. American Society of Agronomy, Madison, Wisconsin, 770 p.

Bouwer, H. and R.D. Jackson. 1974. Determining Soil Properties. Drainage for Agriculture, edited by J. van Schilfgaarde. American Society of Agronomy, Madison, Wis., pp. 611-672.

Bowman, B.T. and W.W. Sans. 1983. Determination of Octanol-Water Partitioning Coefficients of 61 Organophosphorous and Carbonate Insecticides and their Relationship to Respective Water Solubility Values. Journal of Environmental Science and Health, Volume B18, Number 6, pp. 667-683.

Brady, N.C. 1974. The Nature and Properties of Soils, 8th Edition. MacMillan Publishing Co., Inc., New York, 639 p.

Braester, C. 1972. Vertical Infiltration at Constant Flux at the Soil Surface. Second Annual Report (Part 1), in: Development of Methods, Tools, and Solutions for Unsaturated Flow with Application to Watershed Hydrology and Other Fields. Technion-Israel Institute of Technology, 48 p.

Brown, R.H., A.A. Konoplyantsev, J. Ineson and U.S. Kovalevsky. 1972. Ground Water Studies: An International Guide for Research and Practice, Studies and Reports in Hydrology, UNESCO, Volume 7, Number 10, pp. 1-18.

Campbell, G.S., W.D. Zollinger and S.A. Taylor. 1966. Sample Changer for Thermocouple Psychrometer: Construction and some Applications. Journal of Agronomy, Volume 58, pp. 315-318.

Cochran, W.G. 1977. Sampling Techniques. John Wiley and Sons, Inc., New York, 413 p.

Code of Federal Regulations. 1982. Part 141.11-141.16 and Part 143.3. Published by the Office of the Federal Register, U.S. Government Printing Office, Washington, D.C.

Code of Federal Regulations. 1983. Volume 48, No. 194. Published by the Office of the Federal Register, U.S. Government Printing Office, Washington, D.C.

Crank, J. 1975. The Mathematics of Diffusion, Second Edition, Claredon Press, Oxford, 414 p.

Davis, J.C. 1973. Statistics and Data Analysis in Geology. John Wiley and Sons, New York, 550 p.

Davis, S.N. and R.J. DeWiest. 1966. Hydrogeology. John Wiley and Sons, Inc., New York, 463 p.

Davis, S.N. 1969. Porosity and Permeability of Natural Materials. Flow Through Porous Media, ed. R.J.M. DeWiest. Academic Press, New York, pp. 54-89.

DeWiest, R.M. 1965. Geohydrology. John Wiley and Sons, Inc., New York, 366 p.

Drost, W., D. Klotz, A. Koch, H. Moser, F. Neumaier and W. Rauert. 1968. Point Dilution Methods of Investigating Ground Water Flow by Means of Radioisotopes. Water Resources Research, Volume 4, pp. 125-146.

Duursma, E.K. 1966. Molecular Diffusion of Radioisotopes in Interstitial Water of Sediments. International Atomic Energy Agency, Vienna, IAEA SM-72/20.

Eakin, T.E., D. Price, and J.R. Harrill. 1976. Summary Appraisals of the Nation's Ground Water Resources-Great Basin Region. U.S. Geological Survey Professional Paper 813-G, 37 p.

Elprince, A.M. and P.R. Day. 1977. Fitting Solute Breakthrough Equations to Data Using Two Adjustable Parameters. Soil Science Society of America Journal, Volume 41, Number 1, pp. 39-41.

Ferguson, H. and W. Gardner. 1962. Water Content Measurement in Soil Columns by Gamma Ray Absorption. Soil Science Society of America Proceedings, Volume 26, pp. 11-18.

Fetter, C.W., Jr. 1980. Applied Hydrogeology. Charles E. Merrill Publishing Co., Columbus, Ohio, 488 p.

Fetter, C.W., Jr. 1981. Determination of the Direction of Ground Water Flow. Ground Water Monitoring Review, Volume 1, Number 3, pp. 28-31.

Fox, W.E. and D.S. Page-Hanify. 1959. A Method of Determining Bulk Density of Soil. Soil Science, Volume 88, Number 3, pp. 168-171.

Fox, W.E. 1959. An Instrument for the Determination of Soil Volume. Soil Science, Volume 88, pp. 349-352.

Freeze, R.A. and J.A. Cherry. 1979. Ground Water. Prentice-Hall, Inc., Englewood Cliffs, N.J., 604 p.

Fried, J.J. 1975. Groundwater Pollution. Elsevier Scientific Publishing Company, New York, 330 p.

Gardner, W. and D. Kirkham. 1952. Determination of Soil Moisture by Neutron Scattering. Soil Science, Volume 73, pp. 391-401.

Gaspar, E. and M. Oncescu. 1972. Radioactive Tracers in Hydrology. American Elsevier, New York, 90 p.

Gelhar, L.W. and C.J. Axness. 1981. Stochastic Analysis of Macro-Dispersion in Three-Dimensionally Heterogeneous Aquifers. Report No. H-8, Hydraulic Research Program, New Mexico Institute of Mining and Technology, Soccorro, New Mexico, 140 p.

Gelhar, L.W. and C.L. Axness. 1983. Three-Dimensional Stochastic Analysis of Microdispersion. Water Resources Research, Volume 19, Number 1, pp. 161-180.

Gelhar, L.W., A. Mantoglou, C. Welty and K.R. Rehfeldt. 1985. A Review of Field Scale Subsurface Solute Transport Processes Under Saturated and Unsaturated Conditions. Electric Power Research Institute, Palo Alto, California. (In Press.). 107 p.

Gibson, R.E. 1966. A Note on the Constant Head Test to Measure Soil Permeability In-situ. Geotechnique, Volume 16, Number 3.

Gill, H.E. and J. Vecchioli. 1965. Availability of Ground Water in Morris County, New Jersey, U.S. Geological Survey Special Report 25.

Gillham, R.W., E.A. Sudicky, J.A. Cherry and E.O. Frind. 1984. An Advection-Diffusion Concept for Solute Transport in Heterogeneous Unconsolidated Geological Deposits. Water Resources Research, Volume 20, Number 3, pp. 369-378.

Golder, H.Q. and A.A. Gass. 1963. Field Tests for Determining Permeability of Soil Strata. A.S.T.M. Special Publication 322 (Field Testing of Soils).

Grisak, G.E., W.F. Merritt and D.W. Williams. 1977. A Fluoride Borehole Dilution Apparatus for Ground Water Velocity Measurements. Canadian Geotechnique Journal, Volume 14, pp. 554-561.

Gurr, C.G. 1962. Use of Gamma Rays in Measuring Water Content and Permeability in Unsaturated Columns of Soil. Soil Science, Volume 94, pp. 224-229.

Guyod, H. 1966. Interpretation of Electric and Gamma Ray Logs in Water Wells. Well Log Analyst, January-March.

Halevy, E., H. Moser, O. Zellhofer and A. Zuber. 1967. Borehole Dilution Techniques: A Critical Review. Isotopes in Hydrology. IAEA, Vienna, pp. 531-564.

Hall, H.N. 1953. Compressibility of Reservoir Rocks. Transactions AIME, Volume 198, pp. 309-316.

Hanson, R.L. 1973. Evaluating the Reliability of Specific Yield Determinations. Journal of Research of the U.S. Geological Survey, Volume 1, Number 3, pp. 371-376.

Hantush, M.S. 1956. Analysis of Data from Pumping Tests in Leaky Aquifers. Transactions of the American Geophysical Union, Volume 37, Number 6, pp. 702-714.

Harleman, D.R., P.F. Mehlhorn and R.R. Rumer. 1963. Dispersion-Permeability Correlation in Porous Media. Journal of Hydraulics Division of the American Society of Civil Engineering, Number HY2, Volume 89, pp. 67-85.

Hillel, D. 1971. Soil and Water, Academic Press, New York, 288 p.

Hoopes, J.A. and D.R.F. Harleman. 1965. Waste Water Recharge and Dispersion in Porous Media, Technical Report Number 75, Hydrodynamic Lab., Massachusetts Institute of Technology, Cambridge, Mass.

Hoopes, J.A. and D.R.F. Harleman. 1967. Dispersion in Radial Flow from a Recharge Well, Journal of Geophysical Research, Volume 72, Number 14, pp. 3595-3607.

Hough, B.K. 1957. Basic Soils Engineering. Ronald Press, New York, 513 p.

Hvorslev, M.J. 1951. Time Lag and Soil Permeability in Ground Water Observations. Bulletin Number 36, U.S. Waterways Experimental Station, Vicksburg.

Johnson, A.I., R.C. Prill and D.A. Morris. 1963. Specific Yield: Column Drainage and Centrifuge Moisture Content. U.S. Geological Survey Water-Supply Paper 1662-A, 69 p.

Johnson, A.I. 1967. Specific Yield-Compilation of Specific Yields for Various Materials. U.S. Geological Survey Water-Supply Paper 1662-D, 74 p.

Jones, O.R. and A.D. Schneider. 1969. Determining Specific Yield of the Ogallala Aquifer by the Neutron Method. Water Resources Research, Volume 5, Number 6, pp. 1267-1272.

Jumikis, A.R. 1962. Soil Mechanics, D. Van Nostrand Company, Inc., Princeton, N.J.

Kaufman, A.M., L.L. Edwards and W.J. O'Connell. 1980. A Repository Post-Sealing Risk Analysis using MACRO, in Waste Management '80, Edited by R.G. Post, Arizona Board of Regents, Tucson, pp. 109-123.

Kemper, W.D. 1959. Estimation of Osmotic Stress in Soil Water from the Electrical Resistance of Finely Porous Ceramic Units. Soil Science, Volume 87, pp. 345-349.

Kerfoot, W.B. 1982. Comparison of 2-D and 3-D Ground Water Flow Meter Probes in Fully Penetrating Monitoring Wells. Proceedings of the Second National Symposium on Aquifer Restoration and Ground Water Monitoring, May 26-28, 1982, Columbus, Ohio, pp. 264-268.

Kincaid, C.T., J. T. Morrey, and C.J. Hostetler. 1983. Geohydrochemical Models for Solute Migration. Vol. I EA-3417. Electric Power Research Institute, Palo Alto, CA.

Kirkham, D. 1964. Soil Physics. Handbook of Applied Hydrology, edited by V.T. Chow. McGraw-Hill, New York, pp. 5.1-5.26.

Klock, G.O., L. Boersma and L.W. DeBacker. 1969. Pore Size Distributions as Measured by the Mercury Intrusion Method and their Use in Predicting Permeability. Soil Science Society of America Proceedings, Volume 33, Number 1, pp. 12-15.

Klotz, D., H. Moser and P. Trimborn. 1978. Single-Borehole Techniques: Present Status and Examples of Recent Applications in Isotope Hydrology. Volume 1, International Atomic Energy Agency, pp. 159-179.

Klute, A. 1965. Laboratory Measurements of Hydraulic Conductivity of Unsaturated Soil. Methods of Soil Analysis, Part I, edited by C.A. Black. American Society of Agronomy, Madison, Wis., pp. 253-261.

Klute, A. 1972. The Determination of Hydraulic Conductivity and Diffusivity of Unsaturated Soils. Science, Volume 113, Number 4, pp. 264-276.

Knutson, G. 1966. Tracers for Ground Water Investigations. Ground Water Problems (Proceedings of the International Symposium, Stockholm, Sweden). Pergamon Press, Oxford.

Krumbein, W.C. and G.D. Monk. 1943. Permeability as a Function of the Size Parameters of Unconsolidated Sand. Transactions of the American Institute of Minerology and Meterology Engineers, Volume 151, pp. 153-163.

Kruseman, G.P. and N.A. deRidder. 1970. Analysis and Evaluation of Pumping Test Data. International Institute for Land Reclamation and Improvement, Bulletin 11, Wageningen, The Netherlands.

Lacroix, Y. 1960. Notes on the Determination of Coefficients of Permeability in the Laboratory In-situ. Polytechnic School, Zurich (unpublished).

Lallemand-Barres, A. and P. Peaudecerf. 1978. Recherche des Relations Entre La Valeur de la Dispersivite Macroscopique D'un Milieu Aquifere, Ses Autres Caracteristiques et les Conditions de Mesure. Bulletin de Recherches Geologiques et Minieres, 2e Serie, Section III, Number 4, Orleans, France.

Lambe, T.W. 1951. Soil Testing for Engineers. John Wiley and Sons, N.Y., 165 p.

Lee, D.R. and J.A. Cherry. 1978. A Field Exercise on Ground Water Flow Using Seepage Meters and Mini-Piezometers. Journal of Geology Education, Volume 27, pp. 6-10.

Liakopoulos, A.C. 1965. Variation of the Permeability Tensor Ellipsoid in Homogeneous Anisotropic Soils. Water Resources Research, Volume 1, Number 1, pp. 135-141.

Lohman, S.W. 1972. Ground Water Hydraulics, U.S.G.S. Professional Paper Number 708, 70 p.

Londe, P. 1973. Water Seepage in Rock Slopes. Quarterly Journal of Engineering Geology, Volume 6, Number 1.

Loudon, A.G., 1952. The Computation of Permeability from Simple Soil Tests. Geotechnique, Volume 3, Number 4.

Milligan, V. 1976. Field Measurement of Permeability in Soil And Rock. Proceedings of the Conference on In-Situ Measurements of Soil Properties, Volume II, June 1-4, 1975. American Society of Civil Engineers, pp. 3-37.

Mills, W.B., V. Kwong, L. Mok, and M.D. Ungs. 1985. Microcomputer Methods for Toxicants in Ground Waters and Rivers. Presented at National Conference on Environmental Engineering, Boston, Mass.

Moench, A.F. and A. Ogata. 1981. A Numerical Inversion of the Laplace Transform Solution to Radial Dispersion in a Porous Medium, Water Resources Research, Volume 17, Number 1, pp. 250-252.

Molz, F.J., O. Guven and J.G. Melville. 1983. An Examination of Scale-Dependent Dispersion Coefficients. Ground Water, Volume 21, Number 6, pp. 715-725.

Mood, A.M., F.A. Graybill and D.C. Boes. 1974. Introduction to the Theory of Statistics, Third Edition, McGraw-Hill, Inc., New York. 564 p.

Morris, D.A. and A.I. Johnson. 1967. Summary of Hydrologic and Physical Properties of Rock and Soil Materials, as Analyzed by the Hydrologic Laboratory of the U.S. Geological Survey. 1948-1960, U.S. Geological Survey Water-Supply Paper 1839-D, 42 p.

Mualem, Y. 1976. A New Model for Predicting the Hydraulic Conductivity of Unsaturated Porous Media. Water Resources Research, Volume 12, Number 3, pp. 513-522.

Nelson, J.D. and R.C. Ward. 1981. Statistical Considerations and Sampling Techniques for Ground Water Monitoring. Ground Water, Volume 19, Number 6, pp. 617-625.

Nofziger, D.L. 1978. Errors in Gamma-Ray Measurements of Water Content and Bulk Density in Nonuniform Soils. Soil Science Society of America Proceedings, Volume 42, pp. 845-850.

Nye, P.H. and P.B. Tinker. 1977. Solute Movement in the Soil-Root System. University of California Press, Berkeley, 342 p.

Ogata, A. and R.B. Banks. 1961. A Solution of the Differential Equation of Longitudinal Dispersion in Porous Media. U.S. Geological Survey, Professional Paper 411-A. 7 p.

Ogata, A. 1970. Theory of Dispersion in a Granular Medium. U.S. Geological Survey, Professional Paper 411-I. 134 p.

Olea, R.A. 1975. Optimum Mapping Techniques Using Regionalized Variable Theory. Number Two Series on Spatial Analysis, Kansas Geological Survey, Lawrence, Kansas, 137 p.

Oster, C.A. 1982. Review of Ground Water Flow and Transport Models in the Unsaturated Zone. PNL-4427, NUREG/CR-2917, U.S. Nuclear Regulatory Commission, Washington, D.C.

Pettyjohn, W.A., J.R.L. Studlick, R.C. Bain and J.H. Lehr. 1979. A Ground Water Quality Atlas of the United States. National Demonstration Project, 272 p.

Phillips, K.J. and L.W Gelhar. 1978. Contaminant Transport to Deep Wells, Journal of the Hydraulics Division, ASCE, Volume 104, Number HY6, pp. 807-819.

Pickens, J.F. and G.E. Grisak. 1981a. Scale-Dependent Dispersion in a Stratified Granular Aquifer. Water Resources Research, Volume 17, Number 4, pp. 1191-1211.

Pickens, J.F. and G.E. Grisak. 1981b. Modeling of Scale-Dependent Dispersion in Hydrogeologic Systems. Water Resources Research, Volume 17, Number 6, pp. 1701-1711.

Piersol, R.J., L.E. Workman and M.C. Watson. 1940. Porosity, Total Liquid Saturation, and Permeability of Illinois Oil Sands. Illinois Geological Survey Report Investigation 67.

Pinder, G.F. and W.G. Gray. 1977. Finite Element Simulation in Surface and Subsurface Hydrology. Academic Press, New York, 295 p.

Rai, D. and J.M. Zachara. 1984. Chemical Attenuation Rates, Coefficients and Constants in Leachate Migration, Volume 1: A Critical Review. Electric Power Research Institute, Report EPRI EA-3356, Volume I, Palo Alto, California, 336 p.

Raimondi, P.G., H.G. Gradner and C.G. Petrick. 1959. Effect of Pore Structure and Molecular Diffusion on the Mixing of Misible Liquids Flowing in Porous Media. Paper presented at the American Institute of Chemical Engineers and Society of Petroleum Engineers Joint Symposium on Oil Recovery Methods, San Francisco, Preprint 43.

Rawls, W.J. and L.E. Asmussen. 1973. Neutron Probe Field Calibration for Soils in the Georgia Coastal Plain. Soil Science, Volume 110, pp. 262-265.

Reynolds, S.G. 1970a. The Gravimetric Method of Soil Moisture Determination, I, A Study of Equipment and Methodological Problems. Journal of Hydrology, Volume 11, pp. 258-273.

Reynolds, S.G. 1970b. The Gravimetric Method of Soil Moisture Determination, III, An Examination of Factors Influencing Soil Moisture Variability. Journal of Hydrology, Volume 11, pp. 288-300.

Rice, R. 1969. A Fast-Response, Field Tensiometer System. Transactions of the American Society of Agricultural Engineering, Volume 12, pp. 48-50.

Richards, L.A. and G. Ogata. 1961. Psychrometric Measurements of Soil Samples Equilibrated on Pressure Membranes. Soil Science Society of America Proceedings, Volume 25, pp. 456-459.

Richards, L.A. 1965. Physical Condition of Water in Soil. Methods of Soil Analysis, Part 1, Edited by C.A. Black. American Society of Agronomy, Madison, Wis., pp. 128-152.

Richards, S.J. 1965. Soil Suction Measurements with Tensiometers in Methods of Soil Analysis. Agronomy, Volume 9, pp. 153-163.

Robinson, V.K. 1974. Low Cost Geophysical Well Logs for Hydrogeological Investigations. Quarterly Journal of Engineering Geology, Volume 7, Number 2.

Ross, B. and C.R. Faust. 1982. Analysis of Uncertainty in Contaminant Migration Prediction. Report prepared by GeoTrans, Inc., for the U.S. EPA, 33 p.

Rowe, P.W. 1972. The Relevance of Soil Fabric to Site Investigation Practice. Twelfth Rankine Lecture, Geotechnique, Volume 22, Number 2.

Sampson, R.J. 1978. SURFACE II Graphics System (revised). Number One Series on Spatial Analysis, Kansas Geological Survey, Lawrence, Kansas, 240 p.

Scalf, M.R., J.F. McNabb, W.J. Dunlap, R.L. Cosby and J. Fryberger. 1981. Manual of Ground Water Sampling Procedures. U.S. EPA Robert S. Kerr Laboratory and National Water Well Association. 93 p.

Scheidegger, A.E. 1961. General Theory of Dispersion in Porous Media. Journal of Geophysical Research, Volume 66, Number 10, pp. 3273-3278.

Schmugge, T.J., T.J. Jackson and H.L. McKin. 1980. Survey of Methods for Soil Moisture Determination. Water Resources Research, Volume 16, Number 6, pp. 961-979.

Science Applications, Inc. 1982. Planning Workshop on Solute Migration from Utility Solid Wastes. Electric Power Research Institute, Palo Alto, California, Report No. EA-2415, 126 p.

Selig, E.T., D.C. Wobschall, S. Mansukhani and A. Motiwala. 1975. Capacitance Sensor for Soil Moisture Measurement, Record 532, Transaction of the Reserve Board, Washington, D.C., p. 64.

Sharp, J.C. 1970. Fluid Flow Through Fissured Media. Ph. D. Thesis, University of London.

Sherard, J.L., R.J. Woodward, S.F. Gizienski and W.A. Clevenger. 1963. Earth and Earth-Rock Dams. John Wiley and Sons, New York.

Simmons, C.S. and G.W. Gee. 1981. Simulation of Water Flow and Retention in Earthen Cover Materials Overlying Uranium Mill Tailings. Report Number PNL-3877, Pacific Northwest Laboratory (Battelle), Richland, Washington, 78 p.

Smith, L. and F.W. Schwartz. 1980. Mass Transport: Part 1, A Stochastic Analysis of Macroscopic Dispersion. Water Resources Research, Volume 16, Number 2, pp. 303-313.

Stallman, R.W. 1971. Aquifer-Test Design, Observation and Data Analysis. Techniques of Water Resources Investigations of the U.S. Geological Survey, Chapter B1. Government Printing Office, Washington, D.C.

Sudicky, E.A. 1983. An Advection-Diffusion Theory of Contaminant Transport for Stratified Porous Media. Ph.D. Thesis, University of Waterloo, Waterloo, Ontario, Canada, 203 p.

Sudicky, E.A., J.A. Cherry and E.O. Frind. 1983. Migration of Contaminants in Groundwater at a Landfill: A Case Study, Part 4. A Natural-Gradient Dispersion Test. Journal of Hydrology, Volume 63, pp. 81-108.

Summers, K., S. Gherini and C. Chen. 1980. Methodology to Evaluate the Potential for Ground Water Contamination from Geothermal Fluid Releases. EPA Report Number EPA-600/7-80-117, 168 p.

Summers, K. and G. Rupp. 1982a. Assessment Methods for Predicting Existence and Transport of Ground Water Contamination. Tetra Tech Report. 47 p.

Summers, K. and G. Rupp. 1982b. Selection and Use of Assessment Methods for Ground Water Contamination. Paper in State, County, Regional and Municipal Jurisdiction of Ground Water Protection: Proceedings of the Sixth National Ground Water Quality Symposium, September 22-24, 1982, Atlanta, GA. p. 209-218.

Tang, D.H. and D.K. Babu. 1979. Analytical Solution of a Velocity Dependent Dispersion Problem, Water Resources Research, Volume 15, Number 6, pp. 1471-1478.

Taylor, S.A. and G.L. Ashcroft. 1972. Physical Edaphology, W.H. Freeman and Company, San Francisco, 533 p.

Terzaghi, K. 1960. Storage Dam Founded on Landslide Debris. Journal of the Boston Society of Civil Engineering. January.

Tetra Tech. 1977. Stream-Aquifer Model of Carlls River Basin Long Island, New York. 85 p.

Tetra Tech. 1984a. Ground Water Data Analyses at Utility Waste Disposal Sites. EPRI Research Project RP2283-2. Electric Power Research Institute, Palo Alto, California.

Tetra Tech. 1984b. Proceedings of First SWES Technology Transfer Seminar on Solute Migration in Ground Water at Utility Waste Disposal Sites. Project Manager-Ishwar P. Muraka. Electric Power Research Institute, Palo Alto, California.

Thomas, H.E. 1951. Ground Water Regions of the United States.

Thomas, A. 1963. In-Situ Measurement of Moisture in Soil and Similar Substance by Fringe Capacitance. Journal of Scientific Instrumentation, Volume 43, p. 996.

Thomas, S.D., B. Ross and J.W. Mercer. 1982. A Summary of Repository Siting Models. NUREG/CR-2782, U.S. Nuclear Regulatory Commission, Washington, D.C.

Todd, D.K. 1959. Ground Water Hydrology. John Wiley and Sons, Inc., New York, 336 p.

Todd, D.K. 1980. Ground Water Hydrology, Second Edition. John Wiley and Sons, New York, 535 p.

Todorovic, P. 1975. A Stochastic Model of Dispersion in a Porous Medium. Water Resources Research, Volume 11, Number 2, pp. 348-354.

(USBR) United States Department of Interior, Bureau of Reclamation. 1968. Earth Manual, Denver, Colorado.

U.S. Environmental Protection Agency. 1977a. National Interim Primary Drinking Water Regulations. U.S. Government Printing Office, Washington, D.C.

U.S. Environmental Protection Agency. 1977b. National Secondary Drinking Water Regulations - Proposed Rules. Federal Register, Volume 42, Number 62.

U.S. Environmental Protection Agency. 1979a. Draft Report to Congress: Water Supply-Wastewater Treatment Coordination Study. EPA Contract No. 68-01-5033. 375 p.

U.S. Environmental Protection Agency. 1979b. Handbook for Analytical Quality Control in Water and Wastewater Laboratories, U.S. EPA EMSL Cincinnati, Ohio. EPA Report No. EPA-600/4-79-019.

U.S. Environmental Protection Agency. 1980. Procedures Manual for Ground Water Monitoring at Solid Waste Disposal Facilities. Report No. SW-611. 2nd Edition. 269 p.

U.S. Environmental Protection Agency. 1984. Ground Water Protection Strategy. Washington, D.C.

Vachaud, G., J.M. Royer and J.D. Cooper. 1977. Comparison of Methods of Calibration of a Neutron Probe by Gravimetry on Neutron-Capture Model. Journal of Hydrology, Volume 34, pp. 343-356.

van Bavel, C.H.M. 1961. Calibration and Characteristics of Two Neutron Moisture Probes. Soil Science Society of America Proceedings, Volume 25, pp. 329-334.

van Bavel, C.H.M. 1962. Accuracy and Source Strength in Soil Moisture Neutron Probes. Soil Science Society of America Proceedings, Volume 26, p. 405.

van Everdingen, R.O. 1963. Groundwater Flow-Diagrams in Sections with Exaggerated Vertical Scale. Geological Survey of Canada Paper 63-27, 21 p.

van Genuchten, M.Th. 1978. Proceedings of the Fourth Annual Hazardous Waste Management Symposium, Southwest Research Institute and U.S. EPA, San Antonio, Texas, March 6-8, 1978.

van Genuchten, M.Th. 1980. A Closed-Form Equation for Predicting the Hydraulic Conductivity of Unsaturated Soils. Soil Science Society of America Proceedings, Volume 44, pp. 892-898.

van Genuchten, M.T. and W.J. Alves. 1982. Analytical Solutions of the One-Dimensional Convective-Dispersive Solute Transport Equation. USDA Agricultural Research Service, Technical Bulletin, Number 1661, 149 p.

Walker, F.C. 1955. Experience in the Evaluation and Treatment of Seepage from Operating Reservoirs. Fifth International Congress on Large Dams, Paris.

Walton, W.C. 1970. Groundwater Resource Evaluation. McGraw-Hill Book Co., New York, 664 p.

Weast, R.C. 1969. Handbook of Chemistry and Physics, 50th Edition. The Chemical Rubber Co., Cleveland, Ohio, 2356 p.

Weeks, E.P. 1969. Determining the Ratio of Horizontal to Vertical Permeability by Aquifer Test Analysis. Water Resources Research, Volume 5, pp. 196-214.

Whitaker, S. 1967. Diffusion and Dispersion in Porous Media. Journal of the American Institute of Chemical Engineering, Volume 13, Number 3, pp. 420-427.

Wilkes, P.F. 1974. Permeability Tests in Alluvial Deposits and the Determination of K_0. Geotechnique, Volume 24, Number 1.

Williams, T.H.L. 1978. An Automatic Scanning and Recording Tensiometer System. Journal of Hydrology, Volume 39, pp. 175-183.

Wilson, J.T. and J.F. McNabb. 1981. Biodegradation of Contaminants in the Subsurface. First International Conference on Ground Water Quality Research, October 7-10, 1981, Houston, Texas.

Wilson, J.L. and P.J. Miller. 1978. Two-Dimensional Plume in Uniform Ground-Water Flow. Journal of the Hydraulic Division, ASCE, Volume 104, Number 4, pp. 503-514.

Wilson, L.G. 1981. Monitoring in the Vadose Zone, Part 1: Storage Changes. Ground Water Monitoring Review, Volume 1, Number 3, pp. 32-41.

Wood, P.R., R.F. Lang, I.L. Payan and J. DeMarco. 1981. Anaerobic Transformation, Transport and Removal of Volatile Chlorinated Organics in Ground Water. First International Conference on Ground Water Quality Research, October 7-10, 1981, Houston, Texas.

Yeh, G. 1981. AT123D: Analytical Transient One, Two and Three-Dimensional Simulation of Waste Transport in the Aquifer System. Oak Ridge National Laboratory, ORNL-5602; Publication Number 1439, Environmental Sciences Division, Oak Ridge, Tennessee, 79 p.

Zalkin, F., M. Wilkerson and R.J. Oshima. 1984. Pesticide Movement to Groundwater, Volume II: Pesticide Contamination in the Soil Profile at DBCP, EDB, Simazine and Carbofuran Application Sites. Environmental Hazards Assessment Program, California Department of Food and Agriculture, Sacramento, California, 168 p.

Additional References on Ground Water Sampling

Barcelona, M.J., J.A. Helfrich, E.E. Garske, and J.P. Gibb. A Laboratory Evaluation of Ground Water Sampling Mechanisms. Ground Water Monitoring Review. 4:32-41.

Barcelona, M.J., J.P. Gibb, and R.A. Miller. 1983. A Guide to the Selection of Materials for Monitoring Well Construction and Ground Water Sampling. Illinois State Water Survey Contract. Report 327:78.

Claassen, H.C. 1982. Guidelines and Techniques for Obtaining Water Samples that Accurately Represent the Water Chemistry of an Aquifer. U.S. Geological Survey. Open-File Report 82-1 024, 49 p.

Ford, P.J., P.J. Turina, D.E. Seely. 1983. Characterization of Hazardous Waste Sites--A Methods Manual Vol II Available Sampling Methods. EPA Report No. EPA-600/4-83-040. 215 p.

Gibb, J.P., R.M. Schuller, and R.A. Griffin. 1981. Procedures for the Collection of Representative Water Quality Data from Monitoring Wells. Illinois State Water Survey and Geological Survey. 70 p.

Gillham, R.W., M.J.L. Robin, J.F. Barker, and J.A. Cherry. 1983. Groundwater Monitoring and Sampling Bias. Department of Earth Sciences, University of Waterloo, Ontario. Prepared for American Petroleum Institute. 206 p.

Keely, J.F. 1982. Chemical Time-Series Sampling. Ground Water Monitoring Review. 2: 29-38.

Philip, J.R. 1957. Evaporation and Moisture and Heat Fields in the Soil. J. Meteorology. Vol. 14, No. 4.

Stolzenburg, T.R., D.G. Nichols, and I. Murarka. 1984. Evaluation of Chemical Changes in Ground Water Samples due to Sampling Mechanism. Electric Power Research Institute, Palo Alto, CA (In Press).

U.S. Environmental Protection Agency. 1983. Ground Water Monitoring Guidance to Owners and Operators of Interim Status Facilities. (Draft). USEPA SW-963.

U.S. Geological Survey. 1980. Ground Water. National Handbook of Recommended Methods for Water Data Acquisition. Chapter 2. Reston, VA.

Appendix A, Monthly Distributor of Rainfall Erosivity Factor R, which appears in the first two editions of this manual., is now out of date and has been deleted.

Appendix B, Methods for Predicting Soil Erodibility Index K, which appears in the first two editions of this manual, is now out of date and has been deleted.

Appendix C, Stream and River Data, which appears in the first two editions of this manual, is now out of date and has been deleted.

APPENDIX D

IMPOUNDMENT THERMAL PROFILES

Thermal profile plots are provided (on microfiche in the enclosed envelope for EPA-published manual, or as Part 3, EPA-600/6-82-004c for paper copies purchased from the National Technical Information Service) for a variety of impoundment sizes and geographic locations throughout the United States. The locations are arranged in alphabetical order. Within each location set, the plots are ordered by depth and hydraulic residence time. An index to the plots is provided below, and the modeling approach is described in Appendix F.

APPENDIX E

MODELING THERMAL STRATIFICATION IN IMPOUNDMENTS

E.1 IMPOUNDMENT THERMAL PROFILE MODEL: BACKGROUND

The model used for computation of impoundment temperature profiles is based on the Lake Ecologic Model originally developed by Chen and Orlob (1975). The model was modified for this application to compute temperature alone. The purpose of the model application was to simulate the effects of mixing, impoundment physical characteristics, hydraulic residence time, and climate on the vertical profiles of temperature.

Physical Representation

Each configuration simulated was idealized as a number of horizontally mixed layers. Natural vertical mixing is computed by the use of dispersion coefficients in the vertical mass transport equation. Values of the dispersion coefficients for different size lakes were estimated from previous studies (Water Resources Engineers, Inc., 1969).

Temperature

Temperatures were computed as a function of depth according to Equation (E-1):

$$\bar{v}\frac{\partial T}{\partial t} = \frac{1}{c\rho}\frac{\partial}{\partial z}\left(A_z D_z \frac{\partial T}{\partial z}\right) - \frac{\partial}{\partial z}(QT) + \frac{A_s}{c\rho}(\mu-\lambda T) + \frac{\theta}{c\rho} - T\frac{\partial \bar{v}}{\partial t} \qquad \text{(E-1)}$$

where T = the local water temperature
c = specific heat
ρ = fluid density
A_z = cross-sectional area at the fluid element boundary
t = time
z = vertical distance
D_z = the eddy diffusion coefficient in the vertical direction
Q = advection across the fluid element boundaries
A_s = cross-sectional area of the surface fluid element
μ, λ = coefficients describing heat transfer across air-water interface
θ = sum of all external additions of heat to fluid volume of fluid element
$\bar{v}$ = element volume.

Application/Verification

The model has recently been used in a lake aeration study (Lorenzen and Fast, 1976). In that study, the model was applied to Kezar Lake in New Hampshire and El Capitan Reservoir in California to verify that artificial mixing could be adequately simulated.

Computed temperature profiles were compared to observed values as shown in

Figures E-1 and E-2. The model performance was judged to be good for the intended purpose of providing guidance for further study.

E.2 PREPARATION OF THERMAL PROFILES

The thermal profiles in Appendix D of this report were prepared by inputting the selected climatological conditions, inflow rate, impoundment physical conditions, and wind. Of these, only wind warrants special discussion here. The remaining model parameters are discussed in the text of Chapter 5.

Wind-Induced Mixing and the Eddy Diffusion Coefficient

Figure E-3 is a plot of the eddy conductivity coefficient versus stability. It was used to obtain coefficients for wind mixing for the model runs. The upper envelope represents high wind mixing conditions and the lower envelope represents low wind mixing conditions. Note that the plot in Figure E-3 was developed for this model, and the model was then verified with data from Hungry Horse Reservoir, which is located on the South Fork of the Flathead River in northwestern Montana. Accordingly, the extremes of wind mixing and the effects on impoundment stability are as found for Hungry Horse Reservoir. The coefficients should be applicable elsewhere, however, because the eddy diffusion coefficient is relatively insensitive to climate and location.

The significance of the eddy conductivity coefficient and its implications for wind mixing may be understood by examining an equation describing transport within the system. Mixing implies the transfer of materials or properties within a system from points of high concentration to points of low concentration, and vice versa. For a system which is undergoing forced convection, it has been observed that the time rate of transport, F, of a property, S, through the system is proportional (other things being equal) to the rate of change of concentration of this property with distance, z. In equation form, this rule is expressed as:

$$F = - D \frac{\partial S}{\partial z} \qquad \text{(E-2)}$$

where

D = coefficient of proportionality.

The mixing process as defined by Equation E-2 is variously called "effective diffusion," "eddy diffusion," or the "diffusion analogy" because it is identical in form to the equation describing the process of molecular diffusion. The difference between the two processes, however, is that for molecular diffusion, D is constant, while for turbulent transfer, D is a function of the dynamic character, or the turbulence level, of the system. In general, D is a temporal and spatial variable, and thus will be referred to here as D(z,t). Equation E-2 rewritten for heat flow over the reservoir vertical axis is:

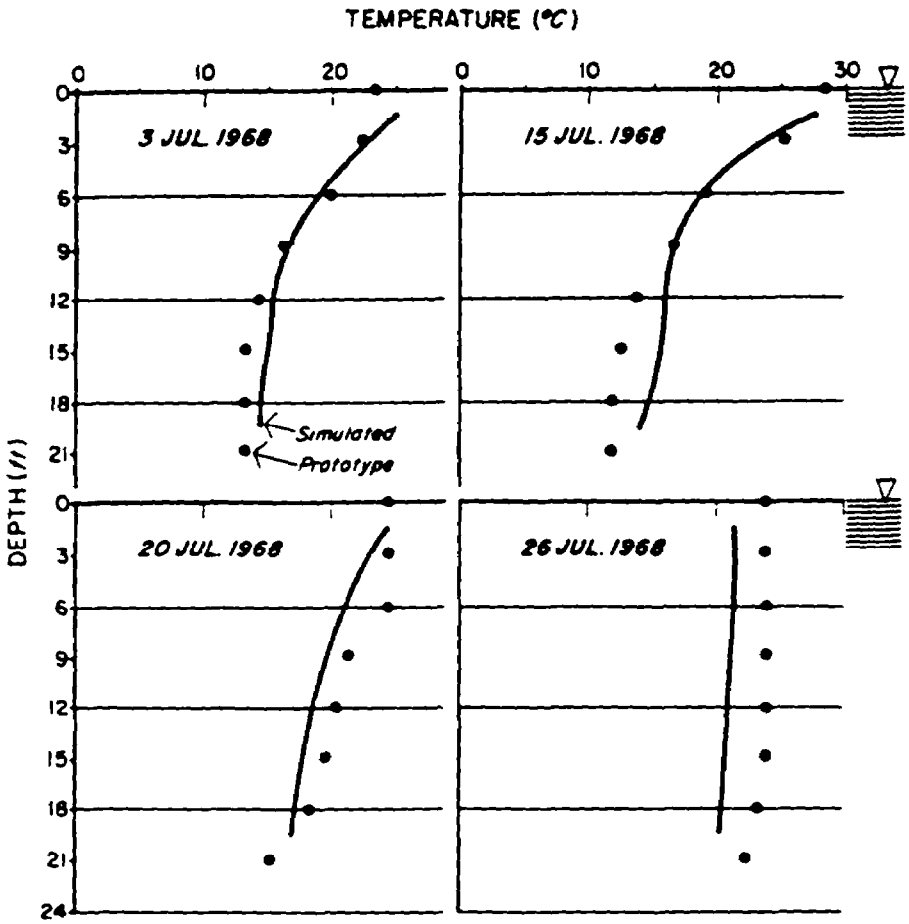

FIGURE E-1 COMPARISON OF COMPUTED AND OBSERVED TEMPERATURE PROFILES IN KEZAR LAKE

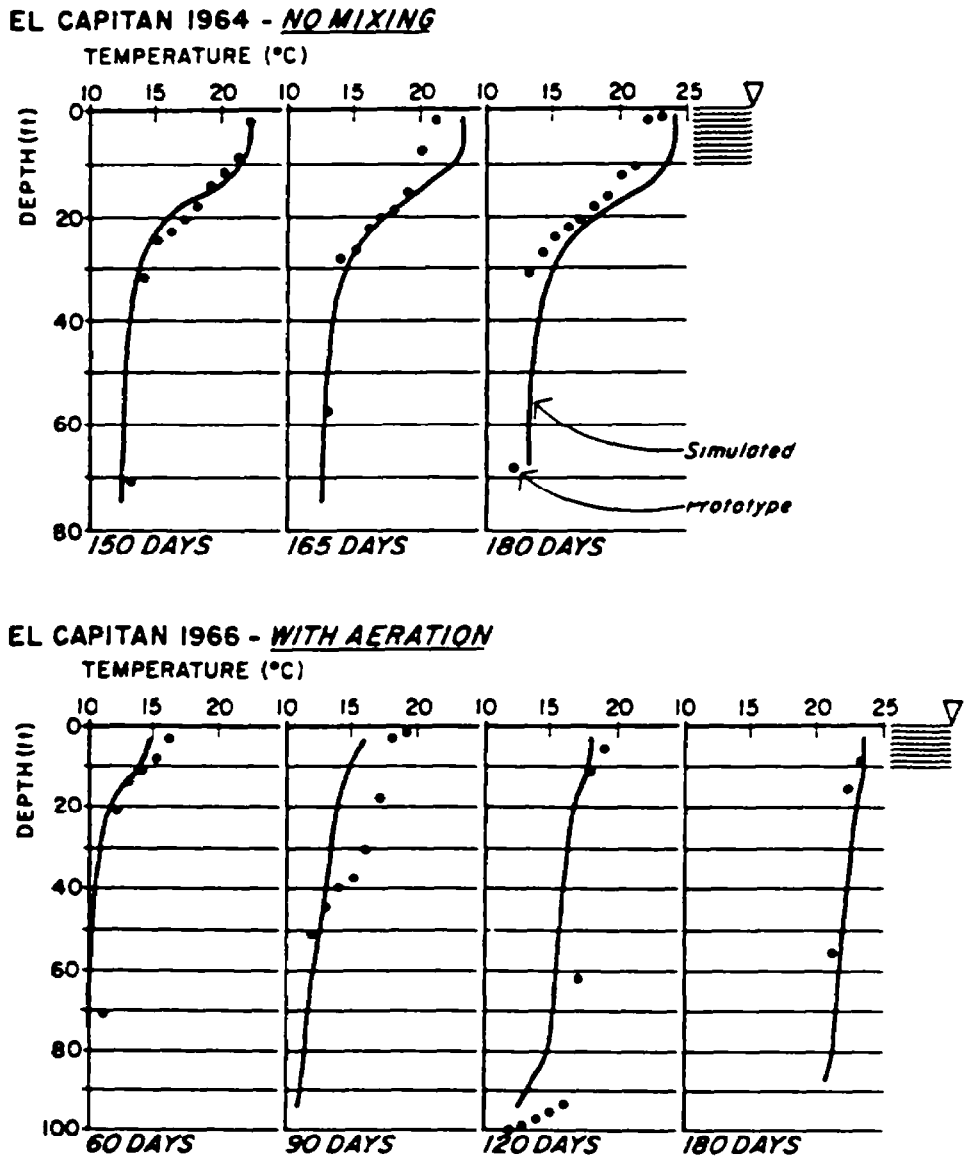

FIGURE E-2 COMPARISON OF COMPUTED AND OBSERVED TEMPERATURE PROFILES IN EL CAPITAN RESERVOIR

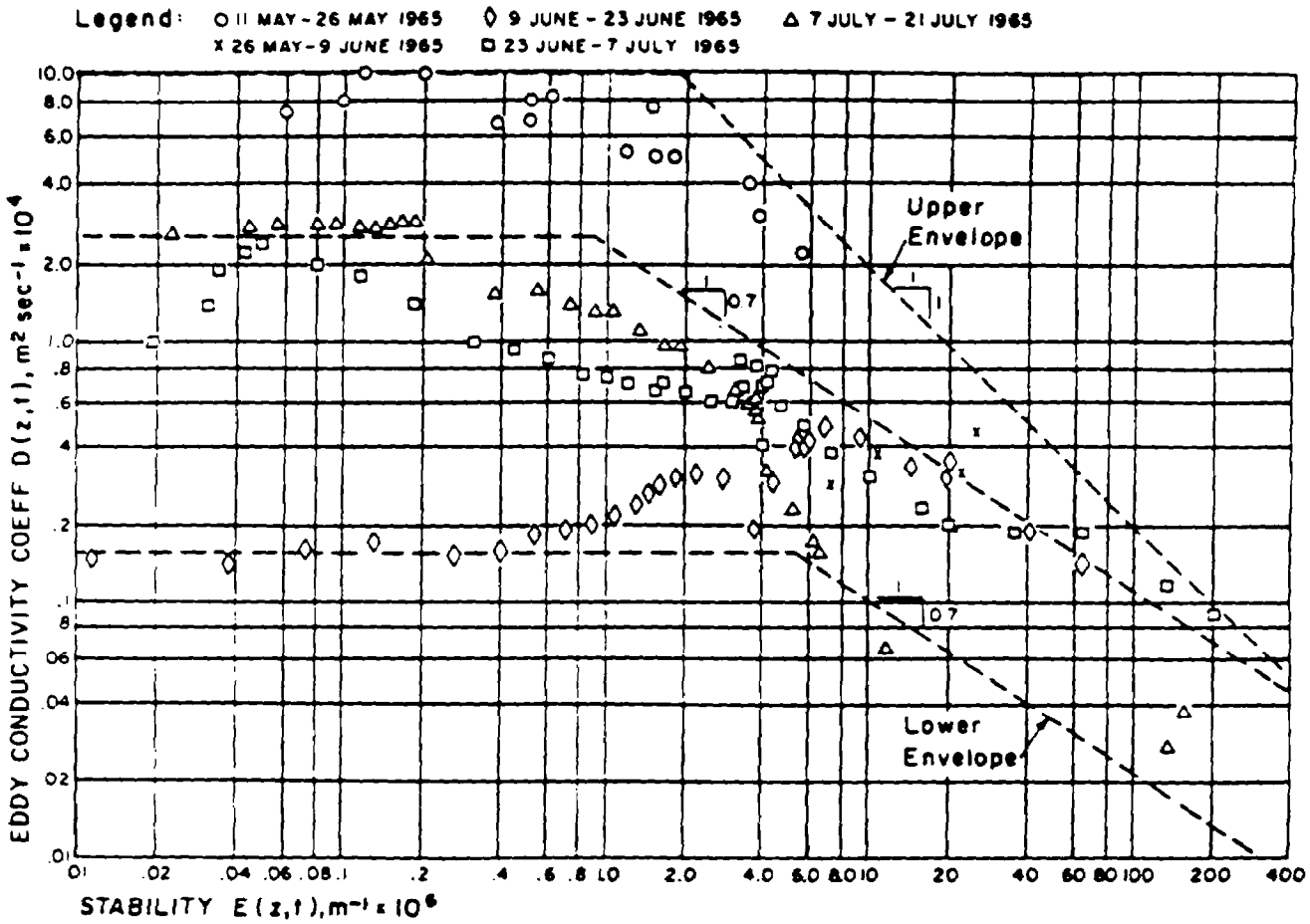

FIGURE E-3 PLOT OF THE EDDY CONDUCTIVITY COEFFICIENT, D(Z,T) VERSUS STABILITY, E(Z,T) FOR HUNGRY HORSE RESERVOIR DATA (AFTER WATER RESOURCES, INC., 1969)

$$H = -\rho c D(z,t) \frac{\partial T}{\partial z} \qquad \text{(E-3)}$$

where H = heat flux, $HL^{-2}T^{-1}$

ρ = density of water, ML^{-3}

c = heat capacity of water, $HM^{-1}D^{-1}$

$D(z,t)$ = coefficient of eddy conductivity, $L^{2}T^{-1}$

T = temperature, D

z = elevation in the reservoir, L

t = time T.

From Equation E-3, therefore, it may be seen that the rate of heat flux (H), which describes the rate of energy transfer vertically in an impoundment, is a function of the temperature gradient over depth ($\frac{\partial T}{\partial z}$) and the degree of turbulence (induced by wind and other factors) and is characterized by the eddy diffusion coefficient D(z,t) in the equation. It is this coefficient, D(z,t) which is plotted on the ordinate (stability is on the abscissa) in Figure E-3.

Surface Heat Flux

The simulation of temperature involves the following steps:

1. The heat transfer at the air-water interface is evaluated for all surface nodes as a function of the meterological variables and nodal temperatures.
2. The heat input due to shortwave solar radiation is distributed with depth according to the light transmissibility characteristics of the water (which are a function of the suspended particulates).
3. Heat is distributed within the water body by hydrodynamic transport (advection and dispersion) in the same manner as conservative dissolved constituents.

The net rate of heat transfer across the air-water interface is computed according to the following heat budget equation:

$$H = q_{sn} + q_{at} - q_{w} - q_{e} \pm q_{c} \qquad \text{(E-4)}$$

where

H = net rate of heat transfer ($Kcal/m^2/sec$)

q_{sn} = net shortwave solar radiation across the air-water interface, including losses by absorption and scattering in the atmosphere, and reflection at the water surface ($Kcal/m^2/sec$)

a_{at} = atmospheric long wave radiation across the air-water interface ($Kcal/m^2/sec$)

q_{w} = long wave back radiation from the water surface to the atmosphere ($Kcal/m^2/sec$)

a_e = evaporative heat loss (Kcal/m^2/sec)

q_c = convective heat exchange between the water surface and the atmosphere (Kcal/m^2/sec).

The heat transfer terms for long wave back radiation, evaporative heat loss, and convective heat exchange depend on the water temperature in the surface nodes (λ values), while the solar radiation and atmospheric long wave radiation (μ values) are independent of water temperature. Algorithms for the various terms of Equation E-2 are used for separate computation and then summed as shown in Equation E-1.

NOTE:

For a more detailed description of the model, its applicability, and the eddy diffusion coefficient, the reader is referred to a report entitled "Mathematical Models for the Prediction of Thermal Energy Changes in Impoundments." (See the list of references at the end of this Appendix.)

REFERENCES FOR APPENDIX E

Chen, C.W., and G.T. Orlob. 1975. Ecologic Simulation for Aquatic Environments in Systems Analysis and Simulation in Ecology. Academic Press, New York, San Franciso, and London. III:475-588.

Lorenzen, M.W., and A. Fast. 1976. A Guide to Aeration/Circulation Techniques for Lake Management. For U.S. Environmental Protection Agency, Corvallis, OR.

Water Resources Engineers, Inc. 1969. Mathematical Models for the Prediction of Thermal Energy Changes in Impoundments. Water Quality Office, U.S. Environmental Protection Agency, Washington, D.C.

APPENDIX F

RESERVOIR SEDIMENT DEPOSITION SURVEYS

Summaries of data from known reliable reservoir sedimentation surveys made in the United States through 1970 are presented in this Appendix, together with an explanation of the summary table. Additional data from surveys made after 1970 are included for some reservoirs. The reservoirs are grouped according to the 79 drainage areas into which the United States is divided in the publication: "River Basin Maps Showing Hydrologic Stations", compiled under the auspices of the Subcommittee on Hydrology, Federal Inter-Agency River Basin Committee. An index map of these drainage areas is shown on page F-78. An index to the surveys is provided below. Appendix F is available on microfiche in the enclosed envelope for the EPA-published manual, or as Part 3, for paper copies purchased from the National Technical Information Service.

APPENDIX G

INITIAL DILUTION TABLES

Appendix G consists of Initial Dilution Tables. Page G-1 provides information for choosing the appropriate table. These follow in numerical order beginning on pp. G-2 through G-101. The Appendix is available on microfiche in the enclosed envelope for the EPA-published manual, or as Part 3 for paper copies purchased from the National Technical Information Service.

APPENDIX H

EQUIVALENTS OF COMMONLY USED UNITS OF MEASUREMENT

English Unit	Multiplier	SI Unit
acre	X4.046.724→ ← 2.471X10^{-4}X	m^2
acre	X0.405→ ← 2.471X	ha*
acre-ft	X1,233.5→ ← 8.11X10^{-4}X	m^3
Btu	X1.055→ ← 0.9478X	kJ
Btu	X0.252→ ← 3.968X	kg-cal*
Btu/hr/sq ft	X3.158→ ← 0.316X	J/s-m^2
Btu/lb	X0.555→ ← 1.80X	kg-cal/kg*
cfm	X0.028→ ← 35.71X	m^3/min
cfs	X1.7→ ← 0.588X	m^3/min
cfs/sq miles	X0.657→ ← 1.522X	m^3/min km^2
cu ft	X0.028→ ← 35.314X	m^3
cu ft	X28.32→ ← 0.0353X	l*
cu in.	X16.39→ ← 0.061X	cm^3
cu yd	X0.75→ ← 1.3709X	m^3
^oF	0.555(^oF−32)→ ← 1.8(^oC)+32	^oC
^oC	plus 273→ ← minus 273	K
ft	X0.3048→ ← 3.28X	m
ft-lb	X1.356→ ← 0.737X	J
gal	X3.785→ ← 0.264X	l*
gal	X0.003785→ ← 264.2X	m^3
gpd/acre	X0.9365→ ← 1.068X	m^3/day km^2
gpd/ft	X0.0124→ ← 80.65X	m^3/day m
gpd/sq ft	X0.0408→ ← 24.51X	m^3/day m^2
gpm	X0.0631→ ← 15.85X	cm^3/s
gpm	X0.0631→ ← 15.85X	l*/s
gpm/sq ft	X40.7→ ← 0.0245X	l*/min m^2
hp	X0.7454→ ← 1.341X	kW
hp-hr	X2.684→ ← 0.372X	MJ
in.	X2.54→ ← 0.3937X	cm
lb/day/acre-ft	X3.68→ ← 0.2717X	g/day m^3
lb/1,000 cu ft	X16.0→ ← 0.0625X	g/m^3
lb/day/cu ft	X16→ ← 0.0625X	kg/day m^3
lb/mil gal	X0.92→ ← 8.333X	g/m^3
mil gal	X3,785→ ← 2.64X10^{-4}X	m^3
mgd	X3,785→ ← 2.64X10^{-4}X	m^3/day
mgd	X0.0438→ ← 22.82X	m^3/s
mile	X1.61→ ← 0.621X	km
ppb	X10^{-3}→ ← 1,000X	mg/l*
ppm	approximately equal to	mg/l*
sq ft	X0.0929→ ← 10.76X	m^2
sq in.	X645.2→ ← 0.00155	mm^2
sq miles	X2.590→ ← 0.3861X	km^2

Other commonly used conversions:

1 MGD = 1.55cfs

1 MW = 3.414 X 10^6 BTU/hr

1 BTU = 252 cal

γc_p = 62.4 BTU/ft^3/^oF

1 BTU = 778 ft-lb

1 Langley/day = 3.7 BTU/$ft.^2$/day

*Not an SI unit, but a term commonly used and preferred as a wastewater unit of expression.

APPENDIX I

ADDITIONAL AQUIFER PARAMETERS

Physical Properties of Water

The density of a fluid is defined as the mass of fluid per unit volume. The viscosity of a fluid is a measure of the resistance of the fluid to deform when moving. The kinematic viscosity ν is defined as the viscosity μ divided by the density of the fluid ρ_w:

$$\nu = \mu/\rho_w$$

Compressibility β_w is the relative change of a unit volume of fluid per unit increase in pressure. Thus β_w relates the volumetric strain to the stress induced in water by a change in fluid pressure.

Upon examining Table I-1, the viscosity μ is most affected by temperature changes and μ decreases by about 3 percent per degree Celsius rise in temperature. The properties of water are also a function of pressure, but they are even less sensitive to changes in pressure than to changes in temperature. However, in most situations that are encountered in ground water problems, the physical properties of water are considered as constants.

Particle Density

Particle density, $\rho_s(g/cm^3)$, of a soil is defined as the mass of soil solids $M_s(g)$ divided by the volume of the soil solids $V_s(cm^3)$:

$$\rho_s = M_s/V_s$$

The particle density for most mineral soils varies between 2.6 and 2.75 g/cm^3. Table I-2 gives a list of typical values for various materials. Note that organic matter has a much lower particle density, between 1.2 and 1.5 g/cm^3. Thus, surface soils usually have a lower particle density than subsoils.

Sometimes the density of a soil is expressed in terms of the specific gravity. The specific gravity G (unitless) is equal to the ratio of the particle density $\rho_s(g/cm^3)$ of the material to that of water $\rho_w(g/cm^3)$ at 4 degrees Celsius and at atmospheric pressure:

$$G = \rho_s/\rho_w$$

However, since the density of water under these conditions is 1 g/cm^3 (see Table I-2), the specific gravity is numerically (although not dimensionally) equal to the particle density.

The average particle density ρ_s (g/cm^3) of a soil can be determined in the laboratory by the picnometer method (i.e., water displacement test) (Fox, 1959; Taylor and Ashcroft, 1972). Typical values for various materials are given in Table VII-3.

TABLE I-1

PHYSICAL PROPERTIES OF PURE WATER AT ONE ATMOSPHERE

Temperature ^{o}C	Density (g/cm^3)	Viscosity (g/cm sec)	Kinematic Viscosity (cm^2/sec)	Compressibility (cm sec^2/g)
0	.99987	.01787	.0179	5.098×10^{-11}
4	1.00000	.01567	.0157	4.959×10^{-11}
5	.99999	.01519	.0152	4.928×10^{-11}
10	.99973	.01307	.0131	4.789×10^{-11}
15	.99913	.01139	.0114	4.678×10^{-11}
20	.99823	.01002	.01004	4.591×10^{-11}
25	.99708	.00890	.00893	4.524×10^{-11}
30	.99568	.00798	.00801	4.475×10^{-11}
35	.99406	.00719	.00723	4.442×10^{-11}

Reference: Weast (1969).

Specific Yield

Specific yield can be used as an estimate of effective porosity. Specific yield is also used to predict the drawdown of the water table and the local velocity field around a pumping well. It is an essential parameter for the analysis of the performance of a recovery well field.

The specific yield S_y (unitless) of an unconfined aquifer is a measure of the "water-yielding" capacity of the porous medium. The specific yield is defined as the volume of water that will discharge per unit area of saturated porous medium under a unit drop in hydraulic head. Specific yield can be expressed as either a ratio or as a percentage. That part of the water retained by molecular and surface tension forces in the void spaces of a gravity drained material is known as retained water. The "water-retaining" capacity of porous media is called the specific retention S_r (unitless). Hence, the porosity of a saturated, unconfined aquifer is equal to the sum of the specific yield and the specific retention:

$$p = S_y + S_r$$

Gravity drainage from most unconfined aquifers is not instantaneous. If the hydraulic conductivity is low, the water-yielding capacity can increase up to the

TABLE I-2

RANGE AND MEAN VALUES OF PARTICLE DENSITY

Material	Range (g/cm^3)	Mean (g/cm^3)
clay	2.51 - 2.77	2.67
silt	2.47 - 2.79	2.62
sand, fine	2.54 - 2.77	2.67
sand, medium	2.60 - 2.77	2.66
sand, coarse	2.52 - 2.73	2.65
gravel, fine	2.63 - 2.76	2.68
gravel, medium	2.65 - 2.79	2.71
gravel, coarse	2.64 - 2.76	2.69
loess	2.64 - 2.74	2.67
eolian sand	2.63 - 2.70	2.66
till, predominantly clay	2.61 - 2.69	2.65
till, predominantly silt	2.64 - 2.77	2.70
till, predominantly sand	2.63 - 2.73	2.69
till, predominantly gravel	2.67 - 2.78	2.72
glacial drift, predominantly silt	2.70 - 2.73	2.72
glacial drift, predominantly sand	2.65 - 2.75	2.69
glacial drift, predominantly gravel	2.65 - 2.75	2.68
sandstone, fine grained	2.56 - 2.72	2.65
sandstone, medium grained	2.64 - 2.69	2.66
siltstone	2.52 - 2.89	2.65
claystone	2.50 - 2.76	2.66
shale	2.47 - 2.83	2.69
limestone	2.68 - 2.88	2.75
dolomite	2.64 - 2.72	2.69
granite, weathered	2.70 - 2.84	2.74
gabbro, weathered	2.95 - 3.09	3.02
basalt	2.95 - 3.15	3.07
schist	2.70 - 2.84	2.79
slate	2.85 - 3.05	2.94

Reference: Morris and Johnson (1967).

TABLE I-3

RANGE AND MEAN VALUES OF SPECIFIC YIELD

Material[a]	Range (percent)	Mean (percent)
clay	1.1 - 17.6	6
silt	1.1 - 38.6	20
sand, fine	1.0 - 45.9	33
sand, medium	16.2 - 46.2	32
sand, coarse	18.4 - 42.9	30
gravel, fine	12.6 - 39.9	28
gravel, medium	16.9 - 43.5	24
gravel, course	13.2 - 25.2	21
loess	14.1 - 22.0	18
eolian sand (dune sand)	32.3 - 46.7	38
till, predominately silt	0.5 - 13.0	6
till, predominately sand	1.9 - 31.2	16
till, predominately gravel	5.1 - 34.2	16
glacial drift, predominately silt	33.2 - 48.1	40
glacial drift, predominately sand	29.0 - 48.2	41
sandstone, fine grained	2.1 - 39.6	21
sandstone, medium grained	11.9 - 41.1	27
siltstone	0.9 - 32.7	12
shale[b]	0.5 - 5	--
limestone	0.2 - 35.8	14
schist	21.9 - 33.2	26

[a]Reference: Morris and Johnson (1967).

[b]Reference: Walton (1970).

specific yield at a diminishing rate as the time of drainage increases.

Values of specific yield depend on grain size, shape and distribution of pores, compaction of the stratum and time of drainage. The range and mean values of laboratory measured specific yields for various geologic materials are given in Table I-3.

Specific Storage

The specific storage or elastic storage coefficient S_s of a confined aquifer is defined as the volume of water released from storage per unit volume of aquifer per unit decline in hydraulic head. This release is due to the compaction of the aquifer's granular skeleton and the expansion of pore water when the water pressure is reduced by pumping. S_s has the units of cm^{-1} and is normally a small quantity ($1 \times 10^{-5} cm^{-1}$ or less). Typical values of specific storage S_s are given for various geologic materials in Table I-4.

Storativity

Storativity or storage coefficient, S, is also defined as the volume of water that is released from storage per unit horizontal area of aquifer per unit decline of hydraulic head. It is a dimensionless quantity. This parameter is obtained in addition to transmissivity from pumping tests. It is used to compute aquifer yields and to compute drawdowns of individual wells.

For confined aquifers, storativity is due to water being released from the compression of the granular skeleton and expansion of the pore water. S is mathematically defined as the product of the specific storage, S_s (cm^{-1}) and the aquifer thickness, b(cm):

$$S = S_s b$$

The value of the storativity for confined aquifers is generally small, falling between the range of 0.00005 and 0.005 (Todd, 1980). Hence, large pressure changes over an extensive area of aquifer are required before substantial water is released.

For unconfined aquifers, storativity is due to the release of water from gravity drainage of voids (i.e., yield) and from the compressibility of the granular skeleton (i.e., elastic storage).

This is mathematically defined as:

$$S = S_y + hS_s$$

where S_y is the specific yield (dimensionless), h is the saturated thickness of the water-table aquifer (cm) and S_s is the specific storage (cm^{-1}). The value of S_y is usually several orders of magnitude larger than hS_s, except for fine-grained aquifers where S_y may approach the value of hS_s. Storativity S of unconfined aquifers ranges from 0.01 to 0.30.

TABLE I-4

RANGE OF VALUES FOR COMPRESSIBILITY AND
SPECIFIC STORAGE OF VARIOUS GEOLOGIC MATERIALS

Material	Specific Storage S_s (cm^{-1})
plastic clay	$2.0 \times 10^{-4} - 2.5 \times 10^{-5}$
stiff clay	$2.5 \times 10^{-5} - 1.3 \times 10^{-5}$
medium-hard clay	$1.3 \times 10^{-5} - 6.9 \times 10^{-6}$
loose sand	$9.8 \times 10^{-6} - 5.1 \times 10^{-6}$
dense sand	$2.1 \times 10^{-6} - 1.3 \times 10^{-6}$
dense sandy gravel	$9.8 \times 10^{-7} - 5.1 \times 10^{-7}$
rock, fissured, jointed	$6.9 \times 10^{-7} - 3.2 \times 10^{-8}$
rock, sound	less than 3.2×10^{-8}

Reference: Jumikis (1962) and Walton (1970).

Measuring Specific Yield, Specific Storage and Storativity

Although most field methods determine specific yield directly, most laboratory methods determine specific retention by the centrifuge-moisture method (Johnson et al. 1963), and specific yield S_y (unitless) is found indirectly by subtracting the specific retention S_r (unitless) from the porosity p (unitless):

$$S_y = p - S_r$$

Other laboratory methods are discussed by Johnson (1967). However, laboratory samples may be disturbed or may not be representative of the aquifer.

Several field methods are available to estimate specific yield, including drawdown tests, recharge tests, the neutron moisture methods and tracer methods. Jones and Schneider (1969) discuss the neutron moisture method and compare it to five other methods for the Ogallala aquifer in Texas. They concluded that pumping and recharge methods underestimate the specific yield by 50% compared to the other methods. Hanson (1973) also concludes that pumping will underestimate the specific yield if the pumping test is done over too short a period of time. However, Todd (1980) believes that methods based on an analysis of the time - drawdown data from well-pumping tests generally give the most reliable results.

Specific storage S_s is a function of the solid matrix and fluid compressibility. Compressibility can be determined in the laboratory by means of a consolidation

apparatus called a loading cell. Either a fixed-ring or a floating-ring container type loading cell can be used (Hall, 1953; Lambe, 1951). In the field, specific storage is generally measured indirectly as storativity S by pumping tests. If the saturated thickness b(cm) of the confined aquifer and storativity S (unitless) are known, then the specific storage S_s (cm^{-1}) can be solved as shown below:

$$S_s = S/b$$

The contribution of specific storage to storativity in unconfined aquifers is generally negligible.

Storativity can be determined directly from pumping tests of wells and from ground water fluctuations in response to atmospheric pressure or ocean tide variations and river level fluctuations. An extensive discussion of the various types of pumping tests and the procedures for calculating the storativity from them is given by Todd (1980), Walton (1970), and Lohman (1972).

APPENDIX J

MATHEMATICAL FUNCTIONS

Complimentary Error Function

The complimentary error function (erfc) is defined as follows:

$$\text{erfc}(x) = \frac{2}{\sqrt{\pi}} \int_x^\infty e^{-z^2} dz$$

In addition, erfc has the following properties:

$$\text{erfc}(x) = 1 - \text{erf}(x)$$

$$\text{erf}(-x) = -\text{erf}(x)$$

$$\text{erfc}(-x) = 2 - \text{erfc}(x)$$

$$\text{erfc}(0) = 1$$

$$\text{erfc}(\infty) = 0$$

$$\text{erfc}(-\infty) = 2$$

where erf is the error function. A list of the error function and complimentary error function for various values of x are given in Table J-1. A method for numerically computing erfc is shown in Table J-2.

The following trick should be used when using erfc and exponential functions multiplied together:

$$e^a \cdot \text{erfc}(x) = ?$$

when $a \to \infty$

$x \to \infty$

Use the following solution:

$$e^a \cdot \text{erfc}(x) = (a_1 t + a_2 t^2 + a_3 t^3 + a_4 t^4 + a_5 t^5) e^{a-x^2}$$

where $a_1 \ldots a_5$ and t are given in Table J-2. Note that the trick is to evaluate the combined exponential argument e^{a-x^2} rather than $e^a \cdot e^{-x^2}$. For example:

$$e^{100} \cdot \text{erfc}(9) = 1.15 \times 10^{7}$$

$$e^{100} \cdot \text{erfc}(10) = 5.86 \times 10^{-2}$$

$$e^{100} \cdot \text{erfc}(11) = 4.08 \times 10^{-11}$$

TABLE J-1

TABLE OF THE ERROR FUNCTION (erf) AND THE COMPLIMENTARY ERROR FUNCTION (erfc)

x	erf(x)	erfc(x)	x	erf(x)	erfc(x)
0	0	1.0	1.1	0.880205	0.119795
0.05	0.056372	0.943628	1.2	0.910314	0.089686
0.1	0.112463	0.887537	1.3	0.934008	0.065992
0.15	0.167996	0.832004	1.4	0.952285	0.047715
0.2	0.222703	0.777297	1.5	0.966105	0.033895
0.25	0.276326	0.723674	1.6	0.976348	0.023652
0.3	0.328627	0.671373	1.7	0.983790	0.016210
0.35	0.379382	0.620618	1.8	0.989091	0.010909
0.4	0.428392	0.571608	1.9	0.992790	0.007210
0.45	0.475482	0.524518	2.0	0.995322	0.004678
0.5	0.520500	0.479500	2.1	0.997021	0.002979
0.55	0.563323	0.436677	2.2	0.998137	0.001863
0.6	0.603856	0.396144	2.3	0.998857	0.001143
0.65	0.642029	0.357971	2.4	0.999311	0.000689
0.7	0.677801	0.322199	2.5	0.999593	0.000407
0.75	0.711156	0.288844	2.6	0.999764	0.000236
0.8	0.742101	0.257899	2.7	0.999866	0.000134
0.85	0.770668	0.229332	2.8	0.999925	0.000075
0.9	0.796908	0.203092	2.9	0.999959	0.000041
0.95	0.820891	0.179109	3.0	0.999978	0.000022
1.0	0.842701	0.157299	infinite	1.000000	0.000000

$\text{erfc}(x) = 1 - \text{erf}(x)$
$\text{erfc}(-x) = 2 - \text{erfc}(x)$
$\text{erf}(-x) = -\text{erf}(x)$

Reference: Crank (1975).

TABLE J-2

NUMERICAL COMPUTATION OF THE COMPLIMENTARY ERROR FUNCTION

$$\text{erfc}(x) = (a_1 t + a_2 t^2 + a_3 t^3 + a_4 t^4 + a_5 t^5) e^{-x^2} + \varepsilon(x)$$

$$\text{where} \quad t = \frac{1}{(1 + px)}$$

$$\text{error term} \quad |\varepsilon(x)| \leq 1.5 \times 10^{-7}$$

$$\text{and} \quad p = .3275911$$

$$a_1 = .254829592$$

$$a_2 = -.284496736$$

$$a_3 = 1.421413741$$

$$a_4 = -1.453152027$$

$$a_5 = 1.061405429$$

Reference: page 299, Eq. 7.1.26 of Abramowitz and Stegun (1964).

Leaky Well Function of Hantush

The leaky well function of Hantush is defined as follows:

$$W(u,r/B) = \int_u^\infty \frac{\exp}{t} \left(-t - \frac{r^2}{4B^2 t} \right) dt$$

where W(:) has the limits:

$W(o,r/B) = 2K_o(r/B)$ (modified Bessel function of zero order)

$W(u,o) = E_1(u)$ (exponential integral)

$W(\infty,r/B) = 0$

exp(:) = exponential function

The leaky well function has been extensively tabulated by Hantush (1956) and is given in Table J-3. For large values of r/B (i.e., r/B > 1), Wilson and Miller (1978) have developed the following approximation to W:

TABLE J-3

THE LEAKY WELL FUNCTION OF HANTUSH

$W(u,r/B)$

u	r/B																	
	0.01	0.015	0.03	0.05	0.075	0.10	0.15	0.2	0.3	0.4	0.5	0.6	0.7	0.8	0.9	1.0	1.5	2.0	2.5
0.000001	9.4425	8.6319	7.2471	6.2705	5.4270	4.9541	4.0601	3.5954	2.7449	2.2791	1.8468	1.5550	1.3210	1.1307	0.9735	0.8420	0.4276	0.2270	0.1247
0.000005	9.0413	8.6119	7.2471	6.2705	5.4270	4.9541	4.0601	3.5954	2.7449	2.2791	1.8468	1.5550	1.3210	1.1307	0.9735	0.8420	0.4276	0.2270	0.1247
0.00001	9.4270	8.6313	7.2471	6.2705	5.4270	4.9541	4.0601	3.5954	2.7449	2.2791	1.8468	1.5550	1.3210	1.1307	0.9735	0.8420	0.4276	0.2270	0.1247
0.00005	8.8827	8.0533	7.2456	6.2705	5.4270	4.9541	4.0601	3.5954	2.7449	2.2791	1.8468	1.5550	1.3210	1.1307	0.9735	0.8420	0.4276	0.2270	0.1247
0.0001	8.3903	8.0419	7.2122	6.2703	5.4270	4.9541	4.0601	3.5954	2.7449	2.2791	1.8468	1.5550	1.3210	1.1307	0.9735	0.8420	0.4276	0.2270	0.1247
0.0005	6.9750	6.9152	6.6210	6.0871	5.4057	4.9530	4.0601	3.5954	2.7449	2.2791	1.8468	1.5550	1.3210	1.1307	0.9735	0.8420	0.4276	0.2270	0.1247
0.001	6.3369	6.2765	6.1707	5.7965	5.3870	4.9297	4.0595	3.5954	2.7449	2.2791	1.8468	1.5550	1.3210	1.1307	0.9735	0.8420	0.4276	0.2270	0.1247
0.005	4.7212	4.7152	4.6879	4.6004	4.4713	4.2960	3.8871	3.4967	2.7429	2.2790	1.8468	1.5550	1.3210	1.1307	0.9735	0.8420	0.4276	0.2270	0.1247
0.01	4.0356	4.0320	4.0167	3.9795	3.9091	3.8150	3.5775	3.2975	2.7104	2.2751	1.8466	1.5550	1.3210	1.1307	0.9735	0.8420	0.4276	0.2270	0.1247
0.05	2.4675	2.4670	2.4647	2.4576	2.4440	2.4273	2.3776	2.3110	2.1781	2.0675	1.8927	1.7055	1.7055	1.1210	0.9700	0.8400	0.4276	0.2270	0.1247
0.1	1.8227	1.8225	1.8213	1.8184	1.8130	1.8050	1.7829	1.7527	1.6904	1.5644	1.4022	1.3115	1.1701	1.0666	0.9297	0.8190	0.4271	0.2270	0.1247
0.5	0.5598	0.5597	0.5595	0.5594	0.5588	0.5581	0.5561	0.5532	0.5453	0.5340	0.5206	0.5044	0.4860	0.4656	0.4440	0.4230	0.3087	0.1964	0.1170
1.0	0.2196	0.2196	0.2193	0.2193	0.2191	0.2190	0.2186	0.2179	0.2161	0.2135	0.2103	0.2065	0.2020	0.1970	0.1914	0.1856	0.1560	0.1139	0.0803
5.0	0.0011	0.0011	0.0011	0.0011	0.0011	0.0011	0.0011	0.0011	0.0011	0.0011	0.0011	0.0011	0.0011	0.0011	0.0011	0.0011	0.0010	0.0010	0.0008

Reference: Hantush (1956).

$$W(u,r/B) = \left(\frac{\pi B}{2r}\right)^{\frac{1}{2}} \exp\left(-\frac{r}{B}\right)\operatorname{erfc}\left(-\frac{\left(\frac{r}{B} - 2u\right)}{2\sqrt{u}}\right)$$

in which erfc is the complementary error function (see Table J-1). This expression for W is reasonably accurate (within 10 percent) for $r/B > 1$ and is very accurate (within 1 percent) for $r/B > 10$.

Note that at large times (i.e., as u goes to zero) the leaky well function reduces to the modified Bessel function K_0:

$$W(0,r/B) = 2K_0(r/B)$$

If r/B is larger than one, the following approximation for the Bessel function can be made:

$$K_0(r/B) = \left(\frac{\pi B}{2r}\right)^{\frac{1}{2}} \exp\left(-\frac{r}{B}\right)$$

• U.S. GOVERNMENT PRINTING OFFICE 1988 - 550-111/80679